Nonlinear scale-dependent deformation behaviour of beam and plate structures

Ali Farajpour Ouderji

School of Mechanical Engineering

The University of Adelaide

Adelaide, Australia

A thesis submitted in fulfilment of the requirements

for the degree of Ph.D. in Mechanical Engineering

Summary

Improving the knowledge of the mechanics of small-scale structures is important in many microelectromechanical and nanoelectromechanical systems. Classical continuum mechanics cannot be utilised to determine the mechanical response of small-scale structures, since size effects become significant at small-scale levels. Modified elasticity models have been introduced for the mechanics of ultra-small structures. It has recently been shown that higher-order models, such as nonlocal strain gradient and integral models, are more capable of incorporating scale influences on the mechanical characteristics of small-scale structures than the classical continuum models. In addition, some scale-dependent models are restricted to a specific range of sizes. For instance, nonlocal effects on the mechanical behaviour vanish after a particular length. Scrutinising the available literature indicates that the large amplitude vibrations of small-scale beams and plates using two-parameter scale-dependent models and nonlocal integral models have not been investigated yet. In addition, no two-parameter continuum model with geometrical nonlinearity has been introduced to analyse the influence of a geometrical imperfection on the vibration of small-scale beams. Analysing these systems would provide useful results for small-scale mass sensors, resonators, energy harvesters and actuators using small-scale beams and plates.

In this thesis, scale-dependent nonlinear continuum models are developed for the time-dependent deformation behaviour of beam-shaped structures. The models contain two completely different size parameters, which make it able to describe both the reduction and increase in the total stiffness. The first size parameter accounts for the nonlocality of the stress, while the second one describes the strain gradient effect. Geometrical nonlinearity on the vibrations of small-scale beams is captured through the strain-displacement equations. The small-scale beam is assumed to possess geometrical imperfections. Hamilton's approach is utilised for deriving the corresponding differential equations. The coupled nonlinear motion equations are solved numerically employing Galerkin's method of discretisation and the continuation scheme of solution. It is concluded that geometrical imperfections

would substantially alter the nonlinear vibrational response of small-scale beams. When there is a relatively small geometrical imperfection in the structure, the small-scale beam exhibits a hardening-type nonlinearity while a combined hardening- and softening-type nonlinearity is found for beams with large geometrical imperfections. The strain gradient influence is associated with an enhancement in the beam stiffness, leading to higher nonlinear resonance frequencies. By contrast, the stress nonlocality is related to a remarkable reduction in the total stiffness, and consequently lower nonlinear resonance frequencies. In addition, a scale-dependent model of beams is proposed in this thesis to analyse the influence of viscoelasticity and geometrical nonlinearity on the vibration of small-scale beams. A nonlocal theory incorporating strain gradients is used for describing the problem in a mathematical form. Implementing the classical continuum model of beams causes a substantial overestimation in the beam vibrational amplitude. In addition, the nonlinear resonance frequency computed by the nonlocal model is less than that obtained via the classical model. When the forcing amplitude is comparatively low, the linear and nonlinear damping mechanisms predict almost the same results. However, when forcing amplitudes become larger, the role of nonlinear viscoelasticity in the vibrational response increases. The resonance frequency of the scale-dependent model with a nonlinear damping mechanism is lower than that of the linear one.

To simulate scale effects on the mechanical behaviour of ultra-small plates, a novel scale-dependent model of plates is developed. The static deflection and oscillation of rectangular plates at small-scale levels are analysed via a two-dimensional stress-driven nonlocal integral model. A reasonable kernel function, which fulfil all necessary criteria, is introduced for rectangular small-scale plates for the first time. Hamilton and Leibniz integral rules are used for deriving the non-classical motion equations of the structure. Moreover, two types of edge conditions are obtained for the linear vibration. The first type is the well-known classical boundary condition while the second type is the non-classical edge condition associated with the curvature nonlocality. The differential quadrature technique as a powerful numerical approach for implementing complex boundary conditions is used. It is found that while the Laplacian-based nonlocal model cannot predict size influences on the

bending of small-scale plates subject to uniform lateral loading, the bending response is remarkably size-dependent based on the stress-driven plate model. When the size influence increases, the difference between the resonance frequency obtained via the stress-driven model and that of other theories substantially increases. Moreover, the resonance frequency is higher when the curvature nonlocality increases due to an enhancement in the plate stiffness. It is also concluded that more constraint on the small-scale plate causes the system to vibrate at a relatively high frequency. In addition to the linear vibration, the time-dependent large deformation of small-scale plates incorporating size influences is studied. The stress-driven theory is employed to formulate the problem at small-scale levels. Geometrical nonlinearity effects are taken into account via von Kármán's theory. Three types of edge conditions including one conventional and two non-conventional conditions are presented for nonlinear vibrations. The first non-classical edge condition is associated with the curvature nonlocality while the second one is related to nonlocal in-plane strain components. A differential quadrature technique and an appropriate iteration method are used to compute the nonlinear natural frequencies and maximum in-plane displacements. Molecular dynamics simulations are also performed for verification purposes. Nonlinear frequency ratios are increased when vibration amplitudes increase. Furthermore, the curvature nonlocality would cause the small-scale pate to vibrate at a lower nonlinear frequency ratio. By contrast, the nonlocal in-plane strain has the opposite effect on the small-scale system.

The outcomes from this thesis will be useful for engineers to design vibrating small-scale resonators and sensors using ultra-small plates.

Thesis declaration

I certify that this work contains no material which has been accepted for the award of any other degree or diploma in my name, in any university or other tertiary institution and, to the best of my knowledge and belief, contains no material previously published or written by another person, except where due reference has been made in the text. In addition, I certify that no part of this work will, in the future, be used in a submission in my name, for any other degree or diploma in any university or other tertiary institution without the prior approval of the University of Adelaide and where applicable, any partner institution responsible for the joint-award of this degree.

I acknowledge that copyright of published works contained within this thesis resides with the copyright holder(s) of those works.

I also give permission for the digital version of my thesis to be made available on the web, via the University's digital research repository, the Library Search and also through web search engines, unless permission has been granted by the University to restrict access for a period of time.

I acknowledge the support I have received for my research through the provision of an Australian Government Research Training Program Scholarship.

Ali Farajpour Ouderji

18/2/2021

Acknowledgments

I would like to express that I am very grateful for my family's unconditional assistance throughout my life. Without their love and guidance, I could not follow my heart and dreams in this world. I owe everything in my life to my father Hossein, my mother Tayebeh and my brother Mohammad Reza. They give me endless love, inspiration, motivation and support at every second of my life from dawn to dusk. This thesis is lovingly and respectfully dedicated to them, although nothing can compensate for their love and support. Also, I am very thankful to my grandmother Hayat for her prayers and attention to me. I would like to recall the great memories of my grandparents Mehdi, Akbar and Sefora as well as my uncle Mohammad. Although they passed away, their memories, braveness, kindness and extremely valuable lessons will be with me for ever.

I would like to sincerely thank my excellent supervisors Professor Carl Howard and Dr William Robertson for their wonderful and precious help and guidance during my study at the University of Adelaide. Their support and knowledge have helped me a lot to complete this thesis and be hopeful for a better future. In addition, I am really grateful to them for the proof-reading of the thesis and papers and for their valuable comments, which have assisted me a lot to increase my knowledge. Also, I am very thankful for Dr. Paul Medwell's help and advice. I will not forget his significant assistance during one of the most difficult moments of my life.

Finally, I would like to appreciate the help of all other persons who have assisted me to complete this thesis. I have learned a lot from them, and I would use these valuable lessons in my life.

Table of contents

Chapter 1
Introduction

Chapter overview

This chapter provides an introductory background and motivation about the research conducted in this thesis. Next, an introduction about size-dependent theoretical tools such as nonlocal and strain gradient elasticity, and the basic concept of molecular dynamics are introduced. The scope, aims and objectives of the present work are then specified. The overall structure of this thesis is presented at the end of this chapter.

1 Introduction

1.1 Motivation

Flexible thin-walled structures are often used in mechanical and civil engineering applications. The deformation behaviour of flexible thin-walled structures, such as elastic plates and beams at both macroscale and small-scale levels, has been the focus of many research studies in the literature due to their applications in biomedical, civil, and mechanical engineering. Developing theoretical models using continuum mechanics is beneficial to predicting the deformation behaviour of these thin-walled structures. The deformation can either be amplified or mitigated depending on the application. When the deformation is large compared to the thickness of the structure, theories based on a linear response are not valid, and theories that account for non-linearities in the physics need to be utilised. As a 'rule-of-thumb', linear theoretical models are only applicable for deformations less than 5% of the thickness of a structure [1]. For MEMS and other ultra-small devices, this threshold is frequently exceeded, and impresses the need for utilising non-linear structural mechanics models. For small-scale structures, developing a modified continuum model that incorporates 'size effects' is essential.

Nanoscale structures including nanoscale rods , rings [2], beams [3-5], plates [6, 7], and shells [8, 9] have been utilised as the structural parts of nanoelectromechanical systems (NEMS). Nanomechanical resonators [10, 11], nanoscale mass sensors [12], electromechanical nano-actuators [13], and nano-energy harvesters [14] are examples of these NEMS-based devices. These nanoscale devices have applications in areas of nanotechnology such as nano-electronics, nano-machines and nano-medicine. To achieve a better performance of nano-devices, a better understanding of the mechanical characteristics of nanostructures is important, as these ultra-small structures are usually subject to mechanical loads, pressure or stresses. In addition, in nano-devices such as nanoscale generators [15, 16], the mechanical energy is converted into electricity, hence an analysis on the electro-mechanical behaviour is essential.

Performing accurate experimental measurements at nanoscale levels is challenging, and therefore continuum-based modelling and molecular dynamics (MD) simulations of nanostructures have attracted a considerable amount of attention. Using continuum-based models and the results of MD simulations, the number of required experimental measurements for the validations of models can be reduced. Compared to MD simulations, the continuum modelling of nanostructures is less computationally expensive. Particularly, performing MD simulations on a nanostructure with a large number of molecules requires a high computational effort. Using continuum models, the mechanical characteristics can be formulated and estimated. In this way, the computational costs of MD simulations can be reduced by eliminating unnecessary simulations. In addition, the results from continuum-based modelling of nanostructures complement and can help clarify the results of experimental measurements and molecular dynamics simulations.

Accounting for scale effects has a crucial role in the mechanics of nanostructures, as opposed to in macrostructures [17, 18]. Thus, traditional continuum-based theories, which are scale-free, have been modified in order to capture size effects. Various size-dependent theories for examining the mechanical characteristics of nanostructures have been introduced in recent years. Since the mechanical behaviour of structures at microscale levels [19, 20] is different from that observed at nanoscale levels, the modified continuum-based theories of microstructures are different from those of nanostructures [21]. In general, structural stiffness hardening is observed at microscale levels whereas the mechanics of nanostructures is usually governed by stiffness softening. Therefore, size-dependent models, including the couple stress [22, 23] and strain gradient elasticities [24], are often used to analyse the mechanical behaviour of microstructures including microbeams, microbars, and microplates, while the nonlocal elasticity theory [25, 26] is applied to nanoscale structures. However, to have a more general size-dependent continuum-based model capable of predicting size effects at different small scales, a combination of these modified elasticity theories [27] can be employed. In addition, more recently, a number of nonlocal integral continuum models [28, 29] with non-classical

3

constitutive boundary conditions have been used for ultra-small structures, which do not exhibit the drawbacks of conventional scale-dependent models.

1.2 Size-dependent continuum mechanics

In this section, size-dependent [30, 31] elasticity theories, including nonlocal elasticity and nonlocal strain gradient elasticity, which are commonly applied to nanoscale structures, are reviewed. Firstly, the basic concept of nonlocal elasticity is clarified, and then both the integral and differential nonlocal constitutive relations are discussed. Finally, the theory of the nonlocal strain gradient elasticity is introduced.

The main advantage of advanced elasticity approaches such as nonlocal strain gradient theory (NSGT) and stress-driven integral elasticity (SDIE) compared to the classical elasticity theory (CET) is size dependency. The CET is scale-free, and thus can only predict size-independent mechanical characteristics. As a result, the application of this theory to small-scale beam and plate structures is not recommended. By contrast, the NSGT and SDIE contain at least on scale parameter that accounts for size effects. These scale-dependent theories are valid at a wide range of sizes from ultrasmall to macroscale levels. However, the computational costs of the NSGT and SDIE are higher than the CET. The NSGT has two size parameters (one related to stress nonlocalities and the other associated with strain gradients) while one parameter illustrates size effects in the SDIE. On the other side, constitutive boundary conditions are captured in the SDIE whereas the NSGT and CET do not include these extra boundary conditions.

Consider a carbon nanotube of length L as a small-scale beam. The fundamental building block of the carbon nanotube is a carbon hexagon with bond length a. Both internal and external characteristic lengths (i.e. a and L) affect the mechanical behaviour of the carbon nanotube, in contrast to large-scale tubes, where only the external characteristic length (L) is important. In nonlocal elasticity, mechanical stress (σ_{ij}^{nl}) is a function of strain components at all locations. From the mathematical point of view, stress is related to strain by an integral relation, which contains the ratio

4

of a to L as a scale parameter. In the next subsection, more details are given on how to capture size effects using advanced elasticity models.

1.2.1 Nonlocal elasticity theory

The nonlocal elasticity theory was introduced by Eringen [32, 33], almost two decades before the invention of carbon nanotubes (CNTs). However, this valuable theory did not attract much attention until the synthesis of nanostructures such as CNTs and graphene sheets (GSs) emerged. Peddieson et al. [34] first suggested that the theory can be used to analyse the size-dependent mechanical response of nanostructures. In the classical elasticity theory, which is not able to predict size effects, the stress at a location is only dependent on the strain at that location. By contrast with classical elasticity, strains at all locations affect the stress at one arbitrary location in nonlocal elasticity as shown in Fig. 1. This basic assumption allows this theory to capture intermolecular interactions, leading to a size-dependent theory of elasticity. Ignoring body forces, the nonlocal integral constitutive relation is given by

$$\sigma_{ij}^{nl} = \iiint_V \varphi(|x - x'|, \eta)\sigma_{ij}^l dV, \tag{1}$$

where σ_{ij}^{nl}, σ_{ij}^l, φ and η stand for the nonlocal stress, local stress, kernel function and small-scale coefficient, respectively; $|x - x'|$ is the distance from x to x', and V denotes the volume of the body. The nonlocal coefficient is expressed as

$$\eta = \frac{e_0 a}{L}, \tag{2}$$

in which e_0, a and L are respectively the calibration coefficient, and internal and external characteristic lengths. Each nanostructure has internal and external characteristic lengths. For example, the c-c bond length in graphene is commonly chosen as the internal characteristic length, as shown in Fig. 2. The calibration coefficient is obtained either from experimental measurements or molecular dynamics (MD). The classical (local) stress is obtained as

$$\sigma_{ij}^l = C_{ijkl}\varepsilon_{kl}, \tag{3}$$

where C_{ijkl} and ε_{kl} stand for the elasticity tensor and the strain tensor, respectively.
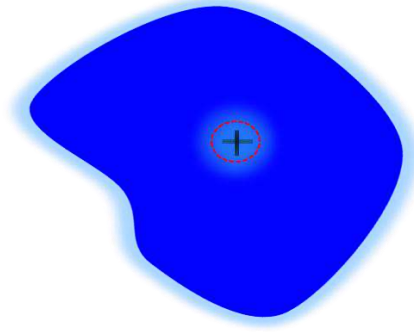
Fig. 1. Stress at a spot of a nanostructure is dependent on strains at all spots according to the nonlocal elasticity theory.
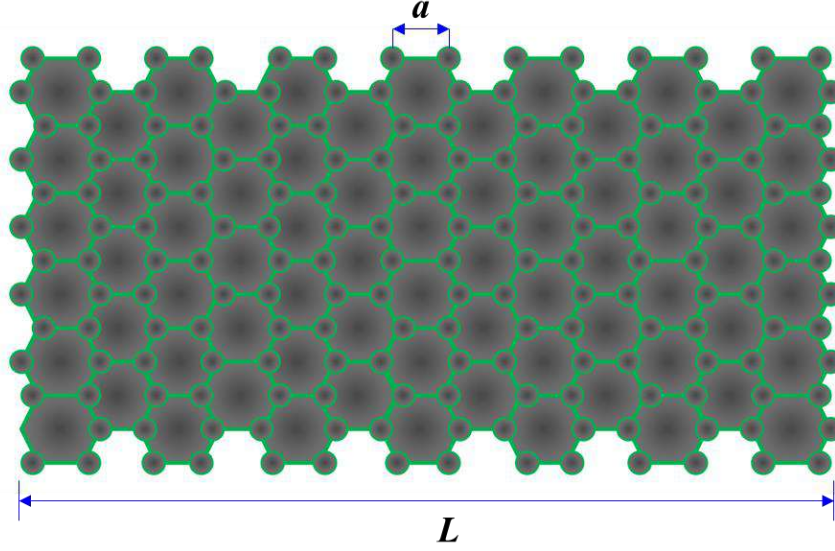
Fig. 2. Internal characteristic length (a) as well as the external characteristic length (L) for graphene.

Since the nonlocal constitutive Eq. (1) must reduce to that of the classical elasticity theory for very large external characteristic length, the kernel function (nonlocal modulus) has the following property

$$\lim_{\eta \to 0} \varphi(|x - x'|, \eta) = \delta(|x - x'|). \tag{4}$$

Here, δ denotes the Dirac delta function. Eringen [35] introduced some kernel functions for nonlocal problems. One of the most popular kernel functions is given by

$$\varphi(|x|, \eta) = (2\pi L^2 \eta^2)^{-1} K_0 \left(\frac{|x|}{L\eta} \right), \tag{5}$$

in which K_0 denotes the modified Bessel function. Since the implementation of the integral nonlocal constitutive equation, shown in Eq. (1), in formulating the mechanics of nanostructures is difficult, a nonlocal operator (L_{nl}) with the following property is introduced

$$L_{nl} \varphi(|x - x'|, \eta) = \delta(|x - x'|). \tag{6}$$

Applying the nonlocal operator to Eq. (1), one can obtain

6

$$L_{nl}\sigma_{ij}^{nl} = \sigma_{ij}^{l}. \tag{7}$$

Using the above equations, Eringen [33, 35] obtained the following relation for the nonlocal operator

$$L_{nl}(*) = [1 - (e_0 a)^2 \nabla^2](*). \tag{8}$$

Here, ∇^2 is the Laplace operator. Equations (7) and (8) have been extensively used to develop size-dependent continuum models in order to estimate the mechanical response of nanostructures [26, 36-38].

1.2.2 Nonlocal strain gradient elasticity

There are two limitations associated with the nonlocal elasticity theory. Firstly, nonlocal effects disappear after a certain length. For instance, scale effects predicted by the nonlocal elasticity on the axial vibration of uniform nanorods disappear for $L>20$ nm [37]. Secondly, nonlocal elasticity can only predict stiffness softening of small-scale structures. However, stiffness hardening has been observed in some small-scale structures, especially at higher lengths. This stiffness hardening can be estimated incorporating surface effects [39-43] or strain gradients [44-47]. For example, it was found that the pure nonlocal plate model cannot completely predict the buckling instability of circular graphene sheets subject to axisymmetric radial loading [48] by employing MD simulations. To overcome the shortcomings of the nonlocal elasticity, Lim et al. [27] introduced a nonlocal strain gradient theory (NSGT) using two kernel functions. The new theory is able to describe both stiffness softening and hardening at small-scale levels. In addition, the scale effect predicted by the NSGT appears in a wider range of lengths in comparison with nonlocal effects. However, the computational costs of the nonlocal elasticity is less than those of the NSGT due to the fact that strain gradient terms are also incorporated.

According to the nonlocal theory of strain gradients, the basic relation of small-scale structures can be written as

$$\sigma_{ij}^{nl(0)} = \iiint_V H_0\left(|x - x'|, \chi_{nl}^{(0)}\right) C_{ijkl}\varepsilon_{kl}dV, \tag{9}$$

$$\sigma_{ij}^{nl(1)} = \ell_{sg}^2 \iiint_V H_1\left(|x - x'|, \chi_{nl}^{(1)}\right) C_{ijkl}\nabla\varepsilon_{kl}dV. \tag{10}$$

7

Here $\sigma_{ij}^{nl(0)}$ and $\sigma_{ij}^{nl(1)}$ show the nonlocal stresses of zeroth and first orders; H_0 and H_1 represent the nonlocal moduli corresponding to $\sigma_{ij}^{nl(0)}$ and $\sigma_{ij}^{nl(1)}$, respectively; ∇, ℓ_{sg}, $\chi_{nl}^{(0)}$ and $\chi_{nl}^{(1)}$ are the gradient operator, strain gradient constant, zeroth- and first-order nonlocal constants, respectively. For nonlocal stresses, one can write

$$\sigma_{ij}^{nl(t)} = \sigma_{ij}^{nl(0)} - \nabla \sigma_{ij}^{nl(1)}. \tag{11}$$

In the above relation, $\sigma_{ij}^{nl(t)}$ denotes the total nonlocal stress. Furthermore, the nonlocal parameters are defined by

$$\chi_{nl}^{(0)} = \frac{e_0 \ell_{ic}}{\ell_{ec}}, \tag{12}$$

$$\chi_{nl}^{(1)} = \frac{e_1 \ell_{ic}}{\ell_{ec}}, \tag{13}$$

in which e_0 and e_1 are two calibration parameters associated with the zeroth-order and first-order nonlocal scale coefficients, respectively. Following Eringen [35] and assuming $e=e_0=e_1$, Lim et al. [27] used a differential form for the scale-dependent basic relation of small-scale structures given by

$$L_{nl} \sigma_{ij}^{nl} = L_{sg} \sigma_{ij}^{cl}. \tag{14}$$

Here L_{nl} and L_{sg} represent the nonlocal and strain gradient operators which are defined by

$$L_{nl}(*) = (*) - (e\ell_{ic})^2 \nabla^2(*),$$

$$L_{sg}(*) = (*) - \ell_{sg}^2 \nabla^2(*). \tag{15}$$

It should be noticed that the effect of axial inertia (in-plane inertia) on the mechanics of beams (plates) is negligible when the maximum deformation is small enough. However, in large amplitude problems, these effects become significant since large displacements in one direction can induce deformation along other directions as well. In the present work, the equation of motion in axial direction (in-plane directions) is derived in conjunction with the main motion equation of beams (plates), and then a system of nonlinear coupled equations are solved using a numerical technique such as the differential quadrature or Galerkin methods.

1.3 Molecular dynamics

Molecular dynamics (MD) is a powerful approach to determine the mechanical, electrical and thermal properties of ultra-small structures. In this method, the positions of the molecules of an ultra-small system are estimated by solving Newton's motion equations at each time step of numerical simulation. The forces, which affect the motion of each particle, are calculated from the appropriate potential energies, which include all intermolecular interactions. MD simulations can be performed to indicate the accuracy of the results of the developed advanced continuum model. The deformation of a small-scale structure can be predicted through MD simulations. LAMMPS software is commonly utilised for obtaining the scale-dependent deformation behaviour. A Velocity-Verlet approach can be used for integrating the motion equations of small-scale particles. In this way, the trajectories of small-scale particles are determined at each time. The suitable potential energy, which plays an important role in obtaining accurate MD results, are chosen for the system based on the type of molecules inside the system.

1.4 Research gaps

It has been recently shown that conventional scale-dependent models are not capable of comprehensively incorporating size effects on the mechanical characteristics of structures at ultra-small levels [49]. In addition, a conventional model is restricted to a specific range of sizes. For example, nonlocal effects on the mechanical behaviour vanish after a particular length. Scrutinising the available literature review indicates that the number of advanced two-parameter scale-dependent models and integral models are limited compared to one-parameter ones. Particularly, the large amplitude vibration of small-scale beams with geometrical imperfections and viscoelasticity using a higher-order two-parameter model has not been investigated yet. Analysing these systems would provide useful results for small-scale mass sensors using vibrating microscale/nanoscale beams.

A majority of the available analysis on the deformation behaviour of beams and plates at nanoscales is restricted to either a simple linear investigation or nonlinear models with a single-mode

solution procedure. Nonetheless, large deformations are very likely in a real situation due to large mechanical loads. Thus, linear scale-dependent models are not adequately accurate for these structures. In addition, a single-mode solution procedure for solving nonlinear differential equations results in an overly approximate solution which is not reliable, especially for small-scale structures. Developing a precise nonlinear model and solution procedure for taking into account the effect of geometrical nonlinearity provides a platform for understanding the mechanics of the building blocks of small-scale devices during operation of a realistic situation.

Previous studies performed on the time-dependent deformation of small-scale plates using advanced scale-dependent models based on stress-driven elasticity are restricted to only circular and annular nanoplates with a one-dimensional kernel function. However, in real applications, other geometry types such as rectangular small-scale plates are also found. Thus, linear scale-dependent models available for annular nanoplates are extended in this thesis to rectangular small-scale plates, by introducing a reasonable two-dimensional kernel function. Additional non-classical edge conditions associated with the curvature nonlocality are presented for the mechanical analysis of rectangular nanoplates for the first time.

In many of the available continuum models of small-scale plates, only small deflections have been taken into consideration [36, 38, 50]. By contrast, the mechanical response of small-scale plate structures are usually nonlinear due to different causes such unavoidable large loading and strong intermolecular interactions. Thus, to better describe the mechanics of small-scale plates, there is a growing need to develop a scale-dependent model incorporating nonlinearity effects. No nonlinear analysis has been reported on these systems using a stress-driven scale-dependent model. Understanding the time-dependent deformation of small-scale plates with geometrical nonlinearity would be useful in the design of small-scale systems such as ultra-small resonators and actuators.

1.5 Aims and objectives

The first aim of this project was to analyse the nonlinear scale-dependent time-dependent deformation of beams at ultra-small levels. Accordingly, the first objective was developing a continuum model for the vibration of straight ultra-small beams incorporating nonlinearly coupled transverse/axial motion and scale impacts. This continuum modelling is conducted taking into account two completely different size parameters. The nonlocality of the stress as well as the strain gradient effect are captured. Nonlinear terms appearing in coupled differential equations of motions are rooted in the geometrical nonlinearity. Developing a comprehensive continuum model is also performed by incorporating both transverse and axial displacements via a high-dimensional coupled DOF ensuring converged and reliable results. The second objective is to derive a scale-dependent continuum model for the vibrations of geometrically imperfect ultra-small beams and obtaining their vibration response by including the nonlinearity of geometric type due to the stretching of the beam centreline. Eringen's type of elasticity is adopted for nonlocality effects. Moreover, the influence of strain gradients is incorporated, leading to a comprehensive continuum modelling for small-scale beams. Both displacements are considered in the nonlinear model. A precise numerical solution is presented for large deformations. The third objective of this project is to study the large time-dependent deformation of small-scale viscoelastic beams. The influences of geometric imperfections and internal energy loss on the vibrational behaviour of small-scale beams are examined in detail via a nonlinear scale-dependent model.

The second aim of this project was to examine the vibrational behaviour of small-scale plates via an advanced scale-dependent model. Firstly, a linear stress-driven model is presented for the deformation of rectangular plates at small-scale levels taking into consideration the influence of the curvature nonlocality. Extra edge conditions related to the non-classical constitutive equations are obtained. Higher-order non-classical motion equations are solved implementing extra edge conditions using the differential quadrature technique. Secondly, scale-dependent nonlinear continuum

modelling of the large-amplitude vibrations of ultra-small plates is performed based on an integral size-dependent model. Incorporating both in-plane and transverse displacements, as well as geometrical nonlinearity, an accurate elasticity model is presented. The curvature nonlocality and in-plane nonlocality are taken into account. Developing a continuum model by incorporating these effects enables the proposed model to precisely predict the vibration response of the system at ultra-small levels. A reliable solution using a numerical technique with a high number of DOF for the coupled transverse/axial motion is obtained. MD simulation is conducted to evaluate the precision of the models for the scale-dependent deformation behaviour of plates using LAMMPS software. In addition, visual molecular dynamics (VMD) software will be used to visually observe the deformation of the ultra-small structure. To verify the results of the developed model, a graphene sheet as a nanoplate will be used in MD simulations.

1.6 Chapter outline

There are seven chapters in this thesis. The first chapter gives an introductory background about the research undertaken in this project. The motivation of the present work is elaborated in this chapter. In addition, size-dependent continuum approaches including nonlocal and strain gradient elasticity are briefly explained. The basic concept of molecular dynamics technique and popular related software packages are also given. The research gaps, aims and objectives of the present work are listed, followed by this section that described the structure of the thesis.

A comprehensive literature review on the mechanical modelling of structures at small-scales is presented in chapter 2. The available studies on various types of ultra-small structures including rods, rings, beams, tubes, plates and shells are investigated. Particular attention is paid to static deformation, wave propagation, vibrations and instability analysis at small-scales. More information and details about the basic concepts and mathematical modelling tools such as nonlocal continuum mechanics are given in the second chapter. This chapter together with chapter one give a detailed overview of

the available research methods and works on the mechanics of small-scale structures to an interested reader.

Chapter 3 deals with the nonlinear vibrations of ultra-small beams with geometrical imperfections. An advanced continuum model is proposed via a nonlocal model including strain gradients. The roles of size, nonlinearity and imperfections in the scale-dependent deformation of beams are illustrated. This study fulfils the initial objectives of the project.

In chapter 4, a nonlinear scale-dependent model with viscoelasticity effects is presented. Strain gradients, stress nonlocality and a geometrical imperfection in the small-scale beam are assumed in order for the analysis to be original and more comprehensive. The nonlinear viscoelasticity modelling performed in this chapter together with the mathematical framework given in chapter three provide a comprehensive nonlinear continuum model of ultrasmall beams.

In chapter 5, the size-dependent deformation behaviour of small-scale plates is studied via developing a stress-driven model. The linear resonance frequency is computed by applying a differential solution technique. The influences of various parameters on the vibrational response is analysed in this chapter. This chapter covers one of the main objectives of the project, which is the scale-dependent mechanics of ultrasmall plates.

In chapter 6, an advanced nonlinear plate model is proposed for the oscillations of small-scale plates. Graphene sheets are taken into account to conduct MD simulations on. The accuracy of the proposed nonlinear model is examined using MD results. The coupled equations with higher-order nonlinearity are solved by a differential quadrature approach and an iteration technique. All non-classical edge conditions related to both curvature nonlocality and in-plane strain components are presented in this chapter. The influences of size, maximum deflection and geometric parameters on the nonlinear frequencies and in-plane displacements are studied. In chapter six, the linear continuum model presented in the previous chapter is extended to nonlinear small-scale problems. In chapter six, the linear scale-dependent model presented in the previous chapter is extended to nonlinear small-scale plate problems.

In the final chapter 7, the most important findings of the present work and some possible future research that can be conducted to continue this study are listed. The results of all scale-dependent models of beam and plate structures as well as numerical molecular dynamics simulations performed in previous chapters are reviewed.

In addition to the nonlinear vibration analysis of nanobeams and nanoplates, the large-amplitude oscillation of nanotubes conveying fluid is analysed by developing an advanced mathematical framework in the Appendix. The mathematical models of small-scale tubes presented in the main body of the thesis are extended to their fluid-structure interaction counterparts. This part is a complementary study to chapters 3 and 4, and provide a useful platform for engineers and researchers who design and fabricate microelectromechanical and nanoelectromechanical systems using fluid-conveying nanotubes such as fluid filtration nanosystems, nanopipettes and microfluidic devices.

References

[1] Reddy JN. An Introduction to Nonlinear Finite Element Analysis: with applications to heat transfer, fluid mechanics, and solid mechanics: OUP Oxford; 2014.

[2] Cui L, Gu H, Xu H, Shi D. Synthesis and characterization of superparamagnetic composite nanorings. Materials Letters. 2006;60(24):2929-32.

[3] Iijima S, Ichihashi T. Single-shell carbon nanotubes of 1-nm diameter. nature. 1993;363(6430):603.

[4] Barretta R, Čanađija M, Luciano R, de Sciarra FM. Stress-driven modeling of nonlocal thermoelastic behavior of nanobeams. International Journal of Engineering Science. 2018;126:53-67.

[5] She G-L, Ren Y-R, Yuan F-G, Xiao W-S. On vibrations of porous nanotubes. International Journal of Engineering Science. 2018;125:23-35.

[6] Geim AK, Novoselov KS. The rise of graphene. Nanoscience and Technology: A Collection of Reviews from Nature Journals: World Scientific; 2010. p. 11-9.

[7] Jalaei MH, Arani AG, Tourang H. On the dynamic stability of viscoelastic graphene sheets. International Journal of Engineering Science. 2018;132:16-29.

[8] Loo C, Lowery A, Halas N, West J, Drezek R. Immunotargeted nanoshells for integrated cancer imaging and therapy. Nano letters. 2005;5(4):709-11.

[9] Faleh NM, Ahmed RA, Fenjan RM. On vibrations of porous FG nanoshells. International Journal of Engineering Science. 2018;133:1-14.

[10] Eichler A, Moser J, Chaste J, Zdrojek M, Wilson-Rae I, Bachtold A. Nonlinear damping in mechanical resonators made from carbon nanotubes and graphene. Nature nanotechnology. 2011;6(6):339.

[11] Farokhi H, Païdoussis MP, Misra AK. Nonlinear behaviour of cantilevered carbon nanotube resonators based on a new nonlinear electrostatic load model. Journal of Sound and Vibration. 2018;419:604-29.

[12] Zhao Q, Gan Z, Zhuang Q. Electrochemical sensors based on carbon nanotubes. Electroanalysis: An International Journal Devoted to Fundamental and Practical Aspects of Electroanalysis. 2002;14(23):1609-13.

[13] Fennimore A, Yuzvinsky T, Han W-Q, Fuhrer M, Cumings J, Zettl A. Rotational actuators based on carbon nanotubes. Nature. 2003;424(6947):408.

[14] Briscoe J, Dunn S. Piezoelectric nanogenerators–a review of nanostructured piezoelectric energy harvesters. Nano Energy. 2015;14:15-29.

[15] Chu H, Jang H, Lee Y, Chae Y, Ahn J-H. Conformal, graphene-based triboelectric nanogenerator for self-powered wearable electronics. Nano Energy. 2016;27:298-305.

[16] Kwon J, Sharma BK, Ahn J-H. Graphene based nanogenerator for energy harvesting. Japanese Journal of Applied Physics. 2013;52(6S):06GA2.

[17] Ghayesh MH, Amabili M, Paidoussis M. Nonlinear vibrations and stability of an axially moving beam with an intermediate spring support: two-dimensional analysis. Nonlinear Dynamics. 2012;70(1):335-54.

[18] Ghayesh MH. On the natural frequencies, complex mode functions, and critical speeds of axially traveling laminated beams: parametric study. Acta Mechanica Solida Sinica. 2011;24(4):373-82.

[19] Farokhi H, Ghayesh MH. Supercritical nonlinear parametric dynamics of Timoshenko microbeams. Communications in Nonlinear Science and Numerical Simulation. 2018;59:592-605.

[20] Dehrouyeh-Semnani AM, Nikkhah-Bahrami M, Yazdi MRH. On nonlinear stability of fluid-conveying imperfect micropipes. International Journal of Engineering Science. 2017;120(Supplement C):254-71.

[21] Lei J, He Y, Guo S, Li Z, Liu D. Size-dependent vibration of nickel cantilever microbeams: Experiment and gradient elasticity. AIP Advances. 2016;6(10):105202.

[22] Farokhi H, Ghayesh MH. Nonlinear mechanics of electrically actuated microplates. International Journal of Engineering Science. 2018;123:197-213.

[23] Ghayesh MH. Dynamics of functionally graded viscoelastic microbeams. International Journal of Engineering Science. 2018;124:115-31.

[24] Akgöz B, Civalek Ö. Free vibration analysis of axially functionally graded tapered Bernoulli–Euler microbeams based on the modified couple stress theory. Composite Structures. 2013;98:314-22.

[25] Pradhan S, Phadikar J. Nonlocal elasticity theory for vibration of nanoplates. Journal of Sound and Vibration. 2009;325(1-2):206-23.

[26] Reddy J. Nonlocal theories for bending, buckling and vibration of beams. International Journal of Engineering Science. 2007;45(2-8):288-307.

[27] Lim C, Zhang G, Reddy J. A higher-order nonlocal elasticity and strain gradient theory and its applications in wave propagation. Journal of the Mechanics and Physics of Solids. 2015;78:298-313.

[28] Barretta R, Faghidian SA, de Sciarra FM. Stress-driven nonlocal integral elasticity for axisymmetric nano-plates. International Journal of Engineering Science. 2019;136:38-52.

[29] Barretta R, Fabbrocino F, Luciano R, de Sciarra FM, Ruta G. Buckling loads of nano-beams in stress-driven nonlocal elasticity. Mechanics of Advanced Materials and Structures. 2019:1-7.

[30] Ghayesh MH, Farokhi H, Hussain S. Viscoelastically coupled size-dependent dynamics of microbeams. International Journal of Engineering Science. 2016;109:243-55.

[31] Farokhi H, Ghayesh MH. Size-dependent parametric dynamics of imperfect microbeams. International Journal of Engineering Science. 2016;99:39-55.

[32] Eringen AC, Edelen D. On nonlocal elasticity. International Journal of Engineering Science. 1972;10(3):233-48.

[33] Eringen AC. Nonlocal continuum field theories: Springer Science & Business Media; 2002.

[34] Peddieson J, Buchanan GR, McNitt RP. Application of nonlocal continuum models to nanotechnology. International Journal of Engineering Science. 2003;41(3-5):305-12.

[35] Eringen AC. On differential equations of nonlocal elasticity and solutions of screw dislocation and surface waves. Journal of applied physics. 1983;54(9):4703-10.

[36] Arash B, Wang Q. A review on the application of nonlocal elastic models in modeling of carbon nanotubes and graphenes. Computational materials science. 2012;51(1):303-13.

[37] Aydogdu M. Axial vibration of the nanorods with the nonlocal continuum rod model. Physica E: Low-dimensional Systems and Nanostructures. 2009;41(5):861-4.

[38] Murmu T, Pradhan S. Buckling analysis of a single-walled carbon nanotube embedded in an elastic medium based on nonlocal elasticity and Timoshenko beam theory and using DQM. Physica E: Low-dimensional Systems and Nanostructures. 2009;41(7):1232-9.

[39] Yan Z, Jiang L. The vibrational and buckling behaviors of piezoelectric nanobeams with surface effects. Nanotechnology. 2011;22(24):245703.

[40] Guo J-G, Zhao Y-P. The size-dependent bending elastic properties of nanobeams with surface effects. Nanotechnology. 2007;18(29):295701.

[41] Malekzadeh P, Shojaee M. Surface and nonlocal effects on the nonlinear free vibration of non-uniform nanobeams. Composites Part B: Engineering. 2013;52:84-92.

[42] Jiang L, Yan Z. Timoshenko beam model for static bending of nanowires with surface effects. Physica E: Low-dimensional systems and Nanostructures. 2010;42(9):2274-9.

[43] Assadi A. Size dependent forced vibration of nanoplates with consideration of surface effects. Applied Mathematical Modelling. 2013;37(5):3575-88.

[44] Akgöz B, Civalek Ö. Strain gradient elasticity and modified couple stress models for buckling analysis of axially loaded micro-scaled beams. International Journal of Engineering Science. 2011;49(11):1268-80.

[45] Mindlin RD, Eshel N. On first strain-gradient theories in linear elasticity. International Journal of Solids and Structures. 1968;4(1):109-24.

[46] Wang B, Zhou S, Zhao J, Chen X. A size-dependent Kirchhoff micro-plate model based on strain gradient elasticity theory. European Journal of Mechanics-A/Solids. 2011;30(4):517-24.

[47] Askes H, Aifantis EC. Gradient elasticity and flexural wave dispersion in carbon nanotubes. Physical Review B. 2009;80(19):195412.

[48] Farajpour A, Dehghany M, Shahidi A. Surface and nonlocal effects on the axisymmetric buckling of circular graphene sheets in thermal environment. Composites Part B: Engineering. 2013;50:333-43.

[49] Li L, Hu Y, Ling L. Wave propagation in viscoelastic single-walled carbon nanotubes with surface effect under magnetic field based on nonlocal strain gradient theory. Physica E: Low-dimensional Systems and Nanostructures. 2016;75:118-24.

[50] Mohammadi M, Farajpour A, Goodarzi M, Heydarshenas R. Levy type solution for nonlocal thermo-mechanical vibration of orthotropic mono-layer graphene sheet embedded in an elastic medium. Journal of Solid Mechanics. 2013;5(2):116-32.

Chapter 2
Literature review

Chapter overview

A literature review on the scale-dependent modelling of fundamental structural components at small-scales is given in this chapter. The available models on the mechanical behaviour of different types of small-scale components including micro/nanorods, micro/nanorings, micro/nanobeams, micro/nanoplates and micro/nanoshells are described. The focus of attention in this chapter is the static deformation, wave propagation, vibration and instability analysis at ultra-small levels. This literature review has been published in "International Journal of Engineering Science" as:

A. Farajpour, M.H. Ghayesh, H. Farokhi, "A review on the mechanics of nanostructures", International Journal of Engineering Science, volume 133, pages 231-263 (2018).

Statement of Authorship

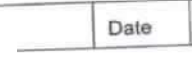| Title of Paper	A review on the mechanics of nanostructures
Publication Status	☑ Published ☐ Accepted for Publication ☐ Submitted for Publication ☐ Unpublished and Unsubmitted work written in manuscript style
Publication Details	A Farajpour, MH Ghayesh, H Farokhi, A review on the mechanics of nanostructures, International Journal of Engineering Science 133, 231–263 (2018).

Principal Author

Name of Principal Author (Candidate)	Ali Farajpour Ouderji
Contribution to the Paper	- Research - Doing the literature review - Reviewing and developing all available relevant models - Writing all parts of the paper and analysing the data of available models - Preparing the revised version of the paper
Overall percentage (%)	70%
Certification:	This paper reports on original research I conducted during the period of my Higher Degree by Research candidature and is not subject to any obligations or contractual agreements with a third party that would constrain its inclusion in this thesis. I am the primary author of this paper.
Signature	Date 2/6/2020

Co-Author Contributions

By signing the Statement of Authorship, each author certifies that:

   i.   the candidate's stated contribution to the publication is accurate (as detailed above);

   ii.   permission is granted for the candidate in include the publication in the thesis; and

   iii.   the sum of all co-author contributions is equal to 100% less the candidate's stated contribution.

Name of Co-Author	Mergen H. Ghayesh
Contribution to the Paper	- Supervising the work including preparing the paper - Correspondence with the reviewers and editor of the journal - Editing and evaluating the paper before submission
Signature	Date 21/06/2020

Name of Co-Author	Hamed Farokhi
Contribution to the Paper	- Participation in supervising the work - Participation in evaluating the paper before submission
Signature	Date 19/06/2020

Please cut and paste additional co-author panels here as required.
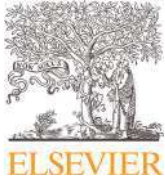
Review

A review on the mechanics of nanostructures

Ali Farajpour[a], Mergen H. Ghayesh[a,*], Hamed Farokhi[b]

[a] School of Mechanical Engineering, University of Adelaide, South Australia 5005, Australia
[b] Department of Mechanical and Construction Engineering, Northumbria University, Newcastle upon Tyne NE1 8ST, UK

A B S T R A C T

Understanding the mechanical behaviour of nanostructures is of great importance due to their applications in nanodevices such as in nanomechanical resonators, nanoscale mass sensors, electromechanical nanoactuators and nanogenerators. Due to the difficulties of performing accurate experimental measurements at nanoscales and the high computational costs associated with the molecular dynamics simulations, the continuum modelling of nanostructures has attracted a considerable amount of attention. Since size influences have a crucial role in the mechanics of structures at nanoscale levels, classical continuum-based theories have been modified to incorporate these effects. Among various modified continuum-based theories, the nonlocal elasticity and the nonlocal strain gradient elasticity have been employed to estimate the mechanical behaviour of nanostructures. In this review paper, first these two modified elasticity theories are briefly explained. Then, the nonlocal motion equations for different nanostructures including nanorods, nanorings, nanobeams, nanoplates and nanoshells are derived. Several papers which reported on the size-dependent mechanical behaviour of nanostructures using modified continuum models are reviewed. Furthermore, important results reported on the vibration, bending and buckling of nanostructures as well as the results of size-dependent wave propagation analyses are discussed.

© 2018 Elsevier Ltd. All rights reserved.

1. Introduction

Nanoscale structures including nanoscale rods (Xu et al., 2004), rings (Cui, Gu, Xu & Shi, 2006), beams (Iijima & Ichihashi, 1993, Barretta, Čanađija, Luciano & de Sciarra, 2018, Barretta & Marotti de Sciarra, 2018, Hadi, Nejad & Hosseini, 2018, She, Ren, Yuan & Xiao, 2018, Khaniki, 2018), plates (Geim & Novoselov, 2010, Jalaei, Arani & Tourang, 2018), and shells (Loo et al., 2005, Faleh, Ahmed & Fenjan, 2018) have been utilised as the fundamental structural parts of many nanoelectromechanical systems (NEMS). Nanomechanical resonators (Eichler et al., 2011, Farokhi, Païdoussis & Misra, 2018), nanoscale mass sensors (Zhao, Gan & Zhuang, 2002), electromechanical nanoactuators (Fennimore et al., 2003), and nanoenergy harvesters (Briscoe & Dunn, 2015) are salient examples of these NEMS-based devices. These valuable nanoscale devices have broad applications in different areas of nanotechnology such as nanoelectronics, nanomachines and nanomedicine. To achieve a better performance for the nanodevice, a better understanding of the mechanical characteristics of nanostructures as these ultrasmall structures are usually subject to mechanical loads, pressure or stresses. In addition, in nanodevices such as nanoscale generators (Chu et al., 2016, Kwon, Sharma & Ahn, 2013), the mechanical energy is converted into electricity, hence an analysis on the mechanical behaviour is essential.

---

* Corresponding author.
  E-mail addresses: ali.farajpourouderji@adelaide.edu.au (A. Farajpour), mergen.ghayesh@adelaide.edu.au (M.H. Ghayesh), hamed.farokhi@northumbria.ac.uk (H. Farokhi).

Since performing an accurate experimental measurement at nanoscale levels is challenging, continuum-based modelling and molecular dynamics (MD) simulations of nanostructures have attracted a considerable amount of attention. Using continuum-based models and the results of MD simulations, the number of required experimental measurements can be reduced. Compared to MD simulations, the continuum modelling of nanostructures is less computationally expensive. Particularly, performing MD simulations on a nanostructure with a large number of molecules requires a high computational effort. Using continuum models, the mechanical characteristics can be formulated and estimated. In this way, the computational costs of MD simulations can be reduced by eliminating unnecessary simulations. In addition, the continuum-based modelling of nanostructures can help us to better understand the results of experimental measurements or molecular dynamics.

Scale effects have a crucial role to play in the mechanics of nanostructures, as opposed in macrostructures (Ghayesh, Païdoussis & Amabili, 2013, Ghayesh & Amabili, 2012, Ghayesh & Amabili, 2013, Ghayesh, Amabili & Paidoussis, 2012, Ghayesh, 2009, Ghayesh, 2011, Gholipour, Ghayesh, Zander & Mahajan, 2018). Thus, traditional continuum-based theories, which are scale-free, have been modified in order to capture size effects. Various size-dependent theories for examining the mechanical characteristics of nanostructures have been introduced in recent years. Since the mechanical behaviour of structures at microscale levels (Ghayesh & Farokhi, 2015, Gholipour, Farokhi & Ghayesh, 2015, Ghayesh, Amabili & Farokhi, 2013, Ghayesh, Farokhi & Amabili, 2013, Ghayesh, Farokhi & Amabili, 2014, Ghayesh & Farokhi, 2015, Farokhi & Ghayesh, 2015, Farokhi & Ghayesh, 2015, Ghayesh, Farokhi & Gholipour, 2017, Farokhi & Ghayesh, 2018, Ghayesh, Farokhi, Gholipour & Tavallaeinejad, 2018, Dehrouyeh-Semnani, Nikkhah-Bahrami & Yazdi, 2017, Ghayesh & Farokhi, 2017) is different from that observed at nanoscale levels, the modified continuum-based theories of microstructures are different from those of nanostructures (Lei et al., 2016). In general, the structural stiffness hardening is observed at microscale levels whereas the mechanics of nanostructures is usually governed by the stiffness softening. Therefore, size-dependent models including the couple stress (Farokhi, Ghayesh & Amabili, 2013, Ghayesh, Farokhi & Alici, 2015, Farokhi, Ghayesh, Gholipour & Hussain, 2017, Ghayesh & Farokhi, 2017, Farokhi & Ghayesh, 2018, Farokhi & Ghayesh, 2018, Ghayesh, 2018, Ghayesh & Farokhi, 2018, Ghayesh, Farokhi & Alici, 2016, Ghayesh, Farokhi & Amabili, 2013, Ghayesh, Farokhi & Gholipour, 2017) and strain gradient elasticities (Ghayesh, Amabili & Farokhi, 2013, Akgöz & Civalek, 2011, Akgöz & Civalek, 2013) are often used to analyse the mechanical behaviour of microstructures including microbeams, microbars and microplates while the nonlocal elasticity theory (Pradhan & Phadikar, 2009, Reddy, 2007, Farajpour, Shahidi & Farajpour, 2018, Asemi & Farajpour, 2014) is applied to nanoscale structures. However, to have a more general size-dependent continuum-based model capable of predicting size effects at different small scales, a combination of these modified elasticity theories (Lim, Zhang & Reddy, 2015) can be employed.

This review article is organised as follows: In Section 2, concise information is given about different size-dependent elasticity theories utilised for investigating the mechanical characteristics of structures at nanoscale levels including the pure nonlocal and nonlocal strain gradient elasticities. In Section 3, first the size-dependent motion equations of various types of nanoscale structures such as nanoscale rods, rings, beams, plates and shells are developed via the nonlocal elasticity. Then, studies on the size-dependent modelling of the mechanical behaviour of these structures are reviewed; particular attention is paid to the size-dependent bending, buckling and vibration of nanoscale structures as well as size-dependent wave propagations in these small-scale structures. Finally, Section 4 concludes on the size-dependent continuum theories of nanostructures, and the most important findings to date are highlighted.

2. Size-dependent continuum mechanics

In this section, size-dependent (Ghayesh, Farokhi & Hussain, 2016, Farokhi & Ghayesh, 2016, Ghayesh & Amabili, 2014, Ghayesh, 2018, Ghayesh, 2018, Ghayesh, Farokhi, Gholipour & Tavallaeinejad, 2017, Ghayesh, Farokhi, Gholipour & Hussain, 2017, Farokhi, Ghayesh, Gholipour & Tavallaeinejad, 2017, Farokhi, Ghayesh & Gholipour, 2017, Ghayesh, Farokhi & Farajpour, 2018) elasticity theories including the nonlocal elasticity and the nonlocal strain gradient elasticity, which are commonly applied to nanoscale structures, are reviewed. Firstly, the basic concept of the nonlocal elasticity is clarified, and then both the integral and differential nonlocal constitutive relations are discussed. Finally, the theory of the nonlocal strain gradient elasticity is introduced.

2.1. Nonlocal elasticity theory

The nonlocal elasticity was introduced by Eringen (Eringen & Edelen, 1972, Eringen & Nonlocal, 2002) almost two decades before the invention of carbon nanotubes (CNTs). However, this valuable theory did not attract much attention until the synthesis of nanostructures such as CNTs and graphene sheets (GSs) emerged. Peddieson et al. (Peddieson, Buchanan & McNitt, 2003) first suggested that the theory can be used to analyse the size-dependent mechanical response of nanostructures. In the classical elasticity theory, which is not able to predict size effects, the stress at a spot is only dependent on the strain at that spot. By contrast, in the nonlocal elasticity, strains at all spots affect the stress at one arbitrary spot as shown in Fig. 1. This basic assumption allows this theory to capture intermolecular interactions, leading to a size-dependent theory of elasticity. Ignoring body forces, the nonlocal integral constitutive relation is given by

$$\sigma_{ij}^{nl} = \int \int_V \int \varphi\big(\left|\mathbf{X} - \mathbf{X}'\right|, \eta\big)\sigma_{ij}^l dV, \tag{1}$$
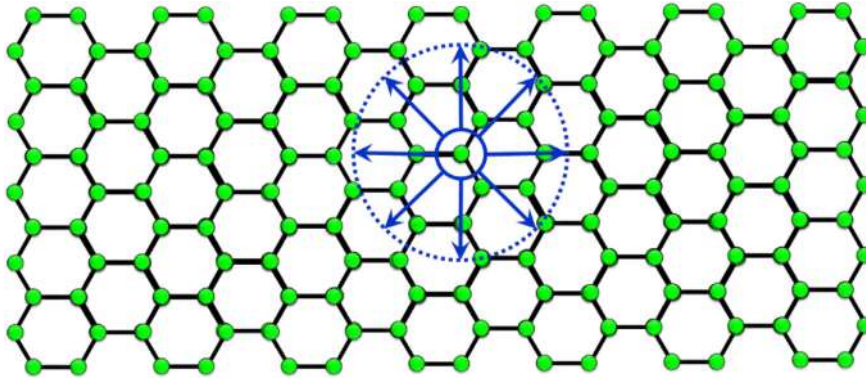
Fig. 1. Stress at a spot of a nanostructure is dependent on strains at all spots according to the nonlocal elasticity theory.
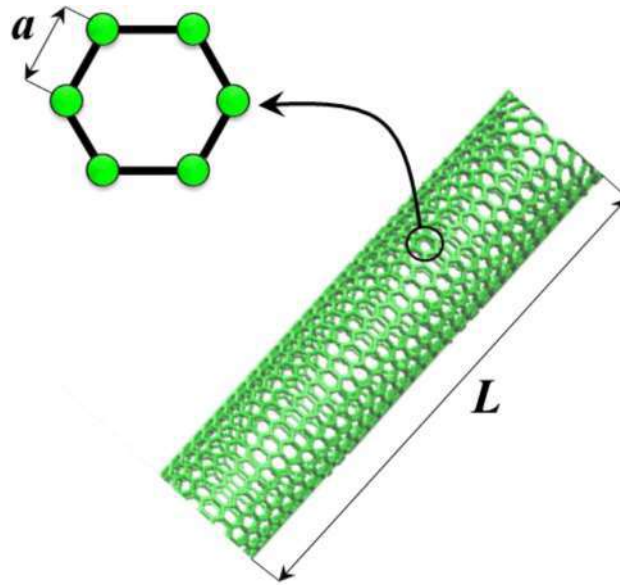
Fig. 2. Internal characteristics length (a) as well as the external characteristics length (L) for CNTs.

where σ_{ij}^{nl}, σ_{ij}^{l}, φ and η stand for the nonlocal stress, local stress, kernel function and small-scale coefficient, respectively; $|\mathbf{x} - \mathbf{x}'|$ is the distance from $\mathbf{x}$ to $\mathbf{x}'$, and V denotes the volume of the body. The nonlocal coefficient is expressed as

$$\eta = \frac{e_0 a}{L}, \tag{2}$$

in which e_0, a and L are respectively the calibration coefficient, and internal and external characteristic lengths. Each nanostructure has internal and external characteristic lengths. For example, for carbon nanotubes, the c-c bond length is commonly chosen as the internal characteristic length (see Fig. 2). The calibration coefficient is obtained either from experimental measurements or molecular dynamics (MD). The classical (local) stress is obtained as

$$\sigma_{ij}^{l} = C_{ijkl} \varepsilon_{kl}, \tag{3}$$

where C_{ijkl} and ε_{kl} stand for the elasticity tensor and the strain tensor, respectively.

Since the nonlocal constitutive Eq. (1) must reduce to that of the classical elasticity theory for very large external characteristic length, the kernel function (nonlocal modulus) has the following property

$$\lim_{\eta \to 0} \varphi(|\mathbf{x} - \mathbf{x}'|, \eta) = \delta(|\mathbf{x} - \mathbf{x}'|). \tag{4}$$

Here δ denotes the Dirac delta. Eringen (Eringen, 1983) introduced some kernel functions for nonlocal problems. One of the most popular kernel functions is given by

$$\varphi(|\mathbf{x}|, \eta) = \left(2\pi L^2 \eta^2\right)^{-1} K_0\left(\frac{\sqrt{\mathbf{x}.\mathbf{x}}}{L\eta}\right), \tag{5}$$

in which K_0 denotes the modified Bessel function. Since the implementation of the integral nonlocal constitutive equation (i.e. Eq. (1)) in formulating the mechanics of nanostructures is difficult, a nonlocal operator (L_{nl}) with the following property is introduced

$$L_{nl}\varphi\left(\left|x-x'\right|,\eta\right) = \delta\left(\left|x-x'\right|\right). \tag{6}$$

Applying the nonlocal operator to Eq. (1), one can obtain

$$L_{nl}\sigma_{ij}^{nl} = \sigma_{ij}^{l}. \tag{7}$$

Using the above equations, Eringen (Eringen and Nonlocal, 2002, Eringen, 1983) obtained the following relation for the nonlocal operator

$$L_{nl}(*) = \left[1 - (e_0 a)^2 \nabla^2\right](*). \tag{8}$$

Here ∇^2 stands for the Laplace operator. Eqs. (7) and (8) are extensively used to develop size-dependent continuum models in order to estimate the mechanical response of nanostructures.

2.2. Nonlocal strain gradient elasticity

There are two limitations associated with the nonlocal elasticity theory. Firstly, nonlocal effects disappear after a certain length. For instance, scale effects predicted by the nonlocal elasticity on the axial vibration of uniform nanorods disappear for $L > 20$ nm (Aydogdu, 2009). Secondly, the nonlocal elasticity can only predict the stiffness softening of small-scale structures. However, stiffness hardening has been observed in some small-scale structures, especially at higher lengths. This stiffness hardening can be estimated incorporating surface effects (Yan & Jiang, 2011, Gheshlaghi & Hasheminejad, 2011, Guo & Zhao, 2007, Malekzadeh & Shojaee, 2013, Jiang & Yan, 2010, Assadi, 2013) or strain gradients (Ghayesh, Amabili & Farokhi, 2013, Akgöz & Civalek, 2011, Mindlin & Eshel, 1968, Farajpour, Shahidi, Tabataba'i-Nasab & Farajpour, 2018, Wang, Zhou, Zhao & Chen, 2011, Askes & Aifantis, 2009, Ghayesh & Farajpour, 2018, Farajpour & Rastgoo, 2017). For example, it was found that the pure nonlocal plate model cannot completely predict the buckling instability of circular graphene sheets subject to an axisymmetric loading (Farajpour, Dehghany & Shahidi, 2013) by employing MD simulations. To overcome the shortcomings of the nonlocal elasticity, Lim et al. (Lim, Zhang & Reddy, 2015) introduced a nonlocal strain gradient theory (NSGT) using two kernel functions. The new theory is able to describe both stiffness softening and hardening at small-scale levels. In addition, the scale effect predicted by the NSGT appears in a wider range of lengths in comparison with nonlocal effects. However, the computational costs of the nonlocal elasticity is less than those of the NSGT due to the fact that strain gradient terms are also incorporated.

3. Types of different nanostructures

In the following sub-sections, the size-dependent continuum models of various types of nanoscale structures including nanorods, nanorings, nanobeams, nanoplates and nanoshells as well as the literature on the mechanics of these nanostructures are reviewed. Furthermore, size-dependent differential equations for the mechanical behaviours of these structures such as their buckling, vibration, bending and wave propagation responses are presented via the nonlocal elasticity. Various types of nanostructures, involving nanorods, nanorings, nanobeams, nanoplates, and nanoshells, are considered in this paper (see Fig. 3).

3.1. Nanorods

In this section, modified continuum models reported on the mechanical behaviour of nanorods are reviewed. Nanorods (Ye et al., 2012) are one-dimensional nanoscale structures which can be made by various techniques such as vapour-phase transport (Xu et al., 2004), hydrothermal synthesis (Choy et al., 2004) and seed-mediated growth (Nikoobakht & El-Sayed, 2003) (see Fig. 4). The length of nanorods can vary from 1 nm to 3000 nm (Wen et al., 2003). These small-scale structures have been extensively utilised in various devices including nanosensors (John, 2005), drug delivery systems (Alkilany et al., 2012) and solar cells (Liu & Aydil, 2009). To better design nanosystems using nanorods, it is advised to enhance knowledge about the mechanics of these structures since the overall performance of a nanosystem is affected by the mechanical characteristics of its parts.

3.1.1. Nonlocal rod model

Aydogdu (Aydogdu, 2009) developed a nonlocal model for the linear longitudinal vibration of nanoscale rods. Following him, one can write the nonlocal stress of nanorods as

$$\sigma_{xx}^{nl} - (e_0 a)^2 \frac{\partial^2 \sigma_{xx}^{nl}}{\partial x^2} = E\varepsilon_{xx}, \tag{9}$$

where E is the elasticity modulus. Using Eq. (9), the force resultant of nanorods (i.e. $N_{xx} = \int_A \sigma_{xx}^{nl} dA$) can be expressed as

$$N_{xx} - (e_0 a)^2 \frac{\partial^2 N_{xx}}{\partial x^2} = EA\frac{\partial u}{\partial x}, \tag{10}$$
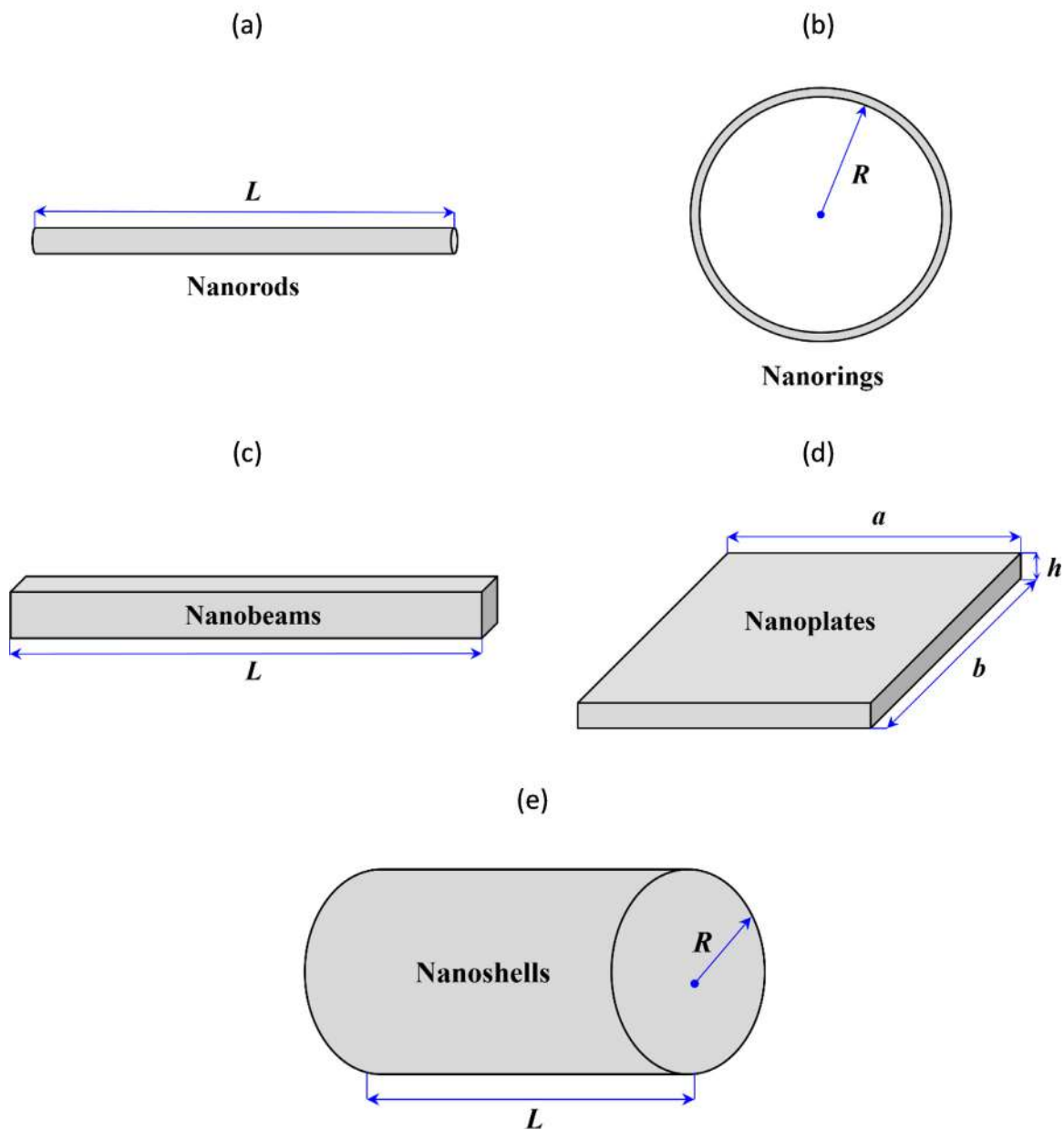
Fig. 3. Different types of nanostructures: (a) nanorods, (b) nanorings, (c) nanobeams, (d) nanoplates, and (e) nanoshells.
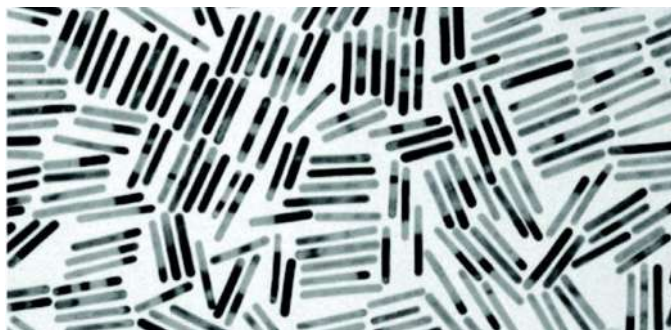
Fig. 4. A set of gold nanorods (Ye et al., 2012). Reprinted with permission from ACS. Copyright (2012) American Chemical Society.
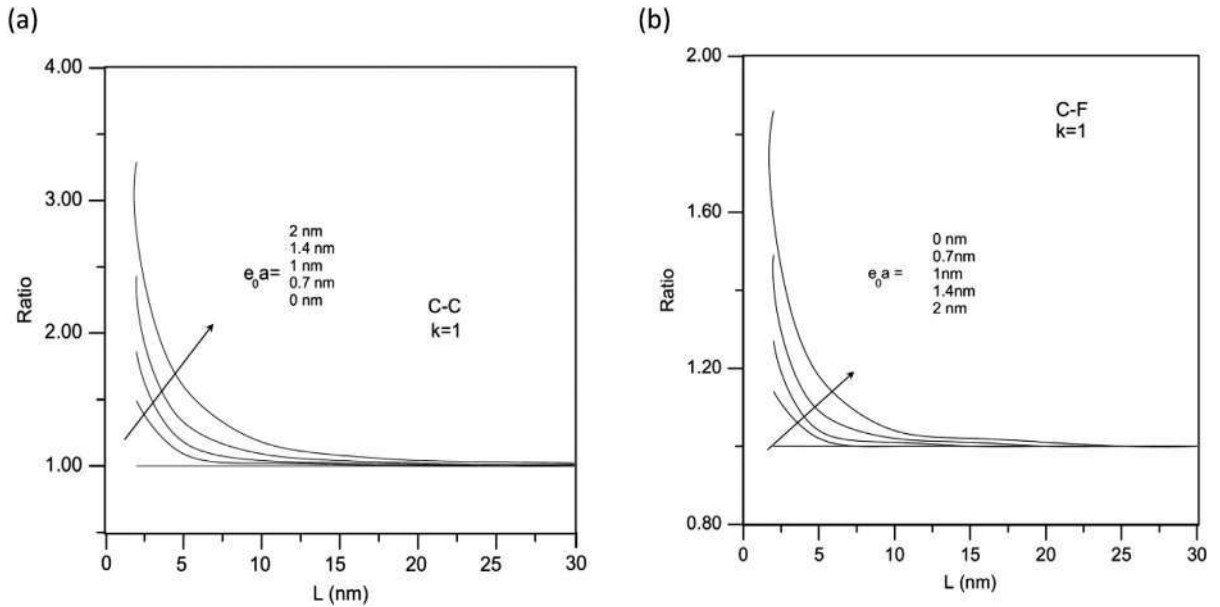
Fig. 5. Scale effects on the longitudinal vibration of nanorods for (a) C–C and (b) C-F ends (Aydogdu, 2009). Reprinted with permission from Elsevier.

where A and u denote the area of the rod cross-section and the axial displacement, respectively. Now employing the Hamilton principle, one can obtain the motion equation of nanorods as

$$\frac{\partial N_{xx}}{\partial x} = m\frac{\partial^2 u}{\partial t^2}. \tag{11}$$

Here m represents the mass per unit length of the nanorod. Using Eqs. (10) and (11), the following explicit relation is obtained for the stress resultant

$$N_{xx} = EA\frac{\partial u}{\partial x} + (e_0 a)^2 m\frac{\partial^3 u}{\partial x \partial t^2}. \tag{12}$$

Substituting Eq. (12) into Eq. (11), one obtains

$$EA\frac{\partial^2 u}{\partial x^2} + m(e_0 a)^2 \frac{\partial^4 u}{\partial x^2 \partial t^2} = m\frac{\partial^2 u}{\partial t^2}. \tag{13}$$

Eq. (13) governs the axial vibration of nanoscale rods incorporating size effects. This equation was first derived by Aydogdu (Aydogdu, 2009). He solved the equation analytically and presented explicit expressions for two different boundary conditions. Fig. 5 shows the ratio of the local natural frequency to the nonlocal one for various scale parameters. The frequency ratios are calculated for clamped-clamped (C–C) and clamped-free (C-F) nanorods. It is found that for small lengths, scale effects are noticeable while the nonlocal and local frequencies are approximately the same after a certain length ($L > 20$ nm). More recently, the nonlocal rod model has been employed to analyse the longitudinal free vibration of nanorods for different boundary conditions including an attached mass and an attached spring (Numanoğlu, Akgöz & Civalek, 2018); it was found that the mass attachment reduces the axial frequency of nanorods.

3.1.2. Size-dependent mechanics of nanorods

There are various types of nanoscale rods such as uniform, non-uniform and nonhomogeneous. In addition to simple uniform nanorods, the axial vibrations of tapered nanorods (Danesh, Farajpour & Mohammadi, 2012) and double-nanorod systems (Murmu & Adhikari, 2010) were also investigated in the literature. Moreover, the axial vibration of nonhomogeneous rods at nanoscale levels was studied utilising the nonlocal elasticity (Chang, 2013, Şimşek, 2012); shown was that the material non-homogeneity can greatly affect the axial vibration of nanorods. Depending on the value of elasticity modulus ratio, the natural frequency of nanorods can decrease or increase with increasing power-law exponent (Şimşek, 2012).

In addition to the axial vibration of nanorods, other mechanical responses of these small-scale structures have been also investigated using size-dependent continuum models. For instance, wave propagations in nanorods were studied via help of the nonlocal elasticity (Narendar & Gopalakrishnan, 2010, Aydogdu, 2012); it was reported that the scale parameter greatly affects the wave propagation in nanorods. The size coefficient causes a certain region associated with the band gap in longitudinal wave modes. The nonlocal elasticity was also employed for analysing the size-dependent torsion of cracked nanorods (Loya, Aranda-Ruiz & Fernández-Sáez, 2014); the presence of a circumferential crack reduces the natural frequencies.
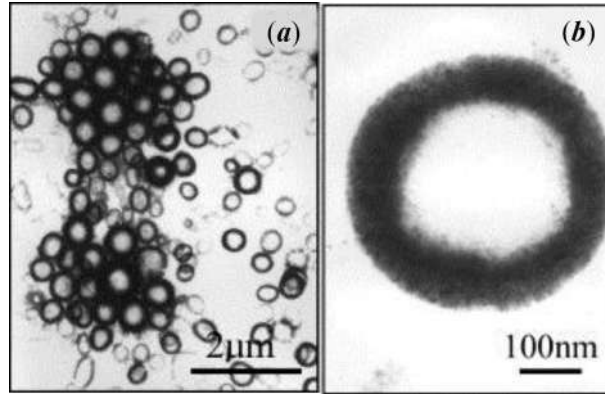
Fig. 6. (*a*) A system of nanorings and (*b*) a single nanoring (Cui, Gu, Xu & Shi, 2006). Reprinted with permission from Elsevier.
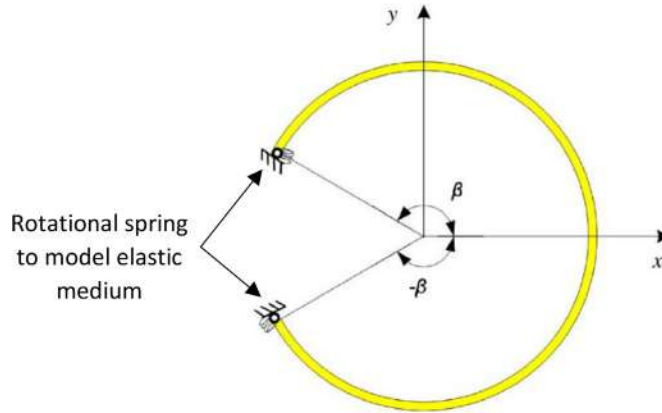

Fig. 7. A nanoscale arch embedded in an elastic medium (Wang & Duan, 2008). Reprinted with permission from AIP Publishing.

The majority of size-dependent continuum models of nanorods have been developed via the nonlocal theory of elasticity. However, more recently, the NSGT has been employed for describing the longitudinal vibration (Li, Hu & Li, 2016) and tension (Zhu & Li, 2017) of nanorods; the modified rod model was successfully calibrated employing MD results.

3.2. Nanorings

Another nanoscale structure with a remarkable potential applications in nanoelectromechanical systems (NEMS) is nanorings. Fig. 6 illustrate a system of circular nanorings as well as a single nanoring. Compared to nanobeams and nanoplates, few theoretical studies have been reported on the mechanical behaviour of nanorings using size-dependent continuum models. Wang & Duan (2008) developed a nonlocal model to explore the oscillations of nanoscale rings; exact results were obtained for the size-dependent natural frequencies. Assuming the flexural vibration of nanorings without extension, the nonlocal differential equation is obtained as (Wang & Duan, 2008)

$$\frac{\partial^6 v}{\partial \theta^6} + 2\frac{\partial^4 v}{\partial \theta^4} + \frac{\partial^2 v}{\partial \theta^2} = \frac{mR^4}{EI}\left[\frac{e_0 a}{R}\frac{\partial^6 v}{\partial t^2 \partial \theta^4} - \left(1 + \frac{e_0 a}{R}\right)\frac{\partial^4 v}{\partial t^2 \partial \theta^2} + \frac{\partial^2 v}{\partial t^2}\right], \tag{14}$$

where v, R and θ are the tangential displacement, the radius of the nanoring and the angle between the horizontal line and the line drawn from the ring centre, respectively; E, m, I and $e_0 a$ are the elasticity modulus, mass per unit length, inertia moment and the nonlocal parameter, respectively. In a paper by Wang and Duan (Wang & Duan, 2008), the oscillation of nanoscale arches (see Fig. 7) was also examined using the nonlocal elasticity. The variation of the frequency parameter versus the opening angle (2β) for various nonlocal parameters ($\alpha = e_0 a/R$) for (a) asymmetric and (b) symmetric modes is plotted in Fig. 8. The frequency parameter is defined as $\Omega = mR^4\omega^2/EI$ where ω is the dimensional natural frequency of the nanosystem. Increasing opening angle reduces the natural frequency of nanoarches. In addition, stronger nonlocal effects lead to lower natural frequencies since increasing nonlocal parameter results in a reduction in the stiffness of nanostructures.

In addition to the above-mentioned valuable study, the nonlocal elasticity theory was also utilised in Refs. (Moosavi, Mohammadi, Farajpour & Shahidi, 2011, Wang, Xiang, Yang & Kitipornchai, 2012, Arefi, Mirdamadi & Salimi, 2012) in order to derive size-dependent differential equations for investigating the mechanical behaviour of nanoscale rings. Moosavi et al.
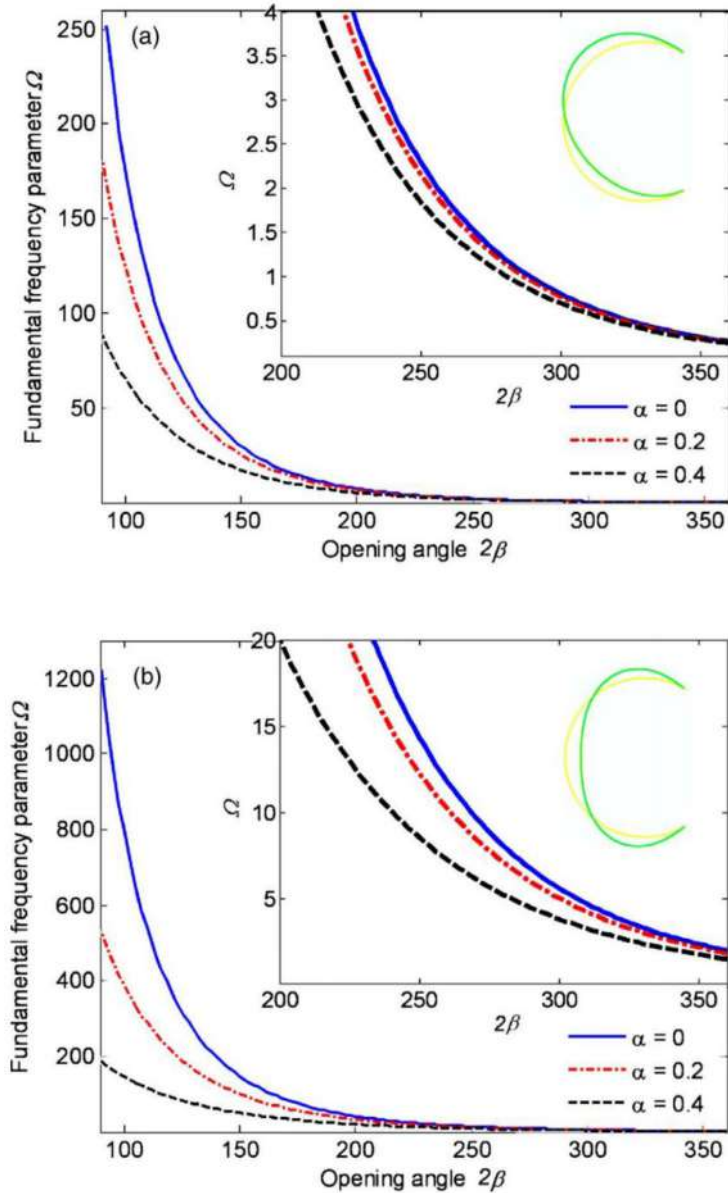
Fig. 8. Frequency parameter versus the opening angle for various nonlocal parameters for (*a*) asymmetric and (*b*) symmetric modes (Wang & Duan, 2008). Reprinted with permission from AIP Publishing.

(Moosavi, Mohammadi, Farajpour & Shahidi, 2011) developed a nonlocal shear deformation theory of rings for the in-plane free vibrations of nanorings; they found that the change in the natural frequency obtained by the classical theory and the shear deformation one is significant for small radii and larger nonlocal parameters. Furthermore, the size-dependent buckling of nanorings and nanoarches was analysed via help of the nonlocal elasticity in Refs. (Wang, Xiang, Yang & Kitipornchai, 2012) and (Arefi, Mirdamadi & Salimi, 2012); increasing the scale parameter reduces the buckling force.

3.3. Nanobeams

Nanobeams (García-Sánchez et al., 2007, Babaei Gavan et al., 2009, Baghani, Mohammadi & Farajpour, 2016) such as carbon nanotubes, silicon and silver nanobeams have various promising applications in different nanoscale devices such as small-scale mechanical sensors (Zhao, Gan & Zhuang, 2002), resonators (Eichler et al., 2011, Farokhi, Païdoussis & Misra, 2018) and actuators (Fennimore et al., 2003) (see Fig. 9). Since the small-scale system operates based on mechanical mechanisms in these applications, understanding the size-dependent mechanical characteristics of nanoscale beams is importance. In early studies on the mechanics of nanoscale beams, especially carbon nanotubes, size effects were not taken into con-
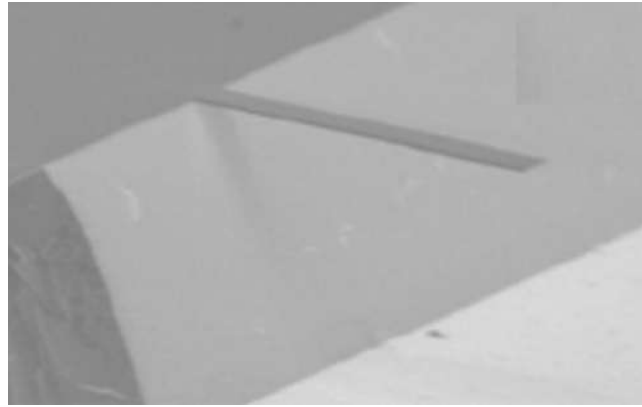
Fig. 9. A schematic representation of a cantilever nanobeam (Babaei Gavan et al., 2009). Reprinted with permission from AIP Publishing.

sideration (Fu, Hong & Wang, 2006, Yoon, Ru & Mioduchowski, 2005, Yoon, Ru & Mioduchowski, 2003, Wang, Ru & Mioduchowski, 2005). For the first time, Peddieson et al. (Peddieson, Buchanan & McNitt, 2003) utilised the nonlocal continuum mechanics so as to capture size effects on the bending of nanobeams; particularly size-dependent bending of cantilever nanobeams was examined because of their wide applications in nanoscale actuators. In the following, the bending, vibration and buckling of nanobeams as well as the wave propagation in them are reviewed. Both size-dependent linear and nonlinear studies are considered.

3.3.1. Nonlocal beam model

Applying the nonlocal theory, the modified constitutive equation of a nanoscale beam can be expressed as

$$\left[1 - (e_0 a)^2 \nabla^2\right]\sigma_{xx} = E\varepsilon_{xx}. \tag{15}$$

On the other hand, applying the theory of Euler–Bernoulli beams, the axial strain is given by

$$\varepsilon_{xx}(x, z, t) = \frac{\partial u(x, t)}{\partial x} - z\frac{\partial^2 w(x, t)}{\partial x^2}, \tag{16}$$

where w and u indicate the mid-surface transverse and axial displacements of the nanobeam, respectively (Dehghany & Farajpour, 2014). The force and couple stress resultants of nanobeams are defined as

$$N_{xx} = \int_A \sigma_{xx}dA, \, M_{xx} = \int_A z\sigma_{xx}dA, \tag{17}$$

in which A is the cross-sectional area. For nanobeams, the following equations are derived via Hamilton's principle

$$\frac{\partial N_{xx}}{\partial x} = m\frac{\partial^2 u}{\partial t^2}, \tag{18}$$

$$\frac{\partial^2 M_{xx}}{\partial x^2} + \frac{\partial}{\partial x}\left(N_{xx}\frac{\partial w}{\partial x}\right) + q = m\frac{\partial^2 w}{\partial t^2}. \tag{19}$$

Here m and q represent the mass per unit length and the transverse loading, respectively. In view of Eq. (15), one can write

$$\left[1 - (e_0 a)^2 \nabla^2\right]M_{xx} = -EI\frac{\partial^2 w}{\partial x^2}. \tag{20}$$

Using Eqs. (18)–(20), the following differential equation is derived for the linear transverse vibration of nonlocal beams subject to an external loading

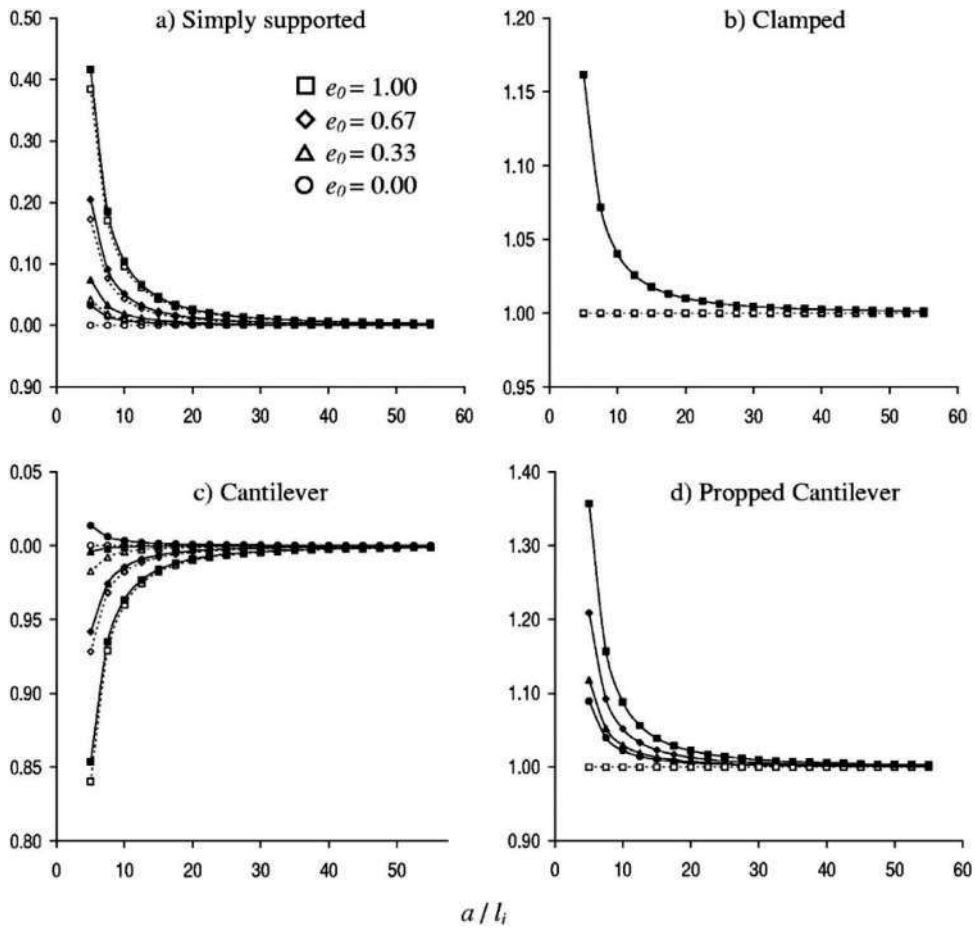$$-EI\frac{\partial^4 w}{\partial x^4} + \frac{\partial}{\partial x}\left(N_{xx}\frac{\partial w}{\partial x}\right) - (e_0 a)^2\frac{\partial^3}{\partial x^3}\left(N_{xx}\frac{\partial w}{\partial x}\right)$$

$$+q - (e_0 a)^2\frac{\partial^2 q}{\partial x^2} = m\frac{\partial^2 w}{\partial t^2} - m(e_0 a)^2\frac{\partial^4 w}{\partial x^2 \partial t^2}. \tag{21}$$

Fig. 10. The ratio of the maximum transverse displacement calculated via the Timoshenko model of beams to that calculated via the Euler–Bernoulli model against the ratio of the length to the internal characteristic length for (a) simply supported, (b) clamped, (c) cantilever and (d) propped cantilever nanobeams subject to a uniform transverse load (a dashed line indicates the Euler–Bernoulli model while a solid line indicates Timoshenko beam model) (Reddy & Pang, 2008). Reprinted with permission from AIP Publishing.

3.3.2. Size-dependent bending of nanobeams

Different modified beam models such as Reddy, Timoshenko, Euler–Bernoulli and Levinson were proposed for investigating the *bending* of nanoscale beams via the nonlocal continuum mechanics (Reddy, 2007, Reddy & Pang, 2008, Aydogdu, 2009, Thai & Vo, 2012). Fig. 10 shows the ratio of the maximum deflection of nanobeams under uniformly transverse loading obtained by the Timoshenko theory to that of the Euler–Bernoulli one with the ratio of the length (a) to the internal characteristic length (l_i) for various boundary conditions and various calibration coefficients (e_0) (Reddy & Pang, 2008). In all cases, the influence of the calibration coefficient disappears after a certain length. Furthermore, explicit expressions were obtained in Refs. (Khajeansari, Baradaran & Yvonnet, 2012, Yan et al., 2015, Zenkour & Sobhy, 2015) in order to analyse the linear bending of nanobeams using the nonlocal elasticity as a size-dependent theory. The influence of the surface energy on the bending of nanobeams was also studied in the literature (Jiang & Yan, 2010, Ansari & Sahmani, 2011); it was found that the surface influence is more significant for slender nanobeams.

In addition, the nonlocal elasticity has been utilised to explore the size-dependent bending behaviour of *non-homogeneous* nanobeams (Şimşek & Yurtcu, 2013, Nejad & Hadi, 2016). More recently, a NSGT-based beam model has been proposed by Li et al. (Li et al., 2017) for the mechanical behaviour of non-homogeneous nanoscale beams. Fig. 11 indicates the maximum deflection of a non-homogeneous nanobeam with simply supported boundary conditions subject to sinusoidal applied load in the transverse direction. Different strain gradient coefficients (i.e. $\zeta = \ell/L$ in which ℓ is the strain gradient parameter) and various nonlocal coefficients (i.e $\tau = e_0 a/L$) are considered. Increasing strain gradient parameter reduces the maximum deflection of non-homogeneous nanobeams since higher strain gradient parameters increase the stiffness of nanostructures. By contrast, the maximum deflection notably increases with increasing nonlocal coefficient.

In addition to linear size-dependent models, *nonlinear* studies have been also reported on the static behaviour of nanoscale beams (Reddy, 2010, Preethi, Rajagopal & Reddy, 2015, Li, Hu & Ling, 2016). Reddy (Reddy, 2010) presented both
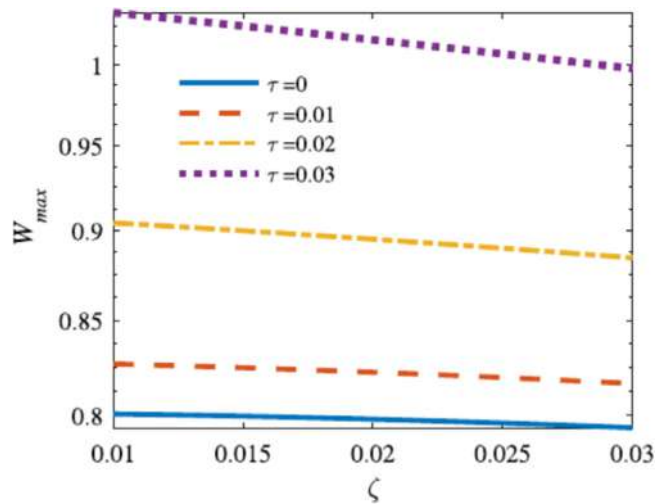
Fig. 11. Maximum deflection of a non-homogeneous nanoscale beam with simply supported boundary conditions subject to sinusoidal applied load for different strain gradient coefficients and various nonlocal coefficients (Li et al., 2017). Reprinted with permission from Elsevier.
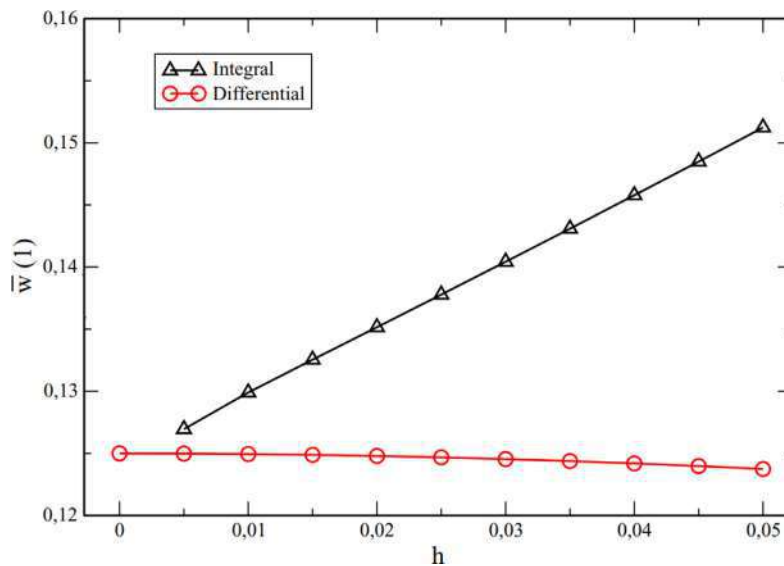
Fig. 12. Integral and differential nonlocal models for the bending of cantilever nanobeams (h is the nonlocal coefficient defined as $h = e_0 a/L$) (Fernández-Sáez, Zaera, Loya & Reddy, 2016). Reprinted with permission from Elsevier.

classical and shear deformable beam models incorporating the geometric nonlinearity as well as the size effects by nonlocal elasticity as well as von Kármán's assumptions. Moreover, a nonlinear size-dependent finite element formulation incorporating both surface and nonlocal effects was proposed by Preethi et al. (Preethi, Rajagopal & Reddy, 2015) via use of the Timoshenko theory of beams. The nonlinear bending of nanoscale non-homogeneous beams has been lately examined by Li and Hu (Li, Hu & Ling, 2016) using the NSGT as a size-dependent elasticity theory.

More recently, an *integral* size-dependent formulation has been developed by Fernández-Sáez et al. (Fernández-Sáez, Zaera, Loya & Reddy, 2016) so as to describe the bending of nanobeams using the nonlocal integral constitutive relation and the Euler–Bernoulli theory of beams. Using the integral nonlocal formulation, the paradox observed in cantilever nanobeams when the differential nonlocal elasticity is used (namely, the increasing effect of the nonlocal parameter on the nanobeam stiffness) was resolved as shown in Fig. 12. Moreover, Tuna and Kirca (2016) examined the static deformation of nanobeams using the nonlocal integral model; exact results were obtained for both Euler–Bernoulli and Timoshenko nanobeams.

3.3.3. Size-dependent buckling of nanobeams

Size-dependent elasticity models have been also proposed for the *buckling* of nanoscale beams, especially carbon nanotubes. The majority of continuum models have been developed using the nonlocal elasticity (Zhang, Liu & Wang, 2004,
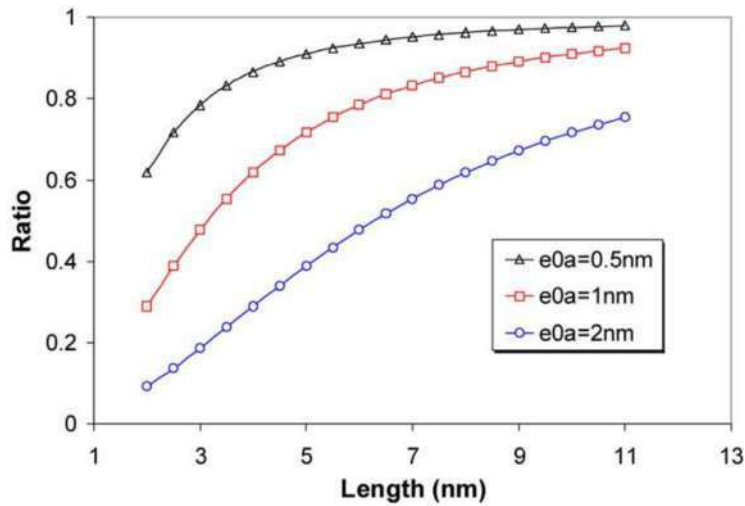
Fig. 13. The nonlocal-to-local buckling ratio of CNTs against their length for various $e_0 a$ (Wang, Varadan & Quek, 2006). Reprinted with permission from Elsevier.
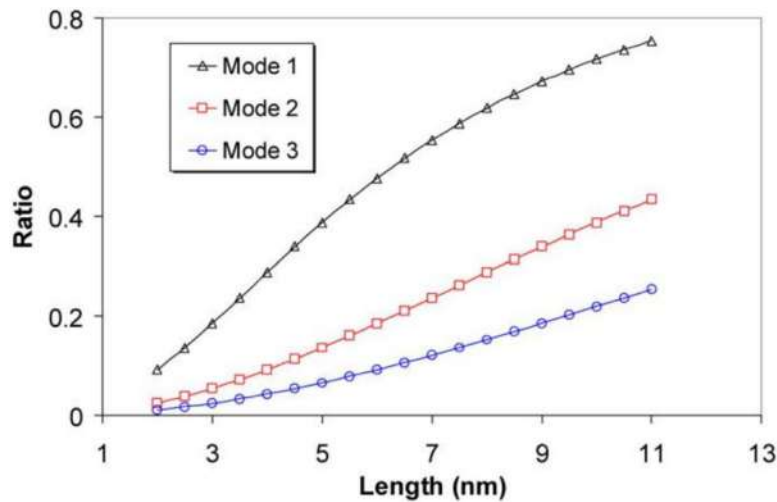
Fig. 14. The nonlocal-to-local buckling ratio of CNTs against their length for different mode numbers (Wang, Varadan & Quek, 2006). Reprinted with permission from Elsevier.

Murmu & Pradhan, 2009, Pradhan & Reddy, 2011, Benguediab, Tounsi, Zidour & Semmah, 2014, Hao, Guo & Wang, 2010, Eltaher, Emam & Mahmoud, 2013, Nejad, Hadi & Rastgoo, 2016, Murmu & Adhikari, 2011). For instance, Sudak (Sudak, 2003) explored the linear stability of multi-walled carbon nanotubes (MWCNTs) via help of the nonlocal elasticity; nonlocal influences have a crucial role to play in the buckling of MWCNTs. In addition, Wang et al. (Wang, Varadan & Quek, 2006) introduced a linear nonlocal theory for the stability of single-walled carbon nanotubes (SWCNTs). The variation of the nonlocal-to-local buckling ratio with the length is plotted in Fig. 13 for different nonlocal parameters. As the length increases, the effect of the length scale significantly decreases. Furthermore, higher values of $e_0 a$ reduces the buckling load ratio since the difference between the two theories increases when the nonlocal influence becomes stronger. Fig. 14 illustrates the change of the buckling ratio with the length for different model numbers. It is observed that the influence of size is greater for higher mode numbers. This is due to the fact that at higher buckling modes, the interaction between molecules increases.

At nanoscale levels, the surface-to-bulk ratio of structures is high, and thus *surface influences* on the mechanical characteristics of nanostructures become important. The surface influence on the stability of nanoscale beams has been investigated using modified beam models (Wang & Feng, 2009, Wang, 2012, Attia, 2017). Wang and Feng (Wang & Feng, 2009) proposed a modified Euler model so as to examine the influence of surface elastic constants and surface residual stress on the buckling of nanowires subject to uniaxial compression. Wang (Wang, 2012) carried out a nonlinear analysis on the buckling of nanobeams conveying fluid flow; the nonlinear buckling of the fluid-conveying nanosystem was considerably affected by the surface elastic constant. More lately, the effects of surface energy on the mechanics of non-homogeneous nanobeams
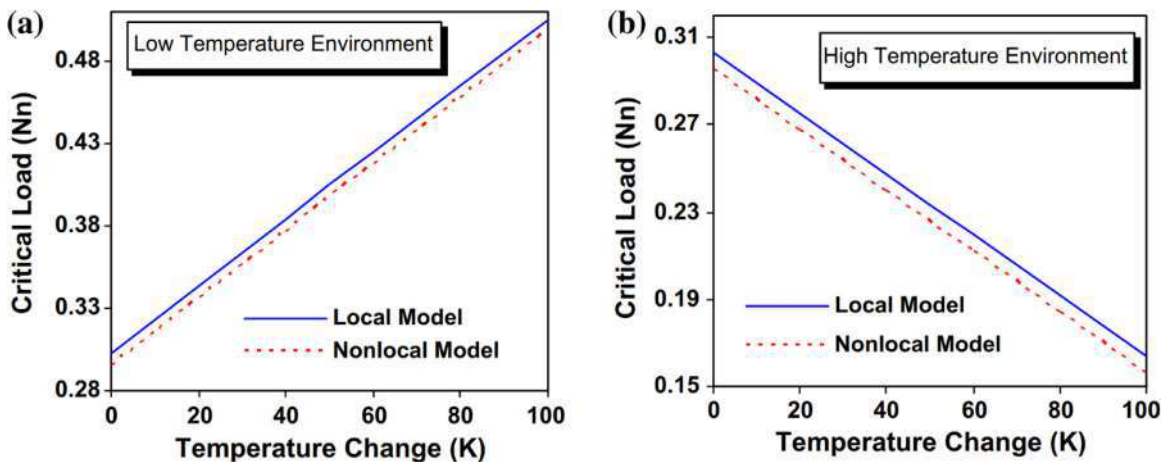
Fig. 15. The critical buckling load versus the temperature change for (a) low temperature environment, and (b) for high temperature environment (Murmu & Pradhan, 2010). Reprinted with permission from Elsevier.

have been analysed based on two different size-dependent theories; surface effects become more prominent as the material gradient index of non-homogeneous nanobeams increases.

It has been shown that the critical buckling load of different types of nanobeams such as CNTs and non-homogeneous nanobeams is sensitive to *temperature changes* (Murmu & Pradhan, 2010, Amara, Tounsi & Mechab, 2010, Narendar & Gopalakrishnan, 2011, Ebrahimi & Salari, 2015, Yu, Xue, Li & Tian, 2016). Fig. 15 shows temperature effects on the linear stability of CNTs. The temperature change affects the buckling force of SWCNTs. At low temperatures, the buckling force increases when the temperature change increases whereas increasing temperature change reduces the buckling force at a high temperature environment. This is because the thermal expansion constant of SWCNTs is negative at low temperatures while it is positive at high temperatures (Jiang, Liu, Huang & Hwang, 2004).

The *post-buckling* analysis of nanoscale beams has been the focus of many studies in the literature (Emam, 2013, Dai, Wang, Abdelkefi & Ni, 2015, She, Yuan, Ren & Xiao, 2017). For example, Setoodeh et al. (Setoodeh, Khosrownejad & Malekzadeh, 2011) determined exact analytical solutions for the post-buckling of SWCNTs within the framework of the nonlocal elasticity as well as the Euler–Bernoulli beam theory; the nonlinearity related to the stretching of the mid-plane is more profound for higher modes. In addition, the NSGT was utilised in order to examine the nonlinear buckling of nanoscale beams (Li & Hu, 2015); both the nonlocal and strain gradient parameters significantly affect the nonlinear buckling loads. The post-buckling of non-homogeneous nanobeams was also studied via the NSGT (Li & Hu, 2017); it was found that both hardening and softening responses can occur for the stiffness of the nanoscale beam depending on size coefficient values.

3.3.4. Size-dependent vibration of nanobeams

The nonlocal elasticity theory has been broadly utilised for analysing the *vibration characteristics* of nanobeams (Chakraverty & Behera, 2015, Murmu, McCarthy & Adhikari, 2012, Apuzzo et al., 2017, Kiani, 2010, Murmu & Adhikari, 2010, Murmu, Adhikari & Wang, 2011, Lei, Adhikari & Friswell, 2013, Fernández-Sáez & Zaera, 2017). Some pioneering studies are briefly reviewed in the following. Wang and Varadan (Wang & Varadan, 2006) proposed a linear nonlocal beam theory for the size-dependent oscillations of both single- and double-walled CNTs. The ratio of the nonlocal natural frequency to the local one decreases with increasing the nonlocal parameter as seen from Fig. 16 (Pradhan & Murmu, 2009). Murmu and Pradhan (Murmu & Pradhan, 2009) analysed the oscillation of SWCNTs surrounded by a linear elastic medium employing the nonlocal elasticity incorporating thermal influences; the small scale influence becomes less important with increasing Winkler stiffness constant of the elastic medium (see Fig. 17). In addition, a nonlocal beam model was presented by Simsek (Şimşek, 2010) for the size-dependent vibration of CNTs subject to a moving load; the nonlocal dynamic deflection is larger than the local one since the small scale effect has a decreasing effect on the nanotube stiffness. Benzair et al. (Benzair et al., 2008) examined temperature influences on the vibrations of CNTs via help of the nonlocal elasticity; temperature influences on the natural frequency decrease with increasing vibration mode number. Duan et al. (Duan, Wang & Zhang, 2007) employed the molecular dynamics to calibrate the nonlocal beam model of CNTs for the vibration analysis; it was found that the calibration coefficient of the nonlocal beam model depends on the geometrical features, mode number and edge conditions.

In addition to the stress nonlocality, *surface influences* on the vibration of nanoscale beams have been studied based on modified continuum models (Yan & Jiang, 2011, Gheshlaghi & Hasheminejad, 2011, Attia & Rahman, 2018, Kiani, 2016, Sharabiani & Yazdi, 2013, Lee & Chang, 2010, Lei, Natsuki, Shi & Ni, 2012); it was concluded that surface effects can account for the stiffness hardening, which cannot be described by the nonlocal elasticity theory. In addition, recently size-dependent
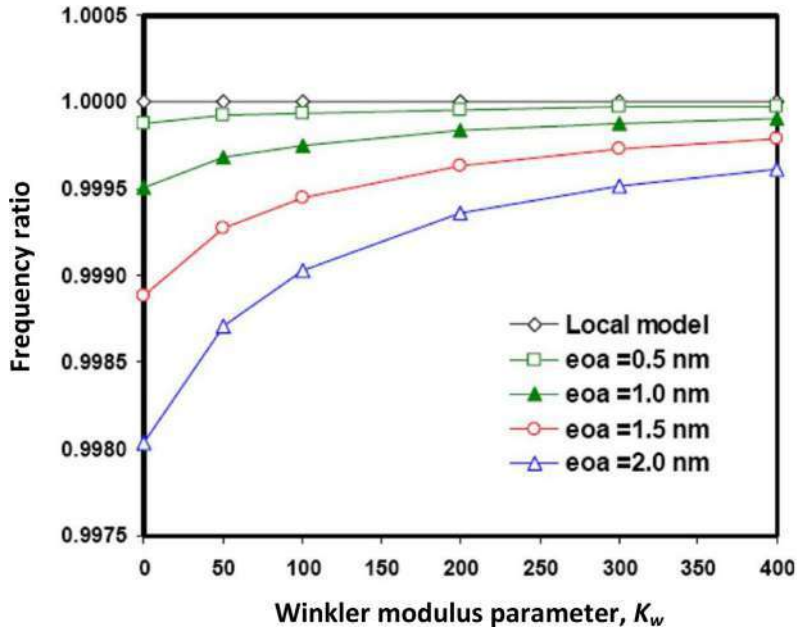
Fig. 16. The ratio of the nonlocal frequency to the local one versus the Winkler parameter for various nonlocal coefficients (Pradhan & Murmu, 2009). Reprinted with permission from AIP Publishing.
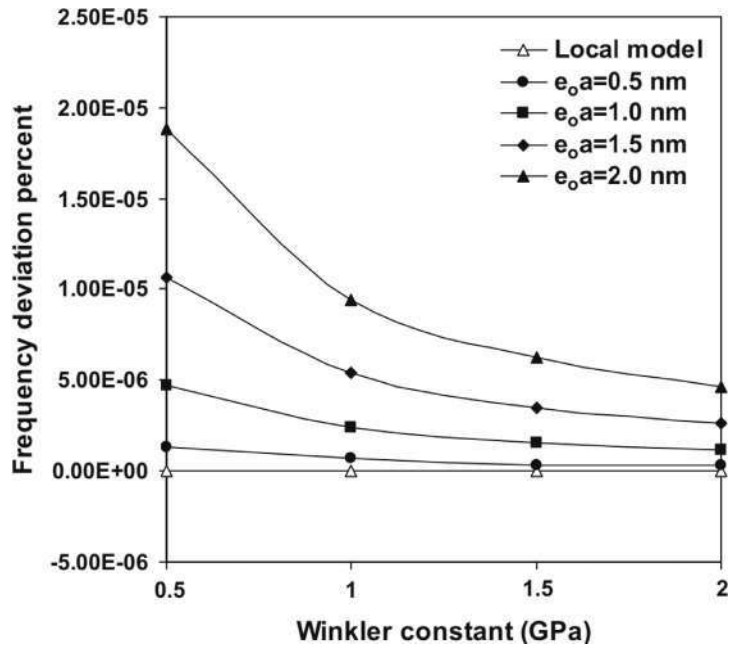
Fig. 17. The frequency difference between the local and nonlocal models versus the Winkler constant for different nonlocal parameters (Murmu & Pradhan, 2009). Reprinted with permission from Elsevier.

continuum models incorporating surface and nonlocal effects have been developed for the vibration of *smart* nanoscale beams such as piezoelectric and magneto-electro-elastic nanobeams (Ebrahimi & Barati, 2018, Ke & Wang, 2014, Ebrahimi & Barati, 2016, Ke, Wang & Wang, 2012, Arefi & Zenkour, 2017, Yan & Jiang, 2013) as well as *non-homogeneous* nanoscale beams (Attia, 2017, Shafiei, Kazemi, Safi & Ghadiri, 2016, Şimşek, 2016, Rahmani & Pedram, 2014, Nejad, Hadi & Farajpour, 2017).

More recently, NSGT-based continuum models have been introduced for the vibration of nanobeams (Farajpour, Shahidi, Tabataba'i-Nasab & Farajpour, 2018, Li et al., 2017, Şimşek, 2016, Lu, Guo & Zhao, 2017, Ebrahimi & Barati, 2017, Lu, Guo & Zhao, 2017, Ghayesh & Farajpour, 2018). Various modified theories of elasticity are compared in Fig. 18; CT, NT and SGT
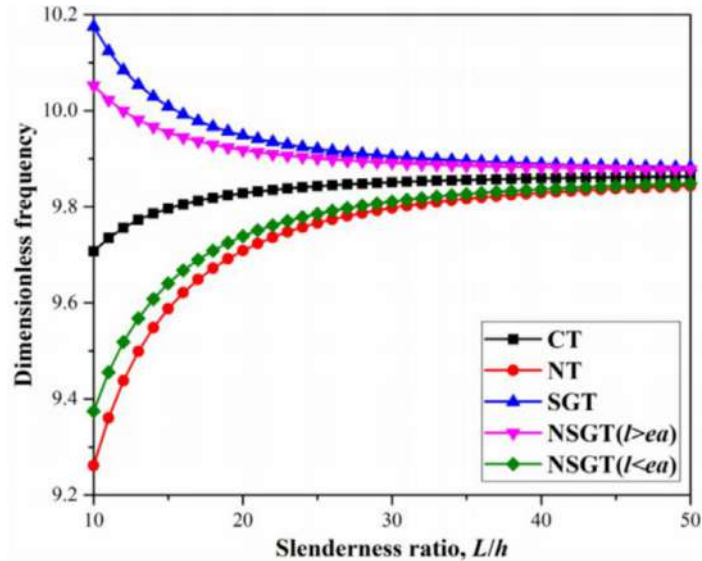
Fig. 18. Dimensionless frequency versus the slenderness ratio of nanoscale beams for various elasticity theories (Lu, Guo & Zhao, 2017). Reprinted with permission from Elsevier.

stand for the classical, nonlocal, and strain gradient theories, respectively. It is found that the NT gives the lowest natural frequencies while the SGT leads to the highest ones. The results of the NSGT are greatly dependent on the relative values of size parameters. For $ea > l$, the natural frequency obtained by the NSGT is higher than that of the NT but lower than that obtained by the CT. However, for $ea < l$, the NSGT leads to the natural frequency which is higher than that obtained by the CT but lower than that of the SGT.

In addition to linear modified continuum models, *nonlinear* size-dependent models have been presented in the literature for the free and forced vibrations of nanobeams using the nonlocal elasticity (Shafiei, Kazemi, Safi & Ghadiri, 2016, Yang, Ke & Kitipornchai, 2010, Ke, Xiang, Yang & Kitipornchai, 2009, Arani et al., 2012, Şimşek, 2014, Fang, Zhen, Zhang & Tang, 2013, Soltani & Farshidianfar, 2012), the surface elasticity (Malekzadeh & Shojaee, 2013, Hosseini-Hashemi, Nazemnezhad & Rokni, 2015) and the NSGT (Li, Hu & Ling, 2016, Şimşek, 2016, Ghayesh & Farajpour, 2018). Furthermore, different solution methods such as the differential quadrature method (DQM) (Malekzadeh & Shojaee, 2013, Yang, Ke & Kitipornchai, 2010), the Homotopy perturbation method (Shafiei, Kazemi, Safi & Ghadiri, 2016), the continuation scheme (Ghayesh & Farajpour, 2018) and the Hamiltonian approach (Şimşek, 2016) have been utilised for solving the derived nonlinear equations of motion. Fig. 19 shows the frequency-amplitude response of tubes at nanoscales via the NSGT; q_1, ω_1 and Ω denote the first generalised coordinate, the linear natural frequency and the non-dimensional excitation frequency, respectively. Perfectly straight nanotubes exhibit a hardening-type nonlinear response with two saddle nodes.

3.3.5. Size-dependent wave propagations in nanobeams

Wave propagations in nanobeams have been also analysed via help of size-dependent models including the nonlocal elasticity theory (NET) (Wang, 2005, Heireche et al., 2008, Wang, Zhou & Lin, 2006, Narendar & Gopalakrishnan, 2009), the surface elasticity (Zhang et al., 2015, Assadi & Farshi, 2011) and the NSGT (Lim, Zhang & Reddy, 2015, Li, Hu & Ling, 2016, Li, Hu & Ling, 2015, She, Yuan & Ren, 2018, Barati, 2017). Fig. 20 illustrates the change of the phase velocity with the wave number for various modified theories such as the classical elasticity theory (CET), NSGT, SGT and NET; the results of MD calculations are also plotted in the figure. The NSGT results are very close to those calculated by the MD simulations.

3.4. Nanoplates

Nanoplates such as graphene sheets (Geim & Novoselov, 2010), silver nanoplates (Chen & Carroll, 2002) and metallic carbon nanosheets (Zhang, Wang, Chen & Jena, 2013) have an extensive range of promising applications in various fields of nanotechnology. In applications such as nanomechanical resonators (Bunch et al., 2007, Jiang, Park & Rabczuk, 2014, Rhoads, Shaw & Turner, 2008, Asemi, Farajpour & Mohammadi, 2014), nanoscale mass sensors (Dai, Kim & Eom, 2012, Shen, Tang, Li & Tang, 2012, Farajpour, Rastgoo, Farajpour & Mohammadi, 2016) and actuators (Park, An, Suk & Ruoff, 2010, Kong & Chen, 2014), mechanical characteristics of nanoplates play an important role in the general performance of the nanoscale device. Fig. 21 shows the application of graphene sheets as a resonating nanomechanical sensor (Murmu & Adhikari, 2013). So far many modified theoretical models have been reported on the mechanics of various nanoplates. In the following, first
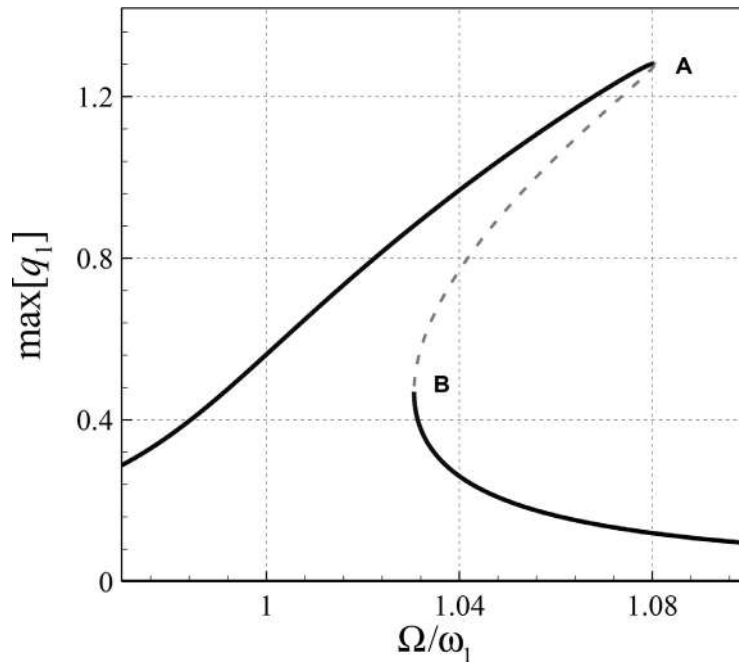
Fig. 19. Frequency-amplitude response of tubes at nanoscales via the NSGT (Ghayesh & Farajpour, 2018). Reprinted with permission from Elsevier.
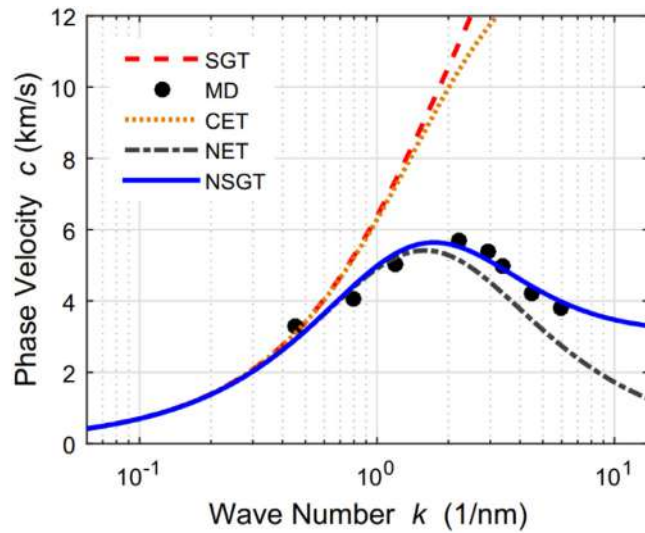
Fig. 20. Wave propagations in SWCNTs based on different modified theories (Li, Hu & Ling, 2016). Reprinted with permission from Elsevier.
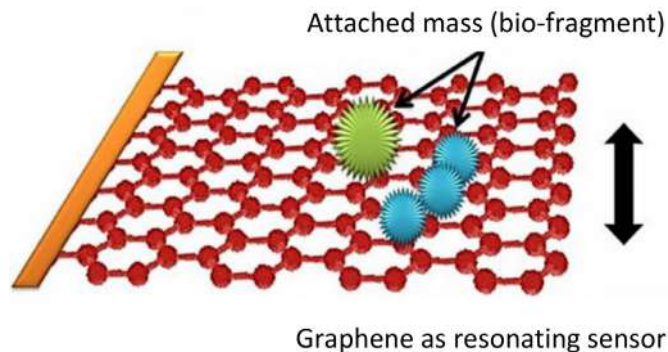
Fig. 21. Application of graphene sheets as a resonating nanosensor (Murmu & Adhikari, 2013). Reprinted with permission from Elsevier.
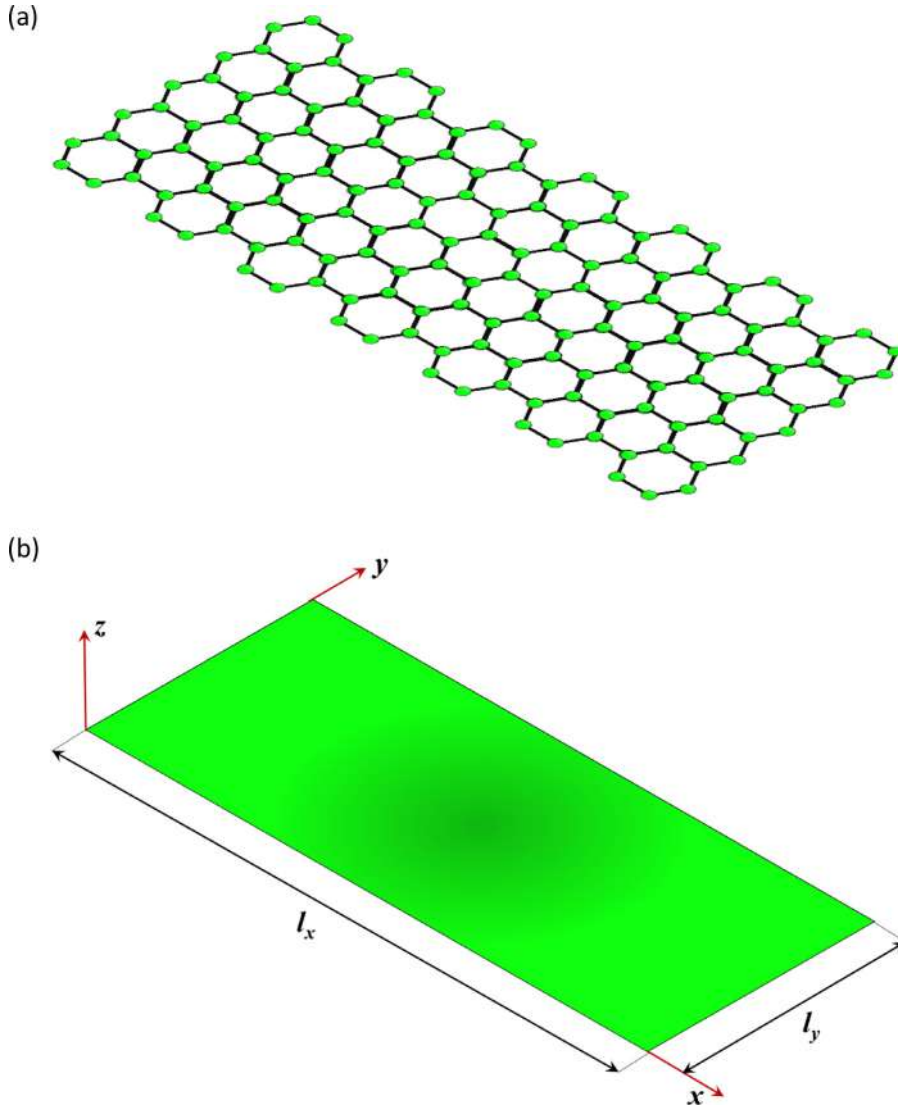
Fig. 22. (a) A SLGS with length l_x and width l_y, and (b) its equivalent continuum model.

the linear motion equations for the mechanics of nanoplates are presented. Then, important size-dependent studies on the vibration, stability and static deformation of nanoscale plates as well as wave propagations in them are discussed.

3.4.1. Nonlocal plate model

In Fig. 22, a typical single-layered graphene sheet (SLGS) with length l_x and width l_y is shown. Based on the NET, the constitutive equations of orthotropic nanoplates are expressed as

$$\left[1 - (e_0 a)^2 \nabla^2\right]\sigma_{xx} = \frac{E_1}{1 - v_{12}v_{21}}\varepsilon_{xx} + \frac{v_{12}E_2}{1 - v_{12}v_{21}}\varepsilon_{yy}, \ \left[1 - (e_0 a)^2 \nabla^2\right]\sigma_{yy} = \frac{v_{12}E_2}{1 - v_{12}v_{21}}\varepsilon_{xx} + \frac{E_2}{1 - v_{12}v_{21}}\varepsilon_{yy},$$

$$\left[1 - (e_0 a)^2 \nabla^2\right]\sigma_{xy} = 2G_{12}\varepsilon_{xy}, \tag{22}$$

where E_i, v_{ij} and G_{ij} stand for the elasticity modulus along the i direction, Poisson's ratio and the shear elasticity modulus of the nanoplate, respectively. The strain components of the orthotropic nanoplate are as

$$\varepsilon_{xx} = \frac{\partial u}{\partial x} - z\frac{\partial^2 w}{\partial x^2}, \varepsilon_{yy} = \frac{\partial v}{\partial y} - z\frac{\partial^2 w}{\partial y^2},$$

$$\varepsilon_{xy} = \frac{1}{2}\left(\frac{\partial u}{\partial y} + \frac{\partial v}{\partial x}\right) - z\frac{\partial^2 w}{\partial x \partial y}, \tag{23}$$

in which w, v and u, respectively, indicate the mid-surface displacements in z, y and x axes. The stress resultants are as

$$\langle N_{xx}, N_{yy}, N_{xy} \rangle = \int_{-h/2}^{h/2} \langle \sigma_{xx}, \sigma_{yy}, \sigma_{xy} \rangle dz, \quad \langle M_{xx}, M_{yy}, M_{xy} \rangle = \int_{-h/2}^{h/2} \langle \sigma_{xx}, \sigma_{yy}, \sigma_{xy} \rangle z dz. \tag{24}$$

Here h denotes the thickness of the orthotropic nanoplate. Using Eqs. (22)-(24), the stress resultants of the orthotropic nanoplate are obtained as

$$\left[1 - (e_0 a)^2 \nabla^2\right] N_{xx} = S_{11} \frac{\partial u}{\partial x} + S_{12} \frac{\partial v}{\partial y}, \quad \left[1 - (e_0 a)^2 \nabla^2\right] N_{yy} = S_{12} \frac{\partial u}{\partial x} + S_{22} \frac{\partial v}{\partial y},$$

$$\left[1 - (e_0 a)^2 \nabla^2\right] N_{xy} = S_{33} \left(\frac{\partial u}{\partial y} + \frac{\partial v}{\partial x} \right), \tag{25}$$

$$\left[1 - (e_0 a)^2 \nabla^2\right] M_{xx} = -D_{11} \frac{\partial^2 w}{\partial x^2} - D_{12} \frac{\partial^2 w}{\partial y^2}, \quad \left[1 - (e_0 a)^2 \nabla^2\right] M_{yy} = -D_{12} \frac{\partial^2 w}{\partial x^2} - D_{22} \frac{\partial^2 w}{\partial y^2},$$

$$\left[1 - (e_0 a)^2 \nabla^2\right] M_{xy} = -2D_{33} \frac{\partial^2 w}{\partial x \partial y}, \tag{26}$$

where

$$S_{11} = \frac{E_1 h}{1 - \nu_{12} \nu_{21}}, S_{12} = \frac{\nu_{12} E_2 h}{1 - \nu_{12} \nu_{21}}, S_{22} = \frac{E_2 h}{1 - \nu_{12} \nu_{21}}, S_{33} = G_{12} h,$$

$$D_{11} = \frac{E_1 h^3}{12(1 - \nu_{12} \nu_{21})}, D_{12} = \frac{\nu_{12} E_2 h^3}{12(1 - \nu_{12} \nu_{21})}, D_{22} = \frac{E_2 h^3}{12(1 - \nu_{12} \nu_{21})}, D_{33} = \frac{G_{12} h^3}{12}, \tag{27}$$

in which S_{ij} and D_{ij} stand for the in-plane and flexural stiffnesses of the nanoscale plate. Using Hamilton's law, the motion equations in terms of stress resultants are obtained as

$$\frac{\partial N_{xx}}{\partial x} + \frac{\partial N_{xy}}{\partial y} = \rho h \frac{\partial^2 u}{\partial t^2}, \frac{\partial N_{yy}}{\partial y} + \frac{\partial N_{xy}}{\partial x} = \rho h \frac{\partial^2 v}{\partial t^2}, \frac{\partial^2 M_{xx}}{\partial x^2} + \frac{\partial^2 M_{yy}}{\partial y^2} + 2 \frac{\partial^2 M_{xy}}{\partial x \partial y} + q + \frac{\partial}{\partial x} \left(N_{xy} \frac{\partial w}{\partial y} + N_{xx} \frac{\partial w}{\partial x} \right)$$

$$+ \frac{\partial}{\partial y} \left(N_{xy} \frac{\partial w}{\partial x} + N_{yy} \frac{\partial w}{\partial y} \right) = \rho h \frac{\partial^2 w}{\partial t^2}, \tag{28}$$

where q and ρ are the distributed transverse load and the nanoplate mass density, respectively. Substituting Eq. (26) into Eq. (28), one obtains

$$-D_{11} \frac{\partial^4 w}{\partial x^4} - 2(D_{12} + 2D_{33}) \frac{\partial^4 w}{\partial x^2 \partial y^2} - D_{22} \frac{\partial^4 w}{\partial y^4}$$

$$+ \left[1 - (e_0 a)^2 \nabla^2\right] q + \left[1 - (e_0 a)^2 \nabla^2\right] \frac{\partial}{\partial x} \left(N_{xy} \frac{\partial w}{\partial y} + N_{xx} \frac{\partial w}{\partial x} \right)$$

$$+ \left[1 - (e_0 a)^2 \nabla^2\right] \frac{\partial}{\partial y} \left(N_{xy} \frac{\partial w}{\partial x} + N_{yy} \frac{\partial w}{\partial y} \right) = \left[1 - (e_0 a)^2 \nabla^2\right] \rho h \frac{\partial^2 w}{\partial t^2} \tag{29}$$

3.4.2. Size-dependent bending of nanoplates

Nonlocal continuum mechanics has been utilised to analyse the *static deformation* of nanoscale plates. For instance, Duan and Wang (Duan & Wang, 2007) obtained exact solutions for the axisymmetric static deformation of circular SLGSs subject to transverse loading by decoupling nonlocal equations for both clamped and simply-supported edges. In addition, an exact solution was presented by Yan et al. (Yan et al., 2015) for the bending of rectangular nanoplates via the NET. Aghababaei and Reddy (Aghababaei & Reddy, 2009) explored the static deformation of rectangular nanoplates incorporating size effects via use of the NET; a modified third-order theory of shear deformations was proposed for nanoplates. Huang et al. (Huang, Han & Liang, 2012) determined the scale parameter for the bending of SLGSs using the molecular dynamics. Moreover, a nonlinear nonlocal plate model was proposed for the large deflection of monolayer graphene sheets (Golmakani & Rezatalab, 2014) as well as bilayer graphene sheets (Far & Golmakani, 2018, Xu, Shen & Zhang, 2013). Surface influences on the size-dependent bending of nanoscale plates have been also examined (Shaat, Mahmoud, Gao & Faheem, 2014, Zhang & Jiang, 2014, Wang & Wang, 2013); a positive value of surface constant reduces the nanoplate deflection. In Fig. 23, the results of the nonlocal and local plate models as well as MD results for the bending of nanoplates are compared (Yan et al., 2015). The results of the nonlocal plate model are in a very good agreement with those calculated by MD simulations.
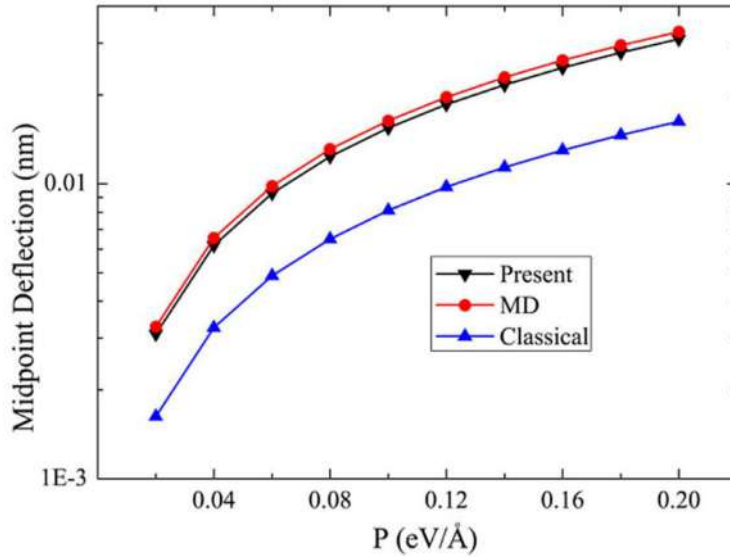
Fig. 23. Comparison of the nonlocal and local plate models as well as MD results (Yan et al., 2015). Reprinted with permission from Elsevier.
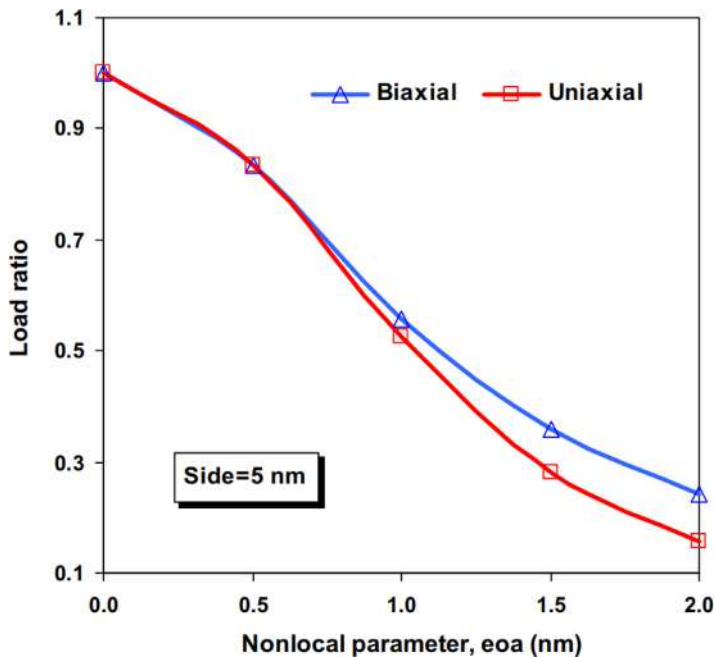
Fig. 24. Buckling load ratio versus the nonlocal parameter for both biaxially amd uniaxially compressed nanoplates (Pradhan & Murmu, 2009). Reprinted with permission from Elsevier.

3.4.3. Size-dependent buckling of nanoplates

NET-based models have been employed for the *linear buckling* of nanoplates in recent years due to the simplicity and capability of these models in the size-dependent analysis of structures at nanoscale levels. Various solution methods such as analytical solution techniques (Aksencer & Aydogdu, 2011, Zenkour & Sobhy, 2013, Murmu, McCarthy & Adhikari, 2013, Murmu & Pradhan, 2009, Farajpour, Mohammadi, Shahidi & Mahzoon, 2011, Pradhan, 2009, Radić & Jeremić, 2016), the DQM (Malekzadeh, Setoodeh & Beni, 2011, Pradhan & Murmu, 2009, Farajpour, Shahidi, Mohammadi & Mahzoon, 2012), Galerkin's approach (Babaei & Shahidi, 2011, Farajpour, Danesh & Mohammadi, 2011) and the finite strip method (Sarrami-Foroushani & Azhari, 2014) have been applied to the nonlocal governing differential equations of nanoscale plates. Fig. 24 shows the nonlocal-to-local buckling load ratio versus the scale parameter for nanoplates subject to uniaxial and biaxial
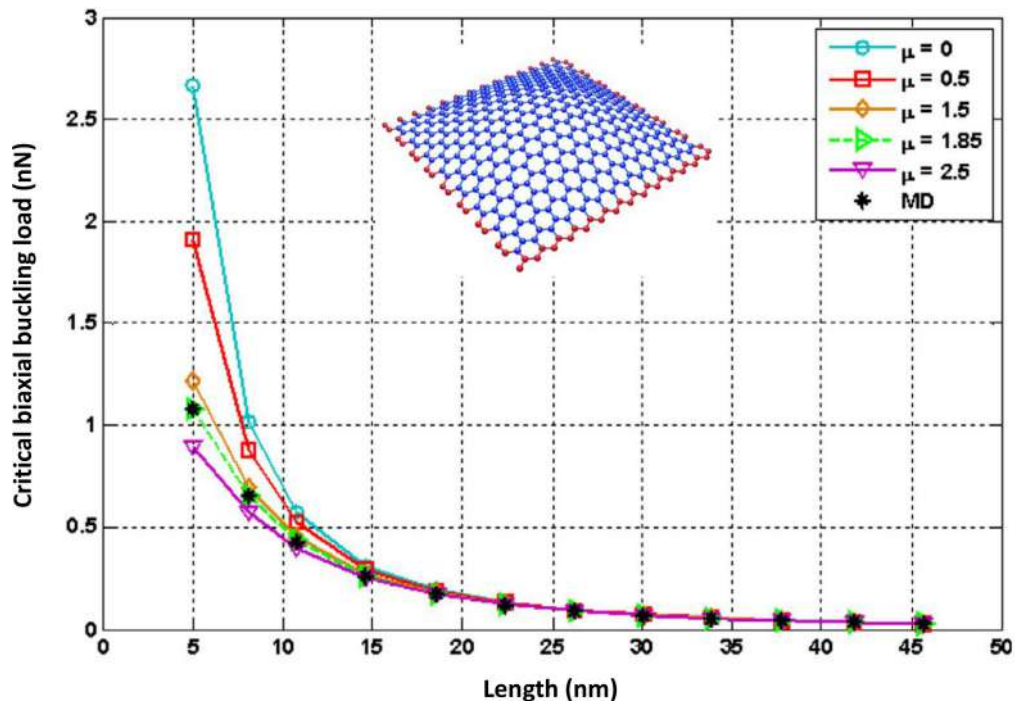
Fig. 25. Accuracy of nonlocal continuum modelling of SLGSs via MD simulations (Ansari & Sahmani, 2013). Reprinted with permission from Elsevier.

loading conditions; the nonlocal buckling load is lower than the local one. This is because the nonlocal effect reduces the structural stiffness of nanoplates, and thus the buckling load declines. The accuracy and reliability of the nonlocal continuum modelling of nanoplates have been shown by performing MD simulations (Farajpour, Dehghany & Shahidi, 2013, Ansari & Sahmani, 2013). In Fig. 25, the buckling force of square SLGSs versus the length is plotted for different size parameters (i.e. $\mu = (e_0 a)^2$); the MD results are also shown. It is observed that the nonlocal plate model with a reasonable size parameter can accurately predict the critical buckling force of nanoscale plates.

In addition to the NET, the surface elasticity theory (Farajpour, Dehghany & Shahidi, 2013, Cheng & Chen, 2015, Karimi, Mirdamadi & Shahidi, 2017, Lu, Guo & Zhao, 2018) and the NSGT (Farajpour, Yazdi, Rastgoo & Mohammadi, 2016) have also been utilised for the stability of nanoscale plates, especially GSs. It has been shown that surface or strain gradient effects should be taken into consideration to capture the stiffness hardening behaviour observed in the stability of circular GSs subject to axisymmetric radial loads. Furthermore, nonlinear nonlocal models (Shen, 2011, Farajpour, Solghar & Shahidi, 2013, Naderi & Saidi, 2014) and nonlinear continuum models incorporating surface effects (Wang & Wang, 2013, Sahmani, Bahrami, Aghdam & Ansari, 2015) have been developed in the literature to analyse the size-dependent post-buckling of nanoplates.

3.4.4. Size-dependent vibration of nanoplates

Various nonlocal plate models such as the Kirchhoff plate theory (Wang, Li & Kishimoto, 2011, Pradhan & Phadikar, 2009, Pouresmaeeli, Ghavanloo & Fazelzadeh, 2013, Wang, Murmu & Adhikari, 2011, Farajpour, Shahidi & Farajpour, 2018), first-order shear deformation model (Pradhan & Phadikar, 2009, Hosseini-Hashemi, Zare & Nazemnezhad, 2013), two-variable refined theory of plates (Malekzadeh & Shojaee, 2013, Karimi, Haddad & Shahidi, 2015) and higher-order shear deformation model (Pradhan & Sahu, 2010, Daneshmehr, Rajabpoor & Hadi, 2015, Kiani, 2014) have been employed so as to examine the *linear vibration* of nanoscale plates. On the other hand, to solve the size-dependent differential equations of these nonlocal plate models, different solution methods such as analytical approaches (Mohammadi, Goodarzi, Ghayour & Farajpour, 2013, Arani & Jalaei, 2016, Hosseini-Hashemi, Bedroud & Nazemnezhad, 2013), Galerkin's method (Babaei & Shahidi, 2013, Malekzadeh & Farajpour, 2012), the DQM (Farajpour, Shahidi & Farajpour, 2018, Pradhan & Kumar, 2011, Malekzadeh, Setoodeh & Beni, 2011), the finite element method (Phadikar & Pradhan, 2010, Natarajan et al., 2012) and the kp-Ritz method (Zhang, Zhang & Liew, 2017, Zhang et al., 2015). The variation of the fundamental frequency of square SLGSs with the width for various nonlocal parameters is illustrated in Fig. 26. The results of MD simulations, local and nonlocal plate models are given. Firstly, the results of the NET match MD results while the CET leads to overestimated results especially for SLGSs with small widths. Secondly, increasing nonlocal parameter reduces the fundamental frequency since increasing nonlocal effects reduces the structural stiffness. Moreover, it is found that the nonlocal influence gradually disappears as the width of the nanoplate increases.
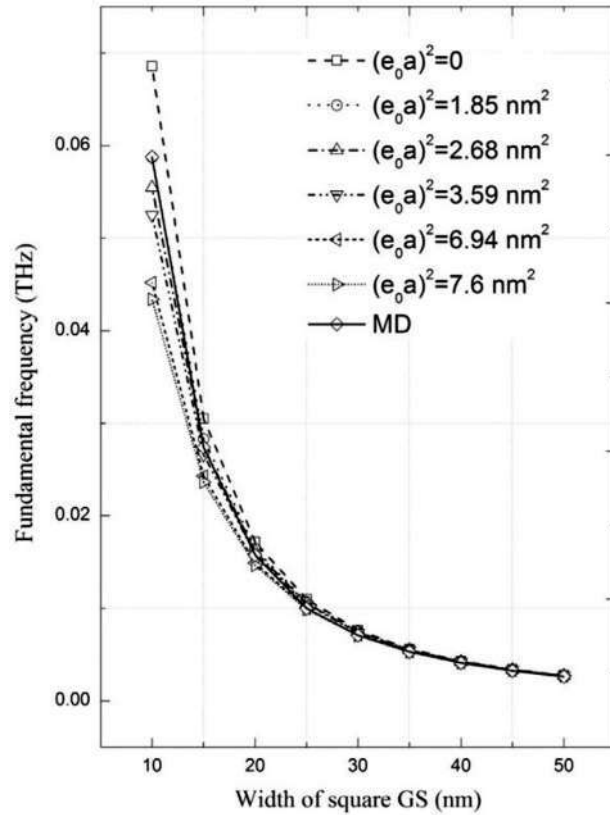
Fig. 26. Fundamental frequencies of SLGSs with four edges simply supported versus the width for different nonlocal parameters (Zhang et al., 2015). Reprinted with permission from Elsevier.

The influences of *surface energy, residual surface tension* and *strain gradients* affect the vibration characteristics of nanoplates. In recent years, size-dependent plate models incorporating surface effects (Assadi, 2013, Ansari & Sahmani, 2011, Wang & Wang, 2011, Barati & Shahverdi, 2017) as well as NSGT-based models (Shahverdi & Barati, 2017, Ebrahimi & Barati, 2017) have been developed for the vibration of nanoplates. It has been shown that the stiffness-hardening behaviour can be described using these size-dependent plate models.

In addition to linear size-dependent plate models, *nonlinear* models have been proposed to analyse the large-amplitude vibration of nanoscale plates using the surface elasticity theory (Ebrahimi & Hosseini, 2017, Ebrahimi & Heidari, 2017) and the NET (Shen, Shen & Zhang, 2010, Jomehzadeh & Saidi, 2011, Farajpour, Shahidi, Hadi & Farajpour, 2018, Shen, Xu & Zhang, 2013). Fig. 27 indicates the size influence on the nonlinear vibration of SLGSs with four edges simply supported. The non-linear frequency ratio is defined as ω/ω_L where ω and ω_L indicate the nonlinear and linear nonlocal frequencies, respectively. It is found that the as the scale parameter increases the influence of the geometrical nonlinearity. More recently, size-dependent nonlinear plate models have been utilised for investigating the large-amplitude vibration of smart nanoscale plates such as piezoelectric (Asemi, Farajpour & Mohammadi, 2014, Liu et al., 2016, Liu, Ke, Wang & Yang, 2015) & magneto-electro-elastic ultrathin plates (Ansari & Gholami, 2016, Farajpour et al., 2016).

3.4.5. Size-dependent wave propagations in nanoplates

Wave propagations in nanoscale plates such as graphene sheets (Arash, Wang & Liew, 2012, Wang, Li & Kishimoto, 2010), smart (Ebrahimi & Dabbagh, 2017) and inhomogeneous (Karami, Shahsavari & Janghorban, 2018) nanoplates have been examined using size-dependent plate models. The majority of size-dependent studies on the wave propagation analysis have been carried out via use of the NET (Wang, Li & Kishimoto, 2010, Narendar & Gopalakrishnan, 2012, Wang, Li & Kishimoto, 2010). The surface elasticity theory (Narendar & Gopalakrishnan, 2012, Zhang, Liu, Fang & Nie, 2014) and the NSGT (Ebrahimi, Barati & Dabbagh, 2016, Ebrahimi & Dabbagh, 2017) have been also utilised to explore the size-dependent wave propagation in nanoplates. It was found that increasing nonlocal parameter strengthens the dispersion degree. In addition, strengthened dispersion degrees for nanoplates can be achieved by increasing wave numbers.
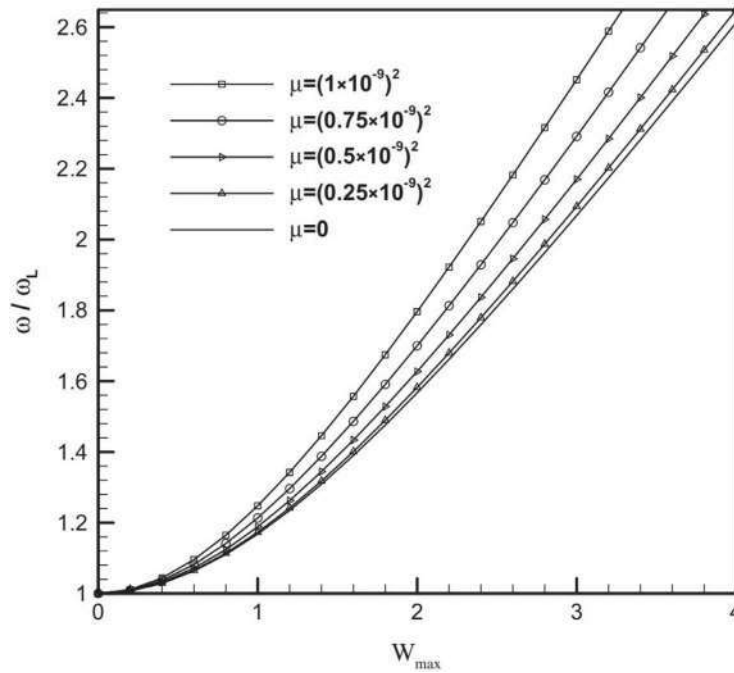
Fig. 27. Nonlinear frequency ratio of SLGSs against maximum deflection for different scale parameters ($\mu = (e_0 a)^2$) (Jomehzadeh & Saidi, 2011). Reprinted with permission from Elsevier.

3.5. Nanoshells

In addition to size-dependent beam models, the mechanical behaviour of nanotubes including CNTs (Iijima & Ichihashi, 1993), boron nitride nanoscale tubes (BNNTs) (Chopra et al., 1995) can be estimated via size-dependent shell models. In general, modified shell theories result in a more accurate estimation of the mechanical characteristics of nanotubes compared to modified beam theories. However, size-dependent shell models are more complex in terms of mathematical formulation as well as solution methods. Moreover, they require high computational costs compared to size-dependent beam models.

3.5.1. Nonlocal shell model

At nanoscale levels, the NET is usually employed in order to incorporate the size effect into a continuum-based shell model. Based on the NET and the classical shell theory, one can write

$$\left[1 - (e_0 a)^2 \nabla^2\right] \begin{Bmatrix} \sigma_{xx} \\ \sigma_{\theta\theta} \\ \sigma_{zz} \\ \sigma_{\theta z} \\ \sigma_{xz} \\ \sigma_{x\theta} \end{Bmatrix} = \begin{bmatrix} C_{11} & C_{12} & C_{13} & 0 & 0 & 0 \\ C_{12} & C_{22} & C_{23} & 0 & 0 & 0 \\ C_{13} & C_{23} & C_{33} & 0 & 0 & 0 \\ 0 & 0 & 0 & C_{44} & 0 & 0 \\ 0 & 0 & 0 & 0 & C_{55} & 0 \\ 0 & 0 & 0 & 0 & 0 & C_{66} \end{bmatrix} \begin{Bmatrix} \varepsilon_{xx} \\ \varepsilon_{\theta\theta} \\ \varepsilon_{zz} \\ \gamma_{\theta z} \\ \gamma_{xz} \\ \gamma_{x\theta} \end{Bmatrix}, \tag{30}$$

where C_{ij} are the elasticity constants of the nanoscale shell. From the above equation, the normal strain along the z direction is obtained as $\varepsilon_{zz} = -(1/C_{33})(C_{13}\varepsilon_{xx} + C_{23}\varepsilon_{\theta\theta})$. Substituting this relation into Eq. (30), one obtains

$$\left[1 - (e_0 a)^2 \nabla^2\right] \begin{Bmatrix} \sigma_{xx} \\ \sigma_{\theta\theta} \\ \sigma_{x\theta} \end{Bmatrix} = \begin{bmatrix} \tilde{C}_{11} & \tilde{C}_{12} & 0 \\ \tilde{C}_{12} & \tilde{C}_{22} & 0 \\ 0 & 0 & \tilde{C}_{66} \end{bmatrix} \begin{Bmatrix} \varepsilon_{xx} \\ \varepsilon_{\theta\theta} \\ \gamma_{x\theta} \end{Bmatrix}, \tag{31}$$

where

$$\tilde{C}_{11} = C_{11} - \frac{C_{13}^2}{C_{33}}, \tilde{C}_{22} = C_{22} - \frac{C_{23}^2}{C_{33}}, \tilde{C}_{12} = C_{12} - \frac{C_{13}C_{23}}{C_{33}}, \tilde{C}_{66} = C_{66}. \tag{32}$$

Applying Hamilton's law, the motion equations of the nanoscale shell in terms of stress resultants are obtained as

$$\frac{1}{R}\frac{\partial N_{x\theta}}{\partial \theta} + \frac{\partial N_{xx}}{\partial x} = \rho h \frac{\partial^2 u}{\partial t^2}, \tag{33}$$

$$\frac{1}{R}\frac{\partial N_{\theta\theta}}{\partial \theta} + \frac{\partial N_{x\theta}}{\partial x} + \frac{1}{R}\left(\frac{\partial M_{x\theta}}{\partial x} + \frac{1}{R}\frac{\partial M_{\theta\theta}}{\partial \theta}\right) = \rho h \frac{\partial^2 v}{\partial t^2}, \tag{34}$$

$$\frac{\partial^2 M_{xx}}{\partial x^2} + \frac{1}{R}\left(\frac{1}{R}\frac{\partial^2 M_{\theta\theta}}{\partial \theta^2} + 2\frac{\partial^2 M_{x\theta}}{\partial x\partial\theta} - N_{\theta\theta}\right) + q + N_{xx}^t \frac{\partial^2 w}{\partial x^2} + \frac{N_{\theta\theta}^t}{R^2}\frac{\partial^2 w}{\partial \theta^2} = \rho h \frac{\partial^2 w}{\partial t^2}, \tag{35}$$

where

$$\begin{Bmatrix} N_{xx} \\ N_{\theta\theta} \\ N_{x\theta} \end{Bmatrix} = \int_{-h/2}^{h/2} \begin{Bmatrix} \sigma_{xx} \\ \sigma_{\theta\theta} \\ \sigma_{x\theta} \end{Bmatrix} dz, \quad \begin{Bmatrix} M_{xx} \\ M_{\theta\theta} \\ M_{x\theta} \end{Bmatrix} = \int_{-h/2}^{h/2} \begin{Bmatrix} \sigma_{xx} \\ \sigma_{\theta\theta} \\ \sigma_{x\theta} \end{Bmatrix} z dz, \tag{36}$$

in which h and ρ indicate the thickness and mass density of the nanoscale shell, respectively; also, $N_{\theta\theta}^t$ and N_{xx}^t are respectively the total circumferential and axial loads. R and q represent the average radius of the nanoshell and the radial loading, respectively. Using Eqs. (31) and (36), one can obtain

$$\left[1 - (e_0 a)^2 \nabla^2\right] \begin{Bmatrix} N_{xx} \\ N_{\theta\theta} \\ N_{x\theta} \end{Bmatrix} = \begin{bmatrix} \tilde{S}_{11} & \tilde{S}_{12} & 0 \\ \tilde{S}_{12} & \tilde{S}_{22} & 0 \\ 0 & 0 & \tilde{S}_{66} \end{bmatrix} \begin{Bmatrix} \frac{\partial u}{\partial x} \\ \frac{1}{R}\left(\frac{\partial v}{\partial \theta} + w\right) \\ \frac{1}{R}\frac{\partial u}{\partial \theta} + \frac{\partial v}{\partial x} \end{Bmatrix},$$

$$\left[1 - (e_0 a)^2 \nabla^2\right] \begin{Bmatrix} M_{xx} \\ M_{\theta\theta} \\ M_{x\theta} \end{Bmatrix} = -\begin{bmatrix} \tilde{D}_{11} & \tilde{D}_{12} & 0 \\ \tilde{D}_{12} & \tilde{D}_{22} & 0 \\ 0 & 0 & \tilde{D}_{66} \end{bmatrix} \begin{Bmatrix} \frac{\partial^2 w}{\partial x^2} \\ \frac{1}{R^2}\left(\frac{\partial^2 w}{\partial \theta^2} - \frac{\partial v}{\partial \theta}\right) \\ \frac{1}{R}\left(2\frac{\partial^2 w}{\partial x\partial\theta} - \frac{\partial v}{\partial x}\right) \end{Bmatrix}, \tag{37}$$

where

$$\langle \tilde{S}_{11}, \tilde{S}_{12}, \tilde{S}_{22}, \tilde{S}_{66}\rangle = \langle \tilde{C}_{11}, \tilde{C}_{12}, \tilde{C}_{22}, \tilde{C}_{66}\rangle h, \quad \langle \tilde{D}_{11}, \tilde{D}_{12}, \tilde{D}_{22}, \tilde{D}_{66}\rangle = \langle \tilde{C}_{11}, \tilde{C}_{12}, \tilde{C}_{22}, \tilde{C}_{66}\rangle \frac{h^3}{12}. \tag{38}$$

Substituting Eq. (37) into Eqs. (33)-(35), the differential motion equations of the nanoshell are derived as

$$\tilde{S}_{11}\frac{\partial^2 u}{\partial x^2} + \frac{\tilde{S}_{66}}{R^2}\frac{\partial^2 u}{\partial \theta^2} + \frac{1}{R}\left(\tilde{S}_{12} + \tilde{S}_{66}\right)\frac{\partial^2 v}{\partial x\partial\theta} + \frac{\tilde{S}_{12}}{R}\frac{\partial w}{\partial x} = \tilde{m}\left[1 - (e_0 a)^2 \nabla^2\right]\frac{\partial^2 u}{\partial t^2}, \tag{39}$$

$$\frac{1}{R}\left(\tilde{S}_{12} + \tilde{S}_{66}\right)\frac{\partial^2 u}{\partial x\partial\theta} + \left(\tilde{S}_{66} + \frac{\tilde{D}_{66}}{R^2}\right)\frac{\partial^2 v}{\partial x^2} + \frac{1}{R^2}\left(\tilde{S}_{22} + \frac{\tilde{D}_{22}}{R^2}\right)\frac{\partial^2 v}{\partial \theta^2}$$
$$+ \frac{1}{R^2}\left\{\tilde{S}_{22}\frac{\partial w}{\partial \theta} - \left[\frac{\tilde{D}_{22}}{R^2}\frac{\partial^3 w}{\partial \theta^3} + \left(\tilde{D}_{12} + 2\tilde{D}_{66}\right)\frac{\partial^3 w}{\partial x^2\partial\theta}\right]\right\} = \tilde{m}\left[1 - (e_0 a)^2 \nabla^2\right]\frac{\partial^2 v}{\partial t^2}, \tag{40}$$

$$-\frac{1}{R}\left(\tilde{S}_{12}\frac{\partial u}{\partial x} + \frac{\tilde{S}_{22}}{R}\frac{\partial v}{\partial \theta}\right) + \frac{1}{R^2}\left[\left(\tilde{D}_{12} + 2\tilde{D}_{66}\right)\frac{\partial^3 v}{\partial x^2\partial\theta} + \frac{\tilde{D}_{22}}{R^2}\frac{\partial^3 v}{\partial \theta^3}\right]$$
$$-\left\{\tilde{D}_{11}\frac{\partial^4 w}{\partial x^4} + \frac{1}{R^2}\left[2\left(\tilde{D}_{12} + 2\tilde{D}_{66}\right)\frac{\partial^4 w}{\partial x^2\partial\theta^2} + \frac{\tilde{D}_{22}}{R^2}\frac{\partial^4 w}{\partial \theta^4} + \tilde{S}_{22}w\right]\right\}$$
$$+\left[1 - (e_0 a)^2 \nabla^2\right]\left(q + \frac{N_{\theta\theta}^t}{R^2}\frac{\partial^2 w}{\partial \theta^2} + N_{xx}^t\frac{\partial^2 w}{\partial x^2}\right) = \tilde{m}\left[1 - (e_0 a)^2 \nabla^2\right]\frac{\partial^2 w}{\partial t^2}, \tag{41}$$

in which $\tilde{m} = \rho h$. The above coupled differential equations govern the size-dependent mechanical behaviour of nanoshells based on the NET.

3.5.2. Size-dependent mechanics of nanoshells

Size-dependent shell models have recently been utilised for analysing the mechanics of CNTs (Wang & Varadan, 2007, Hu et al., 2008, Ansari, Rouhi & Sahmani, 2011), BNNTs (Arani, Amir, Shajari & Mozdianfard, 2012), piezoelectric nanotubes (Ke, Wang & Reddy, 2014, Sahmani, Aghdam & Akbarzadeh, 2016) and magneto-electro-elastic nanotubes (Ke, Wang, Yang & Kitipornchai, 2014, Farajpour, Rastgoo & Farajpour, 2017). To modify the traditional shell theories for capturing size influences, various modified theories including the NET (Wang & Varadan, 2007, Hu et al., 2008, Wang, Hu & Guo, 2006), the surface elasticity (Altenbach & Eremeyev, 2011, Sahmani, Bahrami & Aghdam, 2016) and the NSGT (Sahmani & Aghdam, 2018, Zeighampour, Beni & Karimipour, 2017) can be used. The NET can predict the stiffness softening while the surface elasticity with positive surface properties can account for the stiffness hardening. The NSGT takes into account both the softening and hardening of the structural stiffness. To solve the motion equations of nanotubes using modified shell models, various solution techniques such as the DQM (Arani, Kolahchi & Maraghi, 2013, Farajpour, Rastgoo & Mohammadi, 2017), perturbation
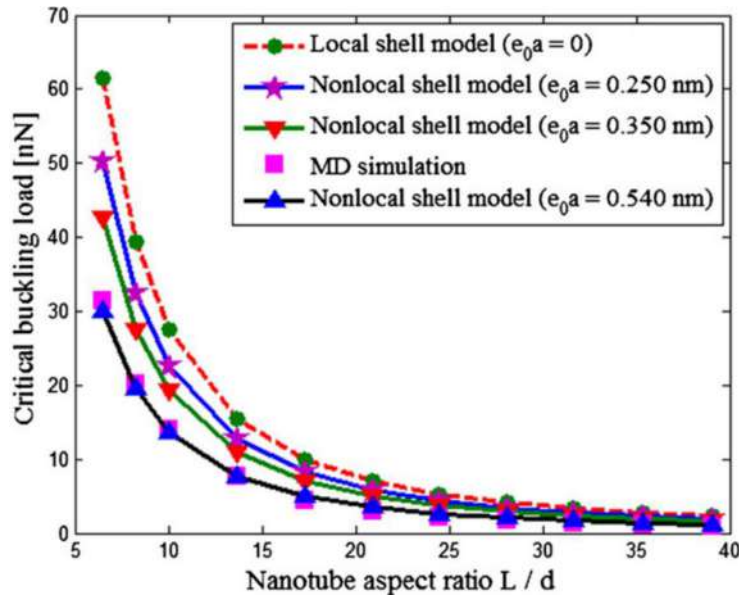
Fig. 28. Comparison between the nonlocal and local shell models for simply-supported SWCNTs (Ansari, Sahmani & Rouhi, 2011). Reprinted with permission from Elsevier.
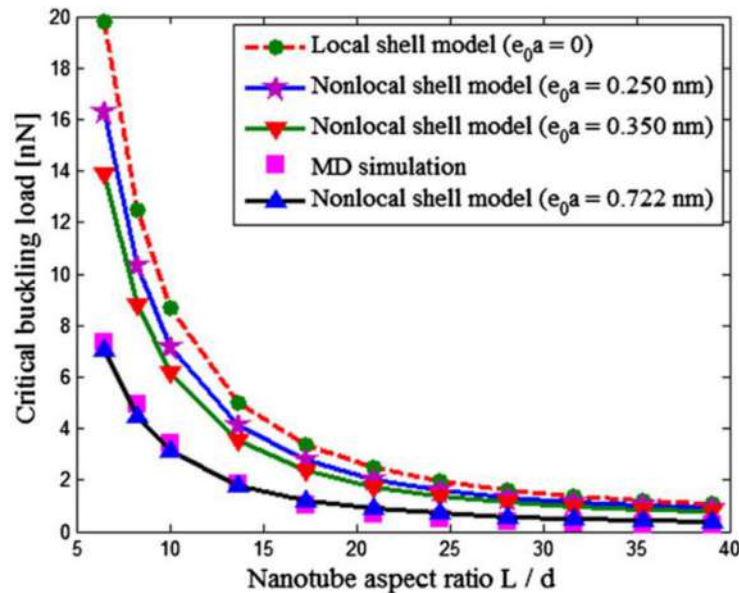
Fig. 29. Comparison between the nonlocal and local shell models for clamped-free SWCNTs (Ansari, Sahmani & Rouhi, 2011). Reprinted with permission from Elsevier.

schemes (Sahmani & Aghdam, 2018, Shen & Zhang, 2010), analytical methods (Wang, Hu & Guo, 2006, Khademolhosseini, Rajapakse & Nojeh, 2010, Farajpour & Rastgoo, 2017) were employed.

The appropriate value of the nonlocal parameter has a significant role in the correct prediction of the mechanical characteristics of nanotubes, especially CNTs. Wang and Wang (Wang & Wang, 2007) formulated the constitutive equations of CNTs via use of the nonlocal elasticity; they also proposed a general range for the nonlocal parameter (i.e. $0 \text{ nm} \leq e_0 a \leq 2 \text{ nm}$), which has been extensively applied to the nonlocal continuum models of CNTs and GSs. Particularly, Ansari et al. (Ansari, Sahmani & Rouhi, 2011) calibrated a nonlocal shear deformable shell model for the buckling of SWCNTs applying the MD. The value of the nonlocal parameter ranges from 0.5 to 0.8 nm depending on the bending rigidity and the boundary conditions. Figs. 28 and 29 show the change of the buckling force with *L/d* for both local and nonlocal shell models for clamped-free and simply-supported edges. The local shell model fails to correctly predict the buckling behaviour of SWCNTs while the nonlocal shell model with a calibrated scale parameter gives a reasonable estimation of the critical buckling force. Tables 1

Table 1
Calibrated scale parameters for the mechanics of CNTs via the NET.

Mechanical behaviour	Continuum model	Calibration parameter (e_0)	Nonlocal parameter (nm)
Mechanics	NET-based shell and beam models (Wang & Wang, 2007)	—-	0–2
Wave propagation	NET-based shell model (Hu et al., 2008)	0.2–0.6	—-
Vibration	NET-based beam model (Duan, Wang & Zhang, 2007)	0–19	—-
Wave propagation	NET-based rod model (Aydogdu, 2012)	0–0.386	—-
Axial buckling	NET-based shell model (Ansari, Sahmani & Rouhi, 2011)	—-	0.531–0.780

Table 2
Calibrated scale parameters for the mechanics of GSs via the NET.

Mechanical behaviour	Continuum model	Nonlocal parameter (nm)
Buckling	NET-based plate model (Ansari & Sahmani, 2013)	1.33–1.36
Vibration	NET-based plate model (Shen, Shen & Zhang, 2010)	0.22–0.67
Post-buckling	NET-based nonlinear plate model (Farajpour, Solghar & Shahidi, 2013)	0.25–1

Table 3
Calibrated scale parameters for the mechanics of CNTs via the NSGT.

Mechanical behaviour	Continuum model	Strain gradient parameter (nm)	Nonlocal parameter (nm)
Buckling	NSGT-based shell model (Mehralian, Beni & Zeverdejani, 2017)	0.4–0.9	1–1.5
Vibration	NSGT-based shell model (Mehralian, Beni & Zeverdejani, 2017)	0.1–0.4	3.3–3.5
Wave propagation	NSGT-based beam model (Li, Hu & Ling, 2016)	0.175	0.8

and 2 list the calibrated scale parameters of CNTs and GSs for the NET, respectively. In addition, the calibrated values for the scale parameters of CNTs for the NSGT are given in Table 3.

4. Conclusions

Nanostructures have extensively been utilised in NEMS-based devices including nanomechanical resonators, mass nanosensors, nanoenergy harvesters, and nanogenerators due to their excellent physical characteristics. To properly design and manufacture these small-scale devices, it is important to estimate how nanostructures respond to mechanical/electrical excitation loads. Due to the problems associated with performing experiments at nanoscales and conducting MD simulations, the size-dependent continuum models of nanostructures have received a considerable attention.

The NET and NSGT have widely been applied for estimating the mechanical characteristics of nanoscale structures. In the present paper, first these size-dependent elasticity theories were briefly reviewed. Then, the NET-based equations of motion were derived for nanorods, nanorings, nanobeams, nanoplates and nanoshells. Pioneering studies conducted on the size-dependent continuum modelling of nanostructures with and without incorporating surface effects on the basis of the NET and NSGT were reviewed. Important findings on the mechanical behaviour of these nanostructures are summarised as

- Scale effects predicted by the NSGT appear in a wider range of lengths compared to nonlocal effects.
- The computational cost of the NET is less than that of the NSGT.
- Surface effects are more significant for slender nanobeams.
- Increasing strain gradient parameter reduces the transverse deflection of nanobeams while the transverse deflection increases with increasing nonlocal coefficient.
- For cantilever nanobeams, integral nonlocal models can better describe the bending behaviour than a differential nonlocal model.
- Nonlocal effects reduce the critical buckling loads of nanostructures due to the reduction of the structural stiffness.
- Increasing nonlocal parameter notably reduces the natural frequencies of nanostructure.
- Strengthened dispersion degrees for nanoplates can be achieved by increasing the nonlocal parameter as well as increasing the wave number.
- For circular nanoplates, a combination of the NET and surface elasticity or the NSGT is required in order to accurately predict the critical buckling loads.
- Size-dependent shell models lead to a more accurate estimation of the mechanical characteristics of nanotubes compared to size-dependent beam models.
- Size-dependent shell models are more mathematically complex and require high computational effort compared to size-dependent beam models.

Further effort is required in order to calibrate the available size-dependent continuum models of nanostructures by performing MD simulations or experiments. In addition, compared to nanobeams, the mechanical behaviour of nanorings has not been studied comprehensively. More analysis can be carried out to explore the size-dependent mechanical response

of nanorings, especially in thermal environment. Moreover, most size-dependent studies on the mechanics of nanorods are linear. Modified continuum models can be developed to examine the nonlinear vibration of nanorods.

References

Aghababaei, R., & Reddy, J. (2009). Nonlocal third-order shear deformation plate theory with application to bending and vibration of plates. *Journal of Sound and Vibration, 326,* 277–289.

Akgöz, B., & Civalek, Ö. (2011). Strain gradient elasticity and modified couple stress models for buckling analysis of axially loaded micro-scaled beams. *International Journal of Engineering Science, 49,* 1268–1280.

Akgöz, B., & Civalek, Ö. (2013). Free vibration analysis of axially functionally graded tapered Bernoulli–Euler microbeams based on the modified couple stress theory. *Composite Structures, 98,* 314–322.

Aksencer, T., & Aydogdu, M. (2011). Levy type solution method for vibration and buckling of nanoplates using nonlocal elasticity theory. *Physica E: Low-dimensional Systems and Nanostructures, 43,* 954–959.

Alkilany, A. M., Thompson, L. B., Boulos, S. P., Sisco, P. N., & Murphy, C. J. (2012). Gold nanorods: their potential for photothermal therapeutics and drug delivery, tempered by the complexity of their biological interactions. *Advanced drug delivery reviews, 64,* 190–199.

Altenbach, H., & Eremeyev, V. A. (2011). On the shell theory on the nanoscale with surface stresses. *International Journal of Engineering Science, 49,* 1294–1301.

Amara, K., Tounsi, A., & Mechab, I. (2010). Nonlocal elasticity effect on column buckling of multiwalled carbon nanotubes under temperature field. *Applied Mathematical Modelling, 34,* 3933–3942.

Ansari, R., & Gholami, R. (2016). Size-dependent nonlinear vibrations of first-order shear deformable magneto-electro-thermo elastic nanoplates based on the nonlocal elasticity theory. *International Journal of Applied Mechanics, 8,* 1650053.

Ansari, R., & Sahmani, S. (2011). Bending behavior and buckling of nanobeams including surface stress effects corresponding to different beam theories. *International Journal of Engineering Science, 49,* 1244–1255.

Ansari, R., & Sahmani, S. (2011). Surface stress effects on the free vibration behavior of nanoplates. *International Journal of Engineering Science, 49,* 1204–1215.

Ansari, R., & Sahmani, S. (2013). Prediction of biaxial buckling behavior of single-layered graphene sheets based on nonlocal plate models and molecular dynamics simulations. *Applied Mathematical Modelling, 37,* 7338–7351.

Ansari, R., Rouhi, H., & Sahmani, S. (2011). Calibration of the analytical nonlocal shell model for vibrations of double-walled carbon nanotubes with arbitrary boundary conditions using molecular dynamics. *International Journal of Mechanical Sciences, 53,* 786–792.

Ansari, R., Sahmani, S., & Rouhi, H. (2011). Rayleigh–Ritz axial buckling analysis of single-walled carbon nanotubes with different boundary conditions. *Physics Letters A, 375,* 1255–1263.

Apuzzo, A., Barretta, R., Luciano, R., de Sciarra, F. M., & Penna, R. (2017). Free vibrations of Bernoulli-Euler nano-beams by the stress-driven nonlocal integral model. *Composites Part B: Engineering, 123,* 105–111.

Arani, A. G., & Jalaei, M. (2016). Transient behavior of an orthotropic graphene sheet resting on orthotropic visco-Pasternak foundation. *International Journal of Engineering Science, 103,* 97–113.

Arani, A. G., Atabakhshian, V., Loghman, A., Shajari, A., & Amir, S. (2012). Nonlinear vibration of embedded SWBNNTs based on nonlocal Timoshenko beam theory using DQ method. *Physica B: Condensed Matter, 407,* 2549–2555.

Arani, A. G., Amir, S., Shajari, A., & Mozdianfard, M. (2012). Electro-thermo-mechanical buckling of DWBNNTs embedded in bundle of CNTs using nonlocal piezoelasticity cylindrical shell theory. *Composites Part B: Engineering, 43,* 195–203.

Arani, A. G., Kolahchi, R., & Maraghi, Z. K. (2013). Nonlinear vibration and instability of embedded double-walled boron nitride nanotubes based on nonlocal cylindrical shell theory. *Applied Mathematical Modelling, 37,* 7685–7707.

Arash, B., Wang, Q., & Liew, K. M. (2012). Wave propagation in graphene sheets with nonlocal elastic theory via finite element formulation. *Computer Methods in Applied Mechanics and Engineering, 223,* 1–9.

Arefi, M., & Zenkour, A. M. (2017). Wave propagation analysis of a functionally graded magneto-electro-elastic nanobeam rest on Visco-Pasternak foundation. *Mechanics Research Communications, 79,* 51–62.

Arefi, A., Mirdamadi, H., & Salimi, M. (2012). Stability Analysis of Circular Nanorings Under Different Loading Behavior by Nonlocal Elasticity Theory. *Journal of Computational and Theoretical Nanoscience, 9,* 794–801.

Asemi, S. R., & Farajpour, A. (2014). Vibration characteristics of double-piezoelectric-nanoplate-systems, in: Micro & Nano Letters. *Institution of Engineering and Technology,* 280–285.

Asemi, S., Farajpour, A., & Mohammadi, M. (2014). Nonlinear vibration analysis of piezoelectric nanoelectromechanical resonators based on nonlocal elasticity theory. *Composite Structures, 116,* 703–712.

Askes, H., & Aifantis, E. C. (2009). Gradient elasticity and flexural wave dispersion in carbon nanotubes. *Physical Review B, 80,* 195412.

Assadi, A., & Farshi, B. (2011). Size-dependent longitudinal and transverse wave propagation in embedded nanotubes with consideration of surface effects. *Acta mechanica, 222,* 27.

Assadi, A. (2013). Size dependent forced vibration of nanoplates with consideration of surface effects. *Applied Mathematical Modelling, 37,* 3575–3588.

Attia, M. A., & Rahman, A. A. A. (2018). On vibrations of functionally graded viscoelastic nanobeams with surface effects. *International Journal of Engineering Science, 127,* 1–32.

Attia, M. A. (2017). On the mechanics of functionally graded nanobeams with the account of surface elasticity. *International Journal of Engineering Science, 115,* 73–101.

Aydogdu, M. (2009). Axial vibration of the nanorods with the nonlocal continuum rod model. *Physica E: Low-dimensional Systems and Nanostructures, 41,* 861–864.

Aydogdu, M. (2009). A general nonlocal beam theory: its application to nanobeam bending, buckling and vibration. *Physica E: Low-dimensional Systems and Nanostructures, 41,* 1651–1655.

Aydogdu, M. (2012). Longitudinal wave propagation in nanorods using a general nonlocal unimodal rod theory and calibration of nonlocal parameter with lattice dynamics. *International Journal of Engineering Science, 56,* 17–28.

Babaei, H., & Shahidi, A. (2011). Small-scale effects on the buckling of quadrilateral nanoplates based on nonlocal elasticity theory using the Galerkin method. *Archive of Applied Mechanics, 81,* 1051–1062.

Babaei, H., & Shahidi, A. (2013). Free vibration analysis of quadrilateral nanoplates based on nonlocal continuum models using the Galerkin method: the effects of small scale. *Meccanica, 48,* 971–982.

Babaei Gavan, K., Westra, H. J., van der Drift, E. W., Venstra, W. J., & van der Zant, H. S. (2009). Size-dependent effective Young's modulus of silicon nitride cantilevers. *Applied Physics Letters, 94,* 233108.

Baghani, M., Mohammadi, M., & Farajpour, A. (2016). Dynamic and stability analysis of the rotating nanobeam in a nonuniform magnetic field considering the surface energy. *International Journal of Applied Mechanics, 8,* 1650048.

Barati, M. R., & Shahverdi, H. (2017). Vibration analysis of multi-phase nanocrystalline silicon nanoplates considering the size and surface energies of nanograins/nanovoids. *International Journal of Engineering Science, 119,* 128–141.

Barati, M. R. (2017). On wave propagation in nanoporous materials. *International Journal of Engineering Science, 116,* 1–11.

Barretta, R., & Marotti de Sciarra, F. (2018). Constitutive boundary conditions for nonlocal strain gradient elastic nano-beams. *International Journal of Engineering Science, 130,* 187–198.

Barretta, R., Čanađija, M., Luciano, R., & de Sciarra, F. M. (2018). Stress-driven modeling of nonlocal thermoelastic behavior of nanobeams. *International Journal of Engineering Science, 126,* 53–67.

Benguediab, S., Tounsi, A., Zidour, M., & Semmah, A. (2014). Chirality and scale effects on mechanical buckling properties of zigzag double-walled carbon nanotubes. *Composites Part B: Engineering, 57*, 21–24.

Benzair, A., Tounsi, A., Besseghier, A., Heireche, H., Moulay, N., & Boumia, L. (2008). The thermal effect on vibration of single-walled carbon nanotubes using nonlocal Timoshenko beam theory. *Journal of Physics D: Applied Physics, 41*, 225404.

Briscoe, J., & Dunn, S. (2015). Piezoelectric nanogenerators–a review of nanostructured piezoelectric energy harvesters. *Nano Energy, 14*, 15–29.

Bunch, J. S., Van Der Zande, A. M., Verbridge, S. S., Frank, I. W., Tanenbaum, D. M., Parpia, J. M., et al. (2007). Electromechanical resonators from graphene sheets. *Science, 315*, 490–493.

Chakraverty, S., & Behera, L. (2015). Free vibration of non-uniform nanobeams using Rayleigh–Ritz method. *Physica E: Low-dimensional Systems and Nanostructures, 67*, 38–46.

Chang, T.-P. (2013). Axial vibration of non-uniform and non-homogeneous nanorods based on nonlocal elasticity theory. *Applied Mathematics and Computation, 219*, 4933–4941.

Chen, S., & Carroll, D. L. (2002). Synthesis and characterization of truncated triangular silver nanoplates. *Nano letters, 2*, 1003–1007.

Cheng, C.-H., & Chen, T. (2015). Size-dependent resonance and buckling behavior of nanoplates with high-order surface stress effects. *Physica E: Low-dimensional Systems and Nanostructures, 67*, 12–17.

Chopra, N. G., Luyken, R., Cherrey, K., Crespi, V. H., Cohen, M. L., Louie, S. G., et al. (1995). Boron nitride nanotubes. *Science, 269*, 966–967.

Choy, J.-H., Jang, E.-S., Won, J.-H., Chung, J.-H., Jang, D.-J., & Kim, Y.-W. (2004). Hydrothermal route to ZnO nanocoral reefs and nanofibers. *Applied physics letters, 84*, 287–289.

Chu, H., Jang, H., Lee, Y., Chae, Y., & Ahn, J.-H. (2016). Conformal, graphene-based triboelectric nanogenerator for self-powered wearable electronics. *Nano Energy, 27*, 298–305.

Cui, L., Gu, H., Xu, H., & Shi, D. (2006). Synthesis and characterization of superparamagnetic composite nanorings. *Materials Letters, 60*, 2929–2932.

Dai, M. D., Kim, C.-W., & Eom, K. (2012). Nonlinear vibration behavior of graphene resonators and their applications in sensitive mass detection. *Nanoscale research letters, 7*, 499.

Dai, H., Wang, L., Abdelkefi, A., & Ni, Q. (2015). On nonlinear behavior and buckling of fluid-transporting nanotubes. *International Journal of Engineering Science, 87*, 13–22.

Danesh, M., Farajpour, A., & Mohammadi, M. (2012). Axial vibration analysis of a tapered nanorod based on nonlocal elasticity theory and differential quadrature method. *Mechanics Research Communications, 39*, 23–27.

Daneshmehr, A., Rajabpoor, A., & Hadi, A. (2015). Size dependent free vibration analysis of nanoplates made of functionally graded materials based on nonlocal elasticity theory with high order theories. *International Journal of Engineering Science, 95*, 23–35.

Dehghany, M., & Farajpour, A. (2014). Free vibration of simply supported rectangular plates on Pasternak foundation: An exact and three-dimensional solution. *Engineering Solid Mechanics, 2*, 29–42.

Dehrouyeh-Semnani, A. M., Nikkhah-Bahrami, M., & Yazdi, M. R. H. (2017). On nonlinear stability of fluid-conveying imperfect micropipes. *International Journal of Engineering Science, 120*, 254–271.

Duan, W., & Wang, C. M. (2007). Exact solutions for axisymmetric bending of micro/nanoscale circular plates based on nonlocal plate theory. *Nanotechnology, 18*, 385704.

Duan, W., Wang, C., & Zhang, Y. (2007). Calibration of nonlocal scaling effect parameter for free vibration of carbon nanotubes by molecular dynamics. *Journal of applied physics, 101*, 024305.

Ebrahimi, F., & Barati, M. R. (2016). A nonlocal higher-order refined magneto-electro-viscoelastic beam model for dynamic analysis of smart nanostructures. *International Journal of Engineering Science, 107*, 183–196.

Ebrahimi, F., & Barati, M. R. (2017). Vibration analysis of viscoelastic inhomogeneous nanobeams resting on a viscoelastic foundation based on nonlocal strain gradient theory incorporating surface and thermal effects. *Acta Mechanica, 228*, 1197–1210.

Ebrahimi, F., & Barati, M. R. (2017). Damping vibration analysis of smart piezoelectric polymeric nanoplates on viscoelastic substrate based on nonlocal strain gradient theory. *Smart Materials and Structures, 26*, 065018.

Ebrahimi, F., & Barati, M. R. (2018). Vibration analysis of smart piezoelectrically actuated nanobeams subjected to magneto-electrical field in thermal environment. *Journal of Vibration and Control, 24*, 549–564.

Ebrahimi, F., & Dabbagh, A. (2017). Nonlocal strain gradient based wave dispersion behavior of smart rotating magneto-electro-elastic nanoplates. *Materials Research Express, 4*, 025003.

Ebrahimi, F., & Dabbagh, A. (2017). On flexural wave propagation responses of smart FG magneto-electro-elastic nanoplates via nonlocal strain gradient theory. *Composite Structures, 162*, 281–293.

Ebrahimi, F., & Heidari, E. (2017). Surface effects on nonlinear vibration of embedded functionally graded nanoplates via higher order shear deformation plate theory. *Mechanics of Advanced Materials and Structures*, 1–29.

Ebrahimi, F., & Hosseini, S. (2017). Surface effects on nonlinear dynamics of NEMS consisting of double-layered viscoelastic nanoplates. *The European Physical Journal Plus, 132*, 172.

Ebrahimi, F., & Salari, E. (2015). Thermal buckling and free vibration analysis of size dependent Timoshenko FG nanobeams in thermal environments. *Composite Structures, 128*, 363–380.

Ebrahimi, F., Barati, M. R., & Dabbagh, A. (2016). A nonlocal strain gradient theory for wave propagation analysis in temperature-dependent inhomogeneous nanoplates. *International Journal of Engineering Science, 107*, 169–182.

Eichler, A., Moser, J., Chaste, J., Zdrojek, M., Wilson-Rae, I., & Bachtold, A. (2011). Nonlinear damping in mechanical resonators made from carbon nanotubes and graphene. *Nature nanotechnology, 6*, 339.

Eltaher, M., Emam, S. A., & Mahmoud, F. (2013). Static and stability analysis of nonlocal functionally graded nanobeams. *Composite Structures, 96*, 82–88.

Emam, S. A. (2013). A general nonlocal nonlinear model for buckling of nanobeams. *Applied Mathematical Modelling, 37*, 6929–6939.

Eringen, A. C., & Edelen, D. (1972). On nonlocal elasticity. *International Journal of Engineering Science, 10*, 233–248.

Eringen, A. C., & Nonlocal (2002). continuum field theories. *Springer Science & Business Media.*

Eringen, A. C. (1983). On differential equations of nonlocal elasticity and solutions of screw dislocation and surface waves. *Journal of applied physics, 54*, 4703–4710.

Faleh, N. M., Ahmed, R. A., & Fenjan, R. M. (2018). On vibrations of porous FG nanoshells. *International Journal of Engineering Science, 133*, 1–14.

Fang, B., Zhen, Y.-X., Zhang, C.-P., & Tang, Y. (2013). Nonlinear vibration analysis of double-walled carbon nanotubes based on nonlocal elasticity theory. *Applied Mathematical Modelling, 37*, 1096–1107.

Far, M. S., & Golmakani, M. (2018). Large deflection of thermo-mechanical loaded bilayer orthotropic graphene sheet in/on polymer matrix based on nonlocal elasticity theory. *Computers & Mathematics with Applications.*

Farajpour, A., & Rastgoo, A. (2017). Influence of carbon nanotubes on the buckling of microtubule bundles in viscoelastic cytoplasm using nonlocal strain gradient theory. *Results in physics, 7*, 1367–1375.

Farajpour, A., & Rastgoo, A. (2017). Size-dependent static stability of magneto-electro-elastic CNT/MT-based composite nanoshells under external electric and magnetic fields. *Microsystem Technologies, 23*, 5815–5832.

Farajpour, A., Yazdi, M. H., Rastgoo, A., Loghmani, M., & Mohammadi, M. (2016). Nonlocal nonlinear plate model for large amplitude vibration of magneto–electro-elastic nanoplates. *Composite Structures, 140*, 323–336.

Farajpour, A., Danesh, M., & Mohammadi, M. (2011). Buckling analysis of variable thickness nanoplates using nonlocal continuum mechanics. *Physica E: Low-dimensional Systems and Nanostructures, 44*, 719–727.

Farajpour, A., Dehghany, M., & Shahidi, A. (2013). Surface and nonlocal effects on the axisymmetric buckling of circular graphene sheets in thermal environment. *Composites Part B: Engineering, 50*, 333–343.

Farajpour, A., Mohammadi, M., Shahidi, A., & Mahzoon, M. (2011). Axisymmetric buckling of the circular graphene sheets with the nonlocal continuum plate model. *Physica E: Low-dimensional Systems and Nanostructures, 43*, 1820–1825.

Farajpour, A., Rastgoo, A., & Farajpour, M. (2017). Nonlinear buckling analysis of magneto-electro-elastic CNT-MT hybrid nanoshells based on the nonlocal continuum mechanics. *Composite Structures, 180*, 179–191.

Farajpour, A., Rastgoo, A., & Mohammadi, M. (2017). Vibration, buckling and smart control of microtubules using piezoelectric nanoshells under electric voltage in thermal environment. *Physica B: Condensed Matter, 509*, 100–114.

Farajpour, M. R., Rastgoo, A., Farajpour, A., & Mohammadi, M. (2016). Vibration of piezoelectric nanofilm-based electromechanical sensors via higher-order non-local strain gradient theory. *Micro & Nano Letters, 11*, 302–307.

Farajpour, M. R., Shahidi, A., & Farajpour, A. (2018). Resonant frequency tuning of nanobeams by piezoelectric nanowires under thermo-electro-magnetic field: a theoretical study, in: Micro & Nano Letters. *Institution of Engineering and Technology*.

Farajpour, M., Shahidi, A., & Farajpour, A. (2018). A nonlocal continuum model for the biaxial buckling analysis of composite nanoplates with shape memory alloy nanowires. *Materials Research Express, 5*, 035026.

Farajpour, M., Shahidi, A., Hadi, A., & Farajpour, A. (2018). Influence of initial edge displacement on the nonlinear vibration, electrical and magnetic insta-bilities of magneto-electro-elastic nanofilms. *Mechanics of Advanced Materials and Structures*, 1–13.

Farajpour, A., Shahidi, A., Mohammadi, M., & Mahzoon, M. (2012). Buckling of orthotropic micro/nanoscale plates under linearly varying in-plane load via nonlocal continuum mechanics. *Composite Structures, 94*, 1605–1615.

Farajpour, M., Shahidi, A., Tabataba'i-Nasab, F., & Farajpour, A. (2018). Vibration of initially stressed carbon nanotubes under magneto-thermal environment for nanoparticle delivery via higher-order nonlocal strain gradient theory. *The European Physical Journal Plus, 133*, 219.

Farajpour, A., Solghar, A. A., & Shahidi, A. (2013). Postbuckling analysis of multi-layered graphene sheets under non-uniform biaxial compression. *Physica E: Low-dimensional Systems and Nanostructures, 47*, 197–206.

Farajpour, A., Yazdi, M. H., Rastgoo, A., & Mohammadi, M. (2016). A higher-order nonlocal strain gradient plate model for buckling of orthotropic nanoplates in thermal environment. *Acta Mechanica, 227*, 1849–1867.

Farokhi, H., & Ghayesh, M. H. (2015). Thermo-mechanical dynamics of perfect and imperfect Timoshenko microbeams. *International Journal of Engineering Science, 91*, 12–33.

Farokhi, H., & Ghayesh, M. H. (2015). Nonlinear dynamical behaviour of geometrically imperfect microplates based on modified couple stress theory. *International Journal of Mechanical Sciences, 90*, 133–144.

Farokhi, H., & Ghayesh, M. H. (2016). Size-dependent parametric dynamics of imperfect microbeams. *International Journal of Engineering Science, 99*, 39–55.

Farokhi, H., & Ghayesh, M. H. (2018). Supercritical nonlinear parametric dynamics of Timoshenko microbeams. *Communications in Nonlinear Science and Numerical Simulation, 59*, 592–605.

Farokhi, H., & Ghayesh, M. H. (2018). Nonlinear mechanical behaviour of microshells. *International Journal of Engineering Science, 127*, 127–144.

Farokhi, H., & Ghayesh, M. H. (2018). Nonlinear mechanics of electrically actuated microplates. *International Journal of Engineering Science, 123*, 197–213.

Farokhi, H., Ghayesh, M. H., & Amabili, M. (2013). Nonlinear dynamics of a geometrically imperfect microbeam based on the modified couple stress theory. *International Journal of Engineering Science, 68*, 11–23.

Farokhi, H., Ghayesh, M. H., & Gholipour, A. (2017). Dynamics of functionally graded micro-cantilevers. *International Journal of Engineering Science, 115*, 117–130.

Farokhi, H., Ghayesh, M. H., Gholipour, A., & Hussain, S. (2017). Motion characteristics of bilayered extensible Timoshenko microbeams. *International Journal of Engineering Science, 112*, 1–17.

Farokhi, H., Ghayesh, M. H., Gholipour, A., & Tavallaeinejad, M. (2017). Nonlinear oscillations of viscoelastic microplates. *International Journal of Engineering Science, 118*, 56–69.

Farokhi, H., Païdoussis, M. P., & Misra, A. K. (2018). Nonlinear behaviour of cantilevered carbon nanotube resonators based on a new nonlinear electrostatic load model. *Journal of Sound and Vibration, 419*, 604–629.

Fennimore, A., Yuzvinsky, T., Han, W.-Q., Fuhrer, M., Cumings, J., & Zettl, A. (2003). Rotational actuators based on carbon nanotubes. *Nature, 424*, 408.

Fernández-Sáez, J., & Zaera, R. (2017). Vibrations of Bernoulli-Euler beams using the two-phase nonlocal elasticity theory. *International Journal of Engineering Science, 119*, 232–248.

Fernández-Sáez, J., Zaera, R., Loya, J., & Reddy, J. (2016). Bending of Euler–Bernoulli beams using Eringen's integral formulation: a paradox resolved. *International Journal of Engineering Science, 99*, 107–116.

Fu, Y., Hong, J., & Wang, X. (2006). Analysis of nonlinear vibration for embedded carbon nanotubes. *Journal of Sound and Vibration, 296*, 746–756.

García-Sánchez, D., San Paulo, A., Esplandiú, M. J., Perez-Murano, F., Forró, L., Aguasca, A., et al. (2007). Mechanical detection of carbon nanotube resonator vibrations,. *Physical review letters, 99*, 085501.

Geim, A. K., & Novoselov, K. S. (2010). The rise of graphene, in: Nanoscience and Technology: A Collection of Reviews from Nature Journals. *World Scientific*, 11–19.

Ghayesh, M. H., & Amabili, M. (2012). Nonlinear dynamics of axially moving viscoelastic beams over the buckled state. *Computers & Structures, 112–113*, 406–421.

Ghayesh, M. H., & Amabili, M. (2013). Nonlinear vibrations and stability of an axially moving Timoshenko beam with an intermediate spring support. *Mechanism and Machine Theory, 67*, 1–16.

Ghayesh, M. H., & Amabili, M. (2014). Coupled longitudinal-transverse behaviour of a geometrically imperfect microbeam. *Composites Part B: Engineering, 60*, 371–377.

Ghayesh, M. H., & Farajpour, A. (2018). Nonlinear coupled mechanics of nanotubes incorporating both nonlocal and strain gradient effects. *Mechanics of Advanced Materials and Structures*, 1–10.

Ghayesh, M. H., & Farajpour, A. (2018). Nonlinear mechanics of nanoscale tubes via nonlocal strain gradient theory. *International Journal of Engineering Science, 129*, 84–95.

Ghayesh, M. H., & Farokhi, H. (2015). Chaotic motion of a parametrically excited microbeam. *International Journal of Engineering Science, 96*, 34–45.

Ghayesh, M. H., & Farokhi, H. (2015). Nonlinear dynamics of microplates. *International Journal of Engineering Science, 86*, 60–73.

Ghayesh, M. H., & Farokhi, H. (2017). Global dynamics of imperfect axially forced microbeams. *International Journal of Engineering Science, 68*, 188–202.

Ghayesh, M. H., & Farokhi, H. (2017). Nonlinear mechanics of doubly curved shallow microshells. *International Journal of Engineering Science, 119*, 288–304.

Ghayesh, M. H., & Farokhi, H. (2018). On the viscoelastic dynamics of fluid-conveying microtubes. *International Journal of Engineering Science, 127*, 186–200.

Ghayesh, M. H. (2009). Stability characteristics of an axially accelerating string supported by an elastic foundation. *Mechanism and Machine Theory, 44*, 1964–1979.

Ghayesh, M. H. (2011). On the natural frequencies, complex mode functions, and critical speeds of axially traveling laminated beams: parametric study. *Acta Mechanica Solida Sinica, 24*, 373–382.

Ghayesh, M. H. (2018). Dynamics of functionally graded viscoelastic microbeams. *International Journal of Engineering Science, 124*, 115–131.

Ghayesh, M. H. (2018). Functionally graded microbeams: Simultaneous presence of imperfection and viscoelasticity. *International Journal of Mechanical Sciences, 140*, 339–350.

Ghayesh, M. H. (2018). Nonlinear vibration analysis of axially functionally graded shear-deformable tapered beams. *Applied Mathematical Modelling, 59*, 583–596.

Ghayesh, M. H., Amabili, M., & Farokhi, H. (2013). Three-dimensional nonlinear size-dependent behaviour of Timoshenko microbeams. *International Journal of Engineering Science, 71*, 1–14.

Ghayesh, M. H., Amabili, M., & Farokhi, H. (2013). Nonlinear forced vibrations of a microbeam based on the strain gradient elasticity theory. *International Journal of Engineering Science, 63*, 52–60.

Ghayesh, M. H., Amabili, M., & Paidoussis, M. (2012). Nonlinear vibrations and stability of an axially moving beam with an intermediate spring support: two-dimensional analysis. *Nonlinear Dynamics, 70*, 335–354.

Ghayesh, M. H., Farokhi, H., & Alici, G. (2015). Subcritical parametric dynamics of microbeams. *International Journal of Engineering Science, 95*, 36–48.

Ghayesh, M. H., Farokhi, H., & Alici, G. (2016). Size-dependent performance of microgyroscopes. *International Journal of Engineering Science, 100*, 99–111.

Ghayesh, M. H., Farokhi, H., & Amabili, M. (2013). Nonlinear dynamics of a microscale beam based on the modified couple stress theory. *Composites Part B: Engineering, 50*, 318–324.

Ghayesh, M. H., Farokhi, H., & Amabili, M. (2013). Nonlinear behaviour of electrically actuated MEMS resonators. *International Journal of Engineering Science, 71*, 137–155.

Ghayesh, M. H., Farokhi, H., & Amabili, M. (2014). In-plane and out-of-plane motion characteristics of microbeams with modal interactions. *Composites Part B: Engineering, 60*, 423–439.

Ghayesh, M. H., Farokhi, H., & Farajpour, A. (2018). Chaotic oscillations of viscoelastic microtubes conveying pulsatile fluid. *Microfluid Nanofluid, 22*, 72.

Ghayesh, M. H., Farokhi, H., & Gholipour, A. (2017). Oscillations of functionally graded microbeams. *International Journal of Engineering Science, 110*, 35–53.

Ghayesh, M. H., Farokhi, H., & Gholipour, A. (2017). Vibration analysis of geometrically imperfect three-layered shear-deformable microbeams. *International Journal of Mechanical Sciences, 122*, 370–383.

Ghayesh, M. H., Farokhi, H., & Hussain, S. (2016). Viscoelastically coupled size-dependent dynamics of microbeams. *International Journal of Engineering Science, 109*, 243–255.

Ghayesh, M. H., Farokhi, H., Gholipour, A., & Hussain, S. (2017). On the nonlinear mechanics of layered microcantilevers. *International Journal of Engineering Science, 120*, 1–14.

Ghayesh, M. H., Farokhi, H., Gholipour, A., & Tavallaeinejad, M. (2017). Nonlinear bending and forced vibrations of axially functionally graded tapered microbeams. *International Journal of Engineering Science, 120*, 51–62.

Ghayesh, M. H., Farokhi, H., Gholipour, A., & Tavallaeinejad, M. (2018). Nonlinear oscillations of functionally graded microplates. *International Journal of Engineering Science, 122*, 56–72.

Ghayesh, M. H., Païdoussis, M. P., & Amabili, M. (2013). Nonlinear dynamics of cantilevered extensible pipes conveying fluid. *Journal of Sound and Vibration, 332*, 6405–6418.

Gheshlaghi, B., & Hasheminejad, S. M. (2011). Surface effects on nonlinear free vibration of nanobeams. *Composites Part B: Engineering, 42*, 934–937.

Gholipour, A., Farokhi, H., & Ghayesh, M. H. (2015). In-plane and out-of-plane nonlinear size-dependent dynamics of microplates. *Nonlinear Dynamics, 79*, 1771–1785.

Gholipour, A., Ghayesh, M. H., Zander, A., & Mahajan, R. (2018). Three-dimensional biomechanics of coronary arteries. *International Journal of Engineering Science, 130*, 93–114.

Golmakani, M., & Rezatalab, J. (2014). Nonlinear bending analysis of orthotropic nanoscale plates in an elastic matrix based on nonlocal continuum mechanics. *Composite Structures, 111*, 85–97.

Guo, J.-G., & Zhao, Y.-P. (2007). The size-dependent bending elastic properties of nanobeams with surface effects. *Nanotechnology, 18*, 295701.

Hadi, A., Nejad, M. Z., & Hosseini, M. (2018). Vibrations of three-dimensionally graded nanobeams. *International Journal of Engineering Science, 128*, 12–23.

Hao, M., Guo, X., & Wang, Q. (2010). Small-scale effect on torsional buckling of multi-walled carbon nanotubes. *European Journal of Mechanics-A/Solids, 29*, 49–55.

Heireche, H., Tounsi, A., Benzair, A., Maachou, M., & Bedia, E. A. (2008). Sound wave propagation in single-walled carbon nanotubes using nonlocal elasticity. *Physica E: Low-dimensional Systems and Nanostructures, 40*, 2791–2799.

Hosseini-Hashemi, S., Bedroud, M., & Nazemnezhad, R. (2013). An exact analytical solution for free vibration of functionally graded circular/annular Mindlin nanoplates via nonlocal elasticity. *Composite Structures, 103*, 108–118.

Hosseini-Hashemi, S., Nazemnezhad, R., & Rokni, H. (2015). Nonlocal nonlinear free vibration of nanobeams with surface effects. *European Journal of Mechanics-A/Solids, 52*, 44–53.

Hosseini-Hashemi, S., Zare, M., & Nazemnezhad, R. (2013). An exact analytical approach for free vibration of Mindlin rectangular nano-plates via nonlocal elasticity. *Composite Structures, 100*, 290–299.

Hu, Y.-G., Liew, K. M., Wang, Q., He, X., & Yakobson, B. (2008). Nonlocal shell model for elastic wave propagation in single-and double-walled carbon nanotubes. *Journal of the Mechanics and Physics of Solids, 56*, 3475–3485.

Huang, L., Han, Q., & Liang, Y. (2012). Calibration of nonlocal scale effect parameter for bending single-layered graphene sheet under molecular dynamics. *Nano, 7*, 1250033.

Iijima, S., & Ichihashi, T. (1993). Single-shell carbon nanotubes of 1-nm diameter. *nature, 363*, 603.

Jalaei, M. H., Arani, A. G., & Tourang, H. (2018). On the dynamic stability of viscoelastic graphene sheets. *International Journal of Engineering Science, 132*, 16–29.

Jiang, L., & Yan, Z. (2010). Timoshenko beam model for static bending of nanowires with surface effects. *Physica E: Low-dimensional systems and Nanostructures, 42*, 2274–2279.

Jiang, H., Liu, B., Huang, Y., & Hwang, K. (2004). Thermal expansion of single wall carbon nanotubes. *Journal of engineering materials and technology, 126*, 265–270.

Jiang, J.-W., Park, H. S., & Rabczuk, T. (2014). MoS 2 nanoresonators: intrinsically better than graphene? *Nanoscale, 6*, 3618–3625.

John, H. (2005). Fluorescence properties of gold nanorods and their application for DNA biosensing. *Chemical communications*, 3924–3926.

Jomehzadeh, E., & Saidi, A. (2011). A study on large amplitude vibration of multilayered graphene sheets. *Computational materials science, 50*, 1043–1051.

Karami, B., Shahsavari, D., & Janghorban, M. (2018). Wave propagation analysis in functionally graded (FG) nanoplates under in-plane magnetic field based on nonlocal strain gradient theory and four variable refined plate theory. *Mechanics of Advanced Materials and Structures, 25*, 1047–1057.

Karimi, M., Haddad, H. A., & Shahidi, A. R. (2015). Combining surface effects and non-local two variable refined plate theories on the shear/biaxial buckling and vibration of silver nanoplates. *Micro & Nano Letters, 10*, 276–281.

Karimi, M., Mirdamadi, H. R., & Shahidi, A. R. (2017). Shear vibration and buckling of double-layer orthotropic nanoplates based on RPT resting on elastic foundations by DQM including surface effects. *Microsystem Technologies, 23*, 765–797.

Ke, L.-L., & Wang, Y.-S. (2014). Free vibration of size-dependent magneto-electro-elastic nanobeams based on the nonlocal theory. *Physica E: Low-Dimensional Systems and Nanostructures, 63*, 52–61.

Ke, L., Wang, Y., & Reddy, J. (2014). Thermo-electro-mechanical vibration of size-dependent piezoelectric cylindrical nanoshells under various boundary conditions. *Composite Structures, 116*, 626–636.

Ke, L.-L., Wang, Y.-S., & Wang, Z.-D. (2012). Nonlinear vibration of the piezoelectric nanobeams based on the nonlocal theory. *Composite Structures, 94*, 2038–2047.

Ke, L.-L., Wang, Y.-S., Yang, J., & Kitipornchai, S. (2014). The size-dependent vibration of embedded magneto-electro-elastic cylindrical nanoshells. *Smart Materials and Structures, 23*, 125036.

Ke, L., Xiang, Y., Yang, J., & Kitipornchai, S. (2009). Nonlinear free vibration of embedded double-walled carbon nanotubes based on nonlocal Timoshenko beam theory. *Computational Materials Science, 47*, 409–417.

Khademhosseini, F., Rajapakse, R., & Nojeh, A. (2010). Torsional buckling of carbon nanotubes based on nonlocal elasticity shell models. *Computational materials science, 48*, 736–742.

Khajeansari, A., Baradaran, G., & Yvonnet, J. (2012). An explicit solution for bending of nanowires lying on Winkler–Pasternak elastic substrate medium based on the Euler–Bernoulli beam theory. *International journal of engineering science, 52*, 115–128.

Khaniki, H. B. (2018). On vibrations of nanobeam systems. *International Journal of Engineering Science, 124*, 85–103.

Kiani, K. (2010). A meshless approach for free transverse vibration of embedded single-walled nanotubes with arbitrary boundary conditions accounting for nonlocal effect. *International Journal of Mechanical Sciences, 52*, 1343–1356.

Kiani, K. (2014). Free vibration of conducting nanoplates exposed to unidirectional in-plane magnetic fields using nonlocal shear deformable plate theories. *Physica E: Low-dimensional Systems and Nanostructures, 57*, 179–192.

Kiani, K. (2016). Thermo-elasto-dynamic analysis of axially functionally graded non-uniform nanobeams with surface energy. *International Journal of Engineering Science, 106*, 57–76.

Kong, L., & Chen, W. (2014). Carbon Nanotube and Graphene based Bioinspired Electrochemical Actuators. *Advanced materials, 26*, 1025–1043.

Kwon, J., Sharma, B. K., & Ahn, J.-H. (2013). Graphene based nanogenerator for energy harvesting. *Japanese Journal of Applied Physics, 52*, 06GA02.

Lee, H.-L., & Chang, W.-J. (2010). Surface and small-scale effects on vibration analysis of a nonuniform nanocantilever beam. *Physica E: Low-Dimensional Systems and Nanostructures, 43*, 466–469.

Lei, J., He, Y., Guo, S., Li, Z., & Liu, D. (2016). Size-dependent vibration of nickel cantilever microbeams: Experiment and gradient elasticity. *AIP Advances, 6*, 105202.

Lei, Y., Adhikari, S., & Friswell, M. (2013). Vibration of nonlocal Kelvin–Voigt viscoelastic damped Timoshenko beams. *International Journal of Engineering Science, 66*, 1–13.

Lei, X.-w., Natsuki, T., Shi, J.-x, & Ni, Q.-q (2012). Surface effects on the vibrational frequency of double-walled carbon nanotubes using the nonlocal Timoshenko beam model. *Composites Part B: Engineering, 43*, 64–69.

Li, L., & Hu, Y. (2015). Buckling analysis of size-dependent nonlinear beams based on a nonlocal strain gradient theory. *International Journal of Engineering Science, 97*, 84–94.

Li, L., & Hu, Y. (2017). Post-buckling analysis of functionally graded nanobeams incorporating nonlocal stress and microstructure-dependent strain gradient effects. *International Journal of Mechanical Sciences, 120*, 159–170.

Li, X., Li, L., Hu, Y., Ding, Z., & Deng, W. (2017). Bending, buckling and vibration of axially functionally graded beams based on nonlocal strain gradient theory. *Composite Structures, 165*, 250–265.

Li, L., Hu, Y., & Li, X. (2016). Longitudinal vibration of size-dependent rods via nonlocal strain gradient theory. *International Journal of Mechanical Sciences, 115*, 135–144.

Li, L., Hu, Y., & Ling, L. (2015). Flexural wave propagation in small-scaled functionally graded beams via a nonlocal strain gradient theory. *Composite Structures, 133*, 1079–1092.

Li, L., Hu, Y., & Ling, L. (2016). Wave propagation in viscoelastic single-walled carbon nanotubes with surface effect under magnetic field based on nonlocal strain gradient theory. *Physica E: Low-dimensional Systems and Nanostructures, 75*, 118–124.

Lim, C., Zhang, G., & Reddy, J. (2015). A higher-order nonlocal elasticity and strain gradient theory and its applications in wave propagation. *Journal of the Mechanics and Physics of Solids, 78*, 298–313.

Liu, B., & Aydil, E. S. (2009). Growth of oriented single-crystalline rutile TiO2 nanorods on transparent conducting substrates for dye-sensitized solar cells. *Journal of the American Chemical Society, 131*, 3985–3990.

Liu, C., Ke, L.-L., Yang, J., Kitipornchai, S., & Wang, Y.-S. (2016). Nonlinear vibration of piezoelectric nanoplates using nonlocal Mindlin plate theory. *Mechanics of Advanced Materials and Structures*, 1–13.

Liu, C., Ke, L.-L., Wang, Y.-S., & Yang, J. (2015). Nonlinear vibration of nonlocal piezoelectric nanoplates. *International Journal of Structural Stability and Dynamics, 15*, 1540013.

Loo, C., Lowery, A., Halas, N., West, J., & Drezek, R. (2005). Immunotargeted nanoshells for integrated cancer imaging and therapy. *Nano letters, 5*, 709–711.

Loya, J., Aranda-Ruiz, J., & Fernández-Sáez, J. (2014). Torsion of cracked nanorods using a nonlocal elasticity model. *Journal of Physics D: Applied Physics, 47*, 115304.

Lu, L., Guo, X., & Zhao, J. (2017). Size-dependent vibration analysis of nanobeams based on the nonlocal strain gradient theory. *International Journal of Engineering Science, 116*, 12–24.

Lu, L., Guo, X., & Zhao, J. (2017). A unified nonlocal strain gradient model for nanobeams and the importance of higher order terms. *International Journal of Engineering Science, 119*, 265–277.

Lu, L., Guo, X., & Zhao, J. (2018). On the mechanics of Kirchhoff and Mindlin plates incorporating surface energy. *International Journal of Engineering Science, 124*, 24–40.

Malekzadeh, P., & Farajpour, A. (2012). Axisymmetric free and forced vibrations of initially stressed circular nanoplates embedded in an elastic medium. *Acta Mechanica, 223*, 2311–2330.

Malekzadeh, P., & Shojaee, M. (2013). Surface and nonlocal effects on the nonlinear free vibration of non-uniform nanobeams. *Composites Part B: Engineering, 52*, 84–92.

Malekzadeh, P., & Shojaee, M. (2013). Free vibration of nanoplates based on a nonlocal two-variable refined plate theory. *Composite Structures, 95*, 443–452.

Malekzadeh, P., Setoodeh, A., & Beni, A. A. (2011). Small scale effect on the thermal buckling of orthotropic arbitrary straight-sided quadrilateral nanoplates embedded in an elastic medium. *Composite Structures, 93*, 2083–2089.

Malekzadeh, P., Setoodeh, A., & Beni, A. A. (2011). Small scale effect on the free vibration of orthotropic arbitrary straight-sided quadrilateral nanoplates. *Composite Structures, 93*, 1631–1639.

Mehralian, F., Beni, Y. T., & Zeverdejani, M. K. (2017). Calibration of nonlocal strain gradient shell model for buckling analysis of nanotubes using molecular dynamics simulations. *Physica B: Condensed Matter, 521*, 102–111.

Mehralian, F., Beni, Y. T., & Zeverdejani, M. K. (2017). Nonlocal strain gradient theory calibration using molecular dynamics simulation based on small scale vibration of nanotubes. *Physica B: Condensed Matter, 514*, 61–69.

Mindlin, R. D., & Eshel, N. (1968). On first strain-gradient theories in linear elasticity. *International Journal of Solids and Structures, 4*, 109–124.

Mohammadi, M., Goodarzi, M., Ghayour, M., & Farajpour, A. (2013). Influence of in-plane pre-load on the vibration frequency of circular graphene sheet via nonlocal continuum theory. *Composites Part B: Engineering, 51*, 121–129.

Moosavi, H., Mohammadi, M., Farajpour, A., & Shahidi, S. (2011). Vibration analysis of nanorings using nonlocal continuum mechanics and shear deformable ring theory. *Physica E: Low-dimensional Systems and Nanostructures, 44*, 135–140.

Murmu, T., & Adhikari, S. (2010). Nonlocal effects in the longitudinal vibration of double-nanorod systems. *Physica E: Low-dimensional Systems and Nanostructures, 43*, 415–422.

Murmu, T., & Adhikari, S. (2010). Nonlocal transverse vibration of double-nanobeam-systems. *Journal of Applied Physics, 108*, 083514.

Murmu, T., & Adhikari, S. (2011). Axial instability of double-nanobeam-systems. *Physics Letters A, 375*, 601–608.

Murmu, T., & Adhikari, S. (2013). Nonlocal mass nanosensors based on vibrating monolayer graphene sheets. *Sensors and Actuators B: Chemical, 188*, 1319–1327.

Murmu, T., & Pradhan, S. (2009). Buckling analysis of a single-walled carbon nanotube embedded in an elastic medium based on nonlocal elasticity and Timoshenko beam theory and using DQM. *Physica E: Low-dimensional Systems and Nanostructures, 41*, 1232–1239.

Murmu, T., & Pradhan, S. (2009). Thermo-mechanical vibration of a single-walled carbon nanotube embedded in an elastic medium based on nonlocal elasticity theory. *Computational Materials Science, 46*, 854–859.

Murmu, T., & Pradhan, S. (2009). Buckling of biaxially compressed orthotropic plates at small scales. *Mechanics Research Communications, 36*, 933–938.

Murmu, T., & Pradhan, S. (2010). Thermal effects on the stability of embedded carbon nanotubes. *Computational Materials Science, 47*, 721–726.

Murmu, T., Adhikari, S., & Wang, C. (2011). Torsional vibration of carbon nanotube–buckyball systems based on nonlocal elasticity theory. *Physica E: Low-dimensional Systems and Nanostructures, 43*, 1276–1280.

Murmu, T., McCarthy, M., & Adhikari, S. (2012). Vibration response of double-walled carbon nanotubes subjected to an externally applied longitudinal magnetic field: a nonlocal elasticity approach,. *Journal of Sound and Vibration, 331*, 5069–5086.

Murmu, T., McCarthy, M., & Adhikari, S. (2013). In-plane magnetic field affected transverse vibration of embedded single-layer graphene sheets using equivalent nonlocal elasticity approach. *Composite Structures, 96*, 57–63.

Naderi, A., & Saidi, A. (2014). Nonlocal postbuckling analysis of graphene sheets in a nonlinear polymer medium. *International Journal of Engineering Science, 81*, 49–65.

Narendar, S., & Gopalakrishnan, S. (2009). Nonlocal scale effects on wave propagation in multi-walled carbon nanotubes. *Computational Materials Science, 47*, 526–538.

Narendar, S., & Gopalakrishnan, S. (2010). Nonlocal scale effects on ultrasonic wave characteristics of nanorods. *Physica E: Low-dimensional Systems and Nanostructures, 42*, 1601–1604.

Narendar, S., & Gopalakrishnan, S. (2011). Critical buckling temperature of single-walled carbon nanotubes embedded in a one-parameter elastic medium based on nonlocal continuum mechanics. *Physica E: Low-dimensional Systems and Nanostructures, 43*, 1185–1191.

Narendar, S., & Gopalakrishnan, S. (2012). Temperature effects on wave propagation in nanoplates. *Composites Part B: Engineering, 43*, 1275–1281.

Narendar, S., & Gopalakrishnan, S. (2012). Study of terahertz wave propagation properties in nanoplates with surface and small-scale effects. *International Journal of Mechanical Sciences, 64*, 221–231.

Natarajan, S., Chakraborty, S., Thangavel, M., Bordas, S., & Rabczuk, T. (2012). Size-dependent free flexural vibration behavior of functionally graded nanoplates. *Computational Materials Science, 65*, 74–80.

Nejad, M. Z., & Hadi, A. (2016). Eringen's non-local elasticity theory for bending analysis of bi-directional functionally graded Euler–Bernoulli nano-beams. *International Journal of Engineering Science, 106*, 1–9.

Nejad, M. Z., Hadi, A., & Farajpour, A. (2017). Consistent couple-stress theory for free vibration analysis of Euler-Bernoulli nano-beams made of arbitrary bi-directional functionally graded materials. *Structural Engineering and Mechanics, 63*, 161–169.

Nejad, M. Z., Hadi, A., & Rastgoo, A. (2016). Buckling analysis of arbitrary two-directional functionally graded Euler–Bernoulli nano-beams based on nonlocal elasticity theory. *International Journal of Engineering Science, 103*, 1–10.

Nikoobakht, B., & El-Sayed, M. A. (2003). Preparation and growth mechanism of gold nanorods (NRs) using seed-mediated growth method. *Chemistry of Materials, 15*, 1957–1962.

Numanoğlu, H. M., Akgöz, B., & Civalek, Ö. (2018). On dynamic analysis of nanorods. *International Journal of Engineering Science, 130*, 33–50.

Park, S., An, J., Suk, J. W., & Ruoff, R. S. (2010). Graphene based actuators. *Small, 6*, 210–212.

Peddieson, J., Buchanan, G. R., & McNitt, R. P. (2003). Application of nonlocal continuum models to nanotechnology. *International Journal of Engineering Science, 41*, 305–312.

Phadikar, J., & Pradhan, S. (2010). Variational formulation and finite element analysis for nonlocal elastic nanobeams and nanoplates. *Computational materials science, 49*, 492–499.

Pouresmaeeli, S., Ghavanloo, E., & Fazelzadeh, S. (2013). Vibration analysis of viscoelastic orthotropic nanoplates resting on viscoelastic medium. *Composite structures, 96*, 405–410.

Pradhan, S., & Kumar, A. (2011). Vibration analysis of orthotropic graphene sheets using nonlocal elasticity theory and differential quadrature method. *Composite Structures, 93*, 774–779.

Pradhan, S., & Murmu, T. (2009). Small-scale effect on vibration analysis of single-walled carbon nanotubes embedded in an elastic medium using nonlocal elasticity theory. *Journal of Applied Physics, 105*, 124306.

Pradhan, S., & Murmu, T. (2009). Small scale effect on the buckling of single-layered graphene sheets under biaxial compression via nonlocal continuum mechanics. *Computational materials science, 47*, 268–274.

Pradhan, S., & Phadikar, J. (2009). Nonlocal elasticity theory for vibration of nanoplates. *Journal of Sound and Vibration, 325*, 206–223.

Pradhan, S., & Phadikar, J. (2009). Small scale effect on vibration of embedded multilayered graphene sheets based on nonlocal continuum models. *Physics letters A, 373*, 1062–1069.

Pradhan, S., & Reddy, G. (2011). Buckling analysis of single walled carbon nanotube on Winkler foundation using nonlocal elasticity theory and DTM. *Computational Materials Science, 50*, 1052–1056.

Pradhan, S., & Sahu, B. (2010). Vibration of single layer graphene sheet based on nonlocal elasticity and higher order shear deformation theory. *Journal of Computational and Theoretical Nanoscience, 7*, 1042–1050.

Pradhan, S. (2009). Buckling of single layer graphene sheet based on nonlocal elasticity and higher order shear deformation theory. *Physics Letters A, 373*, 4182–4188.

Preethi, K., Rajagopal, A., & Reddy, J. N. (2015). Surface and non-local effects for non-linear analysis of Timoshenko beams. *International Journal of Non-Linear Mechanics, 76*, 100–111.

Radić, N., & Jeremić, D. (2016). Thermal buckling of double-layered graphene sheets embedded in an elastic medium with various boundary conditions using a nonlocal new first-order shear deformation theory. *Composites Part B: Engineering, 97*, 201–215.

Rahmani, O., & Pedram, O. (2014). Analysis and modeling the size effect on vibration of functionally graded nanobeams based on nonlocal Timoshenko beam theory. *International Journal of Engineering Science, 77*, 55–70.

Reddy, J., & Pang, S. (2008). Nonlocal continuum theories of beams for the analysis of carbon nanotubes. *Journal of Applied Physics, 103*, 023511.

Reddy, J. (2007). Nonlocal theories for bending, buckling and vibration of beams. *International Journal of Engineering Science, 45*, 288–307.

Reddy, J. (2010). Nonlocal nonlinear formulations for bending of classical and shear deformation theories of beams and plates. *International Journal of Engineering Science, 48*, 1507–1518.

Rhoads, J. F., Shaw, S. W., & Turner, K. L. (2008). Nonlinear dynamics and its applications in micro-and nanoresonators, in: ASME 2008 Dynamic Systems and Control Conference. *American Society of Mechanical Engineers*, 1509–1538.

Sahmani, S., & Aghdam, M. (2018). Nonlocal strain gradient shell model for axial buckling and postbuckling analysis of magneto-electro-elastic composite nanoshells. *Composites Part B: Engineering, 132*, 258–274.

Sahmani, S., Aghdam, M., & Akbarzadeh, A. (2016). Size-dependent buckling and postbuckling behavior of piezoelectric cylindrical nanoshells subjected to compression and electrical load. *Materials & Design, 105*, 341–351.

Sahmani, S., Bahrami, M., & Aghdam, M. (2016). Surface stress effects on the nonlinear postbuckling characteristics of geometrically imperfect cylindrical nanoshells subjected to torsional load. *Composites Part B: Engineering, 84*, 140–154.

Sahmani, S., Bahrami, M., Aghdam, M., & Ansari, R. (2015). Postbuckling behavior of circular higher-order shear deformable nanoplates including surface energy effects. *Applied Mathematical Modelling, 39*, 3678–3689.

Sarrami-Foroushani, S., & Azhari, M. (2014). Nonlocal vibration and buckling analysis of single and multi-layered graphene sheets using finite strip method including van der Waals effects. *Physica E: Low-dimensional Systems and Nanostructures, 57*, 83–95.

Setoodeh, A., Khosrownejad, M., & Malekzadeh, P. (2011). Exact nonlocal solution for postbuckling of single-walled carbon nanotubes. *Physica E: Low-dimensional Systems and Nanostructures, 43*, 1730–1737.

Shaat, M., Mahmoud, F., Gao, X.-L., & Faheem, A. F. (2014). Size-dependent bending analysis of Kirchhoff nano-plates based on a modified couple-stress theory including surface effects. *International Journal of Mechanical Sciences, 79*, 31–37.

Shafiei, N., Kazemi, M., Safi, M., & Ghadiri, M. (2016). Nonlinear vibration of axially functionally graded non-uniform nanobeams. *International Journal of Engineering Science, 106*, 77–94.

Shahverdi, H., & Barati, M. R. (2017). Vibration analysis of porous functionally graded nanoplates. *International Journal of Engineering Science, 120*, 82–99.

Sharabiani, P. A., & Yazdi, M. R. H. (2013). Nonlinear free vibrations of functionally graded nanobeams with surface effects. *Composites Part B: Engineering, 45*, 581–586.

She, G.-L., Ren, Y.-R., Yuan, F.-G., & Xiao, W.-S. (2018). On vibrations of porous nanotubes. *International Journal of Engineering Science, 125*, 23–35.

She, G.-L., Yuan, F.-G., & Ren, Y.-R. (2018). On wave propagation of porous nanotubes. *International Journal of Engineering Science, 130*, 62–74.

She, G.-L., Yuan, F.-G., Ren, Y.-R., & Xiao, W.-S. (2017). On buckling and postbuckling behavior of nanotubes. *International Journal of Engineering Science, 121*, 130–142.

Shen, H.-S., & Zhang, C.-L. (2010). Torsional buckling and postbuckling of double-walled carbon nanotubes by nonlocal shear deformable shell model. *Composite Structures, 92*, 1073–1084.

Shen, H.-S. (2011). Nonlocal plate model for nonlinear analysis of thin films on elastic foundations in thermal environments. *Composite Structures, 93*, 1143–1152.

Shen, L., Shen, H.-S., & Zhang, C.-L. (2010). Nonlocal plate model for nonlinear vibration of single layer graphene sheets in thermal environments. *Computational Materials Science, 48*, 680–685.

Shen, Z.-B., Tang, H.-L., Li, D.-K., & Tang, G.-J. (2012). Vibration of single-layered graphene sheet-based nanomechanical sensor via nonlocal Kirchhoff plate theory. *Computational Materials Science, 61*, 200–205.

Shen, H.-S., Xu, Y.-M., & Zhang, C.-L. (2013). Prediction of nonlinear vibration of bilayer graphene sheets in thermal environments via molecular dynamics simulations and nonlocal elasticity. *Computer Methods in Applied Mechanics and Engineering, 267*, 458–470.

Şimşek, M., & Yurtcu, H. (2013). Analytical solutions for bending and buckling of functionally graded nanobeams based on the nonlocal Timoshenko beam theory. *Composite Structures, 97*, 378–386.

Şimşek, M. (2010). Vibration analysis of a single-walled carbon nanotube under action of a moving harmonic load based on nonlocal elasticity theory. *Physica E: Low-dimensional Systems and Nanostructures, 43*, 182–191.

Şimşek, M. (2012). Nonlocal effects in the free longitudinal vibration of axially functionally graded tapered nanorods. *Computational Materials Science, 61*, 257–265.

Şimşek, M. (2014). Large amplitude free vibration of nanobeams with various boundary conditions based on the nonlocal elasticity theory. *Composites Part B: Engineering, 56*, 621–628.

Şimşek, M. (2016). Nonlinear free vibration of a functionally graded nanobeam using nonlocal strain gradient theory and a novel Hamiltonian approach. *International Journal of Engineering Science, 105*, 12–27.

Soltani, P., & Farshidianfar, A. (2012). Periodic solution for nonlinear vibration of a fluid-conveying carbon nanotube, based on the nonlocal continuum theory by energy balance method. *Applied Mathematical Modelling, 36*, 3712–3724.

Sudak, L. (2003). Column buckling of multiwalled carbon nanotubes using nonlocal continuum mechanics. *Journal of applied physics, 94*, 7281–7287.

Thai, H.-T., & Vo, T. P. (2012). A nonlocal sinusoidal shear deformation beam theory with application to bending, buckling, and vibration of nanobeams. *International Journal of Engineering Science, 54*, 58–66.

Tuna, M., & Kirca, M. (2016). Exact solution of Eringen's nonlocal integral model for bending of Euler–Bernoulli and Timoshenko beams. *International Journal of Engineering Science, 105*, 80–92.

Wang, C., & Duan, W. (2008). Free vibration of nanorings/arches based on nonlocal elasticity. *Journal of Applied Physics, 104*, 014303.

Wang, G.-F., & Feng, X.-Q. (2009). Surface effects on buckling of nanowires under uniaxial compression. *Applied physics letters, 94*, 141913.

Wang, Q., & Varadan, V. (2006). Vibration of carbon nanotubes studied using nonlocal continuum mechanics. *Smart Materials and Structures, 15*, 659.

Wang, Q., & Varadan, V. (2007). Application of nonlocal elastic shell theory in wave propagation analysis of carbon nanotubes. *Smart Materials and Structures, 16*, 178.

Wang, Q., & Wang, C. (2007). The constitutive relation and small scale parameter of nonlocal continuum mechanics for modelling carbon nanotubes. *Nanotechnology, 18*, 075702.

Wang, K., & Wang, B. (2011). Vibration of nanoscale plates with surface energy via nonlocal elasticity. *Physica E: Low-dimensional Systems and Nanostructures, 44*, 448–453.

Wang, K., & Wang, B. (2013). A finite element model for the bending and vibration of nanoscale plates with surface effect. *Finite Elements in Analysis and Design, 74*, 22–29.

Wang, K., & Wang, B. (2013). Effect of surface energy on the non-linear postbuckling behavior of nanoplates. *International Journal of Non-Linear Mechanics, 55*, 19–24.

Wang, Q. (2005). Wave propagation in carbon nanotubes via nonlocal continuum mechanics. *Journal of Applied physics, 98*, 124301.

Wang, L. (2012). Surface effect on buckling configuration of nanobeams containing internal flowing fluid: A nonlinear analysis. *Physica E: Low-dimensional Systems and Nanostructures, 44*, 808–812.

Wang, L., Hu, H., & Guo, W. (2006). Validation of the non-local elastic shell model for studying longitudinal waves in single-walled carbon nanotubes. *Nanotechnology, 17*, 1408.

Wang, Y.-Z., Li, F.-M., & Kishimoto, K. (2010). Flexural wave propagation in double-layered nanoplates with small scale effects. *Journal of Applied Physics, 108*, 064519.

Wang, Y.-Z., Li, F.-M., & Kishimoto, K. (2010). Scale effects on the longitudinal wave propagation in nanoplates. *Physica E: Low-dimensional Systems and Nanostructures, 42*, 1356–1360.

Wang, Y.-Z., Li, F.-M., & Kishimoto, K. (2010). Scale effects on flexural wave propagation in nanoplate embedded in elastic matrix with initial stress. *Applied Physics A, 99*, 907–911.

Wang, Y.-Z., Li, F.-M., & Kishimoto, K. (2011). Thermal effects on vibration properties of double-layered nanoplates at small scales. *Composites Part B: Engineering, 42*, 1311–1317.

Wang, C., Murmu, T., & Adhikari, S. (2011). Mechanisms of nonlocal effect on the vibration of nanoplates. *Applied Physics Letters, 98*, 153101.

Wang, C., Ru, C., & Mioduchowski, A. (2005). Axisymmetric and beamlike vibrations of multiwall carbon nanotubes. *Physical Review B, 72*, 075414.

Wang, Q., Varadan, V., & Quek, S. (2006). Small scale effect on elastic buckling of carbon nanotubes with nonlocal continuum models. *Physics Letters A, 357*, 130–135.

Wang, C. M., Xiang, Y., Yang, J., & Kitipornchai, S. (2012). Buckling of nano-rings/arches based on nonlocal elasticity. *International Journal of Applied Mechanics, 4*, 1250025.

Wang, Q., Zhou, G., & Lin, K. (2006). Scale effect on wave propagation of double-walled carbon nanotubes. *International Journal of Solids and Structures, 43*, 6071–6084.

Wang, B., Zhou, S., Zhao, J., & Chen, X. (2011). A size-dependent Kirchhoff micro-plate model based on strain gradient elasticity theory. *European Journal of Mechanics-A/Solids, 30*, 517–524.

Wen, J., Lao, J., Wang, D., Kyaw, T., Foo, Y., & Ren, Z. (2003). Self-assembly of semiconducting oxide nanowires, nanorods, and nanoribbons. *Chemical Physics Letters, 372*, 717–722.

Xu, C., Sun, X. W., Dong, Z. L., Yu, M., My, T., Zhang, X., et al. (2004). Zinc oxide nanowires and nanorods fabricated by vapour-phase transport at low temperature. *Nanotechnology, 15*, 839.

Xu, Y.-M., Shen, H.-S., & Zhang, C.-L. (2013). Nonlocal plate model for nonlinear bending of bilayer graphene sheets subjected to transverse loads in thermal environments. *Composite Structures, 98*, 294–302.

Yan, Z., & Jiang, L. (2011). The vibrational and buckling behaviors of piezoelectric nanobeams with surface effects. *Nanotechnology, 22*, 245703.

Yan, Z., & Jiang, L. (2013). Size-dependent bending and vibration behaviour of piezoelectric nanobeams due to flexoelectricity. *Journal of Physics D: Applied Physics, 46*, 355502.

Yan, J., Tong, L., Li, C., Zhu, Y., & Wang, Z. (2015). Exact solutions of bending deflections for nano-beams and nano-plates based on nonlocal elasticity theory. *Composite Structures, 125*, 304–313.

Yang, J., Ke, L., & Kitipornchai, S. (2010). Nonlinear free vibration of single-walled carbon nanotubes using nonlocal Timoshenko beam theory. *Physica E: Low-dimensional Systems and Nanostructures, 42*, 1727–1735.

Ye, X., Jin, L., Caglayan, H., Chen, J., Xing, G., Zheng, C., et al. (2012). Improved size-tunable synthesis of monodisperse gold nanorods through the use of aromatic additives. *ACS nano, 6*, 2804–2817.

Yoon, J., Ru, C., & Mioduchowski, A. (2003). Vibration of an embedded multiwall carbon nanotube. *Composites Science and Technology, 63*, 1533–1542.

Yoon, J., Ru, C., & Mioduchowski, A. (2005). Vibration and instability of carbon nanotubes conveying fluid. *Composites Science and Technology, 65*, 1326–1336.

Yu, Y. J., Xue, Z.-N., Li, C.-L., & Tian, X.-G. (2016). Buckling of nanobeams under nonuniform temperature based on nonlocal thermoelasticity. *Composite Structures, 146*, 108–113.

Zeighampour, H., Beni, Y. T., & Karimipour, I. (2017). Wave propagation in double-walled carbon nanotube conveying fluid considering slip boundary condition and shell model based on nonlocal strain gradient theory. *Microfluidics and Nanofluidics, 21*, 85.

Zenkour, A., & Sobhy, M. (2013). Nonlocal elasticity theory for thermal buckling of nanoplates lying on Winkler–Pasternak elastic substrate medium. *Physica E: Low-dimensional Systems and Nanostructures, 53*, 251–259.

Zenkour, A. M., & Sobhy, M. (2015). A simplified shear and normal deformations nonlocal theory for bending of nanobeams in thermal environment. *Physica E: Low-Dimensional Systems and Nanostructures, 70*, 121–128.

Zhang, Z., & Jiang, L. (2014). Size effects on electromechanical coupling fields of a bending piezoelectric nanoplate due to surface effects and flexoelectricity. *Journal of Applied Physics, 116*, 134308.

Zhang, Y.-W., Chen, J., Zeng, W., Teng, Y.-Y., Fang, B., & Zang, J. (2015). Surface and thermal effects of the flexural wave propagation of piezoelectric functionally graded nanobeam using nonlocal elasticity. *Computational Materials Science, 97*, 222–226.

Zhang, Y., Lei, Z., Zhang, L., Liew, K., & Yu, J. (2015). Nonlocal continuum model for vibration of single-layered graphene sheets based on the element-free kp-Ritz method. *Engineering Analysis with Boundary Elements, 56*, 90–97.

Zhang, Y., Liu, G., & Wang, J. (2004). Small-scale effects on buckling of multiwalled carbon nanotubes under axial compression. *Physical review B, 70*, 205430.

Zhang, L., Liu, J., Fang, X., & Nie, G. (2014). Effects of surface piezoelectricity and nonlocal scale on wave propagation in piezoelectric nanoplates. *European Journal of Mechanics-A/Solids, 46*, 22–29.

Zhang, S., Wang, Q., Chen, X., & Jena, P. (2013). Stable three-dimensional metallic carbon with interlocking hexagons. In *Proceedings of the National Academy of Sciences: 110* (pp. 18809–18813).

Zhang, L., Zhang, Y., & Liew, K. (2017). Vibration analysis of quadrilateral graphene sheets subjected to an in-plane magnetic field based on nonlocal elasticity theory. *Composites Part B: Engineering, 118*, 96–103.

Zhao, Q., Gan, Z., & Zhuang, Q. (2002). Electrochemical sensors based on carbon nanotubes. *Electroanalysis: An International Journal Devoted to Fundamental and Practical Aspects of Electroanalysis, 14*, 1609–1613.

Zhu, X., & Li, L. (2017). Closed form solution for a nonlocal strain gradient rod in tension. *International Journal of Engineering Science, 119*, 16–28.

Chapter 3

Nonlinear vibration of small-scale beams with geometrical imperfections

---

Chapter overview

In this chapter, the first objective of this project, which is the nonlinear vibration of geometrically imperfect beams at small-scale levels, is analysed. For this purpose, an advanced scale-dependent model is developed by assuming stress nonlocality and taking into consideration strain gradients in the constitutive equations of the structure. To simulate a geometrical imperfection, an initial deformation is assumed in the small-scale beam prior to vibrations. The geometrical nonlinearity is modelled through strain-displacement relations. Potential and kinetic energies of the small-scale system are used to conduct an energy balance and obtain the coupled motion equations. Using a Galerkin-based technique, the nonlinear vibrational response of the imperfect beam is numerically estimated. It is found that the resonance frequency is highly influenced by both geometrical imperfections and scale effects. This work was published in "International Journal of Mechanical Sciences" as:

A. Farajpour, M.H. Ghayesh, H. Farokhi, "Large-amplitude coupled scale-dependent behaviour of geometrically imperfect NSGT nanotubes", International Journal of Mechanical Sciences, volume 150, pages 510-525 (2019).

Statement of Authorship

Title of Paper	Large-amplitude coupled scale-dependent behaviour of geometrically imperfect NSGT nanotubes
Publication Status	☑ Published ☐ Accepted for Publication ☐ Submitted for Publication ☐ Unpublished and Unsubmitted work written in manuscript style
Publication Details	A Farajpour, MH Ghayesh, H Farokhi, Large-amplitude coupled scale-dependent behaviour of geometrically imperfect NSGT nanotubes, International Journal of Mechanical Sciences 150, 510-525 (2019).

Principal Author

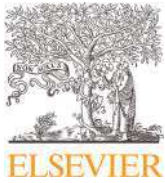|	
Name of Principal Author (Candidate)	Ali Farajpour Ouderji
Contribution to the Paper	- Research and doing the literature review of the paper - Developing the model (i.e. derivation of nonlinear coupled partial differential equations of motion via Hamilton's principle) - Incorporating size effects using a refined scale-dependent approach - Incorporating the influence of geometrical imperfection and nonlinearity into the model - Writing all parts of the paper and analysing the data - Correspondence with the reviewers and editor of the journal, - Preparing the revised version of the paper
Overall percentage (%)	60%
Certification:	This paper reports on original research I conducted during the period of my Higher Degree by Research candidature and is not subject to any obligations or contractual agreements with a third party that would constrain its inclusion in this thesis. I am the primary author of this paper.
Signature	Date 2/6/2020

Co-Author Contributions

By signing the Statement of Authorship, each author certifies that:
i. the candidate's stated contribution to the publication is accurate (as detailed above);
ii. permission is granted for the candidate in include the publication in the thesis; and
iii. the sum of all co-author contributions is equal to 100% less the candidate's stated contribution.

Name of Co-Author	Mergen H. Ghayesh
Contribution to the Paper	- Supervising the work including preparing the paper - Contribution to the development of the ideas and concepts of the paper - Editing and evaluating the paper before submission - Discretising and solving the equations of motions, and obtaining frequency response curves
Signature	Date 21/06/2090

Name of Co-Author	Hamed Farokhi
Contribution to the Paper	- Participation in supervising the work - Contribution to the development of the concepts of the paper - Discretising and solving the equations of motions, and obtaining frequency response curves
Signature	Date 19/06/2020

Large-amplitude coupled scale-dependent behaviour of geometrically imperfect NSGT nanotubes

Ali Farajpour [a,*], Mergen H. Ghayesh [a], Hamed Farokhi [b]

[a] School of Mechanical Engineering, University of Adelaide, South Australia 5005, Australia
[b] Department of Mechanical and Construction Engineering, Northumbria University, Newcastle upon Tyne NE1 8ST, UK

ARTICLE INFO

ABSTRACT

In this paper, a scale-dependent coupled nonlinear continuum-based model is developed for the mechanical behaviour of imperfect nanoscale tubes incorporating both the effect of the stress nonlocality and strain gradient effects. The scale effects on the nonlinear mechanics are taken into consideration employing a modified elasticity theory on the basis of a refined combination of Eringen's elasticity and the strain gradient theory. According to the Euler–Bernoulli theory of beams, the nonlocal strain gradient theory (NSGT) and Hamilton's principle, the potential energy, kinetic energy and the work performed by harmonic loads are formulated, and then the coupled scale-dependent equations of the imperfect nanotube are derived. Finally, Galerkin's scheme, as a discretisation technique, and the continuation method, as a solution procedure for ordinary differential equations, are used. The effects of geometrical imperfections in conjunction with other nanosystem parameters such as the nonlocal coefficient as well as the strain gradient coefficient on the coupled large-amplitude mechanical behaviour are explored and discussed.

1. Introduction

Nanostructures such as nanorings, nanotubes and nanosheets which form the fundamental building blocks of some nanoelectromechanical systems (NEMS) are scarcely a perfect structural element. During the fabrication process, a geometric imperfection is likely to be formed in the structure of nanomaterials since manufacturing at nanoscale levels is difficult to be implemented with high precision. Therefore, it is important to take these imperfections into account in a theoretical model or molecular dynamics (MD) simulations so as to obtain more accurate results.

In addition to experimental measurements and MD simulations, theoretical modelling of nanoscale structures has attracted researchers' attention in recent years due to its simplicity and low computational costs [1–7]. In addition to microscale structures [8–10], various size-dependent continuum-based models for nanoscale structures have been proposed [11–16]. For instance, Guo et al. [17] examined the influence of length scale on the mechanical response of nanoscale beams while moving in the axial direction and rotating; the critical velocity of rotation is greater for forward waves than that of backward waves. Li et al. [18] studied the influence of the nonlocality along the thickness of nanoscale beams; analytical expressions were proposed for the buckling behaviour. More recently, wave propagations in smart nanoscale tubes

and shells have been investigated using a size-dependent continuum-based formulation [19]. Lei et al. [20] examined the size-dependent elasticity of cantilever small-scale beams carrying out experiments. In addition, in an interesting article, an experimental scheme was proposed by Li et al. [21] for obtaining the scale parameter of a size-dependent theory. Now previous studies related to the continuum-based modelling of size-dependent imperfect nanostructures are reviewed. Farshidianfar and Soltani [22] used the nonlocal continuum mechanics to investigate the transverse dynamics of a geometrically imperfect fluid-conveying carbon nanotube (CNT) with both edges immovable; they obtained an approximate explicit expression for the nonlinear natural frequencies employing a multi-scale perturbation technique. Wang et al. [23] also developed a nonlocal beam model in order to examine the large-amplitude forced dynamics of imperfect single-walled CNTs; they utilised a one-term Galerkin approximation and the precise integration scheme to describe the nonlinear behaviour of the CNT. In another study, Mohammadi et al. [24] applied Eringen's elasticity theory to nanoscale beams with a geometrical imperfection resting on an elastic foundation so as to explore their post-buckling behaviour. In order to examine the stability response of metal foam nanoscale beams with an initial deflection in the presence of structural porosities, a nonlinear nonlocal analysis was also performed by Barati and Zenkour [25]. The effect of out-of-plane defects on the free dynamics of a single-layered graphene sheets was investigated by Jalali et al. [26] via use of Erin-

---

gen's elasticity theory; they reported that out-of-plane defects have an important role to play in the free vibration of graphene sheets. Furthermore, Rafiee et al. [27] used the classical (local) continuum mechanics in conjunction with the first-order shear deformation theory in order to explore the large-amplitude dynamic instability of imperfect piezo-electric functionally graded (FG) plates reinforced by CNTs. A nonlocal beam model was also developed by Arefi and Salimi [28] to study the influence of the small initial curvature on the mechanical behaviour of single-walled CNTs. In addition, the effects of geometrical imperfections on the vibration response of graphene sheets [29] and on the large-amplitude instability of FG nanopanels [30] have been investigated. In addition, size influences have been studied on the nonlinear mechanics of microscale structures in recent years [31–33].

Recently, it has been reported that taking into account both the stress nonlocality and strain gradients leads to a more reliable size-dependent theoretical model for nanorods [34], nanobeams [35–37], functionally graded nanostructures [38,39], protein microtubules [40] and graphene sheets [41]. However, all of the above-described valuable theoretical models of size-dependent imperfect nanoscale structures contain only one scale parameter (mainly only one nonlocal parameter) which is incapable of incorporating the size effect thoroughly. In the present study, for the first time, a nonlinear size-dependent nanobeam model is developed for imperfect nanotubes with consideration of both the stress nonlocality and strain gradients. The effect of being nanosized is incorporated into the modified continuum model within the framework of the nonlocal counterpart of the classical continuum mechanics as well as a strain gradient-based theory. The Euler–Bernoulli beam theory (EBBT), as a deformation model, is employed together with Hamilton's principle, as a work/energy law, for the derivation of the coupled scale-dependent equations of geometrically imperfect nanoscale tubes. The nonlinear mechanical behaviour of the imperfect nanosystem is obtained on the basis of Galerkin's scheme and a continuation-based approach. It is predicted that the present modified continuum-based model would be useful in design and manufacturing of NEMS devices using different nanotubes such as silver, carbon and silicon nanotubes.

2. Size-dependent formulation and solution technique

Fig. 1 illustrates a nanoscale tube with a geometrical imperfection subject to external harmonic force. The geometrical imperfection is described by an arbitrary initial curvature as shown in the figure. The length and thickness of the nanotube are respectively denoted by L and h while the inner and outer radii are indicated by R_i and R_o, respectively. Moreover, the area and the inertia moment of the cross-section of the tube are denoted by A and I, respectively. E, ρ and ν also represent the elasticity modulus, the mass density and Poisson's ratio of the nanoscale tube, respectively.

According the EBBT, the nonlinear axial strain (ε_{xx}) of the geometrically imperfect nanoscale tube is obtained as

$$\varepsilon_{xx} = \frac{\partial u}{\partial x} + \frac{1}{2}\left(\frac{\partial w}{\partial x}\right)^2 + \frac{\partial w}{\partial x}\frac{dw_0}{dx} - z\frac{\partial^2 w}{\partial x^2}, \tag{1}$$

in which u, w and w_0 represent the longitudinal, transverse and initial transverse displacements of the imperfect nanosystem, respectively; x, z and t are the longitudinal coordinate, the transverse coordinate and the time, respectively. There are various size-dependent theories for nanoscale structures [42–46] as well as modified elasticity theories for microscale structures [47–49]. In this paper, the NSGT [38,50,51] is utilised for capturing size effects. The nonlocal strain gradient constitutive equation of the nanotube can be formulated as [52,53]

$$t_{xx} - (e_0 a)^2 \nabla^2 t_{xx} = E\varepsilon_{xx} - El_{sg}^2 \nabla^2 \varepsilon_{xx}, \tag{2}$$

where t_{xx}, l_{sg} and $e_0 a$ are the total stress along the axial direction, the strain gradient parameter and the nonlocal parameter, respectively; ∇^2 indicates the Laplace operator; e_0 and a are a scale parameter for calibrating the theoretical model and the internal characteristics length of the nanotube, respectively [54,55]. The strain gradient parameter and the nonlocal parameter are determined using experimental measurements or MD simulations [21,56,57]. For instance, Li et al. [35] obtained the scale parameters of carbon nanotubes for the wave propagation analysis via MD simulations. Using Eqs. (1) and (2), one can derive the following relations

$$\left[1 - (e_0 a)^2 \nabla^2\right] N_{xx} = EA\left(1 - l_{sg}^2 \nabla^2\right)\left[\frac{\partial u}{\partial x} + \frac{1}{2}\left(\frac{\partial w}{\partial x}\right)^2 + \frac{\partial w}{\partial x}\frac{dw_0}{dx}\right], \tag{3a}$$

$$\left[1 - (e_0 a)^2 \nabla^2\right] M_{xx} = -EI\left(1 - l_{sg}^2 \nabla^2\right)\frac{\partial^2 w}{\partial x^2}, \tag{3b}$$

with N_{xx} being the longitudinal force resultant and M_{xx} being the bending couple resultant, which are defined by

$$\left\{\begin{matrix} N_{xx} \\ M_{xx} \end{matrix}\right\} = \int_A \left\{\begin{matrix} 1 \\ z \end{matrix}\right\} t_{xx} dA. \tag{4}$$

Applying the nonlocal strain gradient theory (NSGT) to the imperfect nanoscale tube, the variation of the elastic energy is obtained as

$$\delta U = \int_0^L \int_A \left(\sigma_{xx}\delta\varepsilon_{xx} + \sigma_{xx}^{(1)}\nabla\delta\varepsilon_{xx}\right)dAdx = \int_0^L \int_A t_{xx}\delta\varepsilon_{xx}dAdx + \left[\int_A \sigma_{xx}^{(1)}\delta\varepsilon_{xx}dA\right]_0^L, \tag{5}$$

in which σ_{xx} and $\sigma_{xx}^{(1)}$ are respectively the traditional nonlocal axial stress and the higher-order nonlocal axial stress, and ∇ represents the gradient operator; U stands for the elastic energy of the nanotube. It should be noted that the relation between the various stress components is given by $t_{xx} = \sigma_{xx} - \nabla\sigma_{xx}^{(1)}$ on the basis of the NSGT. Consider a nanoscale tube of mass per unit length m subject to the harmonic transverse loading
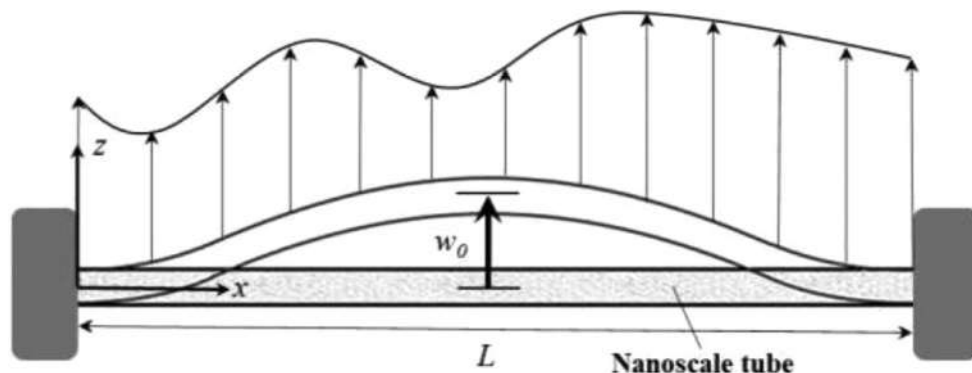

Fig. 1. Schematic representation of a geometrically imperfect nanoscale tube subject to a harmonic loading.

$F(x)\cos(\omega t)$ in which F and ω represent the force amplitude and frequency, respectively. The corresponding motion and work variations can be written as

$$\delta K = m \int_0^L \left(\frac{\partial u}{\partial t} \delta \frac{\partial u}{\partial t} + \frac{\partial w}{\partial t} \delta \frac{\partial w}{\partial t} \right) dx, \tag{6a}$$

$$\delta W_F = \int_0^L F(x)\cos(\omega t)\delta w \, dx. \tag{6b}$$

Here K and W_F are the motion energy and the external work associated with the transverse harmonic force, respectively. To derive the differential equations of motion, the following steps are taken:

(1) Substituting Eqs. (5) and (6) into $\int_{t_1}^{t_2} (\delta K + \delta W_F - \delta U)dt = 0$ (i.e., Hamilton's principle).
(2) Integrating by parts and collecting the coefficient of δu and δw.

The resultant differential equations of motion are as

$$\frac{\partial N_{xx}}{\partial x} = m\frac{\partial^2 u}{\partial t^2}, \tag{7a}$$

$$\frac{\partial^2 M_{xx}}{\partial x^2} + \frac{\partial}{\partial x}\left[N_{xx}\left(\frac{\partial w}{\partial x} + \frac{dw_0}{dx} \right) \right] = m\frac{\partial^2 w}{\partial t^2} - F(x)\cos(\omega t). \tag{7b}$$

The related boundary conditions are also obtained as

$$N_{xx} = 0 \text{ or } u = 0, \; N_{xx}\left(\frac{\partial w}{\partial x} + \frac{dw_0}{dx} \right) + \frac{\partial M_{xx}}{\partial x} = 0 \text{ or } w = 0, \; M_{xx} = 0 \text{ or } \frac{\partial w}{\partial x} = 0, \tag{8a}$$

$$N_{xx}^{(1)} = 0 \text{ or } \frac{\partial u}{\partial x} = 0, \; N_{xx}^{(1)}\left(\frac{\partial w}{\partial x} + \frac{dw_0}{dx} \right) = 0 \text{ or } \frac{\partial w}{\partial x} = 0, \; M_{xx}^{(1)} = 0 \text{ or } \frac{\partial^2 w}{\partial x^2} = 0, \tag{8b}$$

where

$$\left\{ \begin{matrix} N_{xx}^{(1)} \\ M_{xx}^{(1)} \end{matrix} \right\} = \int_A \left\{ \begin{matrix} 1 \\ z \end{matrix} \right\} \sigma_{xx}^{(1)} dA. \tag{9}$$

Using the relations of stress resultants (i.e., Eq. (3)) and the above differential equations (i.e., Eq. (7)), the following explicit relations are obtained

$$N_{xx} = EA\left(1 - l_{sg}^2 \nabla^2\right)\left[\frac{\partial u}{\partial x} + \frac{1}{2}\left(\frac{\partial w}{\partial x} \right)^2 + \frac{\partial w}{\partial x}\frac{dw_0}{dx} \right] + m(e_0 a)^2 \frac{\partial^3 u}{\partial x \partial t^2}, \tag{10a}$$

$$\begin{aligned} M_{xx} &= -EI\left(1 - l_{sg}^2 \nabla^2\right)\frac{\partial^2 w}{\partial x^2} + m(e_0 a)^2 \frac{\partial^2 w}{\partial t^2} \\ &\quad - (e_0 a)^2 F(x)\cos(\omega t) - (e_0 a)^2 \frac{\partial}{\partial x}\left[N_{xx}\left(\frac{\partial w}{\partial x} + \frac{dw_0}{dx} \right) \right]. \end{aligned} \tag{10b}$$

Substituting Eq. (10) into Eq. (7) leads to the following NSGT-based coupled nonlinear equations for the geometrically imperfect nanoscale tube

$$\begin{aligned} EA&\left[\frac{\partial^2 u}{\partial x^2} + \frac{\partial w}{\partial x}\frac{\partial^2 w}{\partial x^2} + \frac{\partial^2 w}{\partial x^2}\frac{dw_0}{dx} + \frac{\partial w}{\partial x}\frac{d^2 w_0}{dx^2} - l_{sg}^2\left(\frac{\partial^4 u}{\partial x^4} + 3\frac{\partial^2 w}{\partial x^2}\frac{\partial^3 w}{\partial x^3} + \frac{\partial w}{\partial x}\frac{\partial^4 w}{\partial x^4} \right.\right. \\ &\left.\left. + \frac{\partial^4 w}{\partial x^4}\frac{dw_0}{dx} + 3\frac{\partial^3 w}{\partial x^3}\frac{d^2 w_0}{dx^2} + 3\frac{\partial^2 w}{\partial x^2}\frac{d^3 w_0}{dx^3} + \frac{\partial w}{\partial x}\frac{d^4 w_0}{dx^4} \right) \right] = m\frac{\partial^2 u}{\partial t^2} - m(e_0 a)^2 \frac{\partial^4 u}{\partial x^2 \partial t^2}, \end{aligned} \tag{11}$$

$$\begin{aligned} EI&\left(l_{sg}^2 \frac{\partial^6 w}{\partial x^6} - \frac{\partial^4 w}{\partial x^4} \right) + EA\left[\frac{\partial^2 w}{\partial x^2} + \frac{d^2 w_0}{dx^2} - (e_0 a)^2\left(\frac{\partial^4 w}{\partial x^4} + \frac{d^4 w_0}{dx^4} \right) \right]\left[\frac{\partial u}{\partial x} + \frac{1}{2}\left(\frac{\partial w}{\partial x} \right)^2 + \frac{\partial w}{\partial x}\frac{dw_0}{dx} \right] \\ &+ EA\left[\frac{\partial w}{\partial x} + \frac{dw_0}{dx} - 3(e_0 a)^2\left(\frac{\partial^3 w}{\partial x^3} + \frac{d^3 w_0}{dx^3} \right) \right]\left(\frac{\partial^2 u}{\partial x^2} + \frac{\partial w}{\partial x}\frac{\partial^2 w}{\partial x^2} + \frac{\partial^2 w}{\partial x^2}\frac{dw_0}{dx} + \frac{\partial w}{\partial x}\frac{d^2 w_0}{dx^2} \right) \\ &- EA\left\{ \left[l_{sg}^2 + 3(e_0 a)^2 \right]\left(\frac{\partial^2 w}{\partial x^2} + \frac{d^2 w_0}{dx^2} \right) - (e_0 a)^2 l_{sg}^2\left(\frac{\partial^4 w}{\partial x^4} + \frac{d^4 w_0}{dx^4} \right) \right\} \\ &\times \left[\frac{\partial^3 u}{\partial x^3} + \left(\frac{\partial^2 w}{\partial x^2} \right)^2 + \frac{\partial w}{\partial x}\frac{\partial^3 w}{\partial x^3} + \frac{\partial^3 w}{\partial x^3}\frac{dw_0}{dx} + 2\frac{\partial^2 w}{\partial x^2}\frac{d^2 w_0}{dx^2} + \frac{\partial w}{\partial x}\frac{d^3 w_0}{dx^3} \right] \\ &- EA\left\{ \left[l_{sg}^2 + (e_0 a)^2 \right]\left(\frac{\partial w}{\partial x} + \frac{dw_0}{dx} \right) - 3(e_0 a)^2 l_{sg}^2\left(\frac{\partial^3 w}{\partial x^3} + \frac{d^3 w_0}{dx^3} \right) \right\} \\ &\times \left(\frac{\partial^4 u}{\partial x^4} + 3\frac{\partial^2 w}{\partial x^2}\frac{\partial^3 w}{\partial x^3} + \frac{\partial w}{\partial x}\frac{\partial^4 w}{\partial x^4} + \frac{\partial^4 w}{\partial x^4}\frac{dw_0}{dx} + 3\frac{\partial^3 w}{\partial x^3}\frac{d^2 w_0}{dx^2} + 3\frac{\partial^2 w}{\partial x^2}\frac{d^3 w_0}{dx^3} + \frac{\partial w}{\partial x}\frac{d^4 w_0}{dx^4} \right) \\ &+ 3EAl_{sg}^2 (e_0 a)^2\left(\frac{\partial^2 w}{\partial x^2} + \frac{d^2 w_0}{dx^2} \right)\left[\frac{\partial^5 u}{\partial x^5} + 3\left(\frac{\partial^3 w}{\partial x^3} \right)^2 + 4\frac{\partial^2 w}{\partial x^2}\frac{\partial^4 w}{\partial x^4} + \frac{\partial w}{\partial x}\frac{\partial^5 w}{\partial x^5} + \frac{\partial^5 w}{\partial x^5}\frac{dw_0}{dx} \right. \\ &\left. + 4\frac{\partial^4 w}{\partial x^4}\frac{d^2 w_0}{dx^2} + 6\frac{\partial^3 w}{\partial x^3}\frac{d^3 w_0}{dx^3} + 4\frac{\partial^2 w}{\partial x^2}\frac{d^4 w_0}{dx^4} + \frac{\partial w}{\partial x}\frac{d^5 w_0}{dx^5} \right] \\ &+ EAl_{sg}^2 (e_0 a)^2\left(\frac{\partial w}{\partial x} + \frac{dw_0}{dx} \right)\left(\frac{\partial^6 u}{\partial x^6} + 10\frac{\partial^3 w}{\partial x^3}\frac{\partial^4 w}{\partial x^4} + 5\frac{\partial^2 w}{\partial x^2}\frac{\partial^5 w}{\partial x^5} + \frac{\partial w}{\partial x}\frac{\partial^6 w}{\partial x^6} \right. \\ &\left. + \frac{\partial^6 w}{\partial x^6}\frac{dw_0}{dx} + 5\frac{\partial^5 w}{\partial x^5}\frac{d^2 w_0}{dx^2} + 10\frac{\partial^4 w}{\partial x^4}\frac{d^3 w_0}{dx^3} + 10\frac{\partial^3 w}{\partial x^3}\frac{d^4 w_0}{dx^4} + 5\frac{\partial^2 w}{\partial x^2}\frac{d^5 w_0}{dx^5} + \frac{\partial w}{\partial x}\frac{d^6 w_0}{dx^6} \right) \end{aligned} \tag{12}$$

$$- m(e_0a)^2 \left(\frac{\partial w}{\partial x} + \frac{d w_0}{dx} \right) \left[(e_0a)^2 \frac{\partial^6 u}{\partial x^4 \partial t^2} - \frac{\partial^4 u}{\partial x^2 \partial t^2} \right] - 3m(e_0a)^4 \left(\frac{\partial^3 w}{\partial x^3} + \frac{d^3 w_0}{dx^3} \right) \frac{\partial^4 u}{\partial x^2 \partial t^2}$$

$$- m(e_0a)^2 \left(\frac{\partial^2 w}{\partial x^2} + \frac{d^2 w_0}{dx^2} \right) \left[3(e_0a)^2 \frac{\partial^5 u}{\partial x^3 \partial t^2} - \frac{\partial^3 u}{\partial x \partial t^2} \right] - m(e_0a)^4 \left(\frac{\partial^4 w}{\partial x^4} + \frac{d^4 w_0}{dx^4} \right) \frac{\partial^3 u}{\partial x \partial t^2}$$

$$= m \frac{\partial^2 w}{\partial t^2} - m(e_0a)^2 \frac{\partial^4 w}{\partial x^2 \partial t^2} - F(x) \cos(\omega t) + (e_0a)^2 \frac{\partial^2}{\partial x^2} [F(x) \cos(\omega t)].$$

Assuming the amplitude of the harmonic loading as $F(x) = F_1$, and applying the following non-dimensional parameters to Eqs. (11) and (12)

$$x^* = \frac{x}{L}, u^* = \frac{u}{r}, w^* = \frac{w}{r}, w_0^* = \frac{w_0}{r}, \chi_{nl} = \frac{e_0a}{L}, \chi_{sg} = \frac{l_{sg}}{L},$$
$$\beta = \frac{L}{r}, r = \sqrt{\frac{I}{A}}, F_1^* = \frac{F_1 L^3}{EI}, t^* = \frac{t}{L^2} \sqrt{\frac{EI}{m}}, \Omega = \sqrt{\frac{L^4 m}{EI}} \omega, \tag{13}$$

one can obtain the non-dimensional equations of motions as

$$\beta \left[\beta \frac{\partial^2 u}{\partial x^2} + \frac{\partial w}{\partial x} \frac{\partial^2 w}{\partial x^2} + \frac{\partial^2 w}{\partial x^2} \frac{d w_0}{dx} + \frac{\partial w}{\partial x} \frac{d^2 w_0}{dx^2} - \chi_{sg}^2 \left(\beta \frac{\partial^4 u}{\partial x^4} + 3 \frac{\partial^2 w}{\partial x^2} \frac{\partial^3 w}{\partial x^3} + \frac{\partial w}{\partial x} \frac{\partial^4 w}{\partial x^4} \right. \right.$$
$$\left. \left. + \frac{\partial^4 w}{\partial x^4} \frac{d w_0}{dx} + 3 \frac{\partial^3 w}{\partial x^3} \frac{d^2 w_0}{dx^2} + 3 \frac{\partial^2 w}{\partial x^2} \frac{d^3 w_0}{dx^3} + \frac{\partial w}{\partial x} \frac{d^4 w_0}{dx^4} \right) \right] = \frac{\partial^2 u}{\partial t^2} - \chi_{nl}^2 \frac{\partial^4 u}{\partial x^2 \partial t^2}, \tag{14}$$

$$\chi_{sg}^2 \frac{\partial^6 w}{\partial x^6} - \frac{\partial^4 w}{\partial x^4} + \left[\frac{\partial^2 w}{\partial x^2} + \frac{d^2 w_0}{dx^2} - \chi_{nl}^2 \left(\frac{\partial^4 w}{\partial x^4} + \frac{d^4 w_0}{dx^4} \right) \right] \left[\beta \frac{\partial u}{\partial x} + \frac{1}{2} \left(\frac{\partial w}{\partial x} \right)^2 + \frac{\partial w}{\partial x} \frac{d w_0}{dx} \right]$$

$$+ \left[\frac{\partial w}{\partial x} + \frac{d w_0}{dx} - 3 \chi_{nl}^2 \left(\frac{\partial^3 w}{\partial x^3} + \frac{d^3 w_0}{dx^3} \right) \right] \left(\beta \frac{\partial^2 u}{\partial x^2} + \frac{\partial w}{\partial x} \frac{\partial^2 w}{\partial x^2} + \frac{\partial^2 w}{\partial x^2} \frac{d w_0}{dx} + \frac{\partial w}{\partial x} \frac{d^2 w_0}{dx^2} \right)$$

$$- \left[\left(\chi_{sg}^2 + 3 \chi_{nl}^2 \right) \left(\frac{\partial^2 w}{\partial x^2} + \frac{d^2 w_0}{dx^2} \right) - \chi_{nl}^2 \chi_{sg}^2 \left(\frac{\partial^4 w}{\partial x^4} + \frac{d^4 w_0}{dx^4} \right) \right]$$

$$\times \left[\beta \frac{\partial^3 u}{\partial x^3} + \left(\frac{\partial^2 w}{\partial x^2} \right)^2 + \frac{\partial w}{\partial x} \frac{\partial^3 w}{\partial x^3} + \frac{\partial^3 w}{\partial x^3} \frac{d w_0}{dx} + 2 \frac{\partial^2 w}{\partial x^2} \frac{d^2 w_0}{dx^2} + \frac{\partial w}{\partial x} \frac{d^3 w_0}{dx^3} \right]$$

$$- \left[\left(\chi_{sg}^2 + \chi_{nl}^2 \right) \left(\frac{\partial w}{\partial x} + \frac{d w_0}{dx} \right) - 3 \chi_{nl}^2 \chi_{sg}^2 \left(\frac{\partial^3 w}{\partial x^3} + \frac{d^3 w_0}{dx^3} \right) \right] \left(\beta \frac{\partial^4 u}{\partial x^4} + 3 \frac{\partial^2 w}{\partial x^2} \frac{\partial^3 w}{\partial x^3} \right.$$

$$\left. + \frac{\partial w}{\partial x} \frac{\partial^4 w}{\partial x^4} + \frac{\partial^4 w}{\partial x^4} \frac{d w_0}{dx} + 3 \frac{\partial^3 w}{\partial x^3} \frac{d^2 w_0}{dx^2} + 3 \frac{\partial^2 w}{\partial x^2} \frac{d^3 w_0}{dx^3} + \frac{\partial w}{\partial x} \frac{d^4 w_0}{dx^4} \right)$$

$$+ 3 \chi_{nl}^2 \chi_{sg}^2 \left(\frac{\partial^2 w}{\partial x^2} + \frac{d^2 w_0}{dx^2} \right) \left[\beta \frac{\partial^5 u}{\partial x^5} + 3 \left(\frac{\partial^3 w}{\partial x^3} \right)^2 + 4 \frac{\partial^2 w}{\partial x^2} \frac{\partial^4 w}{\partial x^4} + \frac{\partial w}{\partial x} \frac{\partial^5 w}{\partial x^5} + \frac{\partial^5 w}{\partial x^5} \frac{d w_0}{dx} \right.$$

$$\left. + 4 \frac{\partial^4 w}{\partial x^4} \frac{d^2 w_0}{dx^2} + 6 \frac{\partial^3 w}{\partial x^3} \frac{d^3 w_0}{dx^3} + 4 \frac{\partial^2 w}{\partial x^2} \frac{d^4 w_0}{dx^4} + \frac{\partial w}{\partial x} \frac{d^5 w_0}{dx^5} \right]$$

$$+ \chi_{nl}^2 \chi_{sg}^2 \left(\frac{\partial w}{\partial x} + \frac{d w_0}{dx} \right) \left(\beta \frac{\partial^6 u}{\partial x^6} + 10 \frac{\partial^3 w}{\partial x^3} \frac{\partial^4 w}{\partial x^4} + 5 \frac{\partial^2 w}{\partial x^2} \frac{\partial^5 w}{\partial x^5} + \frac{\partial w}{\partial x} \frac{\partial^6 w}{\partial x^6} + \frac{\partial^6 w}{\partial x^6} \frac{d w_0}{dx} \right.$$

$$\left. + 5 \frac{\partial^5 w}{\partial x^5} \frac{d^2 w_0}{dx^2} + 10 \frac{\partial^4 w}{\partial x^4} \frac{d^3 w_0}{dx^3} + 10 \frac{\partial^3 w}{\partial x^3} \frac{d^4 w_0}{dx^4} + 5 \frac{\partial^2 w}{\partial x^2} \frac{d^5 w_0}{dx^5} + \frac{\partial w}{\partial x} \frac{d^6 w_0}{dx^6} \right)$$

$$- \frac{\chi_{nl}^2}{\beta} \left(\frac{\partial w}{\partial x} + \frac{d w_0}{dx} \right) \left(\chi_{nl}^2 \frac{\partial^6 u}{\partial x^4 \partial t^2} - \frac{\partial^4 u}{\partial x^2 \partial t^2} \right) - 3 \frac{\chi_{nl}^4}{\beta} \left(\frac{\partial^3 w}{\partial x^3} + \frac{d^3 w_0}{dx^3} \right) \frac{\partial^4 u}{\partial x^2 \partial t^2}$$

$$- \frac{\chi_{nl}^2}{\beta} \left(\frac{\partial^2 w}{\partial x^2} + \frac{d^2 w_0}{dx^2} \right) \left(3 \chi_{nl}^2 \frac{\partial^5 u}{\partial x^3 \partial t^2} - \frac{\partial^3 u}{\partial x \partial t^2} \right) - \frac{\chi_{nl}^4}{\beta} \left(\frac{\partial^4 w}{\partial x^4} + \frac{d^4 w_0}{dx^4} \right) \frac{\partial^3 u}{\partial x \partial t^2}$$

$$= \frac{\partial^2 w}{\partial t^2} - \chi_{nl}^2 \frac{\partial^4 w}{\partial x^2 \partial t^2} - F_1 \beta \cos(\Omega t). \tag{15}$$

Here asterisk superscripts are neglected for convenience purposes. β, r, χ_{nl} and χ_{sg} stand for the slenderness ratio, the gyration radius, the nonlocal coefficient and the strain gradient coefficient, respectively. Furthermore, Ω represents the non-dimensional harmonic excitation frequency. In order to obtain a numerical solution for Eqs. (14) and (15), first Galerkin's procedure [58–61] as a discretisation method is utilised [66–69]. In this way, the longitudinal and transverse displacements are as

$$u(x,t) = \sum_{j=1}^{N_x} r_j(t) \hat{u}_j(x), \tag{16a}$$

$$w(x,t) = \sum_{j=1}^{N_z} q_j(t) \hat{w}_j(x), \tag{16b}$$

where N_x and N_z denote the number of shape functions along the x and z axes, respectively; r_j and $\hat{u}_j$ represent the axial generalized coordinate and the axial shape function of the imperfect nanotube; also, q_j and $\hat{w}_j$ stand for the transverse generalized coordinate and the transverse shape function, respectively. Let us consider a geometric imperfection as $w_0 = A_0 \hat{w}_1(x)$ for the nanotube; A_0 indicates the imperfection amplitude. Assuming

clamped-clamped (C–C) boundary conditions for the tube, the appropriate shape functions are

$$\begin{Bmatrix} \hat{w}_j(x) \\ \hat{u}_j(x) \end{Bmatrix} = \begin{Bmatrix} -\left[\dfrac{\cosh\lambda_j - \cos\lambda_j}{\sinh\lambda_j - \sin\lambda_j}\right]\left[\sinh(\lambda_j x) - \sin(\lambda_j x)\right] + \cosh(\lambda_j x) - \cos(\lambda_j x) \\ \sin(j\pi x) \end{Bmatrix}, \tag{17}$$

in which λ_j stand for the jth root of the classical frequency equation for C–C beams. It is worth mentioning that $\hat{w}_1(x)$ is obtained from Eq. (17) when j is set to 1. Inserting Eq. (16) into Eqs. (14) and (15) and then applying the Galerkin discretisation technique, one obtains

$$\beta^2 \sum_{j=1}^{N_x} r_j \left(\int_0^1 \hat{u}_k \hat{u}_j'' dx\right) + \beta \sum_{j=1}^{N_z}\sum_{i=1}^{N_z} q_i q_j \left(\int_0^1 \hat{u}_k \hat{w}_i'' \hat{w}_j' dx\right) + \beta A_0 \sum_{j=1}^{N_z} q_j \left(\int_0^1 \hat{u}_k \hat{w}_j'' \hat{w}_1' dx\right)$$

$$+ \beta A_0 \sum_{j=1}^{N_z} q_j \left(\int_0^1 \hat{u}_k \hat{w}_j' \hat{w}_1'' dx\right) - \beta\chi_{sg}^2 \left[\beta \sum_{j=1}^{N_x} r_j \left(\int_0^1 \hat{u}_k \hat{u}_j'''' dx\right) + 3\sum_{i=1}^{N_z}\sum_{j=1}^{N_z} q_i q_j \left(\int_0^1 \hat{u}_k \hat{w}_i'' \hat{w}_j''' dx\right)\right.$$

$$+ \sum_{j=1}^{N_z}\sum_{i=1}^{N_z} q_i q_j \left(\int_0^1 \hat{u}_k \hat{w}_i' \hat{w}_j'''' dx\right) + A_0 \sum_{j=1}^{N_z} q_j \left(\int_0^1 \hat{u}_k \hat{w}_j'''' \hat{w}_1' dx\right) + 3A_0 \sum_{j=1}^{N_z} q_j \left(\int_0^1 \hat{u}_k \hat{w}_j''' \hat{w}_1'' dx\right) \tag{18}$$

$$\left. + 3A_0 \sum_{j=1}^{N_z} q_j \left(\int_0^1 \hat{u}_k \hat{w}_j'' \hat{w}_1''' dx\right) + A_0 \sum_{j=1}^{N_z} q_j \left(\int_0^1 \hat{u}_k \hat{w}_j' \hat{w}_1'''' dx\right)\right]$$

$$= \sum_{j=1}^{N_x} \ddot{r}_j \left(\int_0^1 \hat{u}_k \hat{u}_j dx\right) - \chi_{nl}^2 \sum_{j=1}^{N_x} \ddot{r}_j \left(\int_0^1 \hat{u}_k \hat{u}_j'' dx\right) \text{ for } k = 1, 2, \cdots N_x,$$

$$\int_0^1 \hat{w}_k \left[\chi_{sg}^2 \sum_{j=1}^{N_z} q_j \hat{w}_j^{(6)} - \sum_{j=1}^{N_z} q_j \hat{w}_j''''\right] dx$$

$$+ \int_0^1 \left\{\hat{w}_k \left[\sum_{j=1}^{N_z} q_j \hat{w}_j'' + A_0 \hat{w}_1'' - \chi_{nl}^2 \left(\sum_{j=1}^{N_z} q_j \hat{w}_j'''' + A_0 \hat{w}_1''''\right)\right]\right.$$

$$\left. \times \left[\beta \sum_{j=1}^{N_x} r_j \hat{u}_j' + \frac{1}{2}\sum_{i=1}^{N_z}\sum_{j=1}^{N_z} q_i q_j \hat{w}_i' \hat{w}_j' + A_0 \sum_{j=1}^{N_z} q_j \hat{w}_j' \hat{w}_1'\right] dx\right\}$$

$$+ \int_0^1 \left\{\hat{w}_k \left[\sum_{j=1}^{N_z} q_j \hat{w}_j' + A_0 \hat{w}_1' - 3\chi_{nl}^2 \left(\sum_{j=1}^{N_z} q_j \hat{w}_j''' + A_0 \hat{w}_1'''\right)\right]\right.$$

$$\left. \times \left(\beta \sum_{j=1}^{N_x} r_j \hat{u}_j'' + \sum_{i=1}^{N_z}\sum_{j=1}^{N_z} q_i q_j \hat{w}_j'' \hat{w}_i' + A_0 \sum_{j=1}^{N_z} q_j \left(\hat{w}_1' \hat{w}_j'' + \hat{w}_1'' \hat{w}_j'\right)\right) dx\right\}$$

$$- \int_0^1 \left\{\hat{w}_k \left[\left(\chi_{sg}^2 + 3\chi_{nl}^2\right)\left(\sum_{j=1}^{N_z} q_j \hat{w}_j'' + A_0 \hat{w}_1''\right) - \chi_{nl}^2 \chi_{sg}^2 \left(\sum_{j=1}^{N_z} q_j \hat{w}_j'''' + A_0 \hat{w}_1''''\right)\right]\right.$$

$$\left. \times \left[\beta \sum_{j=1}^{N_x} r_j \hat{u}_j''' + \sum_{i=1}^{N_z}\sum_{j=1}^{N_z} q_i q_j \left(\hat{w}_j'' \hat{w}_i'' + \hat{w}_j''' \hat{w}_i'\right) + A_0 \sum_{j=1}^{N_z} q_j \left(\hat{w}_j''' \hat{w}_1' + 2\hat{w}_j'' \hat{w}_1'' + \hat{w}_j' \hat{w}_1'''\right)\right] dx\right\}$$

$$- \int_0^1 \left\{\hat{w}_k \left[\left(\chi_{sg}^2 + \chi_{nl}^2\right)\left(\sum_{j=1}^{N_z} q_j \hat{w}_j' + A_0 \hat{w}_1'\right) - 3\chi_{nl}^2 \chi_{sg}^2 \left(\sum_{j=1}^{N_z} q_j \hat{w}_j''' + A_0 \hat{w}_1'''\right)\right]\left[\beta \sum_{j=1}^{N_x} r_j \hat{u}_j''''\right.\right.$$

$$\left.\left. + \sum_{i=1}^{N_z}\sum_{j=1}^{N_z} q_i q_j \left(3\hat{w}_j''' \hat{w}_i'' + \hat{w}_i' \hat{w}_j''''\right) + A_0 \sum_{j=1}^{N_z} q_j \left(\hat{w}_j'''' \hat{w}_1' + 3\hat{w}_j''' \hat{w}_1'' + 3\hat{w}_j'' \hat{w}_1''' + \hat{w}_j' \hat{w}_1''''\right)\right] dx\right\} \tag{19}$$

$$+ 3\chi_{nl}^2 \chi_{sg}^2 \int_0^1 \left\{\hat{w}_k \left(\sum_{j=1}^{N_z} q_j \hat{w}_j'' + A_0 \hat{w}_1''\right)\left[\beta \sum_{j=1}^{N_x} r_j \hat{u}_j^{(5)} + \sum_{i=1}^{N_z}\sum_{j=1}^{N_z} q_i q_j \left(3\hat{w}_i''' \hat{w}_j''' + 4\hat{w}_i'' \hat{w}_j'''' + \hat{w}_i' \hat{w}_j^{(5)}\right)\right.\right.$$

$$\left.\left. + A_0 \sum_{j=1}^{N_z} q_j \left(\hat{w}_j^{(5)} \hat{w}_1' + 4\hat{w}_j'''' \hat{w}_1'' + 6\hat{w}_j''' \hat{w}_1''' + 4\hat{w}_j'' \hat{w}_1'''' + \hat{w}_j' \hat{w}_1^{(5)}\right)\right] dx\right\}$$

$$+ \chi_{nl}^2 \chi_{sg}^2 \int_0^1 \left\{\hat{w}_k \left(\sum_{j=1}^{N_z} q_j \hat{w}_j' + A_0 \hat{w}_1'\right)\left[\beta \sum_{j=1}^{N_x} r_j \hat{u}_j^{(6)} + \sum_{i=1}^{N_z}\sum_{j=1}^{N_z} q_i q_j \left(10\hat{w}_i''' \hat{w}_j'''' + 5\hat{w}_i'' \hat{w}_j^{(5)} + \hat{w}_i' \hat{w}_j^{(6)}\right)\right.\right.$$

$$\left.\left. + A_0 \sum_{j=1}^{N_z} q_j \left(\hat{w}_1' \hat{w}_j^{(6)} + 5\hat{w}_j^{(5)} \hat{w}_1'' + 10\hat{w}_j'''' \hat{w}_1''' + 10\hat{w}_j''' \hat{w}_1'''' + 5\hat{w}_j'' \hat{w}_1^{(5)} + \hat{w}_j' \hat{w}_1^{(6)}\right)\right] dx\right\}$$

$$- \frac{\chi_{nl}^2}{\beta} \int_0^1 \hat{w}_k \left[\left(\sum_{j=1}^{N_z} q_j \hat{w}_j' + A_0 \hat{w}_1'\right)\sum_{j=1}^{N_x} \ddot{r}_j \left(\chi_{nl}^2 \hat{u}_j'''' - \hat{u}_j''\right) + 3\chi_{nl}^2 \left(\sum_{j=1}^{N_z} q_j \hat{w}_j''' + A_0 \hat{w}_1'''\right)\sum_{j=1}^{N_x} \ddot{r}_j \hat{u}_j''\right] dx$$

$$- \frac{\chi_{nl}^2}{\beta} \int_0^1 \hat{w}_k \left(\sum_{j=1}^{N_z} q_j \hat{w}_j'' + A_0 \hat{w}_1''\right)\left(3\chi_{nl}^2 \sum_{j=1}^{N_x} \ddot{r}_j \hat{u}_j''' - \sum_{j=1}^{N_x} \ddot{r}_j \hat{u}_j'\right) dx$$

$$- \frac{\chi_{nl}^4}{\beta} \int_0^1 \left[\hat{w}_k \left(\sum_{j=1}^{N_z} q_j \hat{w}_j'''' + A_0 \hat{w}_1''''\right)\sum_{j=1}^{N_x} \ddot{r}_j \hat{u}_j'\right] dx$$

$$= \int_0^1 \hat{w}_k \left(\sum_{j=1}^{N_z} \ddot{q}_j \hat{w}_j - \chi_{nl}^2 \sum_{j=1}^{N_z} \ddot{q}_j \hat{w}_j''\right) dx - \left(\int_0^1 \hat{w}_k dx\right) F_1 \beta \cos(\Omega t) \text{ for } k = 1, 2, \cdots N_x.$$
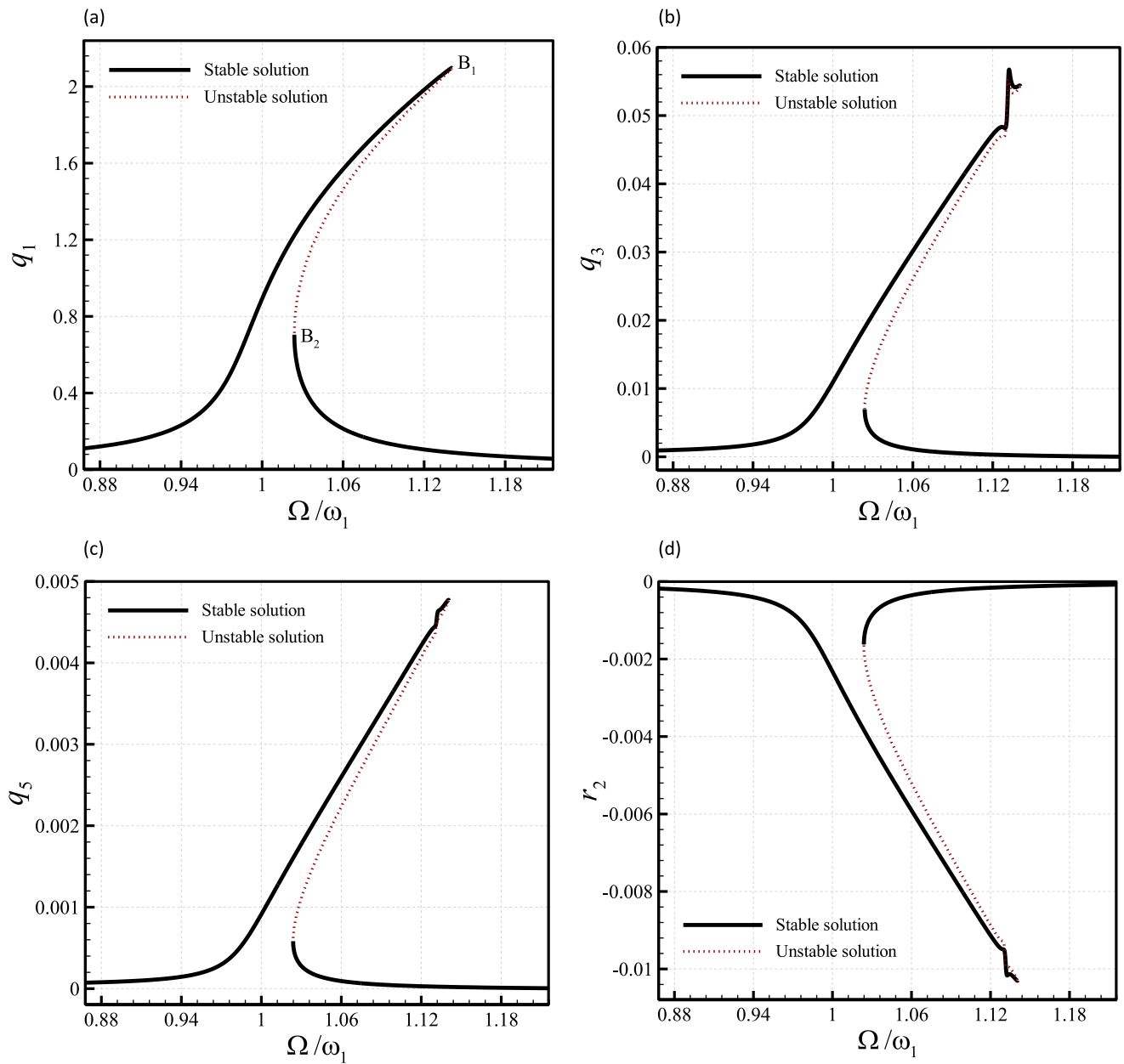
Fig. 2. Frequency-amplitude plots of the geometrically imperfect nanotube; (a–c) the maximum of q_1, q_2, and q_3, respectively; (d) the minimum of r_2; for non-zero χ_{sg} and $A_0 = 0.8$.
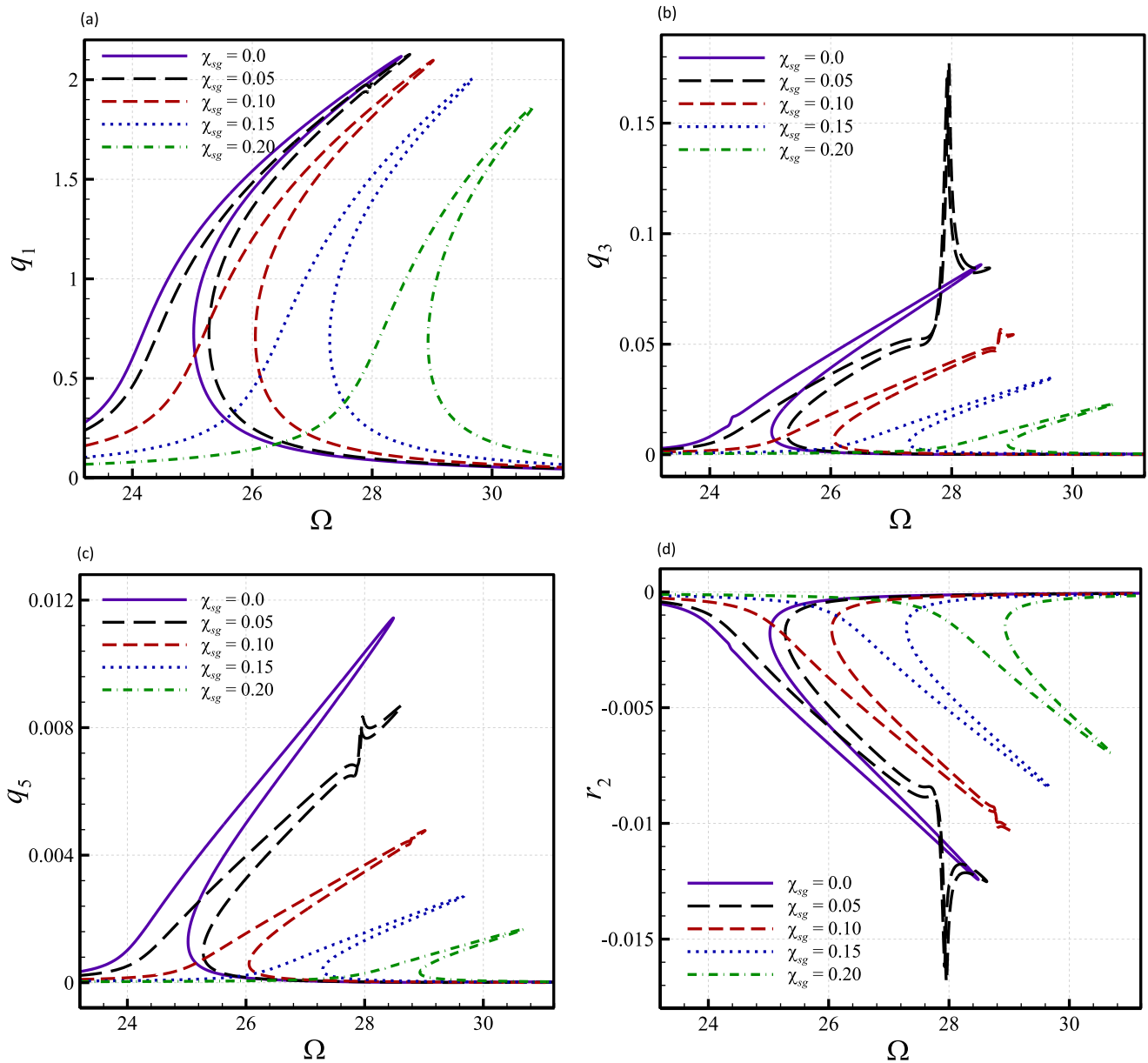
Fig. 3. Strain gradient effects on frequency-amplitude plots of the geometrically imperfect nanotube; (a–c) the maximum of q_1, q_2, and q_3, respectively; (d) the minimum of r_2 for $A_0 = 0.8$.
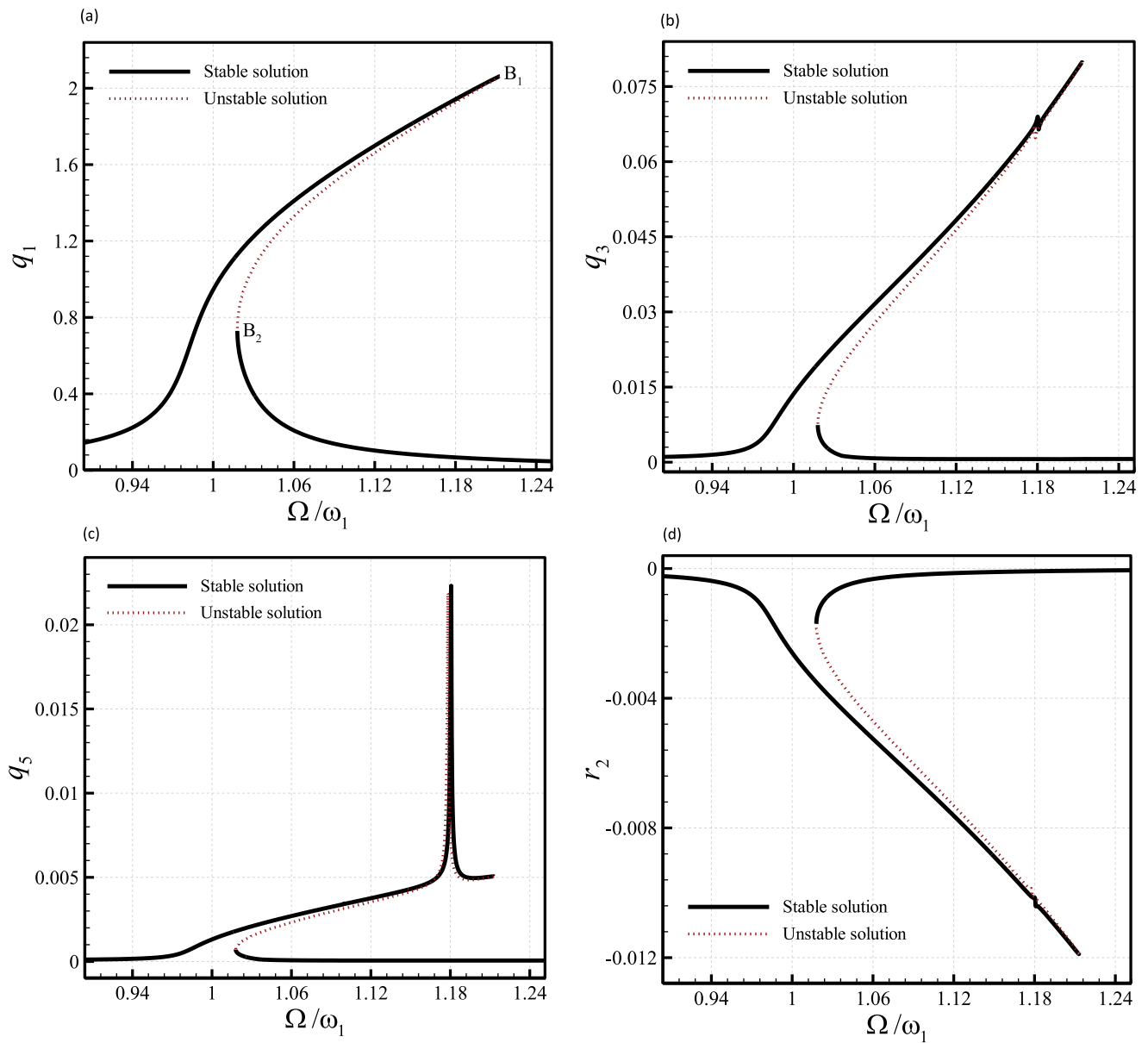
Fig. 4. Frequency-amplitude plots of the geometrically imperfect nanotube; (a–c) the maximum of q_1, q_2, and q_3, respectively; (d) the minimum of r_2 for non-zero χ_{nl} and $A_0 = 0.8$.
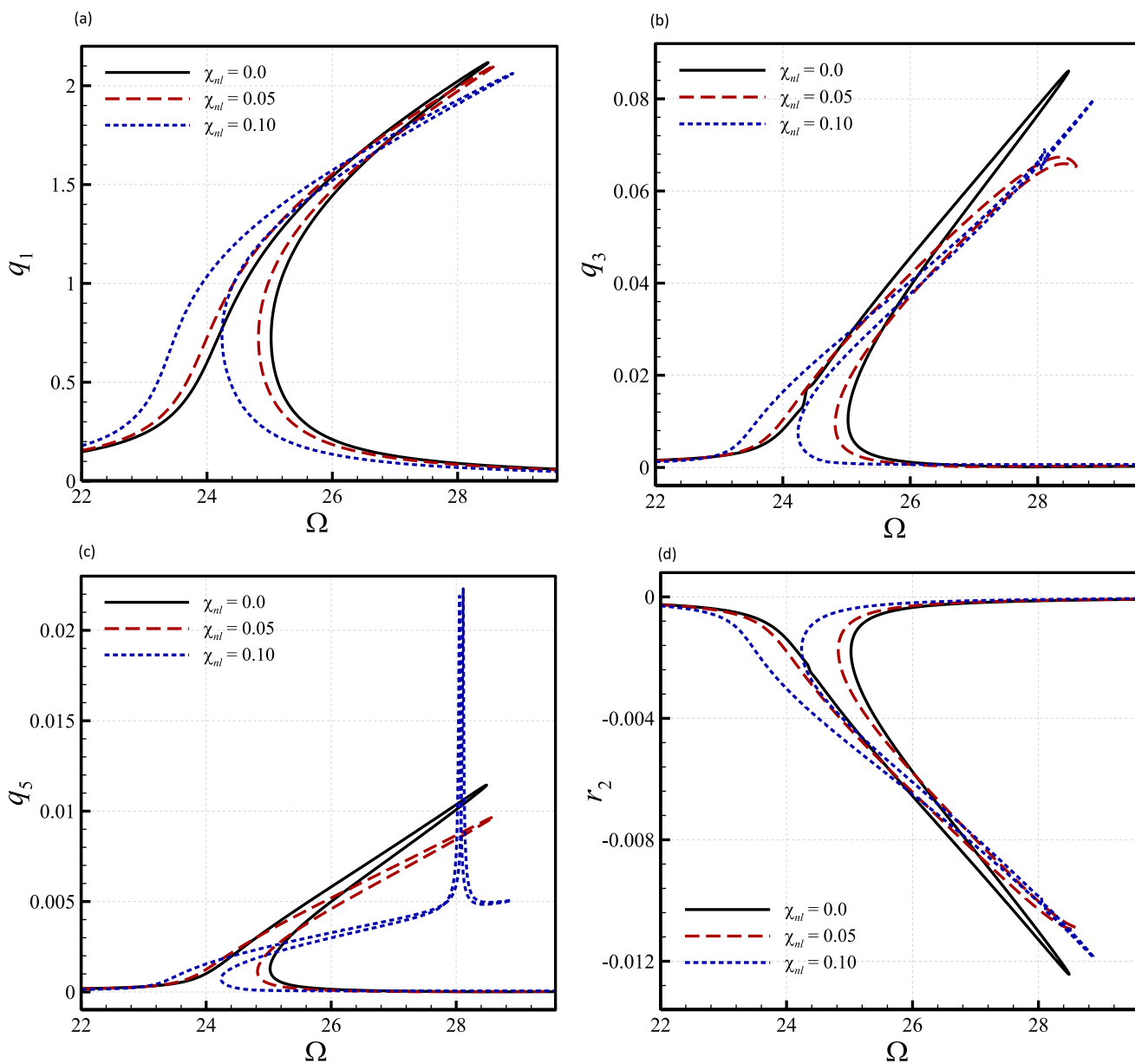
Fig. 5. Nonlocal effects on frequency-amplitude plots of the geometrically imperfect nanotube; (a–c) the maximum of q_1, q_2, and q_3, respectively; (d) the minimum of r_2 for $A_0 = 0.8$.
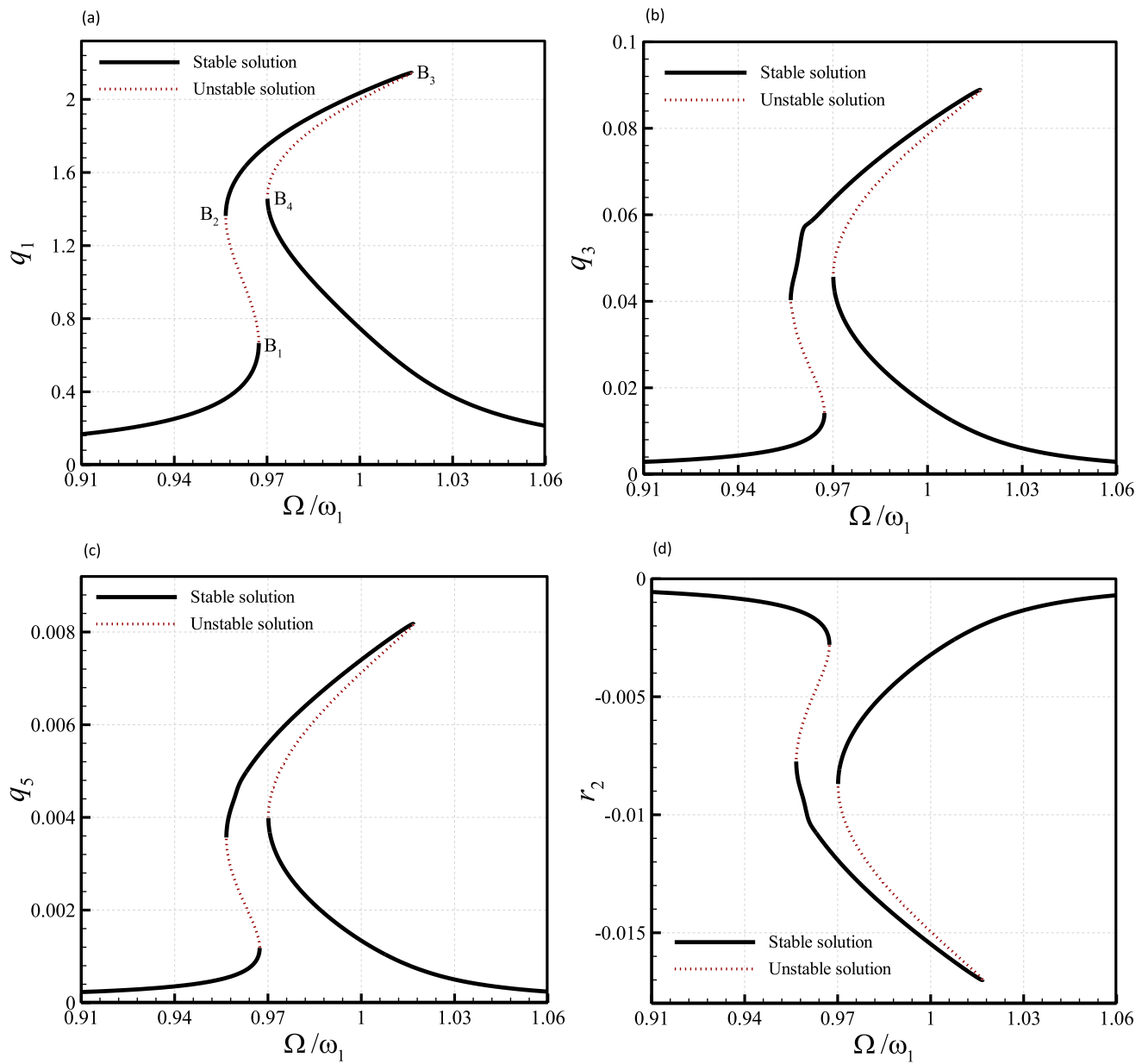
Fig. 6. Frequency-amplitude plots of the geometrically imperfect nanotube; (a–c) the maximum of q_1, q_2, and q_3, respectively; (d) the minimum of r_2 for non-zero χ_{sg} and $A_0 = 1.5$.
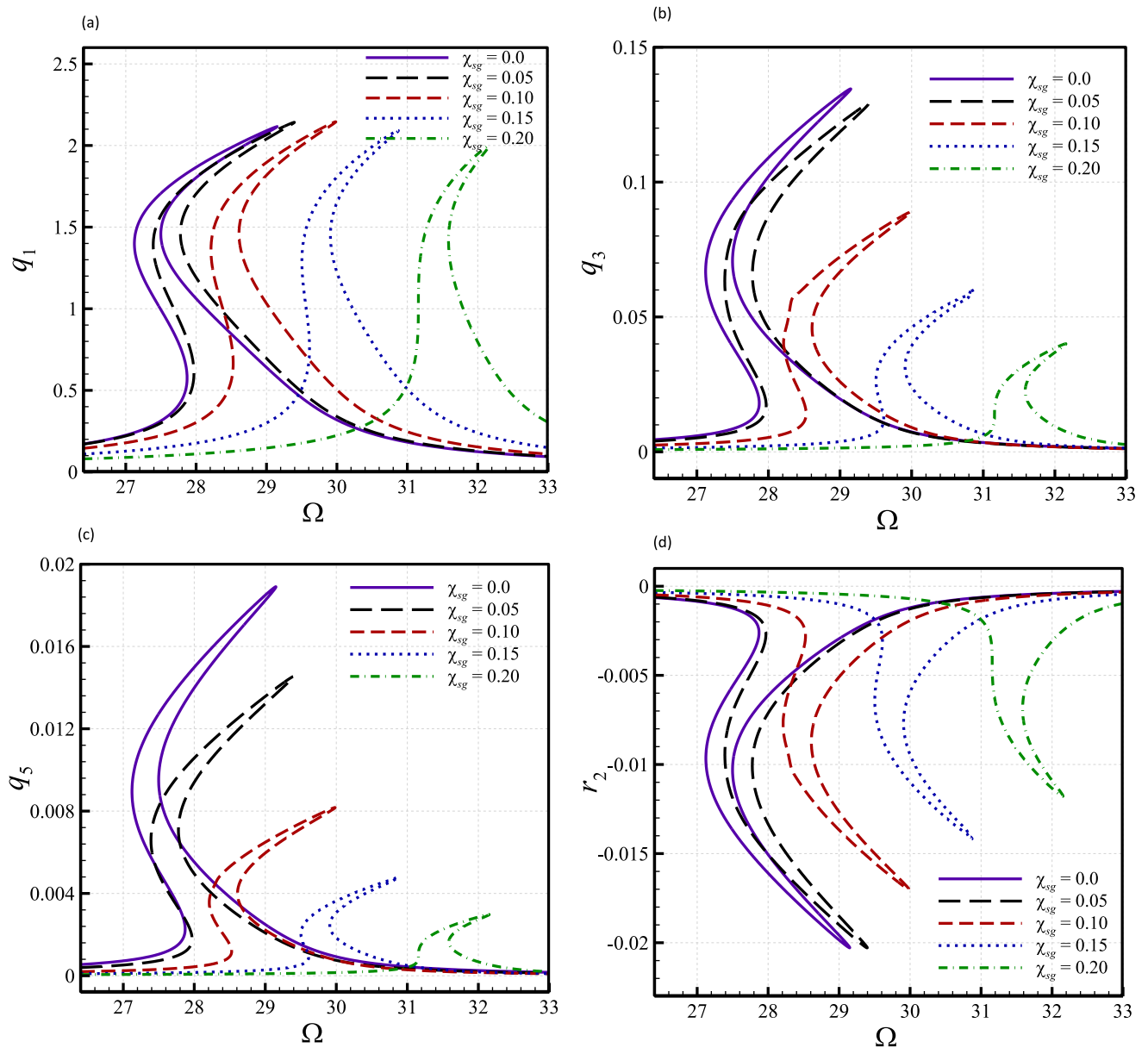
Fig. 7. Strain gradient effects on frequency-amplitude plots of the geometrically imperfect nanotube; (a–c) the maximum of q_1, q_2, and q_3, respectively; (d) the minimum of r_2 for $A_0 = 1.5$.

Fig. 8. Frequency-amplitude plots of the geometrically imperfect nanotube; (a–c) the maximum of q_1, q_2, and q_3, respectively; (d) the minimum of r_2 for non-zero χ_{nl} and $A_0 = 1.5$.

Fig. 9. Nonlocal effects on frequency-amplitude plots of the geometrically imperfect nanotube; (a–c) the maximum of q_1, q_2, and q_3, respectively; (d) the minimum of r_2 for $A_0 = 1.5$.
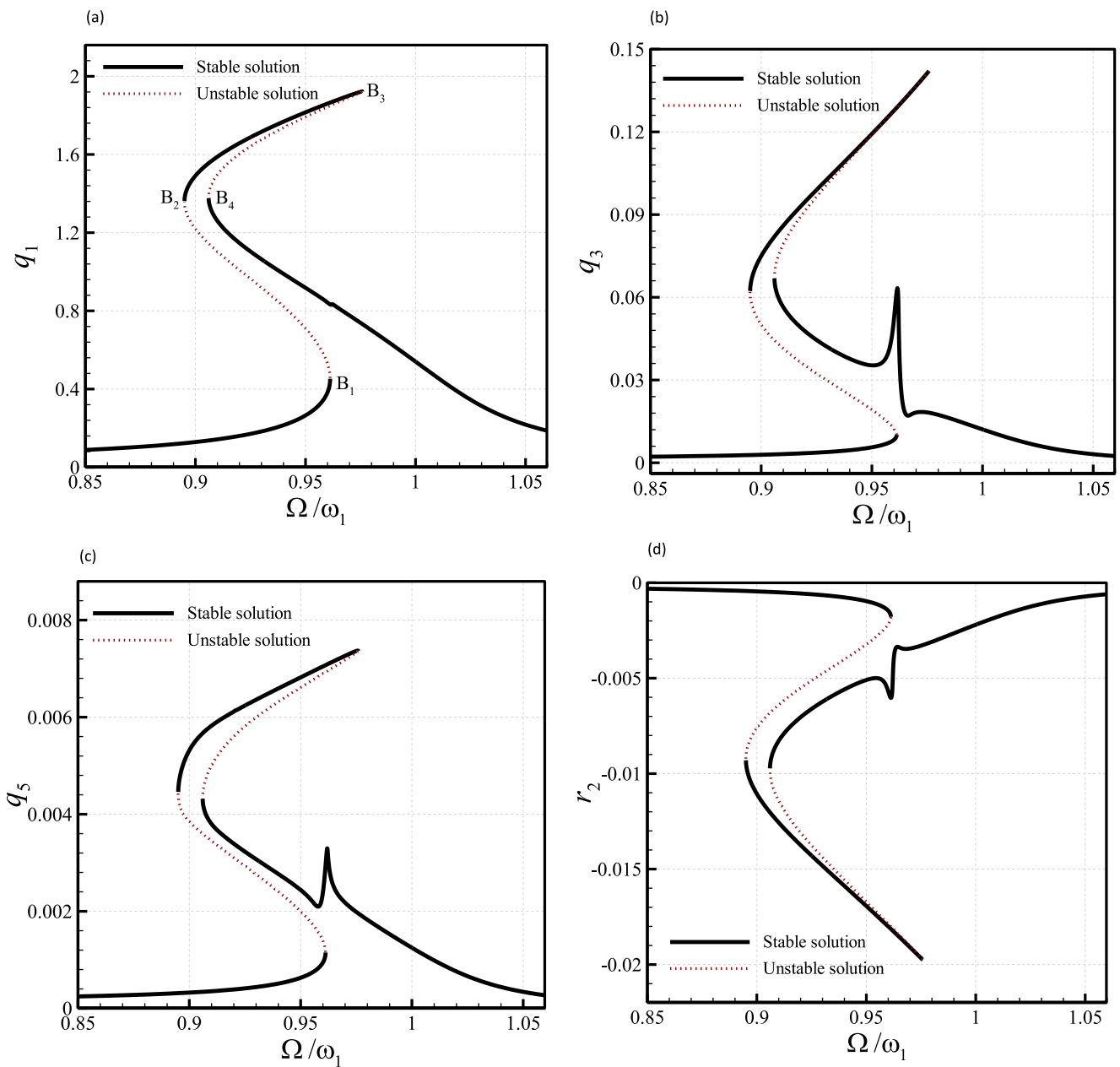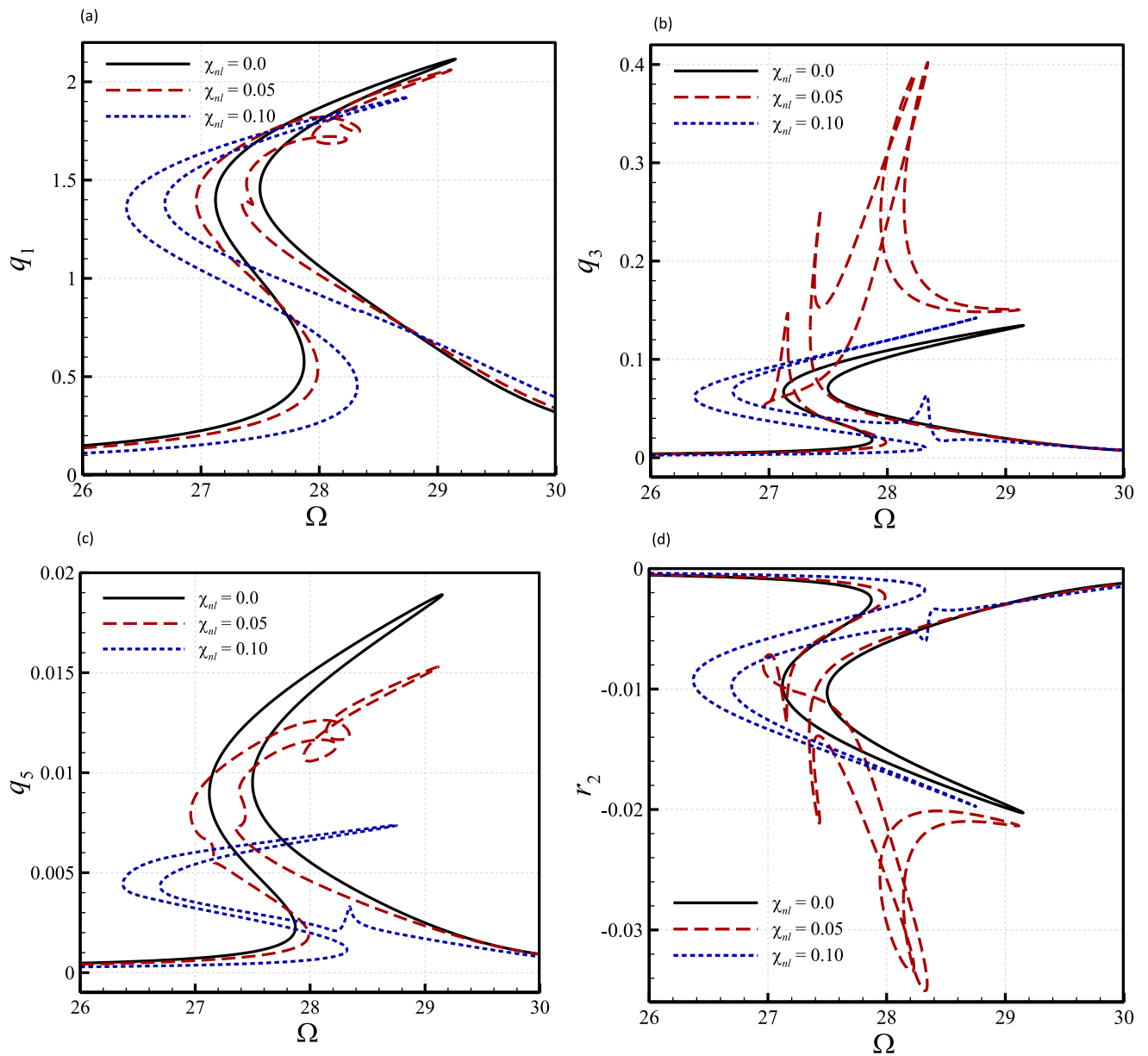
To determine the large-amplitude mechanical characteristics [70–79] of geometrically imperfect nanotubes subject to a harmonic loading, a numerical scheme in the context of a continuation-based technique is employed [62,63]. In the present nonlinear analysis, a convergence test is carried out, indicating that eight base functions for each displacement component are sufficient to meet the requirement of calculation precision [80–84]. In general, a system of sixteen base functions is considered (eight base functions for u and eight base functions for w).

3. Numerical results

The influence of a geometric imperfection together with other parameters such as the nonlocal and strain gradient coefficients on the large-amplitude mechanical behaviour of nanoscale tubes is studied in this section. Let us consider an imperfect nanoscale tube of length 100 nm. The material properties are taken as $E = 1.0$ TPa, $v = 0.19$, and $\rho = 2300$ kg/m^3. The outer and inner radii of the tube are, respectively, assumed as 0.84 and 0.5 nm. The slenderness ratio is determined as $\beta = 204.5935$. In the nonlinear analysis, the modal damping ratio is chosen as $\zeta = 0.005$.

The variation of the maximum values of some transverse generalised coordinates as well as the minimum value of the second axial generalised coordinate versus the excitation-to-natural frequency ratio (excitation frequency ratio) is shown in Fig. 2. The values of the strain gradient and nonlocal coefficients are, respectively, taken as $\chi_{sg} = 0.1$ and $\chi_{nl} = 0$. The force and imperfection amplitudes are assumed as $F_1 = 0.1$ and $A_0 = 0.8$, respectively. A hardening-type nonlinearity with two saddle points (B_1 and B_2) is found for the geometrically imperfect nanoscale tube. As the excitation frequency ratio increases, the maximum value of q_1 increases until point B_1 (the first saddle point) in which the nanotube experiences a dramatic jump to a lower value of the transverse amplitude. Decreasing the excitation frequency first increases the maximum value of q_1, and then at point B_2 (the second saddle point), the nanosystem displays a sudden increase followed by a gradual reduction in q_1. In addition, from Fig. 2, modal interactions [64] around the first saddle point are clearly observed for higher generalised coordinates.

Fig. 3 illustrates the effect of χ_{sg} on the frequency-amplitude plots for imperfect nanoscale tubes. The force and imperfection amplitudes are taken as $F_1 = 0.1$ and $A_0 = 0.8$, respectively. The nonlocal effect is neglected in this figure (i.e., $\chi_{nl} = 0$). The resonant frequency of the geometrically imperfect nanotube is higher when higher values are chosen for the strain gradient coefficient. Nonetheless, the peak amplitude of the imperfect nanosystem is lower for higher values of χ_{sg}. In addition, strong modal interactions are observed, especially for higher generalised coordinates, when the strain gradient coefficient is set to $\chi_{sg} = 0.05$. However, increasing the strain gradient effect can gradually eliminates the modal interactions.

The variation of some transverse and axial generalised coordinates of the imperfect nanoscale tube versus the excitation frequency ratio is depicted in Fig. 4; but this time, only the nonlocal effect is incorporated. The imperfection and force amplitudes are the same as those of Fig. 2. A nonlocal coefficient of 0.1 is selected for the nanotube while the strain gradient coefficient is zero. Again, a hardening-type nonlinearity with two saddle points is observed for geometrically imperfect nanotubes. However, stronger modal interactions are seen in Fig. 4 in comparison with those of Fig. 2, especially for the fifth generalised coordinate along the transverse direction. It means that the modal interaction may be overestimated when only the nonlocal effect is taken into consideration.

Fig. 5 depicts the influence of χ_{nl} on the frequency-amplitude plots of imperfect nanoscale tubes. The strain gradient coefficient is set to zero. A value of 0.8 is chosen for the non-dimensional imperfection amplitude while the dimensionless force amplitude is $F_1 = 0.1$. It is found that imperfect nanotubes with higher nonlocal coefficients undergo resonance at lower excitation frequencies. Another interesting finding is that for
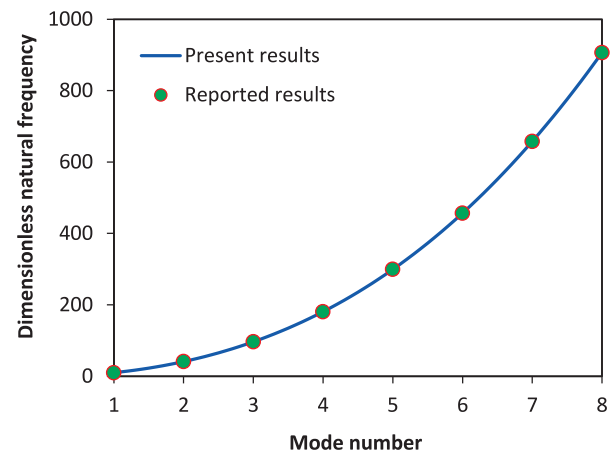

Fig. 10. Comparison of the present results with those reported in Ref. [53] for linear perfect NSGT nanobeams.

higher nonlocal effects, the imperfect nanotube exhibits strong modal interactions (see Fig. 5c).

The variation of maximum values of some transverse generalised coordinates and the minimum value of the second axial generalised coordinate of the nanotube versus the excitation frequency ratio is demonstrated in Fig. 6; a larger imperfection amplitude ($A_0 = 1.5$) is taken into account. A value of $F_1 = 0.14$ is taken for the force amplitude. The strain gradient coefficient is taken as $\chi_{sg} = 0.1$ while the nonlocal coefficient is assumed to be zero. A combination of softening and hardening nonlinearities with four saddle points is observed in this case. Initially, the nonlinear mechanical behaviour is of softening type which is followed by a hardening-type nonlinearity. The transverse amplitude of the imperfect nanotube increases gradually with increasing the excitation frequency ratio until point B_1 (the first saddle point) where it suddenly increases. Then, the transverse amplitude continuously increases until point B_3 (the third saddle point) in which the imperfect nanotube jumps to a lower transverse amplitude. By comparing Fig. 2 with Fig. 6, it can be concluded that a small increase in the imperfection amplitude can substantially change the nonlinear mechanical behaviour.

Fig. 7 shows the influence of χ_{sg} on the large-amplitude mechanical behaviour of geometrically imperfect nanoscale tubes. The nonlocal effect is not taken into account. The imperfection amplitude and the force amplitude are set to $A_0 = 1.5$, and $F_1 = 0.14$, respectively. Imperfect nanotubes with higher strain gradient coefficients undergo resonance at higher excitation frequencies. Moreover, higher values of the strain gradient coefficient reduces the peak amplitude of both the motions along the x and z axes.

The variation of the maximum values of some transverse generalised coordinates and the minimum value of the second axial generalised coordinate versus the excitation frequency ratio is depicted in Fig. 8; only the effect of the nonlocal coefficient is taken into consideration (i.e. $\chi_{sg} = 0.0$, $\chi_{nl} = 0.1$). The imperfection and force amplitudes are the same as those mentioned above for Fig. 6. It is observed that the nonlinear behaviour is still a combination of softening and hardening types with four saddle points. Increasing the excitation frequency ratio gradually increases q_1 until point B_1 where the value of the first transverse generalised coordinate suddenly increases. Then, the value of q_1 decreases with increasing Ω/ω_1. By comparing Figs. 6–8, it is seen that although the general nonlinear mechanical characteristics of the imperfect nanotube such as the number of saddle points remain the same, some details are different. Fig. 9 illustrates the influence of χ_{nl} on the frequency-amplitude plots of imperfect nanoscale tubes for $\chi_{sg} = 0.0$, $A_0 = 1.5$, and $f_1 = 0.14$. It is found that in this case, non-zero nonlocal coefficients are associated with strong modal interactions, especially for higher generalised coordinates.

4. Conclusions

A nonlinear analysis has been performed in order to investigate the effect of geometrical imperfection on the large-amplitude mechanical behaviour of nanoscale tube subject to transverse distributed harmonic loading. A NSGT-based model incorporating both nonlocal and strain gradient effects was proposed to better describe the size-dependent softening and hardening behaviors of the stiffness. The EBBT as well as the Hamilton principle were utilised for deriving the coupled nonlinear equations. Galerkin's procedure as well as a continuation-based approach were lastly used to discretise the differential equations and to determine the large-amplitude mechanical characteristics, respectively.

A geometrical imperfection can significantly change the nonlinear dynamic behaviour of nanoscale tubes. When the amplitude of the geometrical imperfection is low, the nanotube displays a hardening-type nonlinearity with two saddle points. However, when a large imperfection amplitude is taken into consideration, the nanotube displays a combination of softening and hardening nonlinearities with four saddle points. Higher strain gradient coefficients are associated with higher resonant frequencies. Furthermore, it was found that increasing the strain gradient coefficient can eliminate the modal interactions. On the other hand, higher nonlocal coefficients make the imperfect nanotube undergo resonances at lower excitation frequencies. The modal interaction is overestimated by incorporating only the nonlocal effect.

Appendix A. Verification study

To verify the present results, a linear NSGT nanotube without any geometrical imperfections is considered. For this nanotube, Eqs. (14) and (15) are reduced to only one motion equation along the transverse direction. In Fig. 10, the results are compared with those obtained by Li et al. [53] for the linear vibration of nanobeams employing the NSGT. The material and geometrical properties are given in Refs. [53,65]. A very good agreement is observed between the reported results and the available results in the literature.

References

[1] Wang Q, Wang C. The constitutive relation and small scale parameter of nonlocal continuum mechanics for modelling carbon nanotubes. Nanotechnology 2007;18:075702.

[2] Arash B, Wang Q. A review on the application of nonlocal elastic models in modeling of carbon nanotubes and graphenes. Comput Mater Sci 2012;51:303–13.

[3] Saadatnia Z, Esmailzadeh E. Nonlinear harmonic vibration analysis of fluid-conveying piezoelectric-layered nanotubes. Compos Part B Eng 2017;123:193–209.

[4] Gul U, Aydogdu M. Noncoaxial vibration and buckling analysis of embedded double-walled carbon nanotubes by using doublet mechanics. Compos Part B Eng 2018;137:60–73.

[5] Zhang Y, Liew K, Hui D. Characterizing nonlinear vibration behavior of bilayer graphene thin films. Compos Part B Eng 2018;145:197–205.

[6] Barretta R, Feo L, Luciano R, de Sciarra FM, Penna R. Functionally graded Timoshenko nanobeams: a novel nonlocal gradient formulation. Compos Part B Eng 2016;100:208–19.

[7] Romano G, Barretta R, Diaco M. On nonlocal integral models for elastic nano-beams. Int J Mech Sci 2017;131:490–9.

[8] Gholipour A, Farokhi H, Ghayesh MH. In-plane and out-of-plane nonlinear size-dependent dynamics of microplates. Nonlinear Dyn 2015;79:1771–85.

[9] Ghayesh MH, Amabili M, Farokhi H. Three-dimensional nonlinear size-dependent behaviour of Timoshenko microbeams. Int J Eng Sci 2013;71:1–14.

[10] Ghayesh MH, Farokhi H. Nonlinear dynamics of microplates. Int J Eng Sci 2015;86:60–73.

[11] Reddy J. Nonlocal theories for bending, buckling and vibration of beams. Int J Eng Sci 2007;45:288–307.

[12] Preethi K, Rajagopal A, Reddy JN. Surface and non-local effects for non-linear analysis of Timoshenko beams. Int J Nonlinear Mech 2015;76:100–11.

[13] Farajpour A, Rastgoo A, Mohammadi M. Vibration, buckling and smart control of microtubules using piezoelectric nanoshells under electric voltage in thermal environment. Phys B Condens Matter 2017;509:100–14.

[14] Farajpour MR, Shahidi A, Farajpour A. Resonant frequency tuning of nanobeams by piezoelectric nanowires under thermo-electro-magnetic field: a theoretical study. Micro Nano Lett 2018. doi:10.1049/mnl.2018.5286.

[15] Guo S, He Y, Liu D, Lei J, Shen L, Li Z. Torsional vibration of carbon nanotube with axial velocity and velocity gradient effect. Int J Mech Sci 2016;119:88–96.

[16] Eptaimeros K, Koutsoumaris CC, Tsamasphyros G. Nonlocal integral approach to the dynamical response of nanobeams. Int J Mech Sci 2016;115:68–80.

[17] Guo S, He Y, Liu D, Lei J, Li Z. Dynamic transverse vibration characteristics and vibro-buckling analyses of axially moving and rotating nanobeams based on nonlocal strain gradient theory. Microsyst Technol 2018;24:963–77.

[18] Li L, Tang H, Hu Y. The effect of thickness on the mechanics of nanobeams. Int J Eng Sci 2018;123:81–91.

[19] Ma L, Ke L, Reddy J, Yang J, Kitipornchai S, Wang Y. Wave propagation characteristics in magneto-electro-elastic nanoshells using nonlocal strain gradient theory. Compos Struct 2018;199:10–23.

[20] Lei J, He Y, Guo S, Li Z, Liu D. Size-dependent vibration of nickel cantilever microbeams: experiment and gradient elasticity. AIP Adv 2016;6:105202.

[21] Li Z, He Y, Lei J, Guo S, Liu D, Wang L. A standard experimental method for determining the material length scale based on modified couple stress theory. Int J Mech Sci 2018;141:198–205.

[22] Farshidianfar A, Soltani P. Nonlinear flow-induced vibration of a SWCNT with a geometrical imperfection. Comput Mater Sci 2012;53:105–16.

[23] Wang B, Z-c Deng, Zhang K. Nonlinear vibration of embedded single-walled carbon nanotube with geometrical imperfection under harmonic load based on nonlocal Timoshenko beam theory. Appl Math Mech 2013;34:269–80.

[24] Mohammadi H, Mahzoon M, Mohammadi M, Mohammadi M. Postbuckling instability of nonlinear nanobeam with geometric imperfection embedded in elastic foundation. Nonlinear Dyn 2014;76:2005–16.

[25] Barati MR, Zenkour AM. Investigating post-buckling of geometrically imperfect metal foam nanobeams with symmetric and asymmetric porosity distributions. Compos Struct 2017;182:91–8.

[26] Jalali S, Jomehzadeh E, Pugno N. Influence of out-of-plane defects on vibration analysis of graphene: molecular dynamics and non-local elasticity approaches. Superlattices Microstruct 2016;91:331–44.

[27] Rafiee M, He X, Liew K. Non-linear dynamic stability of piezoelectric functionally graded carbon nanotube-reinforced composite plates with initial geometric imperfection. Int J Nonlinear Mech 2014;59:37–51.

[28] Arefi A, Salimi M. Investigations on vibration and buckling of carbon nanotubes with small initial curvature by nonlocal elasticity theory. Fuller Nanotub Carbon Nanostruct 2015;23:105–12.

[29] Wang C, Lan L, Liu Y, Tan H, He X. Vibration characteristics of wrinkled single-layered graphene sheets. Int J Solids Struct 2013;50:1812–23.

[30] Sahmani S, Fattahi A. Imperfection sensitivity of the size-dependent nonlinear instability of axially loaded FGM nanopanels in thermal environments. Acta Mech 2017;228:3789–810.

[31] Farokhi H, Ghayesh MH, Amabili M. Nonlinear dynamics of a geometrically imperfect microbeam based on the modified couple stress theory. Int J Eng Sci 2013;68:11–23.

[32] Farokhi H, Ghayesh MH. Thermo-mechanical dynamics of perfect and imperfect Timoshenko microbeams. Int J Eng Sci 2015;91:12–33.

[33] Farokhi H, Ghayesh MH. Nonlinear dynamical behaviour of geometrically imperfect microplates based on modified couple stress theory. Int J Mech Sci 2015;90:133–44.

[34] Zhu X, Li L. Closed form solution for a nonlocal strain gradient rod in tension. Int J Eng Sci 2017;119:16–28.

[35] Li L, Hu Y, Ling L. Wave propagation in viscoelastic single-walled carbon nanotubes with surface effect under magnetic field based on nonlocal strain gradient theory. Phys E Low-dimens Syst Nanostruct 2016;75:118–24.

[36] Wang J, Shen H, Zhang B, Liu J, Zhang Y. Complex modal analysis of transverse free vibrations for axially moving nanobeams based on the nonlocal strain gradient theory. Phys E Low-dimens Syst Nanostruct 2018;101:85–93.

[37] Wang J, Shen H, Zhang B, Liu J. Studies on the dynamic stability of an axially moving nanobeam based on the nonlocal strain gradient theory. Modern Phys Lett B 2018:1850167.

[38] Şimşek M. Nonlinear free vibration of a functionally graded nanobeam using nonlocal strain gradient theory and a novel Hamiltonian approach. Int J Eng Sci 2016;105:12–27.

[39] Sahmani S, Aghdam M. Nonlocal strain gradient shell model for axial buckling and postbuckling analysis of magneto-electro-elastic composite nanoshells. Compos Part B Eng 2018;132:258–74.

[40] Farajpour A, Rastgoo A. Influence of carbon nanotubes on the buckling of microtubule bundles in viscoelastic cytoplasm using nonlocal strain gradient theory. Results Phys 2017;7:1367–75.

[41] Ebrahimi F, Barati MR. Vibration analysis of nonlocal strain gradient embedded single-layer graphene sheets under nonuniform in-plane loads. J Vib Control 2017;24(20):4751–63.

[42] Eringen AC. Nonlocal continuum field theories. Springer Science & Business Media; 2002.

[43] Farajpour M, Shahidi A, Farajpour A. A nonlocal continuum model for the biaxial buckling analysis of composite nanoplates with shape memory alloy nanowires. Mater Res Express 2018;5:035026.

[44] Farajpour A, Shahidi A, Hadi A, Farajpour A. Influence of initial edge displacement on the nonlinear vibration, electrical and magnetic instabilities of magneto-electro-elastic nanofilms. Mech Adv Mater Struct 2018:1–13.

[45] Farajpour A, Rastgoo A, Farajpour M. Nonlinear buckling analysis of magneto-electro-elastic CNT-MT hybrid nanoshells based on the nonlocal continuum mechanics. Compos Struct 2017;180:179–91.

[46] Reddy J. Nonlocal nonlinear formulations for bending of classical and shear deformation theories of beams and plates. Int J Eng Sci 2010;48:1507–18.

[47] Ghayesh MH, Amabili M, Farokhi H. Nonlinear forced vibrations of a microbeam based on the strain gradient elasticity theory. Int J Eng Sci 2013;63:52–60.

[48] Ghayesh MH, Farokhi H, Amabili M. Nonlinear dynamics of a microscale beam based on the modified couple stress theory. Compos Part B Eng 2013;50:318–24.

[49] Ghayesh MH, Farokhi H. Chaotic motion of a parametrically excited microbeam. Int J Eng Sci 2015;96:34–45.

[50] Farajpour M, Shahidi A, Tabataba'i-Nasab F, Farajpour A. Vibration of initially stressed carbon nanotubes under magneto-thermal environment for nanoparticle delivery via higher-order nonlocal strain gradient theory. Eur Phys J Plus 2018;133:219.

[51] Farajpour MR, Rastgoo A, Farajpour A, Mohammadi M. Vibration of piezoelectric nanofilm-based electromechanical sensors via higher-order non-local strain gradient theory. Micro Nano Lett 2016;11:302–7.

[52] Lim C, Zhang G, Reddy J. A higher-order nonlocal elasticity and strain gradient theory and its applications in wave propagation. J Mech Phys Solids 2015;78:298–313.

[53] Li X, Li L, Hu Y, Ding Z, Deng W. Bending, buckling and vibration of axially functionally graded beams based on nonlocal strain gradient theory. Compos Struct 2017;165:250–65.

[54] Zhang L, Zhang Y, Liew K. Vibration analysis of quadrilateral graphene sheets subjected to an in-plane magnetic field based on nonlocal elasticity theory. Compos Part B Eng 2017;118:96–103.

[55] Mercan K, Civalek Ö. Buckling analysis of Silicon carbide nanotubes (SiCNTs) with surface effect and nonlocal elasticity using the method of HDQ. Compos Part B: Eng 2017;114:34–45.

[56] Mehralian F, Beni YT, Zeverdejani MK. Nonlocal strain gradient theory calibration using molecular dynamics simulation based on small scale vibration of nanotubes. Phys B Condens Matter 2017;514:61–9.

[57] Mehralian F, Beni YT, Zeverdejani MK. Calibration of nonlocal strain gradient shell model for buckling analysis of nanotubes using molecular dynamics simulations. Phys B Condens Matter 2017;521:102–11.

[58] Ghayesh MH, Farokhi H, Amabili M. Nonlinear behaviour of electrically actuated MEMS resonators. Int J Eng Sci 2013;71:137–55.

[59] Ghayesh MH, Farokhi H, Alici G. Size-dependent performance of microgyroscopes. Int J Eng Sci 2016;100:99–111.

[60] Malekzadeh P, Farajpour A. Axisymmetric free and forced vibrations of initially stressed circular nanoplates embedded in an elastic medium. Acta Mech 2012;223:2311–30.

[61] Ghayesh MH, Farokhi H, Farajpour A. Chaotic oscillations of viscoelastic microtubes conveying pulsatile fluid. Microfluid Nanofluidics 2018;22:72.

[62] Allgower EL, Georg K. Introduction to numerical continuation methods. SIAM; 2003.

[63] Mittelmann H, Roose D. Continuation techniques and bifurcation problems, Birkhäuser Verlag, Basel, 1989.

[64] Ghayesh MH, Farokhi H, Amabili M. In-plane and out-of-plane motion characteristics of microbeams with modal interactions. Compos Part B Eng 2014;60:423–39.

[65] Li L, Li X, Hu Y. Free vibration analysis of nonlocal strain gradient beams made of functionally graded material. Int J Eng Sci 2016;102:77–92.

[66] Farokhi H, Ghayesh MH, Gholipour A, Hussain SH. Motion characteristics of bilayered extensible Timoshenko microbeams. Int J Eng Sci 2017;112:1–17.

[67] Ghayesh MH, Farokhi H, Gholipour A. Oscillations of functionally graded microbeams. Int J Eng Sci 2017;110:35–53.

[68] Ghayesh MH, Farokhi H, Gholipour A. Vibration analysis of geometrically imperfect three-layered shear-deformable microbeams. Int J Mech Sci 2017;122:370–83.

[69] Farokhi H, Ghayesh MH. Supercritical nonlinear parametric dynamics of Timoshenko microbeams. Commun Nonlinear Sci Numer Simul 2018;59:592–605.

[70] Ghayesh MH, Paidoussis MP, Amabili M. Nonlinear dynamics of cantilevered extensible pipes conveying fluid. J Sound Vib 2013;332:6405–18.

[71] Ghayesh MH, Farokhi H, Hussain SH. Viscoelastically coupled size-dependent dynamics of microbeams. Int J Eng Sci 2016;109:243–55.

[72] Ghayesh MH, Amabili M. Nonlinear dynamics of axially moving viscoelastic beams over the buckled state. Comput Struct 2012;112–113:406–21.

[73] Ghayesh MH, Amabili M, Paidoussis MP. Nonlinear vibrations and stability of an axially moving beam with an intermediate spring support: Two-dimensional analysis. Nonlinear Dyn 2012;70(1):335–54.

[74] Farokhi H, Ghayesh MH. Size-dependent parametric dynamics of imperfect microbeams. Int J Eng Sci 2016;99:39–55.

[75] Ghayesh MH, Amabili M. Coupled longitudinal-transverse behaviour of a geometrically imperfect microbeam. Compos Part B Eng 2014;60:371–7.

[76] Ghayesh MH. Stability characteristics of an axially accelerating string supported by an elastic foundation. Mech Mach Theory 2009;44:1964–79.

[77] Ghayesh MH. On the natural frequencies, complex mode functions, and critical speeds of axially traveling laminated beams: Parametric study. Acta Mech Solida Sin 2011;24(4):373–82.

[78] Gholipour A, Ghayesh MH, Zander A. Nonlinear biomechanics of bifurcated atherosclerotic coronary arteries. Int J Eng Sci 2018;133:60–83.

[79] Gholipour A, Ghayesh MH, Zander A, Mahajan R. Three-dimensional biomechanics of coronary arteries. Int J Eng Sci 2018;130:93–114.

[80] Farokhi H, Ghayesh MH. Nonlinear mechanics of electrically actuated microplates. Int J Eng Sci 2018;123:197–213.

[81] Ghayesh MH, Farokhi H, Gholipour A, Tavallaeinejad M. Nonlinear oscillations of functionally graded microplates. Int J Eng Sci 2018;122:56–72.

[82] Ghayesh MH. Functionally graded microbeams: simultaneous presence of imperfection and viscoelasticity. Int J Mech Sci 2018;140:339–50.

[83] Ghayesh MH. Nonlinear vibration analysis of axially functionally graded shear-deformable tapered beams. Appl Math Model 2018;59:583–96.

[84] Ghayesh MH. Dynamics of functionally graded viscoelastic microbeams. Int J Eng Sci 2018;124:115–31.

Chapter 4

Nonlinear vibration of small-scale imperfect beams incorporating viscoelasticity effects

Chapter overview

Chapter 4 deals with the second objective of this project, which is the nonlinear vibration of geometrically imperfect beams with viscoelasticity at small-scales. To formulate the problem, a scale-dependent model, which is based on a non-classical constitutive equation, is proposed. Strain gradients and nonlocality in stress components are simulated in the beam constitutive equations in order for the model to better describe size dependency. To model the internal energy loss in the structure, the Kelvin-Voigt theory is used. Potential and kinetic energies as well as viscous work are implemented into a work/energy balance, yielding the coupled motion equations. This investigation together with the previous analysis presented in chapter 3 provide a comprehensive study on the large-amplitude vibration of beams at nanoscales. This study would be helpful in the analysis of electromechanical small-scale systems using vibrating carbon nanotubes. The work was published in International Journal of Engineering Science as:

Statement of Authorship

Title of Paper	Nonlocal nonlinear mechanics of imperfect carbon nanotubes
Publication Status	☑ Published ☐ Accepted for Publication ☐ Submitted for Publication ☐ Unpublished and Unsubmitted work written in manuscript style
Publication Details	A Farajpour, MH Ghayesh, H Farokhi, Nonlocal nonlinear mechanics of imperfect carbon nanotubes, International Journal of Engineering Science 142, 201-215 (2019).

Principal Author

Name of Principal Author (Candidate)	Ali Farajpour Ouderji
Contribution to the Paper	- Research and doing the literature review of the paper - Developing the model (i.e. derivation of nonlinear coupled partial differential equations of motion via Hamilton's principle) - Incorporating size effects using a modified elasticity theory - Incorporating the influence of geometrical nonlinearity into the model - Incorporating viscoelasticity effects into the model - Writing all parts of the paper and analysing the data
Overall percentage (%)	60%
Certification:	This paper reports on original research I conducted during the period of my Higher Degree by Research candidature and is not subject to any obligations or contractual agreements with a third party that would constrain its inclusion in this thesis. I am the primary author of this paper.
Signature	Date 2/6/2020

Co-Author Contributions

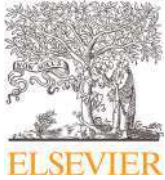By signing the Statement of Authorship, each author certifies that:

i.   the candidate's stated contribution to the publication is accurate (as detailed above);

ii. permission is granted for the candidate in include the publication in the thesis; and

iii. the sum of all co-author contributions is equal to 100% less the candidate's stated contribution.

Name of Co-Author	Mergen H. Ghayesh
Contribution to the Paper	- Supervising the work including preparing the paper - Contribution to the development of the ideas and concepts of the paper - Editing and evaluating the paper before submission - Correspondence with the reviewers and editor of the journal - Discretising and solving the equations of motions, and obtaining frequency response curves
Signature	Date 21/06/2020

Name of Co-Author	Hamed Farokhi
Contribution to the Paper	- Participation in supervising the work - Contribution to the development of the concepts of the paper - Discretising and solving the equations of motions, and obtaining frequency response curves
Signature	Date 19/06/2020

Nonlocal nonlinear mechanics of imperfect carbon nanotubes

Ali Farajpour[a], Mergen H. Ghayesh[a,*], Hamed Farokhi[b]

[a] School of Mechanical Engineering, University of Adelaide, South Australia 5005, Australia
[b] Department of Mechanical and Construction Engineering, Northumbria University, Newcastle upon Tyne NE1 8ST, UK

ABSTRACT

In this article, for the first time, a coupled nonlinear model incorporating scale influences is presented to simultaneously investigate the influences of viscoelasticity and geometrical imperfections on the nonlocal coupled mechanics of carbon nanotubes; large deformations, stress nonlocality and strain gradients are captured in the model. The Kelvin-Voigt model is also applied in order to ascertain the viscoelasticity effects on the mechanics of the initially imperfect nanoscale system. The modified coupled equations of motion are then derived via the Hamilton principle. A solution approach for the derived coupled equations is finally developed applying a decomposition-based procedure in conjunction with a continuation-based scheme. The significance of many parameters such as size parameters, initial imperfections, excitation parameters and linear and nonlinear damping effects in the nonlinear mechanical response of the initially imperfect viscoelastic carbon nanotube is assessed. The present results can be useful for nanoscale devices using carbon nanotubes since the viscoelasticity and geometrical imperfection are simultaneously included in the proposed model.

© 2019 Elsevier Ltd. All rights reserved.

1. Introduction

Micro and nano structures have been widely used in micro/nano devices (Farajpour, Ghayesh, & Farokhi, 2018; Ruzziconi, Bataineh, Younis, Cui, & Lenci, 2013). Among them, carbon nanostructures have been used in a wide range of applications in nanotechnology, biotechnology and nanoengineering since they display interesting electrical, mechanical and chemical properties. Some important carbon nanostructures are carbon nanotubes (CNTs), graphene sheets and buckyballs. To appropriately use these precious nanostructures in different applications, especially in nanoengineering, our level of understanding of their mechanical properties should be increased. This is due to the fact that the overall performance of a nanoelectromechanical system (NEMS) depends greatly on the mechanical behaviour of its building blocks such as CNTs.

Scale-dependent models have been utilised for the investigation of the mechanics of many small-scale structures such as microbeams (Dehrouyeh-Semnani, Nikkhah-Bahrami, & Yazdi, 2017; Demir and Civalek, 2017; Farokhi, Ghayesh, & Gholipour, 2017; Farokhi, Ghayesh, Gholipour, & Hussain, 2017; Ghayesh, Farokhi, Gholipour, & Hussain, 2017; Pourasghar & Chen, 2019; Qi, Huang, Fu, Zhou, & Jiang, 2018), microplates (Farokhi & Ghayesh, 2018b; Farokhi & Ghayesh, 2018a; Ghayesh, Farokhi, Gholipour, & Tavallaeinejad, 2018; Rahaeifard & Mojahedi, 2017), nanobeams (Attia & Abdel Rahman, 2018; Barretta, Čanađija, Luciano, & de Sciarra, 2018; Karami & Janghorban, 2019; Khaniki, 2018; Khaniki, 2019; Li, Tang, & Hu, 2018; She, Ren, Yuan, & Xiao, 2018) and nanoplates (Barretta, Faghidian, & Marotti de Sciarra, 2019; Jalaei, Arani, & Tourang, 2018; Lu, Guo, & Zhao, 2018; Natsuki & Natsuki, 2018; Shahverdi & Barati, 2017). A particular attention has been paid to the mechanics

---

* Corresponding author.
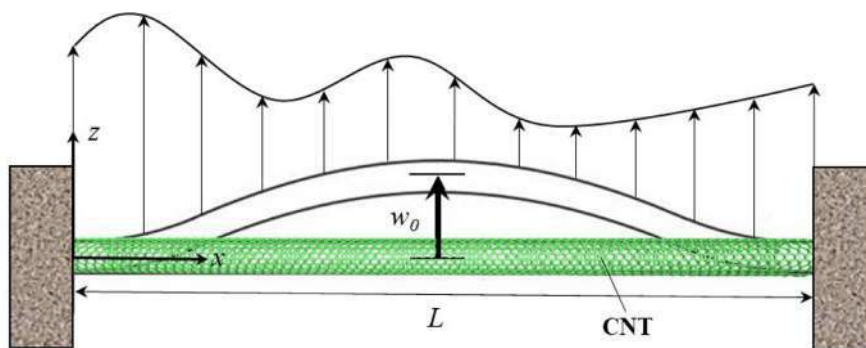 *E-mail address:* mergen.ghayesh@adelaide.edu.au (M.H. Ghayesh).

Fig. 1. An initially imperfect viscoelastic CNT with clamped-clamped edges.

of CNTs. Although CNTs display a viscoelastic response when they are subject to an applied load (Suhr, Koratkar, Keblinski, & Ajayan, 2005; Xu, Futaba, Yamada, Yumura, & Hata, 2010), many size-dependent theoretical models in the literature have not considered the effects of viscoelasticity. As some examples, a few size-dependent models for the mechanical response of elastic CNTs are reviewed. Setoodeh, Khosrownejad, and Malekzadeh (2011) obtained an exact solution for the buckling instability of elastic CNTs with large deformations by applying a classical nonlocal model. Aydogdu (2012) presented a size-dependent nonlocal rod theory to ascertain the axial vibration characteristics of nanorods. In addition, Malekzadeh and Sho-jaee (2013) proposed a non-classical continuum theory to explore the free vibration of non-uniform beams at the nanoscale level. The nonlocal oscillations of mass nanosensors employing elastic CNTs with small deformations were also examined by Aydogdu and Filiz (2011). In addition to these interesting papers, a few studies have been carried out on the viscoelastic response of CNTs under mechanical stresses. Chang and Lee (2012) developed a nonlocal model to study the viscoelas-tic vibration characteristics of carbon nanotubes. In another analysis, a linear study was performed by Lei, Adhikari, and Friswell (2013) on the damping effect on the vibration response of CNTs using a combination of the Kelvin-Voigt model and the Eringen theory. The time-dependent deformation of fluid-conveying CNTs taking into account the internal energy loss was also explored by Bahaadini and Hosseini (2016). Furthermore, the effect of initial stresses on the vibration of vis-coelastic beams at nanoscale levels was investigated by Zhang, Pang, and Fan (2016). Karličić, Murmu, Cajić, Kozić, and Adhikari (2014) also proposed a non-classical model for the dynamic characteristics of a CNT-based composite viscoelastic system under the action of a magnetic field.

The use of the classical nonlocal theory of elasticity for nanoscale structures such as CNTs is limited to a particular range of lengths since nonlocal effects usually disappear after a certain length. To overcome this problem, Lim, Zhang, and Reddy (2015) has recently introduced a modified nonlocal elasticity theory by incorporating the strain gradient influences. Using the molecular dynamics, it has been indicated that this modified theory is able to better estimate the size-dependent mechanics of CNTs compared to the classical nonlocal theory (Li, Hu, & Ling, 2016). However, few research papers have been reported on the size-dependent deformation of CNTs with consideration of viscoelastic effects using this modified nonlocal theory. Some linear models have been merely developed for the wave propagation analysis of viscoelastic carbon nanotubes (Li & Hu, 2016; Tang, Liu, & Zhao, 2016; Zhen & Zhou, 2017).

In addition to the influence of viscoelasticity, the influence of geometrical imperfections becomes more and more impor-tant when large deformations are taken into consideration since these imperfections can change the nonlinear mechanical characteristics of ultrasmall structures.

In the current investigation, *for the first time*, the effects of viscoelasticity as well as geometrical imperfections on the mechanics of CNTs with large deformations are analysed via a modified nonlocal elasticity model. The consideration of both viscoelasticity and geometrical imperfections leads to a more comprehensive scale-dependent model for CNTs. Furthermore, the proposed model can be used in a wide range of lengths since the stiffness hardening and softening are included. As a viscoelastic theory, the Kelvin-Voigt model is applied in the analysis. The coupled nonlinear equations of ultrasmall tubes are presented applying the Hamilton principle together with a beam model. A solution approach is developed with the application of a decomposition-based procedure in conjunction with a continuation-based method. The importance of many parameters such as the size parameter, the initial imperfection, the excitation loading as well as the linear and nonlinear damping effects in the size-dependent coupled mechanics of the initially imperfect viscoelastic carbon nanotube with large deflections is explained.

2. Formulation

Shown in Fig. 1 is a clamped-clamped single-walled carbon nanotube with an initial deformation as a geometric imper-fection. The viscoelastic and elastic constants of the CNT are denoted by η and E, respectively. Moreover, Poisson's ratio, the length and the mass density are denoted by v, L and ρ, respectively. w_0 denotes the initial deflection of the viscoelastic CNT while the axial and transverse time-dependent displacements are described by u and w, respectively. A harmonic load in

the form of $q(x, t) = \cos(\omega t)F(x)$ is applied on the imperfect nanoscale system along the transverse direction; ω and F are the forcing frequency and amplitude, respectively.

To model the mechanics of nanostructures such as CNTs, scale-dependent continuum mechanics can be used (Bahaadini, Saidi, & Hosseini, 2018; Ebrahimi & Barati, 2016; Faleh, Ahmed, & Fenjan, 2018; Hadi, Nejad, & Hosseini, 2018; Lu, Guo, & Zhao, 2017b; Zhu and Li, 2017b). For a single-walled CNT with an initial deformation, the axial strain (ε_{xx}) is given by

$$\varepsilon_{xx} = \frac{\partial u}{\partial x} + \frac{1}{2}\left(\frac{\partial w}{\partial x}\right)^2 + \frac{\partial w}{\partial x}\frac{dw_0}{dx} - z\frac{\partial^2 w}{\partial x^2}. \tag{1}$$

On the other hand, based on the modified nonlocal elasticity, the total axial stress of the imperfect viscoelastic CNT (t_{xx}) is expressed as (Ebrahimi, Barati, & Dabbagh, 2016; Lu, Guo, & Zhao, 2017a; Şimşek, 2016; Zhu & Li, 2017a)

$$\left[1 - (e_0 a)^2\nabla^2\right]t_{xx} = \left(1 - l_{sg}^2\nabla^2\right)\left(t_{xx(el)}^{cl} + t_{xx(vis)}^{cl}\right), \tag{2}$$

where $t_{xx(el)}^{cl}$ and $t_{xx(vis)}^{cl}$ are respectively the elastic and viscoelastic parts of the classical (local) stress; e_0, a, l_{sg} and ∇^2 stand for the calibration parameter associated with the nonlocal stress (Malekzadeh & Shojaee, 2015), the internal characteristic length, the strain gradient parameter and the Laplace operator, respectively (Ghayesh & Farajpour, 2018; Ghayesh & Farajpour, 2019). Eq. (2) is the differential scale-dependent constitutive relation of the modified elasticity theory. Recently, integral scale-dependent constitutive relations have also been used for nanostructures (Apuzzo, Barretta, Faghidian, Luciano, & Marotti de Sciarra, 2018; Faghidian, 2018; Fernández-Sáez & Zaera, 2017; Romano and Barretta, 2017). The elastic and viscoelastic parts of the classical stress are

$$t_{xx(el)}^{cl} = E\varepsilon_{xx}, t_{xx(vis)}^{cl} = \eta\frac{\partial\varepsilon_{xx}}{\partial t}. \tag{3}$$

In view of Eqs. (1)–(3), the non-classical stress resultants of the imperfect viscoelastic CNT can be formulated as

$$\left[1 - (e_0 a)^2\nabla^2\right]N_{xx} = EA\left(1 - l_{sg}^2\nabla^2\right)\left[\frac{\partial u}{\partial x} + \frac{1}{2}\left(\frac{\partial w}{\partial x}\right)^2 + \frac{\partial w}{\partial x}\frac{dw_0}{dx}\right]$$
$$+ \eta A\left(1 - l_{sg}^2\nabla^2\right)\left(\frac{\partial^2 u}{\partial t\partial x} + \frac{\partial w}{\partial x}\frac{\partial^2 w}{\partial t\partial x} + \frac{\partial^2 w}{\partial t\partial x}\frac{dw_0}{dx}\right), \tag{4}$$

$$\left[1 - (e_0 a)^2\nabla^2\right]M_{xx} = -EI\left(1 - l_{sg}^2\nabla^2\right)\frac{\partial^2 w}{\partial x^2} - \eta I\left(1 - l_{sg}^2\nabla^2\right)\frac{\partial^3 w}{\partial t\partial x^2}, \tag{5}$$

where

$$\begin{Bmatrix} N_{xx} \\ M_{xx} \end{Bmatrix} = \int_A t_{xx}\begin{Bmatrix} 1 \\ z \end{Bmatrix}dA, \begin{Bmatrix} A \\ I \end{Bmatrix} = \int_A \begin{Bmatrix} 1 \\ z^2 \end{Bmatrix}dA. \tag{6}$$

The relations between different non-classical stresses are described by

$$\begin{Bmatrix} t_{xx} \\ t_{xx(el)} \\ t_{xx(vis)} \end{Bmatrix} = \begin{Bmatrix} \sigma_{xx} \\ \sigma_{xx(el)} \\ \sigma_{xx(vis)} \end{Bmatrix} - \nabla\begin{Bmatrix} \sigma_{xx}^{(1)} \\ \sigma_{xx(el)}^{(1)} \\ \sigma_{xx(vis)}^{(1)} \end{Bmatrix},$$
$$\begin{Bmatrix} t_{xx} \\ \sigma_{xx} \\ \sigma_{xx}^{(1)} \end{Bmatrix} = \begin{Bmatrix} t_{xx(el)} \\ \sigma_{xx(el)} \\ \sigma_{xx(el)}^{(1)} \end{Bmatrix} + \begin{Bmatrix} t_{xx(vis)} \\ \sigma_{xx(vis)} \\ \sigma_{xx(vis)}^{(1)} \end{Bmatrix}, \tag{7}$$

where ∇, $\sigma_{ij(\alpha)}$ and $\sigma_{ij(\alpha)}^{(1)}$ represent the gradient operator, the axial classical nonlocal stress and the axial higher-order nonlocal stress, respectively. The energy variation due to the total elastic stress (δU_{el}) of the imperfect CNT and the work variation due to its total viscoelastic stress (δW_{vis}) are as follows

$$\delta U_{el} = \int_0^L \int_A t_{xx(el)}\delta\varepsilon_{xx}dAdx + \left[\int_A \sigma_{xx(el)}^{(1)}\delta\varepsilon_{xx}dA\right]_0^L, \tag{8}$$

$$\delta W_{vis} = -\int_0^L \int_A t_{xx(vis)}\delta\varepsilon_{xx}dAdx - \left[\int_A \sigma_{xx(vis)}^{(1)}\delta\varepsilon_{xx}dA\right]_0^L. \tag{9}$$

The kinetic energy variation (δK_e) of the imperfect CNT and the work variation (δW_q) due to $q(x, t)$ are also formulated as (Ghayesh, 2018)

$$\delta K_e = m \int_0^L \left(\frac{\partial u}{\partial t} \delta \frac{\partial u}{\partial t} + \frac{\partial w}{\partial t} \delta \frac{\partial w}{\partial t} \right) dx, \tag{10}$$

$$\delta W_q = \int_0^L q(x,t) \delta w \, dx. \tag{11}$$

In Eq. (10), m denotes the mass per unit length of the imperfect CNT. The Hamilton principle is now used for the derivation of the motion equations of the imperfect viscoelastic tube. This principle is generally written as follows

$$\int_{t_1}^{t_2} (\delta K_e + \delta W_q + \delta W_{vis} - \delta U_{el}) dt = 0. \tag{12}$$

Using Eqs. (8)–(11), one obtains the following motion equations

$$\frac{\partial N_{xx}}{\partial x} = m \frac{\partial^2 u}{\partial t^2}, \tag{13}$$

$$\frac{\partial^2 M_{xx}}{\partial x^2} + \frac{\partial}{\partial x} \left[N_{xx} \left(\frac{\partial w}{\partial x} + \frac{dw_0}{dx} \right) \right] + q = m \frac{\partial^2 w}{\partial t^2}. \tag{14}$$

Application of the above equations to Eqs. (4) and (5) gives the following expressions for the non-classical stress resultants

$$N_{xx} = EA \left(1 - l_{sg}^2 \nabla^2 \right) \left[\frac{\partial u}{\partial x} + \frac{1}{2} \left(\frac{\partial w}{\partial x} \right)^2 + \frac{\partial w}{\partial x} \frac{dw_0}{dx} \right]$$
$$+ \eta A \left(1 - l_{sg}^2 \nabla^2 \right) \left(\frac{\partial^2 u}{\partial t \partial x} + \frac{\partial w}{\partial x} \frac{\partial^2 w}{\partial t \partial x} + \frac{\partial^2 w}{\partial t \partial x} \frac{dw_0}{dx} \right) + m(e_0 a)^2 \frac{\partial^3 u}{\partial x \partial t^2}, \tag{15}$$

$$M_{xx} = -EI \left(1 - l_{sg}^2 \nabla^2 \right) \frac{\partial^2 w}{\partial x^2} - \eta I \left(1 - l_{sg}^2 \nabla^2 \right) \frac{\partial^3 w}{\partial t \partial x^2} + (e_0 a)^2 \left\{ m \frac{\partial^2 w}{\partial t^2} - \frac{\partial}{\partial x} \left[N_{xx} \left(\frac{\partial w}{\partial x} + \frac{dw_0}{dx} \right) \right] - q \right\}, \tag{16}$$

Substituting the obtained stress resultants into Eqs. (13) and (14) and assuming the harmonic load as $q = F_1 \cos(\omega t)$, one can obtain

$$EA \left(\frac{\partial^2 u}{\partial x^2} + \frac{\partial w}{\partial x} \frac{\partial^2 w}{\partial x^2} + \frac{\partial^2 w}{\partial x^2} \frac{dw_0}{dx} + \frac{\partial w}{\partial x} \frac{d^2 w_0}{dx^2} \right) - EAl_{sg}^2 \left(\frac{\partial^4 u}{\partial x^4} + 3 \frac{\partial^2 w}{\partial x^2} \frac{\partial^3 w}{\partial x^3} \right.$$
$$\left. + \frac{\partial w}{\partial x} \frac{\partial^4 w}{\partial x^4} + \frac{\partial^4 w}{\partial x^4} \frac{dw_0}{dx} + 3 \frac{\partial^3 w}{\partial x^3} \frac{d^2 w_0}{dx^2} + 3 \frac{\partial^2 w}{\partial x^2} \frac{d^3 w_0}{dx^3} + \frac{\partial w}{\partial x} \frac{d^4 w_0}{dx^4} \right)$$
$$+ \eta A \left(\frac{\partial^3 u}{\partial t \partial x^2} + \frac{\partial^2 w}{\partial t \partial x} \frac{\partial^2 w}{\partial x^2} + \frac{\partial^3 w}{\partial t \partial x^2} \frac{dw_0}{dx} + \frac{\partial w}{\partial x} \frac{\partial^3 w}{\partial t \partial x^2} + \frac{\partial^2 w}{\partial t \partial x} \frac{d^2 w_0}{dx^2} \right)$$
$$- \eta A l_{sg}^2 \left(3 \frac{\partial^3 w}{\partial x^3} \frac{\partial^3 w}{\partial t \partial x^2} + \frac{\partial w}{\partial x} \frac{\partial^5 w}{\partial t \partial x^4} + \frac{\partial^5 u}{\partial t \partial x^4} + \frac{\partial^4 w}{\partial x^4} \frac{\partial^2 w}{\partial t \partial x} + 3 \frac{\partial^2 w}{\partial x^2} \frac{\partial^4 w}{\partial x^3 \partial t} \right.$$
$$\left. + \frac{\partial^5 w}{\partial t \partial x^4} \frac{dw_0}{dx} + 3 \frac{\partial^4 w}{\partial t \partial x^3} \frac{d^2 w_0}{dx^2} + 3 \frac{\partial^3 w}{\partial t \partial x^2} \frac{d^3 w_0}{dx^3} + \frac{\partial^2 w}{\partial t \partial x} \frac{d^4 w_0}{dx^4} \right) = m \left[\frac{\partial^2 u}{\partial t^2} - (e_0 a)^2 \frac{\partial^4 u}{\partial x^2 \partial t^2} \right],$$

$$- EI \left(\frac{\partial^4 w}{\partial x^4} - l_{sg}^2 \frac{\partial^6 w}{\partial x^6} \right) - \eta I \left(\frac{\partial^5 w}{\partial t \partial x^4} - l_{sg}^2 \frac{\partial^7 w}{\partial t \partial x^6} \right)$$
$$+ EA \left[\frac{\partial^2 w}{\partial x^2} + \frac{d^2 w_0}{dx^2} - (e_0 a)^2 \left(\frac{\partial^4 w}{\partial x^4} + \frac{d^4 w_0}{dx^4} \right) \right] \left[\frac{dw_0}{dx} \frac{\partial w}{\partial x} + \frac{1}{2} \left(\frac{\partial w}{\partial x} \right)^2 + \frac{\partial u}{\partial x} \right]$$
$$+ EA \left[\frac{\partial w}{\partial x} + \frac{dw_0}{dx} - 3(e_0 a)^2 \left(\frac{\partial^3 w}{\partial x^3} + \frac{d^3 w_0}{dx^3} \right) \right] \left(\frac{\partial^2 u}{\partial x^2} + \frac{\partial w}{\partial x} \frac{\partial^2 w}{\partial x^2} + \frac{\partial^2 w}{\partial x^2} \frac{dw_0}{dx} + \frac{\partial w}{\partial x} \frac{d^2 w_0}{dx^2} \right)$$
$$- EA \left\{ \left[l_{sg}^2 + 3(e_0 a)^2 \right] \left(\frac{\partial^2 w}{\partial x^2} + \frac{d^2 w_0}{dx^2} \right) - (e_0 a)^2 l_{sg}^2 \left(\frac{\partial^4 w}{\partial x^4} + \frac{d^4 w_0}{dx^4} \right) \right\}$$
$$\times \left[\frac{\partial^3 u}{\partial x^3} + \left(\frac{\partial^2 w}{\partial x^2} \right)^2 + \frac{\partial w}{\partial x} \frac{\partial^3 w}{\partial x^3} + \frac{\partial^3 w}{\partial x^3} \frac{dw_0}{dx} + 2 \frac{\partial^2 w}{\partial x^2} \frac{d^2 w_0}{dx^2} + \frac{\partial w}{\partial x} \frac{d^3 w_0}{dx^3} \right]$$

$$- EA\left\{\left[l_{sg}^2 + (e_0a)^2\right]\left(\frac{\partial w}{\partial x} + \frac{dw_0}{dx}\right) - 3(e_0a)^2 l_{sg}^2\left(\frac{\partial^3 w}{\partial x^3} + \frac{d^3 w_0}{dx^3}\right)\right\}$$

$$\times \left(\frac{\partial w}{\partial x}\frac{\partial^4 w}{\partial x^4} + \frac{d^4 w_0}{dx^4}\frac{\partial w}{\partial x} + \frac{dw_0}{dx}\frac{\partial^4 w}{\partial x^4} + 3\frac{d^2 w_0}{dx^2}\frac{\partial^3 w}{\partial x^3} + \frac{\partial^4 u}{\partial x^4} + 3\frac{\partial^2 w}{\partial x^2}\frac{d^3 w_0}{dx^3} + 3\frac{\partial^2 w}{\partial x^2}\frac{\partial^3 w}{\partial x^3}\right)$$

$$+ 3EAl_{sg}^2(e_0a)^2\left(\frac{\partial^2 w}{\partial x^2} + \frac{d^2 w_0}{dx^2}\right)\left[3\left(\frac{\partial^3 w}{\partial x^3}\right)^2 + \frac{\partial w}{\partial x}\frac{\partial^5 w}{\partial x^5} + \frac{\partial^5 u}{\partial x^5} + 4\frac{\partial^4 w}{\partial x^4}\frac{\partial^2 w}{\partial x^2}\right.$$

$$\left. + \frac{\partial^5 w}{\partial x^5}\frac{dw_0}{dx} + 4\frac{\partial^4 w}{\partial x^4}\frac{d^2 w_0}{dx^2} + 6\frac{\partial^3 w}{\partial x^3}\frac{d^3 w_0}{dx^3} + 4\frac{\partial^2 w}{\partial x^2}\frac{d^4 w_0}{dx^4} + \frac{\partial w}{\partial x}\frac{d^5 w_0}{dx^5}\right]$$

$$+ EA(e_0a)^2 l_{sg}^2\left(\frac{\partial w}{\partial x} + \frac{dw_0}{dx}\right)\left[\frac{\partial^6 u}{\partial x^6} + 10\frac{\partial^3 w}{\partial x^3}\frac{\partial^4 w}{\partial x^4} + 5\frac{\partial^2 w}{\partial x^2}\frac{\partial^5 w}{\partial x^5} + \frac{\partial w}{\partial x}\frac{\partial^6 w}{\partial x^6}\right.$$

$$\left. + \frac{\partial^6 w}{\partial x^6}\frac{dw_0}{dx} + 5\frac{\partial^5 w}{\partial x^5}\frac{d^2 w_0}{dx^2} + 10\frac{\partial^4 w}{\partial x^4}\frac{d^3 w_0}{dx^3} + 10\frac{\partial^3 w}{\partial x^3}\frac{d^4 w_0}{dx^4} + 5\frac{\partial^2 w}{\partial x^2}\frac{d^5 w_0}{dx^5} + \frac{\partial w}{\partial x}\frac{d^6 w_0}{dx^6}\right]$$

$$+ \eta A\left[\frac{\partial^2 w}{\partial x^2} + \frac{d^2 w_0}{dx^2} - (e_0a)^2\left(\frac{\partial^4 w}{\partial x^4} + \frac{d^4 w_0}{dx^4}\right)\right]\left(\frac{dw_0}{dx}\frac{\partial^2 w}{\partial t \partial x} + \frac{\partial^2 u}{\partial t \partial x} + \frac{\partial^2 w}{\partial t \partial x}\frac{\partial w}{\partial x}\right)$$

$$+ \eta A\left[\frac{dw_0}{dx} + \frac{\partial w}{\partial x} - 3(e_0a)^2\left(\frac{\partial^3 w}{\partial x^3} + \frac{d^3 w_0}{dx^3}\right)\right]\left(\frac{\partial^3 u}{\partial x^2 \partial t} + \frac{\partial w}{\partial x}\frac{\partial^3 w}{\partial t \partial x^2} + \frac{\partial^2 w}{\partial x^2}\frac{\partial^2 w}{\partial x \partial t}\right.$$

$$\left. + \frac{\partial^3 w}{\partial t \partial x^2}\frac{dw_0}{dx} + \frac{\partial^2 w}{\partial t \partial x}\frac{d^2 w_0}{dx^2}\right) - \eta A\left\{\left[l_{sg}^2 + 3(e_0a)^2\right]\left(\frac{\partial^2 w}{\partial x^2} + \frac{d^2 w_0}{dx^2}\right) - (e_0a)^2 l_{sg}^2\left(\frac{\partial^4 w}{\partial x^4} + \frac{d^4 w_0}{dx^4}\right)\right\}$$

$$\times \left(2\frac{d^2 w_0}{dx^2}\frac{\partial^3 w}{\partial t \partial x^2} + \frac{\partial^4 u}{\partial t \partial x^3} + \frac{\partial^3 w}{\partial x^3}\frac{\partial^2 w}{\partial t \partial x} + 2\frac{\partial^3 w}{\partial t \partial x^2}\frac{\partial^2 w}{\partial x^2} + \frac{dw_0}{dx}\frac{\partial^4 w}{\partial t \partial x^3} + \frac{\partial w}{\partial x}\frac{\partial^4 w}{\partial t \partial x^3} + \frac{\partial^2 w}{\partial t \partial x}\frac{d^3 w_0}{dx^3}\right)$$

$$- \eta A\left\{\left[l_{sg}^2 + (e_0a)^2\right]\left(\frac{\partial w}{\partial x} + \frac{dw_0}{dx}\right) - 3(e_0a)^2 l_{sg}^2\left(\frac{\partial^3 w}{\partial x^3} + \frac{d^3 w_0}{dx^3}\right)\right\}\left(\frac{\partial^5 u}{\partial t \partial x^4} + \frac{\partial^4 w}{\partial x^4}\frac{\partial^2 w}{\partial t \partial x} + 3\frac{\partial^2 w}{\partial x^2}\frac{\partial^4 w}{\partial t \partial x^3}\right.$$

$$\left. + 3\frac{\partial^3 w}{\partial x^3}\frac{\partial^3 w}{\partial t \partial x^2} + \frac{\partial w}{\partial x}\frac{\partial^5 w}{\partial t \partial x^4} + \frac{\partial^5 w}{\partial t \partial x^4}\frac{dw_0}{dx} + 3\frac{\partial^4 w}{\partial t \partial x^3}\frac{d^2 w_0}{dx^2} + 3\frac{\partial^3 w}{\partial t \partial x^2}\frac{d^3 w_0}{dx^3} + \frac{\partial^2 w}{\partial t \partial x}\frac{d^4 w_0}{dx^4}\right)$$

$$+ 3\eta A(e_0a)^2 l_{sg}^2\left(\frac{\partial^2 w}{\partial x^2} + \frac{d^2 w_0}{dx^2}\right)\left(\frac{\partial^6 u}{\partial t \partial x^5} + \frac{\partial^5 w}{\partial x^5}\frac{\partial^2 w}{\partial t \partial x} + 4\frac{\partial^4 w}{\partial x^4}\frac{\partial^3 w}{\partial t \partial x^2} + 6\frac{\partial^3 w}{\partial x^3}\frac{\partial^4 w}{\partial t \partial x^3} + 4\frac{\partial^2 w}{\partial x^2}\frac{\partial^5 w}{\partial t \partial x^4}\right.$$

$$\left. + \frac{\partial w}{\partial x}\frac{\partial^6 w}{\partial t \partial x^5} + \frac{\partial^6 w}{\partial t \partial x^5}\frac{dw_0}{dx} + 4\frac{\partial^5 w}{\partial t \partial x^4}\frac{d^2 w_0}{dx^2} + 6\frac{\partial^4 w}{\partial t \partial x^3}\frac{d^3 w_0}{dx^3} + 4\frac{\partial^3 w}{\partial t \partial x^2}\frac{d^4 w_0}{dx^4} + \frac{\partial^2 w}{\partial t \partial x}\frac{d^5 w_0}{dx^5}\right)$$

$$+ \eta A(e_0a)^2 l_{sg}^2\left(\frac{\partial w}{\partial x} + \frac{dw_0}{dx}\right)\left(\frac{\partial^7 u}{\partial t \partial x^6} + \frac{\partial^6 w}{\partial x^6}\frac{\partial^2 w}{\partial t \partial x} + 5\frac{\partial^5 w}{\partial x^5}\frac{\partial^3 w}{\partial t \partial x^2} + 10\frac{\partial^4 w}{\partial x^4}\frac{\partial^4 w}{\partial t \partial x^3}\right.$$

$$+ 10\frac{\partial^3 w}{\partial x^3}\frac{\partial^5 w}{\partial t \partial x^4} + \frac{\partial^7 w}{\partial x^6 \partial t}\frac{dw_0}{dx} + 5\frac{\partial^6 w}{\partial t \partial x^5}\frac{\partial^2 w}{\partial x^2} + \frac{\partial^7 w}{\partial t \partial x^6}\frac{\partial w}{\partial x} + 5\frac{\partial^6 w}{\partial t \partial x^5}\frac{d^2 w_0}{dx^2} + 10\frac{\partial^5 w}{\partial t \partial x^4}\frac{d^3 w_0}{dx^3}$$

$$\left. + 10\frac{\partial^4 w}{\partial t \partial x^3}\frac{d^4 w_0}{dx^4} + 5\frac{\partial^3 w}{\partial t \partial x^2}\frac{d^5 w_0}{dx^5} + \frac{\partial^2 w}{\partial t \partial x}\frac{d^6 w_0}{dx^6}\right) \tag{17}$$

$$+ m(e_0a)^2\left[\frac{\partial^2 w}{\partial x^2} + \frac{d^2 w_0}{dx^2} - (e_0a)^2\left(\frac{\partial^4 w}{\partial x^4} + \frac{d^4 w_0}{dx^4}\right)\right]\frac{\partial^3 u}{\partial x \partial t^2}$$

$$+ m(e_0a)^2\left[\frac{\partial w}{\partial x} + \frac{dw_0}{dx} - 3(e_0a)^2\left(\frac{\partial^3 w}{\partial x^3} + \frac{d^3 w_0}{dx^3}\right)\right]\frac{\partial^4 u}{\partial x^2 \partial t^2}$$

$$- 3m(e_0a)^4\left(\frac{\partial^2 w}{\partial x^2} + \frac{d^2 w_0}{dx^2}\right)\frac{\partial^5 u}{\partial x^3 \partial t^2} - m(e_0a)^4\left(\frac{\partial w}{\partial x} + \frac{dw_0}{dx}\right)\frac{\partial^6 u}{\partial x^4 \partial t^2}$$

$$= m\frac{\partial^2 w}{\partial t^2} - m(e_0a)^2\frac{\partial^4 w}{\partial x^2 \partial t^2} - F_1\cos(\omega t). \tag{18}$$

3. Solution method

In this section, a numerical solution procedure is presented for the derived coupled equations of motion given by Eqs. (17) and (18). First of all, it is better to rewrite these differential equations in the non-dimensional form via the following set of parameters

$$x^* = \frac{x}{L}, \langle u^*, w^*, w_0^* \rangle = \frac{1}{R_g} \langle u, w, w_0 \rangle, R_g = \sqrt{\frac{I}{A}}, \langle \chi_{nl}, \chi_{sg} \rangle = \frac{1}{L} \langle e_0 a, l_{sg} \rangle,$$

$$\eta^* = \eta \sqrt{\frac{I}{EmL^4}}, \beta = \frac{L}{R_g}, F_1^* = \frac{F_1 L^3}{EI}, t^* = t \sqrt{\frac{EI}{mL^4}}, \Omega = L^2 \sqrt{\frac{m}{EI}} \omega, \tag{19}$$

in which β represents the ratio of the CNT length (L) to its gyration radius (R_g). In view of these non-dimensional parameters, Eqs. (17) and (18) can be expressed as

$$\frac{\partial^2 u}{\partial t^2} - \chi_{nl}^2 \frac{\partial^4 u}{\partial t^2 \partial x^2} - \beta \left(\frac{\partial^2 w}{\partial x^2} \frac{\partial w}{\partial x} + \frac{\partial w}{\partial x} \frac{d^2 w_0}{dx^2} + \frac{dw_0}{dx} \frac{\partial^2 w}{\partial x^2} + \beta \frac{\partial^2 u}{\partial x^2} \right)$$

$$+ \beta \chi_{sg}^2 \left(\beta \frac{\partial^4 u}{\partial x^4} + \frac{\partial w}{\partial x} \frac{\partial^4 w}{\partial x^4} + 3 \frac{\partial^3 w}{\partial x^3} \frac{\partial^2 w}{\partial x^2} + 3 \frac{d^3 w_0}{dx^3} \frac{\partial^2 w}{\partial x^2} + \frac{\partial^4 w}{\partial x^4} \frac{dw_0}{dx} + 3 \frac{d^2 w_0}{dx^2} \frac{\partial^3 w}{\partial x^3} + \frac{\partial w}{\partial x} \frac{d^4 w_0}{dx^4} \right)$$

$$- \beta \eta \left(\frac{dw_0}{dx} \frac{\partial^3 w}{\partial t \partial x^2} + \frac{\partial^2 w}{\partial t \partial x} \frac{\partial^2 w}{\partial x^2} + \beta \frac{\partial^3 u}{\partial t \partial x^2} + \frac{d^2 w_0}{dx^2} \frac{\partial^2 w}{\partial t \partial x} + \frac{\partial w}{\partial x} \frac{\partial^3 w}{\partial t \partial x^2} \right)$$

$$+ \beta \eta \chi_{sg}^2 \left(\beta \frac{\partial^5 u}{\partial t \partial x^4} + 3 \frac{\partial^3 w}{\partial x^3} \frac{\partial^3 w}{\partial x^2 \partial t} + 3 \frac{\partial^2 w}{\partial x^2} \frac{\partial^4 w}{\partial t \partial x^3} + \frac{\partial^2 w}{\partial t \partial x} \frac{\partial^4 w}{\partial x^4} + \frac{\partial w}{\partial x} \frac{\partial^5 w}{\partial t \partial x^4} \right.$$

$$\left. + 3 \frac{\partial^4 w}{\partial t \partial x^3} \frac{d^2 w_0}{dx^2} + \frac{\partial^5 w}{\partial t \partial x^4} \frac{dw_0}{dx} + 3 \frac{\partial^3 w}{\partial t \partial x^2} \frac{d^3 w_0}{dx^3} + \frac{\partial^2 w}{\partial t \partial x} \frac{d^4 w_0}{dx^4} \right) = 0,$$

$$\frac{\partial^2 w}{\partial t^2} - \chi_{nl}^2 \frac{\partial^4 w}{\partial x^2 \partial t^2} - F_1 \beta \cos(\Omega t) + \frac{\partial^4 w}{\partial x^4} - \chi_{sg}^2 \frac{\partial^6 w}{\partial x^6} + \eta \left(\frac{\partial^5 w}{\partial t \partial x^4} - \chi_{sg}^2 \frac{\partial^7 w}{\partial t \partial x^6} \right)$$

$$- \left[\frac{\partial^2 w}{\partial x^2} + \frac{d^2 w_0}{dx^2} - \chi_{nl}^2 \left(\frac{\partial^4 w}{\partial x^4} + \frac{d^4 w_0}{dx^4} \right) \right] \left[\frac{1}{2} \left(\frac{\partial w}{\partial x} \right)^2 + \frac{dw_0}{dx} \frac{\partial w}{\partial x} + \beta \frac{\partial u}{\partial x} \right]$$

$$- \left[\frac{dw_0}{dx} + \frac{\partial w}{\partial x} - 3 \chi_{nl}^2 \left(\frac{\partial^3 w}{\partial x^3} + \frac{d^3 w_0}{dx^3} \right) \right] \left(\beta \frac{\partial^2 u}{\partial x^2} + \frac{\partial w}{\partial x} \frac{\partial^2 w}{\partial x^2} + \frac{\partial^2 w}{\partial x^2} \frac{dw_0}{dx} + \frac{\partial w}{\partial x} \frac{d^2 w_0}{dx^2} \right)$$

$$+ \left[(\chi_{sg}^2 + 3\chi_{nl}^2) \left(\frac{\partial^2 w}{\partial x^2} + \frac{d^2 w_0}{dx^2} \right) - \chi_{nl}^2 \chi_{sg}^2 \left(\frac{\partial^4 w}{\partial x^4} + \frac{d^4 w_0}{dx^4} \right) \right]$$

$$\times \left[\beta \frac{\partial^3 u}{\partial x^3} + \left(\frac{\partial^2 w}{\partial x^2} \right)^2 + \frac{\partial w}{\partial x} \frac{\partial^3 w}{\partial x^3} + \frac{\partial^3 w}{\partial x^3} \frac{dw_0}{dx} + 2 \frac{\partial^2 w}{\partial x^2} \frac{d^2 w_0}{dx^2} + \frac{\partial w}{\partial x} \frac{d^3 w_0}{dx^3} \right]$$

$$+ \left[(\chi_{sg}^2 + \chi_{nl}^2) \left(\frac{\partial w}{\partial x} + \frac{dw_0}{dx} \right) - 3 \chi_{nl}^2 \chi_{sg}^2 \left(\frac{\partial^3 w}{\partial x^3} + \frac{d^3 w_0}{dx^3} \right) \right]$$

$$\times \left(\beta \frac{\partial^4 u}{\partial x^4} + 3 \frac{\partial^2 w}{\partial x^2} \frac{\partial^3 w}{\partial x^3} + \frac{\partial w}{\partial x} \frac{\partial^4 w}{\partial x^4} + \frac{\partial^4 w}{\partial x^4} \frac{dw_0}{dx} + 3 \frac{\partial^3 w}{\partial x^3} \frac{d^2 w_0}{dx^2} + 3 \frac{\partial^2 w}{\partial x^2} \frac{d^3 w_0}{dx^3} + \frac{\partial w}{\partial x} \frac{d^4 w_0}{dx^4} \right)$$

$$- 3 \chi_{nl}^2 \chi_{sg}^2 \left(\frac{\partial^2 w}{\partial x^2} + \frac{d^2 w_0}{dx^2} \right) \left[\beta \frac{\partial^5 u}{\partial x^5} + 3 \left(\frac{\partial^3 w}{\partial x^3} \right)^2 + 4 \frac{\partial^2 w}{\partial x^2} \frac{\partial^4 w}{\partial x^4} + \frac{\partial w}{\partial x} \frac{\partial^5 w}{\partial x^5} \right.$$

$$\left. + \frac{\partial^5 w}{\partial x^5} \frac{dw_0}{dx} + 4 \frac{\partial^4 w}{\partial x^4} \frac{d^2 w_0}{dx^2} + 6 \frac{\partial^3 w}{\partial x^3} \frac{d^3 w_0}{dx^3} + 4 \frac{\partial^2 w}{\partial x^2} \frac{d^4 w_0}{dx^4} + \frac{\partial w}{\partial x} \frac{d^5 w_0}{dx^5} \right]$$

$$- \chi_{nl}^2 \chi_{sg}^2 \left(\frac{\partial w}{\partial x} + \frac{dw_0}{dx} \right) \left[\beta \frac{\partial^6 u}{\partial x^6} + 10 \frac{\partial^3 w}{\partial x^3} \frac{\partial^4 w}{\partial x^4} + 5 \frac{\partial^2 w}{\partial x^2} \frac{\partial^5 w}{\partial x^5} + \frac{\partial w}{\partial x} \frac{\partial^6 w}{\partial x^6} \right.$$

$$
\begin{aligned}
&+ \frac{\partial^6 w}{\partial x^6}\frac{dw_0}{dx} + 5\frac{\partial^5 w}{\partial x^5}\frac{d^2 w_0}{dx^2} + 10\frac{\partial^4 w}{\partial x^4}\frac{d^3 w_0}{dx^3} + 10\frac{\partial^3 w}{\partial x^3}\frac{d^4 w_0}{dx^4} + 5\frac{\partial^2 w}{\partial x^2}\frac{d^5 w_0}{dx^5} + \frac{\partial w}{\partial x}\frac{d^6 w_0}{dx^6} \Bigg] \\[4pt]
&- \eta\left[\frac{\partial^2 w}{\partial x^2} + \frac{d^2 w_0}{dx^2} - \chi_{nl}^2\left(\frac{\partial^4 w}{\partial x^4} + \frac{d^4 w_0}{dx^4}\right)\right]\left(\frac{\partial w}{\partial x}\frac{\partial^2 w}{\partial t\partial x} + \frac{\partial^2 w}{\partial t\partial x}\frac{dw_0}{dx} + \beta\frac{\partial^2 u}{\partial t\partial x}\right) \\[4pt]
&- \eta\left[\frac{dw_0}{dx} + \frac{\partial w}{\partial x} - 3\chi_{nl}^2\left(\frac{\partial^3 w}{\partial x^3} + \frac{d^3 w_0}{dx^3}\right)\right]\left(\beta\frac{\partial^3 u}{\partial x^2\partial t} + \frac{\partial w}{\partial x}\frac{\partial^3 w}{\partial t\partial x^2} + \frac{\partial^2 w}{\partial x^2}\frac{\partial^2 w}{\partial t\partial x}\right. \\[4pt]
&\left. + \frac{\partial^3 w}{\partial t\partial x^2}\frac{dw_0}{dx} + \frac{\partial^2 w}{\partial t\partial x}\frac{d^2 w_0}{dx^2}\right) + \eta\left[\left(3\chi_{nl}^2 + \chi_{sg}^2\right)\left(\frac{\partial^2 w}{\partial x^2} + \frac{d^2 w_0}{dx^2}\right) - \chi_{nl}^2\chi_{sg}^2\left(\frac{\partial^4 w}{\partial x^4} + \frac{d^4 w_0}{dx^4}\right)\right] \\[4pt]
&\times \left(\frac{\partial^2 w}{\partial t\partial x}\frac{\partial^3 w}{\partial x^3} + \beta\frac{\partial^4 u}{\partial t\partial x^3} + \frac{\partial w}{\partial x}\frac{\partial^4 w}{\partial t\partial x^3} + 2\frac{\partial^3 w}{\partial t\partial x^2}\frac{\partial^2 w}{\partial x^2} + \frac{\partial^4 w}{\partial t\partial x^3}\frac{dw_0}{dx} + 2\frac{\partial^3 w}{\partial t\partial x^2}\frac{d^2 w_0}{dx^2} + \frac{\partial^2 w}{\partial t\partial x}\frac{d^3 w_0}{dx^3}\right) \quad (20)
\end{aligned}
$$

$$
\begin{aligned}
&+ \eta\left[\left(\chi_{sg}^2 + \chi_{nl}^2\right)\left(\frac{\partial w}{\partial x} + \frac{dw_0}{dx}\right) - 3\chi_{nl}^2\chi_{sg}^2\left(\frac{\partial^3 w}{\partial x^3} + \frac{d^3 w_0}{dx^3}\right)\right]\left(\beta\frac{\partial^5 u}{\partial x^4\partial t} + 3\frac{\partial^4 w}{\partial x^3\partial t}\frac{\partial^2 w}{\partial x^2} + \frac{\partial^4 w}{\partial x^4}\frac{\partial^2 w}{\partial t\partial x}\right. \\[4pt]
&\left. + 3\frac{\partial^3 w}{\partial x^3}\frac{\partial^3 w}{\partial t\partial x^2} + \frac{\partial w}{\partial x}\frac{\partial^5 w}{\partial t\partial x^4} + \frac{\partial^5 w}{\partial t\partial x^4}\frac{dw_0}{dx} + 3\frac{\partial^4 w}{\partial t\partial x^3}\frac{d^2 w_0}{dx^2} + 3\frac{\partial^3 w}{\partial t\partial x^2}\frac{d^3 w_0}{dx^3} + \frac{\partial^2 w}{\partial t\partial x}\frac{d^4 w_0}{dx^4}\right) \\[4pt]
&- 3\eta\chi_{nl}^2\chi_{sg}^2\left(\frac{\partial^2 w}{\partial x^2} + \frac{d^2 w_0}{dx^2}\right)\left(\frac{\partial^2 w}{\partial t\partial x}\frac{\partial^5 w}{\partial x^5} + 4\frac{\partial^2 w}{\partial x^2}\frac{\partial^5 w}{\partial t\partial x^4} + \beta\frac{\partial^6 u}{\partial t\partial x^5} + 4\frac{\partial^3 w}{\partial t\partial x^2}\frac{\partial^4 w}{\partial x^4} + 6\frac{\partial^4 w}{\partial t\partial x^3}\frac{\partial^3 w}{\partial x^3}\right. \\[4pt]
&\left. + \frac{\partial w}{\partial x}\frac{\partial^6 w}{\partial t\partial x^5} + \frac{\partial^6 w}{\partial t\partial x^5}\frac{dw_0}{dx} + 4\frac{\partial^5 w}{\partial t\partial x^4}\frac{d^2 w_0}{dx^2} + 6\frac{\partial^4 w}{\partial t\partial x^3}\frac{d^3 w_0}{dx^3} + 4\frac{\partial^3 w}{\partial t\partial x^2}\frac{d^4 w_0}{dx^4} + \frac{\partial^2 w}{\partial t\partial x}\frac{d^5 w_0}{dx^5}\right) \\[4pt]
&- \eta\chi_{nl}^2\chi_{sg}^2\left(\frac{\partial w}{\partial x} + \frac{dw_0}{dx}\right)\left(\beta\frac{\partial^7 u}{\partial t\partial x^6} + \frac{\partial^6 w}{\partial x^6}\frac{\partial^2 w}{\partial t\partial x} + 5\frac{\partial^5 w}{\partial x^5}\frac{\partial^3 w}{\partial t\partial x^2} + 10\frac{\partial^4 w}{\partial x^4}\frac{\partial^4 w}{\partial t\partial x^3}\right. \\[4pt]
&+ 10\frac{\partial^3 w}{\partial x^3}\frac{\partial^5 w}{\partial t\partial x^4} + 5\frac{\partial^2 w}{\partial x^2}\frac{\partial^6 w}{\partial t\partial x^5} + \frac{\partial w}{\partial x}\frac{\partial^7 w}{\partial t\partial x^6} + \frac{\partial^7 w}{\partial t\partial x^6}\frac{dw_0}{dx} + 5\frac{\partial^6 w}{\partial t\partial x^5}\frac{d^2 w_0}{dx^2} \\[4pt]
&\left. + 10\frac{\partial^5 w}{\partial t\partial x^4}\frac{d^3 w_0}{dx^3} + 10\frac{\partial^4 w}{\partial t\partial x^3}\frac{d^4 w_0}{dx^4} + 5\frac{\partial^3 w}{\partial t\partial x^2}\frac{d^5 w_0}{dx^5} + \frac{\partial^2 w}{\partial t\partial x}\frac{d^6 w_0}{dx^6}\right) \\[4pt]
&- \frac{\chi_{nl}^2}{\beta}\left[\frac{\partial^2 w}{\partial x^2} + \frac{d^2 w_0}{dx^2} - \chi_{nl}^2\left(\frac{\partial^4 w}{\partial x^4} + \frac{d^4 w_0}{dx^4}\right)\right]\frac{\partial^3 u}{\partial x\partial t^2} \\[4pt]
&- \frac{\chi_{nl}^2}{\beta}\left[\frac{\partial w}{\partial x} + \frac{dw_0}{dx} - 3\chi_{nl}^2\left(\frac{\partial^3 w}{\partial x^3} + \frac{d^3 w_0}{dx^3}\right)\right]\frac{\partial^4 u}{\partial x^2\partial t^2} \\[4pt]
&+ 3\frac{\chi_{nl}^4}{\beta}\left(\frac{\partial^2 w}{\partial x^2} + \frac{d^2 w_0}{dx^2}\right)\frac{\partial^5 u}{\partial x^3\partial t^2} + \frac{\chi_{nl}^4}{\beta}\left(\frac{\partial w}{\partial x} + \frac{dw_0}{dx}\right)\frac{\partial^6 u}{\partial x^4\partial t^2} = 0. \quad (21)
\end{aligned}
$$

In Eqs. (20) and (21), asterisk superscripts are neglected for the sake of simplification. As the second step, the non-dimensional nonlinear coupled equations are discretised employing the following expressions

$$
u(x,t) = \sum_{i=1}^{N_x} r_i\ [\text{as a function of } t]\Phi_i\ [\text{as a function of } x],
$$

$$
w(x,t) = \sum_{i=1}^{N_z} q_i\ [\text{as a function of } t]\Psi_i\ [\text{as a function of } x]. \quad (22)
$$

Here (r_i, q_i) and (Φ_i, Ψ_i) indicate the generalised coordinates and the shape functions of the imperfect viscoelastic CNT, respectively. Assuming the initial deflection as $w_0 = A_0\Psi_1(x)$ and applying Eq. (22), a set of coupled discretised equations are obtained, where, a continuation-based approach is applied so as to the frequency response of the imperfect viscoelastic CNT is obtained.

4. Numerical results

A nonlinear investigation is performed in the following to examine the effect of initial deflections on the nonlinear coupled response of viscoelastic CNTs. All results are plotted for the case of a zigzag (10, 0) single-walled CNT. The scale
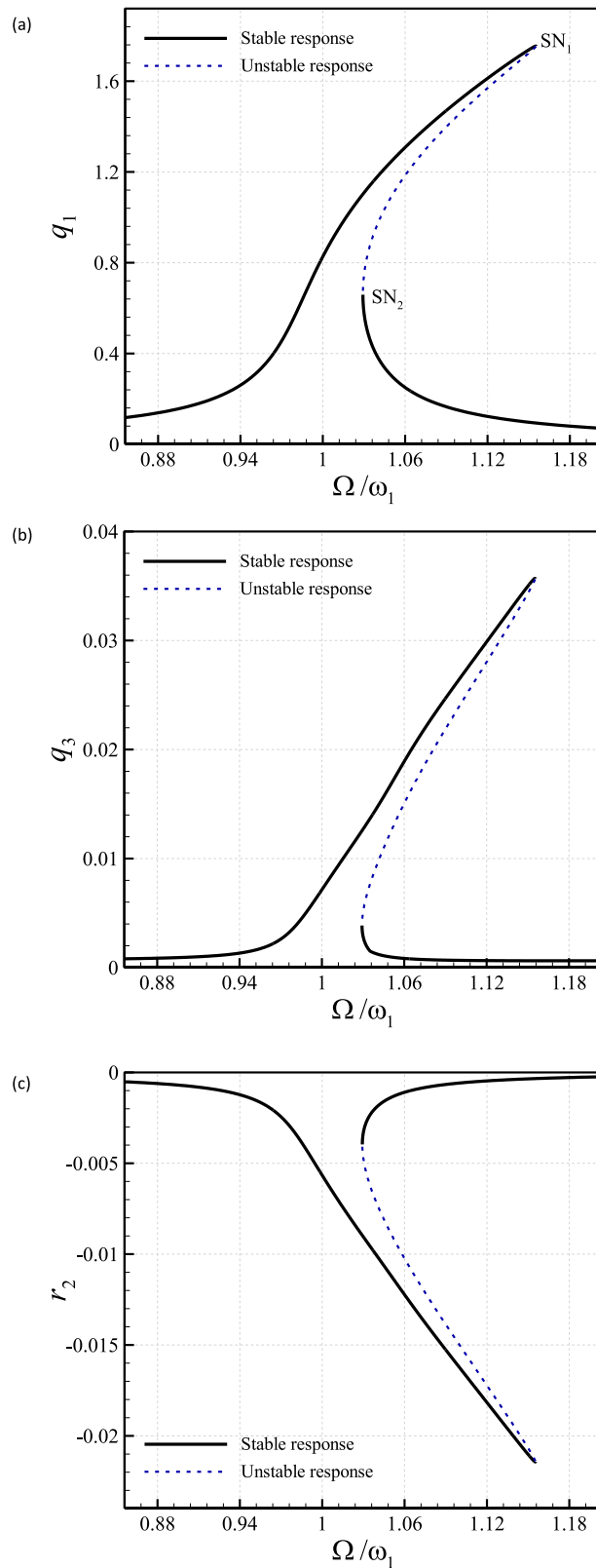
Fig. 2. Frequency-amplitude response of the initially imperfect viscoelastic CNT; (a,b) the maximum of q_1 and q_3, respectively; (c) the minimum of r_2; $A_0 = 0.7$.
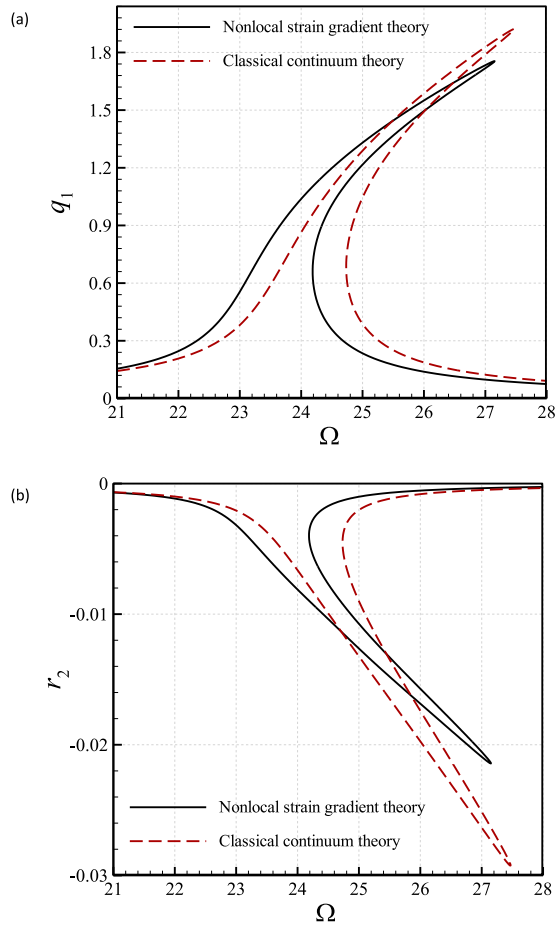
Fig. 3. Comparison of frequency-amplitude responses of the initially imperfect viscoelastic CNT obtained via the nonlocal strain gradient (χ_{nl} = 0.1, χ_{sg} = 0.05) and classical continuum (χ_{nl} = 0, χ_{sg} = 0) theories; (a) the maximum of q_1; (b) the minimum of r_2; A_0 = 0.7.

and geometrical parameters of the imperfect viscoelastic nanosystem are as (χ_{nl} = 0.1, χ_{sg} = 0.05) and (L = 20, h = 0.34, d = 0.7829) nm, respectively. Here the thickness and the average diameter are, respectively, shown by h and d. For the described geometry, the slenderness ratio is as β = 66.2751. The material features of the imperfect viscoelastic zigzag CNT are considered as E = 1.0 TPa, ν = 0.19, η = 0.00045 and ρ = 2300 kg/m^3 for all the cases.

Plotted in Fig. 2 is the size-dependent frequency-amplitude responses of the initially imperfect viscoelastic CNT for χ_{nl} = 0.1, χ_{sg} = 0.05, F_1 = 0.35, A_0 = 0.7, and η = 0.00045. The coupled resonance behaviour of this nanoscale system is of hardening nonlinearity; two saddle nodes at Ω/ω_1 = 1.1554 and Ω/ω_1 = 1.0292 are found. The natural frequency of the initially imperfect viscoelastic CNT is ω_1 = 23.4998. It is worth pointing out that between the two saddle nodes, the nonlinear response is unstable while it is stable in other regions.
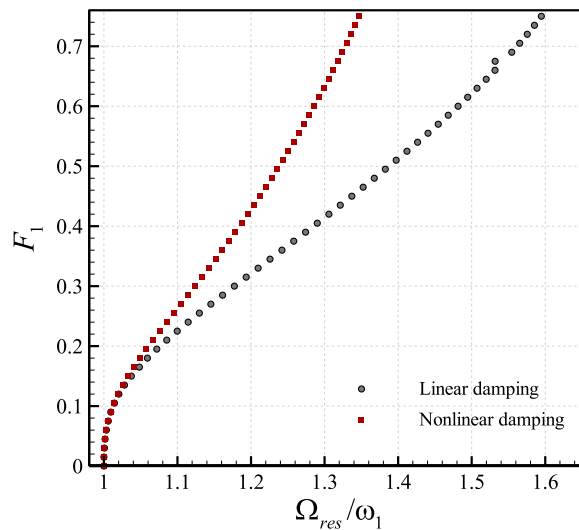
The frequency-amplitude responses of the initially imperfect viscoelastic CNT obtained via the nonlocal strain gradient and classical continuum theories are indicated in Fig. 3. The dimensional parameters of the imperfect viscoelastic nanotube are set to F_1 = 0.35, A_0 = 0.7 and η = 0.00045. Using the classical continuum theory causes overestimated results for the motion amplitudes in both directions (i.e. the axial and transverse ones). In addition, the resonance frequency of the modified nonlocal theory is slightly lower than the frequency estimated by the classical continuum theory.

Shown in Fig. 4 is the force-amplitude responses of the initially imperfect viscoelastic nanotube obtained via the nonlocal strain gradient and classical continuum theories for Ω = 25.0, A_0 = 0.7, and η = 0.00045. The size parameters for the nonlocal strain gradient and classical continuum theories are taken as (χ_{nl} = 0.1, χ_{sg} = 0.05) and (χ_{nl} = 0, χ_{sg} = 0), respectively. Applying the classical continuum theory generally yields higher values of q_1 and r_2. Moreover, ignoring the influence of size parameters causes significantly underestimated results for the value of F_1 related to the saddle node.

Fig. 5 represents the variation of the resonance forcing amplitude versus the resonance frequency for initially imperfect viscoelastic CNTs for two damping mechanisms. For the linear damping, it is assumed that ζ = 0.006 where ζ denotes the modal damping ratio. Moreover, a value of η = 0.00045 is assumed for the nonlinear damping in this figure. For relatively
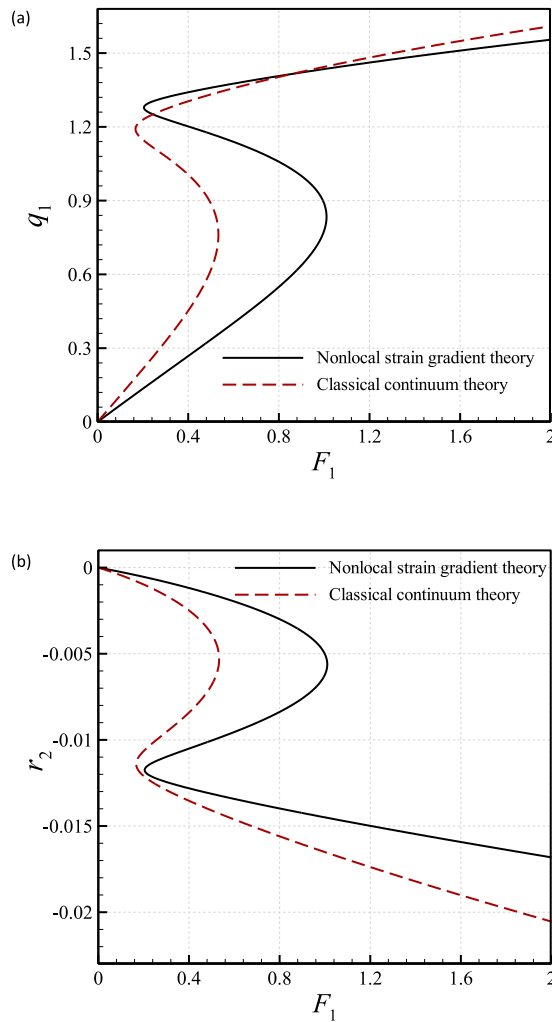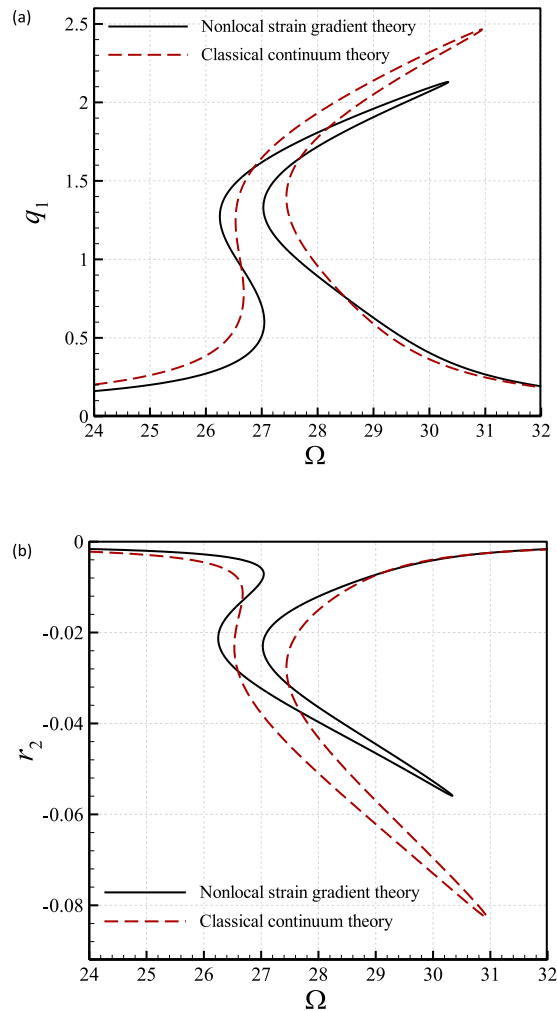
Fig. 4. Comparison of force-amplitude responses of the initially imperfect viscoelastic CNT obtained via the nonlocal strain gradient ($\chi_{nl} = 0.1$, $\chi_{sg} = 0.05$) and classical continuum ($\chi_{nl} = 0$, $\chi_{sg} = 0$) theories; (a) the maximum of q_1; (b) the minimum of r_2; $A_0 = 0.7$.

Fig. 5. Resonance forcing amplitude versus the resonance frequency for two damping mechanisms; a circle denotes the linear damping mechanism ($\zeta = 0.006$) while a square denotes the nonlinear one ($\eta = 0.00045$); $A_0 = 0.7$.
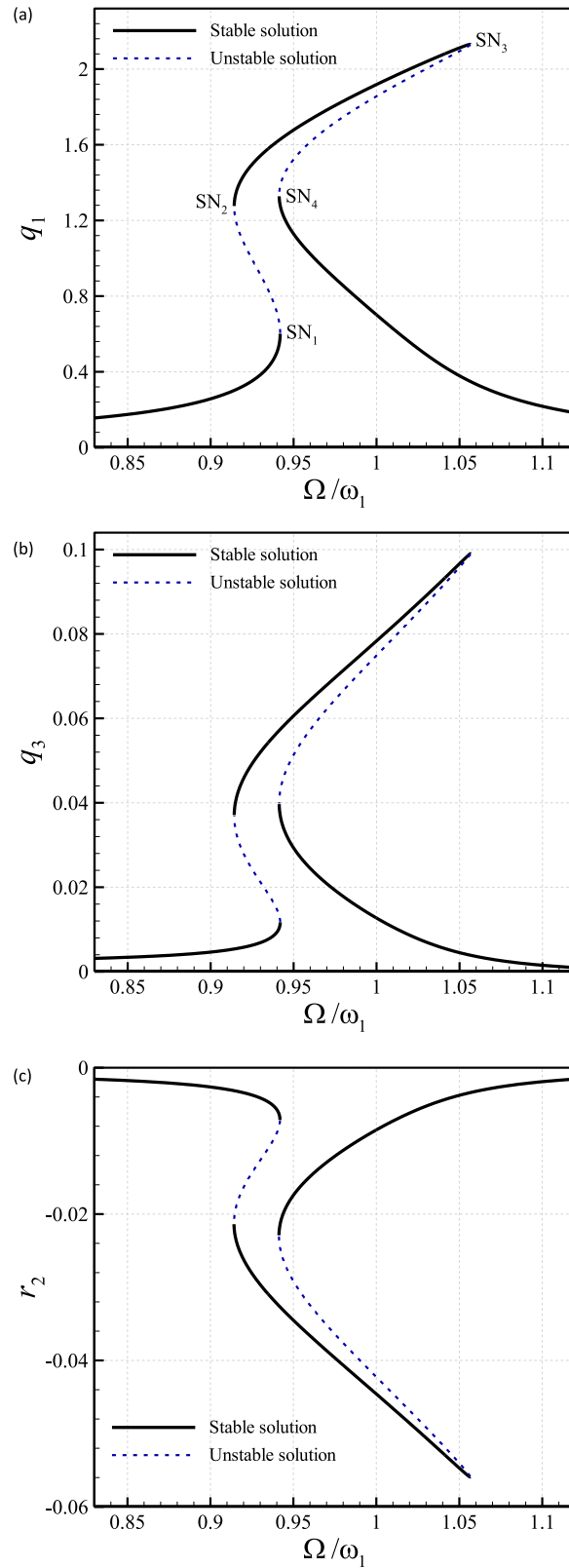
Fig. 6. Frequency-amplitude diagrams of the initially imperfect viscoelastic nanotube; (a,b) the maximum of q_1 and q_3, respectively; (c) the minimum of r_2; $A_0 = 1.4$.
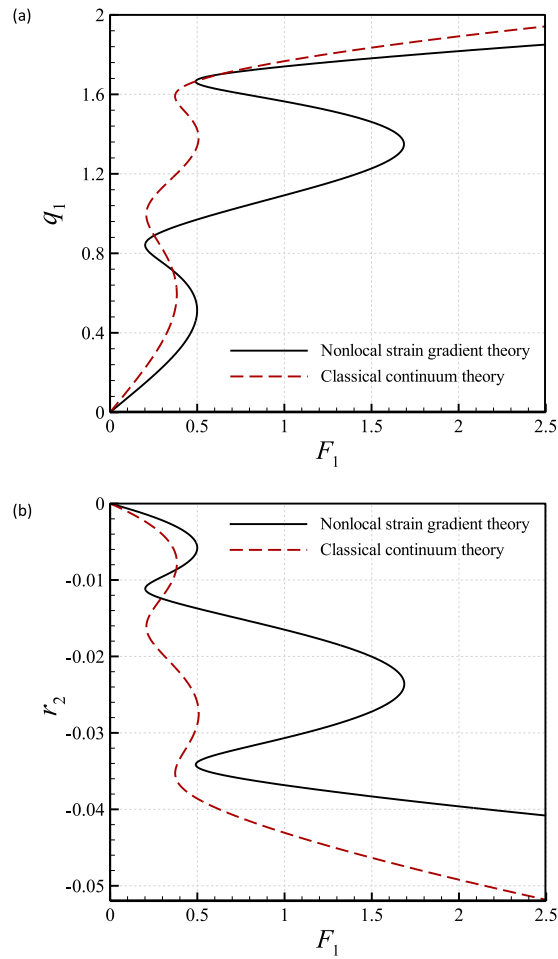
Fig. 7. Comparison of frequency-amplitude responses of the initially imperfect viscoelastic CNT obtained via the nonlocal strain gradient and classical continuum theories; (a) the maximum of q_1; (b) the minimum of r_2; $A_0 = 1.4$.

small values of F_1, there is not an important difference between the results of the two mechanisms. By contrast, for high values of F_1, ignoring nonlinear damping effects causes overestimated results for the resonance frequencies.

Plotted in Fig. 6 is the size-dependent frequency-amplitude responses of the initially imperfect viscoelastic CNT for a higher imperfection amplitude ($A_0 = 1.4$). Other CNT parameters are set to $\chi_{nl} = 0.1$, $\chi_{sg} = 0.05$, $F_1 = 0.80$, and $\eta = 0.00045$. This time the coupled resonance behaviour of the imperfect viscoelastic zigzag CNT is significantly changed. Four saddle nodes at $\Omega/\omega_1 = 0.9419$, 0.9142, 1.0566 and 0.9413 are found for the softening-hardening behaviour. In this case, the natural frequency of the initially imperfect viscoelastic zigzag CNT is as $\omega_1 = 28.7136$. Fig. 7 also represents the frequency-amplitude responses of the initially imperfect viscoelastic nanosystem obtained via the nonlocal strain gradient ($\chi_{nl} = 0.1$, $\chi_{sg} = 0.05$) and classical continuum ($\chi_{nl} = 0$, $\chi_{sg} = 0$) theories for $F_1 = 0.80$, $A_0 = 1.4$, and $\eta = 0.00045$. It is found that the classical continuum theory leads to overestimated results for the motion amplitudes of imperfect viscoelastic zigzag CNTs in both directions.

Fig. 8 indicates the force-amplitude responses of the initially imperfect viscoelastic nanotube obtained via the nonlocal strain gradient and classical continuum theories; this time a larger imperfection amplitude is chosen $A_0 = 1.4$. The excitation frequency and the viscoelastic coefficient are, respectively, set to $\Omega = 27.5$, and $\eta = 0.00045$. Ignoring the size effect generally yields higher values of q_1 and r_2. Plotted in Fig. 5 is the variation of the resonance forcing amplitude versus the resonance frequency for initially imperfect viscoelastic CNTs for two damping mechanisms. For the linear damping, it is assumed that $\zeta = 0.0072$ while a value of $\eta = 0.00045$ is assumed for the nonlinear damping. For small values of F_1, no important difference between the results of the two mechanisms is found. Nonetheless, for relatively high values of F_1, nonlinear damping effects become important. Ignoring them causes highly overestimated results for the resonance frequency.

Fig. 8. Comparison of force-amplitude responses of the initially imperfect viscoelastic CNT obtained via the nonlocal strain gradient ($\chi_{nl} = 0.1$, $\chi_{sg} = 0.05$) and classical continuum ($\chi_{nl} = 0$, $\chi_{sg} = 0$) theories; (a) the maximum of q_1; (b) the minimum of r_2; $A_0 = 1.4$.
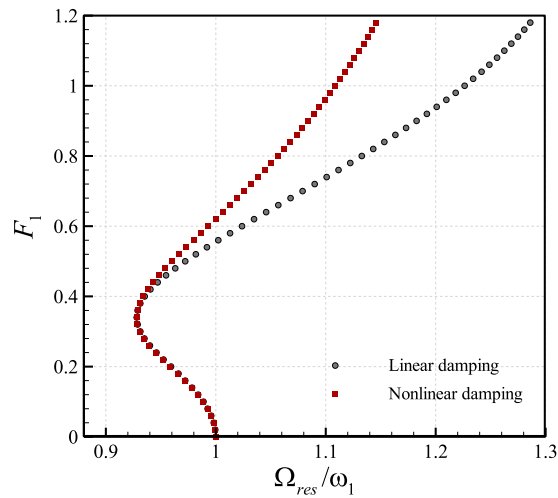
Fig. 9. Resonance forcing amplitude versus the resonance frequency for two damping mechanisms; a circle denotes the linear damping mechanism ($\zeta = 0.006$) while a square denotes the nonlinear one ($\eta = 0.00045$); $A_0 = 1.4$.

5. Concluding remarks

A nonlocal coupled nonlinear beam model was proposed in this paper in order to extract the mechanical response of initially imperfect viscoelastic CNTs. The effect of viscoelasticity was modelled using a viscoelastic model. Moreover, the influence of being geometrically imperfect was captured by considering an initial deflection along the transverse direction. The coupled nonlinear equations of the initially imperfect viscoelastic CNT were derived and solved by applying a work/energy law and a Galerkin procedure.

It was found that the coupled resonance behaviour of viscoelastic CNTs is of hardening nonlinearity with two saddle nodes when a relatively small imperfection is imposed. In addition, using the classical continuum theory causes overestimated amplitudes of motion along both directions. The resonance frequency of the coupled nonlocal model is lower than the frequency estimated by the classical model. For relatively small forcing amplitudes, there is not an important difference between the results of the linear and nonlinear damping mechanisms. By contrast, for high values of this parameter, ignoring nonlinear damping causes overestimated resonance frequencies. It was also seen that a change in the initial deflection can alter the number of the saddle nodes. Four saddle nodes are found for CNTs when a large enough initial deflection is imposed (Fig. 9).

References

Apuzzo, A., Barretta, R., Faghidian, S. A., Luciano, R., & Marotti de Sciarra, F. (2018). Free vibrations of elastic beams by modified nonlocal strain gradient theory. *International Journal of Engineering Science, 133*, 99–108.

Attia, M. A., & Abdel Rahman, A. A. (2018). On vibrations of functionally graded viscoelastic nanobeams with surface effects. *International Journal of Engineering Science, 127*, 1–32.

Aydogdu, M. (2012). Axial vibration analysis of nanorods (carbon nanotubes) embedded in an elastic medium using nonlocal elasticity. *Mechanics Research Communications, 43*, 34–40.

Aydogdu, M., & Filiz, S. (2011). Modeling carbon nanotube-based mass sensors using axial vibration and nonlocal elasticity. *Physica E: Low-dimensional Systems and Nanostructures, 43*, 1229–1234.

Bahaadini, R., & Hosseini, M. (2016). Effects of nonlocal elasticity and slip condition on vibration and stability analysis of viscoelastic cantilever carbon nanotubes conveying fluid. *Computational Materials Science, 114*, 151–159.

Bahaadini, R., Saidi, A. R., & Hosseini, M. (2018). On dynamics of nanotubes conveying nanoflow. *International Journal of Engineering Science, 123*, 181–196.

Barretta, R., Čanađija, M., Luciano, R., & de Sciarra, F. M. (2018). Stress-driven modeling of nonlocal thermoelastic behavior of nanobeams. *International Journal of Engineering Science, 126*, 53–67.

Barretta, R., Faghidian, S. A., & Marotti de Sciarra, F. (2019). Stress-driven nonlocal integral elasticity for axisymmetric nano-plates. *International Journal of Engineering Science, 136*, 38–52.

Chang, W.-J., & Lee, H.-L. (2012). Vibration analysis of viscoelastic carbon nanotubes. *Micro & Nano Letters, 7*, 1308–1312.

Dehrouyeh-Semnani, A. M., Nikkhah-Bahrami, M., & Yazdi, M. R. H. (2017). On nonlinear vibrations of micropipes conveying fluid. *International Journal of Engineering Science, 117*, 20–33.

Demir, Ç., & Civalek, Ö. (2017). On the analysis of microbeams. *International Journal of Engineering Science, 121*, 14–33.

Ebrahimi, F., & Barati, M. R. (2016). A nonlocal higher-order refined magneto-electro-viscoelastic beam model for dynamic analysis of smart nanostructures. *International Journal of Engineering Science, 107*, 183–196.

Ebrahimi, F., Barati, M. R., & Dabbagh, A. (2016). A nonlocal strain gradient theory for wave propagation analysis in temperature-dependent inhomogeneous nanoplates. *International Journal of Engineering Science, 107*, 169–182.

Faghidian, S. A. (2018). Integro-differential nonlocal theory of elasticity. *International Journal of Engineering Science, 129*, 96–110.

Faleh, N. M., Ahmed, R. A., & Fenjan, R. M. (2018). On vibrations of porous FG nanoshells. *International Journal of Engineering Science, 133*, 1–14.

Farajpour, A., Ghayesh, M. H., & Farokhi, H. (2018). A review on the mechanics of nanostructures. *International Journal of Engineering Science, 133*, 231–263.

Farokhi, H., & Ghayesh, M. H. (2018a). Nonlinear mechanics of electrically actuated microplates. *International Journal of Engineering Science, 123*, 197–213.

Farokhi, H., & Ghayesh, M. H. (2018b). On the dynamics of imperfect shear deformable microplates. *International Journal of Engineering Science, 133*, 264–283.

Farokhi, H., Ghayesh, M. H., & Gholipour, A. (2017a). Dynamics of functionally graded micro-cantilevers. *International Journal of Engineering Science, 115*, 117–130.

Farokhi, H., Ghayesh, M. H., Gholipour, A., & Hussain, S. (2017b). Motion characteristics of bilayered extensible Timoshenko microbeams. *International Journal of Engineering Science, 112*, 1–17.

Fernández-Sáez, J., & Zaera, R. (2017). Vibrations of Bernoulli-Euler beams using the two-phase nonlocal elasticity theory. *International Journal of Engineering Science, 119*, 232–248.

Ghayesh, M. H. (2018). Nonlinear vibrations of axially functionally graded Timoshenko tapered beams. *Journal of Computational and Nonlinear Dynamics, 13* 041002-041002-041010.

Ghayesh, M. H., & Farajpour, A. (2018). Nonlinear mechanics of nanoscale tubes via nonlocal strain gradient theory. *International Journal of Engineering Science, 129*, 84–95.

Ghayesh, M. H., & Farajpour, A. (2019). A review on the mechanics of functionally graded nanoscale and microscale structures. *International Journal of Engineering Science, 137*, 8–36.

Ghayesh, M. H., Farokhi, H., Gholipour, A., & Hussain, S. (2017). On the nonlinear mechanics of layered microcantilevers. *International Journal of Engineering Science, 120*, 1–14.

Ghayesh, M. H., Farokhi, H., Gholipour, A., & Tavallaeinejad, M. (2018). Nonlinear oscillations of functionally graded microplates. *International Journal of Engineering Science, 122*, 56–72.

Hadi, A., Nejad, M. Z., & Hosseini, M. (2018). Vibrations of three-dimensionally graded nanobeams. *International Journal of Engineering Science, 128*, 12–23.

Jalaei, M. H., Arani, A. G., & Tourang, H. (2018). On the dynamic stability of viscoelastic graphene sheets. *International Journal of Engineering Science, 132*, 16–29.

Karami, B., & Janghorban, M. (2019). On the dynamics of porous nanotubes with variable material properties and variable thickness. *International Journal of Engineering Science, 136*, 53–66.

Karličić, D., Murmu, T., Cajić, M., Kozić, P., & Adhikari, S. (2014). Dynamics of multiple viscoelastic carbon nanotube based nanocomposites with axial magnetic field. *Journal of Applied Physics, 115*, 234303.

Khaniki, H. B. (2018). On vibrations of nanobeam systems. *International Journal of Engineering Science, 124*, 85–103.

Khaniki, H. B. (2019). On vibrations of FG nanobeams. *International Journal of Engineering Science, 135*, 23–36.

Lei, Y., Adhikari, S., & Friswell, M. (2013). Vibration of nonlocal Kelvin–Voigt viscoelastic damped Timoshenko beams. *International Journal of Engineering Science, 66*, 1–13.

Li, L., & Hu, Y. (2016). Wave propagation in fluid-conveying viscoelastic carbon nanotubes based on nonlocal strain gradient theory. Computational Materials Science, *112*, 282–288.

Li, L., Hu, Y., & Ling, L. (2016). Wave propagation in viscoelastic single-walled carbon nanotubes with surface effect under magnetic field based on nonlocal strain gradient theory. *Physica E: Low-dimensional Systems and Nanostructures, 75*, 118–124.

Li, L., Tang, H., & Hu, Y. (2018). The effect of thickness on the mechanics of nanobeams. *International Journal of Engineering Science, 123*, 81–91.

Lim, C., Zhang, G., & Reddy, J. (2015). A higher-order nonlocal elasticity and strain gradient theory and its applications in wave propagation. *Journal of the Mechanics and Physics of Solids, 78*, 298–313.

Lu, L., Guo, X., & Zhao, J. (2017a). Size-dependent vibration analysis of nanobeams based on the nonlocal strain gradient theory. *International Journal of Engineering Science, 116*, 12–24.

Lu, L., Guo, X., & Zhao, J. (2017b). A unified nonlocal strain gradient model for nanobeams and the importance of higher order terms. *International Journal of Engineering Science, 119*, 265–277.

Lu, L., Guo, X., & Zhao, J. (2018). On the mechanics of Kirchhoff and Mindlin plates incorporating surface energy. *International Journal of Engineering Science, 124*, 24–40.

Malekzadeh, P., & Shojaee, M. (2013). Surface and nonlocal effects on the nonlinear free vibration of non-uniform nanobeams. *Composites Part B: Engineering, 52*, 84–92.

Malekzadeh, P., & Shojaee, M. (2015). A two-variable first-order shear deformation theory coupled with surface and nonlocal effects for free vibration of nanoplates. *Journal of Vibration and Control, 21*, 2755–2772.

Natsuki, T., & Natsuki, J. (2018). Transverse impact analysis of double-layered graphene sheets on an elastic foundation. *International Journal of Engineering Science, 124*, 41–48.

Pourasghar, A., & Chen, Z. (2019). Effect of hyperbolic heat conduction on the linear and nonlinear vibration of CNT reinforced size-dependent functionally graded microbeams. *International Journal of Engineering Science, 137*, 57–72.

Qi, L., Huang, S., Fu, G., Zhou, S., & Jiang, X. (2018). On the mechanics of curved flexoelectric microbeams. *International Journal of Engineering Science, 124*, 1–15.

Rahaeifard, M., & Mojahedi, M. (2017). On the mechanics of laminated microplates. *International Journal of Engineering Science, 119*, 180–188.

Romano, G., & Barretta, R. (2017). Nonlocal elasticity in nanobeams: The stress-driven integral model. *International Journal of Engineering Science, 115*, 14–27.

Ruzziconi, L., Bataineh, A. M., Younis, M. I., Cui, W., & Lenci, S. (2013). Nonlinear dynamics of an electrically actuated imperfect microbeam resonator: Experimental investigation and reduced-order modeling. *Journal of Micromechanics and Microengineering, 23*, 075012.

Setoodeh, A., Khosrownejad, M., & Malekzadeh, P. (2011). Exact nonlocal solution for postbuckling of single-walled carbon nanotubes. *Physica E: Low-dimensional Systems and Nanostructures, 43*, 1730–1737.

Shahverdi, H., & Barati, M. R. (2017). Vibration analysis of porous functionally graded nanoplates. *International Journal of Engineering Science, 120*, 82–99.

She, G.-L., Ren, Y.-R., Yuan, F.-G., & Xiao, W.-S. (2018). On vibrations of porous nanotubes. *International Journal of Engineering Science, 125*, 23–35.

Şimşek, M. (2016). Nonlinear free vibration of a functionally graded nanobeam using nonlocal strain gradient theory and a novel Hamiltonian approach. *International Journal of Engineering Science, 105*, 12–27.

Suhr, J., Koratkar, N., Keblinski, P., & Ajayan, P. (2005). Viscoelasticity in carbon nanotube composites. *Nature materials, 4*, 134.

Tang, Y., Liu, Y., & Zhao, D. (2016). Viscoelastic wave propagation in the viscoelastic single walled carbon nanotubes based on nonlocal strain gradient theory. *Physica E: Low-dimensional Systems and Nanostructures, 84*, 202–208.

Xu, M., Futaba, D. N., Yamada, T., Yumura, M., & Hata, K. (2010). Carbon nanotubes with temperature-invariant viscoelasticity from−196 to 1000 C. *Science, 330*, 1364–1368.

Zhang, Y., Pang, M., & Fan, L. (2016). Analyses of transverse vibrations of axially pretensioned viscoelastic nanobeams with small size and surface effects. *Physics Letters A, 380*, 2294–2299.

Zhen, Y., & Zhou, L. (2017). Wave propagation in fluid-conveying viscoelastic carbon nanotubes under longitudinal magnetic field with thermal and surface effect via nonlocal strain gradient theory. *Modern Physics Letters B, 31*, 1750069.

Zhu, X., & Li, L. (2017a). Closed form solution for a nonlocal strain gradient rod in tension. *International Journal of Engineering Science, 119*, 16–28.

Zhu, X., & Li, L. (2017b). On longitudinal dynamics of nanorods. *International Journal of Engineering Science, 120*, 129–145.

Chapter 5

Vibration and bending of small-scale plates

Chapter overview

In this chapter, the third objective of this project, which is the linear time-dependent deformation of small-scale plates, is investigated. An advanced scale-dependent model is developed by using the stress-driven elasticity theory. To simulate size effects, an integral constitutive equation incorporating curvature nonlocality is used. Introducing an appropriate kernel function and using the Leibniz integral rule, additional non-classical edge conditions are derived. The novel stress-driven nonlocal model is reasonable from mathematical point of view compared to available conventional scale-dependent models. The differential quadrature method is applied as this numerical technique is better capable of implementing complex boundary conditions. While the conventional nonlocal models fail to comprehensively model size dependency in a few cases, the stress-driven integral model can describe size effects in a wide range of small-scale problems. The work was published in International Journal of Engineering Science as:

A. Farajpour, C.Q. Howard, W.S.P. Robertson, "On size-dependent mechanics of nanoplates", International Journal of Engineering Science, volume 156, 103368 (2020).

Statement of Authorship

Title of Paper	On size-dependent mechanics of nanoplates
Publication Status	☑ Published ☐ Accepted for Publication ☐ Submitted for Publication ☐ Unpublished and Unsubmitted work written in manuscript style
Publication Details	Ali Farajpour, Carl Q. Howard, William S.P. Robertson, On size-dependent mechanics of nanoplates, International Journal of Engineering Science 156 (2020) 103368

Principal Author

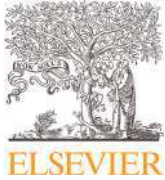| Name of Principal Author (Candidate)	Ali Farajpour Ouderji
Contribution to the Paper	- Doing the literature review of the paper - Deriving the partial differential equations of motion - Incorporating size effects using a scale-dependent continuum approach - Solution procedure - Analysing the results and writing the paper
Overall percentage (%)	80%
Certification:	This paper reports on original research I conducted during the period of my Higher Degree by Research candidature and is not subject to any obligations or contractual agreements with a third party that would constrain its inclusion in this thesis. I am the primary author of this paper.
Signature		Date	2021-2-18

Co-Author Contributions

By signing the Statement of Authorship, each author certifies that:

i.   the candidate's stated contribution to the publication is accurate (as detailed above);

ii.   permission is granted for the candidate in include the publication in the thesis; and

iii.   the sum of all co-author contributions is equal to 100% less the candidate's stated contribution.

Name of Co-Author	Carl Q. Howard
Contribution to the Paper	- Supervising the research work - Contribution to the development of the ideas and concepts of the paper - Editing and evaluating the paper before submission
Signature		Date	2020-10-26

Name of Co-Author	William S.P. Robertson
Contribution to the Paper	- Co-supervising the research work - Contribution to the development of the concepts of the paper - Editing and evaluating the paper before submission
Signature		Date	2020-10-22

Please cut and paste additional co-author panels here as required.

On size-dependent mechanics of nanoplates

Ali Farajpour*, Carl Q. Howard, William S.P. Robertson

School of Mechanical Engineering, University of Adelaide, Adelaide, South Australia 5005, Australia

ARTICLE INFO

ABSTRACT

In this paper, a two-dimensional stress-driven nonlocal integral model is introduced for the bending and transverse vibration of rectangular nanoplates for the first time. An appropriate kernel function, which satisfies all essential properties, is proposed for two-dimensional problems in the Cartesian coordinate system. Using Leibniz integral rule and Hamilton's principle, the curvature-moment relations, classical and constitutive boundary conditions, as well as the equations of motion of rectangular small-scale plates are derived. Two differential quadrature techniques are utilised to implement both classical and non-classical boundary conditions and obtain an accurate numerical solution. The solution is used to simulate the bending and vibration of nanoplates. The Laplacian-based nonlocal strain gradient model of plates is also developed for the sake of comparison. It is found that the stress-driven integral model can better estimate the size-dependent mechanical characteristics of small-scale rectangular plates with various boundary conditions.

© 2020 Elsevier Ltd. All rights reserved.

1. Introduction

Small-scale plates such as graphene sheets, silicene and boron nitride ultrathin films, have shown a wide range of promising applications in nanotechnology and microtechnology (Chen et al., 2013, Zheng, Lee & Feng, 2017). These interesting applications include, but are not limited to, ultrasmall mass detectors, actuators and sensors as well as microscale and nanoscale generators and gyroscopes (Farokhi & Ghayesh, 2018, Ghayesh, Farokhi & Alici, 2016, Kostarelos & Novoselov, 2014, Medina, Gilat & Krylov, 2018). In a considerable number of small-scale devices and systems including those mentioned above, the accurate prediction of the mechanical behaviour of ultrasmall plates plays a crucial role since the performance of these systems is highly dependent on the mechanical characteristics such as critical buckling loads and resonance frequencies (Wang & Arash, 2014).

In addition to experimental techniques, molecular dynamics (MD) approach and modified continuum-based models have been utilised for obtaining the mechanical characteristics of structural components at ultrasmall scales (Farokhi & Ghayesh, 2018, Ghayesh, 2018, Zhao, Guo & Lu, 2018). Due to the high computational requirements and complexity involved in MD simulations, continuum-based models have attracted considerable attention in recent years (El-Borgi et al., 2018, Farokhi & Ghayesh, 2018, Farokhi, Ghayesh, Gholipour & Hussain, 2017, Ghayesh, Farajpour & Farokhi, 2019, Ghayesh, Farokhi, Gholipour & Tavallaeinejad, 2018, Ma, Ke, Wang & Wang, 2018). Early in the 2000s, traditional continuum mechanics was used to study the vibration and buckling of small-scale structures (Ru, 2000, Yoon, Ru & Mioduchowski, 2003). Nonetheless, size effects, which have a significant role in the mechanical behaviour at ultrasmall scales, were not incorporated in the classical continuum mechanics. To handle this limitation, continuum-based models have been modified to include size effects using various assumptions. The most widely used models are Laplacian-based nonlocal elasticity, strain gradient model and couple stress theory.

The Laplacian-based nonlocal elasticity is used as an approximate differential model of the integral nonlocal theory, in which stress components are related to strain components through an integral relationship. The basic assumption of this theory appears promising since there is strong interaction between different parts of a structure at ultrasmall scales. The Laplacian-based nonlocal elasticity has been employed to analyse problems at ultrasmall scales, such as the moderate rotations of nanobeams (Reddy & El-Borgi, 2014), instability and transient responses of graphene sheets (Arani & Jalaei, 2016, Naderi & Saidi, 2014), post-buckling of nanotubes (She, Yuan, Ren & Xiao, 2017), the vibration of non-homogeneous nanostructures (Daneshmehr, Rajabpoor & Hadi, 2015, Nejad & Hadi, 2016, Nejad, Hadi & Rastgoo, 2016, Rahmani & Pedram, 2014, Shafiei, Kazemi, Safi & Ghadiri, 2016), instability analysis of nanotubes transporting fluid (Dai, Wang, Abdelkefi & Ni, 2015), and the mechanical response of smart nanostructures (Ebrahimi & Barati, 2016). In addition to the Laplacian nonlocal elasticity, a refined higher-order scale-dependent model was introduced by combining the differential forms of nonlocal and strain gradient theories (Farajpour, Shahidi, Tabataba'i-Nasab & Farajpour, 2018, Ghayesh & Farajpour, 2018, Lim, Zhang & Reddy, 2015). A number of continuum-based models have been proposed for nanobeams (Hadi, Nejad & Hosseini, 2018, Li, Tang & Hu, 2018, Rajasekaran & Khaniki, 2017), nanotubes (Farajpour, Ghayesh & Farokhi, 2019, Karami & Janghorban, 2019, She et al., 2019, She, Yuan & Ren, 2018), nanoplates (Karami, Shahsavari, Janghorban & Li, 2019, Shahverdi & Barati, 2017) and nanorods (Zhu & Li, 2017) in recent years based on this scale-dependent theory (Lu, Guo & Zhao, 2017, Xu, Zheng & Wang, 2017). Zhu & Li, (2017) obtained analytical solutions for ultrasmall rods subject to axial tension using the Laplacian form of strain gradient nonlocal elasticity. Furthermore, Lu, Guo & Zhao, (2017) used this theory to develop a size-dependent model for the oscillation of nanobeams. More recently, Farajpour, Farokhi, Ghayesh & Hussain, (2018) used an elasticity theory incorporating strain gradients and nonlocality for investigating the large-amplitude dynamics of fluid-conveying nanotubes. This elasticity theory was also employed by Ghayesh, Farokhi & Farajpour, (2019) for global dynamics of tubes conveying fluid at nanoscales. These studies indicate that nonlocal strain gradient models can cover a wider range of size effects, and lead to more reliable results than the Laplacian-based nonlocal elasticity (Li, Hu & Ling, 2016, Mohammadi, Rajabpour & Ghadiri, 2018).

In the integral form of Eringen's model (Eringen, 2002), stress components at an arbitrary point are estimated as a function of strain component at all points (Eringen, 2002, Farajpour, Rastgoo & Farajpour, 2017). Strain components near the given point play a more important role than those far from the point. This assumption is consistent with intermolecular interactions inside a small-scale structure. However, due to the difficulties in applying the integral form of Eringen's model, a Laplacian-based nonlocal theory has commonly been used for small-scale structures (Farajpour, Ghayesh & Farokhi, 2018, Ghayesh & Farajpour, 2019). The application of Laplacian-based nonlocal model is not reliable since several paradoxes, especially in the bending analysis of nanobeams and nanoplates have been reported (Apuzzo et al., 2017, Fernández-Sáez, Zaera, Loya & Reddy, 2016, Romano, Barretta, Diaco & de Sciarra, 2017). To overcome these shortcomings, the integral form of nonlocal elasticity (Koutsoumaris, Eptaimeros & Tsamasphyros, 2017, Tuna & Kirca, 2016), strain- and stress-driven integral models (Apuzzo et al., 2017, Romano & Barretta, 2017, Romano & Barretta, 2017) have been successfully used, yielding more accurate and reliable models for small-scale structures (Romano & Barretta, 2017).

In recent years, stress-driven nonlocal models have been developed for the mechanics of nanorods (Barretta, Faghidian & Luciano, 2019), nanobeams (Barretta, Čanađija, Luciano & de Sciarra, 2018) and axisymmetric annular nanoplates (Barretta, Faghidian & Marotti de Sciarra, 2019). However, all of these problems are limited to one-dimensional small-scale structures. In the case of axisymmetric annular nanoplates, the geometry of the non-classical problem is described by only one coordinate (i.e. radial coordinate) before deformation. Up to now, no scale-dependent continuum models have been proposed for the mechanical behaviour of rectangular nanoplates using the stress-driven integral theory. In the present article, the bending and free vibration of rectangular small-scale plates are examined by developing a stress-driven integral formulation in the Cartesian coordinate system for the first time. For comparison purposes, a nonlocal strain gradient model of plates is also developed for both bending and vibration analyses. An advanced version of the differential quadrature technique is used for solving the sixth-order differential equation of motions. Both classical and non-classical (constitutive) boundary conditions are taken into consideration in both the modelling and solution procedures. Numerical results are calculated for rectangular small-scale plates with various boundary conditions. The influences of parameters including aspect ratio, stress-driven and strain gradient scale coefficients are thoroughly studied.

2. Stress-driven nonlocal integral model of rectangular small-scale plates

A nanoplate of thickness h, width b and length a is shown in Fig. 1. A Cartesian coordinate system is used to measure the response of the small-scale system. It is assumed that the in-plane displacements are negligible compared to transverse deflection, and the effect of geometrical nonlinearity is sufficiently small. Using a Kirchhoff plate model (Leissa, 1969), the strain components (ε_{ij}) are given by

$$\varepsilon_{xx} = -z\frac{\partial^2 w}{\partial x^2} = z\kappa_{xx},$$

$$\varepsilon_{yy} = -z\frac{\partial^2 w}{\partial y^2} = z\kappa_{yy},$$

$$\varepsilon_{xy} = -z\frac{\partial^2 w}{\partial x \partial y} = z\kappa_{xy}, \tag{1}$$
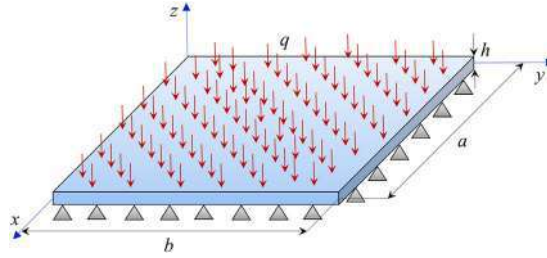
Fig. 1. A rectangular small-scale plate of length a and width b, with a distributed load q applied.

where w and κ_{ij} are transverse deflection and curvature components, respectively.

The strain components is written in terms of stress components as

$$\varepsilon_{xx} = \frac{1}{E}(\sigma_{xx} - \upsilon\sigma_{yy}), \ \ \varepsilon_{yy} = \frac{1}{E}(\sigma_{yy} - \upsilon\sigma_{xx}), \ \ \varepsilon_{xy} = \frac{1}{2G}\sigma_{xy}. \tag{2}$$

where σ_{ij}, G, E and υ denote stress, shear modulus, elasticity modulus and Poisson's ratio, respectively. The components of stress resultants are defined by

$$M_{xx} = \int_{-h/2}^{h/2}(\sigma_{xx}z)dz,$$

$$M_{yy} = \int_{-h/2}^{h/2}(\sigma_{yy}z)dz,$$

$$M_{xy} = \int_{-h/2}^{h/2}(\sigma_{xy}z)dz, \tag{3}$$

in which h is the nanoplate thickness. According to the stress-driven integral elasticity (Barretta, Faghidian & Marotti de Sciarra, 2019, Romano & Barretta, 2017), the curvature components along the x and y axes are expressed as

$$\kappa_{xx}(x,y,t) = (\varphi * H_{xx})(x,y,t) = \int_0^b \int_0^a H_{xx}(\bar{x},\bar{y},t)\varphi(|x - \bar{x}|, |y - \bar{y}|, \lambda_C)d\bar{x}d\bar{y},$$

$$\kappa_{yy}(x,y,t) = (\varphi * H_{yy})(x,y,t) = \int_0^b \int_0^a H_{yy}(\bar{x},\bar{y},t)\varphi(|x - \bar{x}|, |y - \bar{y}|, \lambda_C)d\bar{x}d\bar{y}, \tag{4}$$

where "$*$" represents integral convolution. The parameters $\bar{x}$ and $\bar{y}$ are the variables of integration, φ is the nonlocal kernel function, and λ_C is the stress-driven scale parameter, which is given by $\lambda_C = L_C/\ell_{ext}$, where L_C and ℓ_{ext} are the scale and external characteristic dimensions, respectively. For small-scale plates, the external characteristic dimension is the same as the nanoplate length (i.e. $\ell_{ext} = a$). In addition, H_{xx} and H_{yy} are given by

$$H_{xx}(\bar{x},\bar{y},t) = \frac{1}{D_{11}(1-\upsilon^2)}(M_{xx}(\bar{x},\bar{y},t) - \upsilon M_{yy}(\bar{x},\bar{y},t)), H_{yy}(\bar{x},\bar{y},t) = \frac{1}{D_{11}(1-\upsilon^2)}(M_{yy}(\bar{x},\bar{y},t) - \upsilon M_{xx}(\bar{x},\bar{y},t)), \tag{5}$$

where D_{11} is the bending rigidity, which is obtained by $D_{11} = Eh^3/(12(1-\upsilon^2))$. The shear rigidity of the plate is also given by $D_{33} = Gh^3/12$. The appropriate kernel function for rectangular nanoplates should satisfy the following properties (Barretta, Faghidian & Marotti de Sciarra, 2019):

$$\text{Positivity}: \ \varphi(x,y,\lambda_C) \geq 0, \tag{6}$$

$$\text{Normalisation}: \ \int_{-\infty}^{+\infty}\int_{-\infty}^{+\infty}\varphi(x,y,\lambda_C)dxdy = 1, \tag{7}$$

$$\text{Impulsivity}: \ \lim_{\lambda_C\to 0^+}[\varphi(x,y,\lambda_C)] = \delta(x,y). \tag{8}$$

Here δ is the Dirac delta function. According to the above-mentioned properties, the kernel function of rectangular small-scale plates is

$$\varphi(|x - \bar{x}|, |y - \bar{y}|, \lambda_C) = \frac{1}{4L_C^2}\exp\left(-\frac{1}{L_C}\{|x - \bar{x}| + |y - \bar{y}|\}\right). \tag{9}$$

The bi-exponential kernel function, which is described by Eq. (9), is plotted in Fig. 2 for $L_C = 1/5$. One can easily prove that this nonlocal kernel function fulfils all necessary properties given by Eqs. (6)–(8). Substituting Eq. (9) into the first relation given by Eq. (5), yields

$$\kappa_{xx}(x,y,t) = \frac{1}{4L_C^2}\int_0^b\int_0^a\exp\left(-\frac{1}{L_C}\{|x - \bar{x}| + |y - \bar{y}|\}\right)H_{xx}(\bar{x},\bar{y},t)d\bar{x}d\bar{y}. \tag{10}$$
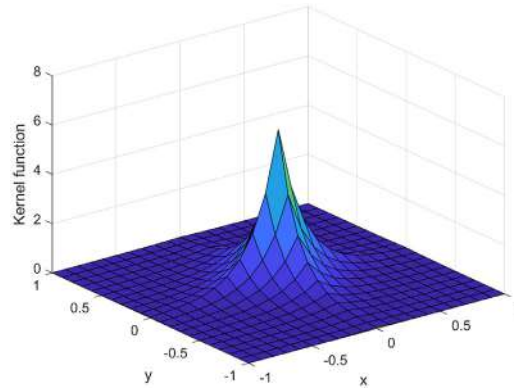
Fig. 2. Nonlocal kernel function for rectangular small-scale plates ($L_c = 1/5$).

Using the Leibniz integral rule, the following differential equation is obtained for the curvature along the x axis:

$$H_{xx} = \kappa_{xx} - L_C^2 \left(\frac{\partial^2 \kappa_{xx}}{\partial x^2} + \frac{\partial^2 \kappa_{xx}}{\partial y^2} \right) + L_C^4 \frac{\partial^4 \kappa_{xx}}{\partial x^2 \partial y^2}. \tag{11}$$

It is important to note that Eq. (11) is equivalent to Eq. (10) and can be used in the mathematical modelling of small-scale plates such as microplates and nanoplates, provided that the following additional boundary conditions are satisfied

$$x = 0 : \ \frac{\partial \kappa_{xx}}{\partial x} = \frac{1}{L_C} \kappa_{xx}, \ x = a : \ \frac{\partial \kappa_{xx}}{\partial x} = -\frac{1}{L_C} \kappa_{xx}. \tag{12}$$

Substituting Eq. (9) into the second relation given by Eq. (5), leads to

$$\kappa_{yy}(x, y, t) = \frac{1}{4L_C^2} \int_0^b \int_0^a \exp\left(-\frac{1}{L_C} \{ |x - \bar{x}| + |y - \bar{y}| \} \right) H_{yy}(\bar{x}, \bar{y}, t) d\bar{x} d\bar{y}. \tag{13}$$

In a similar manner, the following differential equation is obtained

$$H_{yy} = \kappa_{yy} - L_C^2 \left(\frac{\partial^2 \kappa_{yy}}{\partial x^2} + \frac{\partial^2 \kappa_{yy}}{\partial y^2} \right) + L_C^4 \frac{\partial^4 \kappa_{yy}}{\partial x^2 \partial y^2}. \tag{14}$$

Furthermore, the following additional boundary conditions must be satisfied for the curvature along the y axis

$$y = 0 : \ \frac{\partial \kappa_{yy}}{\partial y} = \frac{1}{L_C} \kappa_{yy}, \ y = b : \ \frac{\partial \kappa_{yy}}{\partial y} = -\frac{1}{L_C} \kappa_{yy}, \tag{15}$$

Substituting Eq. (5) into Eqs. (11) and (14), and then substituting Eq. (1) into the resultant equations, one obtains

$$M_{xx} = -D_{11} \frac{\partial^2 w}{\partial x^2} - \upsilon D_{11} \frac{\partial^2 w}{\partial y^2} + D_{11} L_C^2 \left(\frac{\partial^4 w}{\partial x^4} + \frac{\partial^4 w}{\partial x^2 \partial y^2} \right) - D_{11} L_C^4 \frac{\partial^6 w}{\partial x^4 \partial y^2}$$
$$+ \upsilon D_{11} L_C^2 \left(\frac{\partial^4 w}{\partial x^2 \partial y^2} + \frac{\partial^4 w}{\partial y^4} \right) - \upsilon D_{11} L_C^4 \frac{\partial^6 w}{\partial x^2 \partial y^4},$$

$$M_{yy} = -\upsilon D_{11} \frac{\partial^2 w}{\partial x^2} - D_{11} \frac{\partial^2 w}{\partial y^2} + \upsilon D_{11} L_C^2 \left(\frac{\partial^4 w}{\partial x^4} + \frac{\partial^4 w}{\partial x^2 \partial y^2} \right) - \upsilon D_{11} L_C^4 \frac{\partial^6 w}{\partial x^4 \partial y^2} + D_{11} L_C^2 \left(\frac{\partial^4 w}{\partial x^2 \partial y^2} + \frac{\partial^4 w}{\partial y^4} \right) - D_{11} L_C^4 \frac{\partial^6 w}{\partial x^2 \partial y^4},$$

$$M_{xy} = -2D_{33} \frac{\partial^2 w}{\partial x \partial y}, \tag{16}$$

Similarly, the non-classical additional boundary conditions for rectangular small-scale plates are obtained as

$$x = 0 : \ L_C \frac{\partial^3 w}{\partial x^3} = \frac{\partial^2 w}{\partial x^2},$$
$$x = a : \ -L_C \frac{\partial^3 w}{\partial x^3} = \frac{\partial^2 w}{\partial x^2},$$
$$y = 0 : \ L_C \frac{\partial^3 w}{\partial y^3} = \frac{\partial^2 w}{\partial y^2},$$
$$y = b : \ -L_C \frac{\partial^3 w}{\partial y^3} = \frac{\partial^2 w}{\partial y^2}, \tag{17}$$

Employing Hamilton's law, the governing equation is determined as

$$\frac{\partial^2 M_{xx}}{\partial x^2} + 2\frac{\partial^2 M_{xy}}{\partial x \partial y} + \frac{\partial^2 M_{yy}}{\partial y^2} + q = m_0 \frac{\partial^2 w}{\partial t^2} - m_2 \left(\frac{\partial^4 w}{\partial x^2 \partial t^2} + \frac{\partial^4 w}{\partial y^2 \partial t^2} \right), \tag{18}$$

where q is the transverse load per unit area; m_0 and m_2 indicate the mass per unit area and mass moment of inertia, respectively; they are given by

$$m_0 = \int_{-h/2}^{h/2} \rho dz, \ \ m_2 = \int_{-h/2}^{h/2} \rho z^2 dz, \tag{19}$$

in which ρ represents the mass density of the small-scale plate. Substituting Eq. (16) into Eq. (18), leads to the following higher-order differential equation

$$-D_{11}\frac{\partial^4 w}{\partial x^4} - 2(\upsilon D_{11} + 2D_{33})\frac{\partial^4 w}{\partial x^2 \partial y^2} - D_{11}\frac{\partial^4 w}{\partial y^4}$$

$$+ D_{11}L_C^2 \left(\frac{\partial^6 w}{\partial x^6} + \frac{\partial^6 w}{\partial x^4 \partial y^2} + \frac{\partial^6 w}{\partial x^2 \partial y^4} + \frac{\partial^6 w}{\partial y^6} \right)$$

$$+ 2\upsilon D_{11}L_C^2 \left(\frac{\partial^6 w}{\partial x^4 \partial y^2} + \frac{\partial^6 w}{\partial x^2 \partial y^4} \right)$$

$$- D_{11}L_C^4 \left(\frac{\partial^8 w}{\partial x^6 \partial y^2} + 2\upsilon \frac{\partial^8 w}{\partial x^4 \partial y^4} + \frac{\partial^8 w}{\partial x^2 \partial y^6} \right)$$

$$+ q = m_0 \frac{\partial^2 w}{\partial t^2} - m_2 \left(\frac{\partial^4 w}{\partial x^2 \partial t^2} + \frac{\partial^4 w}{\partial y^2 \partial t^2} \right). \tag{20}$$

In Eq. (20), the highest derivative with respect to x is six, namely six boundary conditions are required along the edges perpendicular to x axis. Furthermore, since the highest order of derivatives with respect to y is also six, six boundary conditions in total are needed at the boundaries $y = 0$ and $y = b$. In the stress-driven integral nonlocal elasticity model, the required boundary conditions for small-scale plates can be categorised into two types:

(1) Classical boundary conditions:
Clamped edges:

$$x = 0, a : \ w = 0, \ \ \frac{\partial w}{\partial x} = 0, y = 0, b : \ w = 0, \ \ \frac{\partial w}{\partial y} = 0, \tag{21}$$

Simply supported edges:

$$x = 0, a : \ w = 0, \ M_{xx} = 0, y = 0, b : \ w = 0, \ \ M_{yy} = 0, \tag{22}$$

(2) Non-classical (constitutive) boundary conditions:

$$x = 0 : \ \frac{\partial^3 w}{\partial x^3} - \frac{1}{L_C}\frac{\partial^2 w}{\partial x^2} = 0,$$

$$x = a : \ \frac{\partial^3 w}{\partial x^3} + \frac{1}{L_C}\frac{\partial^2 w}{\partial x^2} = 0,$$

$$y = 0 : \ \frac{\partial^3 w}{\partial y^3} - \frac{1}{L_C}\frac{\partial^2 w}{\partial y^2} = 0,$$

$$y = b : \ \frac{\partial^3 w}{\partial y^3} + \frac{1}{L_C}\frac{\partial^2 w}{\partial y^2} = 0. \tag{23}$$

3. Strain-gradient nonlocal differential model of rectangular small-scale plates

To make a comparison between the integral modelling and available size-dependent models, the governing equations of the strain-gradient nonlocal differential model are derived in this section. Using the strain-gradient nonlocal elasticity and Kirchhoff plate model, the constitutive equations are given by (Lim, Zhang & Reddy, 2015)

$$\sigma_{xx} - (e_0\ell_c)^2 \left(\frac{\partial^2 \sigma_{xx}}{\partial x^2} + \frac{\partial^2 \sigma_{xx}}{\partial y^2} \right) = \frac{E}{(1-\upsilon^2)} \left[\varepsilon_{xx} - \ell_s^2 \left(\frac{\partial^2 \varepsilon_{xx}}{\partial x^2} + \frac{\partial^2 \varepsilon_{xx}}{\partial y^2} \right) \right]$$

$$+ \frac{\upsilon E}{(1-\upsilon^2)} \left[\varepsilon_{yy} - \ell_s^2 \left(\frac{\partial^2 \varepsilon_{yy}}{\partial x^2} + \frac{\partial^2 \varepsilon_{yy}}{\partial y^2} \right) \right], \tag{24}$$

$$\sigma_{yy} - (e_0\ell_c)^2\left(\frac{\partial^2\sigma_{yy}}{\partial x^2} + \frac{\partial^2\sigma_{yy}}{\partial y^2}\right) = \frac{\upsilon E}{(1-\upsilon^2)}\left[\varepsilon_{xx} - \ell_s^2\left(\frac{\partial^2\varepsilon_{xx}}{\partial x^2} + \frac{\partial^2\varepsilon_{xx}}{\partial y^2}\right)\right] + \frac{E}{(1-\upsilon^2)}$$

$$\left[\varepsilon_{yy} - \ell_s^2\left(\frac{\partial^2\varepsilon_{yy}}{\partial x^2} + \frac{\partial^2\varepsilon_{yy}}{\partial y^2}\right)\right], \tag{25}$$

$$\sigma_{xy} - (e_0\ell_c)^2\left(\frac{\partial^2\sigma_{xy}}{\partial x^2} + \frac{\partial^2\sigma_{xy}}{\partial y^2}\right) = 2G\left[\varepsilon_{xy} - \ell_s^2\left(\frac{\partial^2\varepsilon_{xy}}{\partial x^2} + \frac{\partial^2\varepsilon_{xy}}{\partial y^2}\right)\right], \tag{26}$$

where e_0, ℓ_c and G are the calibration coefficient, internal characteristic dimension and shear modulus, respectively. Furthermore, ℓ_s denotes the scale parameter associated with strain gradients (Farajpour & Rastgoo, 2017; Farajpour et al., 2018; Malekzadeh & Farajpour, 2012; Mohammadi et al., 2014). Substituting Eq. (1) into Eqs. (24)–(26), and then using the definitions of the stress resultants given by Eq. (3), one obtains

$$M_{xx} - (e_0a)^2\left(\frac{\partial^2 M_{xx}}{\partial x^2} + \frac{\partial^2 M_{xx}}{\partial y^2}\right) = -D\left[\frac{\partial^2 w}{\partial x^2} - \ell_s^2\left(\frac{\partial^4 w}{\partial x^4} + \frac{\partial^4 w}{\partial x^2\partial y^2}\right)\right] - \upsilon D\left[\frac{\partial^2 w}{\partial y^2} - \ell_s^2\left(\frac{\partial^4 w}{\partial x^2\partial y^2} + \frac{\partial^4 w}{\partial y^4}\right)\right], \tag{27}$$

$$M_{yy} - (e_0a)^2\left(\frac{\partial^2 M_{yy}}{\partial x^2} + \frac{\partial^2 M_{yy}}{\partial y^2}\right) = -\upsilon D\left[\frac{\partial^2 w}{\partial x^2} - \ell_s^2\left(\frac{\partial^4 w}{\partial x^4} + \frac{\partial^4 w}{\partial x^2\partial y^2}\right)\right] - D\left[\frac{\partial^2 w}{\partial y^2} - \ell_s^2\left(\frac{\partial^4 w}{\partial x^2\partial y^2} + \frac{\partial^4 w}{\partial y^4}\right)\right], \tag{28}$$

$$M_{xy} - (e_0a)^2\left(\frac{\partial^2 M_{xy}}{\partial x^2} + \frac{\partial^2 M_{xy}}{\partial y^2}\right) = -(1-\upsilon)D\left[\frac{\partial^2 w}{\partial x\partial y} - \ell_s^2\left(\frac{\partial^4 w}{\partial x^3\partial y} + \frac{\partial^4 w}{\partial x\partial y^3}\right)\right], \tag{29}$$

in which $D = Eh^3/12(1-\upsilon^2)$. Substituting Eqs. (27)–(29) into Eq. (18), yields

$$D\left(\frac{\partial^4 w}{\partial x^4} + 2\frac{\partial^4 w}{\partial x^2\partial y^2} + \frac{\partial^4 w}{\partial y^4}\right) - D\ell_s^2\left(\frac{\partial^6 w}{\partial x^6} + 3\frac{\partial^6 w}{\partial x^4\partial y^2} + 3\frac{\partial^6 w}{\partial x^2\partial y^4} + \frac{\partial^6 w}{\partial y^6}\right)$$

$$+ m_0\frac{\partial^2 w}{\partial t^2} - m_2\left(\frac{\partial^4 w}{\partial x^2\partial t^2} + \frac{\partial^4 w}{\partial y^2\partial t^2}\right) - q + (e_0a)^2\left(\frac{\partial^2 q}{\partial x^2} + \frac{\partial^2 q}{\partial y^2}\right)$$

$$- m_0(e_0a)^2\left(\frac{\partial^4 w}{\partial y^2\partial t^2} + \frac{\partial^4 w}{\partial x^2\partial t^2}\right) + m_2(e_0a)^2\left(\frac{\partial^6 w}{\partial x^4\partial t^2} + 2\frac{\partial^6 w}{\partial x^2\partial y^2\partial t^2} + \frac{\partial^6 w}{\partial y^4\partial t^2}\right) = 0, \tag{30}$$

with the following boundary conditions (Farajpour, Yazdi, Rastgoo & Mohammadi, 2016)

$$x = 0, a: \ w = 0, \quad M_{xx} = 0, \ \text{or} \ \frac{\partial w}{\partial x} = 0, \ \frac{\partial^4 w}{\partial x^4} = 0, y = 0, b: \ w = 0, \quad M_{yy} = 0, \ \text{or} \ \frac{\partial w}{\partial y} = 0, \ \frac{\partial^4 w}{\partial y^4} = 0, \tag{31}$$

4. Solution procedure

4.1. Standard DQ technique

In this section, the differential quadrature (DQ) technique is employed to determine a numerical solution for the governing equation of rectangular nanoplates via the stress-driven integral elasticity theory. It should be noted that the DQ technique is used in this paper since it is a powerful numerical method for handling differential equations with complex boundary conditions.

For brevity, only the DQ-based solution procedure for the bending of small-scale plates using the stress-driven integral nonlocal elasticity is presented. The numerical solution for the vibration analysis can be performed in a similar way. First of all, a set of non-dimensional parameters are given by

$$\bar{w} = \frac{w}{a}, \ \xi = \frac{x}{a}, \ \eta = \frac{y}{b}, \ \beta = \frac{a}{b}, \ \bar{q}_0 = \frac{q_0 a^3}{D}, \ \bar{D}_{33} = \frac{D_{33}}{D_{11}}, \ \lambda_C = \frac{L_C}{a}, \tag{32}$$

where β, $\bar{q}_0$ and λ_C denote the aspect ratio, non-dimensional transverse load and scale coefficient of stress-driven integral nonlocal elasticity, respectively. In view of Eq. (32), one can obtain the following non-dimensional differential equation

$$\frac{\partial^4\bar{w}}{\partial\xi^4} + 2\beta^2\left(\upsilon + 2\bar{D}_{33}\right)\frac{\partial^4\bar{w}}{\partial\xi^2\partial\eta^2} + \beta^4\frac{\partial^4\bar{w}}{\partial\eta^4} - \lambda_C^2\left(\frac{\partial^6\bar{w}}{\partial\xi^6} + \beta^2\frac{\partial^6\bar{w}}{\partial\xi^4\partial\eta^2} + \beta^4\frac{\partial^6\bar{w}}{\partial\xi^2\partial\eta^4} + \beta^6\frac{\partial^6\bar{w}}{\partial\eta^6}\right)$$

$$- 2\upsilon\lambda_C^2\left(\beta^2\frac{\partial^6\bar{w}}{\partial\xi^4\partial\eta^2} + \beta^4\frac{\partial^6\bar{w}}{\partial\xi^2\partial\eta^4}\right) + \beta^2\lambda_C^4\left(\frac{\partial^8\bar{w}}{\partial\xi^6\partial\eta^2} + 2\upsilon\beta^2\frac{\partial^8\bar{w}}{\partial\xi^4\partial\eta^4} + \beta^4\frac{\partial^8\bar{w}}{\partial\xi^2\partial\eta^6}\right) = \bar{q}_0, \tag{33}$$

The boundary condition at each edge of the small-scale plate is clamped. In this section, for brevity, only clamped boundary conditions are considered. However, for other edge conditions, DQ solutions are similarly developed. Using Eq. (32) in conjunction with Eqs. (21) and (23), yields

$$\xi = 0, 1: \ \bar{w} = 0, \ \frac{\partial\bar{w}}{\partial\xi} = 0, \xi = 0: \ \frac{\partial^2\bar{w}}{\partial\xi^2} - \lambda_C\frac{\partial^3\bar{w}}{\partial\xi^3} = 0, \xi = 1: \ \frac{\partial^2\bar{w}}{\partial\xi^2} + \lambda_C\frac{\partial^3\bar{w}}{\partial\xi^3} = 0, \tag{34}$$

$$\eta = 0, 1 : \ \bar{w} = 0, \ \frac{\partial \bar{w}}{\partial \eta} = 0, \eta = 0 : \ \frac{\partial^2 \bar{w}}{\partial \eta^2} - \lambda_C \beta \frac{\partial^3 \bar{w}}{\partial \eta^3} = 0, \eta = 1 : \ \frac{\partial^2 \bar{w}}{\partial \eta^2} + \lambda_C \beta \frac{\partial^3 \bar{w}}{\partial \eta^3} = 0, \tag{35}$$

Based on the DQ technique, the derivatives with respect to ξ and η can be expressed as (Farajpour, Yazdi, Rastgoo & Mohammadi, 2016)

$$\frac{\partial^r \bar{w}}{\partial \xi^r} = \sum_{k=1}^{n_x} C_{i,k}^{(r)} \bar{w}_{k,j},$$

$$\frac{\partial^s \bar{w}}{\partial \eta^s} = \sum_{k=1}^{n_y} \tilde{C}_{j,k}^{(s)} \bar{w}_{i,k},$$

$$\frac{\partial^{(r+s)} \bar{w}}{\partial \xi^r \partial \eta^s} = \sum_{k_2=1}^{n_y} \sum_{k_1=1}^{n_x} C_{i,k_1}^{(r)} \tilde{C}_{j,k_2}^{(s)} \bar{w}_{k_1,k_2}, \tag{36}$$

where $C_{i,k}^{(r)}$ and $\tilde{C}_{j,k}^{(s)}$ represent the weighting coefficients for derivatives with respect to ξ and η, respectively. The numbers of mesh points along ξ and η are, respectively, indicated by n_x and n_y. For first-order derivatives, the weighting coefficients are determined via the relations

$$C_{i,k}^{(1)} = \begin{cases} \frac{M^{(1)}(\xi_i)}{(\xi_i - \xi_k)M^{(1)}(\xi_k)} \ \text{for} \ i \neq k \\ -\sum_{j=1(j\neq i)}^{n_x} C_{i,j}^{(1)} \ \text{for} \ i = k \end{cases}, \tag{37}$$

$$\tilde{C}_{j,k}^{(1)} = \begin{cases} \frac{M^{(1)}(\eta_j)}{(\eta_j - \eta_k)M^{(1)}(\eta_k)} \ \text{for} \ j \neq k \\ -\sum_{m=1(m\neq j)}^{n_y} C_{j,m}^{(1)} \ \text{for} \ j = k \end{cases}, \tag{38}$$

where $M^{(1)}(\xi_i)$ and $M^{(1)}(\eta_j)$ are given by

$$M^{(1)}(\xi_i) = \prod_{k=1(k\neq i)}^{n_x} (\xi_i - \xi_k), M^{(1)}(\eta_j) = \prod_{k=1(k\neq j)}^{n_y} (\eta_j - \eta_k). \tag{39}$$

Higher weighting coefficients are calculated using the following relations

$$C_{i,j}^{(2)} = \sum_{k=1}^{n_x} C_{i,k}^{(1)} C_{k,j}^{(1)},$$

$$C_{i,j}^{(3)} = \sum_{k=1}^{n_x} C_{i,k}^{(2)} C_{k,j}^{(1)},$$

$$C_{i,j}^{(4)} = \sum_{k=1}^{n_x} C_{i,k}^{(2)} C_{k,j}^{(2)},$$

$$C_{i,j}^{(5)} = \sum_{k=1}^{n_x} C_{i,k}^{(3)} C_{k,j}^{(2)},$$

$$C_{i,j}^{(6)} = \sum_{k=1}^{n_x} C_{i,k}^{(3)} C_{k,j}^{(3)}, \tag{40}$$

$$\tilde{C}_{i,j}^{(2)} = \sum_{k=1}^{n_x} \tilde{C}_{i,k}^{(1)} \tilde{C}_{k,j}^{(1)},$$

$$\tilde{C}_{i,j}^{(3)} = \sum_{k=1}^{n_x} \tilde{C}_{i,k}^{(2)} \tilde{C}_{k,j}^{(1)},$$

$$\tilde{C}_{i,j}^{(4)} = \sum_{k=1}^{n_x} C_{i,k}^{(2)} C_{k,j}^{(2)},$$

$$\tilde{C}_{i,j}^{(5)} = \sum_{k=1}^{n_x} \tilde{C}_{i,k}^{(3)} \tilde{C}_{k,j}^{(2)},$$

$$\tilde{C}_{i,j}^{(6)} = \sum_{k=1}^{n_x} \tilde{C}_{i,k}^{(3)} \tilde{C}_{k,j}^{(3)}. \tag{41}$$

The distribution of grid points is important in the implementation of the DQ technique. It has been shown that the Gauss–Chebyshev–Lobatto distribution leads to sufficiently accurate results (Shu, 2012). Using this law of distribution, one can define

$$
\begin{aligned}
\xi_i &= \frac{1}{2}\left\{1 - \cos\left[\frac{\pi(i-1)}{n_x - 1}\right]\right\}, \\
\eta_j &= \frac{1}{2}\left\{1 - \cos\left[\frac{\pi(j-1)}{n_y - 1}\right]\right\}.
\end{aligned}
\tag{42}
$$

To implement all six boundary conditions, the direct method is utilised. Based on this method, all derivatives of the boundary conditions are first discretised, and then substituted into the main discretised governing equations. Applying Eq. (36) to Eqs. (34) and (35), the following relations are obtained

$$
\sum_{k=2}^{n_x-1}(CBCX)_{1,k}\bar{w}_{k,j} = 0, \quad \sum_{k=2}^{n_x-1}(CBCX)_{n_x,k}\bar{w}_{k,j} = 0, \quad \sum_{k=2}^{n_x-1}(NBCX)_{1,k}\bar{w}_{k,j} = 0, \quad \sum_{k=2}^{n_x-1}(NBCX)_{n_x,k}\bar{w}_{k,j} = 0,
\tag{43}
$$

$$
\sum_{k=2}^{n_y-1}(CBCY)_{1,k}\bar{w}_{i,k} = 0, \quad \sum_{k=2}^{n_y-1}(CBCY)_{n_y,k}\bar{w}_{i,k} = 0, \quad \sum_{k=2}^{n_y-1}(NBCY)_{1,k}\bar{w}_{i,k} = 0, \quad \sum_{k=2}^{n_y-1}(NBCY)_{n_y,k}\bar{w}_{i,k} = 0,
\tag{44}
$$

where

$$
\begin{aligned}
(CBCX)_{1,k} &= C_{1,k}^{(1)}, \quad (CBCX)_{n_x,k} = C_{n_x,k}^{(1)}, \\
(NBCX)_{1,k} &= C_{1,k}^{(2)} - \lambda_C C_{1,k}^{(3)}, \quad (NBCX)_{n_x,k} = C_{n_x,k}^{(2)} + \lambda_C C_{n_x,k}^{(3)}, \\
(CBCY)_{1,k} &= \tilde{C}_{1,k}^{(1)}, \quad (CBCY)_{n_y,k} = \tilde{C}_{n_y,k}^{(1)}, \\
(NBCY)_{1,k} &= \tilde{C}_{1,k}^{(2)} - \lambda_C \beta \tilde{C}_{1,k}^{(3)}, \quad (NBCY)_{n_y,k} = \tilde{C}_{n_y,k}^{(2)} + \lambda_C \beta \tilde{C}_{n_y,k}^{(3)}.
\end{aligned}
\tag{45}
$$

Using Eqs. (43) and (44), the following relations are obtained for the transverse deflection near the boundaries of the rectangular small-scale plate

$$
\begin{aligned}
\bar{w}_{2,j} &= -\sum_{k=4}^{n_x-3}(HX)_{1,k}\bar{w}_{k,j}, \quad \bar{w}_{3,j} = -\sum_{k=4}^{n_x-3}(HX)_{2,k}\bar{w}_{k,j}, \\
\bar{w}_{n_x-2,j} &= -\sum_{k=4}^{n_x-3}(HX)_{3,k}\bar{w}_{k,j}, \quad \bar{w}_{n_x-1,j} = -\sum_{k=4}^{n_x-3}(HX)_{4,k}\bar{w}_{k,j},
\end{aligned}
\tag{46}
$$

and

$$
\begin{aligned}
\bar{w}_{i,2} &= -\sum_{k=4}^{n_y-3}(HY)_{1,k}\bar{w}_{i,k}, \quad \bar{w}_{i,3} = -\sum_{k=4}^{n_y-3}(HY)_{2,k}\bar{w}_{i,k}, \\
\bar{w}_{i,n_y-2} &= -\sum_{k=4}^{n_y-3}(HY)_{3,k}\bar{w}_{i,k}, \quad \bar{w}_{i,n_y-1} = -\sum_{k=4}^{n_y-3}(HY)_{4,k}\bar{w}_{i,k}.
\end{aligned}
\tag{47}
$$

The details related to $(HX)_{i,k}$ and $(HY)_{j,k}$ are given in Appendix A. Substituting Eqs. (46) and (47) into Eq. (36), yields

$$
\begin{aligned}
\frac{\partial^r \bar{w}}{\partial x^r} &= \sum_{k=4}^{n_x-3} P_{i,k}^{(r)}\bar{w}_{k,j}, \\
\frac{\partial^s \bar{w}}{\partial y^s} &= \sum_{k=4}^{n_y-3} Q_{j,k}^{(s)}\bar{w}_{i,k}, \\
\frac{\partial^{(r+s)}\bar{w}}{\partial x^r \partial y^s} &= \sum_{k_2=4}^{n_y-3}\sum_{k_1=4}^{n_x-3} F_{i,k_1,k_2,j}^{(r,s)}\bar{w}_{k_1,k_2},
\end{aligned}
\tag{48}
$$

where $P_{i,k}^{(r)}$, $Q_{j,k}^{(s)}$, and $F_{i,k_1,k_2,j}^{(r,s)}$ are defined in Appendix B. Substituting Eq. (48) into Eq. (33), leads to the following discretised equation

$$\sum_{k=4}^{n_x-3} P_{i,k}^{(4)} \bar{w}_{k,j} + 2\beta^2 \sum_{k_2=4}^{n_y-3} \sum_{k_1=4}^{n_x-3} F_{i,k_1,k_2,j}^{(2,2)} \bar{w}_{k_1,k_2} + \beta^4 \sum_{k=4}^{n_y-3} Q_{j,k}^{(4)} \bar{w}_{i,k}$$

$$- \lambda_C^2 \sum_{k=4}^{n_x-3} P_{i,k}^{(6)} \bar{w}_{k,j} - \lambda_C^2 (1+2\upsilon)\beta^2 \sum_{k_2=4}^{n_y-3} \sum_{k_1=4}^{n_x-3} F_{i,k_1,k_2,j}^{(4,2)} \bar{w}_{k_1,k_2}$$

$$- \lambda_C^2 (1+2\upsilon)\beta^4 \sum_{k_2=4}^{n_y-3} \sum_{k_1=4}^{n_x-3} F_{i,k_1,k_2,j}^{(2,4)} \bar{w}_{k_1,k_2} - \lambda_C^2 \beta^6 \sum_{k=4}^{n_y-3} Q_{j,k}^{(6)} \bar{w}_{i,k}$$

$$+ \lambda_C^4 \beta^2 \sum_{k_2=4}^{n_y-3} \sum_{k_1=4}^{n_x-3} F_{i,k_1,k_2,j}^{(6,2)} \bar{w}_{k_1,k_2} + 2\upsilon\lambda_C^4\beta^4 \sum_{k_2=4}^{n_y-3} \sum_{k_1=4}^{n_x-3} F_{i,k_1,k_2,j}^{(4,4)} \bar{w}_{k_1,k_2}$$

$$+ \lambda_C^4 \beta^6 \sum_{k_2=4}^{n_y-3} \sum_{k_1=4}^{n_x-3} F_{i,k_1,k_2,j}^{(2,6)} \bar{w}_{k_1,k_2} = \bar{q}_{ij}, \tag{49}$$

in which $i = 4, 5, \ldots, n_x - 3$ and $j = 4, 5, \ldots, n_x - 3$. It should be noted that for isotropic small-scale plates, Poisson's ratio and shear rigidity have the relationship $\upsilon + 2\bar{D}_{33} = 1$. The non-dimensional deflection of rectangular small-scale plates is determined as

$$\{w_d\} = [K_b]^{-1}\{\bar{q}_{ext}\}, \tag{50}$$

Where $\{w_d\}$, $[K_b]$ and $\{\bar{q}_{ext}\}$ are the inner deflection vector, bending stiffness matrix and external transverse load vector, respectively. Following a similar DQ-based procedure for solving Eq. (20), one finally obtains the relation for the free vibration behaviour of small-scale plates as

$$\left([K_v] - \varpi^2 [M_v]\right)\{w_d\} = \{0\}, \tag{51}$$

where ϖ is the dimensionless frequency of free transverse vibration, which is defined as $\varpi = \omega a^2 \sqrt{m_0/D_{11}}$. The matrices $[K_v]$ and $[M_v]$ denote the stiffness and mass matrices of the small-scale plate, respectively.

4.2. DQ technique *for sixth-order partial differential equations*

An advanced version of the generalised DQ technique, which was proposed by Wu & Liu, (2000) in order to handle sixth-order differential equations, is implemented in this subsection. Based on this technique, partial derivatives are expressed as (Khaniki, 2018, Wu & Liu, 2000)

$$\frac{\partial^r w}{\partial x^r} = \sum_{k=0}^{2} h_{1,k}^{(r)}(x_i) w_{1,j}^{(kx)} + \sum_{k=2}^{n-1} h_{k,0}^{(r)}(x_i) w_{k,j} + \sum_{k=0}^{2} h_{n,k}^{(r)}(x_i) w_{n,j}^{(kx)} = \sum_{k=1}^{n+4} E_{i,k}^{(r)} U_{k,j},$$

$$\frac{\partial^s w}{\partial y^s} = \sum_{k=0}^{2} \tilde{h}_{1,k}^{(s)}(y_j) w_{i,1}^{(ky)} + \sum_{k=2}^{m-1} \tilde{h}_{k,0}^{(s)}(y_j) w_{i,k} + \sum_{k=0}^{2} \tilde{h}_{m,k}^{(s)}(y_j) w_{i,m}^{(ky)} = \sum_{k=1}^{m+4} \tilde{E}_{j,k}^{(s)} U_{i,k}$$

$$\frac{\partial^{(r+s)} \bar{w}}{\partial x^r \partial y^s} = \sum_{k_1=1}^{n+4} \sum_{k_2=1}^{m+4} E_{i,k_1}^{(r)} \tilde{E}_{j,k_2}^{(s)} U_{k_1,k_2} \tag{52}$$

where $h_{i,j}^{(r)}$ and $\tilde{h}_{i,j}^{(s)}$ are the Hermite interpolation shape functions that must satisfy the following relations (Khaniki, 2018)

$$h_{jl}^{(r)}(x_i) = \begin{cases} 1 \text{ if } i = j \text{ and } l = r \\ 0 \text{ otherwise} \end{cases}, \tag{53}$$

$$\tilde{h}_{jl}^{(s)}(y_i) = \begin{cases} 1 \text{ if } i = j \text{ and } l = s \\ 0 \text{ otherwise} \end{cases}, \tag{54}$$

In addition, $E_{i,k}^{(r)}$ and $\tilde{E}_{j,k}^{(r)}$ are the total weighting coefficients of the DQ technique. As can be seen from Eq. (52), along each edge of the small-scale plate, two additional parameters (i.e. the first and second derivatives of the transverse deflection) are incorporated. According to the properties given by the above relations (i.e. Eqs. (53) and (54)), the weighting coefficients are defined as (Khaniki, 2018, Wu & Liu, 2000)

$$h_{1,i}(x) = \frac{(x-x_n)^2}{(x_1-x_n)^2} \left(a_{1i}x^2 + b_{1i}x + c_{1i}\right)\ell_1(x), \quad \text{for } i = 0, 1, 2, \tag{55}$$

$$h_{n,i}(x) = \frac{(x-x_1)^2}{(x_1-x_n)^2} \left(a_{ni}x^2 + b_{ni}x + c_{ni}\right)\ell_n(x), \quad \text{for } i = 0, 1, 2, \tag{56}$$

$$h_{j,0}(x) = \frac{(x - x_1)^2 (x - x_n)^2}{(x_j - x_1)^2 (x_j - x_n)^2} \ell_j(x), \ \ for \ j = 2, 3, \ldots, n - 1, \tag{57}$$

in which $\ell_j(x_i) = \delta_{ij}$. Furthermore, a_{ki}, b_{ki} and c_{ki} $(k = 1, n$ and $i = 0, 1, 2)$ are a number of constant coefficients given in Appendix C. Similarly, the weighting coefficients for partial derivatives with respect to y (i.e. $\tilde{h}_{jl}^{(s)}(y_i)$) are obtained. For brevity purposes, the solution procedure for the bending of clamped rectangular small-scale plates via the stress-driven integral nonlocal elasticity is presented. Inserting Eq. (52) into Eqs. (34) and (35), the following relations are obtained

$$\sum_{k=3}^{n+2} (BCX)_{1,k} U_{k,j} = 0, \ \ \sum_{k=3}^{n+2} (BCX)_{n,k} U_{k,j} = 0,$$

$$\sum_{k=3}^{m+2} (BCY)_{1,k} U_{i,k} = 0, \ \ \sum_{k=3}^{m+2} (BCY)_{m,k} U_{i,k} = 0, \tag{58}$$

where

$$(BCX)_{1,k} = E_{1,k}^{(2)} - \lambda_C E_{1,k}^{(3)},$$

$$(BCX)_{n,k} = E_{n,k}^{(2)} + \lambda_C E_{n,k}^{(3)},$$

$$(BCY)_{1,k} = \tilde{E}_{1,k}^{(2)} - \lambda_C \beta \tilde{E}_{1,k}^{(3)},$$

$$(BCY)_{m,k} = \tilde{E}_{m,k}^{(2)} + \lambda_C \beta \tilde{E}_{m,k}^{(3)}. \tag{59}$$

In view of Eq. (58), the displacement components near the edges of the small-scale plate are determined as follows

$$U_{3,j} = -\sum_{k=4}^{n+1} H_{1,k} U_{k,j}, \ \ U_{n+2,j} = -\sum_{k=4}^{n+1} H_{2,k} U_{k,j},$$

$$U_{i,3} = -\sum_{k=4}^{m+1} H_{3,k} U_{i,k}, \ \ U_{i,m+2} = -\sum_{k=4}^{m+1} H_{4,k} U_{i,k}, \tag{60}$$

where

$$H_{1,k} = (BCXI)_{1,1} (BCX)_{1,k} + (BCXI)_{1,2} (BCX)_{n,k},$$

$$H_{2,k} = (BCXI)_{2,1} (BCX)_{1,k} + (BCXI)_{2,2} (BCX)_{n,k},$$

$$H_{3,k} = (BCYI)_{1,1} (BCY)_{1,k} + (BCYI)_{1,2} (BCY)_{m,k},$$

$$H_{4,k} = (BCYI)_{2,1} (BCY)_{1,k} + (BCYI)_{2,2} (BCY)_{m,k}. \tag{61}$$

Here $(BCXI)_{i,j}$ and $(BCYI)_{i,j}$ are the elements of the inverse of the boundary condition matrices, which are defined in Appendix C. Substituting Eq. (60) into Eq. (52), leads to

$$\frac{\partial^r w}{\partial x^r} = \sum_{k=4}^{n+1} P_{i,k}^{(r)} U_{k,j}, \ \ \frac{\partial^s w}{\partial y^s} = \sum_{k=4}^{m+1} \tilde{P}_{j,k}^{(s)} U_{i,k}, \ \ \frac{\partial^{(r+s)} \bar{w}}{\partial x^r \partial y^s} = \sum_{k_1=4}^{n+1} \sum_{k_2=4}^{m+1} F_{i,k_1,k_2,j}^{(r,s)} U_{k_1,k_2}, \tag{62}$$

where $P_{i,k}^{(r)}$, $\tilde{P}_{j,k}^{(s)}$ and $F_{i,k_1,k_2,j}^{(r,s)}$ are the modified weighting coefficients given in Appendix C. Inserting Eq. (62) into Eq. (33), the following equation is derived for the bending of rectangular small-scale plates subject to transverse loading

$$\sum_{k=4}^{n+1} P_{i,k}^{(4)} U_{k,j} + 2\beta^2 (\upsilon + 2\bar{D}_{33}) \sum_{k_1=4}^{n+1} \sum_{k_2=4}^{m+1} F_{i,k_1,k_2,j}^{(2,2)} U_{k_1,k_2} + \beta^4 \sum_{k=4}^{m+1} \tilde{P}_{j,k}^{(4)} U_{i,k}$$

$$- \lambda_C^2 \sum_{k=4}^{n+1} P_{i,k}^{(6)} U_{k,j} - \lambda_C^2 \beta^2 (1 + 2\upsilon) \sum_{k_1=4}^{n+1} \sum_{k_2=4}^{m+1} F_{i,k_1,k_2,j}^{(4,2)} U_{k_1,k_2} - \lambda_C^2 \beta^4 (1 + 2\upsilon) \sum_{k_1=4}^{n+1} \sum_{k_2=4}^{m+1} F_{i,k_1,k_2,j}^{(2,4)} U_{k_1,k_2} - \lambda_C^2 \beta^6 \sum_{k=4}^{m+1} \tilde{P}_{j,k}^{(6)} U_{i,k}$$

$$+ \beta^2 \lambda_C^4 \sum_{k_1=4}^{n+1} \sum_{k_2=4}^{m+1} F_{i,k_1,k_2,j}^{(6,2)} U_{k_1,k_2} + 2\upsilon \beta^4 \lambda_C^4 \sum_{k_1=4}^{n+1} \sum_{k_2=4}^{m+1} F_{i,k_1,k_2,j}^{(4,4)} U_{k_1,k_2} + \beta^6 \lambda_C^4 \sum_{k_1=4}^{n+1} \sum_{k_2=4}^{m+1} F_{i,k_1,k_2,j}^{(2,6)} U_{k_1,k_2} = \bar{q}_{i,j}, \tag{63}$$

Eq. (63) can be organised in a matrix form for efficient computation. The dimensionless deflection of the plate can be expressed as

$$\{\tilde{w}\} = \left[\tilde{K}_b\right]^{-1} \{\tilde{q}\}, \tag{64}$$

Table 1
First six dimensionless frequencies of SSCC square plates.

ϖ	First natural frequency	Second natural frequency	Third natural frequency	Fourth natural frequency	Fifth natural frequency	Sixth natural frequency
Leissa (Leissa, 1969)	28.946	54.743	69.320	94.584	102.213	129.086
Present method	28.9509	54.7431	69.3270	94.5853	102.2156	129.0951

Table 2
Deflection of CCCC plates subject to uniform loading ($w_{max}D/qb^4$).

Aspect ratio (a/b)	Present method	Imrak and Gerdemeli (Imrak & Gerdemeli, 2007)
1.0	0.0013	0.00127
1.2	0.0017	0.00173
1.4	0.0021	0.00207
1.6	0.0023	0.00230
1.8	0.0024	0.00245
2.0	0.0025	0.00254
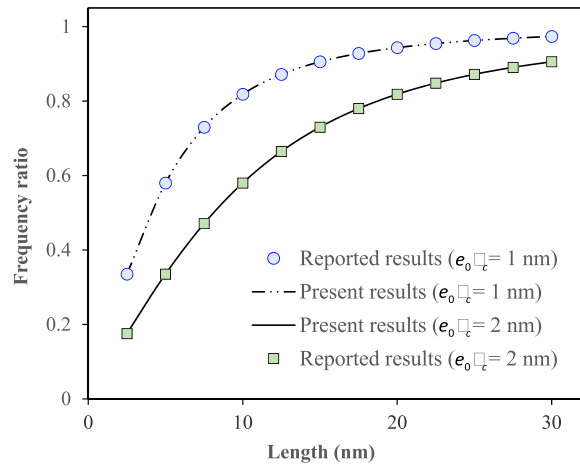
Fig. 3. A verification study for SSSS rectangular nanoplates based on the differential nonlocal model of plates (Aksencer & Aydogdu, 2011).

Similarly, the matrix form for the free transverse vibration based on the advanced DQ technique can be written as

$$\left(\left[\tilde{K}_v \right] - \varpi^2 \left[\tilde{M}_v \right] \right) \{ \tilde{w} \} = \{ 0 \}. \tag{65}$$

In this paper, the computational results were calculated using Matlab (MathWorks Inc., Natick MA, USA).

5. Numerical results

5.1. Verification study

To show the accuracy of the results, several test cases are considered. Table 1 lists the first six dimensionless natural frequencies of local square plates according to classical elasticity theory (Leissa, 1969). The dimensionless frequency is defined by $\varpi = \omega a^2 \sqrt{m_0/D_{11}}$. The boundary conditions of the plate are: simply supported at $x=0$, a, and clamped at $y=0$, b (i.e. SSCC). For simplification, four-letter symbols are used to indicate the boundary conditions of the plate. The first and second letters, respectively, denote the boundary condition at $x = 0$ and $x = a$, while the third and fourth letters represent the boundary condition along boundaries $y = 0$ and $y = b$, respectively. For instance, SCCC plates have one simply supported edge at $x = 0$ and three clamped edges at $x = a$ and $y = 0, b$. The results obtained via standard DQ technique are compared in Table 1 with those obtained by Leissa, (1969). A reasonable agreement is concluded between the results of the present solution procedure and those obtained in the literature.

Table 2 lists the dimensionless transverse deflection of CCCC local plates under uniform distributed loading for various aspect ratios (a/b). The results are compared to those reported by Imrak & Gerdemeli, (2007), and a good match is found. Furthermore, Fig. 3 shows a verification study for the vibration of SSSS rectangular nanoplates for two values of nonlocal parameter. The results are obtained based on Eq. (30) when the strain gradient effect is ignored (i.e. $\ell_s = 0$). The aspect ratio of the nanoplate is set to 2. The ratio of the nonlocal frequency to its local counterpart is defined as the frequency
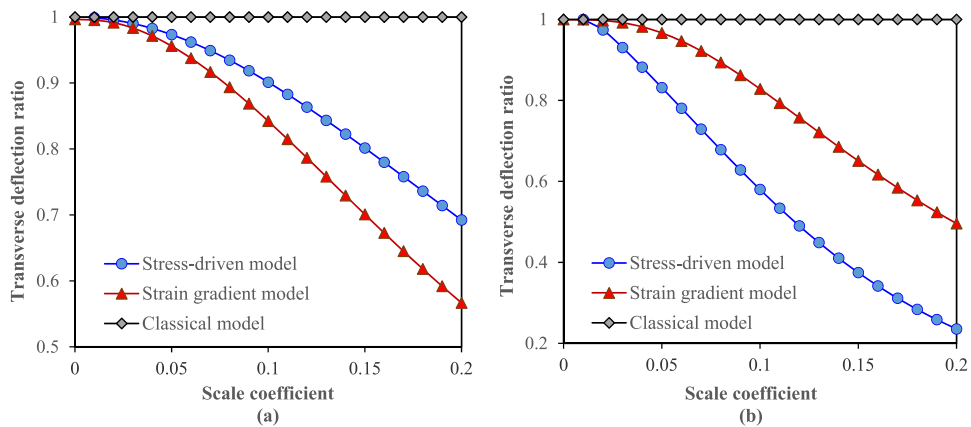
Fig. 4. Transverse deflection ratio of small-scale plates with all edges (a) simply supported, and (b) clamped versus the scale coefficient for stress-driven, strain gradient and classical elasticity theories.
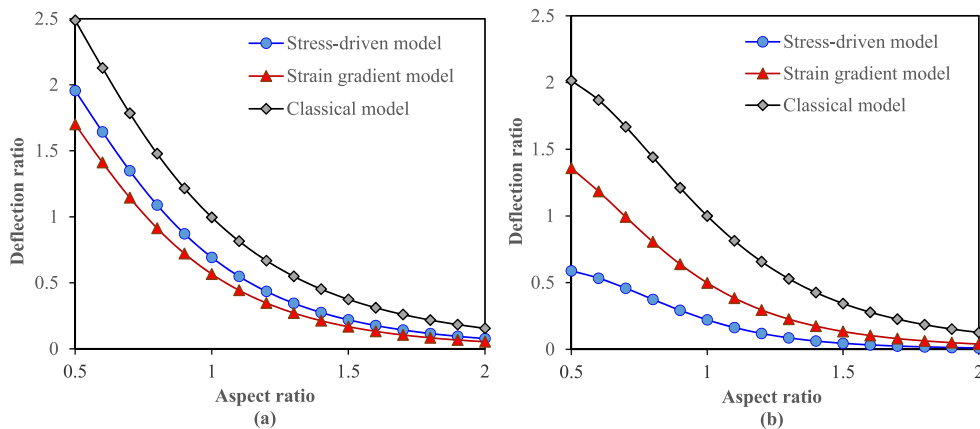
Fig. 5. Deflection ratio of small-scale plates with all edges (a) simply supported, and (b) clamped versus the aspect ratio for stress-driven, strain gradient and classical elasticity theories.

ratio. The results obtained by Aksencer & Aydogdu, (2011) according to the differential nonlocal theory are also presented. An excellent match is seen from Fig. 3 for both nonlocal parameters.

5.2. Bending analysis

The variation of the transverse deflection ratio of simply supported square nanoplates with the scale coefficient for different elasticity theories including the stress-driven, strain gradient and classical theories is plotted in Fig. 4(a). Poisson's ratio and dimensionless transverse loading are set to 0.3 and 1, respectively. Twenty grid points are taken into consideration along each direction of the system for ensuring the convergence of numerical results. It should be noted that the results of the standard and advanced DQ techniques exactly match for a wide range of scale coefficients excluding very small values where the standard method fails to obtain a converged solution. The strain gradient model is obtained from Eq. (30) when the nonlocal parameter is set to zero ($e_0a = 0$). In addition, when the scale parameter of the stress-driven model and its additional (constitutive) boundary conditions are neglected, the classical model is obtained. The transverse deflection ratio is given by $(\bar{w}_{\max})_{nc}/(\bar{w}_{\max})_{cl}$ where "nc" and "cl" stand for non-classical (stress-driven or strain gradient) and classical models, respectively. From Fig. 4(a), it is found that the transverse deflection ratio determined via the stress-driven integral model is significantly different from that of the strain gradient theory. Increasing the scale coefficient dramatically increases the difference between non-classical models, indicating the importance of using the stress-driven theory when the behaviour of the small-scale plate is highly size dependent. A similar trend is observed for clamped square small-scale plates (see Fig. 4(b)). However, this time the stress-driven model leads to lower transverse deflection ratios. It implies that clamped small-scale plates are more influenced by stress-driven effects than simply-supported ones. This is due to the fact that clamped boundary conditions are associated with higher size effects.

Fig. 5(a) and 5(b) indicate the change of the deflection ratio of small-scale plates subject to uniform transverse loading with the aspect ratio for simply supported and clamped cases, respectively. The deflection ratio is defined as $\bar{w}_{\max}/\bar{w}_{\max}^{(0)}$
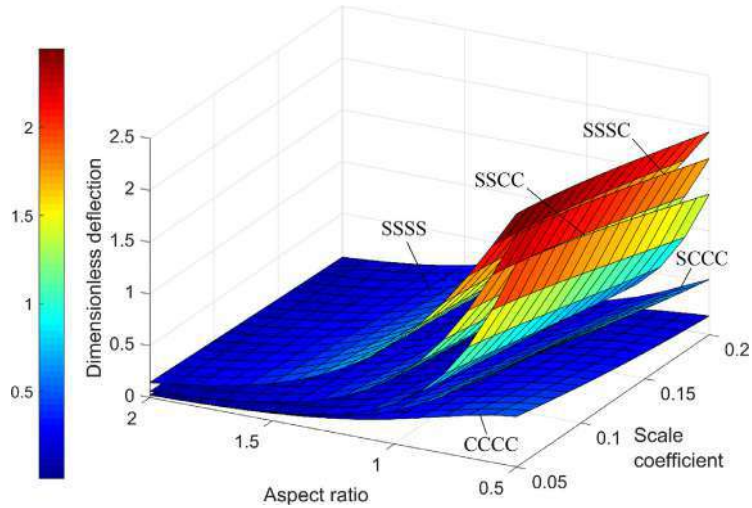
Fig. 6. Dimensionless deflection versus β and λ_C based on the stress-driven integral model.
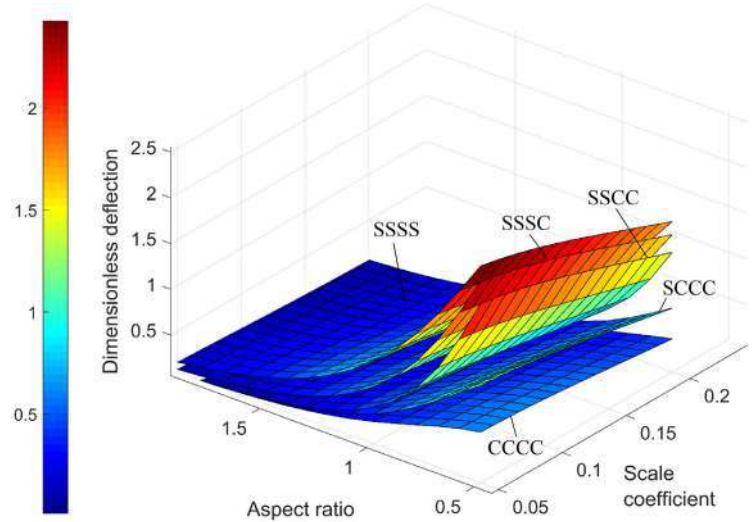

Fig. 7. Dimensionless deflection versus β and ℓ_s/a based on the strain gradient differential model.

in which $\bar{w}_{\max}^{(0)}$ is the maximum dimensionless deflection of a local square plate. The strain gradient parameter and scale coefficient of the stress-driven model are set to 0.2. It can be concluded that when the aspect ratio of the small-scale plate increases, the deflection ratio decreases for both boundary conditions. The stress-driven model predicts relatively higher deflection ratios than the strain gradient model for SSSS nanoplates whereas the opposite is observed for CCCC nanoplates. In fact, clamped boundary conditions lead to higher size effects based on the stress-driven integral modelling. In addition, Figs. 6 and 7 are plotted for investigating the effect of boundary condition on the deflection of ultrasmall plates via the integral and strain gradient models, respectively. The dimensionless defection is given by $\bar{w}_{\max}/\bar{w}_{\max}^{(s)}$ where $\bar{w}_{\max}^{(s)}$ is the maximum deflection of a local square plate with all edges simply supported. It is observed that as more constraint is made on the small-scale plate, the dimensionless deflection decreases.

5.3. Free vibration analysis

The variation of the frequency ratio of simply-supported square nanoplates with the scale coefficient is indicated in Fig. 8(a) for different elasticity theories such as stress-driven and strain gradient models. Poisson's ratio and thickness-to-length ratio are, respectively, taken as 0.3 and 0.05. The frequency ratio is defined as ϖ_{nc}/ϖ_{cl} where "*nc*" and "*cl*" indicate non-classical and classical models, respectively. The difference between the non-classical models significantly increases with increasing the scale coefficient. Fig. 8(b) depicts the frequency ratio of clamped nanoplates versus the scale coefficient for
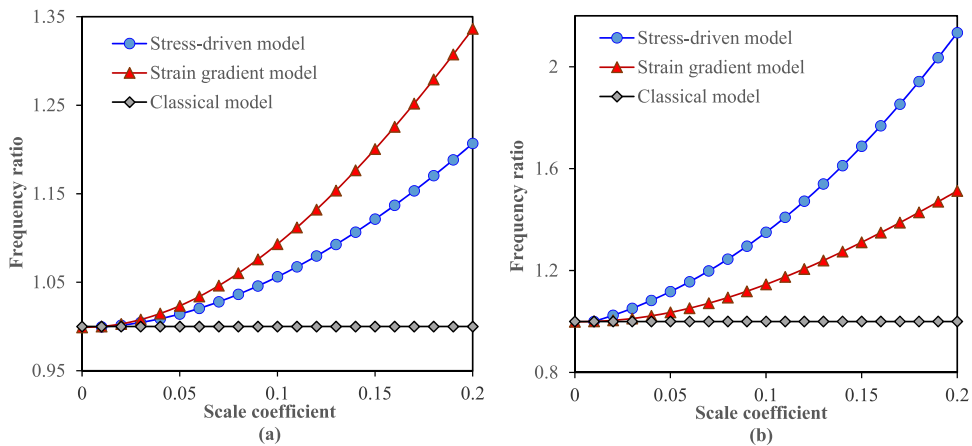
Fig. 8. Frequency ratio of small-scale plates with all edges (a) simply supported, and (b) clamped versus the scale coefficient for stress-driven, strain gradient and classical elasticity theories.
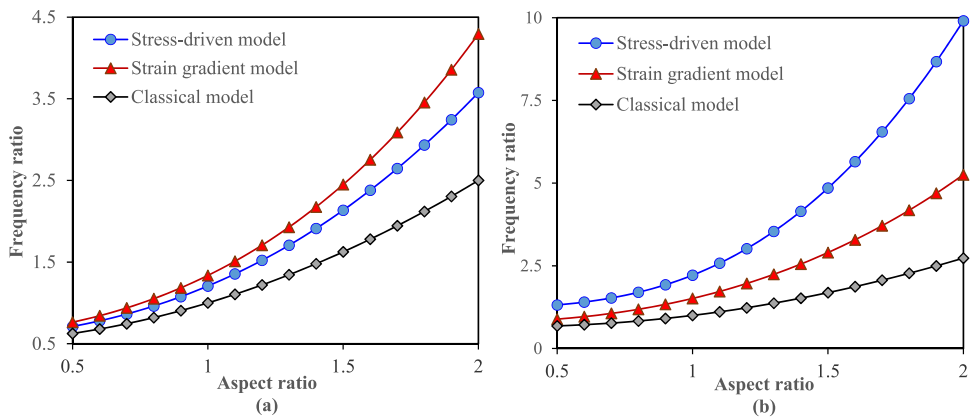
Fig. 9. Frequency ratio of small-scale plates with all edges (a) simply supported, and (b) clamped versus the aspect ratio for stress-driven, strain gradient and classical elasticity theories.

various elasticity models. Frequency ratios increase with increasing the scale coefficient. Comparing Fig. 8(a) and 8(b) indicates that the frequency ratios of clamped nanoplates are higher than those of simply supported ones since the vibration behaviour at small-scale levels is highly affected by size effects when all boundaries of the system are clamped. This observation can be better described by the stress-driven integral theory than the Laplacian-based model incorporating strain gradients as size effects are more pronounced in this model.

To show the influence of geometry on the free vibrations of simply supported small-scale plates, the frequency ratio versus the aspect ratio (i.e. a/b) is plotted in Fig. 9(a) for stress-driven, strain gradient and classical elasticity models. The number of grid points, scale coefficient and thickness-to-length ratio are assumed as 20, 0.2 and 0.05, respectively. The frequency ratio is defined as $\varpi_{nc}/\varpi_{cl}^0$ in which ϖ_{cl}^0 is the dimensionless frequency of a local square plate. Rectangular small-scale plates with higher aspect ratios have higher frequency ratios. In addition, both non-classical models predict higher values for the frequency ratio than the classical plate model since both strain gradient and stress-driven effects lead to a considerable enhancement in the structural stiffness. A similar trend is observed in Fig. 9(b) for the frequency response of clamped small-scale plates. However, in contrast to simply supported nanoplates, the stress-driven model leads to higher frequency ratios than those of the strain gradient model for clamped boundary condition. Figs. 10 and 11 depict the dimensionless frequency versus the aspect ratio and scale coefficient via the stress-driven and strain gradient models, respectively. The dimensionless frequency is defined by $\varpi_{nc}/\varpi_{cl}^{(s)}$ where $\varpi_{cl}^{(s)}$ is the frequency of a simply supported local square plate. The results are calculated for nanoplates with different edge conditions including SSSS, SSSC, SSCC, SCCC and CCCC. It can be concluded that when more constraint is imposed on the system, the dimensionless frequency increases, as expected.
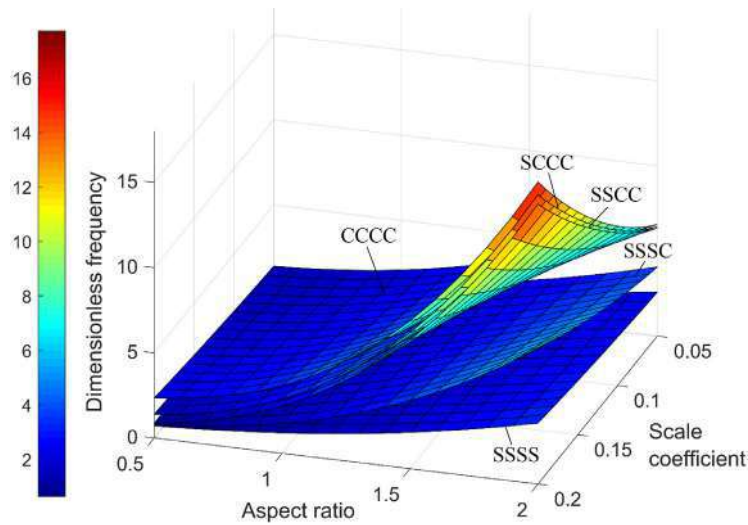
Fig. 10. Dimensionless frequency versus β and λ_C based on the stress-driven integral model.
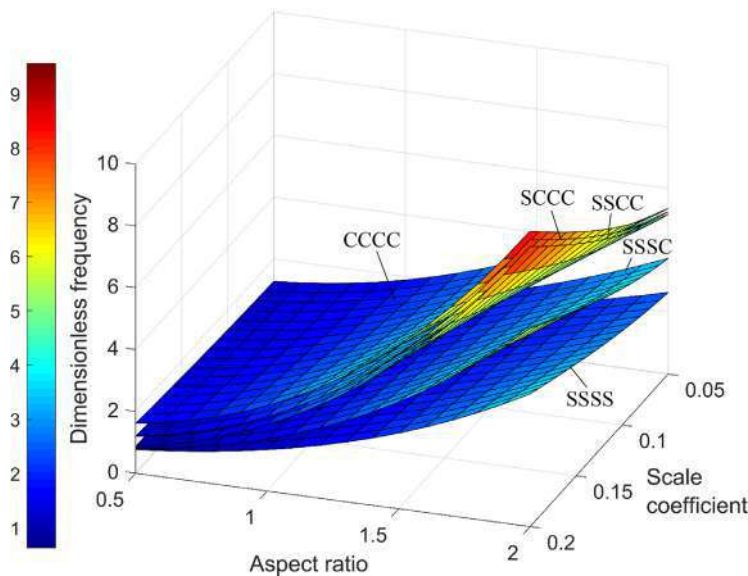

Fig. 11. Dimensionless frequency versus β and ℓ_s/a (the scale coefficient) based on the strain gradient differential model.

6. Conclusions

A stress-driven nonlocal integral model has been developed for the bending and free transverse vibration of rectangular nanoplates using an appropriate two-dimensional kernel function. According to the Leibniz integral rule and Kirchhoff plate model, the curvature-moment relations were derived. The sixth-order partial differential equation of motion, classical and constitutive boundary conditions were explicitly obtained. In addition, the governing differential equations for the static deformation and vibration of a rectangular nanoplate were presented utilising the Laplacian-based model of nonlocal strain gradient elasticity. The maximum transverse deflection and natural frequencies were presented for various boundary conditions and different modified theories such as stress-driven, strain gradient and local models.

It was found that the Laplacian-based nonlocal theory fails to model size effects on the bending behaviour of nanoplates under uniform transverse loading. By contrast, the stress-driven integral elasticity can reliably predict size influences on the statics and vibration of nanoplates with various boundary conditions. Moreover, for clamped nanoplates, the stress-driven model estimates a highly size-dependent response, which is consistent with the fact that when more constraint is imposed on the nanoplate, the effect of intermolecular interactions increases, and thus, size effects increase. The difference between the results of strain gradient elasticity and stress-driven model is higher for higher scale coefficients. In addition, clamped nanoplates are more influenced by the stress-driven effect than simply-supported ones. The stress-driven nonlocal

integral model yields relatively higher scale effects than the strain gradient model for clamped nanoplates. Moreover, it was concluded that stress-driven effects are associated with a notable increase in the structural stiffness of small-scale plates. Furthermore, imposing more constraint on the nanoplate leads to higher dimensionless frequency parameters. The frequency ratios obtained via the stress-driven model are lower than those obtained via the Laplacian-based strain gradient model for simply supported boundary condition.

Declaration of Competing Interest

The authors declare that they have no known competing financial interests or personal relationships that could have appeared to influence the work reported in this paper.

Acknowledgments

Appendix A

The coefficients $(HX)_{i,k}$ are given by

$$(HX)_{1,k} = (BCXI)_{1,1}(CBCX)_{1,k} + (BCXI)_{1,2}(CBCX)_{n_x,k} + (BCXI)_{1,3}(NBCX)_{1,k} + (BCXI)_{1,4}(NBCX)_{n_x,k}, \tag{A1}$$

$$(HX)_{2,k} = (BCXI)_{2,1}(CBCX)_{1,k} + (BCXI)_{2,2}(CBCX)_{n_x,k} + (BCXI)_{2,3}(NBCX)_{1,k} + (BCXI)_{2,4}(NBCX)_{n_x,k}, \tag{A2}$$

$$(HX)_{3,k} = (BCXI)_{3,1}(CBCX)_{1,k} + (BCXI)_{3,2}(CBCX)_{n_x,k} + (BCXI)_{3,3}(NBCX)_{1,k} + (BCXI)_{3,4}(NBCX)_{n_x,k}, \tag{A3}$$

$$(HX)_{4,k} = (BCXI)_{4,1}(CBCX)_{1,k} + (BCXI)_{4,2}(CBCX)_{n_x,k} + (BCXI)_{4,3}(NBCX)_{1,k} + (BCXI)_{4,4}(NBCX)_{n_x,k}, \tag{A4}$$

where

$$[BCX] = \begin{bmatrix} (CBCX)_{1,2} & (CBCX)_{1,3} & (CBCX)_{1,n_x-2} & (CBCX)_{1,n_x-1} \\ (CBCX)_{n_x,2} & (CBCX)_{n_x,3} & (CBCX)_{n_x,n_x-2} & (CBCX)_{n_x,n_x-1} \\ (NBCX)_{1,2} & (NBCX)_{1,3} & (NBCX)_{1,n_x-2} & (NBCX)_{1,n_x-1} \\ (NBCX)_{n_x,2} & (NBCX)_{n_x,3} & (NBCX)_{n_x,n_x-2} & (NBCX)_{n_x,n_x-1} \end{bmatrix} \tag{A5}$$

$$[BCXI] = [BCX]^{-1} = \begin{bmatrix} (BCXI)_{1,1} & (BCXI)_{1,2} & (BCXI)_{1,3} & (BCXI)_{1,4} \\ (BCXI)_{2,1} & (BCXI)_{2,2} & (BCXI)_{2,3} & (BCXI)_{2,4} \\ (BCXI)_{3,1} & (BCXI)_{3,2} & (BCXI)_{3,3} & (BCXI)_{3,4} \\ (BCXI)_{4,1} & (BCXI)_{4,2} & (BCXI)_{4,3} & (BCXI)_{4,4} \end{bmatrix}, \tag{A6}$$

The coefficients $(HY)_{j,k}$ are given by

$$(HY)_{1,k} = (BCYI)_{1,1}(CBCY)_{1,k} + (BCYI)_{1,2}(CBCY)_{n_y,k} + (BCYI)_{1,3}(NBCY)_{1,k} + (BCYI)_{1,4}(NBCY)_{n_y,k}, \tag{A7}$$

$$(HY)_{2,k} = (BCYI)_{2,1}(CBCY)_{1,k} + (BCYI)_{2,2}(CBCY)_{n_y,k} + (BCYI)_{2,3}(NBCY)_{1,k} + (BCYI)_{2,4}(NBCY)_{n_y,k}, \tag{A8}$$

$$(HY)_{3,k} = (BCYI)_{3,1}(CBCY)_{1,k} + (BCYI)_{3,2}(CBCY)_{n_y,k} + (BCYI)_{3,3}(NBCY)_{1,k} + (BCYI)_{3,4}(NBCY)_{n_y,k}, \tag{A9}$$

$$(HY)_{4,k} = (BCYI)_{4,1}(CBCY)_{1,k} + (BCYI)_{4,2}(CBCY)_{n_y,k}(BCYI)_{4,3}(NBCY)_{1,k} + (BCYI)_{4,4}(NBCY)_{n_y,k}, \tag{A10}$$

where

$$[BCY] = \begin{bmatrix} (CBCY)_{1,2} & (CBCY)_{1,3} & (CBCY)_{1,n_y-2} & (CBCY)_{1,n_y-1} \\ (CBCY)_{n_y,2} & (CBCY)_{n_y,3} & (CBCY)_{n_y,n_y-2} & (CBCY)_{n_y,n_y-1} \\ (NBCY)_{1,2} & (NBCY)_{1,3} & (NBCY)_{1,n_y-2} & (NBCY)_{1,n_y-1} \\ (NBCY)_{n_y,2} & (NBCY)_{n_y,3} & (NBCY)_{n_y,n_y-2} & (NBCY)_{n_y,n_y-1} \end{bmatrix}, \tag{A11}$$

$$[BCYI] = [BCY]^{-1} = \begin{bmatrix} (BCYI)_{1,1} & (BCYI)_{1,2} & (BCYI)_{1,3} & (BCYI)_{1,4} \\ (BCYI)_{2,1} & (BCYI)_{2,2} & (BCYI)_{2,3} & (BCYI)_{2,4} \\ (BCYI)_{3,1} & (BCYI)_{3,2} & (BCYI)_{3,3} & (BCYI)_{3,4} \\ (BCYI)_{4,1} & (BCYI)_{4,2} & (BCYI)_{4,3} & (BCYI)_{4,4} \end{bmatrix}, \tag{A12}$$

Appendix B

The modified weighting coefficients of Eq. (48) are calculated by

$$P_{i,k}^{(r)} = C_{i,k}^{(r)} - C_{i,2}^{(r)}(HX)_{1,k} - C_{i,3}^{(r)}(HX)_{2,k} - C_{i,n_x-2}^{(r)}(HX)_{3,k} - C_{i,n_x-1}^{(r)}(HX)_{4,k}, \tag{B1}$$

$$Q_{j,k}^{(s)} = \tilde{C}_{j,k}^{(s)} - \tilde{C}_{j,2}^{(s)}(HY)_{1,k} - \tilde{C}_{j,3}^{(s)}(HY)_{2,k} - \tilde{C}_{j,n_y-2}^{(s)}(HY)_{3,k} - \tilde{C}_{j,n_y-1}^{(s)}(HY)_{4,k}, \tag{B2}$$

$$G_{i,k_1,k_2,j}^{(r,s)} = C_{i,k_1}^{(r)}\tilde{C}_{j,k_2}^{(s)} - C_{i,2}^{(r)}\tilde{C}_{j,k_2}^{(s)}(HX)_{1,k_1} - C_{i,3}^{(r)}\tilde{C}_{j,k_2}^{(s)}(HX)_{2,k_1} - C_{i,n_x-2}^{(r)}\tilde{C}_{j,k_2}^{(s)}(HX)_{3,k_1} - C_{i,n_x-1}^{(r)}\tilde{C}_{j,k_2}^{(s)}(HX)_{4,k_1}, \tag{B3}$$

$$F_{i,k_1,k_2,j}^{(r,s)} = G_{i,k_1,k_2,j}^{(r,s)} - G_{i,k_1,2,j}^{(r,s)}(HY)_{1,k_2} - G_{i,k_1,3,j}^{(r,s)}(HY)_{2,k_2} - G_{i,k_1,n_y-2,j}^{(r,s)}(HY)_{3,k_2} - G_{i,k_1,n_y-1,j}^{(r,s)}(HY)_{4,k_2}, \tag{B4}$$

Appendix C

The coefficients of Hermite interpolation shape functions are given by

$$a_{10} = \left[\ell_1^{(1)}(x_1) + \frac{2}{x_1 - x_n}\right]^2 - \frac{\ell_1^{(2)}(x_1)}{2} - \frac{1}{(x_1 - x_n)^2} - \frac{2\ell_1^{(1)}(x_1)}{x_1 - x_n},$$

$$b_{10} = -\left[\ell_1^{(1)}(x_1) + \frac{2}{x_1 - x_n}\right] - 2x_1 a_{10},$$

$$c_{10} = 1 + a_{10}x_1^2 + x_1\left[\ell_1^{(1)}(x_1) + \frac{2}{x_1 - x_n}\right],$$

$$a_{11} = -\left[\ell_1^{(1)}(x_1) + \frac{2}{x_1 - x_n}\right], \quad b_{11} = 1 - 2a_{11}x_1, \quad c_{11} = x_1(a_{11}x_1 - 1),$$

$$a_{12} = \frac{1}{2}, \quad b_{12} = -x_1, \quad c_{12} = \frac{1}{2}x_n^2. \tag{C1}$$

$$a_{n0} = \left[\ell_n^{(1)}(x_n) - \frac{2}{x_1 - x_n}\right]^2 - \frac{\ell_n^{(2)}(x_n)}{2} - \frac{1}{(x_1 - x_n)^2} + \frac{2\ell_n^{(1)}(x_n)}{x_1 - x_n},$$

$$b_{n0} = -\left[\ell_n^{(1)}(x_n) - \frac{2}{x_1 - x_n}\right] - 2x_n a_{n0},$$

$$c_{n0} = 1 + a_{n0}x_n^2 + x_n\left[\ell_n^{(1)}(x_n) - \frac{2}{x_1 - x_n}\right],$$

$$a_{n1} = -\left[\ell_n^{(1)}(x_n) - \frac{2}{x_1 - x_n}\right], \quad b_{n1} = 1 - 2a_{n1}x_n,$$

$$b_{n2} = -x_n, \quad c_{n2} = \frac{1}{2}x_n^2,$$

$$c_{n1} = x_n(a_{n1}x_n - 1), \quad a_{n2} = \frac{1}{2},$$

$$a_{n0} = \left[\ell_n^{(1)}(x_n) - \frac{2}{x_1 - x_n}\right]^2 - \frac{\ell_n^{(2)}(x_n)}{2} - \frac{1}{(x_1 - x_n)^2} + \frac{2\ell_n^{(1)}(x_n)}{x_1 - x_n},$$

$$b_{n0} = -\left[\ell_n^{(1)}(x_n) - \frac{2}{x_1 - x_n}\right] - 2x_n a_{n0},$$

$$c_{n0} = 1 + a_{n0}x_n^2 + x_n\left[\ell_n^{(1)}(x_n) - \frac{2}{x_1 - x_n}\right],$$

$$a_{n1} = -\left[\ell_n^{(1)}(x_n) - \frac{2}{x_1 - x_n}\right], \quad b_{n1} = 1 - 2a_{n1}x_n,$$

$$c_{n1} = x_n(a_{n1}x_n - 1), \quad a_{n2} = \frac{1}{2}, \quad b_{n2} = -x_n, \quad c_{n2} = \frac{1}{2}x_n^2, \tag{C2}$$

The inverse of boundary condition matrices is calculated by

$$[BCXI] = \begin{bmatrix} (BCX)_{1,3} & (BCX)_{1,n+2} \\ (BCX)_{n,3} & (BCX)_{n,n+2} \end{bmatrix}^{-1} = \begin{bmatrix} (BCXI)_{1,1} & (BCXI)_{1,2} \\ (BCXI)_{2,1} & (BCXI)_{2,2} \end{bmatrix}, \tag{C3}$$

$$[BCYI] = \begin{bmatrix} (BCY)_{1,3} & (BCY)_{1,m+2} \\ (BCY)_{m,3} & (BCY)_{m,m+2} \end{bmatrix}^{-1} = \begin{bmatrix} (BCYI)_{1,1} & (BCYI)_{1,2} \\ (BCYI)_{2,1} & (BCYI)_{2,2} \end{bmatrix}, \tag{C4}$$

The modified weighting coefficients of Eq. (62) are obtained by

$$P_{i,k}^{(r)} = E_{i,k}^{(r)} - E_{i,3}^{(r)} H_{1,k} - E_{i,n+2}^{(r)} H_{2,k}, \tag{C5}$$

$$\tilde{P}_{j,k}^{(s)} = \tilde{E}_{j,k}^{(s)} - \tilde{E}_{j,3}^{(s)} H_{3,k} - \tilde{E}_{j,m+2}^{(s)} H_{4,k}, \tag{C6}$$

$$G_{i,k_1,k_2,j}^{(r,s)} = E_{i,k_1}^{(r)} \tilde{E}_{j,k_2}^{(s)} - E_{i,k_1}^{(r)} \tilde{E}_{j,3}^{(s)} H_{3,k_2} - E_{i,k_1}^{(r)} \tilde{E}_{j,m+2}^{(s)} H_{4,k_2}, \tag{C7}$$

$$F_{i,k_1,k_2,j}^{(r,s)} = G_{i,k_1,k_2,j}^{(r,s)} - G_{i,3,k_2,j}^{(r,s)} H_{1,k_1} - G_{i,n+2,k_2,j}^{(r,s)} H_{2,k_1}, \tag{C8}$$

References

Aksencer, T., & Aydogdu, M. (2011). Levy type solution method for vibration and buckling of nanoplates using nonlocal elasticity theory. *Physica E: Low-dimensional Systems and Nanostructures, 43*, 954–959.
Apuzzo, A., Barretta, R., Luciano, R., de Sciarra, F. M., & Penna, R. (2017). Free vibrations of Bernoulli-Euler nano-beams by the stress-driven nonlocal integral model. *Composites Part B: Engineering, 123*, 105–111.
Arani, A. G., & Jalaei, M. H. (2016). Transient behavior of an orthotropic graphene sheet resting on orthotropic visco-Pasternak foundation. *International Journal of Engineering Science, 103*, 97–113.
Barretta, R., Čanađija, M., Luciano, R., & de Sciarra, F. M. (2018). Stress-driven modeling of nonlocal thermoelastic behavior of nanobeams. *International Journal of Engineering Science, 126*, 53–67.
Barretta, R., Faghidian, S. A., & Luciano, R. (2019). Longitudinal vibrations of nano-rods by stress-driven integral elasticity. *Mechanics of Advanced Materials and Structures, 26*, 1307–1315.
Barretta, R., Faghidian, S. A., & Marotti de Sciarra, F. (2019). Stress-driven nonlocal integral elasticity for axisymmetric nano-plates. *International Journal of Engineering Science, 136*, 38–52.
Chen, C., Lee, S., Deshpande, V. V., Lee, G.-H., Lekas, M., Shepard, K., & Hone, J. (2013). Graphene mechanical oscillators with tunable frequency. *Nature Nanotechnology, 8*, 923.
Dai, H. L., Wang, L., Abdelkefi, A., & Ni, Q. (2015). On nonlinear behavior and buckling of fluid-transporting nanotubes. *International Journal of Engineering Science, 87*, 13–22.
Daneshmehr, A., Rajabpoor, A., & Hadi, A. (2015). Size dependent free vibration analysis of nanoplates made of functionally graded materials based on nonlocal elasticity theory with high order theories. *International Journal of Engineering Science, 95*, 23–35.
Ebrahimi, F., & Barati, M. R. (2016). A nonlocal higher-order refined magneto-electro-viscoelastic beam model for dynamic analysis of smart nanostructures. *International Journal of Engineering Science, 107*, 183–196.
El-Borgi, S., Rajendran, P., Friswell, M., Trabelssi, M., & Reddy, J. (2018). Torsional vibration of size-dependent viscoelastic rods using nonlocal strain and velocity gradient theory. *Composite Structures, 186*, 274–292.
Eringen, A. C. (2002). Nonlocal continuum field theories. *Springer Science & Business Media.*
Farajpour, A., Farokhi, H., Ghayesh, M. H., & Hussain, S. (2018). Nonlinear mechanics of nanotubes conveying fluid. *International Journal of Engineering Science, 133*, 132–143.
Farajpour, A., Ghayesh, M. H., & Farokhi, H. (2018). A review on the mechanics of nanostructures. *International Journal of Engineering Science, 133*, 231–263.
Farajpour, A., Ghayesh, M. H., & Farokhi, H. (2019). Nonlocal nonlinear mechanics of imperfect carbon nanotubes. *International Journal of Engineering Science, 142*, 201–215.
Farajpour, A., Rastgoo, A., & Farajpour, M. (2017). Nonlinear buckling analysis of magneto-electro-elastic CNT-MT hybrid nanoshells based on the nonlocal continuum mechanics. *Composite Structures, 180*, 179–191.
Farajpour, A., & Rastgoo, A. (2017). Influence of carbon nanotubes on the buckling of microtubule bundles in viscoelastic cytoplasm using nonlocal strain gradient theory. *Results in Physics, 7*, 1367–1375.
Farajpour, A., Yazdi, M. H., Rastgoo, A., & Mohammadi, M. (2016). A higher-order nonlocal strain gradient plate model for buckling of orthotropic nanoplates in thermal environment. *Acta Mechanica, 227*, 1849–1867.
Farajpour, M., Shahidi, A., Tabataba'i-Nasab, F., & Farajpour, A. (2018). Vibration of initially stressed carbon nanotubes under magneto-thermal environment for nanoparticle delivery via higher-order nonlocal strain gradient theory. *The European Physical Journal Plus, 133*, 219.
Farajpour, M. R., Shahidi, A. R., & Farajpour, A. (2018). A nonlocal continuum model for the biaxial buckling analysis of composite nanoplates with shape memory alloy nanowires. *Materials Research Express, 5*(3), Article 035026.
Farokhi, H., & Ghayesh, M. H. (2018). Nonlinear mechanical behaviour of microshells. *International Journal of Engineering Science, 127*, 127–144.
Farokhi, H., & Ghayesh, M. H. (2018). On the dynamics of imperfect shear deformable microplates. *International Journal of Engineering Science, 133*, 264–283.
Farokhi, H., & Ghayesh, M. H. (2018). Nonlinear mechanics of electrically actuated microplates. *International Journal of Engineering Science, 123*, 197–213.
Farokhi, H., Ghayesh, M. H., Gholipour, A., & Hussain, S. (2017). Motion characteristics of bilayered extensible Timoshenko microbeams. *International Journal of Engineering Science, 112*, 1–17.
Fernández-Sáez, J., Zaera, R., Loya, J., & Reddy, J. (2016). Bending of Euler–Bernoulli beams using Eringen's integral formulation: a paradox resolved. *International Journal of Engineering Science, 99*, 107–116.
Ghayesh, M. H. (2018). Dynamics of functionally graded viscoelastic microbeams. *International Journal of Engineering Science, 124*, 115–131.
Ghayesh, M. H., & Farajpour, A. (2018). Nonlinear mechanics of nanoscale tubes via nonlocal strain gradient theory. *International Journal of Engineering Science, 129*, 84–95.
Ghayesh, M. H., & Farajpour, A. (2019). A review on the mechanics of functionally graded nanoscale and microscale structures. *International Journal of Engineering Science, 137*, 8–36.
Ghayesh, M. H., Farajpour, A., & Farokhi, H. (2019). Viscoelastically coupled mechanics of fluid-conveying microtubes. *International Journal of Engineering Science, 145*, Article 103139.
Ghayesh, M. H., Farokhi, H., & Alici, G. (2016). Size-dependent performance of microgyroscopes. *International Journal of Engineering Science, 100*, 99–111.

Ghayesh, M. H., Farokhi, H., & Farajpour, A. (2019). Global dynamics of fluid conveying nanotubes. *International Journal of Engineering Science, 135*, 37–57.

Ghayesh, M. H., Farokhi, H., Gholipour, A., & Tavallaeinejad, M. (2018). Nonlinear oscillations of functionally graded microplates. *International Journal of Engineering Science, 122*, 56–72.

Hadi, A., Nejad, M. Z., & Hosseini, M. (2018). Vibrations of three-dimensionally graded nanobeams. *International Journal of Engineering Science, 128*, 12–23.

Imrak, C., & Gerdemeli, I. (2007). An exact solution for the deflection of a clamped rectangular plate under uniform load. *Applied Mathematical Sciences, 1*, 2129–2137.

Karami, B., & Janghorban, M. (2019). On the dynamics of porous nanotubes with variable material properties and variable thickness. *International Journal of Engineering Science, 136*, 53–66.

Karami, B., Shahsavari, D., Janghorban, M., & Li, L. (2019). On the resonance of functionally graded nanoplates using bi-Helmholtz nonlocal strain gradient theory. *International Journal of Engineering Science, 144*, Article 103143.

Khaniki, H. B. (2018). On vibrations of nanobeam systems. *International Journal of Engineering Science, 124*, 85–103.

Kostarelos, K., & Novoselov, K. S. (2014). Graphene devices for life. *Nature nanotechnology, 9*, 744.

Koutsoumaris, C. C., Eptaimeros, K., & Tsamasphyros, G. (2017). A different approach to Eringen's nonlocal integral stress model with applications for beams. *International Journal of Solids and Structures, 112*, 222–238.

Leissa, A. W. (1969). Vibration of plates. *The Ohio State University*.

Li, L., Hu, Y., & Ling, L. (2016). Wave propagation in viscoelastic single-walled carbon nanotubes with surface effect under magnetic field based on nonlocal strain gradient theory. *Physica E: Low-dimensional Systems and Nanostructures, 75*, 118–124.

Li, L., Tang, H., & Hu, Y. (2018). The effect of thickness on the mechanics of nanobeams. *International Journal of Engineering Science, 123*, 81–91.

Lim, C., Zhang, G., & Reddy, J. (2015). A higher-order nonlocal elasticity and strain gradient theory and its applications in wave propagation. *Journal of the Mechanics and Physics of Solids, 78*, 298–313.

Lu, L., Guo, X., & Zhao, J. (2017). Size-dependent vibration analysis of nanobeams based on the nonlocal strain gradient theory. *International Journal of Engineering Science, 116*, 12–24.

Lu, L., Guo, X., & Zhao, J. (2017). A unified nonlocal strain gradient model for nanobeams and the importance of higher order terms. *International Journal of Engineering Science, 119*, 265–277.

Ma, L.-H., Ke, L.-L., Wang, Y.-Z., & Wang, Y.-S. (2018). Wave propagation analysis of piezoelectric nanoplates based on the nonlocal theory. *International Journal of Structural Stability and Dynamics, 18*, Article 1850060.

Malekzadeh, P., & Farajpour, A. (2012). Axisymmetric free and forced vibrations of initially stressed circular nanoplates embedded in an elastic medium. *Acta Mechanica, 223*(11), 2311–2330.

Medina, L., Gilat, R., & Krylov, S. (2018). Bistability criterion for electrostatically actuated initially curved micro plates. *International Journal of Engineering Science, 130*, 75–92.

Mohammadi, K., Rajabpour, A., & Ghadiri, M. (2018). Calibration of nonlocal strain gradient shell model for vibration analysis of a CNT conveying viscous fluid using molecular dynamics simulation. *Computational Materials Science, 148*, 104–115.

Mohammadi, M., Moradi, A., Ghayour, M., & Farajpour, A. (2014). Exact solution for thermo-mechanical vibration of orthotropic mono-layer graphene sheet embedded in an elastic medium. *Latin American Journal of Solids and Structures, 11*(3), 437–458.

Naderi, A., & Saidi, A. R. (2014). Nonlocal postbuckling analysis of graphene sheets in a nonlinear polymer medium. *International Journal of Engineering Science, 81*, 49–65.

Nejad, M. Z., & Hadi, A. (2016). Eringen's non-local elasticity theory for bending analysis of bi-directional functionally graded Euler–Bernoulli nano-beams. *International Journal of Engineering Science, 106*, 1–9.

Nejad, M. Z., Hadi, A., & Rastgoo, A. (2016). Buckling analysis of arbitrary two-directional functionally graded Euler–Bernoulli nano-beams based on nonlocal elasticity theory. *International Journal of Engineering Science, 103*, 1–10.

Rahmani, O., & Pedram, O. (2014). Analysis and modeling the size effect on vibration of functionally graded nanobeams based on nonlocal Timoshenko beam theory. *International Journal of Engineering Science, 77*, 55–70.

Rajasekaran, S., & Khaniki, H. B. (2017). Bending, buckling and vibration of small-scale tapered beams. *International Journal of Engineering Science, 120*, 172–188.

Reddy, J. N., & El-Borgi, S. (2014). Eringen's nonlocal theories of beams accounting for moderate rotations. *International Journal of Engineering Science, 82*, 159–177.

Romano, G., & Barretta, R. (2017). Stress-driven versus strain-driven nonlocal integral model for elastic nano-beams. *Composites Part B: Engineering, 114*, 184–188.

Romano, G., & Barretta, R. (2017). Nonlocal elasticity in nanobeams: the stress-driven integral model. *International Journal of Engineering Science, 115*, 14–27.

Romano, G., Barretta, R., Diaco, M., & de Sciarra, F. M. (2017). Constitutive boundary conditions and paradoxes in nonlocal elastic nanobeams. *International Journal of Mechanical Sciences, 121*, 151–156.

Ru, C. (2000). Column buckling of multiwalled carbon nanotubes with interlayer radial displacements. *Physical Review B, 62*, 16962.

Shafiei, N., Kazemi, M., Safi, M., & Ghadiri, M. (2016). Nonlinear vibration of axially functionally graded non-uniform nanobeams. *International Journal of Engineering Science, 106*, 77–94.

Shahverdi, H., & Barati, M. R. (2017). Vibration analysis of porous functionally graded nanoplates. *International Journal of Engineering Science, 120*, 82–99.

She, G.-L., Yuan, F.-G., Karami, B., Ren, Y.-R., & Xiao, W.-S. (2019). On nonlinear bending behavior of FG porous curved nanotubes. *International Journal of Engineering Science, 135*, 58–74.

She, G.-L., Yuan, F.-G., & Ren, Y.-R. (2018). On wave propagation of porous nanotubes. *International Journal of Engineering Science, 130*, 62–74.

She, G.-L., Yuan, F.-G., Ren, Y.-R., & Xiao, W.-S. (2017). On buckling and postbuckling behavior of nanotubes. *International Journal of Engineering Science, 121*, 130–142.

Shu, C. (2012). Differential quadrature and its application in engineering. *Springer Science & Business Media*.

Tuna, M., & Kirca, M. (2016). Exact solution of Eringen's nonlocal integral model for bending of Euler–Bernoulli and Timoshenko beams. *International Journal of Engineering Science, 105*, 80–92.

Wang, Q., & Arash, B. (2014). A review on applications of carbon nanotubes and graphenes as nano-resonator sensors. *Computational Materials Science, 82*, 350–360.

Wu, T., & Liu, G. (2000). Application of generalized differential quadrature rule to sixth-order differential equations. *Communications in Numerical Methods in Engineering, 16*, 777–784.

Xu, X.-J., Zheng, M.-L., & Wang, X.-C. (2017). On vibrations of nonlocal rods: Boundary conditions, exact solutions and their asymptotics. *International Journal of Engineering Science, 119*, 217–231.

Yoon, J., Ru, C., & Mioduchowski, A. (2003). Vibration of an embedded multiwall carbon nanotube. *Composites Science and Technology, 63*, 1533–1542.

Zhao, J., Guo, X., & Lu, L. (2018). Small size effect on the wrinkling hierarchy in constrained monolayer graphene. *International Journal of Engineering Science, 131*, 19–25.

Zheng, X.-Q., Lee, J., & Feng, P. X.-L. (2017). Hexagonal boron nitride nanomechanical resonators with spatially visualized motion. *Microsystems & Nanoengineering, 3*, 17038.

Zhu, X., & Li, L. (2017). Closed form solution for a nonlocal strain gradient rod in tension. *International Journal of Engineering Science, 119*, 16–28.

Zhu, X., & Li, L. (2017). On longitudinal dynamics of nanorods. *International Journal of Engineering Science, 120*, 129–145.

Chapter 6

Nonlinear vibration behaviour of rectangular small-scale plates

Chapter overview

In chapter 6, the nonlinear vibration of plates at small-scale levels, which is the last objective of this project, is analysed. To conduct this analysis, a nonlinear size-dependent model is presented based on non-classical integral constitutive equations. Curvature nonlocality and in-plane nonlocality are both taken into consideration in the continuum modelling to better estimate size dependency at small-scales. Coupled nonlinear equations with conventional and non-conventional edge conditions are presented by the stress-driven theory. Applying a differential quadrature method and an iteration approach, all edge conditions and coupled nonlinear equations are discretized, and the nonlinear frequencies are computed. Molecular dynamics simulations are also performed to prove that the modelling is valid. This analysis in conjunction with the previous analysis presented in chapter 5 provide a useful benchmark for the vibrations of small-scale plates. This work has been submitted as a journal manuscript for review to "Composites Part B: Engineering".

Statement of Authorship

Title of Paper	A nonlinear stress-driven nonlocal integral model for the vibration of nanoplates
Publication Status	☐ Published ☐ Accepted for Publication ☑ Submitted for Publication ☐ Unpublished and Unsubmitted work written in manuscript style
Publication Details	Ali Farajpour, Carl Q. Howard, William S.P. Robertson, A nonlinear stress-driven nonlocal integral model for the vibration of nanoplates, Composites Part B: Engineering

Principal Author

Name of Principal Author (Candidate)	Ali Farajpour Ouderji
Contribution to the Paper	- Doing the literature review of the paper - Deriving the partial differential equations of motion - Incorporating size effects using a scale-dependent continuum approach - MD simulations - Numerical solution - Analysing the results and writing the paper
Overall percentage (%)	80%
Certification:	This paper reports on original research I conducted during the period of my Higher Degree by Research candidature and is not subject to any obligations or contractual agreements with a third party that would constrain its inclusion in this thesis. I am the primary author of this paper.
Signature	Date 2021-2-18

Co-Author Contributions

By signing the Statement of Authorship, each author certifies that:

i.   the candidate's stated contribution to the publication is accurate (as detailed above);

ii. permission is granted for the candidate in include the publication in the thesis; and

iii. the sum of all co-author contributions is equal to 100% less the candidate's stated contribution.

Name of Co-Author	Carl Q. Howard
Contribution to the Paper	- Supervising the research work - Contribution to the development of the ideas and concepts of the paper - Editing and evaluating the paper before submission
Signature	Date 2020-10-26

Name of Co-Author	William S.P. Robertson
Contribution to the Paper	- Co-supervising the research work - Contribution to the development of the concepts of the paper - Editing and evaluating the paper before submission
Signature	Date 2020-10-22

Please cut and paste additional co-author panels here as required.

A nonlinear stress-driven nonlocal integral model for the vibration of nanoplates

Ali Farajpour[*], Carl Q. Howard, William S.P. Robertson

School of Mechanical Engineering, The University of Adelaide, South Australia 5005, Australia
[*]*Corresponding author: ali.farajpourouderji@adelaide.edu.au (A. Farajpour)*
Email: carl.howard@adelaide.edu.au (C. Howard)
Email: will.robertson@adelaide.edu.au (W.S.P. Robertson)

Abstract

A nonlinear nonlocal integral plate model is introduced in the present article for the first time to investigate the vibrations of graphene sheets. Integral constitutive equations are assumed for both in-plane strain components and nanoplate curvature. Three types of boundary conditions including classical edge condition and non-classical constitutive conditions related to both nonlocal strain components and curvature nonlocality are derived. Application of the stress-driven integral theory and von Kármán's theory of nonlinearity to Kirchhoff's plate model leads to the coupled nonlinear motion equations. The resonance frequencies of the graphene are computed via a differential quadrature technique and an iteration method. All boundary condition types are discretised and implemented in the numerical solution procedure. Furthermore, molecular dynamics simulations are conducted for various maximum transverse amplitudes to verify the nonlinear stress-driven integral plate model. The influences of curvature nonlocality, in-plane nonlocality, maximum transverse deflection, and geometric ratios on the nonlinear frequency ratio and maximum in-plane displacements are studied in detail.

Keywords: *Nonlinear vibration*, *Stress-driven nonlocal integral elasticity*, *Graphene sheets*, *Molecular dynamcis*

1. Introduction

Graphene sheets (GSs), as one of the most common types of nanoplates, have received much interest lately because of their promising mechanical, physical and electrical properties [1, 2]. These ultrasmall plate-shaped structures have been utilised in nanotechnology-based devices and systems from nanoresonators [3] to electrically excited nanoactuators [4] as the basic component. Motion analysis and vibration response of GSs are important in order for these devices to operate efficiently. In a number of unavoidable situations, nonlinear motions and large-amplitude vibrations have been observed in GS-based nanodevices [5, 6].

The vibrational behaviour of GSs with small engineering strain components has been remarkably examined in the open literature due to relatively simple modelling and simulations. In an early continuum-based analysis, Kitipornchai et al. [7] investigated the vibration of GSs by developing a scale-free elasticity model via Kirchhoff's theory; the plate-shaped nanostructure was made of several layers, and the influence of van der Waals force between these layers were taken into account; they found that interlayer forces were strongly dependent on the space between layers. Moreover, Ansari et al. [8] analysed the vibrational response of GSs made of one single layer with small vibration amplitudes via a differential form of nonlocal continuum mechanics; they also determined the calibrated nonlocal parameters, which were independent of the system geometry. Furthermore, molecular mechanics simulations were conducted to analyse the tensile behaviour and linear oscillation of single-layered GSs by Gupta and Batra [9]. A differential nonlocal model incorporating shear deformation and surface energy as well as the nonlocality of stress components were developed by Malekzadeh and Shojaee [10] for the nanoplate vibration; they concluded that surface energy was associated with larger resonance frequencies. Zenkour [11] introduced a mixed nonlocal continuum modelling for the thermomechanical vibrational response of ultrasmall plate-shaped structures;

while the linear frequency decreases with increasing stress nonlocality, the thermal parameter has the opposite effect on the linear frequency.

The number of nonlinear studies carried out on the large-amplitude vibration of GSs is limited compared to widely reported linear studies since the mathematical modelling is more complex, and molecular dynamics simulations require more computational effort. Reddy [12] presented comprehensive nonlinear theoretical formulations for the deformation of beam- and plate-shaped nanostructures via differential nonlocal theory, which can be used as guiding principle for the nonlinear modelling of GSs. Malekzadeh et al. [13] investigated the impacts of geometrical, nonlocal and surface parameters on the nonlinear vibration of skew ultrasmall plates by the differential quadrature method (DQM); they indicated that higher skew angles lead to higher geometrical nonlinearity in the vibrational response of ultrasmall plates. In addition, Farajpour et al. [14] extended the differential nonlocal elasticity to the nonlocal magneto-electro-elasticity for investigating the oscillations of smart nanofilms with large amplitudes. Liu et al. [15] also modelled the nonlinear frequency behaviour of ultrasmall plates with piezoelectric material properties via a differential nonlocal Mindlin theory of plates. Moreover, the influence of geometrical nonlinearity on the vibration of bilayer GSs [16], smart sandwich ultrasmall plates [17], nonhomogeneous nanoplates [18, 19], viscoelastic nanoplates [20, 21], imperfect nanoplates [22] and ultrasmall vibration-based sensors [23].

Recently, the application of integral forms of size-dependent elasticity theories as a more precise theoretical tool, in the continuum modelling of nanostructures has been introduced [24-28]. A number of integral continuum models incorporating size impacts such as stress-driven [29-31], two-phase [32-34] and strain-driven [35] theories have been introduced. These integral size-dependent models include higher-order differential equations of motions with extra non-classical boundary conditions, leading to more accurate theoretical estimations at ultrasmall levels but more time-consuming and complex solution procedures in some cases, compared to

113

the differential nonlocal elasticity. The majority of these research studies using integral models have focused on the linear vibration of nanostructures, especially nanobeams and nanorods. The large-amplitude vibration of plates at nanoscales via the nonlinear stress-driven nonlocal elasticity has not been investigated so far. This work is the first endeavour to develop a nonlinear integral model with size effects for analysing this important problem in nanotechnology. Stress-driven effects are incorporated in both in-plane force resultants and bending moments. The equations of motions are derived via nonlinear Kirchhoff's plate theory and stress-driven integral elasticity. Two sets of higher-order nonlocal edge conditions are obtained for nanoplate motion equations. A DQM-based numerical solution is developed to determine the nonlinear frequency parameters of GSs. Molecular dynamics simulation is also performed to indicate the accuracy of the continuum model. The influences of geometric properties, maximum lateral deflection and size parameters on the nonlinear vibrational behaviour are investigated.

2. A nonlinear stress-driven plate model

Figure 1 shows a single-layered GS of zigzag types with dimensions $(a, h, b)=$(length, thickness, width). The nanoplate is free of any initial stress and initial deflection. The displacements of the GS in z, y and x axis are w, v and u, respectively. Assuming von Kármán's nonlinearity, the strain components are

$$\varepsilon_{xx} = \frac{\partial u}{\partial x} + \frac{1}{2}\left(\frac{\partial w}{\partial x}\right)^2 - z\frac{\partial^2 w}{\partial x^2} = \varepsilon_{xx}^0 + z\kappa_{xx},$$

$$\varepsilon_{yy} = \frac{\partial v}{\partial y} + \frac{1}{2}\left(\frac{\partial w}{\partial y}\right)^2 - z\frac{\partial^2 w}{\partial y^2} = \varepsilon_{yy}^0 + z\kappa_{yy},$$

$$\varepsilon_{xy} = \frac{1}{2}\left(\frac{\partial u}{\partial y} + \frac{\partial v}{\partial x} + \frac{\partial w}{\partial x}\frac{\partial w}{\partial y}\right) - z\frac{\partial^2 w}{\partial x\partial y} = \varepsilon_{xy}^0 + z\kappa_{xy}, \tag{1}$$

where ε_{ij}^0 and κ_{ij} are the in-plane strain and plate curvature, respectively.
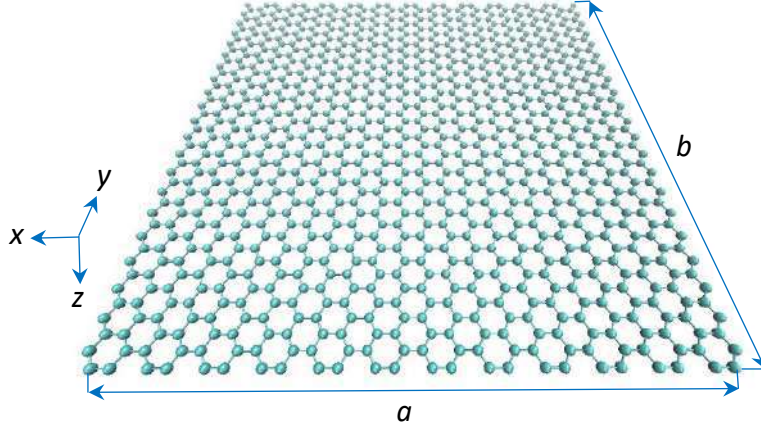
Fig. 1. A single-layered GS prior to time-dependent deformation.

Using the classical model of elasticity, stress components are associated with nonlinear strains as follows

$$\varepsilon_{xx} = \frac{1}{E}(\sigma_{xx} - \upsilon\sigma_{yy}),\ \varepsilon_{yy} = \frac{1}{E}(\sigma_{yy} - \upsilon\sigma_{xx}),\ \varepsilon_{xy} = \frac{1}{2G}\sigma_{xy}, \tag{2}$$

In Eq. (2), E and G indicate Young and shear moduli, respectively; υ denotes Poisson's ratio. However, Eq. (2) is not valid for the stress-driven model, in which size influences are captured via assuming integral constitutive equations for the GS. The in-plane strain components are

$$\varepsilon_{xx}^0 = \int\limits_0^b \int\limits_0^a \varphi(|x - \bar{x}|, |y - \bar{y}|, L_C) F_{xx}(\bar{x}, \bar{y}) d\bar{x} d\bar{y},$$

$$\varepsilon_{yy}^0 = \int\limits_0^b \int\limits_0^a \varphi(|x - \bar{x}|, |y - \bar{y}|, L_C) F_{yy}(\bar{x}, \bar{y}) d\bar{x} d\bar{y},$$

$$\varepsilon_{xy}^0 = \frac{1}{2A_{33}} N_{xy}, \tag{3}$$

where

$$F_{xx} = \frac{1}{A_{11}(1-\upsilon^2)}(N_{xx} - \upsilon N_{yy}),$$
$$F_{yy} = \frac{1}{A_{11}(1-\upsilon^2)}(N_{yy} - \upsilon N_{xx}), \tag{4}$$

115

N_{xx}, N_{yy} and N_{xy} represent force resultants, and A_{ij} denotes the nanoplate in-plane stiffness. In this analysis, N_{ij} and A_{ij} are defied by

$$N_{xx} = \int_{-h/2}^{h/2} \sigma_{xx} dz, \quad N_{yy} = \int_{-h/2}^{h/2} \sigma_{yy} dz, \quad N_{xy} = \int_{-h/2}^{h/2} \sigma_{xy} dz, \tag{5}$$

$$A_{11} = \frac{Eh}{(1-v^2)}, \quad A_{12} = \frac{vEh}{(1-v^2)}, \quad A_{33} = Gh. \tag{6}$$

In Eq. (3), φ and L_{C0} denote the kernel function and the scale parameter associated with in-plane strains, respectively. Similarly, for the plate curvature components, we have

$$\kappa_{xx} = \int_0^b \int_0^a \varphi(|x - \bar{x}|, |y - \bar{y}|, L_C) H_{xx}(\bar{x}, \bar{y}) d\bar{x} d\bar{y},$$

$$\kappa_{yy} = \int_0^b \int_0^a \varphi(|x - \bar{x}|, |y - \bar{y}|, L_C) H_{yy}(\bar{x}, \bar{y}) d\bar{x} d\bar{y},$$

$$\kappa_{xy} = \frac{1}{2D_{33}} M_{xy}, \tag{7}$$

where

$$H_{xx} = \frac{1}{D_{11}(1-v^2)} (M_{xx} - vM_{yy}),$$
$$H_{yy} = \frac{1}{D_{11}(1-v^2)} (M_{yy} - vM_{xx}), \tag{8}$$

where M_{xx}, M_{yy} and M_{xy} represent the couple resultants, and D_{ij} is the rigidity of the GS. L_C denotes the scale parameter associated with the nanoplate curvature, The couple resultants and bending rigidities are given by

$$M_{xx} = \int_{-h/2}^{h/2} z\sigma_{xx} dz, \quad M_{yy} = \int_{-h/2}^{h/2} z\sigma_{yy} dz, \quad M_{xy} = \int_{-h/2}^{h/2} z\sigma_{xy} dz. \tag{9}$$

$$D_{11} = \frac{Eh^3}{12(1-v^2)}, \quad D_{12} = \frac{vEh^3}{12(1-v^2)} = vD_{11}, D_{33} = \frac{Gh^3}{12}. \tag{10}$$

To accurately model the size effect on the mechanics of ultrasmall plate-shaped structures, the kernel function should fulfil the following relations

$$\varphi(|x - \bar{x}|, |y - \bar{y}|, L_C) \geq 0, \tag{11}$$

$$\int_{-\infty}^{+\infty} \int_{-\infty}^{+\infty} \varphi(x, y, L_C) dx dy = 1, \tag{12}$$

$$\lim_{L_C \to 0} \int_{-\infty}^{+\infty} \int_{-\infty}^{+\infty} \varphi[(x - \bar{x}), (y - \bar{y}), L_C] f(\bar{x}, \bar{y}) d\bar{x} d\bar{y} = f(x, y). \tag{13}$$

Here *f(x,y)* is an arbitrary continuous function. An appropriate extension of the one-dimensional bi-exponential kernel function is used as

$$\varphi(|x - \bar{x}|, |y - \bar{y}|, L_C) = \frac{1}{4L_C^2} \exp\left[-\frac{1}{L_C}(|x - \bar{x}| + |y - \bar{y}|)\right]. \tag{14}$$

Substituting Eq. (14) into Eqs. (11)-(13), it can be simply proved that the above-introduced two-dimensional kernel function fully satisfy the required relations. Using Eq. (14) together with Eqs. (3) and (4), one obtains

$$L_{C0}^4 \frac{\partial^4 \varepsilon_{xx}^0}{\partial y^2 \partial x^2} - L_{C0}^2 \left(\frac{\partial^2 \varepsilon_{xx}^0}{\partial y^2} + \frac{\partial^2 \varepsilon_{xx}^0}{\partial x^2}\right) + \varepsilon_{xx}^0 = F_{xx},$$

$$L_{C0}^4 \frac{\partial^4 \varepsilon_{yy}^0}{\partial y^2 \partial x^2} - L_{C0}^2 \left(\frac{\partial^2 \varepsilon_{yy}^0}{\partial y^2} + \frac{\partial^2 \varepsilon_{yy}^0}{\partial x^2}\right) + \varepsilon_{yy}^0 = F_{yy}. \tag{15}$$

with the following boundary conditions

$$x = 0: \frac{\partial \varepsilon_{xx}^0}{\partial x} = \frac{1}{L_{C0}} \varepsilon_{xx}^0,$$

$$x = a: \quad \frac{\partial \varepsilon_{xx}^0}{\partial x} = -\frac{1}{L_{C0}} \varepsilon_{xx}^0,$$

$$y = 0: \quad \frac{\partial \varepsilon_{yy}^0}{\partial y} = \frac{1}{L_{C0}} \varepsilon_{yy}^0,$$

$$y = b: \quad \frac{\partial \varepsilon_{yy}^0}{\partial y} = -\frac{1}{L_{C0}} \varepsilon_{yy}^0. \tag{16}$$

Applying Eqs. (14), (7) and (8), yields the curvature components of the GS

$$L_C^4 \frac{\partial^4 \kappa_{xx}}{\partial y^2 \partial x^2} - L_C^2 \left(\frac{\partial^2 \kappa_{xx}}{\partial y^2} + \frac{\partial^2 \kappa_{xx}}{\partial x^2}\right) + \kappa_{xx} = H_{xx}(x, y),$$

$$L_C^4 \frac{\partial^4 \kappa_{yy}}{\partial y^2 \partial x^2} - L_C^2 \left(\frac{\partial^2 \kappa_{yy}}{\partial y^2} + \frac{\partial^2 \kappa_{yy}}{\partial x^2}\right) + \kappa_{yy} = H_{yy}(x, y), \tag{17}$$

with two extra boundary conditions

$$x = 0: \frac{\partial \kappa_{xx}}{\partial x} = \frac{1}{L_C} \kappa_{xx},$$

$$x = a: \frac{\partial \kappa_{xx}}{\partial x} = -\frac{1}{L_C} \kappa_{xx},$$

$$y = 0: \frac{\partial \kappa_{yy}}{\partial y} = \frac{1}{L_C} \kappa_{yy},$$

$$y = b: \frac{\partial \kappa_{yy}}{\partial y} = -\frac{1}{L_C} \kappa_{yy}. \tag{18}$$

Using Eqs. (4), (8), (15) and (17), the force and couple resultants of the GS are obtained as follows

$$N_{xx} = A_{11}L_{C0}^4 \left[\frac{\partial^5 u}{\partial y^2 \partial x^3} + \frac{\partial w}{\partial x}\frac{\partial^5 w}{\partial y^2 \partial x^3} + 2\frac{\partial^2 w}{\partial x^2}\frac{\partial^4 w}{\partial y^2 \partial x^2} \right.$$

$$\left. + \frac{\partial^3 w}{\partial x^3}\frac{\partial^3 w}{\partial y^2 \partial x} + 2\left(\frac{\partial^3 w}{\partial y \partial x^2}\right)^2 + 2\frac{\partial^2 w}{\partial y \partial x}\frac{\partial^4 w}{\partial y \partial x^3} \right]$$

$$-A_{11}L_{C0}^2 \left[\frac{\partial^3 u}{\partial y^2 \partial x} + \frac{\partial^3 u}{\partial x^3} + \left(\frac{\partial^2 w}{\partial y \partial x}\right)^2 + \frac{\partial w}{\partial x}\frac{\partial^3 w}{\partial y^2 \partial x} + \left(\frac{\partial^2 w}{\partial x^2}\right)^2 + \frac{\partial w}{\partial x}\frac{\partial^3 w}{\partial x^3} \right]$$

$$+A_{11}\left[\frac{\partial u}{\partial x} + \frac{1}{2}\left(\frac{\partial w}{\partial x}\right)^2 \right] + \upsilon A_{11}L_{C0}^4 \left[\frac{\partial^5 v}{\partial y^3 \partial x^2} + \frac{\partial w}{\partial y}\frac{\partial^5 w}{\partial x^2 \partial y^3} + 2\frac{\partial^2 w}{\partial y^2}\frac{\partial^4 w}{\partial x^2 \partial y^2} \right.$$

$$\left. + \frac{\partial^3 w}{\partial y^3}\frac{\partial^3 w}{\partial x^2 \partial y} + 2\left(\frac{\partial^3 w}{\partial x \partial y^2}\right)^2 + 2\frac{\partial^2 w}{\partial x \partial y}\frac{\partial^4 w}{\partial x \partial y^3} \right] - \upsilon A_{11}L_{C0}^2 \left[\frac{\partial^3 v}{\partial x^2 \partial y} + \frac{\partial^3 v}{\partial y^3} \right.$$

$$\left. + \left(\frac{\partial^2 w}{\partial x \partial y}\right)^2 + \frac{\partial w}{\partial y}\frac{\partial^3 w}{\partial x^2 \partial y} + \left(\frac{\partial^2 w}{\partial y^2}\right)^2 + \frac{\partial w}{\partial y}\frac{\partial^3 w}{\partial y^3} \right] + \upsilon A_{11}\left[\frac{\partial v}{\partial y} + \frac{1}{2}\left(\frac{\partial w}{\partial y}\right)^2 \right], \tag{19}$$

$$N_{yy} = A_{11}L_{C0}^4 \left[\frac{\partial^5 v}{\partial y^3 \partial x^2} + \frac{\partial w}{\partial y}\frac{\partial^5 w}{\partial x^2 \partial y^3} + 2\frac{\partial^2 w}{\partial y^2}\frac{\partial^4 w}{\partial x^2 \partial y^2} \right.$$

$$\left. + \frac{\partial^3 w}{\partial y^3}\frac{\partial^3 w}{\partial x^2 \partial y} + 2\left(\frac{\partial^3 w}{\partial x \partial y^2}\right)^2 + 2\frac{\partial^2 w}{\partial x \partial y}\frac{\partial^4 w}{\partial x \partial y^3} \right]$$

$$-A_{11}L_{C0}^2 \left[\frac{\partial^3 v}{\partial x^2 \partial y} + \frac{\partial^3 v}{\partial y^3} + \left(\frac{\partial^2 w}{\partial x \partial y}\right)^2 + \frac{\partial w}{\partial y}\frac{\partial^3 w}{\partial x^2 \partial y} + \left(\frac{\partial^2 w}{\partial y^2}\right)^2 + \frac{\partial w}{\partial y}\frac{\partial^3 w}{\partial y^3} \right]$$

$$+A_{11}\left[\frac{\partial v}{\partial y} + \frac{1}{2}\left(\frac{\partial w}{\partial y}\right)^2 \right] + \upsilon A_{11}L_{C0}^4 \left[\frac{\partial^5 u}{\partial y^2 \partial x^3} + 2\frac{\partial^2 w}{\partial x^2}\frac{\partial^4 w}{\partial y^2 \partial x^2} + \frac{\partial w}{\partial x}\frac{\partial^5 w}{\partial y^2 \partial x^3} \right.$$

$$\left. + \frac{\partial^3 w}{\partial x^3}\frac{\partial^3 w}{\partial y^2 \partial x} + 2\left(\frac{\partial^3 w}{\partial y \partial x^2}\right)^2 + 2\frac{\partial^2 w}{\partial y \partial x}\frac{\partial^4 w}{\partial y \partial x^3} \right] - \upsilon A_{11}L_{C0}^2 \left[\frac{\partial^3 u}{\partial y^2 \partial x} + \frac{\partial^3 u}{\partial x^3} \right.$$

$$\left. + \left(\frac{\partial^2 w}{\partial y \partial x}\right)^2 + \frac{\partial w}{\partial x}\frac{\partial^3 w}{\partial y^2 \partial x} + \left(\frac{\partial^2 w}{\partial x^2}\right)^2 + \frac{\partial w}{\partial x}\frac{\partial^3 w}{\partial x^3} \right] + \upsilon A_{11}\left[\frac{\partial u}{\partial x} + \frac{1}{2}\left(\frac{\partial w}{\partial x}\right)^2 \right], \tag{20}$$

118

$$N_{xy} = A_{33}\left(\frac{\partial u}{\partial y} + \frac{\partial v}{\partial x} + \frac{\partial w}{\partial x}\frac{\partial w}{\partial y}\right), \tag{21}$$

$$M_{xx} = -D_{11}\left[L_C^4\frac{\partial^6 w}{\partial y^2\partial x^4} - L_C^2\left(\frac{\partial^4 w}{\partial y^2\partial x^2} + \frac{\partial^4 w}{\partial x^4}\right) + \frac{\partial^2 w}{\partial x^2}\right]$$

$$-vD_{11}\left[L_C^4\frac{\partial^6 w}{\partial y^4\partial x^2} - L_C^2\left(\frac{\partial^4 w}{\partial y^4} + \frac{\partial^4 w}{\partial y^2\partial x^2}\right) + \frac{\partial^2 w}{\partial y^2}\right], \tag{22}$$

$$M_{yy} = -D_{11}\left[L_C^4\frac{\partial^6 w}{\partial y^4\partial x^2} - L_C^2\left(\frac{\partial^4 w}{\partial y^4} + \frac{\partial^4 w}{\partial y^2\partial x^2}\right) + \frac{\partial^2 w}{\partial y^2}\right]$$

$$-vD_{11}\left[L_C^4\frac{\partial^6 w}{\partial y^2\partial x^4} - L_C^2\left(\frac{\partial^4 w}{\partial y^2\partial x^2} + \frac{\partial^4 w}{\partial x^4}\right) + \frac{\partial^2 w}{\partial x^2}\right], \tag{23}$$

$$M_{xy} = -2D_{33}\frac{\partial^2 w}{\partial x\partial y}. \tag{24}$$

Applying Hamilton's principle results in

$$\frac{\partial N_{xx}}{\partial x} + \frac{\partial N_{xy}}{\partial y} = m_0\frac{\partial^2 u}{\partial t^2}, \tag{25}$$

$$\frac{\partial N_{yy}}{\partial y} + \frac{\partial N_{xy}}{\partial x} = m_0\frac{\partial^2 v}{\partial t^2}, \tag{26}$$

$$\frac{\partial^2 M_{xx}}{\partial x^2} + 2\frac{\partial^2 M_{xy}}{\partial x\partial y} + \frac{\partial^2 M_{yy}}{\partial y^2} + \frac{\partial}{\partial x}\left(N_{xx}\frac{\partial w}{\partial x} + N_{xy}\frac{\partial w}{\partial y}\right)$$

$$+\frac{\partial}{\partial y}\left(N_{yy}\frac{\partial w}{\partial y} + N_{xy}\frac{\partial w}{\partial x}\right) = m_0\frac{\partial^2 w}{\partial t^2}, \tag{27}$$

where $m_0 = \rho h$; the density of the GS is denoted by ρ. Substituting Eqs. (19)-(24) into Eqs. (25)-(27), yields the nonlinear stress-driven equations of motion

$$A_{11}L_{C0}^4\left(\frac{\partial^6 u}{\partial y^2\partial x^4} + 6\frac{\partial^3 w}{\partial y\partial x^2}\frac{\partial^4 w}{\partial y\partial x^3} + 2\frac{\partial^2 w}{\partial y\partial x}\frac{\partial^5 w}{\partial y\partial x^4}\right.$$

$$\left.+\frac{\partial w}{\partial x}\frac{\partial^6 w}{\partial y^2\partial x^4} + 3\frac{\partial^2 w}{\partial x^2}\frac{\partial^5 w}{\partial y^2\partial x^3} + 3\frac{\partial^3 w}{\partial x^3}\frac{\partial^4 w}{\partial y^2\partial x^2} + \frac{\partial^4 w}{\partial x^4}\frac{\partial^3 w}{\partial y^2\partial x}\right)$$

$$+vA_{11}L_{C0}^4\left(\frac{\partial^6 v}{\partial y^3\partial x^3} + 6\frac{\partial^3 w}{\partial x\partial y^2}\frac{\partial^4 w}{\partial x^2\partial y^2} + 3\frac{\partial^3 w}{\partial x^2\partial y}\frac{\partial^4 w}{\partial x\partial y^3}\right.$$

$$\left.+3\frac{\partial^2 w}{\partial x\partial y}\frac{\partial^5 w}{\partial x^2\partial y^3} + \frac{\partial w}{\partial y}\frac{\partial^6 w}{\partial x^3\partial y^3} + 2\frac{\partial^2 w}{\partial y^2}\frac{\partial^5 w}{\partial x^3\partial y^2} + \frac{\partial^3 w}{\partial y^3}\frac{\partial^4 w}{\partial x^3\partial y}\right)$$

$$-A_{11}L_{C0}^2\left(\frac{\partial^4 u}{\partial x^4} + \frac{\partial^4 u}{\partial y^2 \partial x^2} + \frac{\partial w}{\partial x}\frac{\partial^4 w}{\partial x^4} + 3\frac{\partial^2 w}{\partial x^2}\frac{\partial^3 w}{\partial x^3}\right.$$

$$\left.+\frac{\partial w}{\partial x}\frac{\partial^4 w}{\partial y^2 \partial x^2} + \frac{\partial^2 w}{\partial x^2}\frac{\partial^3 w}{\partial y^2 \partial x} + 2\frac{\partial^2 w}{\partial y \partial x}\frac{\partial^3 w}{\partial y \partial x^2}\right)$$

$$-vA_{11}L_{C0}^2\left(\frac{\partial^4 v}{\partial x^3 \partial y} + \frac{\partial^4 v}{\partial x \partial y^3} + 3\frac{\partial^2 w}{\partial x \partial y}\frac{\partial^3 w}{\partial x^2 \partial y} + \frac{\partial w}{\partial y}\frac{\partial^4 w}{\partial x^3 \partial y}\right.$$

$$\left.+\frac{\partial w}{\partial y}\frac{\partial^4 w}{\partial x \partial y^3} + 2\frac{\partial^2 w}{\partial y^2}\frac{\partial^3 w}{\partial x \partial y^2} + \frac{\partial^3 w}{\partial y^3}\frac{\partial^2 w}{\partial x \partial y}\right)$$

$$+A_{11}\left(\frac{\partial^2 u}{\partial x^2} + \frac{\partial w}{\partial x}\frac{\partial^2 w}{\partial x^2}\right) + vA_{11}\left(\frac{\partial^2 v}{\partial x \partial y} + \frac{\partial w}{\partial y}\frac{\partial^2 w}{\partial x \partial y}\right)$$

$$+A_{33}\left(\frac{\partial^2 u}{\partial y^2} + \frac{\partial^2 v}{\partial x \partial y} + \frac{\partial^2 w}{\partial x \partial y}\frac{\partial w}{\partial y} + \frac{\partial w}{\partial x}\frac{\partial^2 w}{\partial y^2}\right) = 0, \tag{28}$$

$$A_{11}L_{C0}^4\left(\frac{\partial^6 v}{\partial y^4 \partial x^2} + 6\frac{\partial^3 w}{\partial x \partial y^2}\frac{\partial^4 w}{\partial x \partial y^3} + 2\frac{\partial^2 w}{\partial x \partial y}\frac{\partial^5 w}{\partial x \partial y^4}\right.$$

$$\left.+\frac{\partial w}{\partial y}\frac{\partial^6 w}{\partial x^2 \partial y^4} + 3\frac{\partial^2 w}{\partial y^2}\frac{\partial^5 w}{\partial x^2 \partial y^3} + 3\frac{\partial^3 w}{\partial y^3}\frac{\partial^4 w}{\partial x^2 \partial y^2} + \frac{\partial^4 w}{\partial y^4}\frac{\partial^3 w}{\partial x^2 \partial y}\right)$$

$$+vA_{11}L_{C0}^4\left(\frac{\partial^6 u}{\partial y^3 \partial x^3} + 6\frac{\partial^3 w}{\partial y \partial x^2}\frac{\partial^4 w}{\partial y^2 \partial x^2} + 3\frac{\partial^2 w}{\partial y \partial x}\frac{\partial^5 w}{\partial y^2 \partial x^3}\right.$$

$$\left.+3\frac{\partial^3 w}{\partial y^2 \partial x}\frac{\partial^4 w}{\partial y \partial x^3} + \frac{\partial w}{\partial x}\frac{\partial^6 w}{\partial y^3 \partial x^3} + 2\frac{\partial^2 w}{\partial x^2}\frac{\partial^5 w}{\partial y^3 \partial x^2} + \frac{\partial^3 w}{\partial x^3}\frac{\partial^4 w}{\partial y^3 \partial x}\right)$$

$$-A_{11}L_{C0}^2\left(\frac{\partial^4 v}{\partial x^2 \partial y^2} + \frac{\partial^4 v}{\partial y^4} + 2\frac{\partial^2 w}{\partial x \partial y}\frac{\partial^3 w}{\partial x \partial y^2} + \frac{\partial w}{\partial y}\frac{\partial^4 w}{\partial y^4}\right.$$

$$\left.+\frac{\partial w}{\partial y}\frac{\partial^4 w}{\partial x^2 \partial y^2} + \frac{\partial^2 w}{\partial y^2}\frac{\partial^3 w}{\partial x^2 \partial y} + 3\frac{\partial^2 w}{\partial y^2}\frac{\partial^3 w}{\partial y^3}\right)$$

$$-vA_{11}L_{C0}^2\left(\frac{\partial^4 u}{\partial y^3 \partial x} + \frac{\partial^4 u}{\partial y \partial x^3} + 3\frac{\partial^2 w}{\partial y \partial x}\frac{\partial^3 w}{\partial y^2 \partial x} + \frac{\partial w}{\partial x}\frac{\partial^4 w}{\partial y \partial x^3}\right.$$

$$\left.+\frac{\partial w}{\partial x}\frac{\partial^4 w}{\partial y^3 \partial x} + 2\frac{\partial^2 w}{\partial x^2}\frac{\partial^3 w}{\partial y \partial x^2} + \frac{\partial^3 w}{\partial x^3}\frac{\partial^2 w}{\partial y \partial x}\right)$$

$$+A_{11}\left(\frac{\partial^2 v}{\partial y^2} + \frac{\partial w}{\partial y}\frac{\partial^2 w}{\partial y^2}\right) + vA_{11}\left(\frac{\partial^2 u}{\partial y \partial x} + \frac{\partial w}{\partial x}\frac{\partial^2 w}{\partial y \partial x}\right)$$

$$+A_{33}\left(\frac{\partial^2 u}{\partial x \partial y} + \frac{\partial^2 v}{\partial x^2} + \frac{\partial^2 w}{\partial x^2}\frac{\partial w}{\partial y} + \frac{\partial w}{\partial x}\frac{\partial^2 w}{\partial x \partial y}\right) = 0, \tag{29}$$

120

$$-D_{11}\left[L_C^4\frac{\partial^8 w}{\partial y^2\partial x^6}-L_C^2\left(\frac{\partial^6 w}{\partial y^2\partial x^4}+\frac{\partial^6 w}{\partial x^6}\right)+\frac{\partial^4 w}{\partial x^4}\right]$$

$$-vD_{11}\left[L_C^4\frac{\partial^8 w}{\partial y^4\partial x^4}-L_C^2\left(\frac{\partial^6 w}{\partial x^2\partial y^4}+\frac{\partial^6 w}{\partial y^2\partial x^4}\right)+\frac{\partial^4 w}{\partial x^2\partial y^2}\right]$$

$$-4D_{33}\frac{\partial^4 w}{\partial x^2\partial y^2}-D_{11}\left[L_C^4\frac{\partial^8 w}{\partial y^6\partial x^2}-L_C^2\left(\frac{\partial^6 w}{\partial y^6}+\frac{\partial^6 w}{\partial y^4\partial x^2}\right)+\frac{\partial^4 w}{\partial y^4}\right]$$

$$-vD_{11}\left[L_C^4\frac{\partial^8 w}{\partial y^4\partial x^4}-L_C^2\left(\frac{\partial^6 w}{\partial y^4\partial x^2}+\frac{\partial^6 w}{\partial y^2\partial x^4}\right)+\frac{\partial^4 w}{\partial y^2\partial x^2}\right]$$

$$+N_{xx}\frac{\partial^2 w}{\partial x^2}+2N_{xy}\frac{\partial^2 w}{\partial x\partial y}+N_{yy}\frac{\partial^2 w}{\partial y^2}=m_0\frac{\partial^2 w}{\partial t^2}. \tag{30}$$

A nanoplate with four clamped edges is considered. There are three sets of boundary conditions: 1) conventional boundary condition (CBC), 2) non-conventional boundary condition (NCBC-e) for in-plane strain components, 3) non-conventional boundary condition (NCBC-k) for curvature components.

CBC:

$$x=0:\quad u=0,\qquad w=0,\qquad \frac{\partial w}{\partial x}=0,$$

$$x=a:\quad u=0,\quad w=0,\qquad \frac{\partial w}{\partial x}=0,$$

$$y=0:\quad v=0,\quad w=0,\qquad \frac{\partial w}{\partial y}=0,$$

$$y=b:\quad v=0,\quad w=0,\qquad \frac{\partial w}{\partial y}=0, \tag{31}$$

NCBC-e:

$$x=0: L_{C0}\left(\frac{\partial^2 u}{\partial x^2}+\frac{\partial w}{\partial x}\frac{\partial^2 w}{\partial x^2}\right)=\frac{\partial u}{\partial x}+\frac{1}{2}\left(\frac{\partial w}{\partial x}\right)^2,$$

$$x=a:\quad L_{C0}\left(\frac{\partial^2 u}{\partial x^2}+\frac{\partial w}{\partial x}\frac{\partial^2 w}{\partial x^2}\right)=-\left[\frac{\partial u}{\partial x}+\frac{1}{2}\left(\frac{\partial w}{\partial x}\right)^2\right],$$

$$y=0: L_{C0}\left(\frac{\partial^2 v}{\partial y^2}+\frac{\partial w}{\partial y}\frac{\partial^2 w}{\partial y^2}\right)=\frac{\partial v}{\partial y}+\frac{1}{2}\left(\frac{\partial w}{\partial y}\right)^2,$$

$$y = b: L_{C0}\left(\frac{\partial^2 v}{\partial y^2} + \frac{\partial w}{\partial y}\frac{\partial^2 w}{\partial y^2}\right) = -\left[\frac{\partial v}{\partial y} + \frac{1}{2}\left(\frac{\partial w}{\partial y}\right)^2\right].$$

(32)

NCBC-k:

$$x = 0: \quad L_C\frac{\partial^3 w}{\partial x^3} = \frac{\partial^2 w}{\partial x^2},$$

$$x = a: L_C\frac{\partial^3 w}{\partial x^3} = -\frac{\partial^2 w}{\partial x^2},$$

$$y = 0: L_C\frac{\partial^3 w}{\partial y^3} = \frac{\partial^2 w}{\partial y^2},$$

$$y = b: L_C\frac{\partial^3 w}{\partial y^3} = -\frac{\partial^2 w}{\partial y^2}.$$

(33)

3. DQM solution

A DQM-based solution procedure is developed in this section for the coupled nonlinear stress-driven equations of motion taking into account both classical and non-classical boundary conditions (i.e. CBC, NCBC-e and NCBC-k). The dimensionless parameters of the GS are given by

$$x' = \frac{x}{a}, \quad y' = \frac{y}{b}, \quad u' = \frac{u}{h}, \quad v' = \frac{v}{h}, \quad w' = \frac{w}{h}, \quad \gamma_{C0} = \frac{L_{C0}}{a}, \quad \gamma_C = \frac{L_C}{a},$$

$$\beta = \frac{a}{b}, \quad \lambda = \frac{h}{a}, \quad t' = \frac{t}{a}\sqrt{\frac{E}{\rho}}, \quad \varpi = a\omega\sqrt{\frac{\rho}{E}}, \quad \bar{N}_{ij} = \frac{N_{ij}a^2}{D}.$$

(34)

Using the relationship between the elasticity and shear moduli and implementing Eq. (34) into Eqs. (28)-(30), one obtains

$$\gamma_{C0}^4\left(\beta^2\frac{\partial^6 u}{\partial y^2\partial x^4} + 6\lambda\beta^2\frac{\partial^3 w}{\partial y\partial x^2}\frac{\partial^4 w}{\partial y\partial x^3} + 2\lambda\beta^2\frac{\partial^2 w}{\partial y\partial x}\frac{\partial^5 w}{\partial y\partial x^4}\right.$$

$$\left. +\lambda\beta^2\frac{\partial w}{\partial x}\frac{\partial^6 w}{\partial y^2\partial x^4} + 3\lambda\beta^2\frac{\partial^2 w}{\partial x^2}\frac{\partial^5 w}{\partial y^2\partial x^3} + 3\lambda\beta^2\frac{\partial^3 w}{\partial x^3}\frac{\partial^4 w}{\partial y^2\partial x^2} + \lambda\beta^2\frac{\partial^4 w}{\partial x^4}\frac{\partial^3 w}{\partial y^2\partial x}\right)$$

$$+v\gamma_{C0}^4\left(\beta^3\frac{\partial^6 v}{\partial y^3\partial x^3} + 6\lambda\beta^4\frac{\partial^3 w}{\partial x\partial y^2}\frac{\partial^4 w}{\partial x^2\partial y^2} + 3\lambda\beta^4\frac{\partial^3 w}{\partial x^2\partial y}\frac{\partial^4 w}{\partial x\partial y^3}\right.$$

122

$$+3\lambda\beta^4 \frac{\partial^2 w}{\partial x \partial y}\frac{\partial^5 w}{\partial x^2 \partial y^3} + \lambda\beta^4 \frac{\partial w}{\partial y}\frac{\partial^6 w}{\partial x^3 \partial y^3} + 2\lambda\beta^4 \frac{\partial^2 w}{\partial y^2}\frac{\partial^5 w}{\partial x^3 \partial y^2} + \lambda\beta^4 \frac{\partial^3 w}{\partial y^3}\frac{\partial^4 w}{\partial x^3 \partial y}\Bigg)$$

$$-\gamma_{C0}^2 \Bigg(\frac{\partial^4 u}{\partial x^4} + \beta^2 \frac{\partial^4 u}{\partial y^2 \partial x^2} + \lambda \frac{\partial w}{\partial x}\frac{\partial^4 w}{\partial x^4} + 3\lambda \frac{\partial^2 w}{\partial x^2}\frac{\partial^3 w}{\partial x^3}$$

$$+\lambda\beta^2 \frac{\partial w}{\partial x}\frac{\partial^4 w}{\partial y^2 \partial x^2} + \lambda\beta^2 \frac{\partial^2 w}{\partial x^2}\frac{\partial^3 w}{\partial y^2 \partial x} + 2\lambda\beta^2 \frac{\partial^2 w}{\partial y \partial x}\frac{\partial^3 w}{\partial y \partial x^2}\Bigg)$$

$$-\upsilon\gamma_{C0}^2 \Bigg(\beta \frac{\partial^4 v}{\partial x^3 \partial y} + \beta^3 \frac{\partial^4 v}{\partial x \partial y^3} + 3\lambda\beta^2 \frac{\partial^2 w}{\partial x \partial y}\frac{\partial^3 w}{\partial x^2 \partial y} + \lambda\beta^2 \frac{\partial w}{\partial y}\frac{\partial^4 w}{\partial x^3 \partial y}$$

$$+\lambda\beta^4 \frac{\partial w}{\partial y}\frac{\partial^4 w}{\partial x \partial y^3} + 2\lambda\beta^4 \frac{\partial^2 w}{\partial y^2}\frac{\partial^3 w}{\partial x \partial y^2} + \lambda\beta^4 \frac{\partial^3 w}{\partial y^3}\frac{\partial^2 w}{\partial x \partial y}\Bigg)$$

$$+\frac{\partial^2 u}{\partial x^2} + \frac{1}{2}(1-\upsilon)\beta^2 \frac{\partial^2 u}{\partial y^2} + \frac{1}{2}\beta(1+\upsilon)\frac{\partial^2 v}{\partial x \partial y} + \lambda \frac{\partial w}{\partial x}\frac{\partial^2 w}{\partial x^2}$$

$$+\frac{1}{2}(1-\upsilon)\lambda\beta^2 \frac{\partial w}{\partial x}\frac{\partial^2 w}{\partial y^2} + \frac{1}{2}(1+\upsilon)\lambda\beta^2 \frac{\partial w}{\partial y}\frac{\partial^2 w}{\partial x \partial y} - (1-\upsilon^2)\frac{\partial^2 u}{\partial t^2} = 0, \tag{35}$$

$$\gamma_{C0}^4 \Bigg(\beta^4 \frac{\partial^6 v}{\partial y^4 \partial x^2} + 6\lambda\beta^5 \frac{\partial^3 w}{\partial x \partial y^2}\frac{\partial^4 w}{\partial x \partial y^3} + 2\lambda\beta^5 \frac{\partial^2 w}{\partial x \partial y}\frac{\partial^5 w}{\partial x \partial y^4}$$

$$+\lambda\beta^5 \frac{\partial w}{\partial y}\frac{\partial^6 w}{\partial x^2 \partial y^4} + 3\lambda\beta^5 \frac{\partial^2 w}{\partial y^2}\frac{\partial^5 w}{\partial x^2 \partial y^3} + 3\lambda\beta^5 \frac{\partial^3 w}{\partial y^3}\frac{\partial^4 w}{\partial x^2 \partial y^2} + \lambda\beta^5 \frac{\partial^4 w}{\partial y^4}\frac{\partial^3 w}{\partial x^2 \partial y}\Bigg)$$

$$+\upsilon\gamma_{C0}^4 \Bigg(\beta^3 \frac{\partial^6 u}{\partial y^3 \partial x^3} + 6\lambda\beta^3 \frac{\partial^3 w}{\partial y \partial x^2}\frac{\partial^4 w}{\partial y^2 \partial x^2} + 3\lambda\beta^3 \frac{\partial^2 w}{\partial y \partial x}\frac{\partial^5 w}{\partial y^2 \partial x^3}$$

$$+3\lambda\beta^3 \frac{\partial^3 w}{\partial y^2 \partial x}\frac{\partial^4 w}{\partial y \partial x^3} + \lambda\beta^3 \frac{\partial w}{\partial x}\frac{\partial^6 w}{\partial y^3 \partial x^3} + 2\lambda\beta^3 \frac{\partial^2 w}{\partial x^2}\frac{\partial^5 w}{\partial y^3 \partial x^2} + \lambda\beta^3 \frac{\partial^3 w}{\partial x^3}\frac{\partial^4 w}{\partial y^3 \partial x}\Bigg)$$

$$-\gamma_{C0}^2 \Bigg(\beta^2 \frac{\partial^4 v}{\partial x^2 \partial y^2} + \beta^4 \frac{\partial^4 v}{\partial y^4} + 2\lambda\beta^3 \frac{\partial^2 w}{\partial x \partial y}\frac{\partial^3 w}{\partial x \partial y^2} + \lambda\beta^5 \frac{\partial w}{\partial y}\frac{\partial^4 w}{\partial y^4}$$

$$+\lambda\beta^3 \frac{\partial w}{\partial y}\frac{\partial^4 w}{\partial x^2 \partial y^2} + \lambda\beta^3 \frac{\partial^2 w}{\partial y^2}\frac{\partial^3 w}{\partial x^2 \partial y} + 3\lambda\beta^5 \frac{\partial^2 w}{\partial y^2}\frac{\partial^3 w}{\partial y^3}\Bigg)$$

$$-\upsilon\gamma_{C0}^2 \Bigg(\beta^3 \frac{\partial^4 u}{\partial y^3 \partial x} + \beta \frac{\partial^4 u}{\partial y \partial x^3} + 3\lambda\beta^3 \frac{\partial^2 w}{\partial y \partial x}\frac{\partial^3 w}{\partial y^2 \partial x} + \lambda\beta \frac{\partial w}{\partial x}\frac{\partial^4 w}{\partial y \partial x^3}$$

$$+\lambda\beta^3 \frac{\partial w}{\partial x}\frac{\partial^4 w}{\partial y^3 \partial x} + 2\lambda\beta \frac{\partial^2 w}{\partial x^2}\frac{\partial^3 w}{\partial y \partial x^2} + \lambda\beta \frac{\partial^3 w}{\partial x^3}\frac{\partial^2 w}{\partial y \partial x}\Bigg)$$

$$+\frac{1}{2}\beta(1+\upsilon)\frac{\partial^2 u}{\partial y \partial x} + \frac{1}{2}(1-\upsilon)\frac{\partial^2 v}{\partial x^2} + \beta^2 \frac{\partial^2 v}{\partial y^2} + \lambda\beta^3 \frac{\partial w}{\partial y}\frac{\partial^2 w}{\partial y^2}$$

$$+\frac{1}{2}\lambda\beta(1+\upsilon)\frac{\partial w}{\partial x}\frac{\partial^2 w}{\partial x \partial y} + \frac{1}{2}\lambda\beta(1-\upsilon)\frac{\partial w}{\partial y}\frac{\partial^2 w}{\partial x^2} - (1-\upsilon^2)\frac{\partial^2 v}{\partial t^2} = 0, \tag{36}$$

$$\frac{\partial^4 w}{\partial x^4} + 2\beta^2 \frac{\partial^4 w}{\partial x^2 \partial y^2} + \beta^4 \frac{\partial^4 w}{\partial y^4}$$

$$-\gamma_C^2 \left[\frac{\partial^6 w}{\partial x^6} + (1+2v)\beta^2 \frac{\partial^6 w}{\partial x^4 \partial y^2} \right.$$

$$\left. +(1+2v)\beta^4 \frac{\partial^6 w}{\partial x^2 \partial y^4} + \beta^6 \frac{\partial^6 w}{\partial y^6} \right]$$

$$+\gamma_C^4 \beta^2 \left(\frac{\partial^8 w}{\partial x^6 \partial y^2} + 2v\beta^2 \frac{\partial^8 w}{\partial x^4 \partial y^4} + \beta^4 \frac{\partial^8 w}{\partial x^2 \partial y^6} \right)$$

$$-\bar{N}_{xx} \frac{\partial^2 w}{\partial x^2} - 2\beta \bar{N}_{xy} \frac{\partial^2 w}{\partial x \partial y} - \beta^2 \bar{N}_{yy} \frac{\partial^2 w}{\partial y^2} + \frac{12}{\lambda^2}(1-v^2)\frac{\partial^2 w}{\partial t^2} = 0, \tag{37}$$

where prime symbol (′) is dropped for simplicity purposes. Furthermore, the dimensionless

force resultants can be expressed as

$$\bar{N}_{xx} = 12\gamma_{C0}^4 \left[\frac{\beta^2}{\lambda} \frac{\partial^5 u}{\partial y^2 \partial x^3} + \beta^2 \frac{\partial w}{\partial x} \frac{\partial^5 w}{\partial y^2 \partial x^3} + 2\beta^2 \frac{\partial^2 w}{\partial x^2} \frac{\partial^4 w}{\partial y^2 \partial x^2} \right.$$

$$\left. +\beta^2 \frac{\partial^3 w}{\partial x^3} \frac{\partial^3 w}{\partial y^2 \partial x} + 2\beta^2 \left(\frac{\partial^3 w}{\partial y \partial x^2} \right)^2 + 2\beta^2 \frac{\partial^2 w}{\partial y \partial x} \frac{\partial^4 w}{\partial y \partial x^3} \right]$$

$$+12v\gamma_{C0}^4 \left[\frac{\beta^3}{\lambda} \frac{\partial^5 v}{\partial y^3 \partial x^2} + \beta^4 \frac{\partial w}{\partial y} \frac{\partial^5 w}{\partial x^2 \partial y^3} + 2\beta^4 \frac{\partial^2 w}{\partial y^2} \frac{\partial^4 w}{\partial x^2 \partial y^2} \right.$$

$$\left. +\beta^4 \frac{\partial^3 w}{\partial y^3} \frac{\partial^3 w}{\partial x^2 \partial y} + 2\beta^4 \left(\frac{\partial^3 w}{\partial x \partial y^2} \right)^2 + 2\beta^4 \frac{\partial^2 w}{\partial x \partial y} \frac{\partial^4 w}{\partial x \partial y^3} \right]$$

$$-12\gamma_{C0}^2 \left[\frac{\beta^2}{\lambda} \frac{\partial^3 u}{\partial y^2 \partial x} + \frac{1}{\lambda} \frac{\partial^3 u}{\partial x^3} + \beta^2 \left(\frac{\partial^2 w}{\partial y \partial x} \right)^2 + \beta^2 \frac{\partial w}{\partial x} \frac{\partial^3 w}{\partial y^2 \partial x} + \left(\frac{\partial^2 w}{\partial x^2} \right)^2 + \frac{\partial w}{\partial x} \frac{\partial^3 w}{\partial x^3} \right]$$

$$-12v\gamma_{C0}^2 \left[\frac{\beta}{\lambda} \frac{\partial^3 v}{\partial x^2 \partial y} + \frac{\beta^3}{\lambda} \frac{\partial^3 v}{\partial y^3} + \beta^2 \left(\frac{\partial^2 w}{\partial x \partial y} \right)^2 + \beta^2 \frac{\partial w}{\partial y} \frac{\partial^3 w}{\partial x^2 \partial y} + \beta^4 \left(\frac{\partial^2 w}{\partial y^2} \right)^2 + \beta^4 \frac{\partial w}{\partial y} \frac{\partial^3 w}{\partial y^3} \right]$$

$$+12 \left[\frac{1}{\lambda} \frac{\partial u}{\partial x} + \frac{v\beta}{\lambda} \frac{\partial v}{\partial y} + \frac{1}{2} \left(\frac{\partial w}{\partial x} \right)^2 + \frac{1}{2} v\beta^2 \left(\frac{\partial w}{\partial y} \right)^2 \right], \tag{38}$$

$$\bar{N}_{yy} = 12\gamma_{C0}^4 \left[\frac{\beta^3}{\lambda} \frac{\partial^5 v}{\partial y^3 \partial x^2} + \beta^4 \frac{\partial w}{\partial y} \frac{\partial^5 w}{\partial x^2 \partial y^3} + 2\beta^4 \frac{\partial^2 w}{\partial y^2} \frac{\partial^4 w}{\partial x^2 \partial y^2} \right.$$

$$\left. +\beta^4 \frac{\partial^3 w}{\partial y^3} \frac{\partial^3 w}{\partial x^2 \partial y} + 2\beta^4 \left(\frac{\partial^3 w}{\partial x \partial y^2} \right)^2 + 2\beta^4 \frac{\partial^2 w}{\partial x \partial y} \frac{\partial^4 w}{\partial x \partial y^3} \right]$$

$$+12v\gamma_{C0}^4 \left[\frac{\beta^2}{\lambda} \frac{\partial^5 u}{\partial y^2 \partial x^3} + \beta^2 \frac{\partial w}{\partial x} \frac{\partial^5 w}{\partial y^2 \partial x^3} + 2\beta^2 \frac{\partial^2 w}{\partial x^2} \frac{\partial^4 w}{\partial y^2 \partial x^2} \right.$$

$$+\beta^2 \frac{\partial^3 w}{\partial x^3}\frac{\partial^3 w}{\partial y^2 \partial x} + 2\beta^2 \left(\frac{\partial^3 w}{\partial y \partial x^2}\right)^2 + 2\beta^2 \frac{\partial^2 w}{\partial y \partial x}\frac{\partial^4 w}{\partial y \partial x^3}\Bigg]$$

$$-12\gamma_{C0}^2 \left[\frac{\beta}{\lambda}\frac{\partial^3 v}{\partial x^2 \partial y} + \frac{\beta^3}{\lambda}\frac{\partial^3 v}{\partial y^3} + \beta^2 \left(\frac{\partial^2 w}{\partial x \partial y}\right)^2 + \beta^2 \frac{\partial w}{\partial y}\frac{\partial^3 w}{\partial x^2 \partial y} + \beta^4 \left(\frac{\partial^2 w}{\partial y^2}\right)^2 + \beta^4 \frac{\partial w}{\partial y}\frac{\partial^3 w}{\partial y^3}\right]$$

$$-12v\gamma_{C0}^2 \left[\frac{\beta^2}{\lambda}\frac{\partial^3 u}{\partial y^2 \partial x} + \frac{1}{\lambda}\frac{\partial^3 u}{\partial x^3} + \beta^2 \left(\frac{\partial^2 w}{\partial y \partial x}\right)^2 + \beta^2 \frac{\partial w}{\partial x}\frac{\partial^3 w}{\partial y^2 \partial x} + \left(\frac{\partial^2 w}{\partial x^2}\right)^2 + \frac{\partial w}{\partial x}\frac{\partial^3 w}{\partial x^3}\right]$$

$$+12\left[\frac{v}{\lambda}\frac{\partial u}{\partial x} + \frac{\beta}{\lambda}\frac{\partial v}{\partial y} + \frac{1}{2}v\left(\frac{\partial w}{\partial x}\right)^2 + \frac{1}{2}\beta^2\left(\frac{\partial w}{\partial y}\right)^2\right], \tag{39}$$

$$\bar{N}_{xy} = 6(1-v)\left(\frac{\beta}{\lambda}\frac{\partial u}{\partial y} + \frac{1}{\lambda}\frac{\partial v}{\partial x} + \beta\frac{\partial w}{\partial x}\frac{\partial w}{\partial y}\right). \tag{40}$$

On the other hand, the dimensionless CBC, NCBC-e and NCBC-k can be written as

$$x = 0: \quad u = 0, \quad w = 0, \quad \frac{\partial w}{\partial x} = 0,$$

$$x = 1: \quad u = 0, \quad w = 0, \quad \frac{\partial w}{\partial x} = 0,$$

$$y = 0: \quad v = 0, \quad w = 0, \quad \frac{\partial w}{\partial y} = 0,$$

$$y = 1: \quad v = 0, \quad w = 0, \quad \frac{\partial w}{\partial y} = 0, \tag{41}$$

$$x = 0: \gamma_{C0}\left(\frac{\partial^2 u}{\partial x^2} + \lambda\frac{\partial w}{\partial x}\frac{\partial^2 w}{\partial x^2}\right) = \frac{\partial u}{\partial x} + \frac{1}{2}\lambda\left(\frac{\partial w}{\partial x}\right)^2,$$

$$x = 1: \quad \gamma_{C0}\left(\frac{\partial^2 u}{\partial x^2} + \lambda\frac{\partial w}{\partial x}\frac{\partial^2 w}{\partial x^2}\right) = -\left[\frac{\partial u}{\partial x} + \frac{1}{2}\lambda\left(\frac{\partial w}{\partial x}\right)^2\right],$$

$$y = 0: \gamma_{C0}\beta\left(\frac{\partial^2 v}{\partial y^2} + \lambda\beta\frac{\partial w}{\partial y}\frac{\partial^2 w}{\partial y^2}\right) = \frac{\partial v}{\partial y} + \frac{1}{2}\lambda\beta\left(\frac{\partial w}{\partial y}\right)^2,$$

$$y = 1: \gamma_{C0}\beta\left(\frac{\partial^2 v}{\partial y^2} + \lambda\beta\frac{\partial w}{\partial y}\frac{\partial^2 w}{\partial y^2}\right) = -\left[\frac{\partial v}{\partial y} + \frac{1}{2}\lambda\beta\left(\frac{\partial w}{\partial y}\right)^2\right]. \tag{42}$$

$$x = 0: \gamma_C \frac{\partial^3 w}{\partial x^3} = \frac{\partial^2 w}{\partial x^2},$$

$$x = 1: \quad \gamma_C \frac{\partial^3 w}{\partial x^3} = -\frac{\partial^2 w}{\partial x^2},$$

$$y = 0: \beta\gamma_C \frac{\partial^3 w}{\partial y^3} = \frac{\partial^2 w}{\partial y^2},$$

$$y = 1: \beta \gamma_C \frac{\partial^3 w}{\partial y^3} = -\frac{\partial^2 w}{\partial y^2}. \tag{43}$$

Implementing all types of edge conditions is essential in order to extract a solution for Eqs.

(35)-(37). Using the DQM, we have [36, 37]

$$\frac{\partial^p u}{\partial x^p} = \sum_{k=1}^{n_x} A_{i,k}^{x(p)} u_{k,j}, \; \frac{\partial^q u}{\partial y^q} = \sum_{k=1}^{n_y} A_{j,k}^{y(q)} u_{i,k}, \; \frac{\partial^{(p+q)} u}{\partial x^p \partial y^q} = \sum_{k=1}^{n_x} \sum_{l=1}^{n_y} A_{i,k}^{x(p)} A_{j,l}^{y(q)} u_{k,l},$$

$$\frac{\partial^p v}{\partial x^p} = \sum_{k=1}^{n_x} A_{i,k}^{x(p)} v_{k,j}, \; \frac{\partial^q v}{\partial y^q} = \sum_{k=1}^{n_y} A_{j,k}^{y(q)} v_{i,k}, \; \frac{\partial^{(p+q)} v}{\partial x^p \partial y^q} = \sum_{k=1}^{n_x} \sum_{l=1}^{n_y} A_{i,k}^{x(p)} A_{j,l}^{y(q)} v_{k,l},$$

$$\frac{\partial^p w}{\partial x^p} = \sum_{k=1}^{n_x} A_{i,k}^{x(p)} w_{k,j}, \; \frac{\partial^q w}{\partial y^q} = \sum_{k=1}^{n_y} A_{j,k}^{y(q)} w_{i,k}, \; \frac{\partial^{(p+q)} w}{\partial x^p \partial y^q} = \sum_{k=1}^{n_x} \sum_{l=1}^{n_y} A_{i,k}^{x(p)} A_{j,l}^{y(q)} w_{k,l},$$
$$\tag{44}$$

where $A_{i,k}^{\alpha(\delta)}$ $(\alpha = x, y)$ is the DQ coefficient; n_α $(\alpha = x, y)$ represents the number of discrete

points. The first-order DQ coefficients are computed by

$$A_{i,k}^{x(1)} = \begin{cases} \dfrac{M^{(1)}(x_i)}{(x_i - x_k) M^{(1)}(x_k)} & for \; i \neq k \\ -\displaystyle\sum_{j=1(j \neq i)}^{n_x} A_{i,j}^{x(1)} & for \; i = k \end{cases}, \tag{45}$$

$$A_{j,k}^{y(1)} = \begin{cases} \dfrac{M^{(1)}(y_j)}{(y_j - y_k) M^{(1)}(y_k)} & for \; j \neq k \\ -\displaystyle\sum_{m=1(m \neq j)}^{n_y} A_{j,m}^{y(1)} & for \; j = k \end{cases}, \tag{46}$$

where

$$M^{(1)}(x_i) = \prod_{k=1(k \neq i)}^{n_x} (x_i - x_k),$$

$$M^{(1)}(y_j) = \prod_{k=1(k \neq j)}^{n_y} (y_j - y_k). \tag{47}$$

The higher-order DQ coefficients for partial derivatives are given by

$$A_{i,j}^{x(2)} = \sum_{k=1}^{n_x} A_{i,k}^{x(1)} A_{k,j}^{x(1)}, \qquad A_{i,j}^{x(3)} = \sum_{k=1}^{n_x} A_{i,k}^{x(2)} A_{k,j}^{x(1)},$$

$$A_{i,j}^{x(4)} = \sum_{k=1}^{n_x} A_{i,k}^{x(2)} A_{k,j}^{x(2)}, \qquad A_{i,j}^{x(6)} = \sum_{k=1}^{n_x} A_{i,k}^{x(3)} A_{k,j}^{x(3)},$$

$$A_{i,j}^{y(2)} = \sum_{k=1}^{n_x} A_{i,k}^{y(1)} A_{k,j}^{y(1)}, \qquad A_{i,j}^{y(3)} = \sum_{k=1}^{n_x} A_{i,k}^{y(2)} A_{k,j}^{y(1)},$$

$$A_{i,j}^{y(4)} = \sum_{k=1}^{n_x} A_{i,k}^{y(2)} A_{k,j}^{y(2)}, \qquad A_{i,j}^{y(6)} = \sum_{k=1}^{n_x} A_{i,k}^{y(3)} A_{k,j}^{y(3)}. \tag{48}$$

According to the Gauss–Chebyshev–Lobatto distribution, x_k and y_k are obtained by [36, 37]

$$x_k = \frac{1}{2} - \frac{1}{2}\cos\left(\frac{\pi(k-1)}{n_x - 1}\right),$$

$$y_k = \frac{1}{2} - \frac{1}{2}\cos\left(\frac{\pi(k-1)}{n_y - 1}\right). \tag{49}$$

Substituting Eq. (44) into Eqs. (35)-(37), the three nonlinear differential equations, which describe the coupled large-amplitude vibration of GSs, can be discretised as

$$\gamma_{C0}^4 \beta^2 \left[\left(\sum_{k=1}^{n_x} \sum_{l=1}^{n_y} A_{i,k}^{x(4)} A_{j,l}^{y(2)} u_{k,l} \right) + 6\lambda \left(\sum_{k=1}^{n_x} \sum_{l=1}^{n_y} A_{i,k}^{x(2)} A_{j,l}^{y(1)} w_{k,l} \right) \left(\sum_{k=1}^{n_x} \sum_{l=1}^{n_y} A_{i,k}^{x(3)} A_{j,l}^{y(1)} w_{k,l} \right) \right.$$

$$+ 2\lambda \left(\sum_{k=1}^{n_x} \sum_{l=1}^{n_y} A_{i,k}^{x(1)} A_{j,l}^{y(1)} w_{k,l} \right) \left(\sum_{k=1}^{n_x} \sum_{l=1}^{n_y} A_{i,k}^{x(4)} A_{j,l}^{y(1)} w_{k,l} \right) + \lambda \left(\sum_{k=1}^{n_x} A_{i,k}^{x(1)} w_{k,j} \right) \left(\sum_{k=1}^{n_x} \sum_{l=1}^{n_y} A_{i,k}^{x(4)} A_{j,l}^{y(2)} w_{k,l} \right)$$

$$+ 3\lambda \left(\sum_{k=1}^{n_x} A_{i,k}^{x(2)} w_{k,j} \right) \left(\sum_{k=1}^{n_x} \sum_{l=1}^{n_y} A_{i,k}^{x(3)} A_{j,l}^{y(2)} w_{k,l} \right) + 3\lambda \left(\sum_{k=1}^{n_x} A_{i,k}^{x(3)} w_{k,j} \right) \left(\sum_{k=1}^{n_x} \sum_{l=1}^{n_y} A_{i,k}^{x(2)} A_{j,l}^{y(2)} w_{k,l} \right)$$

$$\left. + \lambda \left(\sum_{k=1}^{n_x} A_{i,k}^{x(4)} w_{k,j} \right) \left(\sum_{k=1}^{n_x} \sum_{l=1}^{n_y} A_{i,k}^{x(1)} A_{j,l}^{y(2)} w_{k,l} \right) \right] + \upsilon \gamma_{C0}^4 \beta^3 \left[\left(\sum_{k=1}^{n_x} \sum_{l=1}^{n_y} A_{i,k}^{x(3)} A_{j,l}^{y(3)} v_{k,l} \right) + 6\lambda\beta \times \right.$$

$$\left(\sum_{k=1}^{n_x} \sum_{l=1}^{n_y} A_{i,k}^{x(1)} A_{j,l}^{y(2)} w_{k,l} \right) \left(\sum_{k=1}^{n_x} \sum_{l=1}^{n_y} A_{i,k}^{x(2)} A_{j,l}^{y(2)} w_{k,l} \right) + 3\lambda\beta \left(\sum_{k=1}^{n_x} \sum_{l=1}^{n_y} A_{i,k}^{x(2)} A_{j,l}^{y(1)} w_{k,l} \right) \left(\sum_{k=1}^{n_x} \sum_{l=1}^{n_y} A_{i,k}^{x(1)} A_{j,l}^{y(3)} w_{k,l} \right)$$

$$+ 3\lambda\beta \left(\sum_{k=1}^{n_x} \sum_{l=1}^{n_y} A_{i,k}^{x(1)} A_{j,l}^{y(1)} w_{k,l} \right) \left(\sum_{k=1}^{n_x} \sum_{l=1}^{n_y} A_{i,k}^{x(2)} A_{j,l}^{y(3)} w_{k,l} \right) + \lambda\beta \left(\sum_{k=1}^{n_y} A_{j,k}^{y(1)} w_{i,k} \right) \left(\sum_{k=1}^{n_x} \sum_{l=1}^{n_y} A_{i,k}^{x(3)} A_{j,l}^{y(3)} w_{k,l} \right)$$

$$\left. + 2\lambda\beta \left(\sum_{k=1}^{n_y} A_{j,k}^{y(2)} w_{i,k} \right) \left(\sum_{k=1}^{n_x} \sum_{l=1}^{n_y} A_{i,k}^{x(3)} A_{j,l}^{y(2)} w_{k,l} \right) + \lambda\beta \left(\sum_{k=1}^{n_y} A_{j,k}^{y(3)} w_{i,k} \right) \left(\sum_{k=1}^{n_x} \sum_{l=1}^{n_y} A_{i,k}^{x(3)} A_{j,l}^{y(1)} w_{k,l} \right) \right]$$

$$- \gamma_{C0}^2 \left[\sum_{k=1}^{n_x} A_{i,k}^{x(4)} u_{k,j} + \beta^2 \left(\sum_{k=1}^{n_x} \sum_{l=1}^{n_y} A_{i,k}^{x(2)} A_{j,l}^{y(2)} u_{k,l} \right) + \lambda \left(\sum_{k=1}^{n_x} A_{i,k}^{x(1)} w_{k,j} \right) \left(\sum_{k=1}^{n_x} A_{i,k}^{x(4)} w_{k,j} \right) \right.$$

$$+ 3\lambda \left(\sum_{k=1}^{n_x} A_{i,k}^{x(2)} w_{k,j} \right) \left(\sum_{k=1}^{n_x} A_{i,k}^{x(3)} w_{k,j} \right) + \lambda\beta^2 \left(\sum_{k=1}^{n_x} A_{i,k}^{x(1)} w_{k,j} \right) \left(\sum_{k=1}^{n_x} \sum_{l=1}^{n_y} A_{i,k}^{x(2)} A_{j,l}^{y(2)} w_{k,l} \right) + \lambda\beta^2 \times$$

$$\left. \left(\sum_{k=1}^{n_x} A_{i,k}^{x(2)} w_{k,j} \right) \left(\sum_{k=1}^{n_x} \sum_{l=1}^{n_y} A_{i,k}^{x(1)} A_{j,l}^{y(2)} w_{k,l} \right) + 2\lambda\beta^2 \left(\sum_{k=1}^{n_x} \sum_{l=1}^{n_y} A_{i,k}^{x(1)} A_{j,l}^{y(1)} w_{k,l} \right) \left(\sum_{k=1}^{n_x} \sum_{l=1}^{n_y} A_{i,k}^{x(2)} A_{j,l}^{y(1)} w_{k,l} \right) \right]$$

$$- \upsilon \gamma_{C0}^2 \beta \left[\sum_{k=1}^{n_x} \sum_{l=1}^{n_y} A_{i,k}^{x(3)} A_{j,l}^{y(1)} v_{k,l} + \beta^2 \left(\sum_{k=1}^{n_x} \sum_{l=1}^{n_y} A_{i,k}^{x(1)} A_{j,l}^{y(3)} v_{k,l} \right) + 3\lambda\beta \left(\sum_{k=1}^{n_x} \sum_{l=1}^{n_y} A_{i,k}^{x(1)} A_{j,l}^{y(1)} w_{k,l} \right) \right.$$

$$\times \left(\sum_{k=1}^{n_x} \sum_{l=1}^{n_y} A_{i,k}^{x(2)} A_{j,l}^{y(1)} w_{k,l} \right) + \lambda\beta \left(\sum_{k=1}^{n_y} A_{j,k}^{y(1)} w_{i,k} \right) \left(\sum_{k=1}^{n_x} \sum_{l=1}^{n_y} A_{i,k}^{x(3)} A_{j,l}^{y(1)} w_{k,l} \right)$$

$$+ \lambda\beta^3 \left(\sum_{k=1}^{n_y} A_{j,k}^{y(1)} w_{i,k} \right) \left(\sum_{k=1}^{n_x} \sum_{l=1}^{n_y} A_{i,k}^{x(1)} A_{j,l}^{y(3)} w_{k,l} \right) + 2\lambda\beta^3 \left(\sum_{k=1}^{n_y} A_{j,k}^{y(2)} w_{i,k} \right) \left(\sum_{k=1}^{n_x} \sum_{l=1}^{n_y} A_{i,k}^{x(1)} A_{j,l}^{y(2)} w_{k,l} \right)$$

$$+ \lambda\beta^3 \left(\sum_{k=1}^{n_y} A_{j,k}^{y(3)} w_{i,k} \right) \left(\sum_{k=1}^{n_x} \sum_{l=1}^{n_y} A_{i,k}^{x(1)} A_{j,l}^{y(1)} w_{k,l} \right) \Bigg] + \sum_{k=1}^{n_x} A_{i,k}^{x(2)} u_{k,j} + \frac{1}{2}(1-v)\beta^2 \left(\sum_{k=1}^{n_y} A_{j,k}^{y(2)} u_{i,k} \right)$$

$$+ \frac{1}{2}\beta(1+v) \left(\sum_{k=1}^{n_x} \sum_{l=1}^{n_y} A_{i,k}^{x(1)} A_{j,l}^{y(1)} v_{k,l} \right) + \lambda \left(\sum_{k=1}^{n_x} A_{i,k}^{x(1)} w_{k,j} \right) \left(\sum_{k=1}^{n_x} A_{i,k}^{x(2)} w_{k,j} \right) + \frac{1}{2}(1-v)\lambda\beta^2$$

$$\times \left(\sum_{k=1}^{n_x} A_{i,k}^{x(1)} w_{k,j} \right) \left(\sum_{k=1}^{n_y} A_{j,k}^{y(2)} w_{i,k} \right) + \frac{1}{2}(1+v)\lambda\beta^2 \left(\sum_{k=1}^{n_y} A_{j,k}^{y(1)} w_{i,k} \right) \left(\sum_{k=1}^{n_x} \sum_{l=1}^{n_y} A_{i,k}^{x(1)} A_{j,l}^{y(1)} w_{k,l} \right) = 0,$$

$$(50)$$

$$\gamma_{C0}^4 \beta^4 \Bigg[\sum_{k=1}^{n_x} \sum_{l=1}^{n_y} A_{i,k}^{x(2)} A_{j,l}^{y(4)} v_{k,l} + 6\lambda\beta \left(\sum_{k=1}^{n_x} \sum_{l=1}^{n_y} A_{i,k}^{x(1)} A_{j,l}^{y(2)} w_{k,l} \right) \left(\sum_{k=1}^{n_x} \sum_{l=1}^{n_y} A_{i,k}^{x(1)} A_{j,l}^{y(3)} w_{k,l} \right)$$

$$+ 2\lambda\beta \left(\sum_{k=1}^{n_x} \sum_{l=1}^{n_y} A_{i,k}^{x(1)} A_{j,l}^{y(1)} w_{k,l} \right) \left(\sum_{k=1}^{n_x} \sum_{l=1}^{n_y} A_{i,k}^{x(1)} A_{j,l}^{y(4)} w_{k,l} \right) + \lambda\beta \left(\sum_{k=1}^{n_y} A_{j,k}^{y(1)} w_{i,k} \right) \left(\sum_{k=1}^{n_x} \sum_{l=1}^{n_y} A_{i,k}^{x(2)} A_{j,l}^{y(4)} w_{k,l} \right)$$

$$+ 3\lambda\beta \left(\sum_{k=1}^{n_y} A_{j,k}^{y(2)} w_{i,k} \right) \left(\sum_{k=1}^{n_x} \sum_{l=1}^{n_y} A_{i,k}^{x(2)} A_{j,l}^{y(3)} w_{k,l} \right) + 3\lambda\beta \left(\sum_{k=1}^{n_y} A_{j,k}^{y(3)} w_{i,k} \right) \left(\sum_{k=1}^{n_x} \sum_{l=1}^{n_y} A_{i,k}^{x(2)} A_{j,l}^{y(2)} w_{k,l} \right)$$

$$+ \lambda\beta \left(\sum_{k=1}^{n_y} A_{j,k}^{y(4)} w_{i,k} \right) \left(\sum_{k=1}^{n_x} \sum_{l=1}^{n_y} A_{i,k}^{x(2)} A_{j,l}^{y(1)} w_{k,l} \right) \Bigg] + v\gamma_{C0}^4 \beta^3 \Bigg[\sum_{k=1}^{n_x} \sum_{l=1}^{n_y} A_{i,k}^{x(3)} A_{j,l}^{y(3)} u_{k,l} + 6\lambda \times$$

$$\left(\sum_{k=1}^{n_x} \sum_{l=1}^{n_y} A_{i,k}^{x(2)} A_{j,l}^{y(1)} w_{k,l} \right) \left(\sum_{k=1}^{n_x} \sum_{l=1}^{n_y} A_{i,k}^{x(2)} A_{j,l}^{y(2)} w_{k,l} \right) + 3\lambda \left(\sum_{k=1}^{n_x} \sum_{l=1}^{n_y} A_{i,k}^{x(1)} A_{j,l}^{y(1)} w_{k,l} \right) \left(\sum_{k=1}^{n_x} \sum_{l=1}^{n_y} A_{i,k}^{x(3)} A_{j,l}^{y(2)} w_{k,l} \right)$$

$$+ 3\lambda \left(\sum_{k=1}^{n_x} \sum_{l=1}^{n_y} A_{i,k}^{x(1)} A_{j,l}^{y(2)} w_{k,l} \right) \left(\sum_{k=1}^{n_x} \sum_{l=1}^{n_y} A_{i,k}^{x(3)} A_{j,l}^{y(1)} w_{k,l} \right) + \lambda \left(\sum_{k=1}^{n_x} A_{i,k}^{x(1)} w_{k,j} \right) \left(\sum_{k=1}^{n_x} \sum_{l=1}^{n_y} A_{i,k}^{x(3)} A_{j,l}^{y(3)} w_{k,l} \right)$$

$$+ 2\lambda \left(\sum_{k=1}^{n_x} A_{i,k}^{x(2)} w_{k,j} \right) \left(\sum_{k=1}^{n_x} \sum_{l=1}^{n_y} A_{i,k}^{x(2)} A_{j,l}^{y(3)} w_{k,l} \right) + \lambda \left(\sum_{k=1}^{n_x} A_{i,k}^{x(3)} w_{k,j} \right) \left(\sum_{k=1}^{n_x} \sum_{l=1}^{n_y} A_{i,k}^{x(1)} A_{j,l}^{y(3)} w_{k,l} \right) \Bigg]$$

$$-\gamma_{C0}^2\beta^2\left[\sum_{k=1}^{n_x}\sum_{l=1}^{n_y}A_{i,k}^{x(2)}A_{j,l}^{y(2)}v_{k,l}+\beta^2\left(\sum_{k=1}^{n_y}A_{j,k}^{y(4)}v_{i,k}\right)+\lambda\beta^3\left(\sum_{k=1}^{n_y}A_{j,k}^{y(1)}w_{i,k}\right)\left(\sum_{k=1}^{n_y}A_{j,k}^{y(4)}w_{i,k}\right)\right.$$

$$+2\lambda\beta\left(\sum_{k=1}^{n_x}\sum_{l=1}^{n_y}A_{i,k}^{x(1)}A_{j,l}^{y(1)}w_{k,l}\right)\left(\sum_{k=1}^{n_x}\sum_{l=1}^{n_y}A_{i,k}^{x(1)}A_{j,l}^{y(2)}w_{k,l}\right)+3\lambda\beta^3\left(\sum_{k=1}^{n_y}A_{j,k}^{y(2)}w_{i,k}\right)\left(\sum_{k=1}^{n_y}A_{j,k}^{y(3)}w_{i,k}\right)$$

$$\left.+\lambda\beta\left(\sum_{k=1}^{n_y}A_{j,k}^{y(1)}w_{i,k}\right)\left(\sum_{k=1}^{n_x}\sum_{l=1}^{n_y}A_{i,k}^{x(2)}A_{j,l}^{y(2)}w_{k,l}\right)+\lambda\beta\left(\sum_{k=1}^{n_y}A_{j,k}^{y(2)}w_{i,k}\right)\left(\sum_{k=1}^{n_x}\sum_{l=1}^{n_y}A_{i,k}^{x(2)}A_{j,l}^{y(1)}w_{k,l}\right)\right]$$

$$-\nu\gamma_{C0}^2\left[\beta^2\left(\sum_{k=1}^{n_x}\sum_{l=1}^{n_y}A_{i,k}^{x(1)}A_{j,l}^{y(3)}u_{k,l}\right)+\sum_{k=1}^{n_x}\sum_{l=1}^{n_y}A_{i,k}^{x(3)}A_{j,l}^{y(1)}u_{k,l}+3\lambda\beta^2\left(\sum_{k=1}^{n_x}\sum_{l=1}^{n_y}A_{i,k}^{x(1)}A_{j,l}^{y(1)}w_{k,l}\right)\times\right.$$

$$\left(\sum_{k=1}^{n_x}\sum_{l=1}^{n_y}A_{i,k}^{x(1)}A_{j,l}^{y(2)}w_{k,l}\right)+\lambda\left(\sum_{k=1}^{n_x}A_{i,k}^{x(1)}w_{k,j}\right)\left(\sum_{k=1}^{n_x}\sum_{l=1}^{n_y}A_{i,k}^{x(3)}A_{j,l}^{y(1)}w_{k,l}\right)+\lambda\beta^2\left(\sum_{k=1}^{n_x}A_{i,k}^{x(1)}w_{k,j}\right)\times$$

$$\left(\sum_{k=1}^{n_x}\sum_{l=1}^{n_y}A_{i,k}^{x(1)}A_{j,l}^{y(3)}w_{k,l}\right)+2\lambda\left(\sum_{k=1}^{n_x}A_{i,k}^{x(2)}w_{k,j}\right)\left(\sum_{k=1}^{n_x}\sum_{l=1}^{n_y}A_{i,k}^{x(2)}A_{j,l}^{y(1)}w_{k,l}\right)+\lambda\left(\sum_{k=1}^{n_x}A_{i,k}^{x(3)}w_{k,j}\right)\times$$

$$\left.\left(\sum_{k=1}^{n_x}\sum_{l=1}^{n_y}A_{i,k}^{x(1)}A_{j,l}^{y(1)}w_{k,l}\right)\right]+\frac{1}{2}\beta(1+\nu)\left(\sum_{k=1}^{n_x}\sum_{l=1}^{n_y}A_{i,k}^{x(1)}A_{j,l}^{y(1)}u_{k,l}\right)+\frac{1}{2}(1-\nu)\left(\sum_{k=1}^{n_x}A_{i,k}^{x(2)}v_{k,j}\right)$$

$$+\beta^2\left(\sum_{k=1}^{n_y}A_{j,k}^{y(2)}v_{i,k}\right)+\lambda\beta^3\left(\sum_{k=1}^{n_y}A_{j,k}^{y(1)}w_{i,k}\right)\left(\sum_{k=1}^{n_y}A_{j,k}^{y(2)}w_{i,k}\right)+\frac{1}{2}\lambda\beta(1+\nu)\left(\sum_{k=1}^{n_x}A_{i,k}^{x(1)}w_{k,j}\right)$$

$$\times\left(\sum_{k=1}^{n_x}\sum_{l=1}^{n_y}A_{i,k}^{x(1)}A_{j,l}^{y(1)}w_{k,l}\right)+\frac{1}{2}\lambda\beta(1-\nu)\left(\sum_{k=1}^{n_y}A_{j,k}^{y(1)}w_{i,k}\right)\left(\sum_{k=1}^{n_x}A_{i,k}^{x(2)}w_{k,j}\right)=0,$$

$$\tag{51}$$

$$\sum_{k=1}^{n_x}A_{i,k}^{x(4)}w_{k,j}+2\beta^2\left(\sum_{k=1}^{n_x}\sum_{l=1}^{n_y}A_{i,k}^{x(2)}A_{j,l}^{y(2)}w_{k,l}\right)+\beta^4\left(\sum_{k=1}^{n_y}A_{j,k}^{y(4)}w_{i,k}\right)$$

$$-\gamma_C^2\left[\sum_{k=1}^{n_x}A_{i,k}^{x(6)}w_{k,j}+(1+2\nu)\beta^2\left(\sum_{k=1}^{n_x}\sum_{l=1}^{n_y}A_{i,k}^{x(4)}A_{j,l}^{y(2)}w_{k,l}\right)\right.$$

$$\left.+(1+2\nu)\beta^4\left(\sum_{k=1}^{n_x}\sum_{l=1}^{n_y}A_{i,k}^{x(2)}A_{j,l}^{y(4)}w_{k,l}\right)+\beta^6\left(\sum_{k=1}^{n_y}A_{j,k}^{y(6)}w_{i,k}\right)\right]$$

$$
\begin{aligned}
&+\gamma_C^4\beta^2\left[\left(\sum_{k=1}^{n_x}\sum_{l=1}^{n_y}A_{i,k}^{x(6)}A_{j,l}^{y(2)}w_{k,l}\right)+2\upsilon\beta^2\left(\sum_{k=1}^{n_x}\sum_{l=1}^{n_y}A_{i,k}^{x(4)}A_{j,l}^{y(4)}w_{k,l}\right)\right.\\
&+\beta^4\left.\left(\sum_{k=1}^{n_x}\sum_{l=1}^{n_y}A_{i,k}^{x(2)}A_{j,l}^{y(6)}w_{k,l}\right)\right]-\bar{N}_{xx}\left(\sum_{k=1}^{n_x}A_{i,k}^{x(2)}w_{k,j}\right)-\beta^2\bar{N}_{yy}\left(\sum_{k=1}^{n_y}A_{j,k}^{y(2)}w_{i,k}\right)\\
&-2\beta\bar{N}_{xy}\left(\sum_{k=1}^{n_x}\sum_{l=1}^{n_y}A_{i,k}^{x(1)}A_{j,l}^{y(1)}w_{k,l}\right)+\frac{12}{\lambda^2}(1-\upsilon^2)\left(\frac{\partial^2 w}{\partial t^2}\right)_{i,j}=0,
\end{aligned}
$$

$$(52)$$

where $i=1,2,\ldots,n_x$ and $j=1,2,\ldots,n_y$. It should be noticed that in-plane inertia terms are negligible compared to transverse inertia terms [38]. However, time-dependent in-plane displacement components are not ignored in this analysis since large deformations along the transverse direction can induce considerable displacements in the plane of the GS. Substituting Eq. (44) into Eqs. (38)-(40) leads to the following discretised equations for force resultants

$$
\begin{aligned}
(\bar{N}_{xx})_{i,j}=12\gamma_{C0}^4\beta^2&\left[\frac{1}{\lambda}\left(\sum_{k=1}^{n_x}\sum_{l=1}^{n_y}A_{i,k}^{x(3)}A_{j,l}^{y(2)}u_{k,l}\right)+\left(\sum_{k=1}^{n_x}A_{i,k}^{x(1)}w_{k,j}\right)\left(\sum_{k=1}^{n_x}\sum_{l=1}^{n_y}A_{i,k}^{x(3)}A_{j,l}^{y(2)}w_{k,l}\right)\right.\\
&+2\left(\sum_{k=1}^{n_x}A_{i,k}^{x(2)}w_{k,j}\right)\left(\sum_{k=1}^{n_x}\sum_{l=1}^{n_y}A_{i,k}^{x(2)}A_{j,l}^{y(2)}w_{k,l}\right)+\left(\sum_{k=1}^{n_x}A_{i,k}^{x(3)}w_{k,j}\right)\left(\sum_{k=1}^{n_x}\sum_{l=1}^{n_y}A_{i,k}^{x(1)}A_{j,l}^{y(2)}w_{k,l}\right)\\
&+2\left.\left(\sum_{k=1}^{n_x}\sum_{l=1}^{n_y}A_{i,k}^{x(2)}A_{j,l}^{y(1)}w_{k,l}\right)^2+2\left(\sum_{k=1}^{n_x}\sum_{l=1}^{n_y}A_{i,k}^{x(1)}A_{j,l}^{y(1)}w_{k,l}\right)\left(\sum_{k=1}^{n_x}\sum_{l=1}^{n_y}A_{i,k}^{x(3)}A_{j,l}^{y(1)}w_{k,l}\right)\right]\\
+12\upsilon\gamma_{C0}^4\beta^3&\left[\frac{1}{\lambda}\left(\sum_{k=1}^{n_x}\sum_{l=1}^{n_y}A_{i,k}^{x(2)}A_{j,l}^{y(3)}v_{k,l}\right)+\beta\left(\sum_{k=1}^{n_y}A_{j,k}^{y(1)}w_{i,k}\right)\left(\sum_{k=1}^{n_x}\sum_{l=1}^{n_y}A_{i,k}^{x(2)}A_{j,l}^{y(3)}w_{k,l}\right)\right.\\
&+2\beta\left(\sum_{k=1}^{n_y}A_{j,k}^{y(2)}w_{i,k}\right)\left(\sum_{k=1}^{n_x}\sum_{l=1}^{n_y}A_{i,k}^{x(2)}A_{j,l}^{y(2)}w_{k,l}\right)+2\beta\left(\sum_{k=1}^{n_x}\sum_{l=1}^{n_y}A_{i,k}^{x(1)}A_{j,l}^{y(2)}w_{k,l}\right)^2+\beta\times
\end{aligned}
$$

$$\left(\sum_{k=1}^{n_y} A_{j,k}^{y(3)} w_{i,k}\right)\left(\sum_{k=1}^{n_x}\sum_{l=1}^{n_y} A_{i,k}^{x(2)} A_{j,l}^{y(1)} w_{k,l}\right) + 2\beta\left(\sum_{k=1}^{n_x}\sum_{l=1}^{n_y} A_{i,k}^{x(1)} A_{j,l}^{y(1)} w_{k,l}\right)\left(\sum_{k=1}^{n_x}\sum_{l=1}^{n_y} A_{i,k}^{x(1)} A_{j,l}^{y(3)} w_{k,l}\right)\Bigg]$$

$$-12\gamma_{C0}^2\Bigg[\frac{\beta^2}{\lambda}\left(\sum_{k=1}^{n_x}\sum_{l=1}^{n_y} A_{i,k}^{x(1)} A_{j,l}^{y(2)} u_{k,l}\right) + \frac{1}{\lambda}\left(\sum_{k=1}^{n_x} A_{i,k}^{x(3)} u_{k,j}\right) + \beta^2\left(\sum_{k=1}^{n_x}\sum_{l=1}^{n_y} A_{i,k}^{x(1)} A_{j,l}^{y(1)} w_{k,l}\right)^2 + \beta^2\times$$

$$\left(\sum_{k=1}^{n_x} A_{i,k}^{x(1)} w_{k,j}\right)\left(\sum_{k=1}^{n_x}\sum_{l=1}^{n_y} A_{i,k}^{x(1)} A_{j,l}^{y(2)} w_{k,l}\right) + \left(\sum_{k=1}^{n_x} A_{i,k}^{x(2)} w_{k,j}\right)^2 + \left(\sum_{k=1}^{n_x} A_{i,k}^{x(1)} w_{k,j}\right)\left(\sum_{k=1}^{n_x} A_{i,k}^{x(3)} w_{k,j}\right)\Bigg]$$

$$-12\upsilon\gamma_{C0}^2\Bigg[\frac{\beta}{\lambda}\left(\sum_{k=1}^{n_x}\sum_{l=1}^{n_y} A_{i,k}^{x(2)} A_{j,l}^{y(1)} v_{k,l}\right) + \frac{\beta^3}{\lambda}\left(\sum_{k=1}^{n_y} A_{j,k}^{y(3)} v_{i,k}\right) + \beta^2\left(\sum_{k=1}^{n_x}\sum_{l=1}^{n_y} A_{i,k}^{x(1)} A_{j,l}^{y(1)} w_{k,l}\right)^2 + \beta^2\times$$

$$\left(\sum_{k=1}^{n_y} A_{j,k}^{y(1)} w_{i,k}\right)\left(\sum_{k=1}^{n_x}\sum_{l=1}^{n_y} A_{i,k}^{x(2)} A_{j,l}^{y(1)} w_{k,l}\right) + \beta^4\left(\sum_{k=1}^{n_y} A_{j,k}^{y(2)} w_{i,k}\right)^2 + \beta^4\left(\sum_{k=1}^{n_y} A_{j,k}^{y(1)} w_{i,k}\right)\left(\sum_{k=1}^{n_y} A_{j,k}^{y(3)} w_{i,k}\right)\Bigg]$$

$$+12\Bigg[\frac{1}{\lambda}\left(\sum_{k=1}^{n_x} A_{i,k}^{x(1)} u_{k,j}\right) + \frac{\upsilon\beta}{\lambda}\left(\sum_{k=1}^{n_y} A_{j,k}^{y(1)} v_{i,k}\right) + \frac{1}{2}\left(\sum_{k=1}^{n_x} A_{i,k}^{x(1)} w_{k,j}\right)^2 + \frac{1}{2}\upsilon\beta^2\left(\sum_{k=1}^{n_y} A_{j,k}^{y(1)} w_{i,k}\right)^2\Bigg],$$

$$(53)$$

$$(\bar{N}_{yy})_{i,j} = 12\gamma_{C0}^4\beta^3\Bigg[\frac{1}{\lambda}\left(\sum_{k=1}^{n_x}\sum_{l=1}^{n_y} A_{i,k}^{x(2)} A_{j,l}^{y(3)} v_{k,l}\right) + \beta\left(\sum_{k=1}^{n_y} A_{j,k}^{y(1)} w_{i,k}\right)\left(\sum_{k=1}^{n_x}\sum_{l=1}^{n_y} A_{i,k}^{x(2)} A_{j,l}^{y(3)} w_{k,l}\right)$$

$$+2\beta\left(\sum_{k=1}^{n_y} A_{j,k}^{y(2)} w_{i,k}\right)\left(\sum_{k=1}^{n_x}\sum_{l=1}^{n_y} A_{i,k}^{x(2)} A_{j,l}^{y(2)} w_{k,l}\right) + 2\beta\left(\sum_{k=1}^{n_x}\sum_{l=1}^{n_y} A_{i,k}^{x(1)} A_{j,l}^{y(2)} w_{k,l}\right)^2 + \beta\times$$

$$\left(\sum_{k=1}^{n_y} A_{j,k}^{y(3)} w_{i,k}\right)\left(\sum_{k=1}^{n_x}\sum_{l=1}^{n_y} A_{i,k}^{x(2)} A_{j,l}^{y(1)} w_{k,l}\right) + 2\beta\left(\sum_{k=1}^{n_x}\sum_{l=1}^{n_y} A_{i,k}^{x(1)} A_{j,l}^{y(1)} w_{k,l}\right)\left(\sum_{k=1}^{n_x}\sum_{l=1}^{n_y} A_{i,k}^{x(1)} A_{j,l}^{y(3)} w_{k,l}\right)\Bigg]$$

$$+12\upsilon\gamma_{C0}^4\beta^2\Bigg[\frac{1}{\lambda}\left(\sum_{k=1}^{n_x}\sum_{l=1}^{n_y} A_{i,k}^{x(3)} A_{j,l}^{y(2)} u_{k,l}\right) + \left(\sum_{k=1}^{n_x} A_{i,k}^{x(1)} w_{k,j}\right)\left(\sum_{k=1}^{n_x}\sum_{l=1}^{n_y} A_{i,k}^{x(3)} A_{j,l}^{y(2)} w_{k,l}\right)$$

$$+2\left(\sum_{k=1}^{n_x}A_{i,k}^{x(2)}w_{k,j}\right)\left(\sum_{k=1}^{n_x}\sum_{l=1}^{n_y}A_{i,k}^{x(2)}A_{j,l}^{y(2)}w_{k,l}\right)+\left(\sum_{k=1}^{n_x}A_{i,k}^{x(3)}w_{k,j}\right)\left(\sum_{k=1}^{n_x}\sum_{l=1}^{n_y}A_{i,k}^{x(1)}A_{j,l}^{y(2)}w_{k,l}\right)$$

$$+2\left(\sum_{k=1}^{n_x}\sum_{l=1}^{n_y}A_{i,k}^{x(2)}A_{j,l}^{y(1)}w_{k,l}\right)^2+2\left(\sum_{k=1}^{n_x}\sum_{l=1}^{n_y}A_{i,k}^{x(1)}A_{j,l}^{y(1)}w_{k,l}\right)\left(\sum_{k=1}^{n_x}\sum_{l=1}^{n_y}A_{i,k}^{x(3)}A_{j,l}^{y(1)}w_{k,l}\right)\Bigg]$$

$$-12\gamma_{C0}^2\Bigg[\frac{\beta}{\lambda}\left(\sum_{k=1}^{n_x}\sum_{l=1}^{n_y}A_{i,k}^{x(2)}A_{j,l}^{y(1)}v_{k,l}\right)+\frac{\beta^3}{\lambda}\left(\sum_{k=1}^{n_y}A_{j,k}^{y(3)}v_{i,k}\right)+\beta^2\left(\sum_{k=1}^{n_x}\sum_{l=1}^{n_y}A_{i,k}^{x(1)}A_{j,l}^{y(1)}w_{k,l}\right)^2+\beta^2\times$$

$$\left(\sum_{k=1}^{n_y}A_{j,k}^{y(1)}w_{i,k}\right)\left(\sum_{k=1}^{n_x}\sum_{l=1}^{n_y}A_{i,k}^{x(2)}A_{j,l}^{y(1)}w_{k,l}\right)+\beta^4\left(\sum_{k=1}^{n_y}A_{j,k}^{y(2)}w_{i,k}\right)^2+\beta^4\left(\sum_{k=1}^{n_y}A_{j,k}^{y(1)}w_{i,k}\right)\left(\sum_{k=1}^{n_y}A_{j,k}^{y(3)}w_{i,k}\right)\Bigg]$$

$$-12\upsilon\gamma_{C0}^2\Bigg[\frac{\beta^2}{\lambda}\left(\sum_{k=1}^{n_x}\sum_{l=1}^{n_y}A_{i,k}^{x(1)}A_{j,l}^{y(2)}u_{k,l}\right)+\frac{1}{\lambda}\left(\sum_{k=1}^{n_x}A_{i,k}^{x(3)}u_{k,j}\right)+\beta^2\left(\sum_{k=1}^{n_x}\sum_{l=1}^{n_y}A_{i,k}^{x(1)}A_{j,l}^{y(1)}w_{k,l}\right)^2+\beta^2\times$$

$$\left(\sum_{k=1}^{n_x}A_{i,k}^{x(1)}w_{k,j}\right)\left(\sum_{k=1}^{n_x}\sum_{l=1}^{n_y}A_{i,k}^{x(1)}A_{j,l}^{y(2)}w_{k,l}\right)+\left(\sum_{k=1}^{n_x}A_{i,k}^{x(2)}w_{k,j}\right)^2+\left(\sum_{k=1}^{n_x}A_{i,k}^{x(1)}w_{k,j}\right)\left(\sum_{k=1}^{n_x}A_{i,k}^{x(3)}w_{k,j}\right)\Bigg]$$

$$+12\Bigg[\frac{\upsilon}{\lambda}\left(\sum_{k=1}^{n_x}A_{i,k}^{x(1)}u_{k,j}\right)+\frac{\beta}{\lambda}\left(\sum_{k=1}^{n_y}A_{j,k}^{y(1)}v_{i,k}\right)+\frac{1}{2}\upsilon\left(\sum_{k=1}^{n_x}A_{i,k}^{x(1)}w_{k,j}\right)^2+\frac{1}{2}\beta^2\left(\sum_{k=1}^{n_y}A_{j,k}^{y(1)}w_{i,k}\right)^2\Bigg],$$

(54)

$$\left(\bar N_{xy}\right)_{i,j}=6(1-\upsilon)\Bigg[\frac{\beta}{\lambda}\left(\sum_{k=1}^{n_y}A_{j,k}^{y(1)}u_{i,k}\right)+\frac{1}{\lambda}\left(\sum_{k=1}^{n_x}A_{i,k}^{x(1)}v_{k,j}\right)+\beta\left(\sum_{k=1}^{n_x}A_{i,k}^{x(1)}w_{k,j}\right)\left(\sum_{k=1}^{n_y}A_{j,k}^{y(1)}w_{i,k}\right)\Bigg].$$

(54)

In addition to the nonlinear motion equations and in-plane force resultants, the boundary conditions of the single-layered GS including all three types (CBC, NCBC-e and NCBC-k) are discretised as follows

CBC:

$$u_{1,j}=0,\qquad w_{1,j}=0,\qquad \sum_{k=1}^{n_x}A_{1,k}^{x(1)}w_{k,j}=0,$$

$$u_{n_x,j}=0,\qquad w_{n_x,j}=0,\qquad \sum_{k=1}^{n_x}A_{n_x,k}^{x(1)}w_{k,j}=0,$$

$$v_{i,1} = 0, \qquad w_{i,1} = 0, \qquad \sum_{k=1}^{n_y} A_{1,k}^{y(1)} w_{i,k} = 0,$$

$$v_{i,n_y} = 0, \qquad w_{i,n_y} = 0, \qquad \sum_{k=1}^{n_y} A_{n_y,k}^{y(1)} w_{i,k} = 0, \tag{56}$$

NCBC-e:

$$\gamma_{C0} \left[\sum_{k=1}^{n_x} A_{1,k}^{x(2)} u_{k,j} + \lambda \left(\sum_{k=1}^{n_x} A_{1,k}^{x(1)} w_{k,j} \right) \left(\sum_{k=1}^{n_x} A_{1,k}^{x(2)} w_{k,j} \right) \right]$$

$$= \sum_{k=1}^{n_x} A_{1,k}^{x(1)} u_{k,j} + \frac{1}{2} \lambda \left(\sum_{k=1}^{n_x} A_{1,k}^{x(1)} w_{k,j} \right)^2,$$

$$\gamma_{C0} \left[\sum_{k=1}^{n_x} A_{n_x,k}^{x(2)} u_{k,j} + \lambda \left(\sum_{k=1}^{n_x} A_{n_x,k}^{x(1)} w_{k,j} \right) \left(\sum_{k=1}^{n_x} A_{n_x,k}^{x(2)} w_{k,j} \right) \right]$$

$$= - \left[\sum_{k=1}^{n_x} A_{n_x,k}^{x(1)} u_{k,j} + \frac{1}{2} \lambda \left(\sum_{k=1}^{n_x} A_{n_x,k}^{x(1)} w_{k,j} \right)^2 \right],$$

$$\gamma_{C0}\beta \left[\sum_{k=1}^{n_y} A_{1,k}^{y(2)} v_{i,k} + \lambda\beta \left(\sum_{k=1}^{n_y} A_{1,k}^{y(1)} w_{i,k} \right) \left(\sum_{k=1}^{n_y} A_{1,k}^{y(2)} w_{i,k} \right) \right]$$

$$= \sum_{k=1}^{n_y} A_{1,k}^{y(1)} v_{i,k} + \frac{1}{2} \lambda\beta \left(\sum_{k=1}^{n_y} A_{1,k}^{y(1)} w_{i,k} \right)^2,$$

$$\gamma_{C0}\beta \left[\sum_{k=1}^{n_y} A_{n_y,k}^{y(2)} v_{i,k} + \lambda\beta \left(\sum_{k=1}^{n_y} A_{n_y,k}^{y(1)} w_{i,k} \right) \left(\sum_{k=1}^{n_y} A_{n_y,k}^{y(2)} w_{i,k} \right) \right]$$

$$= - \left[\sum_{k=1}^{n_y} A_{n_y,k}^{y(1)} v_{i,k} + \frac{1}{2} \lambda\beta \left(\sum_{k=1}^{n_y} A_{n_y,k}^{y(1)} w_{i,k} \right)^2 \right], \tag{57}$$

NCBC-k:

$$\gamma_C \left(\sum_{k=1}^{n_x} A_{1,k}^{x(3)} w_{k,j} \right) - \left(\sum_{k=1}^{n_x} A_{1,k}^{x(2)} w_{k,j} \right) = 0,$$

$$\gamma_C \left(\sum_{k=1}^{n_x} A_{n_x,k}^{x(3)} w_{k,j} \right) + \left(\sum_{k=1}^{n_x} A_{n_x,k}^{x(2)} w_{k,j} \right) = 0,$$

$$\beta\gamma_C\left(\sum_{k=1}^{n_y}A_{1,k}^{y(3)}w_{i,k}\right)-\left(\sum_{k=1}^{n_y}A_{1,k}^{y(2)}w_{i,k}\right)=0,$$

$$\beta\gamma_C\left(\sum_{k=1}^{n_y}A_{n_y,k}^{y(3)}w_{i,k}\right)+\left(\sum_{k=1}^{n_y}A_{n_y,k}^{y(2)}w_{i,k}\right)=0. \tag{58}$$

To implement the CBC, NCBC-e and NCBC-k, the direct method [36] is employed in this paper. According to this method, Eqs. (56)-(58) are used to obtain the displacement components near the edges of the GS, and then these relations are directly substituted into Eqs. (50)-(55). The resultant reduced equations can be expressed as

$$\langle[\bar{N}_{xx}]\quad[\bar{N}_{xy}]\quad[\bar{N}_{yy}]\rangle=[K_f]\begin{Bmatrix}\{u\}\\\{v\}\end{Bmatrix}+[S(w)], \tag{59}$$

$$[K_{uv}]\begin{Bmatrix}\{u\}\\\{v\}\end{Bmatrix}+[J(w)]=\{0\}, \tag{60}$$

where $[K_f]$ and $[K_{uv}]$ are the stiffness matrices related to in-plane force resultants and in-plane displacements, respectively. Obtaining the in-plane displacement components from Eq. (60), and then substituting the derived equation into Eq. (59), one obtains the resultants as a function of the transverse deflection

$$\langle[\bar{N}_{xx}]\quad[\bar{N}_{xy}]\quad[\bar{N}_{yy}]\rangle=-[K_f][K_{uv}]^{-1}[J(w)]+[S(w)]. \tag{61}$$

Substituting Eq. (61) into the discretised version of the motion equation for w, the following matrix equation is obtained

$$[K_{NL}(\bar{N}_{xx},\bar{N}_{yy},\bar{N}_{xy},w)]\{w\}+[K_L]\{w\}+[M_w]\{\ddot{w}\}=0, \tag{62}$$

where K_{NL} and K_L denote the nonlinear and linear stiffness matrices of the nanoplate, respectively; M_w is the mass matrix of the nanostructure. The nonlinear matrix is a function of the in-plane force resultants and the transverse displacement. However, the mass matrix and linear stiffness depend neither on the force resultant nor on the transverse displacement. Finally, a harmonic balance technique and an iterative method are used to solve Eq. (62), and obtain the nonlinear frequency of the GS. The stopping criteria for the iterative method is [38]

$$\frac{|\varpi_{N+1} - \varpi_N|}{\varpi_N} \leq \varepsilon', \tag{63}$$

where N, ϖ and ε' are the number of iterations, nanoplate dimensionless frequency and a small constant value. In this numerical approach, a value of $\varepsilon' = 0.0001$ is taken.

4. MD simulations

Performing numerical simulations based on the molecular dynamics is a powerful technique for analysing ultrasmall structures such as nanobeams and nanoplates. In this technique, first intermolecular and intramolecular interactions are used to calculate force field, and then motion equations are obtained for each ultrasmall particle. Solving these sets of Newtonian motion equation gives the trajectories of the particles as a function of time. Unlike the continuum modelling, the micro/nanostructure is regarded as a discrete system in MD simulations. In this section, MD simulation is done to verify that the stress-driven model is accurate for the nonlinear vibrations of GSs. Applying the adaptive intermolecular reactive empirical bond order (AIREBO) potential [39], the force field is estimated. According to the AIREBO potential, the entire system energy is expressed as

$$E^{TOT} = \frac{1}{2} \sum_i \sum_{j \neq i} \left(E_{ij}^{REBO} + E_{ij}^{LJ} + \sum_{\substack{m \neq i,j}} \sum_{n \neq i,j,m} E_{mijn}^{TOR} \right), \tag{64}$$

where E represents energy; "*REBO*", "*LJ*" and "*TOR*" denote the reactive empirical bond order, Lennard-Jones, and torsion potentials, respectively. The cut-off distance is set to 0.2 nm in the LAMMPS code. To model the filly clamped nanoplate, four layers of carbon are assumed to be fixed along each side of the GS, as shown in Fig. 2. The time step and ambient temperature are taken as 0.001 ps and 300 K, respectively. An isothermal-isobaric (npt) ensemble with the Nose-Hoover style of time integration is used to perform the relaxation procedure in order for the system to reach the minimum energy state at the beginning of the MD simulation. To induce

nonlinear vibrations, a sufficiently large transverse force is gradually applied to a small group of carbons at the centre of the GS, and then the nanoplate is released to freely vibrate along the transverse direction for 20 ps. Finally, the natural frequencies of a square single-layered GS with size 5 nm are determined via the fast Fourier transform technique.
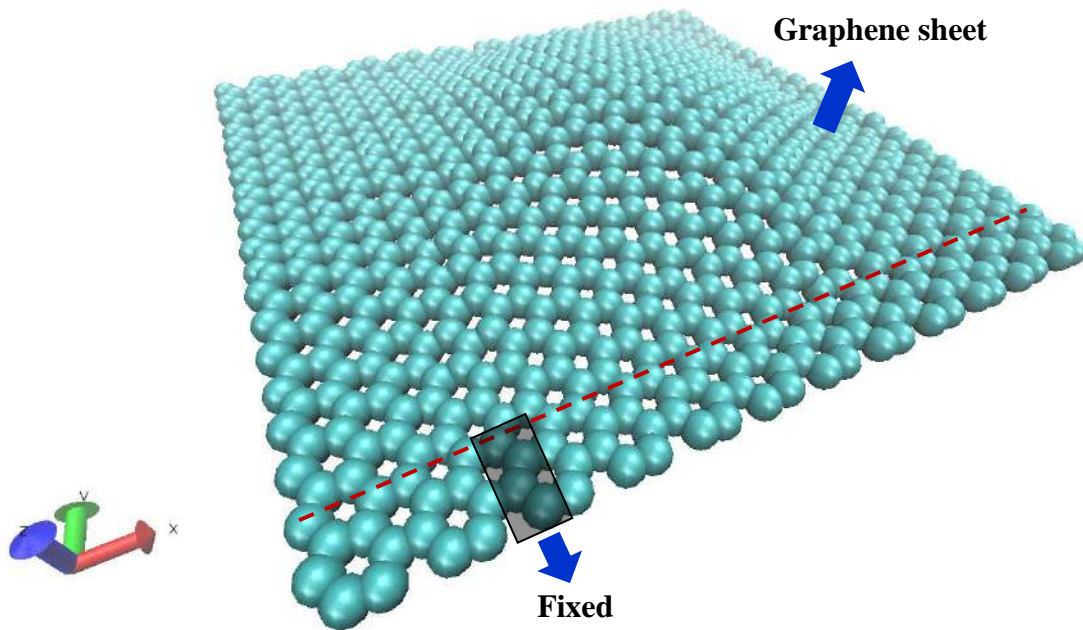

Fig. 2. Four layers of carbon are fixed along each side of the GS to simulate fully clamped boundary conditions in MD simulations.

5. Numerical results

Table 1 lists the linear natural frequencies of a square plate with clamped boundary condition along each edge. Frequency parameters associated with the first vibration modes are presented in this table. The aspect ratio, thickness-to-length ratio and Poisson's ratio are set to 1, 0.05 and 0.3, respectively. The numerical results obtained by the DQM-based solution procedure are compared with those reported by Leissa [40]. A close agreement is found, indicating the accuracy of the solution method. Furthermore, Table 2 provides the nonlinear ratios of clamped square plates for different maximum transverse deflections. To indicate the convergence of the DQ technique, various numbers of grid points are also taken into

consideration. The nonlinear ratio is the ratio of nonlinear fundamental frequency parameter to the linear one (i.e. ω_{nl}/ω_l). After each computed nonlinear ratio, the number of required iteration is also indicated in parentheses. Table 2 compares the present nonlinear ratios to those computed by hierarchical finite element method (HFEM) [41]; a good match is found. In addition, a grid distribution with at least 15 grid points is required for converged results.

Table 1. First six sets of linear frequencies of clamped square plates.

$\omega a^2 \sqrt{\dfrac{\rho}{D}}$	First mode	Second mode	Third mode	Fourth mode	Fifth mode	Sixth mode
Leissa [40]	35.99	73.40	108.22	131.64	132.18	164.99
Present DQ technique	35.9852	73.3938	108.2165	131.5808	132.2048	165.0004

Table 2. The ratio of nonlinear fundamental frequency parameter to its linear counterpart for clamped square plates.

$\dfrac{w_{max}}{h}$	Number of grid points ($n_x = n_y = n$)						HFEM [41]
	7	9	11	15	19	21	
0.21377	1.0064 (2)*	1.0084 (2)	1.0082 (2)	1.0082 (2)	1.0082 (2)	1.0082 (2)	1.0082
0.60780	1.0534 (4)	1.0658 (3)	1.0645 (3)	1.0647 (3)	1.0647 (3)	1.0647 (3)	1.0647
1.0012	1.1498 (5)	1.1696 (3)	1.1666 (3)	1.1668 (3)	1.1668 (3)	1.1668 (3)	1.1668

* The number of required iterations.

Table 3 lists the fundamental nonlinear frequencies of a zigzag GS with size $a=b=5$ nm and $h=0.34$ nm. The results of both MD simulations and stress-driven plate theory are presented in this table. Various values of maximum transverse deflections are taken into account. The appropriate scale parameter of the size-dependent stress-driven plate model is also given in parentheses. More details about the MD simulation are given the previous section. In the stress-

driven continuum modelling, the aspect ratio, density, Poisson's ratio and the number of grid points are 1, 2270 kg/m^3, 0.3 and 19, respectively. The in-plane stiffness of the nanoplate is adopted as 227.46 J/m^2 [42]. The natural frequency obtained via the stress-driven elasticity theory is in a satisfactory agreement with that computed by MD simulations.

Table 3. Comparison of present stress-driven plate model to scale-free nonlinear model and MD simulations.

$\dfrac{w_{max}}{h}$	Nonlinear frequency (THz)		
	MD simulations	Nonlinear stress-driven plate model	Nonlinear classical plate model
0.9438	0.4	0.4150 (0.01,-0.2)*	0.4651
1.2245	0.48	0.4694 (0.02,-0.05)*	0.5021
1.3979	0.55	0.5524 (0.02,0.02)*	0.5281
1.3557	0.55	0.5456 (0.02,0.02)*	0.5216
1.5471	0.60	0.6025 (0.04,0.04)*	0.5519
1.6689	0.65	0.6567 (0.06,0.06)*	0.5723

*Dimensionless scale parameters (γ_c, γ_{c0}).

The nonlinear frequency ratio of the single-layered GS versus the dimensionless maximum transverse deflection (w_{max}/h) is indicated in Fig. 3 for various scale coefficients associated with the plate curvature. The aspect ratio, Poisson's ratio, thickness-to-length ratio are assumed as 1, 0.3 and 0.05, respectively. The scale parameter associated with in-plane nonlocality is taken as 0.1. A grid distribution with nineteen points is assumed for the DQ technique.

Increasing the maximum lateral deflection increases the nonlinear ratio. In fact, the geometrical nonlinearity effect increases when the vibration amplitude gets larger. The second important observation is that the nonlinear ratio dramatically reduces when the curvature nonlocality is higher. As the scale parameter related to the nanoplate curvature increases, the total stiffness enhances, leading to less geometrical nonlinearity effects in the nanoscale structure. The third important finding from this figure is that increasing the dimensionless maximum transverse deflection of the GS results in larger difference between the results of different cases. This indicates that ignoring scale effects at larger transverse deflections is more likely to cause considerable error in the continuum modelling.
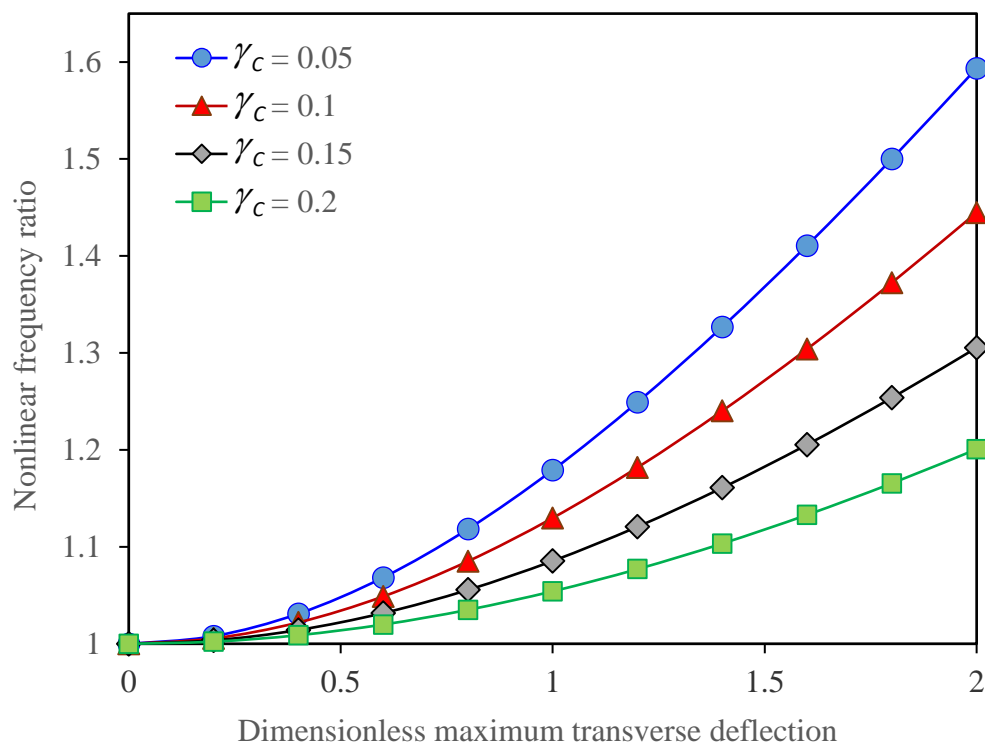
Fig. 3. Nonlinear ratio against the lateral deflection of the GS for various scale parameters associated with the nanoplate curvature.

The influence of the in-plane nonlocality on the large amplitude vibrations of the GS is shown in Fig. 4. Several values of the scale parameter associated with in-plane strain components are taken into account. The aspect ratio, Poisson's ratio, curvature scale parameter, and thickness-to-length ratio are set to 1, 0.3, 0.1, and 0.05, respectively. The nonlinear ratio substantially increases when the GS undergoes larger transverse vibration amplitudes. Furthermore, it is interesting to notice that the nonlinear frequency ratio is higher for higher scale parameters associated with in-plane strain components. This is the opposite of what is observed for the curvature scale parameter. The physical reason behind this finding is that increasing the in-plane strain nonlocality is likely to lead to higher in-pane stiffnesses, which would increase the nonlinearity effect. In a comprehensive continuum model, the scale parameters associated with in-plane strain and curvature should be same. Setting the two scale parameters equal to each other, the nonlinear frequency ratio versus the dimensionless maximum transverse deflection is plotted in Fig. 5. The results of the conventional elasticity are also shown in this figure. The general scale parameter exhibits a decreasing impact on the nonlinear effect. In addition, the difference between the stress-driven and local elasticity models substantially increases with increasing the dimensionless maximum transverse deflection.
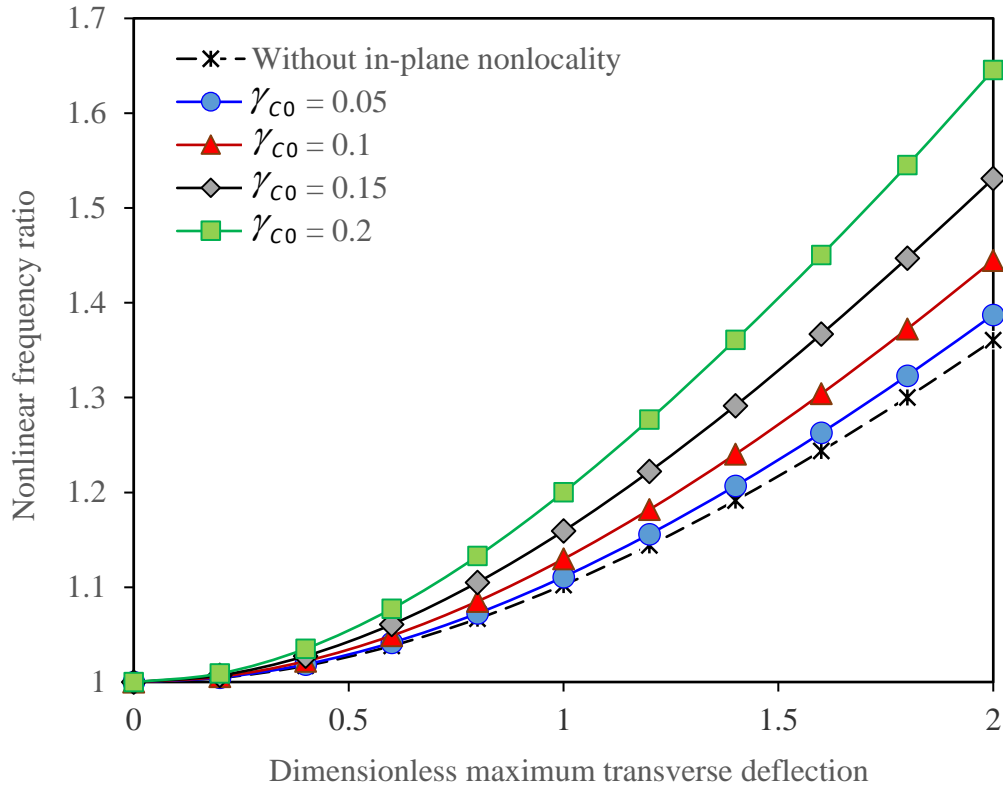
Fig. 4. Nonlinear ratio against the lateral deflection of the GS for various scale parameters associated with the in-plane strains.
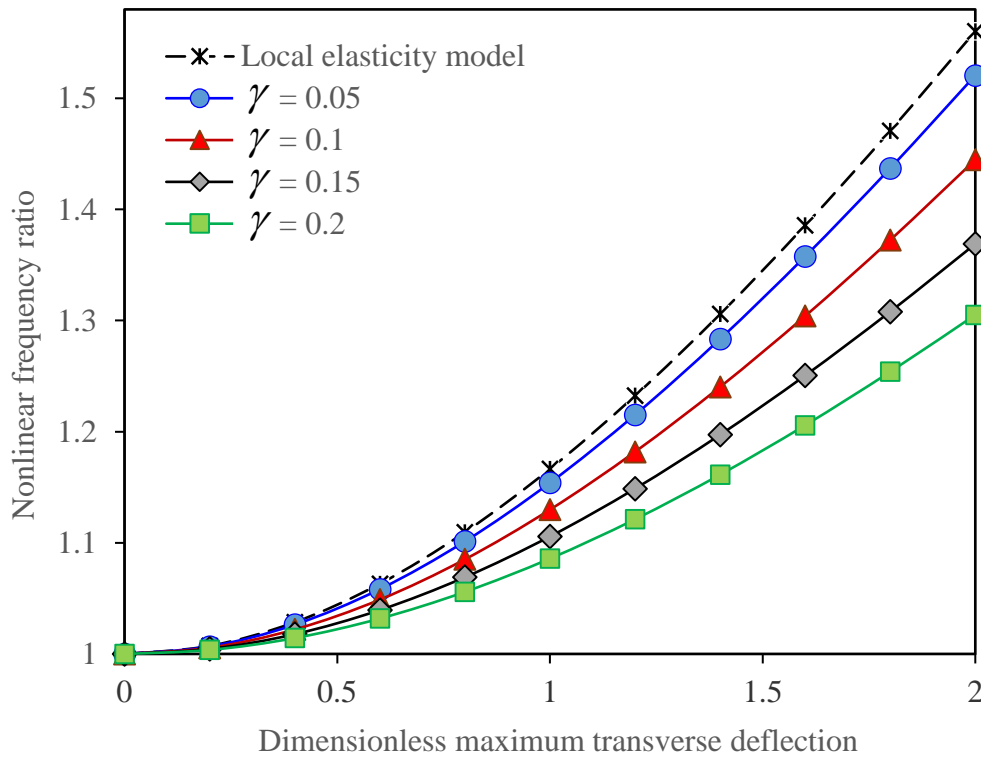

Fig. 5. Nonlinear ratio against the lateral deflection of the GS for various scale parameters $(\gamma = \gamma_c = \gamma_{c0})$.

Figure 6 demonstrates the nonlinear frequency ratio against the dimensionless transverse deflection of the single-layered GS for various aspect (length-to-width) ratios. The thickness-to-length ratio and Poisson's ratio are taken as 0.05 and 0.3, respectively. Size coefficients related to the nanoplate curvature and in-plane strain components are both set to 0.1. Larger aspect ratios lead to lower nonlinear frequency ratios. This trend is more pronounced for large maximum deflections of the GS. To investigate size influences on the in-plane displacement of the nanoplate, the dimensionless maximum displacement components along the x and y axes against the maximum lateral deflection is plotted in Fig. 7 for several scale parameters. The aspect ratio, thickness-to-length ratio and Poisson's ratio are 1.5, 0.05 and 0.3, respectively. Size coefficients related to the curvature and in-plane strain are assumed to be the same. From the figure, it is clear that the scale parameter of the stress-driven plate theory has a slight decreasing impact on the maximum in-plane displacements of the GS along both in-plane directions. This is rooted in the general rule of thumb that when the stress-driven scale parameter increases, the stiffness is increased at small-scale levels.
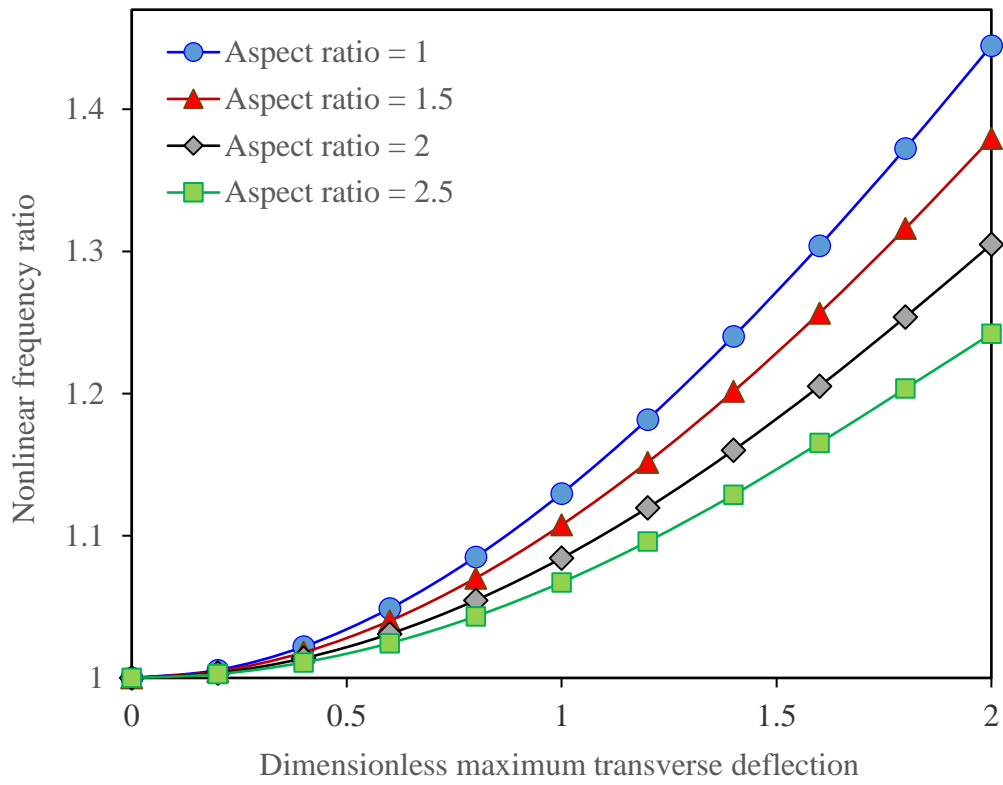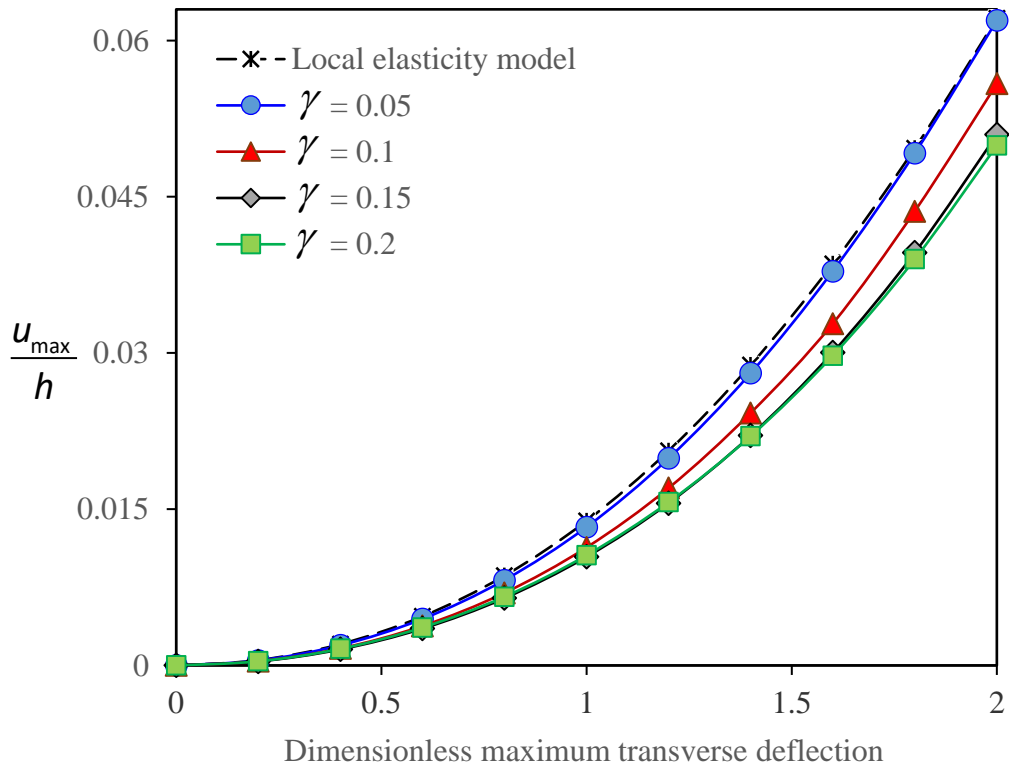
Fig. 6. Nonlinear ratio against the lateral deflection of the GS for various aspect ratios.
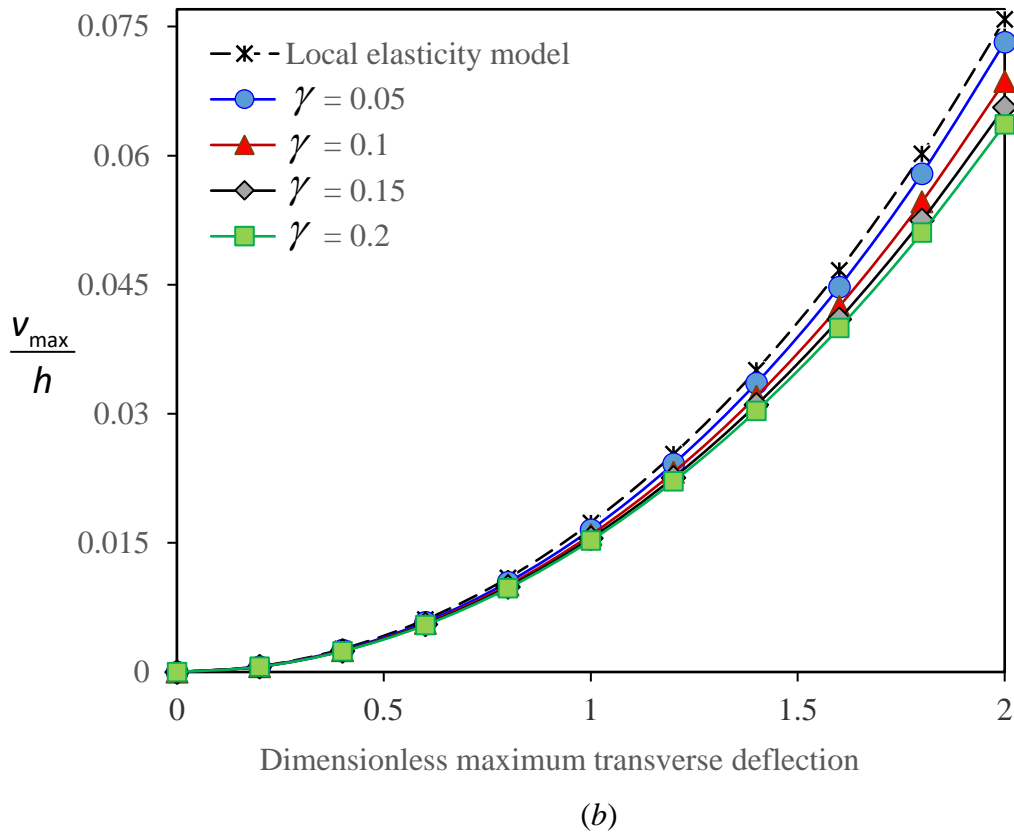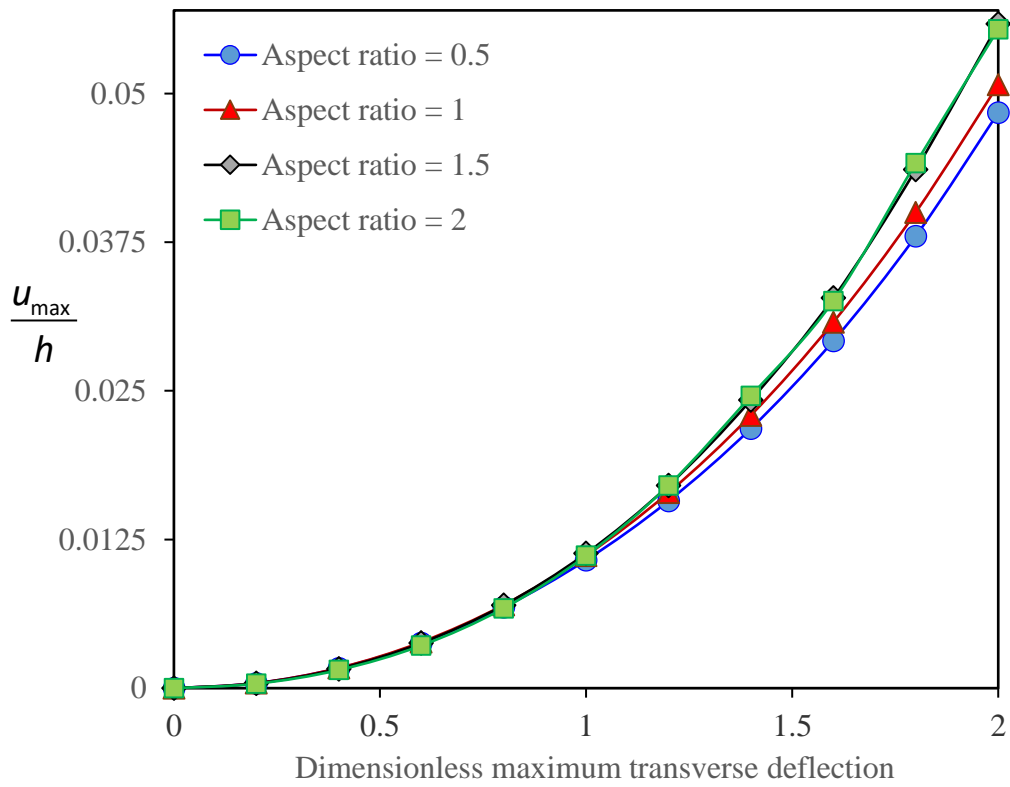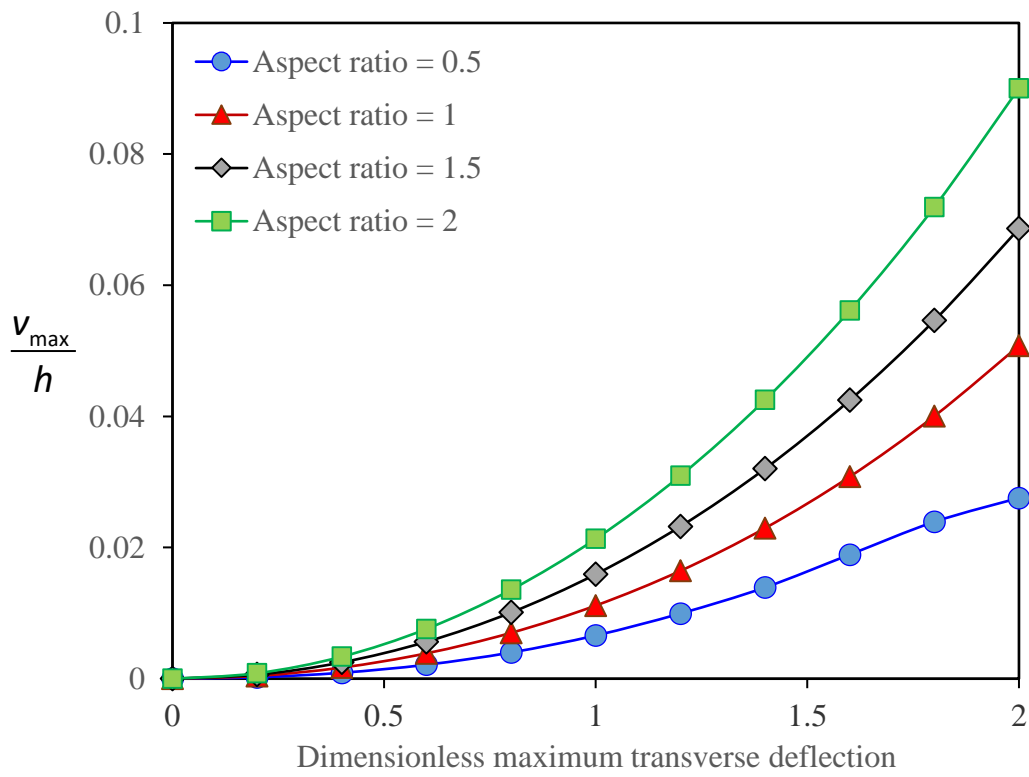

(*a*)

Fig. 7. Maximum displacement in (*a*) *x* and (*b*) *y* axes versus the lateral deflection of the GS for various scale parameters.

The influences of the aspect and thickness-to-length ratios on the dimensionless maximum in-plane displacements are indicated in Figs. 8 and 9, respectively. Both scale parameters are taken as 0.1. The aspect ratio is set to 1.5 when the influence of the other geometric parameter is investigated. On the hand, when aspect ratio effects on in-plane displacements are analysed, the thickness-to-length ratio is taken as 0.05. The geometry of the GS plays a significant role in the in-plane displacements. Both geometric parameters (i.e. the aspect ratio and thickness-to-length ratio) have an increasing effect on the dimensionless maximum in-plane displacements.
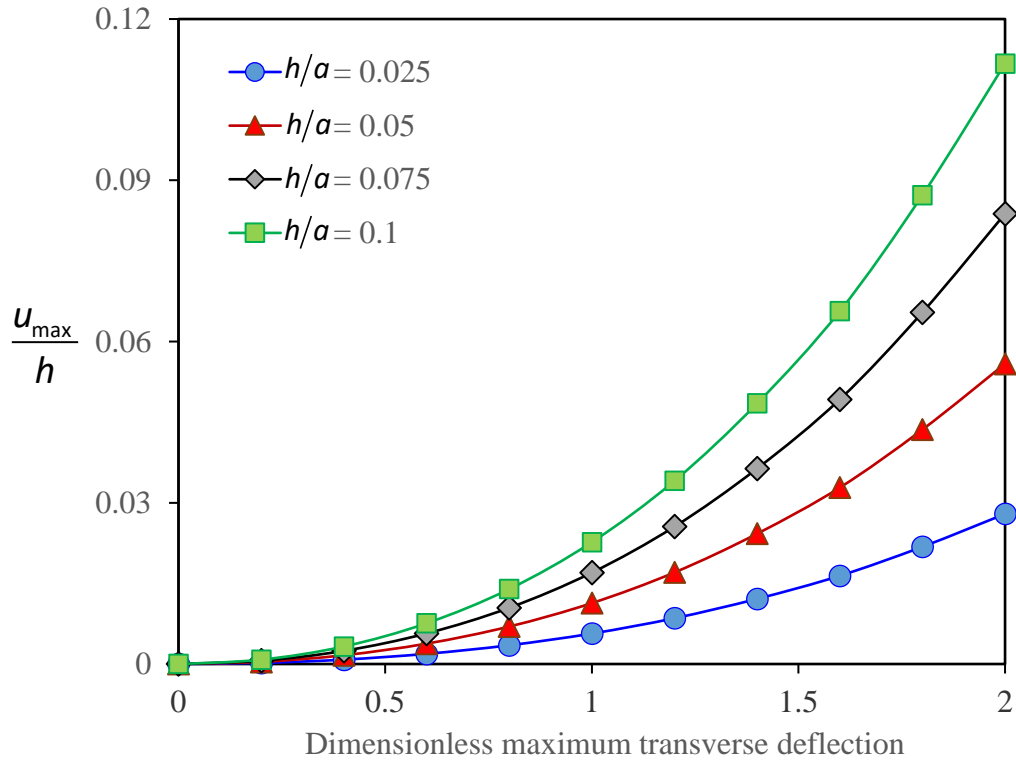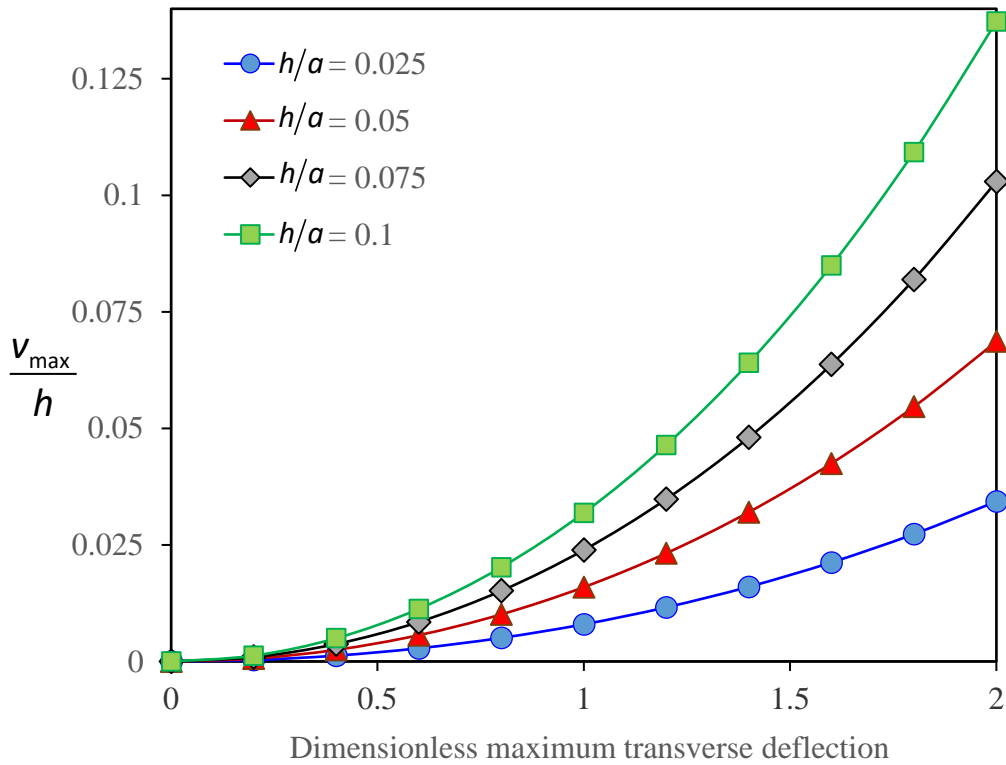
(a)

(b)

Fig. 8. Maximum displacement in (*a*) *x* and (*b*) *y* axes versus the lateral deflection of the GS for various aspect ratios.

Fig. 9. Maximum displacement in (*a*) *x* and (*b*) *y* axes versus the lateral deflection of the GS for various thickness-to-length ratios.

6. Conclusions

A nonlinear stress-driven integral model has been developed for the large-amplitude vibrations of single-layered GSs. The coupled nonlinear equations of motions together with the non-classical and classical constitutive conditions were presented by the von Kármán's theory of nonlinearity and stress-driven elasticity theory. Non-classical constitutive conditions were considered for both in-plane strains as well as nanoplate curvature components. A DQM-based solution procedure in conjunction with an appropriate iteration technique were used to compute the nonlinear frequency parameters of the GS. Furthermore, MD simulation was done for verifying the accuracy of the stress-driven plate model. It was found that the nonlinear frequency ratio is higher when the nanoplate vibration amplitude gets larger. Moreover, the nonlinear frequency ratio substantially reduces with enhancing the curvature nonlocality. Scale effects are more pronounced when the GS undergoes larger transverse vibration amplitudes. In contrast to the scale parameter related to the curvature nonlocality, the other scale parameter, which is associated with nonlocal in-plane strains, has an increasing impact on the nonlinear ratio. In addition, the maximum in-plane displacements of the GS are slightly decreased with increasing the general stress-driven scale parameter.

References

[1] K. Kostarelos, K.S. Novoselov, Graphene devices for life, Nature nanotechnology, 9 (2014) 744.

[2] A.C. Neto, F. Guinea, N.M. Peres, K.S. Novoselov, A.K. Geim, The electronic properties of graphene, Reviews of modern physics, 81 (2009) 109.

[3] S. Adhikari, R. Chowdhury, Zeptogram sensing from gigahertz vibration: Graphene based nanosensor, Physica E: Low-dimensional Systems and Nanostructures, 44 (2012) 1528-1534.

[4] S. Park, J. An, J.W. Suk, R.S. Ruoff, Graphene-based actuators, Small, 6 (2010) 210-212.

[5] J. Atalaya, J.M. Kinaret, A. Isacsson, Nanomechanical mass measurement using nonlinear response of a graphene membrane, EPL (Europhysics Letters), 91 (2010) 48001.

[6] J.F. Rhoads, S.W. Shaw, K.L. Turner, Nonlinear dynamics and its applications in micro- and nanoresonators, Journal of dynamic systems, measurement, and control, 132 (2010).

[7] S. Kitipornchai, X. He, K. Liew, Continuum model for the vibration of multilayered graphene sheets, Physical Review B, 72 (2005) 075443.

[8] R. Ansari, S. Sahmani, B. Arash, Nonlocal plate model for free vibrations of single-layered graphene sheets, Physics Letters A, 375 (2010) 53-62.

[9] S. Gupta, R. Batra, Elastic properties and frequencies of free vibrations of single-layer graphene sheets, Journal of Computational and Theoretical Nanoscience, 7 (2010) 2151-2164.

[10] P. Malekzadeh, M. Shojaee, A two-variable first-order shear deformation theory coupled with surface and nonlocal effects for free vibration of nanoplates, Journal of Vibration and Control, 21 (2015) 2755-2772.

[11] A.M. Zenkour, A novel mixed nonlocal elasticity theory for thermoelastic vibration of nanoplates, Composite Structures, 185 (2018) 821-833.

[12] J. Reddy, Nonlocal nonlinear formulations for bending of classical and shear deformation theories of beams and plates, International Journal of Engineering Science, 48 (2010) 1507-1518.

[13] P. Malekzadeh, M.G. Haghighi, M. Shojaee, Nonlinear free vibration of skew nanoplates with surface and small scale effects, Thin-Walled Structures, 78 (2014) 48-56.

[14] A. Farajpour, M.H. Yazdi, A. Rastgoo, M. Loghmani, M. Mohammadi, Nonlocal nonlinear plate model for large amplitude vibration of magneto-electro-elastic nanoplates, Composite Structures, 140 (2016) 323-336.

[15] C. Liu, L.-L. Ke, J. Yang, S. Kitipornchai, Y.-S. Wang, Nonlinear vibration of piezoelectric nanoplates using nonlocal Mindlin plate theory, Mechanics of Advanced Materials and Structures, 25 (2018) 1252-1264.

[16] Y. Zhang, K. Liew, D. Hui, Characterizing nonlinear vibration behavior of bilayer graphene thin films, Composites Part B: Engineering, 145 (2018) 197-205.

[17] S. Zeng, B. Wang, K. Wang, Nonlinear vibration of piezoelectric sandwich nanoplates with functionally graded porous core with consideration of flexoelectric effect, Composite Structures, 207 (2019) 340-351.

[18] F. Ebrahimi, E. Heidari, Surface effects on nonlinear vibration of embedded functionally graded nanoplates via higher order shear deformation plate theory, Mechanics of Advanced Materials and Structures, 26 (2019) 671-699.

[19] P. Phung-Van, C.H. Thai, H. Nguyen-Xuan, M.A. Wahab, Porosity-dependent nonlinear transient responses of functionally graded nanoplates using isogeometric analysis, Composites Part B: Engineering, 164 (2019) 215-225.

[20] M. Mohammadia, A. Rastgoo, Nonlinear vibration analysis of the viscoelastic composite nanoplate with three directionally imperfect porous FG core, Structural Engineering and Mechanics, 69 (2019) 131-143.

[21] Y. Wang, F. Li, Y. Wang, X. Jing, Nonlinear responses and stability analysis of viscoelastic nanoplate resting on elastic matrix under 3: 1 internal resonances, International Journal of Mechanical Sciences, 128 (2017) 94-104.

[22] E. Ruocco, V. Mallardo, Buckling and vibration analysis nanoplates with imperfections, Applied Mathematics and Computation, 357 (2019) 282-296.

[23] H. Askari, H. Jamshidifar, B. Fidan, High resolution mass identification using nonlinear vibrations of nanoplates, Measurement, 101 (2017) 166-174.

[24] R. Barretta, F.M. de Sciarra, Constitutive boundary conditions for nonlocal strain gradient elastic nano-beams, International Journal of Engineering Science, 130 (2018) 187-198.

[25] M. Fakher, S. Rahmanian, S. Hosseini-Hashemi, On the carbon nanotube mass nanosensor by integral form of nonlocal elasticity, International Journal of Mechanical Sciences, 150 (2019) 445-457.

[26] M.Z. Nejad, A. Hadi, A. Omidvari, A. Rastgoo, Bending analysis of bi-directional functionally graded Euler-Bernoulli nano-beams using integral form of Eringen's non-local elasticity theory, Structural Engineering and Mechanics, 67 (2018) 417-425.

[27] G. Romano, R. Barretta, M. Diaco, F.M. de Sciarra, Constitutive boundary conditions and paradoxes in nonlocal elastic nanobeams, International Journal of Mechanical Sciences, 121 (2017) 151-156.

[28] S.A. Faghidian, Integro-differential nonlocal theory of elasticity, International Journal of Engineering Science, 129 (2018) 96-110.

[29] A. Apuzzo, R. Barretta, R. Luciano, F.M. de Sciarra, R. Penna, Free vibrations of Bernoulli-Euler nano-beams by the stress-driven nonlocal integral model, Composites Part B: Engineering, 123 (2017) 105-111.

[30] P. Jiang, H. Qing, C. Gao, Theoretical analysis on elastic buckling of nanobeams based on stress-driven nonlocal integral model, Applied Mathematics and Mechanics, 41 (2020) 207-232.

[31] R. Barretta, S.A. Faghidian, F.M. de Sciarra, Stress-driven nonlocal integral elasticity for axisymmetric nano-plates, International Journal of Engineering Science, 136 (2019) 38-52.

[32] S. Hosseini-Hashemi, S. Behdad, M. Fakher, Vibration analysis of two-phase local/nonlocal viscoelastic nanobeams with surface effects, The European Physical Journal Plus, 135 (2020) 190.

[33] J. Fernández-Sáez, R. Zaera, Vibrations of Bernoulli-Euler beams using the two-phase nonlocal elasticity theory, International Journal of Engineering Science, 119 (2017) 232-248.

[34] M. Farajpour, A. Shahidi, A. Farajpour, Elastic waves in fluid-conveying carbon nanotubes under magneto-hygro-mechanical loads via a two-phase local/nonlocal mixture model, Materials Research Express, 6 (2019) 0850a0858.

[35] G. Romano, R. Barretta, Stress-driven versus strain-driven nonlocal integral model for elastic nano-beams, Composites Part B: Engineering, 114 (2017) 184-188.

[36] C. Shu, Differential quadrature and its application in engineering, Springer Science & Business Media, 2012.

[37] P. Malekzadeh, A. Setoodeh, A.A. Beni, Small scale effect on the free vibration of orthotropic arbitrary straight-sided quadrilateral nanoplates, Composite Structures, 93 (2011) 1631-1639.

[38] P. Malekzadeh, G. Karami, Large amplitude flexural vibration analysis of tapered plates with edges elastically restrained against rotation using DQM, Engineering structures, 30 (2008) 2850-2858.

[39] S.J. Stuart, A.B. Tutein, J.A. Harrison, A reactive potential for hydrocarbons with intermolecular interactions, The Journal of chemical physics, 112 (2000) 6472-6486.

[40] A.W. Leissa, Vibration of plates, Scientific and Technical Information Division, National Aeronautics and …, 1969.

[41] P. Ribeiro, M. Petyt, Nonlinear vibration of plates by hierarchical finite element and continuation methods, (1997).

[42] C. Reddy, S. Rajendran, K. Liew, Equilibrium configuration and continuum elastic properties of finite sized graphene, Nanotechnology, 17 (2006) 864.

Chapter 7
Conclusions and future works

Chapter overview

The most important findings of the present study on the nonlinear time-dependent deformation of beam- and plate-shaped structures at small-scales are summarized in this chapter. The significance of the present research in engineering applications is also emphasised. In addition, a number of possible future investigations, which can be carried out to continue this thesis are briefly mentioned at the end of this chapter.

7 Conclusions and future works

7.1 Significance

Small-scale devices have many promising applications in scientific fields and modern technologies because of their excellent electromechanical properties. In many small-scale devices, understanding the mechanical characteristics of small-scale beam and plate structures subject to external loads is essential to achieve a reasonable design and manufacturing process since they form the building blocks of these devices. As shown in this thesis, the mechanical characteristics of small-scale structures have been proven to be scale-dependent, and, for the first time, a number of modified continuum models have been provided for the time-dependent deformation of beams and plates at ultrasmall levels. With the help of these modified continuum models, it is now possible to better predict size influences on the mechanical characteristics of ultrasmall devices.

7.2 Conclusions

An advanced scale-dependent model of beams was proposed in chapter 3 to analyse the nonlinear vibrations of nanotubes with an imperfection in the geometry. Strain gradient influences together with stress nonlocality effects were modelled via the NSGT. Both softening- and hardening-stiffness responses could be predicted depending on the values of scale parameters. A scale-dependent type of Euler-Bernoulli theory was implemented to obtain the coupled motion equations. A discretisation solution methodology is utilised for computing the nonlinear natural frequencies. The imperfection in the beam geometry is regarded as an initial transverse deflection. Important observations on the vibrations of small-scale imperfect tubes are:

- Size influences estimated via the NSGT occur in a wider size range in comparison with the stress nonlocality effect. This is because the NSGT concurrently includes strain

gradient and stress nonlocality effects. After a certain length, the latter effect disappears while the former remains active.

- The conventional nonlocal elasticity needs less computational effort than the NSGT.

- Increasing stress nonlocality remarkably decreases the natural frequencies.

- An imperfection in the geometry of the small-scale beam can notably alter the nonlinear vibrational response.

- For systems with low amplitudes of geometrical imperfections, the nanoscale tube exhibits hardening nonlinearity including 2 saddle nodes. By contrast, as imperfections with large amplitudes exist in the structure prior to the time-dependent deformation, the nanoscale tube shows a combined hardening and softening nonlinearity including 4 saddle nodes.

- Higher resonance frequencies are induced by higher strain gradients.

- Enhancing strain gradients would remove modal interactions.

- A larger nonlocal coefficient causes the nanoscale tube to have a resonance response at a lower frequency since stress nonlocalities are associated with a reduction in the structural stiffness.

In chapter 4, using an advanced nonlinear scale-dependent model, the coupled vibrations of small-scale beams with viscoelasticity and imperfections effects were studied. An appropriate work/energy balance was conducted, and the nonlinear motion equations were presented. The stress nonlocality together with the role of strain gradients in the vibrational behaviour of beams at small-scales were simulated in the modelling. Internal energy loss and imperfections in the geometry were estimated via a viscoelastic model and by assuming an

initial transverse deflection, respectively. Using Galerkin's technique, nonlinear frequencies are calculated. The important findings of this study are:

- Imposing a comparatively small imperfection on the small-scale beam, the nonlinear response of the viscoelastic system obeys a hardening type including 2 saddle points.

- The conventional scale-free theory results in an overestimated motion amplitude for the coupled vibration.

- The frequency parameter estimated by the nonlocal theory is less than the one computed via the scale-free theory.

- When the small-scale tube is subject to small loading amplitudes, the linear viscoelasticity would have the same results as the nonlinear viscoelasticity.

- For large magnitudes of loading amplitudes, neglecting nonlinear viscoelasticity leads to overestimated frequency parameters.

- Even a slight decrease in the initial deformation could significantly change the number of saddle points.

- Two saddle points are associated with small initial deflections.

- Two extra saddle points are induced when the small-scale beam is subject to relatively large initial deflections.

The linear vibration and deformation of small-scale plates were investigated in chapter 5 via a stress-driven nonlocal integral model. The one-dimensional kernel function, which had been used for circular and annular small-scale plates, was extended to two-dimensional problems at ultrasmall levels such as the vibration of rectangular nanoplates. The additional non-classical edge conditions related to the curvature nonlocality were obtained. The sixth-order differential equation is presented by implementing Hamilton's law and Kirchhoff plate

model. The differential quadrature technique, as a useful numerical tool for dealing with mathematical problems with complex boundary conditions, is used to compute the natural frequency and transverse deflection of the small-scale plate. The obtained results for various aspect ratios and vibration modes were compared to those reported previously, and an excellent agreement was observed. The following important findings are concluded:

- The Laplacian-based nonlocal model is not able to predict scale influences on the static deformation of small-scale plates subject to uniform load.

- Scale effects on the bending of small-scale plates with different edge conditions can reasonably be described via the stress-driven nonlocal integral model.

- A highly scale-dependent behaviour is found in cases with fully clamped edges based on the stress-driven model. This finding is consistent with a previously reported general law that as stiff conditions are placed on the boundaries at small-scale levels, the influence of intermolecular interaction enhances, and consequently scale effects get more prominent.

- The gap between the strain gradient theory and stress-driven nonlocal theory becomes larger as the scale coefficient increases.

- Clamped small-scale plates are more affected by the size parameter of the continuum model than simply-supported plates.

- The stress-driven model predicts comparatively more size dependency than the model with strain gradients for fully clamped small-scale plates.

- The stress-driven influence induces a remarkable rise in the total stiffness of nanoplates.

- Additional stiff conditions on the small-scale plate would cause the system to vibrate at higher resonance frequencies.

156

Finally, a nonlinear stress-driven model of plates was developed in chapter 6 for the vibrations of nanoplates. Curvature nonlocality was taken into consideration in conjunction with in-plane nonlocality. Three nonlinear coupled motion equations together with three types of edge conditions including one conventional and two non-conventional conditions were obtained. The first additional non-conventional condition was induced due to the curvature nonlocality while the second one was associated with the in-plane nonlocality. A numerical solution was developed based on a differential quadrature method and an iteration technique. Conducting MD simulations via LAMMPS software, the validity of the stress-driven modelling for the vibration of graphene sheets was examined. A very good match was found between the stress-driven and MD results. Important findings on the nonlinear vibrations of small-scale plates are summarised as:

- The nonlinear frequency ratio increases as the small-scale plate experiences vibrations with larger amplitudes.

- Enhancing the curvature nonlocality substantially decreases the nonlinear frequency ratio of the small-scale plate since the curvature nonlinearity is linked to a remarkable enhancement in the stiffness.

- The size influence gets more significant as the graphene sheet displays higher vibration amplitudes, indicating the importance of size effects in the accurate theoretical modelling of nonlinear small-scale structures.

- The scale parameter associated with the in-plane nonlocality exhibits a notable increasing effect on the nonlinear ratio, as opposed to the scale parameter related to the curvature nonlocality.

- Maximum displacements in the plane of the graphene sheet slightly decrease when the general stress-driven parameter increases.

157

7.3 Future works

A number of small-scale rings and rods have been used as the fundamental parts of nanoscale/microscale systems due to their fascinating properties, simple structure, and comparatively straightforward fabrication process. The nonlinear mechanical behaviour of these structures have not been studied comprehensively. Advanced scale-dependent models can be used to carry out more investigations on the nonlinear vibrations of rings and rods at small-scale levels.

The majority of the available scale-dependent continuum models for the vibrations of ultrasmall structures have not been validated yet using experimental measurements since conducting a vibration test at small-scale levels, especially nanoscales, is very challenging and difficult in comparison with the similar test at large-scale levels. More attempt is needed for calibrating the scale-dependent modelling of nanoscale/microscale structures via experiment. To do this, graphene sheets and carbon nanotubes can be used as small-scale plates and beams due to their widespread applications, special mechanical properties and availability.

In addition to small-scale plates and beams, the nonlinear vibrational behaviour of shells at ultrasmall levels can be studied in the future. Developing scale-dependent shell models provides a useful mathematical tool to analyse the vibrational response of a range of ultrasmall structures such as microshells and nanoshells. However, few theoretical investigations have been reported on the mechanics of these ultrasmall structures due to the relative complexity and computational costs with respect to nanoscale/microscale beams and plates.

In the design of many ultrasmall devices such as nanoelectromechanical systems, understanding the mechanical response of fundamental parts to external forces is vital. Particularly, when carbon nanotubes are subject to external axial compressive forces, it is important to compute the critical force corresponding to buckling. To continue the present

study, the linear instability and post-buckling behaviour of nanotubes can be analysed via developing advanced scale-dependent models and MD simulations. In addition, small-scale plates can undergo buckling as an in-plane biaxial or uniaxial compressive load is exerted. The two-dimensional kernel function introduced in the present work, can be used to develop stress-driven models for the linear stability and post-buckling analysis of rectangular plates at small-scale levels.

Appendix A

Additional journal publications

Appendix A1

Nonlinear vibration of small-scale tubes conveying fluid with initial deflection

A1.1 Appendix overview

In this appendix, the influences of initial deflection on the nonlinear vibrations of tubes conveying fluid at small scales are analysed. For this purpose, a higher-order model is presented by assuming nonlocality in stresses and incorporating strain gradients in the non-classical constitutive equations. To simulate slip conditions, the Karniadakis–Beskok technique is employed. Geometrical nonlinearity is modelled through strain-displacement relations. Potential and kinetic energies as well as external work are used to carry out a work/energy balance and obtain the coupled motion equations. The nonlinear vibrational response of the tube is numerically estimated via a Galerkin-based technique. It is found that initial deflections have a crucial impact on the mechanics of fluid-conveying tubes at ultrasmall levels. The continuum models presented in chapters three and four for small-scale beams are extended to their fluid-structure interaction counterparts. This part is a complementary study and provide a useful platform to understand the nonlinear oscillation of nanotubes as one of the most commonly used nanobeams when there is fluid flow inside.

Appendix A1.2

Statement of Authorship

Statement of Authorship

Title of Paper	Frequency response of initially deflected nanotubes conveying fluid via a nonlinear NSGT model
Publication Status	☑ Published ☐ Accepted for Publication ☐ Submitted for Publication ☐ Unpublished and Unsubmitted work written in manuscript style
Publication Details	A Farajpour, MH Ghayesh, H Farokhi, Frequency response of initially deflected nanotubes conveying fluid via a nonlinear NSGT model, Structural Engineering and Mechanics 72, 71-81 (2019).

Principal Author

Name of Principal Author (Candidate)	Ali Farajpour Ouderji
Contribution to the Paper	- Research and doing the literature review of the paper - Developing the model (i.e. derivation of partial differential equations of motion) - Modelling the slip boundary condition using the Beskok–Karniadakis approach - Incorporating axial inertia effects and the influence of an initial deflection - Writing all parts of the paper and analysing the data - Correspondence with the reviewers and editor of the journal - Preparing the revised version of the paper
Overall percentage (%)	60%
Certification:	This paper reports on original research I conducted during the period of my Higher Degree by Research candidature and is not subject to any obligations or contractual agreements with a third party that would constrain its inclusion in this thesis. I am the primary author of this paper.
Signature	Date 2/6/2020

Co-Author Contributions

By signing the Statement of Authorship, each author certifies that:

   i.   the candidate's stated contribution to the publication is accurate (as detailed above);

   ii.   permission is granted for the candidate in include the publication in the thesis; and

   iii.   the sum of all co-author contributions is equal to 100% less the candidate's stated contribution.

Name of Co-Author	Mergen H. Ghayesh
Contribution to the Paper	- Supervising the work including preparing the paper - Contribution to the development of the ideas and concepts of the paper - Editing and evaluating the paper before submission - Discretising and solving the equations of motions, and obtaining frequency response curves
Signature	Date 21/06/2020

Name of Co-Author	Hamed Farokhi
Contribution to the Paper	- Participation in supervising the work - Contribution to the development of the concepts of the paper - Discretising and solving the equations of motions, and obtaining frequency response curves
Signature	Date 19/06/2020

Appendix A1.3

Published journal paper

This work was published in "Structural Engineering and Mechanics" as:

Frequency response of initially deflected nanotubes conveying fluid via a nonlinear NSGT model

Ali Farajpour[*1] , Mergen H. Ghayesh[1a] and Hamed Farokhi[2a]

[1]*School of Mechanical Engineering, University of Adelaide, South Australia 5005, Australia*
[2]*Department of Mechanical and Construction Engineering, Northumbria University, Newcastle upon Tyne NE1 8ST, UK*

Abstract. The objective of this paper is to develop a size-dependent nonlinear model of beams for fluid-conveying nanotubes with an initial deflection. The nonlinear frequency response of the nanotube is analysed via an Euler-Bernoulli model. Size influences on the behaviour of the nanosystem are described utilising the nonlocal strain gradient theory (NSGT). Relative motions at the inner wall of the nanotube is taken into consideration via Beskok–Karniadakis model. Formulating kinetic and elastic energies and then employing Hamilton's approach, the nonlinear motion equations are derived. Furthermore, Galerkin's approach is employed for discretisation, and then a continuation scheme is developed for obtaining numerical results. It is observed that an initial deflection significantly alters the frequency response of NSGT nanotubes conveying fluid. For small initial deflections, a hardening nonlinearity is found whereas a softening-hardening nonlinearity is observed for large initial deflections.

Keywords: nonlinear frequency response; nanotubes; fluid flow; initial deflection

1. Introduction

Nanostructural components such as nanotubes and nanoplates form the basic blocks of many microelectromechanical and nanoelectromechanical systems. Salient examples of these systems are nanoscale/microscale generators, mass sensors and energy harvesters. Furthermore, nanostructures, especially carbon nanotubes and boron nitride nanotubes can be used for the reinforcement of composite plates (Bakhadda, Bouiadjra *et al.* 2018, Draoui, Zidour *et al.* 2019, Semmah, Heireche *et al.* 2019). Developing advanced mathematical modelling for understanding the mechanics of nanostructural components provides a platform to improve the performance of these ultrasmall systems.

Since the mechanical behaviour of ultrasmall structures such as graphene sheets and nanotubes is highly influenced by size effects (Ebrahimi and Barati 2018, Ebrahimi, Haghi *et al.* 2018, Nejad, Hadi *et al.* 2018, Farajpour, Ghayesh *et al.* 2019), the application of the classical continuum mechanics in analysing the mechanical behaviour at ultrasmall levels is not reliable. Therefore, the classical continuum mechanics is modified so as to capture size influences (Ebrahimi and Dabbagh 2018, Farajpour, Ghayesh *et al.* 2018, Arefi 2019, Benahmed, Fahsi *et al.* 2019, Gao, Xiao *et al.* 2019, Karami, Janghorban *et al.* 2019, Mohammadi and Rastgoo 2019, Nebab, Atmane *et al.* 2019). There are a number of size-dependent continuum-, Eringen's theory (Eringen and Edelen 1972, Farajpour,

Shahidi *et al.* 2018) and strain gradient elasticity (Akgöz and Civalek 2013, Ghayesh, Amabili *et al.* 2013, Akgöz and Civalek 2014). In this work, a nonlocal theory incorporating strain gradient effects is used for deriving the motion equations of fluid-conveying nanotubes with an initial deflection.

In the last decade, for the first time, the application of the nonlocal theory to continuum modelling of nanoscale cantilevers was introduced by Peddieson *et al.* (Peddieson, Buchanan *et al.* 2003). Then, many investigations have been performed on the size-dependent continuum modelling of microscale fundamental components (Ghayesh, Amabili *et al.* 2013, Şimşek and Reddy 2013, Farokhi, Ghayesh *et al.* 2016, Farokhi and Ghayesh 2018) and nanoscale fundamental components (Reddy 2010, Farajpour, Rastgoo *et al.* 2017, Farajpour, Shahidi *et al.* 2018) via modifying the continuum mechanics. Various basic problems in solid mechanics at nanoscales such as wave propagation (Tounsi, Heireche *et al.* 2008), thermal buckling (Zenkour and Sobhy 2013), static deflection (Reddy 2010), resonance behaviour (Karami, Shahsavari *et al.* 2019) and vibration analysis with consideration of surface effects (Malekzadeh and Shojaee 2015) as well as homogeneous (Civalek and Akgöz 2013), inhomogeneous (Nejad, Hadi *et al.* 2017) and piezoelectric problems (Asemi and Farajpour 2014), have been studied.

Scale-dependent continuum formulations have been introduced for the mechanics of various types of small-scale structures involving nanoplates (Karami, Janghorban *et al.* 2017, Kadari, Bessaim *et al.* 2018), functionally graded nanoplates (Belkorissat, Houari *et al.* 2015, Bounouara, Benrahou *et al.* 2016, Besseghier, Houari *et al.* 2017, Khetir, Bouiadjra *et al.* 2017, Karami, Janghorban *et al.* 2018, Karami, Janghorban *et al.* 2018, Karami, Janghorban *et al.*

∗Corresponding author, Ph.D. Student
 E-mail: ali.farajpourouderji@adelaide.edu.au

2018), graphene sheets (Bouadi, Bousahla *et al*. 2018, Bourada, Amara *et al*. 2018, Mokhtar, Heireche *et al*. 2018, Yazid, Heireche *et al*. 2018), nanobeams (Chaht, Kaci *et al*. 2015, Bellifa, Benrahou *et al*. 2017, Mouffoki, Bedia *et al*. 2017, Hamza-Cherif, Meradjah *et al*. 2018, Mokhtar, Heireche *et al*. 2018, Youcef, Kaci *et al*. 2018, Bedia, Houari *et al*. 2019), functionally graded nanobeams (Ahouel, Houari *et al*. 2016, Bouafia, Kaci *et al*. 2017), nanoshells (Karami, Janghorban *et al*. 2018), and nanoparticles (Karami, Janghorban *et al*. 2018) as well as microbeams (Al-Basyouni, Tounsi *et al*. 2015, Tlidji, Zidour *et al*. 2019).

Different higher-order theories have been utilised to capture scale influences on the mechanical response of small-scale structural components involving small-scale shells (Farokhi and Ghayesh 2018) and plates (Murmu and Adhikari 2013), panels (Demir, Mercan *et al*. 2016) as well as rods (Numanoğlu, Akgöz *et al*. 2018), beams (Zhang, He *et al*. 2014, Demir and Civalek 2017, Romano, Barretta *et al*. 2017) and tubes (Akgöz and Civalek 2011). Rahmani *et al*. (Rahmani, Refaeinejad *et al*. 2017) assessed different higher-order models with nonlocal influences for the static deformation and instability of functionally graded nanoscale beams; the inclusion of the influences of shear deformations results in a rise in deflection and a decrease in buckling force. Moreover, Akgoz and Civalek (Akgöz and Civalek 2017) examined the influences of shear deformations and temperature change on the vibrations of functionally graded nanoscale microbeams through use of a couple stress model. Malikan (Malikan 2017) also utilised a first-order theory of shear deformations for electromechanical stability analysis of smart nanoplates. In addition, scale-dependent higher-order models have been introduced for Silicon carbide nanotubes (Mercan and Civalek 2017) and boron nitride nanotubes (Mercan and Civalek 2016) as well as nanoscale beams resting on an elastic medium (Demir and Civalek 2017).

In addition to the size-dependent formulation and analysis of solid structural elements at small-scale levels, size effects on the mechanical behaviour of structural elements conveying fluid have been examined in the literature. For instance, the effects of a viscoelastic medium on the flow-induced stability and vibration of a single nanotube (Soltani, Taherian *et al*. 2010), the stability of nanotubes conveying pulsating fluid (Liang and Su 2013), and the flow-induced dynamics of nanotubes (Bahaadini, Saidi *et al*. 2018) as well as elastic waves in fluid-conveying both homogeneous and inhomogeneous nanotubes (Wang, Li *et al*. 2010, Filiz and Aydogdu 2015), have been analysed in recent times. Besides developing size-dependent formulation for fluid-conveying carbon nanotubes, other kinds of nanotubes including boron nitride (Maraghi, Arani *et al*. 2013) and piezoelectric nanotubes (Amiri, Talebitooti *et al*. 2018) conveying nanofluid have been taken into consideration.

As mentioned above, fluid-conveying nanotubes have mainly been analysed in terms of linear mechanics. Nonetheless, a few studies have been done with consideration of nonlinear strain components (Askari and Esmailzadeh 2017). More investigations are required in

order to fully understand the nonlinear frequency response of nanotubes conveying fluid, especially when there is an initial deflection in the system. For the sake of simplification, the influences of an initial deflection on the frequency response of fluid-conveying tubes at nanoscales have not been examined yet. Initial deflections are very significant since in nanoscale electromechanical devices, the fundamental parts are very prone to initial thermomechanical loading, which can consequently cause initial deflections (Farokhi and Ghayesh 2015). In addition, in previous studies, the frequency response was calculated taking into consideration only one trial function for displacements. However, in this paper, a precise solution methodology is presented via consideration of a high number of trail functions.

The aim of this investigation is to examine the influences of an initial deflection on the nonlinear mechanical behaviour of NSGT nanotubes conveying nanofluid flow. A modified Euler-Bernoulli model with strain gradient and nonlocal effects is developed to examine the nonlinear frequency response. To model the relative motions at the inner wall of the nanotube, Beskok–Karniadakis model is also applied. Nonlinear motion equations are presented by formulating kinetic and elastic energies as well as employing Hamilton's approach. For accurately estimating the frequency response, firstly, a system with a high degree of freedom is developed based on Galerkin's approach. Secondly, a continuation method is implemented to extract numerical results in the time domain. The present results would help researchers and engineers with the design of nanoscale electromechanical devices involving nanotubes conveying flow.

2. A nonlocal strain gradient model for tubes conveying flow at nanoscales

Figure 1 shows the schematic configuration of an ultrasmall tube with an initial deflection, which is employed to convey flow at nanoscales. According to the Euler–Bernoulli model, one has the following relation for the nonlinear strain (Ghayesh 2018)

$$\varepsilon_{xx} = \frac{\partial u}{\partial x} - z\frac{\partial^2 w}{\partial x^2} + \frac{\partial w}{\partial x}\frac{dw_0}{dx} + \frac{1}{2}\left(\frac{\partial w}{\partial x}\right)^2 \qquad (1)$$

Here the initial deflection, transverse and axial displacements are denoted by w_0, w and u, respectively. The NSGT-based constitutive relation of nanotubes is given by (Şimşek 2016)

$$t_{xx} - \left(e_0 a\right)^2 \nabla^2 t_{xx} = t_{xx}^{cl} - l_{sg}^2 \nabla^2 t_{xx}^{cl}, \qquad (2)$$

where

$$t_{xx}^{cl} = E\varepsilon_{xx} \qquad (3)$$

where t_{xx}^{cl} indicates the classical stress, and t_{xx} is the total stress; l_{sg}, E and $e_0 a$ represent the scale parameter linked
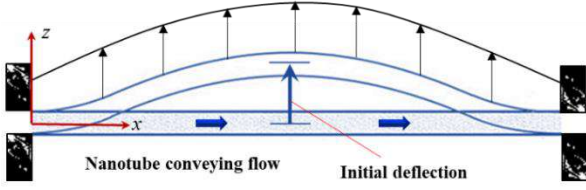
Fig. 1 An initial deflection in a nanotube conveying flow

to strain gradients, elasticity modulus and the scale parameter linked to stress nonlocality, respectively. In the nonlocal parameter, e_0 is a coefficient, which is employed to calibrate the theoretical model, and a is an internal characteristic size of nanotubes (Mohammadi *et al.* 2014, Farajpour *et al.* 2018, Mohammadi *et al.* 2013, farajpour *et al.* 2019, Malekzadeh *et al.* 2012, Farajpour *et al.* 2019). For instance, the internal characteristic size of carbon nanotubes is the bond length between two adjacent carbons. In this case, for the Laplace operator, one has $\nabla^2() = \partial^2()/\partial x^2$. Furthermore, let us consider I and A as the inertia moment and area of cross-section.

The force and moment resultants are

$$\langle N_{xx}, M_{xx} \rangle = \int_A \langle 1, z \rangle t_{xx} dA. \tag{4}$$

In view of the above equations, the force and moment resultants are written as

$$N_{xx} = EA\left(1 - l_{sg}^2 \nabla^2\right)\left[\frac{1}{2}\left(\frac{\partial w}{\partial x}\right)^2 + \frac{\partial u}{\partial x}\right]$$
$$+ EA\left(1 - l_{sg}^2 \nabla^2\right)\left[\frac{\partial w}{\partial x}\frac{dw_0}{dx}\right] + \left(e_0 a\right)^2 \nabla^2 N_{xx}, \tag{5}$$

$$M_{xx} = -EI\left(1 - l_{sg}^2 \nabla^2\right)\left[\frac{\partial^2 w}{\partial x^2}\right] + \left(e_0 a\right)^2 \nabla^2 M_{xx} \tag{6}$$

Based on the NSGT, the elastic energy is (Lim, Zhang *et al.* 2015, Şimşek 2016)

$$\delta U_{el} = \int_0^L \int_A \sigma_{xx} \delta \varepsilon_{xx} dA dx + \int_0^L \int_A \sigma_{xx}^{(1)} \nabla \delta \varepsilon_{xx} dA dx, \tag{7}$$

where the lower- and first-order non-classical stresses are indicated by $\sigma_{xx(\alpha\beta)}$ and $\sigma^{(1)}_{xx(\alpha\beta)}$ represent, respectively; also, L represents the tube length. Assuming ∇ as the gradient operator, the lower- and first-order non-classical stresses are related as (Lim, Zhang *et al.* 2015)

$$t_{xx} = \sigma_{xx} - \nabla \sigma_{xx}^{(1)} \tag{8}$$

Taking into account the effect of the relative motion at the inner wall, the total kinetic energy is obtained as (Paidoussis 1998)

$$T_k = \frac{1}{2}\rho_t \int_A \int_0^L \left(\left(\frac{\partial u}{\partial t}\right)^2 + \left(\frac{\partial w}{\partial t}\right)^2\right) dA dx$$
$$+ \frac{1}{2}\rho_f \int_A \int_0^L \left(\left[\frac{\partial u}{\partial t} + \kappa_{scf} U\left(1 + \frac{\partial u}{\partial x}\right)\right]^2 + \right.$$
$$\left. + \left[\frac{\partial w}{\partial t} + \kappa_{scf} U\left(\frac{\partial w}{\partial x} + \frac{dw_0}{dx}\right)\right]^2\right) dA dx. \tag{9}$$

In Eq. (20), κ_{scf} is the speed correction factor; ρ and U are, respectively, the mass density and fluid speed; "t" and "f" are abbreviations for "tube" and "fluid", respectively. Assuming $F(x)$ as the amplitude of applied loading and ω as the excitation frequency of applied loading, the external work is

$$\delta W_F = \int_0^L F(x)\cos(\omega t)\delta w \, dx. \tag{10}$$

Using Eqs. (7), (9) and (10) together with the following principle

$$\int_{t_1}^{t_2}\left\{\delta W_F + \delta T_k - \delta U_{el}\right\} dt = 0, \tag{11}$$

the nanotube motion equations are derived as

$$\left(M+m\right)\frac{\partial^2 u}{\partial t^2} + M\left(\kappa_{scf}U\right)^2\frac{\partial^2 u}{\partial x^2} + 2M\left(\kappa_{scf}U\right)\frac{\partial^2 u}{\partial t \partial x} - \frac{\partial N_{xx}}{\partial x} = 0 \tag{12}$$

$$\left(M+m\right)\frac{\partial^2 w}{\partial t^2} + M\left(\kappa_{scf}U\right)^2\left(\frac{\partial^2 w}{\partial x^2} + \frac{d^2 w_0}{dx^2}\right)$$
$$+ 2M\left(\kappa_{scf}U\right)\frac{\partial^2 w}{\partial t \partial x} - F(x)\cos(\omega t) - \frac{\partial}{\partial x}\left(N_{xx}\frac{dw_0}{dx}\right) \tag{13}$$
$$- \frac{\partial}{\partial x}\left(N_{xx}\frac{\partial w}{\partial x}\right) - \frac{\partial^2 M_{xx}}{\partial x^2} = 0,$$

in which M is the mass of fluid per length while m denotes the mass of the tube per length (Ghayesh *et al.* 2019, Farajpour *et al.* 2018, Ghayesh *et al.* 2019, Farajpour *et al.* 2019). To derive the differential equations in terms of displacement components, Eqs. (12) and (13) are used together with Eqs. (5) and (6). The derived coupled nonlinear equations are as

$$\left(1 - \left(e_0 a\right)^2 \nabla^2\right)\left[\left(M+m\right)\frac{\partial^2 u}{\partial t^2}\right.$$
$$\left. + M\left(\kappa_{scf}U\right)^2\frac{\partial^2 u}{\partial x^2} + 2M\left(\kappa_{scf}U\right)\frac{\partial^2 u}{\partial t \partial x}\right]$$
$$- EA\left(1 - l_{sg}^2 \nabla^2\right)\left[\frac{\partial w}{\partial x}\frac{\partial^2 w}{\partial x^2} + \frac{\partial^2 u}{\partial x^2}\right] \tag{14}$$
$$- EA\left(1 - l_{sg}^2 \nabla^2\right)\left[\frac{dw_0}{dx}\frac{\partial^2 w}{\partial x^2} + \frac{d^2 w_0}{dx^2}\frac{\partial w}{\partial x}\right] = 0,$$

$$\cos(\omega t)\left[F(x) - \left(e_0 a\right)^2\frac{d^2 F(x)}{dx^2}\right] + EI\left[l_{sg}^2\frac{\partial^6 w}{\partial x^6} - \frac{\partial^4 w}{\partial x^4}\right]$$
$$+ \left[EA\left(1 - \left(e_0 a\right)^2 \nabla^2\right)\right]\left(\left[\frac{d^2 w_0}{dx^2} + \frac{\partial^2 w}{\partial x^2}\right]\left(1 - l_{sg}^2 \nabla^2\right)\times\right.$$
$$\left[\frac{dw_0}{dx}\frac{\partial w}{\partial x} + \frac{1}{2}\left(\frac{\partial w}{\partial x}\right)^2 + \frac{\partial u}{\partial x}\right]\right) + \left[EA\left(1 - \left(e_0 a\right)^2 \nabla^2\right)\right]\times \tag{15}$$
$$\left(\left[\frac{dw_0}{dx} + \frac{\partial w}{\partial x}\right]\left[\frac{\partial}{\partial x}\left(\left(1 - l_{sg}^2 \nabla^2\right)\left[\frac{\partial w}{\partial x}\frac{dw_0}{dx} + \frac{1}{2}\left(\frac{\partial w}{\partial x}\right)^2 + \frac{\partial u}{\partial x}\right]\right)\right]\right)$$
$$+ \left[\left(e_0 a\right)^2\left(1 - \left(e_0 a\right)^2 \nabla^2\right)\right]\left(\left[\frac{\partial^2 w}{\partial x^2} + \frac{d^2 w_0}{dx^2}\right]\times\right.$$

$$\left[(M+m)\frac{\partial^3 u}{\partial x \partial t^2}+M\left(\kappa_{scf}U\right)^2\frac{\partial^3 u}{\partial x^3}+2M\left(\kappa_{scf}U\right)\frac{\partial^3 u}{\partial t \partial x^2}\right]\right]$$

$$+\left[\left(e_0a\right)^2\left(1-\left(e_0a\right)^2\nabla^2\right)\right]\left[\left[\frac{\partial w}{\partial x}+\frac{dw_0}{dx}\right]\times\right.$$

$$\left[(M+m)\frac{\partial^4 u}{\partial x^2 \partial t^2}+2M\left(\kappa_{scf}U\right)\frac{\partial^4 u}{\partial t \partial x^3}+M\left(\kappa_{scf}U\right)^2\frac{\partial^4 u}{\partial x^4}\right]\right]$$

$$=(M+m)\frac{\partial^2 w}{\partial t^2}+M\left(\kappa_{scf}U\right)^2\left(\frac{\partial^2 w}{\partial x^2}+\frac{d^2 w_0}{dx^2}\right)$$

$$+2M\left(\kappa_{scf}U\right)\frac{\partial^2 w}{\partial t \partial x}-\left(e_0a\right)^2\left[(M+m)\frac{\partial^4 w}{\partial x^2 \partial t^2}\right.$$

$$+M\left(\kappa_{scf}U\right)^2\left(\frac{\partial^4 w}{\partial x^4}+\frac{d^4 w_0}{dx^4}\right)+2M\left(\kappa_{scf}U\right)\frac{\partial^4 w}{\partial t \partial x^3}\right].$$

3. Solution technique

To obtain the frequency response of fluid-conveying nanotubes with an initial deflection, a numerical solution technique is developed in this section based on continuation and Galerkin methods (Ghayesh 2012, Kazemirad *et al.* 2013, Farokhi and Ghayesh 2017, Ghayesh *et al.* 2015, Farokhi *et al.* 2017). First of all, a set of dimensionless parameters is introduced as

$$x^*=\frac{x}{L},\ \varphi_{sg}=\frac{l_{sg}}{L},\ \varphi_{nl}=\frac{e_0a}{L},\ w_0^*=\frac{w_0}{d},\ u^*=\frac{u}{d},$$

$$w^*=\frac{w}{d},\ \Xi=L^2\frac{A}{I},\ s=\frac{L}{d},\ F^*=\frac{L^4}{EId}F,\ U^*=L\left(\sqrt{\frac{M}{EI}}\right)U, \quad (16)$$

$$\omega^*=L^2\left(\sqrt{\frac{m+M}{EI}}\right)\omega,\ \Pi_m=\frac{M}{M+m},\ t^*=\frac{1}{L^2}\left(\sqrt{\frac{EI}{m+M}}\right)t.$$

where d is the outer diameter of the nanotube. Moreover, in the present work, h and R are employed to indicate the thickness and outer radius, respectively. Using Eq. (16), the motion equations are first rewritten in a non-dimensional form. Then, applying Galerkin's procedure (Ghayesh and Farokhi 2015, Ghayesh 2018, Ghayesh 2018), the following expressions are used for the sake of discretisation

$$u(x,t)=\sum_{j=1}^{N_x}\phi_j(x)r_j(t),$$

$$w(x,t)=\sum_{j=1}^{N_z}\psi_j(x)q_j(t), \quad (17)$$

in which $(r_j,\ \phi_j)$=(axial generalised coordinate, axial trial function) and $(q_j,\ \psi_j)$=(transverse generalised coordinate, transverse trial function) (Gholipour, Farokhi *et al.* 2015, Ghayesh, Farokhi *et al.* 2016). A clamped-clamped nanotube with an initial deflection in the form of $w_0=A_0\psi_1(x)$ is considered; A_0 denotes the initial deflection coefficient. Employing Eqs. (16) and (17) together with Eqs. (14) and (15) gives

$$\left(\frac{s}{\Xi}\right)\left\{\sum_{j=1}^{N_x}\ddot{r}_j\left(\int_0^1\phi_k\phi_j dx\right)+\left(\kappa_{scf}U\right)^2\sum_{j=1}^{N_x}r_j\left(\int_0^1\phi_k\left(\phi_j\right)'' dx\right)\right.$$

$$\left.+2\left(\kappa_{scf}U\right)\sqrt{\Pi_m}\sum_{j=1}^{N_x}\dot{r}_j\left(\int_0^1\phi_k\left(\phi_j\right)' dx\right)\right\}-\left(\frac{s}{\Xi}\right)\varphi_{nl}^2\times$$

$$\left\{\sum_{j=1}^{N_x}\ddot{r}_j\left(\int_0^1\phi_k\left(\phi_j\right)'' dx\right)+\left(\kappa_{scf}U\right)^2\sum_{j=1}^{N_x}r_j\left(\int_0^1\phi_k\left(\phi_j\right)'''' dx\right)\right.$$

$$\left.+2\left(\kappa_{scf}U\right)\sqrt{\Pi_m}\sum_{j=1}^{N_x}\dot{r}_j\left(\int_0^1\phi_k\left(\phi_j\right)''' dx\right)\right\}$$

$$-\int_0^1\left\{\phi_k\left[A_0\sum_{j=1}^{N_z}\left(\psi_1\right)'\left(\psi_j\right)'q_j+s\sum_{j=1}^{N_x}\left(\phi_j\right)'r_j\right.\right.$$
$$\left.\left.+\frac{1}{2}\sum_{j=1}^{N_z}\sum_{i=1}^{N_z}\left(\psi_j\right)'\left(\psi_i\right)'q_jq_i\right]'\right\}dx$$

$$+\varphi_{sg}^2\int_0^1\left\{\phi_k\left[A_0\sum_{j=1}^{N_z}\left(\psi_1\right)'\left(\psi_j\right)'q_j+s\sum_{j=1}^{N_x}\left(\phi_j\right)'r_j\right.\right.$$
$$\left.\left.+\frac{1}{2}\sum_{j=1}^{N_z}\sum_{i=1}^{N_z}\left(\psi_j\right)'\left(\psi_i\right)'q_jq_i\right]'''\right\}dx=0, \quad (18)$$

$$\sum_{j=1}^{N_z}\left(\int_0^1\psi_k\psi_j dx\right)\ddot{q}_j+2\left(\kappa_{scf}U\right)\sqrt{\Pi_m}\sum_{j=1}^{N_z}\left(\int_0^1\psi_k\left(\psi_j\right)' dx\right)\dot{q}_j$$

$$+\left(\kappa_{scf}U\right)^2\left[\sum_{j=1}^{N_z}\left(\int_0^1\psi_k\left(\psi_j\right)'' dx\right)q_j+A_0\left(\int_0^1\psi_k\left(\psi_1\right)'' dx\right)\right]-\varphi_{nl}^2\times$$

$$\left\{\sum_{j=1}^{N_z}\left(\int_0^1\psi_k\left(\psi_j\right)'' dx\right)\ddot{q}_j+2\left(\kappa_{scf}U\right)\sqrt{\Pi_m}\sum_{j=1}^{N_z}\left(\int_0^1\psi_k\left(\psi_j\right)''' dx\right)\dot{q}_j\right.$$

$$\left.+\left(\kappa_{scf}U\right)^2\left[\sum_{j=1}^{N_z}\left(\int_0^1\psi_k\left(\psi_j\right)'''' dx\right)q_j+A_0\left(\int_0^1\psi_k\left(\psi_1\right)'''' dx\right)\right]\right\}-\varphi_{sg}^2\times$$

$$\sum_{j=1}^{N_z}\left(\int_0^1\psi_k\left(\psi_j\right)^{(6)} dx\right)q_j-\left(\int_0^1\psi_k dx\right)F_1\cos\left(\omega t\right)+\sum_{j=1}^{N_z}\left(\int_0^1\psi_k\left(\psi_j\right)'''' dx\right)q_j$$

$$-\Xi\left(\frac{1}{s}\right)^2\int_0^1\left(\psi_k\left\{\left[\sum_{j=1}^{N_z}\left(\psi_j\right)''q_j+A_0\left(\psi_1\right)''\right]\left[\frac{1}{2}\sum_{j=1}^{N_z}\sum_{i=1}^{N_z}\left(\psi_j\right)'\left(\psi_i\right)'q_jq_i\right.\right.\right.$$

$$\left.+s\sum_{j=1}^{N_x}\left(\phi_j\right)'r_j+A_0\sum_{j=1}^{N_z}\left(\psi_1\right)'\left(\psi_j\right)'q_j\right]+\left(\sum_{j=1}^{N_z}\left(\psi_j\right)'q_j+A_0\left(\psi_1\right)'\right)\times$$

$$\left[s\sum_{j=1}^{N_x}\left(\phi_j\right)'r_j+A_0\sum_{j=1}^{N_z}\left(\psi_1\right)'\left(\psi_j\right)'q_j+\frac{1}{2}\sum_{j=1}^{N_z}\sum_{i=1}^{N_z}\left(\psi_j\right)'\left(\psi_i\right)'q_jq_i\right]'$$

$$-\varphi_{sg}^2\left(\sum_{j=1}^{N_z}\left(\psi_j\right)''q_j+A_0\left(\psi_1\right)''\right)\left[s\sum_{j=1}^{N_x}\left(\phi_j\right)'r_j+A_0\sum_{j=1}^{N_z}\left(\psi_1\right)'\left(\psi_j\right)'q_j\right.$$

$$\left.+\frac{1}{2}\sum_{j=1}^{N_z}\sum_{i=1}^{N_z}\left(\psi_j\right)'\left(\psi_i\right)'q_jq_i\right]''-\varphi_{sg}^2\left(\sum_{j=1}^{N_z}\left(\psi_j\right)'q_j+A_0\left(\psi_1\right)'\right)\times$$

$$\left[s\sum_{j=1}^{N_x}\left(\phi_j\right)'r_j+\frac{1}{2}\sum_{j=1}^{N_z}\sum_{i=1}^{N_z}\left(\psi_j\right)'\left(\psi_i\right)'q_jq_i+A_0\sum_{j=1}^{N_z}\left(\psi_1\right)'\left(\psi_j\right)'q_j\right]'''$$

$$+\left(\frac{s}{\Xi}\right)\varphi_{nl}^2\left(A_0\left(\psi_1\right)''+\sum_{j=1}^{N_z}q_j\left(\psi_j\right)''\right)\left[\left(\kappa_{scf}U\right)^2\sum_{j=1}^{N_x}r_j\left(\phi_j\right)'''\right.$$

$$\left.+\sum_{j=1}^{N_x}\ddot{r}_j\left(\phi_j\right)'+2\left(\kappa_{scf}U\right)\sqrt{\Pi_m}\sum_{j=1}^{N_x}\dot{r}_j\left(\phi_j\right)''\right] \quad (19)$$

$$+\left(\frac{s}{\Xi}\right)\varphi_{nl}^2\left(A_0\left(\psi_1\right)'+\sum_{j=1}^{N_z}q_j\left(\psi_j\right)'\right)\left[\sum_{j=1}^{N_x}\ddot{r}_j\left(\phi_j\right)''+\right.$$

$$\left.\left(\kappa_{scf}U\right)^2\sum_{j=1}^{N_x}r_j\left(\phi_j\right)''''+2\left(\kappa_{scf}U\right)\sqrt{\Pi_m}\sum_{j=1}^{N_x}\dot{r}_j\left(\phi_j\right)'''\right]\right\}\right)dx$$

$$+\Xi\left(\frac{\varphi_{nl}}{s}\right)^2\int_0^1\left(\psi_k\left\{\left(A_0\left(\psi_1\right)''+\sum_{j=1}^{N_z}q_j\left(\psi_j\right)''\right)\times\right.\right.$$

$$\left[s\sum_{j=1}^{N_x}r_j\left(\phi_j\right)'+\frac{1}{2}\sum_{j=1}^{N_z}\sum_{i=1}^{N_z}q_jq_i\left(\psi_j\right)'\left(\psi_i\right)'+A_0\sum_{j=1}^{N_z}q_j\left(\psi_1\right)'\left(\psi_j\right)'\right]$$

$$+\left(A_0\left(\psi_1\right)'+\sum_{j=1}^{N_z}\left(\psi_j\right)'q_j\right)\left[s\sum_{j=1}^{N_x}r_j\left(\phi_j\right)'+A_0\sum_{j=1}^{N_z}q_j\left(\psi_1\right)'\left(\psi_j\right)'\right.$$

$$+\frac{1}{2}\sum_{j=1}^{N_z}\sum_{i=1}^{N_z}q_jq_i\left(\psi_j\right)'\left(\psi_i\right)'\right]'-\varphi_{sg}^2\left(A_0\left(\psi_1\right)''+\sum_{j=1}^{N_z}q_j\left(\psi_j\right)''\right)\times$$

$$\left[s\sum_{j=1}^{N_x}r_j\left(\phi_j\right)'+A_0\sum_{j=1}^{N_z}\left(\psi_1\right)'\left(\psi_j\right)'q_j+\frac{1}{2}\sum_{j=1}^{N_z}\sum_{i=1}^{N_z}q_jq_i\left(\psi_j\right)'\left(\psi_i\right)'\right]''$$

$$-\varphi_{sg}^2\left(A_0\left(\psi_1\right)'+\sum_{j=1}^{N_z}q_j\left(\psi_j\right)'\right)\left[A_0\sum_{j=1}^{N_z}q_j\left(\psi_1\right)'\left(\psi_j\right)'\right.$$

$$+s\sum_{j=1}^{N_x}\left(\phi_j\right)'r_j+\frac{1}{2}\sum_{j=1}^{N_z}\sum_{i=1}^{N_z}q_jq_i\left(\psi_j\right)'\left(\psi_i\right)'\right]''$$

$$+\left(\frac{s}{\Xi}\right)\varphi_{nl}^2\left(A_0\left(\psi_1\right)''+\sum_{j=1}^{N_z}q_j\left(\psi_j\right)''\right)\left[\left(\kappa_{scf}U\right)^2\sum_{j=1}^{N_x}r_j\left(\phi_j\right)'''\right.$$

$$\left.+\sum_{j=1}^{N_x}\ddot{r}_j\left(\phi_j\right)'+2\left(\kappa_{scf}U\right)\sqrt{\Pi_m}\sum_{j=1}^{N_x}\dot{r}_j\left(\phi_j\right)''\right]$$

$$+\left(\frac{s}{\Xi}\right)\varphi_{nl}^2\left(A_0\left(\psi_1\right)'+\sum_{j=1}^{N_z}q_j\left(\psi_j\right)'\right)\times\left[\sum_{j=1}^{N_x}\ddot{r}_j\left(\phi_j\right)''+\right.$$

$$\left.\left(\kappa_{scf}U\right)^2\sum_{j=1}^{N_x}r_j\left(\phi_j\right)''''+2\left(\kappa_{scf}U\right)\sqrt{\Pi_m}\sum_{j=1}^{N_x}\dot{r}_j\left(\phi_j\right)'''\right]\right\}\right)''\right)dx=0.$$

The superscript "*" is neglected for convenience. From Eqs. (18) and (19), a set of discretised coupled differential equations is obtained. The resultant differential equations are numerically solved by a continuation method (Farokhi and Ghayesh 2018, Ghayesh and Farajpour 2018).

4. Results and discussion

Numerical results are presented in the following section for a clamped-clamped nanosystem with 20 degrees of freedom (ten degrees of freedom along each direction). The tube mass density, Poisson's ratio and Young's constant are 1024 kg/m³, 0.3 and 610 MPa, respectively (Shen 2011). These material properties belong to small-scale lipid tubules, which are a class of soft ultrasmall tubes. A dimensionless damping coefficient (c_d=0.25) is introduced in the calculation. Furthermore, the tube geometric features are h=66.0 nm, R=290.5 nm, and L/d=20. The dimensionless parameters are κ_{scf}=1.0788, Π_m=0.5915, Ξ=4006.9411, φ_{sg} = 0.04 and φ_{nl} = 0.08. The nonlinear frequency response of nanotubes with an initial deflection conveying flow is illustrated in Fig. 2 for U=3.65, κ_{scf}=1.0788, A_0=0.10, F_1=2.5, and ω_1=16.3803.

Table 1 Verification study for the linear vibration of simply-supported nanoscale tubes

Mode number	Classical model	Strain gradient model	Nonlocal model	NSGT (present)	NSGT (Li, Li et al. 2017)
1	9.8696	9.9906	9.8502	9.9710	9.97
2	39.4784	41.3808	39.1704	41.0579	41.06
3	88.8264	98.1951	87.2893	96.4957	96.50
4	157.9137	186.4976	153.1508	180.8726	180.87

The maximum values of u and w are plotted versus the frequency ratio (excitation frequency/natural frequency). A hardening-type frequency response involving two distinct bifurcation points at ω/ω_1=1.1194 and 1.0238 is observed. In addition, slight modal interactions are seen in the nonlinear frequency response of the nanotube around ω/ω_1=1.0171 for motions in both directions. Figures 3 and 4 indicates the total transverse displacement of the nanotube in one oscillation period for two important cases, namely when modal interactions are strongest and at peak oscillation amplitude, respectively.

First of all, the accuracy and validity of the present model are demonstrated in Table 1 by making a comparison between the obtained results and those available in the literature for the frequencies values of uniform nanobeams. The difference between the nonlocal, classical, NSGT and strain gradient models can be calculated from this table. For nonlocal, classical, NSGT and strain gradient models, scale parameters are set to $<\varphi_{sg},\varphi_{nl}>$ = $<0,0,02>$, $<\varphi_{sg},\varphi_{nl}>$ = $<0,0>$, $<\varphi_{sg},\varphi_{nl}>$ = $<0.05,0.02>$ and $<\varphi_{sg},\varphi_{nl}>$ = $<0.05,0>$. respectively. For an appropriate comparison, the features of the nanobeam are the same as those assumed in Ref. (Li, Li et al. 2017). From the table, a reasonable agreement is observed, demonstrating the validity of the proposed modelling. Moreover, the strain gradient model leads to the highest dimensionless frequencies $(\omega^*=\omega\sqrt{\rho L^2/E})$ whereas the smallest ones are obtained by the nonlocal model.

The physical explanation for the observed increase in the frequency parameter with increasing strain gradient influence is that the stiffness of structural components at ultrasmall levels is related to strain gradients. The stiffness is higher for stronger strain gradient influences, and this causes the tube to vibrate at a higher natural frequency. However, the nonlocal influence makes the nanosystem experience lower frequency parameters. The physical explanation for this phenomenon is rooted in the reduction of structural stiffness with enhancing nonlocal influences.

The influence of an initial deflection on the nonlinear frequency response of the nanotube conveying flow is illustrated in Fig. 5 for U=4.0 and F_1=2.5. This figure reveals the importance of the consideration of the initial deflection on the frequency response. When there is a slight initial deflection in the nanotube, a hardening-type nonlinearity governs the frequency response. Nonetheless, for larger initial deflections, the frequency response is governed by a softening-hardening response. In fact, the nonlinear frequency response of the system can be tailored by creating an initial deflection during manufacturing
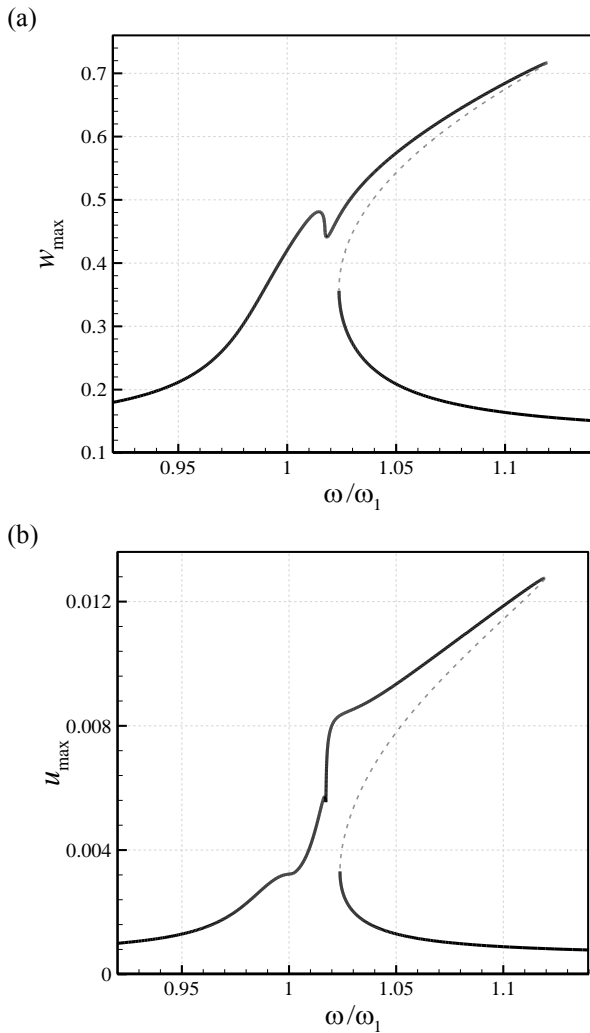
(a)

(b)

Fig. 2 Nonlinear frequency response of the nanotube; (a) w_{max} at x=0.5; (b) u_{max} at x=0.66; dashed line: unstable branch; solid line: stable branch.
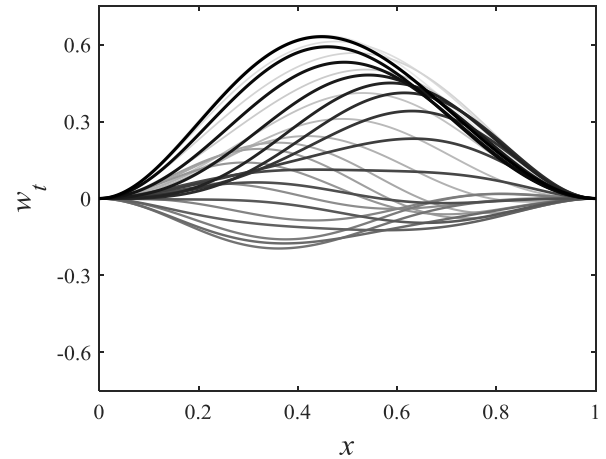

Fig. 3 Total transverse displacement (w_t=w+w_0) of the fluid-conveying nanotube of Fig. 2 in one period of oscillation at ω/ω_1 = 1.0171 (i.e. when modal interactions are strongest).
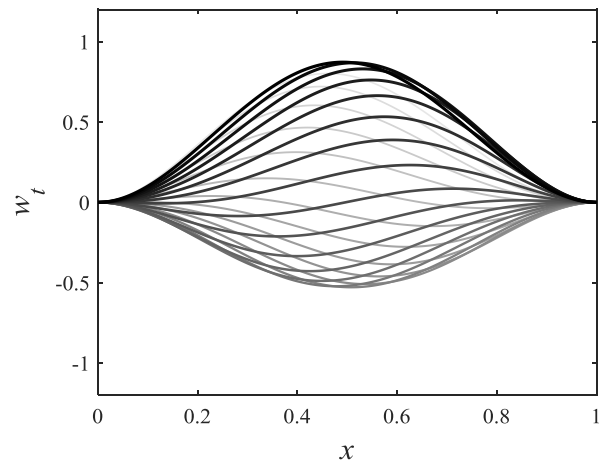

Fig. 4 Total transverse displacement (w_t=w+w_0) of the fluid-conveying nanotube of Fig. 2 in one period of oscillation at ω/ω_1 = 1.1194 (i.e. at peak oscillation amplitude).

process. This is important in ultrasmall electromechanical systems in which there is a fluid-conveying nanotube. Another significant finding is that modal interactions, which are found in the frequency response for small initial deflections (especially, for the axial motion), can be removed by creating higher initial deflections in the nanotube.

The significance of size effects on the coupled nonlinear frequency response of the nanotube conveying flow is indicated in Fig. 6. The initial deflection coefficient and flow speed are, respectively, A_0=0.15 and U=4.0. The speed correction coefficient and the amplitude of applied loading are set to κ_{scf}=1.0788 and F_1=3.0, respectively. The frequency response is plotted for the classical theory (CT) and NSGT. In the CT, size effects are neglected (i.e. φ_{sg} = 0.0 and φ_{nl} = 0.0) while the size parameters of the NSGT are set to φ_{sg} = 0.04 and φ_{nl} = 0.08. The resonance frequency of the CT is noticeably higher than that of the NSGT due to the decreasing effect of stress nonlocality on the stiffness. In addition, the CT overestimates modal interactions, especially for the axial motion.

Figures 7 and 8 illustrate the nonlinear coupled frequency response of the nanotube conveying flow for slip and no-slip conditions. In both figures, the initial deflection coefficient and the amplitude of applied loading are assumed as A_0=0.15 and F_1=2.5, respectively. In Fig. 7, the flow speed is set to U=3.0 whereas a value of 6.50 is considered for the dimensionless flow speed in Fig. 8. Depending on the flow speed, slip condition effect can increase or decrease the resonance frequency. When the flow speed is U=3.0, slip effects result in a reduction in the resonance frequency whereas relative motions at the wall are associated with a substantial increase in the resonance frequency for higher flow speed.

5. Conclusions

This paper dealt with the development of a size-dependent nonlinear model for nanotubes conveying flow when there is an initial deflection in the geometry. The Euler-Bernoulli model was applied in conjunction with the NSGT for formulating the nonlinear frequency response of
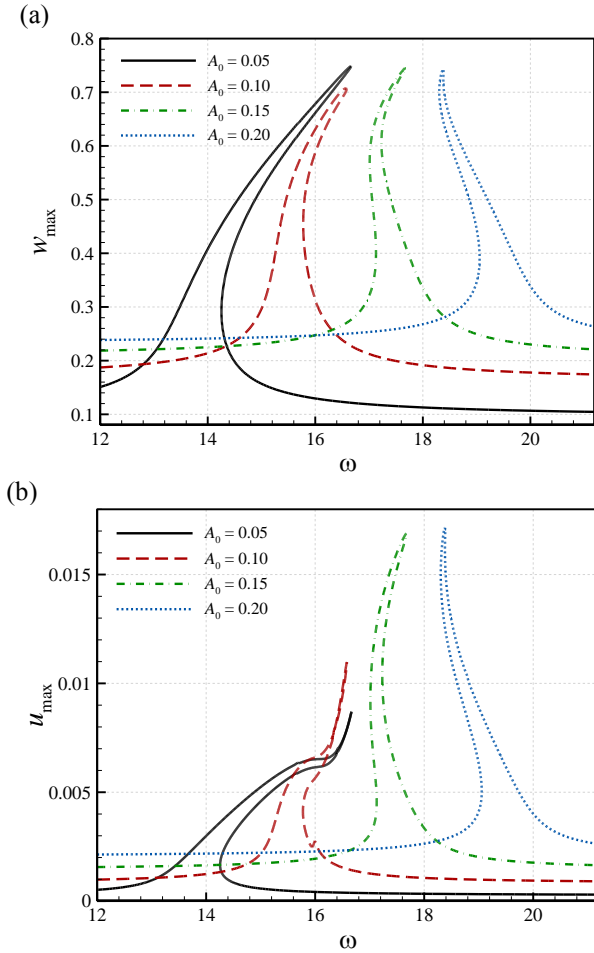
(a)

(b)

Fig. 5 Effect of an initial deflection on the nonlinear frequency response of the nanotube conveying flow; (a) w_{max} at x=0.5 (b) u_{max} at x=0.66
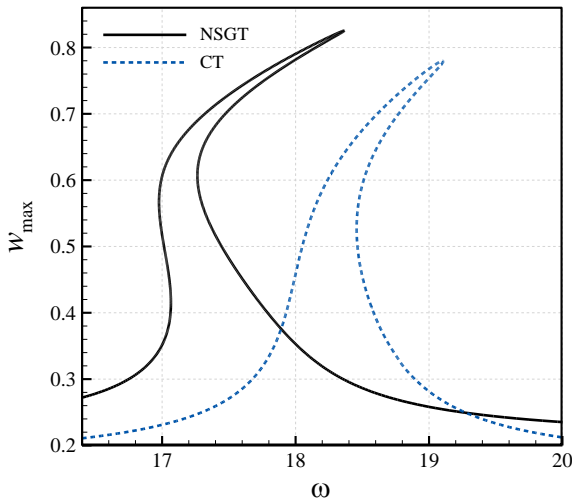

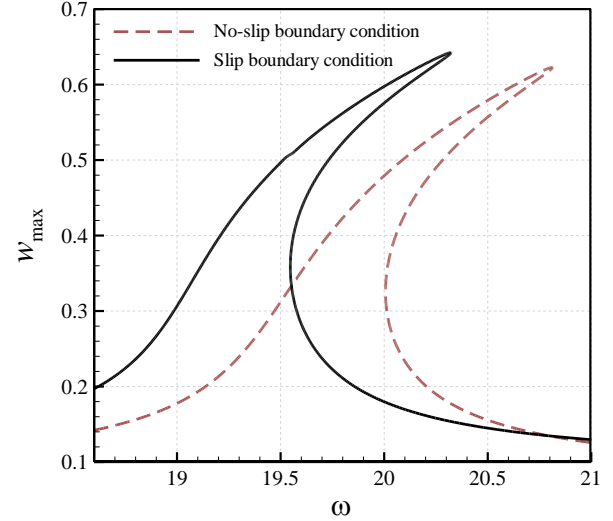Fig. 6 Nonlinear frequency response of the nanotube conveying flow based on the CT and NSGT for w_{max} at x=0.5

Fig. 7. Nonlinear frequency response of the nanosystem for slip and no-slip conditions for w_{max} at x=0.5; U=3.0, A_0=0.15 and F_1=2.5.
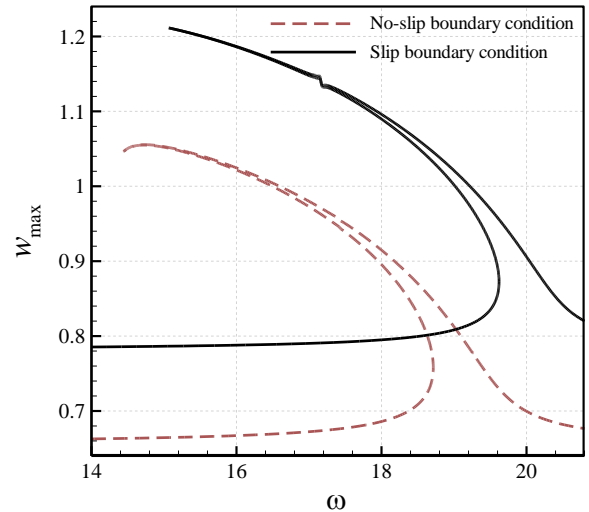

Fig. 8. Nonlinear frequency response of the nanosystem for slip and no-slip conditions for w_{max} at x=0.5; U=6.50, A_0=0.15 and F_1=2.5

given. The discretisation of the motion equations was performed using Galerkin's technique, leading to a system of nonlinear ordinary differential equations. Then, a continuation method of solution was developed for solving the system of equations. The present modelling and methodology would be helpful for different nanoengineering applications such as ultrasmall pipettes, nanofluid filtration, drug delivery and nanofluidics.

Numerical results showed the importance of the effect of initial deflection on the frequency response of nanotubes conveying flow. For a slight initial deflection, the nanosystem displays a hardening-type frequency response. However, when the initial deflection is larger, the frequency response of the nanosystem is governed by a softening-hardening response. Furthermore, it was indicated that enhancing the nonlocal influence reduces the frequency parameter of ultrasmall tubes due to the reduction of their stiffness while boosting the strain gradient influence causes

the nanosystem. To capture slip effects on the nonlinear coupled motion, the Beskok–Karniadakis model was used. Formulating kinetic and elastic energies and applying Hamilton's approach, the nonlinear motion equations were

the opposite trend since it generally improves the tube stiffness. Moreover, modal interactions are substantially influenced by the initial deflection. The CT predicts higher resonance frequencies than the NSGT because of the decreasing influence of stress nonlocality on the stiffness. Furthermore, the CT is not reliable since it overestimates modal interactions. Slip condition effects greatly depend on the flow speed. For comparatively small flow speeds, slip effects reduce the resonance frequency. However, slip effects are linked with a noticeable increase in the resonance frequency of the nanosystem when the flow speed is higher.

References

Ahouel, M., Houari, M.S.A., Bedia, E. and Tounsi, A. (2016), "Size-dependent mechanical behavior of functionally graded trigonometric shear deformable nanobeams including neutral surface position concept", *Steel Compos. Struct.*, **20**(5), 963-981. https://doi.org/10.12989/scs.2016.20.5.963.

Akgöz, B. and Civalek, Ö. (2011), "Buckling analysis of cantilever carbon nanotubes using the strain gradient elasticity and modified couple stress theories", *J. Comput. Theoretical Nanosci.*, **8**(9), 1821-1827.

Akgöz, B. and Civalek, Ö. (2013), "A size-dependent shear deformation beam model based on the strain gradient elasticity theory", *Int. J. Eng. Sci.*, **70**, 1-14. https://doi.org/10.1016/j.ijengsci.2013.04.004.

Akgöz, B. and Civalek, Ö. (2014), "Longitudinal vibration analysis for microbars based on strain gradient elasticity theory", *J. Vib. Control*, **20**(4), 606-616. https://doi.org/10.1177%2F1077546312463752.

Akgöz, B. and Civalek, Ö. (2017), "Effects of thermal and shear deformation on vibration response of functionally graded thick composite microbeams", *Compos. Part B Eng.*, **129**, 77-87. https://doi.org/10.1016/j.compositesb.2017.07.024.

Al-Basyouni, K., Tounsi, A. and Mahmoud, S. (2015), "Size dependent bending and vibration analysis of functionally graded micro beams based on modified couple stress theory and neutral surface position", *Compos. Struct.*, **125**, 621-630. https://doi.org/10.1016/j.compstruct.2014.12.070.

Amiri, A., Talebitooti, R. and Li, L. (2018), "Wave propagation in viscous-fluid-conveying piezoelectric nanotubes considering surface stress effects and Knudsen number based on nonlocal strain gradient theory", *Europe Phys. J. Plus*, **133**(7), 252. https://doi.org/10.1140/epjp/i2018-12077-y.

Arefi, M. (2019), "Static analysis of laminated piezo-magnetic size-dependent curved beam based on modified couple stress theory", *Struct. Eng. Mech.*, **69**(2), 145-153. https://doi.org/10.12989/sem.2019.69.2.145.

Asemi, S.R. and Farajpour, A. (2014), "Vibration characteristics of double-piezoelectric-nanoplate-systems", *IET Micro Nano Lett.*, **9**(4), 280-285. https://doi.org/10.1049/mnl.2013.0741.

Askari, H. and Esmailzadeh, E. (2017), "Forced vibration of fluid conveying carbon nanotubes considering thermal effect and nonlinear foundations", *Compos. Part B Eng.*, **113**, 31-43.

Bahaadini, R., Saidi, A.R. and Hosseini, M. (2018), "On dynamics of nanotubes conveying nanoflow", *Int. J. Eng. Sci.*, **123**, 181-196. https://doi.org/10.1016/j.ijengsci.2017.11.010.

Bakhadda, B., Bouiadjra, M.B., Bourada, F., Bousahla, A.A., Tounsi, A. and Mahmoud, S. (2018), "Dynamic and bending analysis of carbon nanotube-reinforced composite plates with elastic foundation", *Wind Struct.*, **27**(5), 311-324. https://doi.org/10.12989/was.2018.27.5.311.

Bedia, W.A., Houari, M.S.A., Bessaim, A., Bousahla, A.A.,

Tounsi, A., Saeed, T. and Alhodaly, M.S. (2019), "A New Hyperbolic Two-Unknown Beam Model for Bending and Buckling Analysis of a Nonlocal Strain Gradient Nanobeams", *J. Nano Res.*, **57**, 175-191. https://doi.org/10.4028/www.scientific.net/JNanoR.57.175.

Belkorissat, I., Houari, M.S.A., Tounsi, A., Bedia, E. and Mahmoud, S. (2015), "On vibration properties of functionally graded nano-plate using a new nonlocal refined four variable model", *Steel Compos. Struct*, **18**(4), 1063-1081. https://doi.org/10.12989/scs.2015.18.4.1063.

Bellifa, H., Benrahou, K.H., Bousahla, A.A., Tounsi, A. and Mahmoud, S. (2017), "A nonlocal zeroth-order shear deformation theory for nonlinear postbuckling of nanobeams", *Struct. Eng. Mech.*, **62**(6), 695-702. https://doi.org/10.12989/sem.2017.62.6.695.

Benahmed, A., Fahsi, B., Benzair, A., Zidour, M., Bourada, F. and Tounsi, A. (2019), "Critical buckling of functionally graded nanoscale beam with porosities using nonlocal higher-order shear deformation", *Struct. Eng. Mech.*, **69**(4), 457-466. https://doi.org/10.12989/sem.2019.69.4.457.

Besseghier, A., Houari, M.S.A., Tounsi, A. and Mahmoud, S. (2017), "Free vibration analysis of embedded nanosize FG plates using a new nonlocal trigonometric shear deformation theory", *Smart Struct. Syst.*, **19**(6), 601-614. https://doi.org/10.12989/sss.2017.19.6.601.

Bouadi, A., Bousahla, A.A., Houari, M.S.A., Heireche, H. and Tounsi, A. (2018), "A new nonlocal HSDT for analysis of stability of single layer graphene sheet", *Advances in nano research*, **6**(2), 147-162. https://doi.org/10.12989/anr.2018.6.2.147.

Bouafia, K., Kaci, A., Houari, M.S.A., Benzair, A. and Tounsi, A. (2017), "A nonlocal quasi-3D theory for bending and free flexural vibration behaviors of functionally graded nanobeams", *Smart Struct. Syst.*, **19**(2), 115-126. https://doi.org/10.12989/sss.2017.19.2.115.

Bounouara, F., Benrahou, K.H., Belkorissat, I. and Tounsi, A. (2016), "A nonlocal zeroth-order shear deformation theory for free vibration of functionally graded nanoscale plates resting on elastic foundation", *Steel Compos. Struct.*, **20**(2), 227-249. https://doi.org/10.12989/scs.2016.20.2.227.

Bourada, F., Amara, K., Bousahla, A.A., Tounsi, A. and Mahmoud, S. (2018), "A novel refined plate theory for stability analysis of hybrid and symmetric S-FGM plates", *Struct. Eng. Mech.*, **68**(6), 661-675. https://doi.org/10.12989/sem.2018.68.6.661.

Chaht, F.L., Kaci, A., Houari, M.S.A., Tounsi, A., Bég, O.A. and Mahmoud, S. (2015), "Bending and buckling analyses of functionally graded material (FGM) size-dependent nanoscale beams including the thickness stretching effect", *Steel Compos. Struct.*, **18**(2), 425-442. https://doi.org/10.12989/scs.2015.18.2.425.

Civalek, Ö. and Akgöz, B. (2013), "Vibration analysis of micro-scaled sector shaped graphene surrounded by an elastic matrix", *Comput. Mater. Sci.*, **77**, 295-303. https://doi.org/10.1016/j.commatsci.2013.04.055.

Demir, Ç. and Civalek, Ö. (2017), "A new nonlocal FEM via Hermitian cubic shape functions for thermal vibration of nano beams surrounded by an elastic matrix", *Compos. Struct.*, **168**, 872-884. https://doi.org/10.1016/j.compstruct.2017.02.091.

Demir, Ç. and Civalek, Ö. (2017), "On the analysis of microbeams", *Int. J. Eng. Sci.*, **121**, 14-33. https://doi.org/10.1016/j.ijengsci.2017.08.016.

Demir, Ç., Mercan, K. and Civalek, Ö. (2016), "Determination of critical buckling loads of isotropic, FGM and laminated truncated conical panel", *Compos. Part B Eng.*, **94**, 1-10. https://doi.org/10.1016/j.compositesb.2016.03.031.

Draoui, A., Zidour, M., Tounsi, A. and Adim, B. (2019), "Static and Dynamic Behavior of Nanotubes-Reinforced Sandwich

Plates Using (FSDT)", *J. Nano Res.*, **57**, 117-135. https://doi.org/10.4028/www.scientific.net/JNanoR.57.117.

Ebrahimi, F. and Barati, M.R. (2018), "A nonlocal strain gradient refined plate model for thermal vibration analysis of embedded graphene sheets via DQM", *Struct. Eng. Mech.*, **66**(6), 693-701. https://doi.org/10.12989/sem.2018.66.6.693.

Ebrahimi, F. and Dabbagh, A. (2018), "NSGT-based acoustical wave dispersion characteristics of thermo-magnetically actuated double-nanobeam systems", *Struct. Eng. Mech.*, **68**(6), 701-711. https://doi.org/10.12989/sem.2018.68.6.701.

Ebrahimi, F., Haghi, P. and Dabbagh, A. (2018), "Analytical wave dispersion modeling in advanced piezoelectric double-layered nanobeam systems", *Struct. Eng. Mech.*, **67**(2), 175-183. https://doi.org/10.12989/sem.2018.67.2.175.

Eringen, A.C. and Edelen, D. (1972), "On nonlocal elasticity", *Int. J. Eng. Sci.*, **10**(3), 233-248. https://doi.org/10.1016/0020-7225(72)90039-0.

Farajpour, A., Ghayesh, M.H. and Farokhi, H. (2018), "A review on the mechanics of nanostructures", *Int. J. Eng. Sci.*, **133**, 231-263. https://doi.org/10.1016/j.ijengsci.2018.09.006.

Farajpour, A., Ghayesh, M.H. and Farokhi, H. (2019), "Large-amplitude coupled scale-dependent behaviour of geometrically imperfect NSGT nanotubes", *J. Mech. Sci.*, **150**, 510-525. https://doi.org/10.1016/j.ijmecsci.2018.09.043.

Farajpour, A., Rastgoo, A. and Farajpour, M. (2017), "Nonlinear buckling analysis of magneto-electro-elastic CNT-MT hybrid nanoshells based on the nonlocal continuum mechanics", *Compos. Struct.*, **180**, 179-191. https://doi.org/10.1016/j.compstruct.2017.07.100.

Farajpour, M., Shahidi, A. and Farajpour, A. (2018), "A nonlocal continuum model for the biaxial buckling analysis of composite nanoplates with shape memory alloy nanowires", *Mater. Res. Exp.*, **5**(3), 035026. https://doi.org/10.1088/2053-1591/aab3a9.

Farajpour, M., Shahidi, A., Tabataba'i-Nasab, F. and Farajpour, A. (2018), "Vibration of initially stressed carbon nanotubes under magneto-thermal environment for nanoparticle delivery via higher-order nonlocal strain gradient theory", *Europe Phys. J. Plus*, **133**(6), 219. https://doi.org/10.1140/epjp/i2018-12039-5.

Farajpour, M.R., Shahidi, A.R., Tabataba'i-Nasab, F. and Farajpour, A. (2018), "Vibration of initially stressed carbon nanotubes under magneto-thermal environment for nanoparticle delivery via higher-order nonlocal strain gradient theory", *European Phys. J. Plus*, **133**(6), 219. https://doi.org/10.1140/epjp/i2018-12039-5.

Farajpour, M.R., Shahidi, A.R., Hadi, A. and Farajpour, A. (2019), "Influence of initial edge displacement on the nonlinear vibration, electrical and magnetic instabilities of magneto-electro-elastic nanofilms", *Mech. Adv. Mater. Struct.*, **26**(17), 1469-1481. https://doi.org/10.1080/15376494.2018.1432820.

Farajpour, M.R., Shahidi, A.R. and Farajpour, A. (2019), "Influence of shear preload on wave propagation in small-scale plates with nanofibers", *Struct. Eng. Mech.*, **70**(4), 407-420. https://doi.org/10.12989/sem.2019.70.4.407.

Farajpour, A., Farokhi, H., Ghayesh, M.H. and Hussain, S. (2018), "Nonlinear mechanics of nanotubes conveying fluid", *J. Eng. Sci.*, **133**, 132-143. https://doi.org/10.1016/j.ijengsci.2018.08.009.

Farajpour, A., Ghayesh, M.H. and Farokhi, H. (2019), "Large-amplitude coupled scale-dependent behaviour of geometrically imperfect NSGT nanotubes", *J. Mech. Sci.*, **150**, 510-525. https://doi.org/10.1016/j.ijmecsci.2018.09.043.

Farokhi, H. and Ghayesh, M.H. (2015), "Nonlinear dynamical behaviour of geometrically imperfect microplates based on modified couple stress theory", *J. Mech. Sci.*, **90**, 133-144. https://doi.org/10.1016/j.ijmecsci.2014.11.002.

Farokhi, H. and Ghayesh, M.H. (2018), "Nonlinear mechanical behaviour of microshells", *Int. J. Eng. Sci.*, **127**, 127-144. https://doi.org/10.1016/j.ijengsci.2018.02.009.

Farokhi, H. and Ghayesh, M.H. (2018), "Nonlinear mechanics of electrically actuated microplates", *Int. J. Eng. Sci.*, **123**, 197-213. https://doi.org/10.1016/j.ijengsci.2017.08.017.

Farokhi, H. and Ghayesh, M.H. (2018), "Supercritical nonlinear parametric dynamics of Timoshenko microbeams", *Communication Nonlinear Sci. Numeric. Simul.*, **59**, 592-605. https://doi.org/10.1016/j.cnsns.2017.11.033.

Farokhi, H., Ghayesh, M.H. and Hussain, S. (2016), "Large-amplitude dynamical behaviour of microcantilevers", *Int. J. Eng. Sci.*, **106**, 29-41. https://doi.org/10.1016/j.ijengsci.2016.03.002.

Farokhi, H. and Ghayesh, M.H. (2017), "Nonlinear resonant response of imperfect extensible Timoshenko microbeams", *J. Mech. Mater. Design*, **13**(1), 43-55. https://doi.org/10.1007/s10999-015-9316-z.

Farokhi, H., Ghayesh, M.H. and Gholipour, A. (2017), "Dynamics of functionally graded micro-cantilevers", *J. Eng. Sci.*, **115**, 117-130. https://doi.org/10.1016/j.ijengsci.2017.01.004.

Filiz, S. and Aydogdu, M. (2015), "Wave propagation analysis of embedded (coupled) functionally graded nanotubes conveying fluid", *Compos. Struct.*, **132**, 1260-1273. https://doi.org/10.1016/j.compstruct.2015.07.043.

Gao, Y., Xiao, W.S. and Zhu, H. (2019), "Nonlinear vibration of functionally graded nano-tubes using nonlocal strain gradient theory and a two-steps perturbation method", *Struct. Eng. Mech.*, **69**(2), 205-219. https://doi.org/10.12989/sem.2019.69.2.205.

Ghayesh, M.H. (2018), "Dynamics of functionally graded viscoelastic microbeams", *Int. J. Eng. Sci.*, **124**, 115-131. https://doi.org/10.1016/j.ijengsci.2017.11.004.

Ghayesh, M.H. (2018), "Functionally graded microbeams: Simultaneous presence of imperfection and viscoelasticity", *J. Mech. Sci.*, **140**, 339-350. https://doi.org/10.1016/j.ijmecsci.2018.02.037.

Ghayesh, M.H. (2018), "Nonlinear vibration analysis of axially functionally graded shear-deformable tapered beams", *Applied Mathematical Modelling*, **59**, 583-596. https://doi.org/10.1016/j.apm.2018.02.017.

Ghayesh, M.H., Amabili, M. and Farokhi, H. (2013), "Nonlinear forced vibrations of a microbeam based on the strain gradient elasticity theory", *Int. J. Eng. Sci.*, **63**, 52-60. https://doi.org/10.1016/j.ijengsci.2012.12.001.

Ghayesh, M.H., Amabili, M. and Farokhi, H. (2013), "Three-dimensional nonlinear size-dependent behaviour of Timoshenko microbeams", *Int. J. Eng. Sci.*, **71**, 1-14. https://doi.org/10.1016/j.ijengsci.2013.04.003.

Ghayesh, M.H. and Farajpour, A. (2018), "Nonlinear mechanics of nanoscale tubes via nonlocal strain gradient theory", *Int. J. Eng. Sci.*, **129**, 84-95. https://doi.org/10.1016/j.ijengsci.2018.04.003.

Ghayesh, M.H. and Farokhi, H. (2015), "Chaotic motion of a parametrically excited microbeam", *Int. J. Eng. Sci.*, **96**, 34-45. https://doi.org/10.1016/j.ijengsci.2015.07.004.

Ghayesh, M.H., Farokhi, H. and Alici, G. (2016), "Size-dependent performance of microgyroscopes", *Int. J. Eng. Sci.*, **100**, 99-111. https://doi.org/10.1016/j.ijengsci.2015.11.003.

Gholipour, A., Farokhi, H. and Ghayesh, M.H. (2015), "In-plane and out-of-plane nonlinear size-dependent dynamics of microplates", *Nonlinear Dynam.*, **79**(3), 1771-1785. https://doi.org/10.1007/s11071-014-1773-7.

Ghayesh, M.H., Farokhi, H. and Alici, G. (2015), "Subcritical parametric dynamics of microbeams", *J. Eng. Sci.*, **95**, 36-48. https://doi.org/10.1016/j.ijengsci.2015.06.001.

Ghayesh, M.H. (2012), "Subharmonic dynamics of an axially accelerating beam", *Archive Appl. Mech.*, **82**(9), 1169-1181. https://doi.org/10.1007/s00419-012-0609-5.

Ghayesh, M.H. and Farajpour, A. (2019), "A review on the mechanics of functionally graded nanoscale and microscale structures", *J. Eng. Sci.*, **137**, 8-36. https://doi.org/10.1016/j.ijengsci.2018.12.001.

Ghayesh, M.H., Farokhi, H. and Farajpour, A. (2019), "Global dynamics of fluid conveying nanotubes", *J. Eng. Sci.*, **135**, 37-57. https://doi.org/10.1016/j.ijengsci.2018.11.003.

Hamza-Cherif, R., Meradjah, M., Zidour, M., Tounsi, A., Belmahi, S. and Bensattalah, T. (2018), "Vibration analysis of nano beam using differential transform method including thermal effect", *J. Nano Res.*, **54**, 1-14. https://doi.org/10.4028/www.scientific.net/JNanoR.54.1.

Kadari, B., Bessaim, A., Tounsi, A., Heireche, H., Bousahla, A.A. and Houari, M.S.A. (2018), "Buckling analysis of orthotropic nanoscale plates resting on elastic foundations", *J. Nano Res.*, **55**, 42-56. https://doi.org/10.4028/www.scientific.net/JNanoR.55.42.

Karami, B., Janghorban, M., Shahsavari, D. and Tounsi, A. (2018), "A size-dependent quasi-3D model for wave dispersion analysis of FG nanoplates", *Steel Compos. Struct.*, **28**(1), 99-110. https://doi.org/10.12989/scs.2018.28.1.099.

Karami, B., Janghorban, M. and Tounsi, A. (2017), "Effects of triaxial magnetic field on the anisotropic nanoplates", *Steel Compos. Struct.*, **25**(3), 361-374. https://doi.org/10.12989/scs.2017.25.3.361.

Karami, B., Janghorban, M. and Tounsi, A. (2018), "Galerkin's approach for buckling analysis of functionally graded anisotropic nanoplates/different boundary conditions", *Eng. Comput.*, 1-20. https://doi.org/10.1007/s00366-018-0664-9.

Karami, B., Janghorban, M. and Tounsi, A. (2018), "Nonlocal strain gradient 3D elasticity theory for anisotropic spherical nanoparticles", *Steel Compos. Struct.*, **27**(2), 201-216. https://doi.org/10.12989/scs.2018.27.2.201.

Karami, B., Janghorban, M. and Tounsi, A. (2018), "Variational approach for wave dispersion in anisotropic doubly-curved nanoshells based on a new nonlocal strain gradient higher order shell theory", *Thin-Walled Struct.*, **129**, 251-264. https://doi.org/10.1016/j.tws.2018.02.025.

Karami, B., Janghorban, M. and Tounsi, A. (2019), "On exact wave propagation analysis of triclinic material using three-dimensional bi-Helmholtz gradient plate model", *Struct. Eng. Mech.*, **69**(5), 487-497. https://doi.org/10.12989/sem.2019.69.5.487.

Karami, B., Shahsavari, D., Janghorban, M. and Tounsi, A. (2019), "Resonance behavior of functionally graded polymer composite nanoplates reinforced with graphene nanoplatelets", *J. Mech. Sci.*, **156**, 94-105. https://doi.org/10.1016/j.ijmecsci.2019.03.036.

Kazemirad, S., Ghayesh, M.H. and Amabili, M. (2013), "Thermo-mechanical nonlinear dynamics of a buckled axially moving beam", *Archive Appl. Mech.*, **83**(1), 25-42. https://doi.org/10.1007/s00419-012-0630-8.

Khetir, H., Bouiadjra, M.B., Houari, M.S.A., Tounsi, A. and Mahmoud, S. (2017), "A new nonlocal trigonometric shear deformation theory for thermal buckling analysis of embedded nanosize FG plates", *Struct. Eng. Mech.*, **64**(4), 391-402. https://doi.org/10.12989/sem.2017.64.4.391.

Li, X., Li, L., Hu, Y., Ding, Z. and Deng, W. (2017), "Bending, buckling and vibration of axially functionally graded beams based on nonlocal strain gradient theory", *Compos. Struct.*, **165**, 250-265. https://doi.org/10.1016/j.compstruct.2017.01.032.

Liang, F. and Su, Y. (2013), "Stability analysis of a single-walled carbon nanotube conveying pulsating and viscous fluid with nonlocal effect", *Appl. Math. Modell.*, **37**(10-11), 6821-6828. https://doi.org/10.1016/j.apm.2013.01.053.

Lim, C., Zhang, G. and Reddy, J. (2015), "A higher-order nonlocal elasticity and strain gradient theory and its applications in wave propagation", *J. Mech. Phys. Solid.*, **78**, 298-313. https://doi.org/10.1016/j.jmps.2015.02.001.

Malekzadeh, P., Haghighi, M.G. and Shojaee, M. (2014), "Nonlinear free vibration of skew nanoplates with surface and small scale effects", *Thin Wall Struct.*, **78**, 48-56. https://doi.org/10.1016/j.tws.2013.10.027.

Malekzadeh, P. and Shojaee, M. (2015), "A two-variable first-order shear deformation theory coupled with surface and nonlocal effects for free vibration of nanoplates", *J. Vib. Control*, **21**(14), 2755-2772. https://doi.org/10.1177/1077546313516667.

Malekzadeh, P. and Farajpour, A. (2012), "Axisymmetric free and forced vibrations of initially stressed circular nanoplates embedded in an elastic medium", *Acta Mechanica*, **223**(11), 2311-2330. https://doi.org/10.1007/s00707-012-0706-0.

Malikan, M. (2017), "Electro-mechanical shear buckling of piezoelectric nanoplate using modified couple stress theory based on simplified first order shear deformation theory", *Appl. Math. Modell.*, **48**, 196-207. https://doi.org/10.1016/j.apm.2017.03.065.

Maraghi, Z.K., Arani, A.G., Kolahchi, R., Amir, S. and Bagheri, M. (2013), "Nonlocal vibration and instability of embedded DWBNNT conveying viscose fluid", *Compos. Part B Eng.*, **45**(1), 423-432. https://doi.org/10.1016/j.compositesb.2012.04.066.

Mercan, K. and Civalek, Ö. (2016), "DSC method for buckling analysis of boron nitride nanotube (BNNT) surrounded by an elastic matrix", *Compos. Struct.*, **143**, 300-309. https://doi.org/10.1016/j.compstruct.2016.02.040.

Mercan, K. and Civalek, Ö. (2017), "Buckling analysis of Silicon carbide nanotubes (SiCNTs) with surface effect and nonlocal elasticity using the method of HDQ", *Compos. Part B Eng.*, **114**, 34-45. https://doi.org/10.1016/j.compositesb.2017.01.067.

Mohammadi, M. and Rastgoo, A. (2019), "Nonlinear vibration analysis of the viscoelastic composite nanoplate with three directionally imperfect porous FG core", *Struct. Eng. Mech.*, **69**(2), 131-143. https://doi.org/10.12989/sem.2019.69.2.131.

Mohammadi, M., Farajpour, A., Goodarzi, M. and Heydarshenas, R. (2013), "Levy type solution for nonlocal thermo-mechanical vibration of orthotropic mono-layer graphene sheet embedded in an elastic medium", *J. Solid Mech.*, **5**(2), 116-132.

Mohammadi, M., Farajpour, A., Goodarzi, M., Dinari, F. (2014), "Thermo-mechanical vibration analysis of annular and circular graphene sheet embedded in an elastic medium", Latin American J. Solids Struct., **11**(4), 659-682. http://dx.doi.org/10.1590/S1679-78252014000400007.

Mokhtar, Y., Heireche, H., Bousahla, A.A., Houari, M.S.A., Tounsi, A. and Mahmoud, S. (2018), "A novel shear deformation theory for buckling analysis of single layer graphene sheet based on nonlocal elasticity theory", *Smart Struct. Syst.*, **21**(4), 397-405. https://doi.org/10.12989/sss.2018.21.4.397.

Mouffoki, A., Bedia, E., Houari, M.S.A., Tounsi, A. and Mahmoud, S. (2017), "Vibration analysis of nonlocal advanced nanobeams in hygro-thermal environment using a new two-unknown trigonometric shear deformation beam theory", *Smart Struct. Syst.*, **20**(3), 369-383. https://doi.org/10.12989/sss.2017.20.3.369.

Murmu, T. and Adhikari, S. (2013), "Nonlocal mass nanosensors based on vibrating monolayer graphene sheets", *Sensor Actuator B Chem.*, **188**, 1319-1327. https://doi.org/10.1016/j.snb.2013.07.051.

Nebab, M., Atmane, H.A., Bennai, R., Tounsi, A. and Adda Bedia, E.A. (2019), "Vibration response and wave propagation in FG plates resting on elastic foundations using HSDT", *Struct. Eng. Mech.*, **69**(5), 511-525. https://doi.org/10.12989/sem.2019.69.5.511.

Nejad, M.Z., Hadi, A. and Farajpour, A. (2017), "Consistent couple-stress theory for free vibration analysis of Euler-Bernoulli nano-beams made of arbitrary bi-directional functionally graded materials", *Struct. Eng. Mech.*, **63**(2), 161-169. https://doi.org/10.12989/sem.2017.63.2.161.

Nejad, M.Z., Hadi, A., Omidvari, A. and Rastgoo, A. (2018), "Bending analysis of bi-directional functionally graded Euler-Bernoulli nano-beams using integral form of Eringen's non-local elasticity theory", *Struct. Eng. Mech.*, **67**(4), 417-425.

Numanoğlu, H.M., Akgöz, B. and Civalek, Ö. (2018), "On dynamic analysis of nanorods", *Int. J. Eng. Sci.*, **130**, 33-50. https://doi.org/10.1016/j.ijengsci.2018.05.001.

Paidoussis, M.P. (1998), *Fluid-structure interactions: slender structures and axial flow*, Academic press, MA, USA.

Peddieson, J., Buchanan, G.R. and McNitt, R.P. (2003), "Application of nonlocal continuum models to nanotechnology",

Int. J. Eng. Sci., **41**(3-5), 305-312. https://doi.org/10.1016/S0020-7225(02)00210-0.

Rahmani, O., Refaeinejad, V. and Hosseini, S. (2017), "Assessment of various nonlocal higher order theories for the bending and buckling behavior of functionally graded nanobeams", *Steel Compos. Struct*, **23**(3), 339-350. https://doi.org/10.12989/scs.2017.23.3.339.

Reddy, J. (2010), "Nonlocal nonlinear formulations for bending of classical and shear deformation theories of beams and plates", *Int. J. Eng. Sci.*, **48**(11), 1507-1518. https://doi.org/10.1016/j.ijengsci.2010.09.020.

Romano, G., Barretta, R. and Diaco, M. (2017), "On nonlocal integral models for elastic nano-beams", *J. Mech. Sci.*, **131**, 490-499. https://doi.org/10.1016/j.ijmecsci.2017.07.013.

Semmah, A., Heireche, H., Bousahla, A.A. and Tounsi, A. (2019), "Thermal buckling analysis of SWBNNT on Winkler foundation by non local FSDT", *Adv. Nano Res.*, **7**(2), 89-98. https://doi.org/10.12989/anr.2019.7.2.089.

Shen, H.-S. (2011), "Nonlinear analysis of lipid tubules by nonlocal beam model", *J. Theoretical Bio.*, **276**(1), 50-56. https://doi.org/10.1016/j.jtbi.2011.02.001.

Şimşek, M. (2016), "Nonlinear free vibration of a functionally graded nanobeam using nonlocal strain gradient theory and a novel Hamiltonian approach", *Int. J. Eng. Sci.*, **105**, 12-27. https://doi.org/10.1016/j.ijengsci.2016.04.013.

Şimşek, M. and Reddy, J. (2013), "Bending and vibration of functionally graded microbeams using a new higher order beam theory and the modified couple stress theory", *Int. J. Eng. Sci.*, **64**, 37-53. https://doi.org/10.1016/j.ijengsci.2012.12.002.

Soltani, P., Taherian, M. and Farshidianfar, A. (2010), "Vibration and instability of a viscous-fluid-conveying single-walled carbon nanotube embedded in a visco-elastic medium", *J. Phys. D Appl. Phys.*, **43**(42), 425401. https://doi.org/10.1088/0022-3727/43/42/425401.

Tlidji, Y., Zidour, M., Draiche, K., Safa, A., Bourada, M., Tounsi, A., Bousahla, A.A. and Mahmoud, S. (2019), "Vibration analysis of different material distributions of functionally graded microbeam", *Struct. Eng. Mech.*, **69**(6), 637-649. https://doi.org/10.12989/sem.2019.69.6.637.

Tounsi, A., Heireche, H., Berrabah, H., Benzair, A. and Boumia, L. (2008), "Effect of small size on wave propagation in double-walled carbon nanotubes under temperature field", *J. Appl. Phys.*, **104**(10), 104301. https://doi.org/10.1063/1.3018330.

Wang, Y.-Z., Li, F.-M. and Kishimoto, K. (2010), "Wave propagation characteristics in fluid-conveying double-walled nanotubes with scale effects", *Comput. Mater. Sci.*, **48**(2), 413-418. https://doi.org/10.1016/j.commatsci.2010.01.034.

Yazid, M., Heireche, H., Tounsi, A., Bousahla, A.A. and Ahmed Houari, M.S. (2018), "A novel nonlocal refined plate theory for stability response of orthotropic single-layer graphene sheet resting on elastic medium", *Smart Struct. Syst.*, **21**(1), 15-25. https://doi.org/10.12989/sss.2018.21.1.015.

Youcef, D.O., Kaci, A., Benzair, A., Bousahla, A.A. and Tounsi, A. (2018), "Dynamic analysis of nanoscale beams including surface stress effects", *Smart Struct. Syst.*, **21**(1), 65-74. https://doi.org/10.12989/sss.2018.21.1.065.

Zenkour, A. and Sobhy, M. (2013), "Nonlocal elasticity theory for thermal buckling of nanoplates lying on Winkler–Pasternak elastic substrate medium", *Physica E Low-dimensional Syst. Nanostruct.*, **53**, 251-259. https://doi.org/10.1016/j.physe.2013.04.022.

Zhang, B., He, Y., Liu, D., Gan, Z. and Shen, L. (2014), "Non-classical Timoshenko beam element based on the strain gradient elasticity theory", *Finite Elements Anal. Design*, **79**, 22-39. https://doi.org/10.1016/j.finel.2013.10.004.

PL

Appendix A2

Nonlinear dynamics of viscoelastic small-scale tubes conveying fluid

A2.1 Appendix overview

This appendix deals with the dynamics of viscoelastic tubes conveying fluid at small scales. Moreover, the viscoelastic tube is assume to possess a geometrical imperfection. A higher-order scale-dependent model is proposed using non-classical constitutive equations with stress nonlocality and strain gradient. Slip conditions and viscoelasticity effects are simulated via the Karniadakis–Beskok technique and Kelvin–Voigt approach, respectively. Strain-displacement relations are modified to include the influences of geometrical nonlinearity. Potential and kinetic energies together with viscous and external works are used to perform a work/energy balance and derive the motion equations. The nonlinear dynamic response of the tube is predicted by a Galerkin-based method. As the excitation frequency increases, the role of nonlinear damping in the dynamic response increases. This work is a complementary study to the nonlinear vibrations of viscoelastic nanotubes, and would be useful while designing ultrasmall fluid-conveying systems such as microfluidic devices, small-scale fluid filtration systems, and pipettes.

Appendix A2.2

Statement of Authorship

Statement of Authorship

Title of Paper	Local dynamic analysis of imperfect fluid-conveying nanotubes with large deformations incorporating nonlinear damping
Publication Status	☑ Published ☐ Accepted for Publication ☐ Submitted for Publication ☐ Unpublished and Unsubmitted work written in manuscript style
Publication Details	A Farajpour, MH Ghayesh, H Farokhi, Local dynamic analysis of imperfect fluid-conveying nanotubes with large deformations incorporating nonlinear damping, Journal of Vibration and Control 26, 413–429 (2020).

Principal Author

Name of Principal Author (Candidate)	Ali Farajpour Ouderji
Contribution to the Paper	- Research and doing the literature review of the paper - Developing the model (i.e. derivation of partial differential equations of motion) - Modelling the slip boundary condition using the Beskok–Karniadakis approach - Incorporating nonlinear damping and axial inertia effects - Writing all parts of the paper and analysing the data - Correspondence with the reviewers and editor of the journal, - Preparing the revised version of the paper
Overall percentage (%)	60%
Certification:	This paper reports on original research I conducted during the period of my Higher Degree by Research candidature and is not subject to any obligations or contractual agreements with a third party that would constrain its inclusion in this thesis. I am the primary author of this paper.
Signature	Date 2/6/2020

Co-Author Contributions

By signing the Statement of Authorship, each author certifies that:

   i.   the candidate's stated contribution to the publication is accurate (as detailed above);

   ii.   permission is granted for the candidate in include the publication in the thesis; and

   iii.   the sum of all co-author contributions is equal to 100% less the candidate's stated contribution.

Name of Co-Author	Mergen H. Ghayesh
Contribution to the Paper	- Supervising the work including preparing the paper - Contribution to the development of the ideas and concepts of the paper - Editing and evaluating the paper before submission - Discretising and solving the equations of motions, and obtaining frequency response curves
Signature	Date 21/06/2020

Name of Co-Author	Hamed Farokhi
Contribution to the Paper	- Participation in supervising the work - Contribution to the development of the concepts of the paper - Discretising and solving the equations of motions, and obtaining frequency response curves
Signature	Date 19/06/2020

Appendix A2.3

Published journal paper

Local dynamic analysis of imperfect fluid-conveying nanotubes with large deformations incorporating nonlinear damping

Ali Farajpour[1] , Mergen H Ghayesh[1] and Hamed Farokhi[2]

Abstract

An attempt is made in this article to analyse the large-amplitude local dynamics of nanofluid-conveying nanotubes with geometrical imperfections. Each element of the nanotube can have displacements along both longitudinal and transverse directions. A nonlinear damping model is also taken into account utilising the Kelvin–Voigt approach. The stress nonlocality and strain gradient influences are modelled using an advanced scale-dependent theory. Moreover, the Beskok–Karniadakis approach is applied for relative motions at the nanotube wall. To present the coupled motion equations of the coupled nanotube, Hamilton's approach is used. Moreover, to develop a reliable solution procedure, Galerkin's method along with continuation technique is utilised. The effects of nonlinear damping, geometrical imperfection, being at nanoscales, fluid velocity and relative motion at the wall on the large-amplitude local dynamics are investigated.

Keywords

Dynamic analysis, nanotubes, fluid flow, nonlinear damping, imperfection

1. Introduction

Ultrasmall tubes such as carbon nanotubes and boron nitride nanotubes have a substantial promise in conveying fluid due to their perfect hollow circular cross section and excellent mechanical properties. The flow-induced mechanical behaviour of nanotubes raises an attractive research topic, which is significant in order to properly design small-scale systems conveying fluid and particles. Nanofluidic devices, nanopipettes, nanoactuators and nanofluid filtration systems are examples of the application of fluid-conveying ultrasmall systems.

Classical continuum mechanics is not capable of modelling nanostructures and microstructures as size effects are omitted in the classical (local) constitutive relations (Behera and Chakraverty, 2016; Zenkour and Abouelregal, 2014). To take into consideration the effect of being nanosized and microsized, different modified versions of classical continuum mechanics have been introduced. The most popular size-dependent theories are Eringen's theory, theory of strain gradients, couple stress model and theory of surface elasticity. Eringen's theory is widely utilised to capture the influence of being nanosized (Arda and Aydogdu, 2019; Ebrahimi et al., 2018; Farajpour et al., 2017; Ghadiri and Shafiei, 2017; Hosseini et al., 2018), whereas the couple stress and strain gradient models generally account for the

effect of being microsized (Farokhi and Ghayesh, 2018; Farokhi et al., 2018; Ghayesh, 2018a). In this investigation, a nonlocal model with strain gradient effects is utilised for formulating the dynamic behaviour of imperfect coupled tubes conveying fluid at nanoscales.

Investigating size influences on the deformation behaviour of micro/nanoscale structural components has been a topic of major concern in recent years due to the application of these components in microelectromechanical and nanoelectromechanical systems. For instance, Peddieson et al. (2003), as the first researchers, applied Eringen's theory to examine the static deformation of ultrasmall beams. Tounsi et al. (2008) explored the influences of a temperature change on the wave propagation in double-walled tubes at nanoscales; the classical theory (CT) of

---

[1]School of Mechanical Engineering, University of Adelaide, Australia
[2]Department of Mechanical and Construction Engineering, Northumbria University, UK

Corresponding author:
Ali Farajpour, School of Mechanical Engineering, University of Adelaide, North Terrace, Adelaide, South Australia 5005, Australia.
Email: ali.farajpourouderji@adelaide.edu.au

elasticity fails to predict the wave propagation characteristics. Moreover, a nonlocal vibration analysis was conducted by Civalek and Akgöz (2013) on sector graphene sheets. The critical buckling temperature of nanoscale plates was determined by Zenkour and Sobhy (2013); the influences of a Winkler–Pasternak substrate together with size effects on the critical temperature were captured. In addition, based on Eringen's theory, the large deformation of nonlocal plates and beams was formulated by Reddy (2010). The vibration characteristics of functionally graded ultrasmall beams were also determined by Hadi et al. (2018) via help of a modified model of elasticity; they assumed that the material properties of the ultrasmall beam alter along all axes. Malekzadeh and Shojaee (2015) formulated the variation of the natural frequencies of nonlocal plates with surface properties using a modified elasticity model with consideration of shear effects.

Besides the investigation of the mechanics of ultrasmall structural components, the static and dynamic behaviours of small-scale systems conveying fluid have also been studied recently. Particularly, vibration (Soltani et al., 2010), instability (Liang and Su, 2013), linear dynamics (Bahaadini et al., 2018) and wave dispersion behaviour (Filiz and Aydogdu, 2015; Wang et al., 2010) of fluid-conveying nanoscale/microscale tubes have been investigated. In addition to carbon nanotubes, piezoelectric nanoscale/microscale tubes have been employed in fluid transport systems (Amiri et al., 2018; Maraghi et al., 2013). In addition to linear models (Atashafrooz et al., 2018), a few nonlinear continuum models with size effects have been proposed for fluid-conveying nanotubes (Askari and Esmailzadeh, 2017). However, the available size-dependent nonlinear models are limited in terms of geometry and nonlinear damping. First of all, in the available nonlinear models for fluid-conveying systems, it is assumed that nanotubes are perfectly straight. Nonetheless, geometrical imperfections are inevitable in the manufacturing process at small-scale levels. On the other side, the effects of nonlinear damping on the dynamics of fluid-conveying nanotubes have not been incorporated into the size-dependent formulation yet.

In the current study, a nonlinear nonlocal analysis is performed on the large-amplitude dynamics of nanofluid-conveying nanotubes with consideration of an imperfection in the geometry. Both longitudinal and transverse displacements are considered for the size-dependent coupled motion. The influence of nonlinear damping on the nonlinear nonlocal dynamics is captured by employing the Kelvin–Voigt approach. The motion equations of the fluid-conveying nanosystem are presented using an advanced scale-dependent model capturing the stress nonlocality and strain gradients. Based on the Beskok–Karniadakis approach, a speed correction factor is also implemented to incorporate the effect of relative motions at the nanotube wall. Galerkin's method along with continuation technique is used to develop an accurate solution scheme. Numerical results are presented to study the influences of nonlinear damping, imperfections in geometry, fluid speed and relative motion at the nanotube wall on the dynamic behaviour of the nanosystem.

2. Relative motion at the nanotube wall

In order to incorporate the relative motion between the fluid and the nanotube at the inner wall, the Beskok–Karniadakis approach is employed in the following section briefly; an interested reader is referred to Farajpour et al. (2019). It is assumed that the fluid density, velocity vector and pressure are denoted by ρ_f, $\boldsymbol{v}$ and P, respectively. The Navier–Stokes equation for the fluid is expressed as

$$\rho_f \frac{d\boldsymbol{v}}{dt} + \nabla P - \mu_e \nabla^2 \boldsymbol{v} = 0 \qquad (1)$$

in which ∇ and ∇^2 denote the gradient and Laplacian operators, respectively. The effective nanofluid viscosity is denoted by μ_e. It should be mentioned that equation (1) is a linearised version of the Navier–Stokes equation. The nonlinear terms of this equation are insignificant since in this analysis the nanotube possesses geometrical nonlinearity while there is no nonlinearity in the fluid flow. It is assumed that the fluid inside the nanotube is Newtonian and incompressible. In addition, laminar fluid flow is considered for the nanosystem (see Figure 1). The fluid speed in the axial axis is determined as

$$v_x = \left(\frac{r^2}{4\mu_e}\right)\frac{\partial P}{\partial x} + C_0 + C_1 Ln(r) \qquad (2)$$

where C_0 and C_1 are integration constants and r denotes the radial distance from the centre of the nanotube. C_1 must be
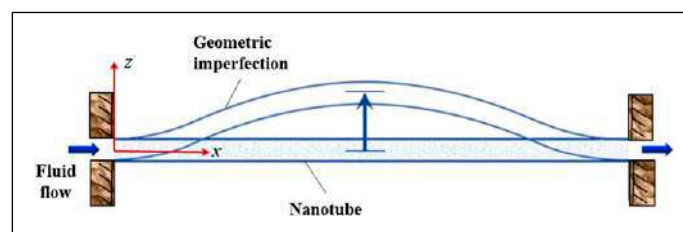
Figure 1. A nanotube with a geometrically imperfect configuration conveying fluid.

zero in order to avoid infinite values at the centre. The slip speed is given by (Beskok and Karniadakis, 1999)

$$(v_x)|_{r=R_i} = \frac{(\sigma_v - 2)R_i Kn}{\sigma_v(1 - \beta Kn)}\left(\frac{\partial v_x}{\partial r}\right)\Big|_{r=R_i} \tag{3}$$

in which R_i and σ_v are, respectively, the nanotube inner radius and tangential momentum accommodation factor. Here, β is commonly set to -1, and Kn is the Knudsen number. Employing equations (2) and (3), the integration constants are obtained as

$$C_0 = -\left(\frac{R_i^2}{4\mu_e}\right)\frac{\partial P}{\partial x} + \left(\frac{R_i^2}{2\mu_e}\right)\left(\frac{Kn}{1 - \beta Kn}\right)\left(\frac{\sigma_v - 2}{\sigma_v}\right)\frac{\partial P}{\partial x},$$

$$C_1 = 0 \tag{4}$$

The speed correction factor related to the relative motion at the inner wall is defined as

$$\kappa_{scf} = \frac{v_{sl}}{v_{nsl}} = \frac{\mu_b}{\mu_e}\left[\frac{4Kn(2 - \sigma_v)}{(1 - \beta Kn)\sigma_v} + 1\right] \tag{5}$$

where v_{sl} and v_{nsl} represent the average slip and no-slip nanofluid speed, respectively. μ_b is the bulk viscosity.

3. Modelling via nonlocal strain gradient theory

In this section, the size-dependent dynamics of imperfect fluid-conveying nanotubes with large deformations is briefly modelled taking into consideration nonlinear; an interested reader is referred to Farajpour et al. (2019) for detailed continuous and discretised equations of Sections 3 and 4. Let us denote the axial strain, axial displacement, transverse deflection and geometrical imperfection by ε_{xx}, u, w and w_0, respectively. Utilising the Euler–Bernoulli theory, the nonlinear strain component is (Farokhi and Ghayesh, 2015, 2016)

$$\varepsilon_{xx} = \frac{\partial u}{\partial x} + \frac{\partial w}{\partial x}\frac{dw_0}{dx} - z\frac{\partial^2 w}{\partial x^2} + \frac{1}{2}\left(\frac{\partial w}{\partial x}\right)^2 \tag{6}$$

Employing the nonlocal strain gradient theory (NSGT), the stress component is written as (Lim et al., 2015)

$$t_{xx} - (e_0 a)^2\nabla^2 t_{xx} = t_{xx(el)}^{cl} - l_{sg}^2\nabla^2 t_{xx(el)}^{cl} + t_{xx(vis)}^{cl} - l_{sg}^2\nabla^2 t_{xx(vis)}^{cl} \tag{7}$$

where

$$t_{xx(el)}^{cl} = E\varepsilon_{xx}, \quad t_{xx(vis)}^{cl} = \eta\frac{\partial\varepsilon_{xx}}{\partial t}, \quad t_{xx} = t_{xx(el)} + t_{xx(vis)},$$

$$t_{xx}^{cl} = t_{xx(el)}^{cl} + t_{xx(vis)}^{cl} \tag{8}$$

In the above equations, 'cl', 'el' and 'vis' stand for classical, elastic and viscoelastic stresses, respectively, and

η, E, l_{sg} and $e_0 a$ denote the viscosity coefficient, Young's modulus, strain gradient and nonlocal size parameters, respectively (Farajpour et al., 2018). Assuming A as the area of the tube cross section, the stress resultants of the tube are

$$\begin{Bmatrix} N_{xx} \\ M_{xx} \end{Bmatrix} = \int_A \begin{Bmatrix} 1 \\ z \end{Bmatrix} t_{xx} dA \tag{9}$$

In view of equations (6)–(8), one obtains

$$t_{xx} - (e_0 a)^2\nabla^2 t_{xx}$$

$$= E\left(1 - l_{sg}^2\nabla^2\right)\left(\frac{\partial u}{\partial x} - z\frac{\partial^2 w}{\partial x^2} + \frac{1}{2}\left(\frac{\partial w}{\partial x}\right)^2\right)$$

$$+ E\left(1 - l_{sg}^2\nabla^2\right)\left(\frac{\partial w}{\partial x}\frac{dw_0}{dx}\right) + \eta\left(1 - l_{sg}^2\nabla^2\right)\left(\frac{\partial^2 w}{\partial t\partial x}\frac{dw_0}{dx}\right)$$

$$+ \eta\left(1 - l_{sg}^2\nabla^2\right)\left(\frac{\partial^2 u}{\partial t\partial x} - z\frac{\partial^3 w}{\partial t\partial x^2} + \frac{\partial w}{\partial x}\frac{\partial^2 w}{\partial t\partial x}\right) \tag{10}$$

Using equations (9) and (10), one can obtain the following relations for the stress resultants

$$N_{xx} - (e_0 a)^2\nabla^2 N_{xx}$$

$$= EA\left(1 - l_{sg}^2\nabla^2\right)\left(\frac{\partial u}{\partial x} + \frac{1}{2}\left(\frac{\partial w}{\partial x}\right)^2\right)$$

$$+ EA\left(1 - l_{sg}^2\nabla^2\right)\left(\frac{\partial w}{\partial x}\frac{dw_0}{dx}\right) + \eta A\left(1 - l_{sg}^2\nabla^2\right)\left(\frac{\partial^2 w}{\partial t\partial x}\frac{dw_0}{dx}\right)$$

$$+ \eta A\left(1 - l_{sg}^2\nabla^2\right)\left(\frac{\partial^2 u}{\partial t\partial x} + \frac{\partial w}{\partial x}\frac{\partial^2 w}{\partial t\partial x}\right) \tag{11}$$

$$M_{xx} - (e_0 a)^2\nabla^2 M_{xx}$$

$$= -\left[EI\left(1 - l_{sg}^2\nabla^2\right)\left(\frac{\partial^2 w}{\partial x^2}\right) + \eta I\left(1 - l_{sg}^2\nabla^2\right)\left(\frac{\partial^3 w}{\partial t\partial x^2}\right)\right] \tag{12}$$

In equation (12), I denotes the second moment of area. For the nanotube, one can write

$$\delta U_{el} = \int_0^L\int_A \sigma_{xx(el)}\delta\varepsilon_{xx}dAdx + \int_0^L\int_A \sigma_{xx(el)}^{(1)}\nabla\delta\varepsilon_{xx}dAdx$$

$$= \int_0^L\int_A \sigma_{xx(el)}\delta\varepsilon_{xx}dAdx + \left[\int_A \sigma_{xx(el)}^{(1)}\delta\varepsilon_{xx}dA\right]_0^L$$

$$- \int_0^L\int_A \nabla\sigma_{xx(el)}^{(1)}\delta\varepsilon_{xx}dAdx \tag{13}$$

where $\sigma_{xx(\alpha\beta)}$ and $\sigma_{xx(\alpha\beta)}^{(1)}$ represent the lower-order and higher-order nonlocal stress components, respectively; U_{el} is the elastic energy; and L stands for the tube length. Similarly, the viscoelastic work is

$$\delta W_{vis} = -\int_0^L \int_A \sigma_{xx(vis)}\delta\varepsilon_{xx}dAdx - \int_0^L \int_A \sigma^{(1)}_{xx(vis)}\nabla\delta\varepsilon_{xx}dAdx$$

$$= -\int_0^L \int_A \sigma_{xx(vis)}\delta\varepsilon_{xx}dAdx - \left[\int_A \sigma^{(1)}_{xx(vis)}\delta\varepsilon_{xx}dA\right]_0^L$$

$$+ \int_0^L \int_A \nabla\sigma^{(1)}_{xx(vis)}\delta\varepsilon_{xx}dAdx$$

(14)

According to the NSGT, the stress components satisfy the following relations

$$\left\{\begin{array}{c} t_{xx} \\ t_{xx(el)} \\ t_{xx(vis)} \end{array}\right\} = \left\{\begin{array}{c} \sigma_{xx} \\ \sigma_{xx(el)} \\ \sigma_{xx(vis)} \end{array}\right\} - \nabla\left\{\begin{array}{c} \sigma^{(1)}_{xx} \\ \sigma^{(1)}_{xx(el)} \\ \sigma^{(1)}_{xx(vis)} \end{array}\right\}$$

(15)

Equation (15) is employed in order to further simplify the elastic energy and viscoelastic work (i.e. equations (13) and (14)). The nanosystem kinetic energy is formulated as

$$T_k = \frac{1}{2}\int_A\int_0^L \rho_t\left(\frac{\partial u}{\partial t}\right)^2 dAdx + \frac{1}{2}\int_A\int_0^L \rho_t\left(\frac{\partial w}{\partial t}\right)^2 dAdx$$

$$+ \frac{1}{2}\int_A\int_0^L \rho_f\left[\frac{\partial u}{\partial t} + \kappa_{scf}U\left(1 + \frac{\partial u}{\partial x}\right)\right]^2 dAdx$$

$$+ \frac{1}{2}\int_A\int_0^L \rho_f\left[\frac{\partial w}{\partial t} + \kappa_{scf}U\left(\frac{\partial w}{\partial x} + \frac{dw_0}{dx}\right)\right]^2 dAdx$$

(16)

where ρ_t and ρ_f are the tube and fluid mass densities, respectively, and U stands for the fluid speed. The external work associated with transverse load $F(x)$ is written as

$$\delta W_F = \int_0^L \cos(\omega t)F(x)\delta w dx$$

(17)

where ω denotes the excitation frequency. The energy/work law is given as follows

$$\int_{t_1}^{t_2}\{\delta W_F + \delta W_{vis} - \delta U_{el} + \delta T_k\}dt = 0$$

(18)

Using equations (13), (14), (16) and (17) together with equation (18) gives

$$\frac{\partial N_{xx}}{\partial x} = (M+m)\frac{\partial^2 u}{\partial t^2} + 2M(\kappa_{scf}U)\frac{\partial^2 u}{\partial t\partial x} + M(\kappa_{scf}U)^2\frac{\partial^2 u}{\partial x^2}$$

(19)

$$\frac{\partial^2 M_{xx}}{\partial x^2} + \frac{\partial}{\partial x}\left(N_{xx}\frac{dw_0}{dx}\right) + F(x)\cos(\omega t) + \frac{\partial}{\partial x}\left(N_{xx}\frac{\partial w}{\partial x}\right)$$

$$= (M+m)\frac{\partial^2 w}{\partial t^2} + 2M(\kappa_{scf}U)\frac{\partial^2 w}{\partial t\partial x}$$

$$+ M(\kappa_{scf}U)^2\left(\frac{\partial^2 w}{\partial x^2} + \frac{d^2 w_0}{dx^2}\right)$$

(20)

where M and m are, respectively, mass per length for fluid and solid parts. Using equations (11) and (12) in conjunction with equations (19) and (20), one obtains

$$N_{xx} = EA\left(1 - l_{sg}^2\nabla^2\right)\left(\frac{\partial u}{\partial x} + \frac{1}{2}\left(\frac{\partial w}{\partial x}\right)^2\right)$$

$$+ EA\left(1 - l_{sg}^2\nabla^2\right)\left(\frac{\partial w}{\partial x}\frac{dw_0}{dx}\right)$$

$$+ \eta A\left(1 - l_{sg}^2\nabla^2\right)\left(\frac{\partial^2 w}{\partial t\partial x}\frac{dw_0}{dx}\right)$$

$$+ \eta A\left(1 - l_{sg}^2\nabla^2\right)\left(\frac{\partial^2 u}{\partial t\partial x} + \frac{\partial w}{\partial x}\frac{\partial^2 w}{\partial t\partial x}\right)$$

$$+ (M+m)(e_0a)^2\frac{\partial^3 u}{\partial x\partial t^2} + 2M(\kappa_{scf}U)(e_0a)^2\frac{\partial^3 u}{\partial t\partial x^2}$$

$$+ M(\kappa_{scf}U)^2(e_0a)^2\frac{\partial^3 u}{\partial x^3}$$

(21)

$$M_{xx} = -\left[EI\left(1 - l_{sg}^2\nabla^2\right)\frac{\partial^2 w}{\partial x^2} + \eta I\left(1 - l_{sg}^2\nabla^2\right)\frac{\partial^3 w}{\partial t\partial x^2}\right]$$

$$- (e_0a)^2\frac{\partial}{\partial x}\left(N_{xx}\frac{dw_0}{dx}\right) - (e_0a)^2 F(x)\cos(\omega t)$$

$$- (e_0a)^2\frac{\partial}{\partial x}\left(N_{xx}\frac{\partial w}{\partial x}\right) + (M+m)(e_0a)^2\frac{\partial^2 w}{\partial t^2}$$

$$+ 2M(\kappa_{scf}U)(e_0a)^2\frac{\partial^2 w}{\partial t\partial x}$$

$$+ M(\kappa_{scf}U)^2(e_0a)^2\left(\frac{\partial^2 w}{\partial x^2} + \frac{d^2 w_0}{dx^2}\right)$$

(22)

Substituting equations (21) and (22) into equations (19) and (20) gives

$$EA\left(1 - l_{sg}^2\nabla^2\right)\frac{\partial^2 u}{\partial x^2} + \eta A\left(1 - l_{sg}^2\nabla^2\right)$$

$$\times \frac{\partial^3 u}{\partial t\partial x^2} - \left(1 - (e_0a)^2\nabla^2\right)$$

$$\times \left[(M+m)\frac{\partial^2 u}{\partial t^2} + 2M(\kappa_{scf}U)\frac{\partial^2 u}{\partial t\partial x} + M(\kappa_{scf}U)^2\frac{\partial^2 u}{\partial x^2}\right]$$

$$= -EA\left(1 - l_{sg}^2\nabla^2\right)$$

$$\times \left(\frac{\partial w}{\partial x}\frac{\partial^2 w}{\partial x^2} + \frac{\partial^2 w}{\partial x^2}\frac{dw_0}{dx} + \frac{\partial w}{\partial x}\frac{d^2 w_0}{dx^2}\right) - \eta A\left(1 - l_{sg}^2\nabla^2\right)$$

$$\times \left(\frac{\partial^2 w}{\partial t\partial x}\frac{\partial^2 w}{\partial x^2} + \frac{\partial w}{\partial x}\frac{\partial^3 w}{\partial t\partial x^2} + \frac{\partial^3 w}{\partial t\partial x^2}\frac{dw_0}{dx} + \frac{\partial^2 w}{\partial t\partial x}\frac{d^2 w_0}{dx^2}\right)$$

(23)

$$EI\left(l_{sg}^2\frac{\partial^6 w}{\partial x^6} - \frac{\partial^4 w}{\partial x^4}\right) + \eta I\left(l_{sg}^2\frac{\partial^7 w}{\partial t\partial x^6} - \frac{\partial^5 w}{\partial t\partial x^4}\right)$$

$$+ \cos(\omega t)\left[F(x) - (e_0 a)^2\frac{d^2 F(x)}{dx^2}\right]$$

$$- \left[(M+m)\frac{\partial^2 w}{\partial t^2} + 2M(\kappa_{scf}U)\frac{\partial^2 w}{\partial t\partial x}\right.$$

$$+ \left. M(\kappa_{scf}U)^2\left(\frac{\partial^2 w}{\partial x^2} + \frac{d^2 w_0}{dx^2}\right)\right]$$

$$+ (e_0 a)^2\left[(M+m)\frac{\partial^4 w}{\partial x^2\partial t^2} + 2M(\kappa_{scf}U)\frac{\partial^4 w}{\partial t\partial x^3}\right.$$

$$+ \left. M(\kappa_{scf}U)^2\left(\frac{\partial^4 w}{\partial x^4} + \frac{d^4 w_0}{dx^4}\right)\right]$$

$$= -EA(1-(e_0 a)^2\nabla^2)\left[\left(\frac{\partial^2 w}{\partial x^2} + \frac{d^2 w_0}{dx^2}\right)(1-l_{sg}^2\nabla^2)\right.$$

$$\times \left.\left(\frac{1}{2}\left(\frac{\partial w}{\partial x}\right)^2 + \frac{\partial w}{\partial x}\frac{dw_0}{dx} + \frac{\partial u}{\partial x}\right)\right] - EA(1-(e_0 a)^2\nabla^2)$$

$$\times \left[\left(\frac{\partial w}{\partial x} + \frac{dw_0}{dx}\right)\left\{\frac{\partial}{\partial x}\left[(1-l_{sg}^2\nabla^2)\left(\frac{1}{2}\left(\frac{\partial w}{\partial x}\right)^2\right.\right.\right.\right.$$

$$+ \left.\left.\left.\left.\frac{\partial w}{\partial x}\frac{dw_0}{dx} + \frac{\partial u}{\partial x}\right)\right]\right\}\right] - \eta A(1-(e_0 a)^2\nabla^2)\left[\left(\frac{\partial^2 w}{\partial x^2}\right.\right.$$

$$+ \left.\frac{d^2 w_0}{dx^2}\right)(1-l_{sg}^2\nabla^2)\left(\frac{\partial^2 w}{\partial t\partial x}\frac{\partial w}{\partial x} + \frac{\partial^2 w}{\partial t\partial x}\frac{dw_0}{dx} + \frac{\partial^2 u}{\partial x\partial t}\right)\right]$$

$$- \eta A(1-(e_0 a)^2\nabla^2)\left[\left(\frac{\partial w}{\partial x} + \frac{dw_0}{dx}\right)\left\{\frac{\partial}{\partial x}\left[(1-l_{sg}^2\nabla^2)\right.\right.\right.$$

$$\times \left.\left.\left.\left(\frac{\partial w}{\partial x}\frac{\partial^2 w}{\partial t\partial x} + \frac{\partial^2 w}{\partial t\partial x}\frac{dw_0}{dx} + \frac{\partial^2 u}{\partial t\partial x}\right)\right]\right\}\right]$$

$$- (e_0 a)^2(1-(e_0 a)^2\nabla^2)\left[\left(\frac{\partial w}{\partial x} + \frac{dw_0}{dx}\right)\right.$$

$$\times \left(\left((M+m)\frac{\partial^4 u}{\partial x^2\partial t^2} + 2M(\kappa_{scf}U)\frac{\partial^4 u}{\partial t\partial x^3}\right.\right.$$

$$+ \left.\left. M(\kappa_{scf}U)^2\frac{\partial^4 u}{\partial x^4}\right)\right] - (e_0 a)^2(1-(e_0 a)^2\nabla^2)$$

$$\times \left[\left(\frac{\partial^2 w}{\partial x^2} + \frac{d^2 w_0}{dx^2}\right)\times\left((M+m)\frac{\partial^3 u}{\partial x\partial t^2}\right.\right.$$

$$+ \left.\left. 2M(\kappa_{scf}U)\frac{\partial^3 u}{\partial t\partial x^2} + M(\kappa_{scf}U)^2\frac{\partial^3 u}{\partial x^3}\right)\right]$$

$$(24)$$

In equations (23) and (24), all linear terms are on the left-hand side of the equal sign, whereas nonlinear terms are on the right-hand side. In equation (23), the first and second terms on the left-hand side are associated with elasticity and viscoelasticity, respectively. Furthermore,

the third, fourth and fifth terms are related to the inertial, Coriolis and parametric forces, respectively. Similar terms in conjunction with the term containing external transverse loading are found on the left-hand side of equation (24). The linear terms in the above-mentioned equations are noticeably different from those of the classical macroscale fluid-conveying pipes. In fact, taking into account size effects leads to terms with higher-order derivatives.

4. Numerical solution

In this section, the nonlinear coupled equations of the nanosystem are first discretised based on Galerkin's scheme, and then the dynamic characteristics are determined via a continuation numerical method. Using the dimensionless parameters given by

$$x^* = \frac{x}{L}, \quad \varphi_{nl} = \frac{e_0 a}{L}, \quad \varphi_{sg} = \frac{l_{sg}}{L}, \quad w^* = \frac{w}{d}, \quad u^* = \frac{u}{d},$$

$$w_0^* = \frac{w_0}{d}, \quad \Xi = L^2\left(\frac{A}{I}\right), \quad t^* = \left(\frac{1}{L^2}\right)\left(\sqrt{\frac{EI}{m+M}}\right)t,$$

$$F^* = \left(\frac{L^4}{EId}\right)F, \quad s = \frac{L}{d}, \quad \Pi_m = \frac{M}{M+m},$$

$$\eta^* = \left(\frac{1}{EL^2}\right)\left(\sqrt{\frac{EI}{m+M}}\right)\eta, \quad U^* = L\left(\sqrt{\frac{M}{EI}}\right)U,$$

$$\omega^* = L^2\left(\sqrt{\frac{m+M}{EI}}\right)\omega$$

$$(25)$$

the coupled nonlinear equations of the nanosystem (i.e. equations (23) and (24)) are rewritten as

$$s\left(\varphi_{sg}^2\frac{\partial^4 u}{\partial x^4} - \frac{\partial^2 u}{\partial x^2}\right) + s\eta\left(\varphi_{sg}^2\frac{\partial^5 u}{\partial t\partial x^4} - \frac{\partial^3 u}{\partial t\partial x^2}\right)$$

$$- \frac{s\varphi_{nl}^2}{\Xi}\left(\frac{\partial^4 u}{\partial x^2\partial t^2} + 2(\kappa_{scf}U)\sqrt{\Pi_m}\,\frac{\partial^4 u}{\partial t\partial x^3} + (\kappa_{scf}U)^2\frac{\partial^4 u}{\partial x^4}\right)$$

$$+ \frac{s}{\Xi}\left(\frac{\partial^2 u}{\partial t^2} + 2(\kappa_{scf}U)\sqrt{\Pi_m}\,\frac{\partial^2 u}{\partial t\partial x} + (\kappa_{scf}U)^2\frac{\partial^2 u}{\partial x^2}\right)$$

$$= \frac{\partial}{\partial x}\left[\frac{1}{2}\left(\frac{\partial w}{\partial x}\right)^2 + \frac{\partial w}{\partial x}\frac{dw_0}{dx}\right] - \varphi_{sg}^2\frac{\partial^3}{\partial x^3}\left[\frac{1}{2}\left(\frac{\partial w}{\partial x}\right)^2\right.$$

$$+ \left.\frac{\partial w}{\partial x}\frac{dw_0}{dx}\right] + \eta\frac{\partial}{\partial x}\left[\frac{\partial^2 w}{\partial t\partial x}\frac{\partial w}{\partial x} + \frac{dw_0}{dx}\frac{\partial^2 w}{\partial t\partial x}\right]$$

$$- \eta\varphi_{sg}^2\frac{\partial^3}{\partial x^3}\left[\frac{\partial w}{\partial x}\frac{\partial^2 w}{\partial t\partial x} + \frac{\partial^2 w}{\partial t\partial x}\frac{dw_0}{dx}\right]$$

$$(26)$$

$$-\varphi_{sg}^2 \frac{\partial^6 w}{\partial x^6} + \frac{\partial^4 w}{\partial x^4} - \eta\varphi_{sg}^2 \frac{\partial^7 w}{\partial t\partial x^6} + \eta\frac{\partial^5 w}{\partial t\partial x^4} - F_1\cos(\omega t) - \varphi_{nl}^2\left(\frac{\partial^4 w}{\partial x^2\partial t^2} + 2\left(\kappa_{scf}U\right)\sqrt{\Pi_m}\frac{\partial^4 w}{\partial t\partial x^3} + \left(\kappa_{scf}U\right)^2\left(\frac{\partial^4 w}{\partial x^4} + \frac{d^4 w_0}{dx^4}\right)\right)$$

$$+ \frac{\partial^2 w}{\partial t^2} + 2\left(\kappa_{scf}U\right)\sqrt{\Pi_m}\frac{\partial^2 w}{\partial t\partial x} + \left(\kappa_{scf}U\right)^2\left(\frac{\partial^2 w}{\partial x^2} + \frac{d^2 w_0}{dx^2}\right)$$

$$= +\Xi\left(\frac{1}{s}\right)^2\left\{\left(\frac{\partial^2 w}{\partial x^2} + \frac{d^2 w_0}{dx^2}\right)\left[\frac{1}{2}\left(\frac{\partial w}{\partial x}\right)^2 + \frac{\partial w}{\partial x}\frac{dw_0}{dx} + s\frac{\partial u}{\partial x}\right] + \left(\frac{\partial w}{\partial x} + \frac{dw_0}{dx}\right)\frac{\partial}{\partial x}\left[\frac{1}{2}\left(\frac{\partial w}{\partial x}\right)^2 + \frac{\partial w}{\partial x}\frac{dw_0}{dx} + s\frac{\partial u}{\partial x}\right]\right.$$

$$-\varphi_{sg}^2\left(\frac{\partial^2 w}{\partial x^2} + \frac{d^2 w_0}{dx^2}\right)\frac{\partial^2}{\partial x^2}\left[\frac{1}{2}\left(\frac{\partial w}{\partial x}\right)^2 + \frac{\partial w}{\partial x}\frac{dw_0}{dx} + s\frac{\partial u}{\partial x}\right] - \varphi_{sg}^2\left(\frac{\partial w}{\partial x} + \frac{dw_0}{dx}\right)\frac{\partial^3}{\partial x^3}\left[\frac{1}{2}\left(\frac{\partial w}{\partial x}\right)^2 + \frac{\partial w}{\partial x}\frac{dw_0}{dx} + s\frac{\partial u}{\partial x}\right]$$

$$+\eta\left(\frac{d^2 w_0}{dx^2} + \frac{\partial^2 w}{\partial x^2}\right)\left(\frac{\partial^2 w}{\partial t\partial x}\frac{\partial w}{\partial x} + \frac{\partial^2 w}{\partial t\partial x}\frac{dw_0}{dx} + s\frac{\partial^2 u}{\partial x\partial t}\right) + \eta\left(\frac{\partial w}{\partial x} + \frac{dw_0}{dx}\right)\frac{\partial}{\partial x}\left(\frac{\partial^2 w}{\partial t\partial x}\frac{\partial w}{\partial x} + \frac{\partial^2 w}{\partial t\partial x}\frac{dw_0}{dx} + s\frac{\partial^2 u}{\partial t\partial x}\right)$$

$$-\varphi_{sg}^2\eta\left(\frac{\partial^2 w}{\partial x^2} + \frac{d^2 w_0}{dx^2}\right)\frac{\partial^2}{\partial x^2}\left(\frac{\partial^2 w}{\partial t\partial x}\frac{\partial w}{\partial x} + \frac{\partial^2 w}{\partial t\partial x}\frac{dw_0}{dx} + s\frac{\partial^2 u}{\partial t\partial x}\right) - \varphi_{sg}^2\eta\left(\frac{\partial w}{\partial x} + \frac{dw_0}{dx}\right)\frac{\partial^3}{\partial x^3}\left(\frac{\partial^2 w}{\partial t\partial x}\frac{\partial w}{\partial x} + \frac{\partial^2 w}{\partial t\partial x}\frac{dw_0}{dx} + s\frac{\partial^2 u}{\partial t\partial x}\right)$$

$$+\frac{s}{\Xi}\varphi_{nl}^2\left(\frac{\partial^2 w}{\partial x^2} + \frac{d^2 w_0}{dx^2}\right)\left[\frac{\partial^3 u}{\partial x\partial t^2} + 2\left(\kappa_{scf}U\right)\sqrt{\Pi_m}\frac{\partial^3 u}{\partial t\partial x^2} + \left(\kappa_{scf}U\right)^2\frac{\partial^3 u}{\partial x^3}\right] + \frac{s}{\Xi}\varphi_{nl}^2\left(\frac{\partial w}{\partial x} + \frac{dw_0}{dx}\right)$$

$$\times\left[\frac{\partial^4 u}{\partial x^2\partial t^2} + 2\left(\kappa_{scf}U\right)\sqrt{\Pi_m}\frac{\partial^4 u}{\partial t\partial x^3} + \left(\kappa_{scf}U\right)^2\frac{\partial^4 u}{\partial x^4}\right]\right\}$$

$$-\Xi\left(\frac{\varphi_{nl}}{s}\right)^2\frac{\partial^2}{\partial x^2}\left\{\left(\frac{\partial^2 w}{\partial x^2} + \frac{d^2 w_0}{dx^2}\right)\left[\frac{1}{2}\left(\frac{\partial w}{\partial x}\right)^2 + \frac{\partial w}{\partial x}\frac{dw_0}{dx} + s\frac{\partial u}{\partial x}\right] + \left(\frac{dw_0}{dx} + \frac{\partial w}{\partial x}\right)\frac{\partial}{\partial x}\left[\frac{1}{2}\left(\frac{\partial w}{\partial x}\right)^2 + \frac{\partial w}{\partial x}\frac{dw_0}{dx} + s\frac{\partial u}{\partial x}\right]\right.$$

$$-\varphi_{sg}^2\left(\frac{\partial^2 w}{\partial x^2} + \frac{d^2 w_0}{dx^2}\right)\frac{\partial^2}{\partial x^2}\left[\frac{1}{2}\left(\frac{\partial w}{\partial x}\right)^2 + \frac{\partial w}{\partial x}\frac{dw_0}{dx} + s\frac{\partial u}{\partial x}\right] - \varphi_{sg}^2\left(\frac{\partial w}{\partial x} + \frac{dw_0}{dx}\right)\frac{\partial^3}{\partial x^3}\left[\frac{1}{2}\left(\frac{\partial w}{\partial x}\right)^2 + \frac{\partial w}{\partial x}\frac{dw_0}{dx} + s\frac{\partial u}{\partial x}\right]$$

$$+\eta\left(\frac{\partial^2 w}{\partial x^2} + \frac{d^2 w_0}{dx^2}\right)\left(\frac{\partial^2 w}{\partial t\partial x}\frac{\partial w}{\partial x} + \frac{\partial^2 w}{\partial t\partial x}\frac{dw_0}{dx} + s\frac{\partial^2 u}{\partial t\partial x}\right) + \eta\left(\frac{\partial w}{\partial x} + \frac{dw_0}{dx}\right)\frac{\partial}{\partial x}\left(\frac{\partial^2 w}{\partial t\partial x}\frac{\partial w}{\partial x} + \frac{\partial^2 w}{\partial t\partial x}\frac{dw_0}{dx} + s\frac{\partial^2 u}{\partial t\partial x}\right)$$

$$-\varphi_{sg}^2\eta\left(\frac{\partial^2 w}{\partial x^2} + \frac{d^2 w_0}{dx^2}\right)\frac{\partial^2}{\partial x^2}\left(\frac{\partial^2 w}{\partial t\partial x}\frac{\partial w}{\partial x} + \frac{\partial^2 w}{\partial t\partial x}\frac{dw_0}{dx} + s\frac{\partial^2 u}{\partial t\partial x}\right) - \varphi_{sg}^2\eta\left(\frac{\partial w}{\partial x} + \frac{dw_0}{dx}\right)\frac{\partial^3}{\partial x^3}\left(\frac{\partial^2 w}{\partial t\partial x}\frac{\partial w}{\partial x} + \frac{\partial^2 w}{\partial t\partial x}\frac{dw_0}{dx} + s\frac{\partial^2 u}{\partial t\partial x}\right)$$

$$+\frac{s}{\Xi}\varphi_{nl}^2\left(\frac{\partial^2 w}{\partial x^2} + \frac{d^2 w_0}{dx^2}\right)\left[\frac{\partial^3 u}{\partial x\partial t^2} + 2\left(\kappa_{scf}U\right)\sqrt{\Pi_m}\frac{\partial^3 u}{\partial t\partial x^2} + \left(\kappa_{scf}U\right)^2\frac{\partial^3 u}{\partial x^3}\right] + \frac{s}{\Xi}\varphi_{nl}^2\left(\frac{\partial w}{\partial x} + \frac{dw_0}{dx}\right)$$

$$\times\left[\frac{\partial^4 u}{\partial x^2\partial t^2} + 2\left(\kappa_{scf}U\right)\sqrt{\Pi_m}\frac{\partial^4 u}{\partial t\partial x^3} + \left(\kappa_{scf}U\right)^2\frac{\partial^4 u}{\partial x^4}\right]\right\}$$

$$\tag{27}$$

The symbol '*' is dropped for convenience purposes. Now, the aforementioned dimensionless motion equations are discretised using the following expressions of displacement components

$$
\begin{aligned}
u &= \sum_{j=1}^{N_x} \phi_j(x)r_j(t), \\
w &= \sum_{j=1}^{N_z} \psi_j(x)q_j(t)
\end{aligned}
\tag{28}
$$

where ϕ_j and r_j stand for the trial function and generalised coordinate of u, respectively. Moreover, ψ_j and q_j indicate the trial function and generalised coordinate of w, respectively (Ghayesh, 2018b; Ghayesh et al., 2013, 2016, 2017). Assuming clamped boundary conditions and using equation (28), the discretised form of equations (26) and (27) is obtained as

$$\frac{s}{\Xi}\left\{\sum_{j=1}^{N_x}\left(\int_0^1\phi_k\phi_j dx\right)\frac{d^2 r_j}{dt^2}+2(\kappa_{scf}U)\sqrt{\Pi_m}\sum_{j=1}^{N_x}\left(\int_0^1\phi_k\frac{d\phi_j}{dx}dx\right)\frac{dr_j}{dt}+(\kappa_{scf}U)^2\sum_{j=1}^{N_x}\left(\int_0^1\phi_k\frac{d^2\phi_j}{dx^2}dx\right)r_j\right\}$$

$$-\frac{s\varphi_{nl}^2}{\Xi}\left\{\sum_{j=1}^{N_x}\left(\int_0^1\phi_k\frac{d^2\phi_j}{dx^2}dx\right)\frac{d^2 r_j}{dt^2}+2(\kappa_{scf}U)\sqrt{\Pi_m}\sum_{j=1}^{N_x}\left(\int_0^1\phi_k\frac{d^3\phi_j}{dx^3}dx\right)\frac{dr_j}{dt}+(\kappa_{scf}U)^2\sum_{j=1}^{N_x}\left(\int_0^1\phi_k\frac{d^4\phi_j}{dx^4}dx\right)r_j\right\}$$

$$-s\int_0^1\left\{\phi_k\frac{d}{dx}\left[\sum_{j=1}^{N_x}\frac{d\phi_j}{dx}r_j\right]\right\}dx+s\varphi_{sg}^2\int_0^1\left\{\phi_k\frac{d^3}{dx^3}\left[\sum_{j=1}^{N_x}\frac{d\phi_j}{dx}r_j\right]\right\}dx$$

$$-s\eta\int_0^1\left\{\phi_k\frac{d}{dx}\left(\sum_{j=1}^{N_x}\frac{d\phi_j}{dx}\frac{dr_j}{dt}\right)\right\}dx+s\eta\varphi_{sg}^2\int_0^1\left\{\phi_k\frac{d^3}{dx^3}\left(\sum_{j=1}^{N_x}\frac{d\phi_j}{dx}\frac{dr_j}{dt}\right)\right\}dx$$

$$=\int_0^1\left\{\phi_k\frac{d}{dx}\left[\frac{1}{2}\sum_{j=1}^{N_z}\sum_{i=1}^{N_z}\frac{d\psi_j}{dx}\frac{d\psi_i}{dx}q_j q_i+A_0\sum_{j=1}^{N_z}\frac{d\psi_1}{dx}\frac{d\psi_j}{dx}q_j\right]\right\}dx$$

$$-\varphi_{sg}^2\int_0^1\left\{\phi_k\frac{d^3}{dx^3}\left[\frac{1}{2}\sum_{j=1}^{N_z}\sum_{i=1}^{N_z}\frac{d\psi_j}{dx}\frac{d\psi_i}{dx}q_j q_i+A_0\sum_{j=1}^{N_z}\frac{d\psi_1}{dx}\frac{d\psi_j}{dx}q_j\right]\right\}dx$$

$$+\eta\int_0^1\left\{\phi_k\frac{d}{dx}\left(\sum_{j=1}^{N_z}\sum_{i=1}^{N_z}\frac{d\psi_j}{dx}\frac{d\psi_i}{dx}\frac{dq_j}{dt}q_i+A_0\sum_{j=1}^{N_z}\frac{d\psi_1}{dx}\frac{d\psi_j}{dx}\frac{dq_j}{dt}\right)\right\}dx$$

$$-\eta\varphi_{sg}^2\int_0^1\left\{\phi_k\frac{d^3}{dx^3}\left(\sum_{j=1}^{N_z}\sum_{i=1}^{N_z}\frac{d\psi_j}{dx}\frac{d\psi_i}{dx}\frac{dq_j}{dt}q_i+A_0\sum_{j=1}^{N_z}\frac{d\psi_1}{dx}\frac{d\psi_j}{dx}\frac{dq_j}{dt}\right)\right\}dx$$

$$\tag{29}$$

$$-\varphi_{sg}^2\sum_{j=1}^{N_z}\left(\int_0^1\psi_k\frac{d^6\psi_j}{dx^6}dx\right)q_j-\eta\varphi_{sg}^2\sum_{j=1}^{N_z}\left(\int_0^1\psi_k\frac{d^6\psi_j}{dx^6}dx\right)\frac{dq_j}{dt}+\sum_{j=1}^{N_z}\left(\int_0^1\psi_k\frac{d^4\psi_j}{dx^4}dx\right)q_j+\eta\sum_{j=1}^{N_z}\left(\int_0^1\psi_k\frac{d^4\psi_j}{dx^4}dx\right)\frac{dq_j}{dt}$$

$$-\left(\int_0^1\psi_k dx\right)F_1\cos(\omega t)+\sum_{j=1}^{N_z}\left(\int_0^1\psi_k\psi_j dx\right)\frac{d^2 q_j}{dt^2}+2(\kappa_{scf}U)\sqrt{\Pi_m}\sum_{j=1}^{N_z}\left(\int_0^1\psi_k\frac{d\psi_j}{dx}dx\right)\frac{dq_j}{dt}$$

$$+(\kappa_{scf}U)^2\left[\sum_{j=1}^{N_z}\left(\int_0^1\psi_k\frac{d^2\psi_j}{dx^2}dx\right)q_j+A_0\left(\int_0^1\psi_k\frac{d^2\psi_1}{dx^2}dx\right)\right]$$

$$-\varphi_{nl}^2\left\{\sum_{j=1}^{N_z}\left(\int_0^1\psi_k\frac{d^2\psi_j}{dx^2}dx\right)\frac{d^2 q_j}{dt^2}+2(\kappa_{scf}U)\sqrt{\Pi_m}\sum_{j=1}^{N_z}\left(\int_0^1\psi_k\frac{d^3\psi_j}{dx^3}dx\right)\frac{dq_j}{dt}\right.$$

$$\left.+(\kappa_{scf}U)^2\left[\sum_{j=1}^{N_z}\left(\int_0^1\psi_k\frac{d^4\psi_j}{dx^4}dx\right)q_j+A_0\left(\int_0^1\psi_k\frac{d^4\psi_1}{dx^4}dx\right)\right]\right\}$$

$$=\Xi\left(\frac{1}{s}\right)^2\int_0^1\left(\psi_k\left\{\left(\sum_{j=1}^{N_z}\frac{d^2\psi_j}{dx^2}q_j+A_0\frac{d^2\psi_1}{dx^2}\right)\left[\frac{1}{2}\sum_{j=1}^{N_z}\sum_{i=1}^{N_z}\frac{d\psi_j}{dx}\frac{d\psi_i}{dx}q_j q_i+A_0\sum_{j=1}^{N_z}\frac{d\psi_1}{dx}\frac{d\psi_j}{dx}q_j+s\sum_{j=1}^{N_x}\frac{d\phi_j}{dx}r_j\right]\right.\right.$$

$$+\left(\sum_{j=1}^{N_z}\frac{d\psi_j}{dx}q_j+A_0\frac{d\psi_1}{dx}\right)\frac{d}{dx}\left[\frac{1}{2}\sum_{j=1}^{N_z}\sum_{i=1}^{N_z}\frac{d\psi_j}{dx}\frac{d\psi_i}{dx}q_j q_i+A_0\sum_{j=1}^{N_z}\frac{d\psi_1}{dx}\frac{d\psi_j}{dx}q_j+s\sum_{j=1}^{N_x}\frac{d\phi_j}{dx}r_j\right]$$

$$-\varphi_{sg}^2\left(\sum_{j=1}^{N_z}\frac{d^2\psi_j}{dx^2}q_j+A_0\frac{d^2\psi_1}{dx^2}\right)\frac{d^2}{dx^2}\left[\frac{1}{2}\sum_{j=1}^{N_z}\sum_{i=1}^{N_z}\frac{d\psi_j}{dx}\frac{d\psi_i}{dx}q_j q_i+A_0\sum_{j=1}^{N_z}\frac{d\psi_1}{dx}\frac{d\psi_j}{dx}q_j+s\sum_{j=1}^{N_x}\frac{d\phi_j}{dx}r_j\right]$$

$$-\varphi_{sg}^2\left(\sum_{j=1}^{N_z}\frac{d\psi_j}{dx}q_j+A_0\frac{d\psi_1}{dx}\right)\frac{d^3}{dx^3}\left[\frac{1}{2}\sum_{j=1}^{N_z}\sum_{i=1}^{N_z}\frac{d\psi_j}{dx}\frac{d\psi_i}{dx}q_j q_i+A_0\sum_{j=1}^{N_z}\frac{d\psi_1}{dx}\frac{d\psi_j}{dx}q_j+s\sum_{j=1}^{N_x}\frac{d\phi_j}{dx}r_j\right]$$

$$+\eta\left(\sum_{j=1}^{N_z}\frac{d^2\psi_j}{dx^2}q_j+A_0\frac{d^2\psi_1}{dx^2}\right)\left(\sum_{j=1}^{N_z}\sum_{i=1}^{N_z}\frac{d\psi_j}{dx}\frac{d\psi_i}{dx}\frac{dq_j}{dt}q_i+A_0\sum_{j=1}^{N_z}\frac{d\psi_1}{dx}\frac{d\psi_j}{dx}\frac{dq_j}{dt}+s\sum_{j=1}^{N_x}\frac{d\phi_j}{dx}\frac{dr_j}{dt}\right)$$

$$+ \eta \left(\sum_{j=1}^{N_z} \frac{d\psi_j}{dx} q_j + A_0 \frac{d\psi_1}{dx} \right) \frac{d}{dx} \left(\sum_{j=1}^{N_z} \sum_{i=1}^{N_z} \frac{d\psi_j}{dx} \frac{d\psi_i}{dx} \frac{dq_j}{dt} q_i + A_0 \sum_{j=1}^{N_z} \frac{d\psi_1}{dx} \frac{d\psi_j}{dx} \frac{dq_j}{dt} + s \sum_{j=1}^{N_x} \frac{d\phi_j}{dx} \frac{dr_j}{dt} \right)$$

$$- \varphi_{sg}^2 \eta \left(\sum_{j=1}^{N_z} \frac{d^2\psi_j}{dx^2} q_j + A_0 \frac{d^2\psi_1}{dx^2} \right) \frac{d^2}{dx^2} \left(\sum_{j=1}^{N_z} \sum_{i=1}^{N_z} \frac{d\psi_j}{dx} \frac{d\psi_i}{dx} \frac{dq_j}{dt} q_i + A_0 \sum_{j=1}^{N_z} \frac{d\psi_1}{dx} \frac{d\psi_j}{dx} \frac{dq_j}{dt} + s \sum_{j=1}^{N_x} \frac{d\phi_j}{dx} \frac{dr_j}{dt} \right)$$

$$- \varphi_{sg}^2 \eta \left(\sum_{j=1}^{N_z} \frac{d\psi_j}{dx} q_j + A_0 \frac{d\psi_1}{dx} \right) \frac{d^3}{dx^3} \left(\sum_{j=1}^{N_z} \sum_{i=1}^{N_z} \frac{d\psi_j}{dx} \frac{d\psi_i}{dx} \frac{dq_j}{dt} q_i + A_0 \sum_{j=1}^{N_z} \frac{d\psi_1}{dx} \frac{d\psi_j}{dx} \frac{dq_j}{dt} + s \sum_{j=1}^{N_x} \frac{d\phi_j}{dx} \frac{dr_j}{dt} \right)$$

$$+ \frac{s}{\Xi} \varphi_{nl}^2 \left(\sum_{j=1}^{N_z} \frac{d^2\psi_j}{dx^2} q_j + A_0 \frac{d^2\psi_1}{dx^2} \right) \left[\sum_{j=1}^{N_x} \frac{d\phi_j}{dx} \frac{d^2 r_j}{dt^2} + \left(\kappa_{scf} U \right)^2 \sum_{j=1}^{N_x} \frac{d^3\phi_j}{dx^3} r_j + 2 \left(\kappa_{scf} U \right) \sqrt{\Pi_m} \sum_{j=1}^{N_x} \frac{d^2\phi_j}{dx^2} \frac{dr_j}{dt} \right]$$

$$+ \frac{s}{\Xi} \varphi_{nl}^2 \left(\sum_{j=1}^{N_z} \frac{d\psi_j}{dx} q_j + A_0 \frac{d\psi_1}{dx} \right) \left[\sum_{j=1}^{N_x} \frac{d^2\phi_j}{dx^2} \frac{d^2 r_j}{dt^2} + 2 \left(\kappa_{scf} U \right) \sqrt{\Pi_m} \sum_{j=1}^{N_x} \frac{d^3\phi_j}{dx^3} \frac{dr_j}{dt} + \left(\kappa_{scf} U \right)^2 \sum_{j=1}^{N_x} \frac{d^4\phi_j}{dx^4} r_j \right] \right\} \right) dx$$

$$- \Xi \left(\frac{\varphi_{nl}}{s} \right)^2 \int_0^1 \left(\psi_k \frac{d^2}{dx^2} \left\{ \left(\sum_{j=1}^{N_z} \frac{d^2\psi_j}{dx^2} q_j + A_0 \frac{d^2\psi_1}{dx^2} \right) \left[\frac{1}{2} \sum_{j=1}^{N_z} \sum_{i=1}^{N_z} \frac{d\psi_j}{dx} \frac{d\psi_i}{dx} q_j q_i + A_0 \sum_{j=1}^{N_z} \frac{d\psi_1}{dx} \frac{d\psi_j}{dx} q_j + s \sum_{j=1}^{N_x} \frac{d\phi_j}{dx} r_j \right] \right. \right.$$

$$+ \left(\sum_{j=1}^{N_z} \frac{d\psi_j}{dx} q_j + A_0 \frac{d\psi_1}{dx} \right) \frac{d}{dx} \left[+ \frac{1}{2} \sum_{j=1}^{N_z} \sum_{i=1}^{N_z} \frac{d\psi_j}{dx} \frac{d\psi_i}{dx} q_j q_i + A_0 \sum_{j=1}^{N_z} \frac{d\psi_1}{dx} \frac{d\psi_j}{dx} q_j + s \sum_{j=1}^{N_x} \frac{d\phi_j}{dx} r_j \right]$$

$$- \varphi_{sg}^2 \left(\sum_{j=1}^{N_z} \frac{d^2\psi_j}{dx^2} q_j + A_0 \frac{d^2\psi_1}{dx^2} \right) \frac{d^2}{dx^2} \left[\frac{1}{2} \sum_{j=1}^{N_z} \sum_{i=1}^{N_z} \frac{d\psi_j}{dx} \frac{d\psi_i}{dx} q_j q_i + A_0 \sum_{j=1}^{N_z} \frac{d\psi_1}{dx} \frac{d\psi_j}{dx} q_j + s \sum_{j=1}^{N_x} \frac{d\phi_j}{dx} r_j \right]$$

$$- \varphi_{sg}^2 \left(\sum_{j=1}^{N_z} \frac{d\psi_j}{dx} q_j + A_0 \frac{d\psi_1}{dx} \right) \frac{d^3}{dx^3} \left[\frac{1}{2} \sum_{j=1}^{N_z} \sum_{i=1}^{N_z} \frac{d\psi_j}{dx} \frac{d\psi_i}{dx} q_j q_i + A_0 \sum_{j=1}^{N_z} \frac{d\psi_1}{dx} \frac{d\psi_j}{dx} q_j + s \sum_{j=1}^{N_x} \frac{d\phi_j}{dx} r_j \right]$$

$$+ \eta \left(\sum_{j=1}^{N_z} \frac{d^2\psi_j}{dx^2} q_j + A_0 \frac{d^2\psi_1}{dx^2} \right) \left(\sum_{j=1}^{N_z} \sum_{i=1}^{N_z} \frac{d\psi_j}{dx} \frac{d\psi_i}{dx} \frac{dq_j}{dt} q_i + A_0 \sum_{j=1}^{N_z} \frac{d\psi_1}{dx} \frac{d\psi_j}{dx} \frac{dq_j}{dt} + s \sum_{j=1}^{N_x} \frac{d\phi_j}{dx} \frac{dr_j}{dt} \right)$$

$$+ \eta \left(\sum_{j=1}^{N_z} \frac{d\psi_j}{dx} q_j + A_0 \frac{d\psi_1}{dx} \right) \frac{d}{dx} \left(\sum_{j=1}^{N_z} \sum_{i=1}^{N_z} \frac{d\psi_j}{dx} \frac{d\psi_i}{dx} \frac{dq_j}{dt} q_i + A_0 \sum_{j=1}^{N_z} \frac{d\psi_1}{dx} \frac{d\psi_j}{dx} \frac{dq_j}{dt} + s \sum_{j=1}^{N_x} \frac{d\phi_j}{dx} \frac{dr_j}{dt} \right)$$

$$- \varphi_{sg}^2 \eta \left(\sum_{j=1}^{N_z} \frac{d^2\psi_j}{dx^2} q_j + A_0 \frac{d^2\psi_1}{dx^2} \right) \frac{d^2}{dx^2} \left(\sum_{j=1}^{N_z} \sum_{i=1}^{N_z} \frac{d\psi_j}{dx} \frac{d\psi_i}{dx} \frac{dq_j}{dt} q_i + A_0 \sum_{j=1}^{N_z} \frac{d\psi_1}{dx} \frac{d\psi_j}{dx} \frac{dq_j}{dt} + s \sum_{j=1}^{N_x} \frac{d\phi_j}{dx} \frac{dr_j}{dt} \right)$$

$$- \varphi_{sg}^2 \eta \left(\sum_{j=1}^{N_z} \frac{d\psi_j}{dx} q_j + A_0 \frac{d\psi_1}{dx} \right) \frac{d^3}{dx^3} \left(\sum_{j=1}^{N_z} \sum_{i=1}^{N_z} \frac{d\psi_j}{dx} \frac{d\psi_i}{dx} \frac{dq_j}{dt} q_i + A_0 \sum_{j=1}^{N_z} \frac{d\psi_1}{dx} \frac{d\psi_j}{dx} \frac{dq_j}{dt} + s \sum_{j=1}^{N_x} \frac{d\phi_j}{dx} \frac{dr_j}{dt} \right)$$

$$+ \frac{s}{\Xi} \varphi_{nl}^2 \left(\sum_{j=1}^{N_z} \frac{d^2\psi_j}{dx^2} q_j + A_0 \frac{d^2\psi_1}{dx^2} \right) \left[\sum_{j=1}^{N_x} \frac{d\phi_j}{dx} \frac{d^2 r_j}{dt^2} + \left(\kappa_{scf} U \right)^2 \sum_{j=1}^{N_x} \frac{d^3\phi_j}{dx^3} r_j + 2 \left(\kappa_{scf} U \right) \sqrt{\Pi_m} \sum_{j=1}^{N_x} \frac{d^2\phi_j}{dx^2} \frac{dr_j}{dt} \right]$$

$$+ \frac{s}{\Xi} \varphi_{nl}^2 \left(\sum_{j=1}^{N_z} \frac{d\psi_j}{dx} q_j + A_0 \frac{d\psi_1}{dx} \right) \left[\sum_{j=1}^{N_x} \frac{d^2\phi_j}{dx^2} \frac{d^2 r_j}{dt^2} + 2 \left(\kappa_{scf} U \right) \sqrt{\Pi_m} \sum_{j=1}^{N_x} \frac{d^3\phi_j}{dx^3} \frac{dr_j}{dt} + \left(\kappa_{scf} U \right)^2 \sum_{j=1}^{N_x} \frac{d^4\phi_j}{dx^4} r_j \right] \right\} \right) dx$$

$$\tag{30}$$

The size-dependent local dynamic characteristics of the system are lastly extracted from equations (29) and (30) via implementation of a numerical continuation technique.

5. Numerical results

To determine the numerical results, nanosystem parameters are assumed as $E = 610$ MPa, $v = 0.3$, $\rho_t = 1024$ kg/m³, $h = 66.0$ nm, $R_o = 290.5$ nm and $L/d_o = 20$ in which v, R_o, h and d_o stand for Poisson's ratio, outer radius, thickness and outer diameter, respectively. In addition, the speed correction factor, dimensionless mass coefficient and dimensionless nanotube geometry factor are $\kappa_{scf} = 1.10$, $\Pi_m = 0.5915$ and

$\Xi = 4006.9411$, respectively. The scale coefficients are set to $(\varphi_{sg}, \varphi_{nl}) = (0.04, 0.10)$. Ten trial functions are assumed for each displacement component.

Figure 2 is plotted to illustrate the nonlinear static transverse response of the fluid-conveying nanotube with increasing fluid speed; various initial imperfection amplitudes are considered. The static transverse response is noticeably affected by the imperfection amplitude. For slow fluid flow, the maximum transverse deflection is higher for higher A_0 while the deflection of the nanotube is lower for higher A_0 for fast fluid flow. It means the influence of geometrical imperfection on the mechanics depends on the value of the fluid speed. Figure 3 shows the fundamental transverse frequency
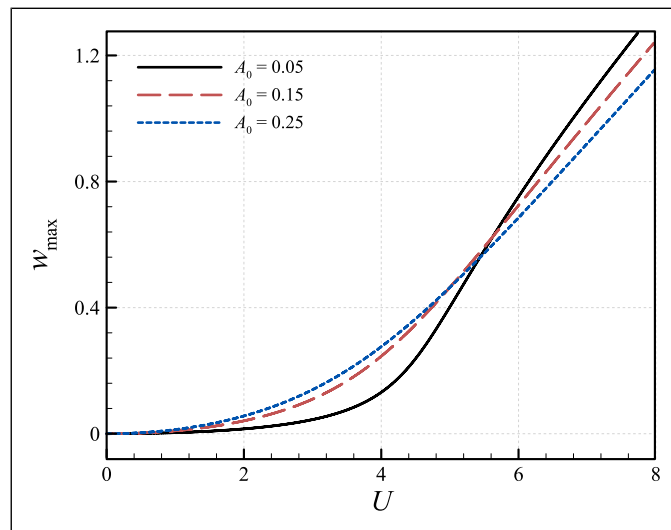
Figure 2. Nonlinear static transverse behaviour of a fluid-conveying tube at nanoscales with increasing fluid speed for different initial imperfection amplitudes.
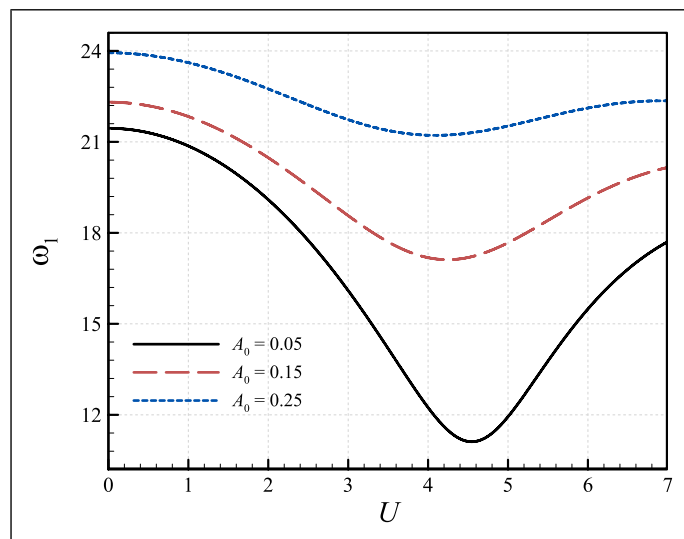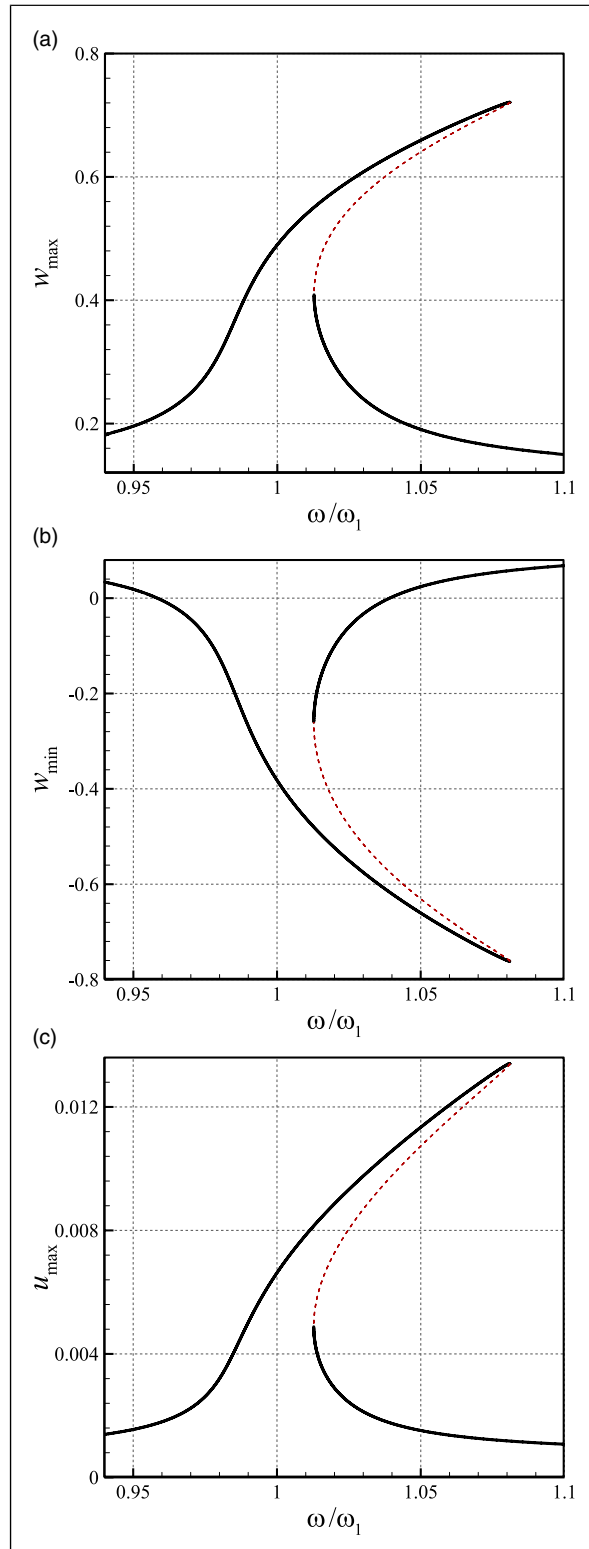

Figure 3. Fundamental transverse frequency of fluid-conveying nanotubes with the fluid speed for different initial imperfection amplitudes.

Figure 4. Nonlinear local dynamics of the fluid-conveying tube at nanoscales; (a, b) maximum and minimum values of *w* at *x* = 0.5; (c) maximum value of *u* at *x* = 0.66.

of nanotubes conveying fluid with the fluid speed; again, various values are considered for the geometric imperfection. As the imperfection amplitude increases, the fundamental frequency substantially increases.
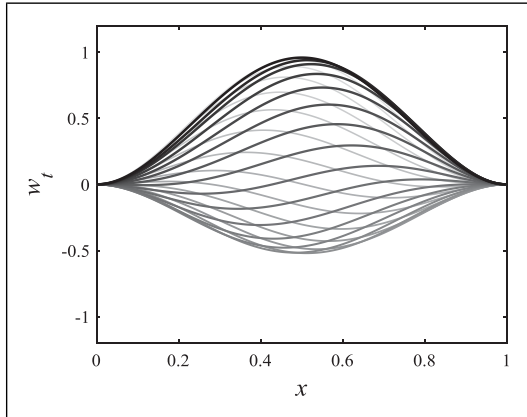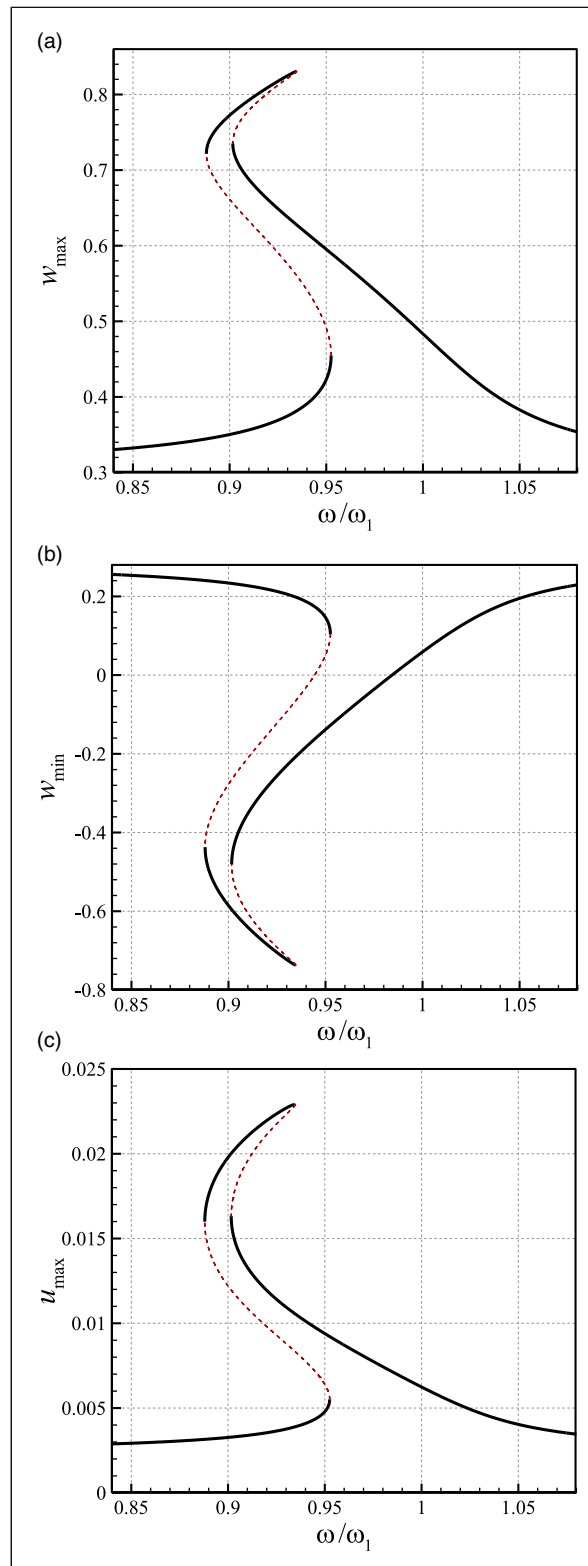

Figure 5. Transverse local oscillation ($w_t = w + w_0$) of the fluid-conveying nanotube of Figure 4 in one period at $\omega/\omega_1 = 1.0810$ (i.e. at peak oscillation amplitude).

The nonlinear local dynamic behaviour of the fluid-conveying tube at nanoscales is shown in Figure 4 for $A_0 = 0.15$, $U = 3.0$, $F_1 = 3.0$, $\kappa_{scf} = 1.10$, $\varphi_{nl} = 0.10$ and $\varphi_{sg} = 0.04$; the fundamental frequency is $\omega_1 = 18.5677$. Two different saddle nodes at $\omega/\omega_1 = 1.0810$ and 1.0128 are found in the nonlinear behaviour. Furthermore, the mechanics is of hardening kind since the amplitude of both axial and transverse motions suddenly decreases at $\omega/\omega_1 = 1.0810$ with the increase in excitation frequency. More details about the coupled motion of Figure 4 at $\omega/\omega_1 = 1.0810$, in which the peak oscillation amplitude occurs, are given in Figures 5 and 6. The total transverse deflection of the nanosystem in one period and the motion characteristics (time histories and phase-plane plots) are, respectively, illustrated in Figures 5 and 6.

In Figure 7, the amplitude of nanotubes conveying fluid is indicated as a function of excitation frequency for $A_0 = 0.15$, $U = 4.25$, $F_1 = 4.0$, $\kappa_{scf} = 1.10$, $\varphi_{nl} = 0.10$ and $\varphi_{sg} = 0.04$; this time, the nonlinear local dynamic behaviour is plotted for a higher fluid speed. The fundamental frequency is $\omega_1 = 17.1162$. In this case, four different saddle nodes at $\omega/\omega_1 = 0.9525$, 0.8880, 0.9346 and 0.9016 are observed in
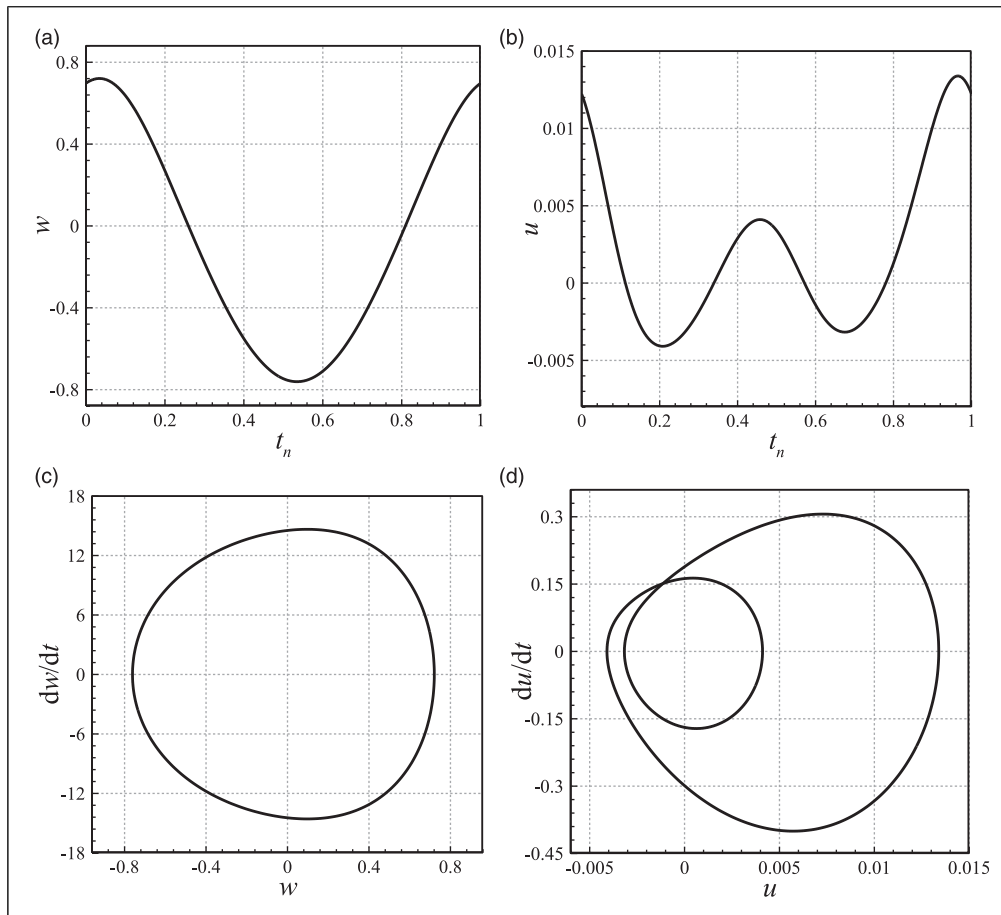

Figure 6. Motion details of Figure 4 at $\omega/\omega_1 = 1.0810$ (i.e. at peak local oscillation amplitude). (a, b) $w - t_n$ at $x = 0.5$ and $u - t_n$ at $x = 0.66$; (c, d) dw/dt at $x = 0.5$ and du/dt at $x = 0.66$; t_n denotes dimensionless time with respect to oscillation period.

Figure 7. Nonlinear local dynamics of the fluid-conveying tube at nanoscales; (a, b) maximum and minimum values of *w* at *x* = 0.5; (c) maximum value of *u* at *x* = 0.66; A_0 = 0.15, *U* = 4.25, F_1 = 4.0 and ω_1 = 17.1162.

the nonlinear local dynamic behaviour. Furthermore, a softening-hardening nonlinearity is found for the system. Comparing Figures 4 and 7 reveals the significance of the fluid speed in the nonlinear dynamics of the nanotube. An
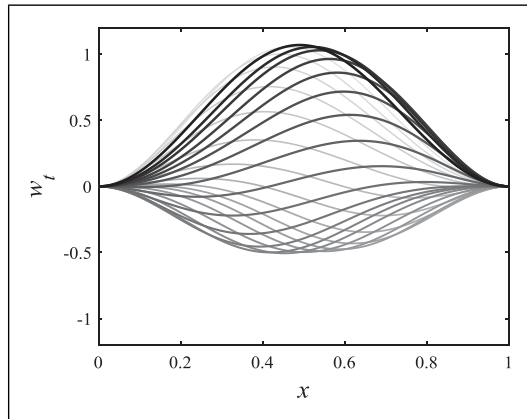

Figure 8. Transverse local oscillation ($w_t = w + w_0$) of the fluid-conveying nanotube of Figure 7 in one period at $\omega/\omega_1 = 0.9346$ (i.e. at peak oscillation amplitude).

increase in the flow speed alters the number of saddle modes and even the type of nonlinearity. Figures 8 and 9 are plotted in order to give more details about the peak oscillation amplitude of the frequency-amplitude diagram of Figure 7. The total transverse deflection and motion characteristics involving time histories and phase-plane plots are illustrated in Figures 8 and 9, respectively.

To investigate the influence of fluid speed on the amplitude-frequency plots of the system, Figure 10 is plotted; $A_0 = 0.15$, $F_1 = 4.0$, $\kappa_{scf} = 1.10$, $\varphi_{nl} = 0.10$ and $\varphi_{sg} = 0.04$. From this figure, it is seen that the type of nonlinearity is very sensitive to the fluid speed. For a relatively small speed (i.e. $U = 3.4$), a completely hardening nonlinear response is observed while the nanotube exhibits a softening-hardening response and softening response for $U = 4.2$ and $U = 5$, respectively.
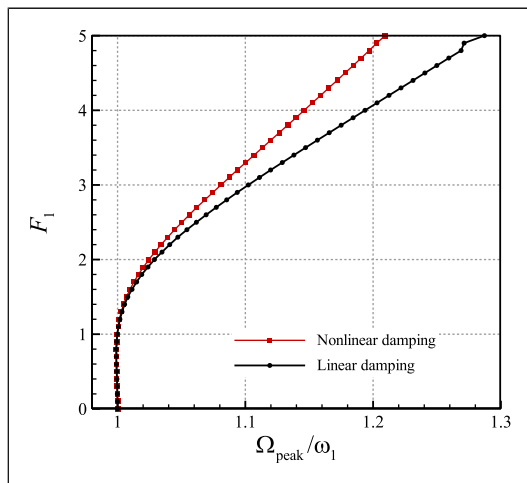
A comparison between the linear and nonlinear damping mechanisms is given in Figure 11; the excitation frequency corresponding to peak oscillation amplitude versus the forcing amplitude is plotted. For comparatively small excitation frequencies, both damping mechanisms result in the same forcing amplitudes. Nonetheless, the Kelvin–Voigt
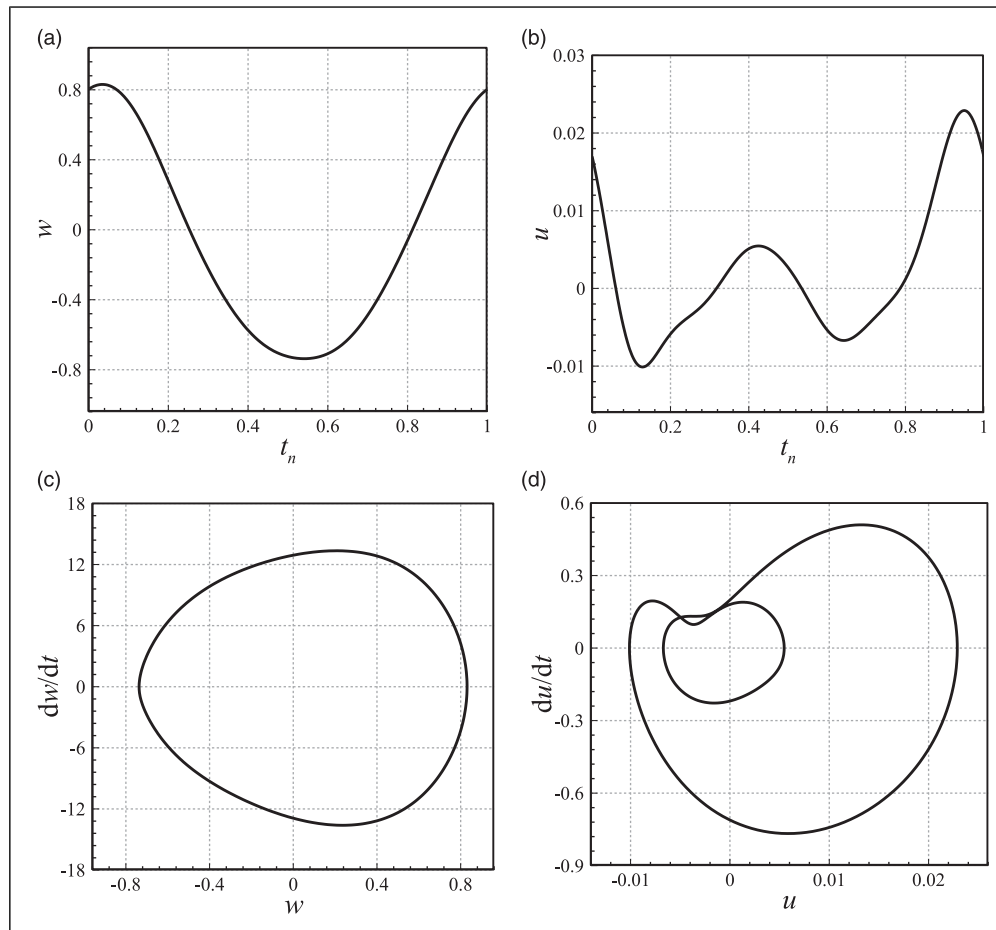
Figure 9. Motion details of Figure 7 at $\omega/\omega_1 = 0.9346$ (i.e. at peak local oscillation amplitude). (a, b) $w - t_n$ at $x = 0.5$ and $u - t_n$ at $x = 0.66$; (c, d) dw/dt at $x = 0.5$ and du/dt at $x = 0.66$; t_n denotes dimensionless time with respect to oscillation period.
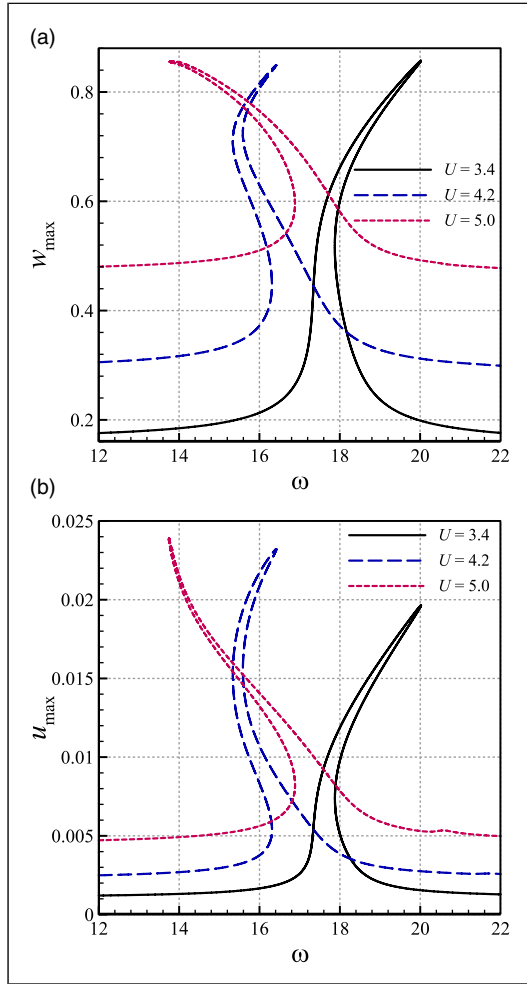
Figure 10. Influence of flow velocity on the nonlinear local dynamics of the fluid-conveying tube at nanoscales; (a) maximum value of w at $x = 0.5$; (b) maximum value of u at $x = 0.66$; $A_0 = 0.15$ and $F_1 = 4.0$.


Figure 11. Excitation frequency corresponding to peak oscillation amplitude versus the forcing amplitude obtained using the Kelvin–Voigt nonlinear damping mechanism (with $\eta = 0.00035$) and a linear viscous damping mechanism (with $c_d = 0.24$).

nonlinear damping mechanism gives higher forcing amplitudes compared to the simple linear viscous damping mechanism. It means that for small excitation frequencies, the linear mechanism can be used while this simple mechanism underestimates the forcing amplitude for comparatively high excitation frequencies.

Figure 12 depicts the role of imperfection amplitude in the amplitude-frequency response of fluid-conveying nanotubes; the flow velocity and forcing amplitude are chosen as $U = 3.5$ and $F_1 = 3.0$, respectively. The imperfection amplitude has an important role in the nonlinear dynamic behaviour of fluid-conveying nanotubes. It can substantially alter the nonlinear dynamics of the nanosystem as shown in Figure 12. Increasing the imperfection amplitude from $A_0 = 0.05$ to $A_0 = 0.25$, the type of nonlinear response gradually turns from hardening to softening.

Figure 13 shows the influence of the relative motion at the inner wall of the nanotube on the nonlinear local dynamic behaviour; the nanosystem parameters are set to $U = 4.2$, $F_1 = 3.5$ and $A_0 = 0.15$. It is found that neglecting the relative motion (i.e. the no-slip condition) yields
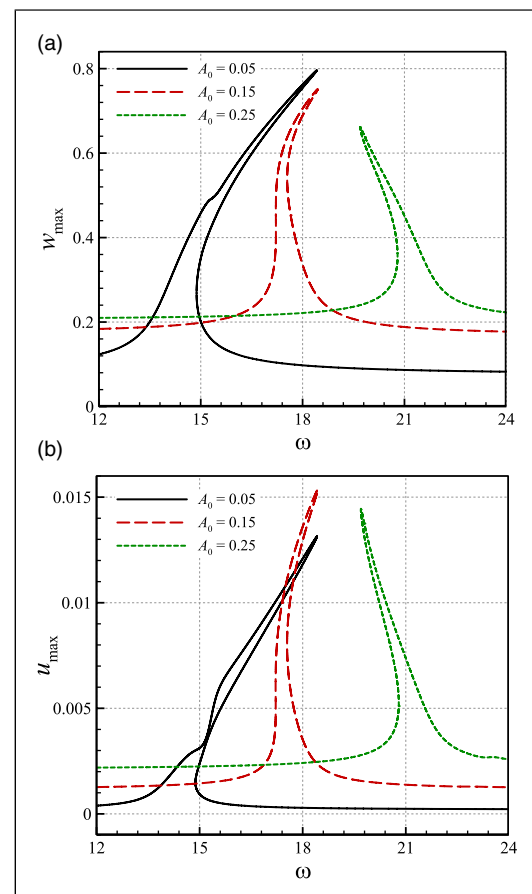
Figure 12. Influence of imperfection amplitude on the nonlinear local dynamics of the fluid-conveying tube at nanoscales; (a) maximum value of w at $x = 0.5$; (b) maximum value of u at $x = 0.66$.
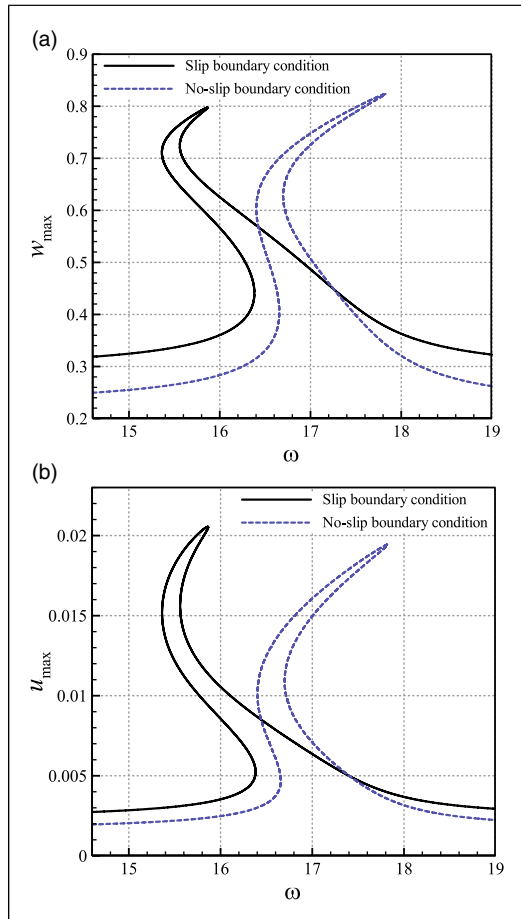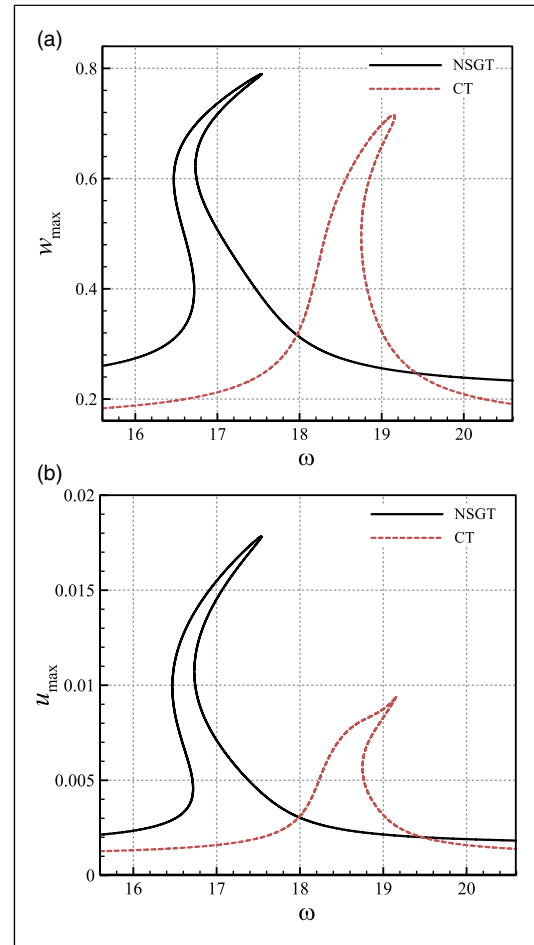
Figure 13. Slip condition influence on the nonlinear local dynamics of the fluid-conveying tube at nanoscales; (a) maximum value of w at $x = 0.5$; (b) maximum value of u at $x = 0.66$.

Figure 14. Nonlinear local dynamics of the fluid-conveying tube at nanoscales calculated by the nonlocal strain gradient theory and classical theory; (a) maximum value of w at $x = 0.5$; (b) maximum value of u at $x = 0.66$; $U = 3.8$, $F_1 = 3.2$ and $A_0 = 0.15$.

overestimated values for the excitation frequency corresponding to the peak oscillation amplitude. Figures 14 and 15 compare the NSGT and the CT for $U = 3.8$ and $U = 6.0$, respectively. For the NSGT, it is assumed that $\varphi_{nl} = 0.10$ and $\varphi_{sg} = 0.04$, whereas both size parameters are set to zero for the CT. It is concluded that neglecting size effects causes a significant error in the estimation of the nonlinear dynamic characteristics of nanotubes conveying fluid.

6. Conclusions

The local dynamic behaviour of a fluid-conveying tube with an imperfection in the geometry has been studied at nanoscales. Both longitudinal and transverse displacements were considered for the motion of each element of the nanotube. Utilising the Kelvin–Voigt approach, a nonlinear damping mechanism was also considered in the size-dependent modelling. Furthermore, applying the NSGT,

the stress nonlocality and strain gradient influences were modelled. The Beskok–Karniadakis approach was used for describing the relative motion at the inner wall of the viscoelastic nanotube. Hamilton's approach, Galerkin's technique and continuation technique were lastly used for deriving, discretising and solving the coupled nonlinear motion equations, respectively. It was found that the fundamental frequency is substantially higher for larger imperfection amplitudes. The type of nonlinearity in the local dynamic behaviour of fluid-conveying nanotubes depends on the fluid speed. For comparatively small fluid speeds, a pure hardening nonlinear response was obtained for the nanotube, whereas the dynamic behaviour gradually turns into a softening response with increasing fluid speed. Furthermore, it was concluded that for relatively small excitation frequencies, the results of the linear damping
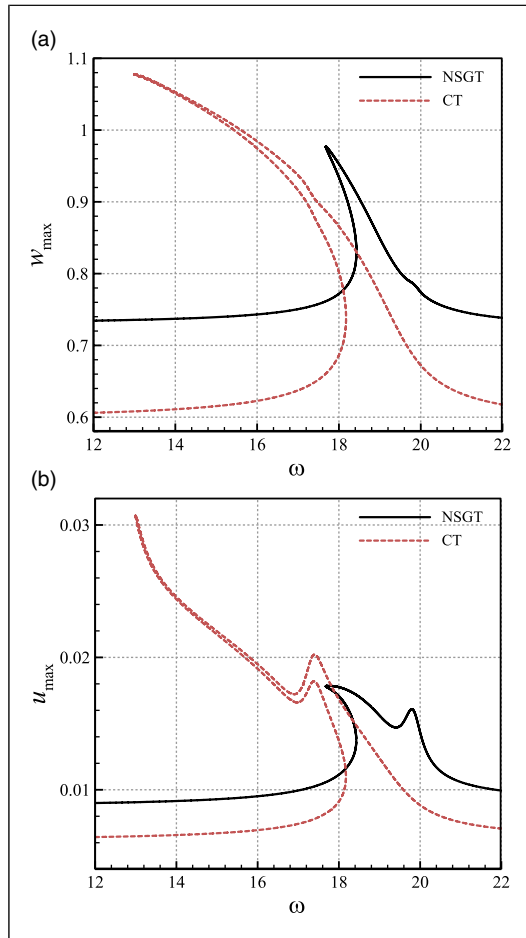
Figure 15. Nonlinear local dynamics of the fluid-conveying tube at nanoscales calculated by the nonlocal strain gradient theory and classical theory; (a) maximum value of *w* at *x* = 0.5; (b) maximum value of *u* at *x* = 0.66; *U* = 6.0, F_1 = 4.5 and A_0 = 0.15.

mechanism are almost the same as those of the nonlinear damping mechanism. However, the nonlinear damping mechanism leads to higher forcing amplitudes compared to the simple linear viscous mechanism for higher values of the excitation frequency.

Declaration of conflicting interests

The author(s) declared no potential conflicts of interest with respect to the research, authorship, and/or publication of this article.

Funding

The author(s) received no financial support for the research, authorship, and/or publication of this article.

ORCID iDs

Ali Farajpour https://orcid.org/0000-0003-1114-7393
Mergen H Ghayesh https://orcid.org/0000-0003-4883-0786

References

Amiri A, Talebitooti R and Li L (2018) Wave propagation in viscous-fluid-conveying piezoelectric nanotubes considering surface stress effects and Knudsen number based on nonlocal strain gradient theory. *The European Physical Journal Plus* 133(7): 252.

Arda M and Aydogdu M (2019) Dynamic stability of harmonically excited nanobeams including axial inertia. *Journal of Vibration and Control* 25(4): 820–833.

Askari H and Esmailzadeh E (2017) Forced vibration of fluid conveying carbon nanotubes considering thermal effect and nonlinear foundations. *Composites Part B: Engineering* 113: 31–43.

Atashafrooz M, Bahaadini R and Sheibani HR (2018) Nonlocal, strain gradient and surface effects on vibration and instability of nanotubes conveying nanoflow. *Mechanics of Advanced Materials and Structures* 1–13.

Bahaadini R, Saidi AR and Hosseini M (2018) On dynamics of nanotubes conveying nanoflow. *International Journal of Engineering Science* 123: 181–196.

Behera L and Chakraverty S (2016) Effect of scaling effect parameters on the vibration characteristics of nanoplates. *Journal of Vibration and Control* 22(10): 2389–2399.

Beskok A and Karniadakis GE (1999) Report: a model for flows in channels, pipes, and ducts at micro and nano scales. *Microscale Thermophysical Engineering* 3(1): 43–77.

Civalek Ö and Akgöz B (2013) Vibration analysis of micro-scaled sector shaped graphene surrounded by an elastic matrix. *Computational Materials Science* 77: 295–303.

Ebrahimi F, Barati MR and Haghi P (2018) Wave propagation analysis of size-dependent rotating inhomogeneous nanobeams based on nonlocal elasticity theory. *Journal of Vibration and Control* 24(17): 3809–3818.

Farajpour A, Ghayesh MH and Farokhi H (2018) A review on the mechanics of nanostructures. *International Journal of Engineering Science* 133: 231–263.

Farajpour A, Ghayesh MH and Farokhi H (2019) Application of nanotubes in conveying nanofluid: a bifurcation analysis with consideration of internal energy loss and geometrical imperfection. *Microsystem Technologies* 25(11): 4357–4371.

Farajpour A, Rastgoo A and Farajpour MR (2017) Nonlinear buckling analysis of magneto-electro-elastic CNT-MT hybrid nanoshells based on the nonlocal continuum mechanics. *Composite Structures* 180: 179–191.

Farokhi H and Ghayesh MH (2015) Thermo-mechanical dynamics of perfect and imperfect Timoshenko microbeams. *International Journal of Engineering Science* 91: 12–33.

Farokhi H and Ghayesh MH (2016) Size-dependent parametric dynamics of imperfect microbeams. *International Journal of Engineering Science* 99: 3955.

Farokhi H and Ghayesh MH (2018) Viscoelastic resonant responses of shear deformable imperfect microbeams. *Journal of Vibration and Control* 24(14): 3049–3062.

Farokhi H, Ghayesh MH, Gholipour A, et al. (2018) Modal interactions and energy transfers in large-amplitude vibrations of functionally graded microcantilevers. *Journal of Vibration and Control* 24(17): 3882–3893.

Filiz S and Aydogdu M (2015) Wave propagation analysis of embedded (coupled) functionally graded nanotubes conveying fluid. *Composite Structures* 132: 1260–1273.

Ghadiri M and Shafiei N (2017) Vibration analysis of a nano-turbine blade based on Eringen nonlocal elasticity applying the differential quadrature method. *Journal of Vibration and Control* 23(19): 3247–3265.

Ghayesh MH (2018a) Dynamics of functionally graded visco-elastic microbeams. *International Journal of Engineering Science* 124: 115–131.

Ghayesh MH (2018b) Functionally graded microbeams: simultaneous presence of imperfection and viscoelasticity. *International Journal of Mechanical Sciences* 140: 339–350.

Ghayesh MH, Amabili M and Farokhi H (2013) Three-dimensional nonlinear size-dependent behaviour of Timoshenko microbeams. *International Journal of Engineering Science* 71: 1–14.

Ghayesh MH, Farokhi H and Gholipour A (2017) Oscillations of functionally graded microbeams. *International Journal of Engineering Science* 110: 35–53.

Ghayesh MH, Farokhi H and Hussain S (2016) Viscoelastically coupled size-dependent dynamics of microbeams. *International Journal of Engineering Science* 109: 243–255.

Hadi A, Nejad MZ and Hosseini M (2018) Vibrations of three-dimensionally graded nanobeams. *International Journal of Engineering Science* 128: 12–23.

Hosseini M, Bahaadini R and Jamali B (2018) Nonlocal instability of cantilever piezoelectric carbon nanotubes by considering surface effects subjected to axial flow. *Journal of Vibration and Control* 24(9): 1809–1825.

Liang F and Su Y (2013) Stability analysis of a single-walled carbon nanotube conveying pulsating and viscous fluid with nonlocal effect. *Applied Mathematical Modelling* 37(10–11): 6821–6828.

Lim CW, Zhang G and Reddy JN (2015) A higher-order nonlocal elasticity and strain gradient theory and its applications in wave propagation. *Journal of the Mechanics and Physics of Solids* 78: 298–313.

Malekzadeh P and Shojaee M (2015) A two-variable first-order shear deformation theory coupled with surface and nonlocal effects for free vibration of nanoplates. *Journal of Vibration and Control* 21(14): 2755–2772.

Maraghi ZK, Arani AG, Kolahchi R, et al. (2013) Nonlocal vibration and instability of embedded DWBNNT conveying viscose fluid. *Composites Part B: Engineering* 45(1): 423–432.

Peddieson J, Buchanan GR and McNitt RP (2003) Application of nonlocal continuum models to nanotechnology. *International Journal of Engineering Science* 41(3–5): 305–312.

Reddy JN (2010) Nonlocal nonlinear formulations for bending of classical and shear deformation theories of beams and plates. *International Journal of Engineering Science* 48(11): 1507–1518.

Soltani P, Taherian MM and Farshidianfar A (2010) Vibration and instability of a viscous-fluid-conveying single-walled carbon nanotube embedded in a visco-elastic medium. *Journal of Physics D: Applied Physics* 43(42): 425401.

Tounsi A, Heireche H, Berrabah HM, et al. (2008) Effect of small size on wave propagation in double-walled carbon nanotubes under temperature field. *Journal of Applied Physics* 104(10): 104301.

Wang Y-Z, Li F-M and Kishimoto K (2010) Wave propagation characteristics in fluid-conveying double-walled nanotubes with scale effects. *Computational Materials Science* 48(2): 413–418.

Zenkour AM and Abouelregal AE (2014) Vibration of FG nanobeams induced by sinusoidal pulse-heating via a nonlocal thermoelastic model. *Acta Mechanica* 225(12): 3409–3421.

Zenkour AM and Sobhy M (2013) Nonlocal elasticity theory for thermal buckling of nanoplates lying on Winkler-Pasternak elastic substrate medium. *Physica E: Low-dimensional Systems and Nanostructures* 53: 251–259.